Structure and Mechanics of Covalent-Permanent and Ionic-Reversible Star Polymer Networks

Dissertation

zur Erlangung des Grades “Doktorin der Naturwissenschaften”

im Promotionsfach Chemie

am Fachbereich Chemie, Pharmazie, Geographie und Geowissenschaften

der Johannes Gutenberg-Universität Mainz

Nora Fribiczer

geboren in Kandel

Mainz, 2024

Die vorliegende Arbeit wurde im Zeitraum von November 2019 bis Dezember 2023 im Rahmen der von der Deutschen Forschungsgemeinschaft (DFG) geförderten Forschergruppe FOR2811 „Adaptive Polymergele mit kontrollierter Netzwerkstruktur ″ im Arbeitskreis von [redacted] am Department Chemie der Johannes Gutenberg-Universität Mainz angefertigt.

1. Gutachter: [redacted]
2. Gutachter: [redacted]

Tag der mündlichen Prüfung: 20.06.2024

Eigenständigkeitserklärung

Hiermit versichere ich, Nora Fribiczer, dass ich die vorliegende Arbeit selbstständig verfasst und keine anderen als die angegebenen schriftlichen und elektronischen Quellen sowie andere Hilfsmittel benutzt habe. Alle Ausführungen, die anderen Schriften wörtlich oder sinngemäß entnommen wurden, habe ich kenntlich gemacht. Weiterhin versichere ich, dass ich die vorliegende Arbeit noch bei keiner anderen Fakultät bzw. einem anderen Fachbereich als Dissertation eingereicht habe.

Mainz, den 14.03.2024	
(Ort, Datum)	(Unterschrift)

„Man merkt nie, was schon getan wurde,

man sieht immer nur, was noch zu tun bleibt.“

— Marie Curie —

DANKSAGUNG

Ein großer Dank geht an [redacted] für die Übertragung des abwechslungsreichen Forschungsthemas, die fachliche und persönliche Unterstützung während der Promotion sowie die gewährte Freiheit in der Ausgestaltung meiner Forschung und das entgegengebrachte Vertrauen in meine Fähigkeiten als Doktorandin des zentralen Serviceprojekts der FOR2811.

Ein weiterer großer Dank geht an [redacted] für die Übernahme des Zweitgutachtens und die wissenschaftlichen und nicht-wissenschaftlichen Diskussionen während der Promotion. Vielen Dank auch an dieser Stelle für die stete Bereitschaft uns Promovierenden den Rücken zu stärken.

Bei den guten Seelen des AK [redacted] namentlich [redacted] und [redacted] bedanke ich mich herzlichst für den steten administrativen und technischen Support. Ganz besonders möchte ich mich hier bei [redacted] bedanken, die mit ihrer guten Laune und ihrem treuen Begleiter [redacted] in jeder Lebenslage etwas Positives zutage gebracht hat und die über die Jahre nicht nur zu einer geschätzten Kollegin, sondern auch zu einer Freundin geworden ist. Auch unserem akademischen Rat [redacted] möchte ich meinen Dank für den wissenschaftlichen Support aussprechen.

Vielen Dank auch an alle ehemaligen und aktuellen Mitglieder des AK [redacted]. Vielen Dank an die *Golden Generation* [redacted] für die tolle Aufnahme damals in den AK, die vielen Gespräche wissenschaftlicher und nicht-wissenschaftlicher Natur und für eure Hilfe in allen Lebenslagen. Auch vielen Dank an [redacted], dessen Alba-Berlin Sticker den AK für immer bereichern werden. Ein riesiges Dankeschön geht auch an die gesamte *Holzklasse* mit [redacted]. Ohne euch wäre meine Promotionszeit nicht dieselbe gewesen und hätte bestimmt nur halb so viel Spaß gemacht. Ein ganz besonderer Dank geht an [redacted], den Arbeitsmann meines Vertrauens, ohne den das Chaos-Büro nie zu seiner vollen Pracht gefunden hätte. Genauso Danke ich [redacted] für die vielen Trash-TV Abende, die ungemein zur Entspannung beigetragen haben. [redacted] danke ich besonders für die gute Zusammenarbeit im Hinblick auf die FOR2811.

Ebenso geht ein Dank an den [redacted] für die lustigen Mittagessen, Kuchennachmittage und Bowle/Secco-Abende.

Des Weiteren möchte ich meinen Mitstreitern der FOR2811 für die gute Zusammenarbeit, den stetigen gegenseitigen Support und den freundschaftlichen Zusammenhalt danken. Ich danke hierbei ganz besonders [redacted] für viele lustige Treffen online und in Persona, die gemeinsame Konferenz in Rom und das Wissen in diesem „Hühnerhaufen“ nicht allein zu sein. Ohne euch wäre meine Promotion im wahrsten Sinne des Wortes nicht möglich gewesen. Ein Dank geht an dieser Stelle auch an [redacted] aus dem [redacted] für die gute Zusammenarbeit.

Abschließend danke ich auch meiner Familie und meinen Freunden für die vollumfängliche Unterstützung auf dem langen Weg zur Promotion, die mir immer Rückhalt gaben und mich in schwierigen Phasen aufgemuntert und bestärkt haben auf dem richtigen Weg zu sein. Meinem Freund [redacted] danke ich für seine stets positive Art, die aufbauenden Worte in stressigen oder schweren Phasen und den Glauben an mich, dass ich alles schaffen kann.

Ich danke ebenso allen Korrekturlesenden dieser Arbeit, den Studierenden, die ich betreuen durfte und allen weiteren Kooperationspartnern und Mitstreitern auf meinem Weg zur Promotion.

Der Deutschen Forschungsgemeinschaft (DFG) danke ich für die finanzielle Unterstützung.

ALLGEMEINE ANMERKUNGEN

Die nachstehende Arbeit wurde im Rahmen der Forschergruppe FOR2811 „Adaptive Polymergele mit kontrollierter Netzwerkstruktur“ durchgeführt. Diese stellt einen Verbund aus mehreren Teilprojekten (TP) dar, die in Syntheseprojekte (TP1–TP2), experimentelle Projekte (TP3–TP5) und Simulationsprojekte (TP6–TP7) unterteilt sind. Das in der 2. Förderperiode (Start im Januar 2023) hinzugestoßene Projekt TP8 befasst sich mit der Eignung der Netzwerke für biomedizinische Anwendungen sowie deren Zellkompatibilität. Die vorliegende Dissertation wurde im Teilprojekt TP4 mit dem initialen Titel „Mesoskopische Netzwerktopologie und Permeabilität Adaptiver Amphiphiler Conetzwerke“ angefertigt. Auf die allgemeine Forschungsfrage und die Ziele der FOR2811 sowie die Rolle und Zielsetzung der vorliegenden Dissertation darin wird im Kapitel *Motivation and Scientific Goal* eingegangen. Ebenso wird dort das Zusammenspiel der einzelnen Teilprojekte zum Erkenntnisgewinn erläutert.

Die nachfolgende Arbeit gliedert sich in eine theoretische Einführung, eine Darstellung des wissenschaftlichen Ziels, einen wissenschaftlichen Hauptteil und eine Zusammenfassung. Die Ergebnisse des wissenschaftlichen Hauptteils (*Chapter I–VI*) wurden wie unten aufgeführt im Peer-Review Verfahren in wissenschaftlichen Fachjournalen veröffentlicht oder zur Veröffentlichung eingereicht. Dabei bilden jeweils die *Chapter I–IV* eine thematische Einheit zu kovalent verknüpften Netzwerken sowie die *Chapter V–VI* zu ionisch-reversibel verknüpften Netzwerken. Weitere Projekte und Publikationen sind im Kapitel *Further Projects* zusammenfasst.

Chapter I:

[redacted], **N. Fribiczer**, [redacted]; *Macromolecules*, **2022**, 55, 15, 6573–6589.

Chapter II:

N. Fribiczer, [redacted];
Macromol. Chem. Phys., **2023**, 2300389

Chapter III:

[redacted], **N. Fribiczer**, [redacted]; *Polym. Chem.,* **2023**, 14, 1965–1977.

Chapter IV:

[redacted], **N. Fribiczer**, [redacted]; *Polymer,* **2024**, *under review*

Chapter V:

[redacted], **N. Fribiczer**, [redacted]; *Polym. Chem.,* **2022**, 13, 4298–4308.

Chapter VI:

[redacted], **N. Fribiczer**, [redacted]; *Macromolecules,* **2024**, *under review*

Zur Einordnung in den Gesamtkontext der Arbeit wird jedem dieser Kapitel eine spezifische Zusammenfassung vorangestellt und die Eigenleistung erläutert. Die zugehörigen *Supporting Information* sind im Appendix dargestellt. Die Nummerierung von Abbildungen, Tabellen und Schemata sowie die Angabe von Literaturstellen erfolgt kapitelweise. Die Adaption der Publikationen geschieht mit der Erlaubnis der Co-Autoren sowie der herausgebenden Verlage.

Die Ergebnisse und Publikationen in der vorliegenden Arbeit wurden aufgrund der Projektstruktur in der FOR2811 kollaborativ und in enger Kooperation mit den anderen Teilprojekten erzielt. Um eine Zuordnung der Mitwirkenden der einzelnen Publikationen zu den Teilprojekten der FOR2811 zu ermöglichen, sind diese in der folgenden Tabelle aufgeschlüsselt. Weitere Informationen sind auf der Website des Verbunds unter „https://www.for2811.uni-mainz.de/“ zugänglich.

Tabelle 1: Zuordnung der Mitwirkenden der einzelnen Teilprojekte der FOR2811.

TP	Titel des Projekts laut Antrag	Name	Rolle
TP1	Synthese von kovalent vernetzten amphiphilen Co-Netzwerken mit Modellcharakter	[redacted]	[redacted]
		[redacted]	[redacted]
TP2	Reversibel elektrostatisch vernetzte amphiphile Conetzwerke aus sternförmigen Blockcopolymeren	[redacted]	[redacted]
		[redacted]	[redacted]
TP3	Netzwerkmaschenstruktur und makroskopische Mechanik von amphiphilen Conetzwerken	[redacted]	[redacted]
		[redacted]	[redacted]
TP4	Mesoskopische Netzwerktopologie und Permeabilität adaptiver amphiphiler Conetzwerke	[redacted]	[redacted]
		[redacted]	[redacted]
TP5	Struktur und ortsaufgelöste Mechanik sowie Rheologie oberflächennaher Bereiche von adaptiven Polymernetzwerken	[redacted]	[redacted]
		[redacted]	[redacted]
TP6	Simulation adaptiver Polymergele mit kontrollierter Netzwerkstruktur	[redacted]	[redacted]
		[redacted]	[redacted]
TP7	Simulation von elektrostatisch reversibel verknüpften Modellnetzwerken	[redacted]	[redacted]
		[redacted]	[redacted]
TP8	Zellkompatibilität amphiphiler Conetzwerke für biomedizinische Anwendungen	[redacted]	[redacted]
		[redacted]	[redacted]

ZUSAMMENFASSUNG

Die Eigenschaften von Polymernetzwerken und -gelen wie Quellung, Mechanik und Permeabilität hängen im Allgemeinen von ihrer zugrundeliegenden Struktur und Zusammensetzung ab. In der vorliegenden Arbeit wird das Zusammenspiel zwischen Synthesebedingungen, resultierender Struktur und damit verbundener Eigenschaften auch in Abhängigkeit der Umgebungsparameter kollaborativ im Rahmen der Forschergruppe FOR2811 untersucht. Hierzu werden kovalent-permanent und ionisch-reversible Modellnetzwerke basierend auf vierarmigen Sternpolymeren hergestellt und eingehend charakterisiert. Im Rahmen der kovalenten Verknüpfung der Bausteine werden amphiphile Polymerconetzwerke (APCN) betrachtet, die sich durch eine umgebungssensitive Viskoelastizität und selektive Permeabilität auszeichnen. Im Kontext der ionisch-reversiblen Verknüpfung werden hingegen rein hydrophile Netzwerke untersucht, um zunächst die Umsetzbarkeit dieser Verknüpfungsweise zu demonstrieren.

Im *ersten Teil* der Arbeit liegt der Fokus auf den heterokomplementär *kovalent verknüpften amphiphilen Polymerconetzwerken* bestehend aus sternförmigen Polymeren beziehungsweise Blockcopolymeren. In einer ersten Studie werden Netzwerke durch heterokomplementäre Verknüpfung von tetra-Poly(ethylenglykol) (t-PEG) und tetra-Poly(ε-caprolacton) (t-PCL) unter verschiedenen Synthesebedingungen hergestellt und grundlegenden charakterisiert. Die Charakterisierung erfolgt ausgehend vom Lösungsverhalten der Netzwerkbausteine über die Netzwerkbildung hin zu den finalen Netzwerken (Quelleigenschaften, Konnektivität und Mechanik).

Eine zweite Studie erweitert diesen Ansatz um Untersuchungen der Netzwerke im gequollenen Zustand sowohl im nicht-selektiven als auch im selektiven Lösungsmittel. Die Mechanik wird auf verschiedenen Längenskalen mittels Rheologie und Rasterkraftmikroskopie sowohl an der Oberfläche als auch im Bulk bestimmt. Durch die Methode der Rasterkraftmikroskopie ist zudem die Oberflächenstruktur zugänglich, wodurch die Detektion einer potenziellen Phasenseparation ermöglicht wird.

Zur gezielten Erzeugung bestimmter Morphologien (sphärisch, lamellar, etc.) und Funktionen (z.B. gerichteter Wirkstofftransport) können die Netzwerke bereits bei der Präparation vorstrukturiert werden. Erreicht wird eine solche Vorstrukturierung durch Nutzung sogenannter Kern-Schale-Systeme aus amphiphilen Blockcopolymeren. Um ein grundsätzliches Verständnis des Verhaltens solcher Blockcopolymere zu erhalten, werden in einer dritten Studie

t-PCL-*b*-PEG Sternpolymere synthetisiert und ihr Lösungsverhalten in verschiedenen Lösungsmitteln mit unterschiedlicher Lösungsmittelqualität charakterisiert. Ein besonderes Augenmerk wird hierbei auf das Verhalten in Wasser gelegt, da hier mizellartige Strukturen zu erwarten sind. Zudem wird der Einfluss der Länge des PEG-Blocks auf das Verhalten in Lösung untersucht.

In einer vierten Studie werden schließlich Netzwerke bestehend aus Blockcopolymeren in den Fokus gerückt. Diese werden durch Vernetzung von t-PEG-*b*-PCL mit heterokomplementären Endgruppen erhalten. Es wird das inverse Blockcopolymer zur vorigen Studie verwendet, da sich die Endgruppenmodifikation im umgekehrten Fall als synthetisch herausfordernd erwiesen hat. Es findet eine umfassende Charakterisierung statt beginnend mit den Netzwerkbausteinen, über die Vernetzung hin zu den Netzwerken und deren Eigenschaften wie Quellverhalten und Mechanik sowohl im Präparationszustand als auch im gequollenen Zustand. Ein Vergleich der Ergebnisse mit den Netzwerken aus separaten hydrophilen und hydrophoben Bausteinen zeigt eine grundsätzliche Übereinstimmung der Netzwerkparameter.

Im *zweiten Teil* der Arbeit wird nun die *ionisch-reversible Verknüpfung der Bausteine* in den Blick genommen. Hierzu sind geeignete ionische Netzwerkbausteine nötig, d.h. Polyelektrolyte oder Polyampholyte, die aus sternförmigen Blockcopolymeren bestehen. Durch diese Architektur ist es möglich die Stärke der Bindung im Netzwerk durch Länge und Art des ionischen Blocks zu variieren. In einer fünften Studie wird daher ein Blockcopolymer bestehend aus t-PEG und Poly(dehydroalanin) (PDha), t-PEG-*b*-PDha, synthetisiert und der Einfluss der Blocklänge des PDha und des Molekulargewichts des PEG-Kerns auf das Verhalten in Lösung untersucht. Durch die ampholytische Natur des PDha kann die Netto-Ladung über den pH-Wert eingestellt und somit die Wechselwirkung zwischen den ionischen Blöcken gesteuert werden. Hiermit wird demonstriert, wie der pH-Wert die Struktur von Polyampholyten in Lösung beeinflusst und wie sich eine Variation der Blocklänge des ionischen Blocks darauf auswirkt.

In einer letzten, sechsten Studie wird nun der Schritt vom ionischen Netzwerkbaustein hin zum fertigen Netzwerk bzw. Gel vollzogen, indem ein t-PEG Kern entweder mit Polycarboxybetainmethacrylamid (PCBAMAA) oder mit Polystyrolsulfonat (PSSNa) Blöcken funktionalisiert und beide Komponenten bei einem geeigneten pH-Wert gemischt werden. Ob die Wechselwirkungen zwischen den Polymeren attraktiv oder repulsiv sind, kann über den pH-Wert gesteuert werden. Damit ist es möglich gezielt sowohl einen Sol-Zustand als auch einen Gel-Zustand einzustellen und die Umsetzbarkeit der Verknüpfungsweise sowie deren mögliche Reversibilität zu demonstrieren.

ABSTRACT

The properties of polymer networks and gels, such as swelling, mechanics and permeability, generally depend on their underlying structure and composition. In the present work, the interplay between synthesis conditions, resulting structure and corresponding properties, also as a function of environmental parameters, is investigated collaboratively within the research unit FOR2811. For this purpose, covalent-permanent and ionic-reversible model networks based on four-armed star polymers are prepared and characterized in detail. In the context of the covalent linkage of the building blocks, amphiphilic polymer co-networks (APCN) are considered, which are characterized by an environmentally sensitive viscoelasticity and selective permeability. In the context of ionic-reversible linkage, however, purely hydrophilic networks are investigated in order to demonstrate an initial proof of concept.

The *first part* of this thesis focuses on hetero-complementary, *covalently crosslinked amphiphilic polymer co-networks* consisting of star-shaped polymers or block copolymers. In a first study, networks of tetra-poly(ethylene glycol) (t-PEG) and tetra-poly(ε-caprolactone) (t-PCL) are prepared by hetero-complementary crosslinking under different synthesis conditions. They are thoroughly characterized starting from the solution behavior of the network building blocks via network formation to the final networks (swelling properties, connectivity of the star polymers, and mechanics).

A second study extends this research by investigating the networks in the swollen state in both a non-selective and a selective solvent. The mechanics are determined on different length scales using rheology and atomic force microscopy both on the surface and in the bulk. The surface structure is also accessible by means of the latter technique, which enables the detection of potential phase separation effects.

The networks can also be pre-structured at preparation to generate specific morphologies (spherical, lamellar, etc.) and functions (e.g. directed drug transport). Such pre-structuring can be achieved by using so-called core-shell systems of amphiphilic block copolymers. In order to gain a basic understanding of the behavior of such block copolymers, t-PCL-*b*-PEG star polymers are synthesized in a third study. Their solution behavior in different solvents with various solvent qualities is characterized. Special attention is paid to the behavior in water, as micellar structures are expected. In addition, the influence of the length of the PEG block on the behavior in solution is investigated.

Finally, a fourth study focuses on networks consisting of block copolymers. These are obtained by crosslinking t-PEG-*b*-PCL with hetero-complementary end linking groups. The inverse block copolymer to the previous study is used, as end group modification in the reverse case proved to be synthetically challenging. A comprehensive characterization is carried out starting with the network building blocks, through the crosslinking reaction to the final networks and their properties such as swelling behavior and mechanics both in the as-prepared and in the swollen state. A comparison of the results with the networks of separate hydrophilic and hydrophobic building blocks reveals a fundamental agreement of the network parameters.

The *second part* of the work focuses on the *ionic-reversible linking of the building blocks*. This requires suitable ionic components, i.e. polyelectrolytes or polyampholytes, which can consist of star-shaped block copolymers. This architecture allows the modification of the bond strength in the network by varying the length and type of ionic block. In a fifth study, a block copolymer consisting of t-PEG and poly(dehydroalanine) (PDha), t-PEG-*b*-PDha, is therefore synthesized and the influence of the block length of the PDha segments and the molecular weight of the PEG core on the solution behavior is investigated. Due to the ampholytic nature of PDha, the net charge can be adjusted via the pH value. This allows control over the interactions between the ion blocks by the pH-value. The study demonstrates how the pH-dependent structure of polyampholytes in solution is affected by the length of the ionic block.

In a final, sixth study, the step from ionic block copolymers to the final network or gel is completed by functionalizing a t-PEG core with either polycarboxybetaine methacrylamide (PCBAMAA) or polystyrene sulfonate (PSSNa) blocks and mixing both components at a suitable pH. Whether the interactions between the polymers are attractive or repulsive can be controlled by the pH value. This allows both a sol state and a gel state to be reached selectively and demonstrates both proof of concept and possible reversibility of this type of crosslinking.

TABLE OF CONTENTS

1. THEORETICAL BACKGROUND

1.1. Introduction

The first polymer networks were produced long before neither the terms polymer, macromolecule, or polymer network nor the underlying structures were known. The first documented appearance of polymer networks in human history dates back to 1600 BC, when natural rubber was used by the South American natives to produce waterproof materials. The next recorded development was the sulfur vulcanization of natural rubber in 1839 by Charles Goodyear, the first ever synthetically crosslinked polymer network.[1]

Only about 100 years later, in 1920, Hermann Staudinger postulated his macromolecular hypothesis that macromolecules with high molecular mass are chain molecules consisting of covalently linked monomeric building blocks. He introduced the term macromolecule and thus initiated modern polymer science.[1–3] Wallace H. Carothers played another important role in the development of polymer chemistry with his work on the controlled production of synthetic polymers by polycondensation and polyaddition. He defined polymerization as "*any chemical combination of a number of similar molecules to form a single molecule*" and thus contributed significantly to the acceptance of the covalent nature of macromolecules.[3–5] In general, the early to mid of the 20th century was characterized by the development and commercialization of polymer-based materials like Bakelite, Epoxies, Polyurethane fibers and foams, Butyl Rubber, and Nylon among others. The acceptance of Staudinger's hypothesis in the 1930s and its understanding paved the way to a rational design of polymeric materials. Inventions before, like Bakelite, were solely based on empirical studies and trial-and-error optimizations.[1,3] Thirty years after the initial hypothesis, Staudinger was finally awarded the Nobel Prize in Chemistry in 1953 "*for his discoveries in the field of macromolecular chemistry*".[3,6]

The terms polymer and macromolecule are often used synonymously but differ in an important structural property. According to the International Union of Pure and Applied Chemistry (IUPAC) the term polymer is defined as "*A molecule of high relative molecular mass, the structure of which essentially comprises the multiple repetition of units derived, actually or conceptually, from molecules of low relative molecular mass*".[3,7] The term macromolecule is more general and is derived from the Greek word "*macro*", meaning large, and the word molecule and is associated with molar masses of 10^4–10^7 g mol^{-1} and sizes of 10–100 nm. A polymer is a type of macromolecule that is composed of many monomeric repeating units. In contrast, a

macromolecule does not have to be composed of repeating monomer units. Thus, every polymer is a macromolecule, but not every macromolecule is a polymer.[8]

1.2. Classification of Polymer Networks and Gels

1.2.1. Polymer Networks

Polymer networks are divided in various classes dependent on the constituting structural units and the type of interactions. In general, according to the IUPAC definition, a **network** in polymer chemistry is "*A highly ramified macromolecule in which essentially each constitutional unit is connected to each other constitutional unit and to the macroscopic phase boundary by many permanent paths through the macromolecule, the number of such paths increasing with the average number of intervening bonds; the paths must on the average be co-extensive with the macromolecule.*

1. Usually, and in all systems that exhibit rubber elasticity, the number of distinct paths is very high, but, in most cases, some constitutional units exist which are connected by a single path only.

2. If the permanent paths through the structure of a network are all formed by covalent bonds, the term covalent network may be used.

3. The term physical network may be used if the permanent paths through the structure of a network are not all formed by covalent bonds but, at least in part, by physical interactions, such that removal of the interactions leaves individual macromolecules or a macromolecule that is not a network."[7]

The additions to the definition already indicate that networks can be classified as **physical** or **chemical** (**covalent**) depending on the type of crosslinking or crosslinking points, respectively. Chemical networks consist of covalently linked building blocks. The network formation occurs either directly during a polymerization reaction or through a crosslinking reaction of the macromonomers after polymerization. Physical networks, in contrast, are of supramolecular nature. In this case, the crosslinking points consist of associations of polymer molecules through hydrogen bonds, Coulomb interactions, Van der Waals interactions or metal-ligand complexation. However, interlocking or entanglement of the polymers with each other, crystallization or other specific interactions can also result in the formation of a physical network. The major difference between the two types of networks is their possible reversibility. While the covalent

linkage is usually permanent and irreversible, the physical linkage can be reversible if the conditions are chosen accordingly [4,7,9–13]

When polymer networks are viewed from a structural perspective, the following can be stated about the crosslinking points: polymer networks are comprised of network junctions or crosslinks, which have three or more groups (branch functionality *f*) emanating from a core, connected by *f* strands. Junctions and strands can be linked together via physical interactions or covalent bonds.[4]

If the linking is of physical nature and based on electrostatics, a further class of polymer networks can be identified. This class of networks is based on polyelectrolytes, i.e. ionic polymeric materials which can be "crosslinked" using suitable oppositely charged segments and suitable environmental conditions (pH, salt concentration).[14] Corresponding, a **polyelectrolyte network** is a "*polymer network containing ionic or ionizable groups in a substantial fraction of its constitutional units*" and is sometimes called a "*crosslinked polyelectrolyte*", but the use of the term is only recommended if "*the polyelectrolyte network is formed by the crosslinking of existing polyelectrolyte macromolecules.*"[7]

The structure of polymer networks can also be viewed on length scales beyond the crosslinking points, as depicted in **Figure 1. 1**.

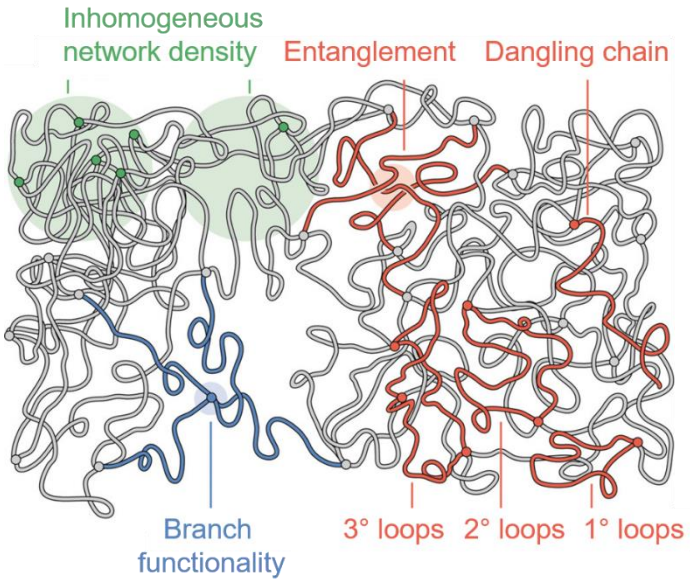

Figure 1. 1: Topological features of amorphous polymer networks on different length-scales: At 10–100 nm the topology is characterized by density inhomogeneities (green), whereas at 1–10 nm dangling chains, loops of different order and entanglements dominate the network structure (red). At the molecular level of < 1 nm, the network features are determined by the branch functionality (blue). (Figure adapted with permission from Ref. [4] ©2019 Wiley-VCH Verlag GmbH & Co. KGaA, Weinheim)

Concentration fluctuations during network formation result in spatial inhomogeneities of junction or strand density on length scales of 10–100 nm. At smaller length scales of 1–10 nm, nanostructural inhomogeneities consist of connectivity defects such as loops and dangling chains as well as mechanical entanglement of polymer chains. Such dangling chains and loop structures are also called network defects. At the molecular scale (< 1 nm), the branch functionality f is a decisive feature which dictates the network structure.[4,7,15,16]

The extent of these inhomogeneities is dependent on the type of building block and chemistry used to prepare the polymer networks. If multi-arm polymers with a narrow molecular weight distribution are end-linked, fairly homogeneous networks can be obtained. A hetero-complementary end-linking approach prevents the formation of primary loops and thus reduces the amount of nanostructural inhomogeneities. Networks prepared with this strategy are referred to as *model networks* in literature.[17–20] This nomenclature corresponds to the respective definition of the IUPAC, which defines a **model network** as "*polymer network synthesized using a reactant or reactants of known molar mass or masses and chemical structure*" and "*prepared […] by crosslinking of existing polymer chains*." It is furthermore stated that "*a model network is not necessarily a perfect network"* due to loose ends resulting from crosslinking of existing polymer chains and occurring "*ring structures as network imperfections*". These imperfections result in a reduction of the concentration of elastically active network chains and thus in a lower modulus compared to theoretical expectations for a perfect network.[7]

A **perfect network**, however, is defined as "*polymer network composed of chains all of which are connected at both their ends to different junction points*." It is further stated that "*If a perfect network is in the rubbery state then, on macroscopic deformation of the network, all of its chains are elastically active and display rubber elasticity.*"[7] With this distinction, the IUPAC clearly separates theoretically perfect networks from experimental reality and at the same time provides a reason why the modulus of experimentally produced model networks is below the theoretical expectations of a perfect network. This definition of a perfect network corresponds to the definition of an **ideal network**. The requirements for an ideal network are: (i) identical length of all network strands; (ii) constant functionality of crosslinking points throughout the entire network; (iii) conformation of network strands obey Gaussian statistics; (iv) macroscopic and microscopic homogeneity; and (v) no entanglement of network strands with each other.[19,21–23]

Model networks according to the above IUPAC definition are therefore also referred to as near-ideal networks.[1,21,24–26] In literature, however, the term model network is sometimes

equated with the term perfect network. Thus, some experimentally prepared networks are termed near-model or quasi-model networks.[13,27,28]

1.2.2. Polymer Gels

Since the early statement by D. Jordan Lloyd "*The colloidal condition, the 'gel', is one which is easier to recognize than to define*", many attempts have been made to define the term polymer gel.[29] The most common description of a polymer gel today is a three-dimensional polymer network structure containing a liquid or swollen in a solvent, respectively. In some cases the addition "*swollen but not dissolved in solvent*" is stated, which only applies to covalently cross-linked polymer networks.[23,30–33] For a more precise definition, we refer again to the standard source for such definitions, the IUPAC, which defines the term gel as follows *"Non-fluid colloidal network or polymer network that is expanded throughout its whole volume by a fluid."*[7] With the corresponding characteristics:

"[…]

2. A gel can contain:

> *1. a covalent polymer network, e.g., a network formed by crosslinking polymer chains or by non-linear polymerization;*
>
> *2. a polymer network formed through the physical aggregation of polymer chains, caused by hydrogen bonds, crystallization, helix formation, complexation, etc, that results in regions of local order acting as the network junction points. The resulting swollen network may be termed a thermoreversible gel if the regions of local order are thermally reversible;*
>
> *3. a polymer network formed through glassy junction points, e.g., one based on block copolymers. If the junction points are thermally reversible glassy domains, the resulting swollen network may also be termed a thermoreversible gel;*
>
> *4. lamellar structures including mesophases, e.g., soap gels, phospholipids and clays;*

[…]"[7]

The definition of a gel thus refers directly to the previous definition of a polymer network. Accordingly, gels can be classified by the type of crosslinking as **physical**ly crosslinked gels and **chemical**ly or covalently crosslinked gels, respectively. With respect to the reversibility, physical gels are also termed **reversible** gels. In addition, polymeric gels can be divided into

natural and **synthetic** gels based on the polymer source. If gels are categorized according to their size, **macro**, **micro** (100 nm–1 μm) and **nano** (< 100 nm) gels can be distinguished. Polymer gels can also be classified depending on the fluid medium; they are termed **hydrogel**, if swollen in water, or **organogel**, if swollen in organic media. In each of these categories, further distinctions can be made on the basis of specific characteristics or properties.[7,11,12,31–33,34]

1.3. Amphiphilic Polymer Co-Networks

The first systematic studies on amphiphilic polymer co-networks (APCN) were published simultaneously by Weber and Stadler[35] as well as Chen, Kennedy and Allen[36] in 1988. The former authors combined polybutadiene and poly(ethylene glycol) whereas the latter ones used polyisobutylene and 2-(dimethylamino)ethyl methacrylate to create first amphiphilic polymer co-networks. Since these early days, APCNs have gained attention and relevance due to their unique properties and rich structural diversity.[37–40]

1.3.1. Definition

According to the name, an amphiphilic polymer co-network consists of a polymer network that contains both hydrophilic and hydrophobic components. The suffix “co” in front of the word “network” refers to the presence of two network components, i.e. a hydrophilic and a hydrophobic one.[13,40]

A quite comprehensive definition of the term can be found in the review by Erdodi and Kennedy who state that “ *amphiphilic co-networks are two-component networks of covalently interconnected hydrophilic/hydrophobic (HI/HO) phases of cocontinuous morphology; as such they swell in water and in hydrocarbons, and respond to changes in the medium by morphology isomerization (‘smart’ networks).”*[40] An important point is the restriction of the definition to covalent linkage of the phases or building blocks, respectively. This excludes systems with dispersed, i.e. not cocontinuous hydrophilic and hydrophobic phases. According to this definition, APCNs are recognized by the following three coexisting properties: (i) simultaneous presence of HI and HO phases in the network; (ii) HI and HO phases are covalently crosslinked resulting in phase cocontinuity; and (iii) microphase separation due to thermodynamic incompatibility between HI and HO.[38,40]

But also more general definitions like "*APCNs comprise hydrophilic and hydrophobic units, with at least one of the two types of units encountered in sufficient long segments*"[18] or definitions based on the swelling ability like "*polymer hydrogels containing hydrophobic units in addition to the hydrophilic ones*"[41] are found in literature. Since swelling in water and hydrocarbons is possible, APCNs can also be classified as hydrogels and organogels in the respective solvent.[40,41]

The term "polymer" is often omitted in the naming or not included in the abbreviation, which is why the abbreviation ACN is used synonymously with the abbreviation APCN for amphiphilic polymer co-networks. In the present work, however, amphiphilic *polymer* co-networks are considered at all times.

1.3.2. Design of APCN

In general, covalently linked APCNs can be prepared either by radical copolymerization with simultaneous crosslinking, by sequential "living" polymerization and crosslinking or by end-linking of suitably functionalized hydrophilic and hydrophobic polymer precursors. The review by Erdodi and Kennedy[40], for example, provides an illustrative overview of these techniques. The key difficulty in APCN synthesis is the thermodynamic incompatibility of the hydrophilic and hydrophobic components, especially if polymeric precursors are used. Due to thermodynamic incompatibility, phase separation may occur, which should be avoided at all costs, otherwise heterogeneous networks will be obtained. To overcome this obstacle, common good solvents for both components are employed or low molecular weight starting materials are used. Other strategies involve the utilization of large hydrophobic protecting groups or the crosslinking of functional amphiphilic multiblock copolymers.[37,40–42]

Within the framework of covalent linkage and the aforementioned synthesis strategies, various APCN designs are obtainable, a selection of which is shown in **Figure 1. 2**. The first possibility is to combine amphiphilic ABA-triblock polymers (1); a second one results from the randomly crosslinking of hydrophobic monomers with hydrophilic monomers or hydrophobic-protected hydrophilic monomers (2 and 6). In addition, crosslinking of telechelic polymers (3), graft polymers (4), a combination of linear and star polymers (5), or star polymers (7) can lead to APCNs. A further design includes the crosslinking of linear polymers with a long crosslinker of the opposite philie (8).[39] The designs 1,3,5, and 7 may lead to model networks if polymers with a known molar mass and low dispersity are used together with a suitable end-linking strategy. One possible end-linking strategy for precise APCN synthesis is 'click'-chemistry, i.e.

in general a hetero-complementary reaction of the corresponding functionalized end-linking groups.[37] A more detailed explanation of click chemistry and its contribution to the synthesis of model networks is given in **Section 1.4**.

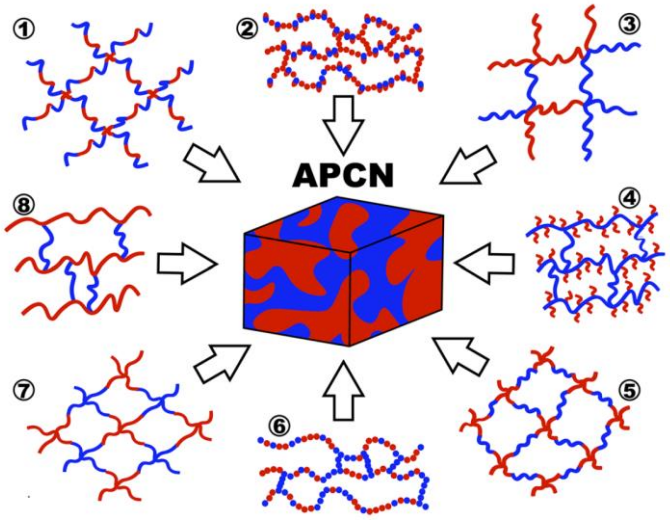

Figure 1. 2: Crosslinking methods used to combine hydrophobic (red) and hydrophilic (blue) building blocks to form APCNs. (1) Crosslinked ABA-triblock polymers. (2) Copolymerized and crosslinked hydrophobic and hydrophobic-protected hydrophilic monomers. (3) Crosslinked telechelic polymers. (4) Crosslinked graft copolymers. (5) Crosslinked hydrophobic star polymers and linear hydrophilic polymers. (6) Copolymerized and crosslinked hydrophobic and hydrophilic monomers. (7) Crosslinked hydrophobic and hydrophilic star polymers. (8) Hydrophobic polymers crosslinked by long hydrophilic crosslinkers. (Reprinted with permission from Ref [39] © The Royal Society of Chemistry 2020.)

1.3.3. Properties and Application

Amphiphilic polymeric co-networks exhibit a variety of properties based on their main characteristics, namely their amphiphilicity, their swelling ability and the possibility of incorporating numerous functional groups (see **Figure 1. 3**). Due to their swelling in water, they can be termed hydrogels. The reduced swelling in water while maintaining biocompatibility is an advantage over conventional hydrogels, which are often used in biological or medical applications. The swelling otherwise leads to a weakening of the gel and at the same time to a damage of the surrounding tissue, which can be reduced by use of APCNs. In the swollen state, the gels are furthermore permeable for diffusive solute transport, e.g. gas, nutrients, drugs, or proteins. The amphiphilicity of the networks leads to self-organization and microphase separation in analogy to non-crosslinked block copolymers (surfactants) with a similar morphology, but in a distorted fashion due to the limitations imposed by crosslinking. The swelling is not only limited to water but is also possible in organic solvents. The selective swelling can lead to selective permeability for respective solute substances and can in addition be utilized for the targeted release of guest

substances. The mechanical properties of the gels are likewise environmental sensitive and change accordingly with a change in the swelling medium. In addition, also simultaneous swelling in both aqueous and organic media is conceivable. The introduction of functional groups into APCNs is a versatile tool to incorporate properties like degradability, self-healing, protein or cell adsorption, enhanced mechanics, and responsiveness to pH, temperature, salt concentration, light, or deformation among others.[24,37,42,43]

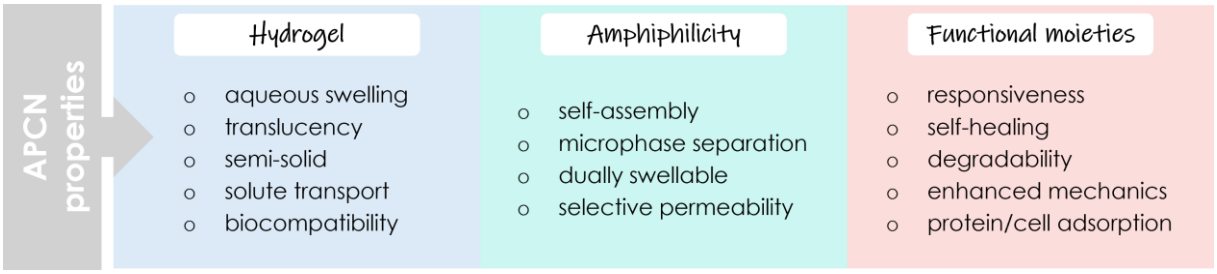

Figure 1. 3: Selection of APCN properties based on the main APCN characteristics.[37]

Due to this variety of adjustable properties, APCNs offer the potential for many possible applications. The most common and commercial application of APCNs are soft contact lenses with extended wear-time. The hydrophobic phase provides high oxygen permeability whereas the hydrophilic phase ensures wettability and on-eye lens movement. The mechanical properties of the lenses are controlled by the crosslinking density and the ratio of hydrophilic and hydrophobic components. In addition, there are many potential biomedical applications for APCNs like drug delivery devices, support for cell proliferation or in general as cell culture surfaces, matrices or membranes for drug or nutrient delivery, tissue engineering, or artificial pancreas.[37,38,40,41] In the field of biomedical applications, many research articles deal with amphiphilic hydrogels based on the hydrophobic polycaprolactone (PCL) and hydrophilic poly (ethylene glycol) (PEG) due to their complementary properties and biocompatibility. PEG is used as hydrophilic phase in most hydrogels because of its good solubility in water and organic solvents, non-toxicity, and absence of antigenicity and immunogenicity. The non-biodegradability of PEG, however, is a severe limitation in bioapplications. The combination with PCL as hydrophobic phase which is biodegradable and biocompatible improves the biodegradability of the respective amphiphilic hydrogels and allows for the transport of hydrophobic substances and drugs. A selection of the synthetic methods for the preparation of networks based on PEG and PCL, the resulting properties and corresponding bioapplications can be found in the review by Dabbaghi et al.[42]

Amphiphilic copolymers in general are also ideal candidates for drug delivery and are being extensively researched for biomedical applications. The review by Perin et al. provides a comprehensive overview of this topic.[42,43] Further potential areas of application for APCNs are chemical and biochemical sensors, membranes for chiral separation, switchable aqueous permeation control, antimicrobial coating, minimal-adhesive surface coatings, antifouling surfaces, and nanoreactors among others.[37,38,40,41,44]

1.4. Synthesis Approaches towards Model Networks

In general polymer networks are formed by chain-growth polymerization (radical polymerization), step-growth polymerization (addition and condensation polymerization), vulcanization, or by end-linking of suitable functionalized prepolymers. Several types of inhomogeneities can be the result of such network formation processes (see also **Section 1.2**): (i) nonuniform spatial distribution of crosslinks; (ii) nonuniform contour length or molecular weight of the network strands; (iii) dangling chains; (iv) loops; and (v) trapped entanglements.[4,15,17]

From all possible network inhomogeneities, loops are the most difficult to control. However, the formation of primary loops can be avoided by use of either rigid monomers or prepolymers with hetero-complementary end-linking which simply cannot react in an intramolecular fashion.[15] The latter approach leads to model networks, which are therefore a promising way to reduce these inhomogeneities and are generally formed by end-linking of suitable prepolymers with a narrow molar mass distribution. For the IUPAC definition of a model network, see **Section 1.2**. The first investigation on model networks were carried out in the 1970s and are based on linear telechelic polymers crosslinked by small molecule crosslinkers with a functionality of $f \geq 3$.[17,45] The first tests with star-shaped instead of linear polymers then took place in the 1980s.[17,46] However, it was not until the 2000s that these became popular as the primary component for model networks.[17,20,47] In particular, end-linking of star polymers with complementary functional groups has been used extensively since then due to the control of branch point functionality.[15,17,25]

Key factors that have to be considered when designing a model network based on the end-linking of star polymers are (**Figure 1. 4**): (i) molecular structure of the stars; (ii) solvent and concentration of the stars; (iii) method of addition of the components; and (iv) end-linking reaction.[17]

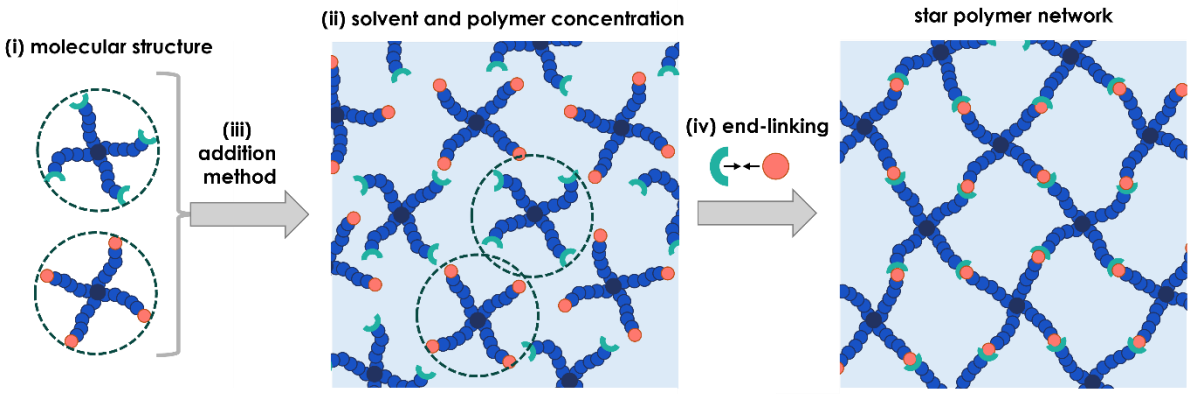

Figure 1. 4: Key factors in the design and synthesis of star polymer networks are the molecular structure of the stars **(i)**, the choice of solvent and polymer concentration **(ii)**, the addition method **(iii)** and the final end-linking chemistry **(iv)**.[17]

(i) The molecular structure comprises structural characteristics like the primary structure of each arm, end group structure, number of arms, and molecular weight. The number of arms must be greater than three and is usually limited to three, four and eight, with four being the most commonly used. The number of arms can affect both the mechanical properties and the network topology. The molecular weight significantly influences the mechanics but also affects the solubility and structure in the pregel solution (see (ii)). The end group structure determines the kind of possible end-linking reaction and influences the solubility of the star polymers. The primary structure, i.e. the type of polymer, determines the nature of the resulting network and its properties (biological and chemical stability, biocompatibility, melting point, glass transition temperature, ...). Of course, the type of polymer also influences the behavior in solution and the choice of solvent and thus the gelation process.[17]

(ii) To ensure a homogeneous mixture of the prepolymers, a common good solvent for both reaction partners should be used. The concentration of the star polymers in the pregel solution affects the homogeneity of the final network; the higher the concentration, the less inhomogeneity is observed. An important parameter that should be considered for the synthesis is the overlap concentration c^* (see also **Section 1.5.1**), as space filling is only achieved at concentrations that are at or above the overlap concentration.[17,28]

(iii) In most cases all components are mixed at a stochiometric ratio and end-linked either spontaneously or by an external stimulus.[17]

(iv) The end-linking process is the most important step in the preparation of a star polymer network. To synthesize a model network, the efficiency of the reaction, i.e. the conversion, should be as high as possible. However, the rate of the reaction should be adjustable or not too high in order to avoid spatial inhomogeneities in the network resulting from frozen concentration fluctuations. Additional requirements can be imposed on the process if the networks are produced for special applications, e.g. in the biological/biomedical field. Here, harsh conditions and toxic additives or byproducts have to be omitted.[17]

As already mentioned, the end-linking process plays a decisive role in avoiding primary loops and in preparing quite homogeneous model networks. A publication by Sakai and coworkers[20] on star polymer networks based on the hetero-complementary end-linking of t-PEG made an important contribution to this in the late 2000s. Here, the end-linking reaction is a condensation reaction of amine-terminated t-PEG and NHS-glutarate-terminated t-PEG. Due to this polymer architecture and functionalization, no intramolecular reactions are possible and therefore no primary loop formation; only higher order loops can be formed by intermolecular reactions. The resulting networks are characterized by high homogeneity and enhanced mechanical properties. After the publication of this study, the number of related research articles increased 5–10-fold in the following years.[18,20,24,25,48] Moreover, the concept was not only used to prepare homopolymer networks, but was also transferred to amphiphilic star polymer networks.[27,39,49]

Next to the aforementioned condensation reaction also **click reactions** have been used for the preparation of model networks. In general click chemistry describes a reaction with the following features: (i) quantitative reaction conversion; (ii) rapid reaction with high thermodynamic driving force; (iii) no byproducts or at least inoffensive byproducts; (iv) stereospecific; (v) selective reaction without side reactions; (vi) functional group tolerance; (vii) mild reaction conditions; (viii) broad applicability; (ix) readily available starting materials; (x) no solvent or non-hazardous solvent; and (xi) minimal synthetic work-up. Exemplary click reactions are Cu^{I}-catalyzed azide-alkyne cycloaddition, Diels–Alder cycloaddition, thiol-ene reaction, and azide-nitrile cycloaddition.[50–52]

The concept of Click Chemistry was developed to "*harness the power of molecular assembly for the widest possible range of applications*".[53] It was first articulated by Sharpless, Kolb, and Finn in a publication in 2001.[50] In 2022, the Nobel Prize in Chemistry was awarded jointly to

Carolyn R. Bertozzi, Morten Meldal and K. Barry Sharpless "*for the development of click chemistry and bioorthogonal chemistry*".[54] In polymer science, click chemistry offers a new way for post polymerization functionalization by incorporation of clickable groups at the chain ends or in the chain backbone. However, the concept can also be applied to the end-linking process of suitable prepolymers in order to build homopolymer networks as well as amphiphilic polymer (co-)networks.[17,37,38,43,51]

This section has provided a brief insight into the variety of synthesis paths to model networks with a controlled structure, especially those based on star polymers. To reduce or eliminate primary loops, hetero-complementary crosslinking is advantageous, which only allows intermolecular reactions, but no intramolecular reactions. This avoids a significant amount of inhomogeneities directly by a suitable choice of the starting material and crosslinking strategy. Due to the controlled and near-ideal structure of model networks, they can be used to study basic physical principles and structure-property relationships as well as the influence of external environmental conditions.

1.5. Characterization Methods

1.5.1. Viscometry

Viscometry is a classical technique in polymer science and polymer characterization. It takes advantage of a change in the viscosity of a dilute polymer solution in comparison to the pure solvent. This effect depends on both the concentration and the molar mass of the polymer.[55–57]

Three basic concentration regimes can be distinguished (see **Figure 1. 5**) based on the polymer concentration, c, or polymer volume fraction, ϕ. The dilute regime **(a)** at low polymer concentration, in which the polymers do not interact or overlap and are thus isolated from each other. If the concentration increases, space filling is obtained at a certain critical concentration, this is the so-called overlap concentration c^* **(b)**. At this concentration the polymer chains start to overlap. Above the overlap concentration **(c)**, the semi-dilute regime is reached in which the chains overlap and may even entangle. At even higher concentrations, a second critical concentration is reached (c^{**}), above which concentrated solutions are found.[23,57–60]

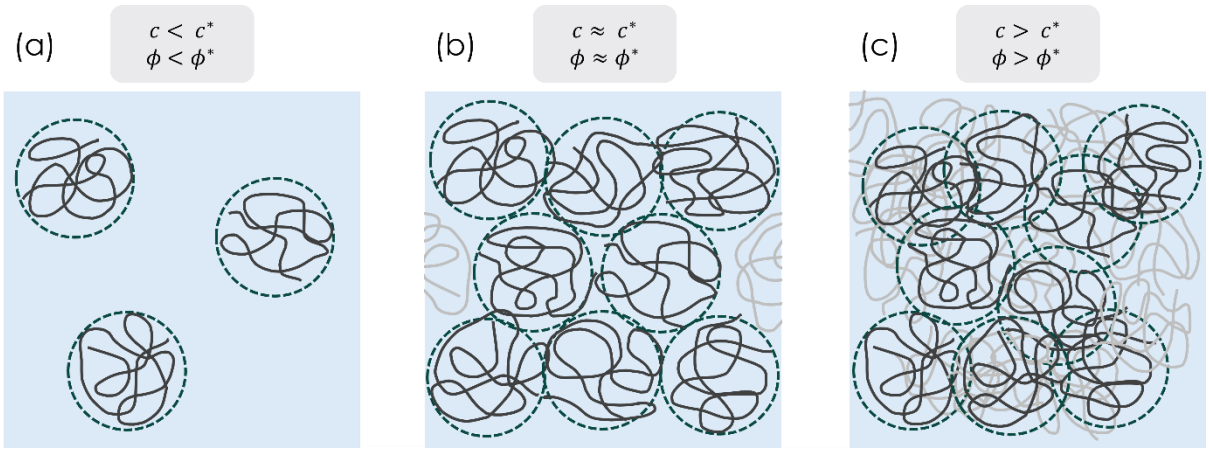

Figure 1. 5: Schematic representation of different concentration regimes below (**a**: dilute), at (**b**) and above (**c**: semi-dilute) the overlap concentration c^*.[23,59,60]

The viscosity increase of a solvent upon addition of a polymer can also be quantified by the intrinsic viscosity $[\eta]$, also known as the Staudinger index, which is a measure of the size and expansion, i.e. the volume, of the polymer in solution. This quantity can be determined using viscosity measurements and is inversely proportional to the overlap concentration outlined in **Figure 1. 5b**.[55–57]

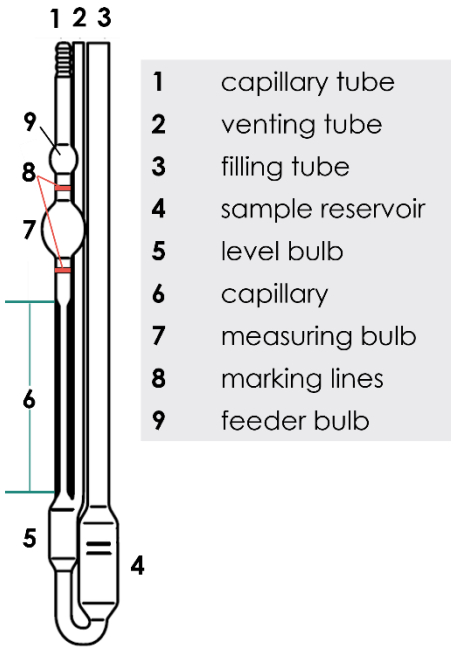

Scheme 1. 1: Ubbelohde viscometer.[61]

For this purpose, an Ubbelohde capillary viscometer (see **Scheme 1. 1**) is used to measure the time required for the solvent and a series of diluted polymer solutions far below the overlap concentration to flow through the capillary at constant temperature. The time measurement is started when the meniscus of the liquid passes the upper marking line and stopped when it reaches the lower marking line (red lines in **Scheme 1. 1**). The measurement is based on the principle of laminar flow and by assuming a similar density of solvent and (polymer) solution, the viscosity can be equated with the times required for the solvent, t_s, or solution, t, to flow through the capillary (see **Equation 1**).

This assumption is justified as very dilute polymer solutions are used. Upon use of Ubbelohde viscometers, attention must also be paid to the range of suitable viscosities for the respective capillary diameter. Corrections of the experimentally measured flow times can be necessary

(Hagenbach-Couette correction) due to additional pressure losses at the capillary ends, which are not considered in the theory.[55,56,58,59,61]

First of all, the specific viscosity, η_{sp}, is determined from the flow times of solvent and solution corresponding to the viscosity of solvent, η_s, and solution, η, as follows[9,56,59]

$$\eta_{\mathrm{sp}} = \frac{\eta - \eta_s}{\eta_s} \approx \frac{t - t_s}{t_s} \tag{1}$$

From this, the reduced viscosity, η_{red}, can be calculated with the respective polymer concentration c.[9,56,59]

$$\eta_{\mathrm{red}} = \frac{\eta_{\mathrm{sp}}}{c} \tag{2}$$

An extrapolation to zero concentration yields the intrinsic viscosity[9,56,59]

$$[\eta] = \lim_{c \to 0} \eta_{\mathrm{red}} \tag{3}$$

This extrapolation can be performed according to a linear equation (4a) by various empirical found extrapolation methods; among those the Schulz–Blaschke approach (4b) and the Huggins approach (4c) are established and well-known. The intrinsic viscosity is obtained from the intercept. The Schulz-Blaschke and Huggins constant, k_{SB} and k_{H}, can be interpreted as a measure of solvent quality, i.e. of the interactions of solvent and polymer molecules. The lower the constant, the better the solvent and the more expanded the polymer chain.[9,58,59,62]

	$\boldsymbol{y}$	=	$m \cdot \boldsymbol{x}$	$+ b$	(4a)
Schulz-Blaschke	$\boldsymbol{\eta_{red}}$	=	$[\eta] \cdot k_{\mathrm{SB}} \cdot \boldsymbol{\eta_{sp}}$	$+ [\eta]$	(4b)
Huggins	$\boldsymbol{\eta_{red}}$	=	$[\eta]^2 \cdot k_{\mathrm{H}} \cdot \boldsymbol{c}$	$+ [\eta]$	(4c)

It is important to keep in mind, that the intrinsic viscosity of branched polymers or star polymers is lower than the one of their linear counterparts of the same molar mass. This is due to their more compact architecture and smaller radius of gyration. This relation is quantified with the so-called contraction factor, g_η, which is defined as follows with the intrinsic viscosity of the branched (index b) and the corresponding linear polymer (index l):[57,63]

$$g_\eta = \frac{[\eta]_\mathrm{b}}{[\eta]_\mathrm{l}} \tag{5}$$

For four-armed star polymers in a good solvent, the contraction factor is found in literature to be g_η = 0.68–0.74.[57,63,64]

Finally, the overlap concentration can be calculated as the reciprocal of the intrinsic viscosity:[57,59,62]

$$c^* = \frac{1}{[\eta]} \tag{6}$$

The overlap concentration can also be determined according to **Equation 7**, which is based on a geometric argument. The polymers are regarded as spherical objects and the overlap concentration corresponds to the concentration of spheres at which space filling is reached. The volume of the spheres is calculated using the radius of gyration, R_g, as the radius of the sphere together with the weight average of the molar mass M_W, and the Avogadro constant N_A.

$$c^* = \frac{3M_\mathrm{W}}{4\pi N_\mathrm{A} R_\mathrm{g}^3} \tag{7}$$

$$\rho = \frac{R_\mathrm{g}}{R_\mathrm{H}} \tag{8}$$

The drawback of this method is that R_g is difficult to access experimentally and is therefore often derived from the hydrodynamic radius R_H according to **Equation 8**. The hydrodynamic radius is much easier to determine experimentally and can be received from dynamic light scattering (DLS), for example. Their ratio, ρ, is a constant for the respective polymer but depends on the polymer architecture and the solvent quality. However, the ratios found experimentally are often approximately 10-20% smaller than the theoretically calculated ones. This results in a relatively high error when using this method, as R_g enters the equation in the third power. In addition, this estimate usually represents the lower limit of the overlap concentration range, while the value determined from viscometry forms the upper limit. The overlap concentration indicates the threshold value at which space filling is reached and a space filling polymer network can be produced by crosslinking. Thus, it is reasonable to use the upper limit if homogeneous networks with a low defect fraction are desired.[28,57,65]

The intrinsic viscosity of polymers does furthermore characteristically depend on the molar mass. This relationship is expressed in the Kuhn-Mark-Houwink-Sakurada equation with the molecular specific constants K_η and a_η:[9,56,57,59,62]

$$[\eta] = K_\eta M^{a_\eta} \tag{9}$$

From the exponent a_η, which depends also on solvent quality, conclusions can be drawn about the geometry of the respective polymer. For flexible linear polymers in a theta-solvent a_η = 0.5 is obtained, whereas values of 0.7–0.8 are expected in a good solvent.[9,56,59]

1.5.2. Rheology

According to its greek origin ("*rheos*" = flow; "*logos*" = study of or understanding), rheology is the study of flow. An important aphorism in this context is "*panta rhei*", which means "everything flows". This phrase alludes to the fact that, depending on the time scale, every material exhibits a dualism between liquid and solid and that the appearance of the material therefore depends on the observation time. The flow characteristics of a material range between the two boundary cases of the ideal elastic solid and the ideal viscous liquid. Polymers exhibit both, solid-like and liquid-like material properties on experimental relevant timescales and are therefore termed viscoelastic.[66,67]

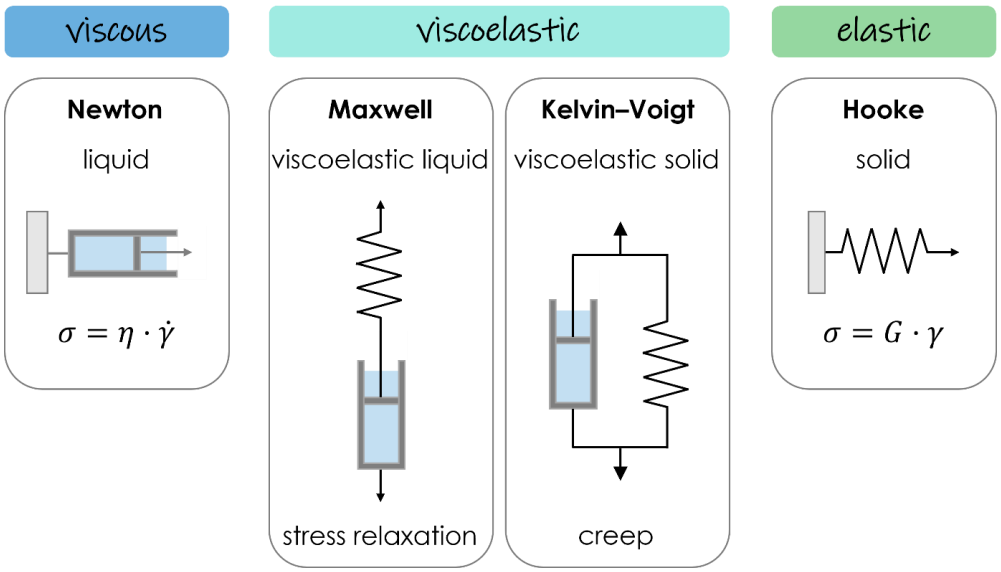

Figure 1. 6: Overview of the three basic cases of rheological behavior: pure viscous liquid, pure elastic solid and viscoelastic materials together with the respective model approaches and corresponding mechanical elements. The viscoelastic case can be further divided into viscoelastic liquids and viscoelastic solids.[9,66–68]

Figure 1. 6 provides an overview of the two boundary cases of an ideal elastic solid and ideal viscous liquid as well as the intermediate case of viscoelastic behavior together with the corresponding mathematical description, mechanical elements, and model approaches. The purely elastic case can be modeled by a spring and described by Hooke's law. Here, for the case of shear deformation, the stress, σ, is proportional to the strain, γ, with the proportionality constant, G, the shear modulus. In contrast, a purely viscous medium can be modeled by a dashpot and obeys Newton's law in which the stress is proportional to the strain rate, $\dot{\gamma}$, with the viscosity, η, serving as proportionality constant.[9,55,67,68]

The two basic mechanical elements spring and dashpot can also be combined linearly or in parallel to model the behavior of viscoelastic materials. The linear arrangement is referred to as Maxwell element and thus corresponds to the Maxwell model for viscoelastic fluids. It is well suited for modeling stress relaxation in such materials. The parallel arrangement of spring and dashpot, on the other hand, corresponds to the Kelvin-Voigt model for viscoelastic solids and is suitable for modeling creep processes.[9,55,66–68]

It is noteworthy, that for polymer solutions, deviations from the ideal Newtonian behavior like shear-thinning and shear-thickening can occur. In these cases, the viscosity is dependent on the shear rate and decreases (shear-thinning) or increases (shear-thickening) from a critical point with increasing shear rate. Other cases of non-Newtonian behavior are rheopexy and thixotropy, where the viscosity increases or decreases with time at a constant shear rate.[58,61,66–68]

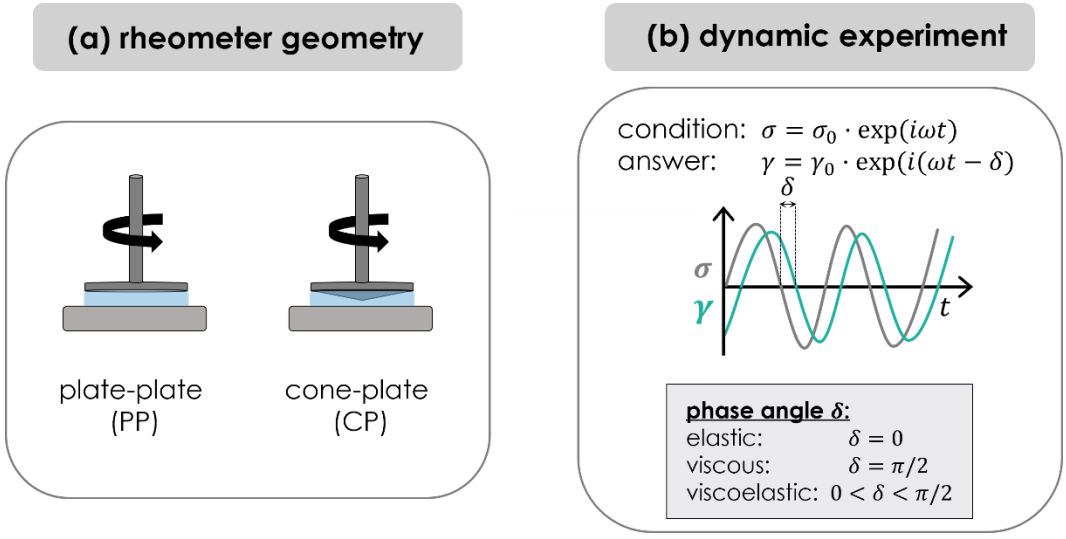

Figure 1. 7: (a) Schematic representation of the set-up for rheological measurements. The plate-plate geometry (PP) is usually chosen for polymer gels and melts, while the cone-plate geometry (CP) is used for polymer solutions. **(b)** Sketch of the applied sinusoidal shear stress and the measured time-dependent shear strain in a dynamic oscillatory shear rheology measurement. The phase angle reflects the elastic, viscous or viscoelastic nature of the material under investigation.[67]

The method of shear rheology is a versatile tool to probe the mechanical and flow properties of polymeric materials by means of stress relaxation, creep, and dynamic experiments. To perform a shear rheological experiment, the sample is placed between an upper and lower geometry. The lower geometry is most commonly an even plate and the upper one can be a plate (PP) or a cone (CP) (see **Figure 1. 7a**). The plate-plate geometry is commonly used for measurements on polymeric gels and the cone-plate geometry for the measurement of polymer solutions. The upper geometry is rotated by the motor of the rheometer and the resulting torque is measured, from which the elastic and viscous contributions to the rheological properties of the material can be derived.[55,66,67]

In case of a dynamic test, the upper geometry is rotated in an oscillating fashion (see **Figure 1. 7b**) and a sinusoidal stress is applied while the resulting time-dependent strain is measured. The phase angle between the applied state and the "answer" of the material, i.e. the measured strain, provides information about the type of rheological behavior (elastic, viscous, viscoelastic).[9,67]

The shear modulus, G, reflects the ratio of stress and strain. In case of the aforementioned dynamic experiment, it is obtained as a complex quantity (G^*) and can be divided in a real part, G', and an imaginary part, G'' according to the following equation.[9,55,62,67]

$$G^* = \frac{\sigma}{\gamma} = G' + iG'' \tag{10}$$

The real part is referred to as the storage modulus and the imaginary part as the loss modulus. The storage modulus represents the elastic contributions, i.e. the energy that is elastically stored upon deformation. The loss modulus, on the other hand, reflects the viscous contributions, i.e. the energy that is dissipated to heat and thus lost. The ratio of loss and storage modulus, $G''/G' = \tan\delta$, is referred to as the loss tangent and is a measure of the elastic and viscous components of the viscoelastic behavior of a material. Values lower than one refer to viscoelastic solids, while values greater than one indicate viscoelastic liquids.[55,62,66,67]

Applying the Maxwell model to such oscillatory shear experiments results in the following expressions for the angular frequency-dependent storage, $G'(\omega)$, and loss modulus, $G''(\omega)$, with the angular frequency, ω, the plateau modulus, G_p, at very high frequencies (see **Figure 1. 8a**), and the terminal relaxation time τ_0.[9,66,67]

$$G'(\omega) = G_p \frac{\omega^2 \tau_0^2}{1 + \omega^2 \tau_0^2} \tag{11a}$$

$$G''(\omega) = G_p \frac{\omega \tau_0}{1 + \omega^2 \tau_0^2} \tag{11b}$$

At low frequencies, the numerators of both equations dominate and a characteristic power-law scaling of $G' \sim \omega^2$ and $G'' \sim \omega^1$ is observed. At high frequencies, the storage modulus gets frequency independent, whereas the loss modulus shows a power law scaling of $G'' \sim \omega^{-1}$ (see **Figure 1. 8a**). From a molecular point of view, the polymeric system has no time to rearrange at short time scales, i.e. at high frequencies, and the elastic properties prevail. Therefore, the storage modulus dominates and converges towards a plateau. On long time scales, i.e. at low frequencies, the polymer chains can slip past each other and relax, the material flows. Here, the viscous behavior dominates and therefore the loss modulus. The time it takes for a polymer to move a distance equal to its own size is called the terminal relaxation time, τ_0, which is located at the intersection point of G' and G''.[9,67]

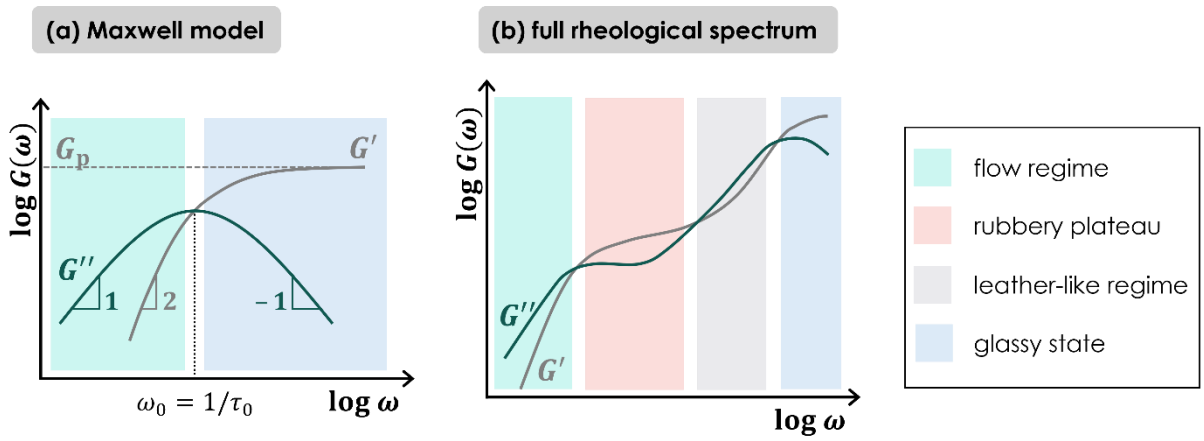

Figure 1. 8: Double-logarithmic representation of the frequency dependent shear-modulus $G(\omega)$ according to the Maxwell model **(a)** and in a full rheological spectrum covering a broad frequency range **(b)**.[62,66–68]

The relaxation time further connects the quantities of shear modulus and viscosity as follows:

$$\eta = G \cdot \tau \tag{12}$$

The viscosity represents how hard it is to rearrange polymeric building blocks, i.e. to flow, and is linearly connected to the shear modulus, which reflects how much energy can be stored initially in a material, and the relaxation time, which represents the time it takes to relax the stored energy.[62,67]

So far, only one relaxation time and thus only one relaxation mode has been discussed. However, polymers have a variety of relaxation modes (relaxation times) and mechanisms on different time and length scales, which is also due to their polydisperse nature. Depending on the time or frequency scale, polymeric materials exhibit a broad rheological spectrum, as depicted in **Figure 1. 8b**. Such a rheological spectrum can basically be divided into four sections, which are from high to low frequency: glassy state, leather-like regime, rubbery elastic plateau, and terminal flow regime. At the glassy state, the polymer behaves like an energy elastic solid and on these very short time scales (very high frequencies), no motion is possible at all. Upon entering the leather-like regime, relaxation modes are sequentially activated, and sequences of monomers can be displaced over distances equal to their own size. Here, the polymer can be described as a viscoelastic solid using the Kelvin-Voigt model. If only short polymer chains without entanglements or chemical crosslinks are considered, the leather-like regime is directly followed by the terminal flow regime. Here, the Maxwell model applies and the polymer resembles a viscoelastic liquid. If, on the other hand, long entangled chains or chemically crosslinked polymers are probed, a rubber-elastic plateau follows at the end of the leather-like regime. Entanglements or crosslinks hinder the relaxation of the polymer chains by trapping them and the deformation energy cannot be relaxed but is stored instead. The trapping by entanglements can be overcome at long timescales by the reptation mechanism leading to terminal viscous flow. In covalently crosslinked polymer networks, however, there is no such terminal flow regime due to the permanent linkage of the chains.[9,66–68]

Such a full spectrum spans over a wide range of frequencies (up to 12 decades) and is only accessible by use of the time–temperature superposition principle. This principle allows the superposition of viscoelastic data sets measured at different temperatures by shifting along the frequency (or time) axis to create the full spectrum. Equating temperature and time is possible because the movement of the polymer chains, i.e. the relaxation modes, are thermally activated and the activation energy is overcome more frequently either at higher temperatures or with a longer observation time and vice versa. Therefore, whether and to what extent the individual sections of the rheological spectrum occur depends not only on the observation time but also on the temperature and, above all, on the polymer system itself.[9,66–68]

Also theoretical approaches have been developed to model the rheological behavior of polymer networks upon deformation. The plateau modulus of the rubbery elastic plateau can be estimated by use of the affine and the phantom network model, which directly correlate the plateau modulus to the number density of elastically active network strands (ν_{eff}).[4,55,62]

The affine network model assumes that the deformation is affine, i.e. that the relative deformation of each network strand is the same as the macroscopic relative deformation of the whole network. The network modulus can be calculated as follows with the Boltzmann constant k_B, the temperature T, the network density ρ, the number-average molar mass of a network strand M_{el}, and the gas constant R.[4,23,55,62]

$$G_{af} = \nu_{eff} \cdot k_B T = \frac{\rho RT}{M_{el}} \tag{13}$$

Instead, the phantom model assumes that the strands of the network can fluctuate around their average position. These fluctuations reduce the conformational constraints and thus the net free energy of the network compared to the affine model. The model also takes into account the branching functionality, f. Therefore, for four-armed star polymers, the affine model modulus is twice as high as the modulus of the phantom network model. However, both models converge for high branch functionalities.[4,23,55,62]

$$G_{ph} = \left(1 - \frac{2}{f}\right) \nu_{eff} \cdot k_B T = \left(1 - \frac{2}{f}\right) \frac{\rho RT}{M_{el}} \tag{14}$$

As already mentioned in **Section 1.2**, even model networks are not necessarily ideal or perfect networks and possess structural inhomogeneities or even defects. The presence of loops and dangling chains significantly reduces the number of elastically active chains and in turn the plateau modulus. Therefore, the theoretically expected values assuming an ideal network are often significantly higher than those determined experimentally.[55,62]

1.5.3. Light Scattering

Light scattering is used as a versatile technique in polymer chemistry to determine either molecular properties such as the weight-average molar mass (M_w) and the radius of gyration (R_g) with static light scattering or molecular dynamics such as the diffusion coefficient (D) with dynamic light scattering. Such measurements are often carried out on dilute polymer solutions in order to avoid interactions between the particles that affect the measurement result.[56,65]

The setup for a typical light scattering experiment is shown in **Figure 1. 9**. The polymer solution or sample of interest is filled into a quartz glass cuvette and the prepared cuvette is placed in a temperature-controlled toluene bath. During sample preparation, the precleaned cuvettes are rinsed with hot acetone and the solutions are filtered to remove dust particles. The incident laser

beam is scattered by the sample particles and the scattering intensity is recorded by a detector in the scattering plane. The detector can also be moved around the setup using a goniometer to measure at different scattering angles, θ. The detector is connected to a computer setup with a suitable software for data processing and analysis.[59,65]

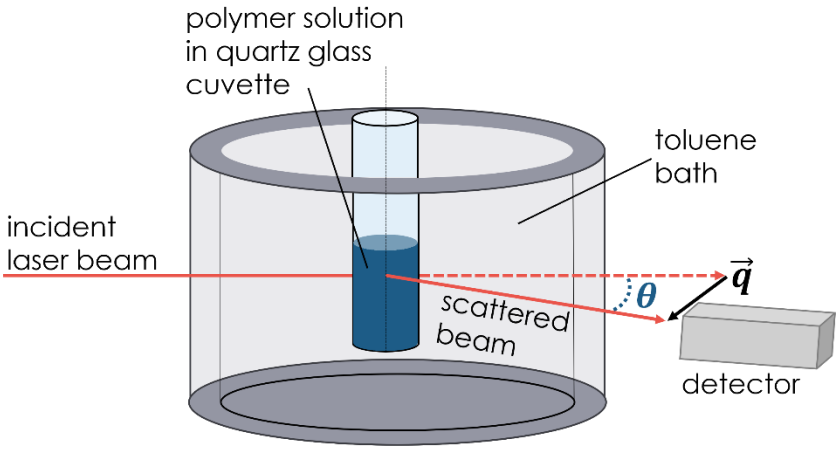

Figure 1. 9: Schematic representation of the setup for a light scattering experiment. The incident laser beam is scattered by the sample solution in the quartz glass cuvette, which in turn is located in a temperature-controlled toluene bath. The scattering intensity is recorded by a detector at specific scattering angles (θ).[59]

The scattering of light is based on the interaction of light as an electromagnetic wave with matter. However, only the electric field is considered here. The electric field, E_i, of the incident light wave, which propagates in x-direction, is given by **Equation 15** with the amplitude, E_0, the angular frequency, ω, and the absolute value of the wave vector, k.[9,56,65,67]

$$E_\mathrm{i} = E_0 \cdot \sin(\omega t - kx) \qquad (15)$$

If a molecule with polarizability α is located in this oscillating electric field, a displacement polarization takes place in which the positive atomic nuclei are deflected against the negative electrons and a Hertzian dipole, μ_ind, is induced. This dipole oscillates at the same frequency as the electric field according to $\mu_\mathrm{ind} = \alpha \cdot E_\mathrm{i}$. The isotropic radiation of this dipole has the same wavelength as the incident light; the scattering processes is elastic.[9,56,65,67]

The scattering vector $\vec{q}$ is an important quantity in light scattering and refers to the optical path difference of incident and scattered laser beam (see also **Figure 1. 9**). Its absolute value, q, is denoted in **Equation 16** with the wavelength of the laser light in vacuum, λ_0, the refractive index of the solvent, n, and the scattering angle θ.[55,56,59,65,69]

$$|\vec{q}| = q = \frac{4\pi n}{\lambda_0} \cdot \sin\left(\frac{\theta}{2}\right) \tag{16}$$

It is important to note that light scattering is only possible if there is sufficient scattering contrast. This contrast results from the relative differences of the refractive indices, n, of the sample and its environment. These differences are generated by density and concentration fluctuations due to thermal movement of the scattering particles.[67]

The detector measures the intensity of the scattered light, I_s, at a certain scattering angle in the scattering plane. The ratio of scattered light intensity and the intensity of the incident laser light depends on the polarizability of the scattering particle, α, and the polarization of the incident light, which is reflected in the angle ϑ. In most cases vertical polarized light is used ($\vartheta = 90°$ and $\sin^2(\vartheta) = 1$). The term ε_0 represents the vacuum dielectric permittivity.[56,59,69]

$$\frac{I_s}{I_i} = \frac{\pi^2\alpha^2}{\varepsilon_0^2\lambda_0^4} \cdot \frac{1}{r^2} \cdot \sin^2(\vartheta) \tag{17}$$

For dilute solutions of small scattering particles ($< \lambda/20$) with only one scattering center per particle, the scattering intensity is independent of the scattering angle. For larger particles, however, intraparticle interference must be taken into account due to multiple scattering centers per particle. The particle form factor, $P(q)$, reflects this interference depending on size and shape of the scattering particle. [9,55,56,59,65,67,69]

$$P(q) = \frac{scattered\ intensity\ at\ scattering\ angle\ \theta}{scattered\ intensity\ without\ interference\ (at\ \theta = 0°)} \tag{18}$$

Static light scattering is one of the few absolute methods to determine the molar mass of polymers in solution. In addition, it can be utilized to determine structural characteristics like the radius of gyration and the second virial coefficient, which gives evidence of the solvent quality and polymer-solvent interactions.[56,65]

For this purpose, the time-averaged scattering intensity is measured as a function of the scattering angle at different concentrations. The aforementioned molecular parameters can then be received from a so-called Zimm-plot according to the Zimm equation (**Equation 19a**). This form of the equation already accounts for scattering from large particles and possible polydispersity effects. The required Rayleigh ratio, R_θ, can be calculated from the scattering intensities of solvent, solution and standard (most commonly toluene) as well as the absolute Rayleigh

ratio of the standard, RR_{standard}, if all intensities are measured using the same experimental setup (see **Equation 19c**). The value of the absolute Rayleigh ratio can be found in literature. The optical constant K (see **Equation 19b**) contains all setup and solvent dependent parameters like the refractive index of the solvent, n, the wavelength of the incident laser light in vacuum, λ_0, the Avogadro constant, N_A, and the refractive index increment, $\frac{\partial n}{\partial c}$.[9,56,65,67]

$$\frac{Kc}{R_\theta} = \frac{1}{M_\text{w}} \cdot \left(1 + \frac{1}{3} q^2 \langle R_\text{g}^2 \rangle_\text{z}\right) + 2A_2 c + \ldots \tag{19a}$$

$$K = \frac{4\pi^2 n^2}{\lambda_0^4 N_\text{A}} \cdot \left(\frac{\partial n}{\partial c}\right)^2 \tag{19b}$$

$$R_\theta = \frac{I_\text{solution} - I_\text{solvent}}{I_\text{standard}} \cdot RR_\text{standard} \tag{19c}$$

To perform an analysis according to the Zimm plot, the data $\frac{Kc}{R_\theta}$ are plotted as a function of $q^2 + k'c$ and extrapolated towards zero scattering angle and zero concentration. The factor k' is a constant, which is arbitrarily chosen to enhance the graphical analysis by spreading the data points equally. The intercept of both extrapolations gives the weight-average molar mass, M_w. From the slope of the extrapolation towards zero scattering angle, the second virial coefficient, A_2, is obtained. Whereas the z-average mean square radius of gyration, $\langle R_\text{g}^2 \rangle_\text{z}$, is received from the slope of the extrapolation towards zero concentration.[9,65,67]

The method of **dynamic light scattering** (DLS), on the other hand, is used to determine the dynamics of scattering particles in solution and thus their diffusion coefficient. For this purpose, the time-dependent fluctuation of the scattering intensity is recorded (see **Figure 1. 10a**), which is caused by Brownian particle motion of the scattering particles (due to thermal density fluctuations of the solvent). The intensity autocorrelation function, $g^{(2)}(q,\tau)$, is introduced to quantitatively analyze these time- and angle-dependent intensity fluctuations. In an autocorrelation, the signal at time t is compared with the signal at time $t + \tau$ (numerator of **Equation 20**) and the degree of self-similarity is determined. The greater the shift in time, i.e. the higher τ, the lower the self-similarity and thus the correlation of the signal. The normalized function shows an exponential decay from 2 to 1 (see **Figure 1. 10b**).[55,57,65,67]

$$g^{(2)}(q,\tau) = \frac{\langle I(q,t) \cdot I(q,t+\tau) \rangle}{\langle I(q,t) \rangle^2} \tag{20}$$

The amplitude autocorrelation function, $g^{(1)}(q,\tau)$, can be obtained from the intensity autocorrelation function using the Siegert relation.[57,65,69]

$$g^{(1)}(q,\tau) = \sqrt{g^{(2)}(q,\tau) - 1} \tag{21}$$

For a more simplified analysis, the amplitude correlation function is commonly plotted in a semi-logarithmic scale as a function of the lag time τ (see **Figure 1. 10c**), with the amplitude, A, and the diffusion coefficient, D. [65,67,69]

$$g^{(1)}(q,\tau) = A \cdot \exp\left(-\frac{\tau}{\tau_R}\right) = A \cdot \exp(-Dq^2\tau) \tag{22}$$

The characteristic relaxation time τ_R marks the decay of the function to $1/e$ of its initial value. If this time is determined for different scattering angles (different q^2), the diffusion coefficient, D, is obtained as the slope of a linear fit to the data according to **Figure 1. 10d**. [65,67]

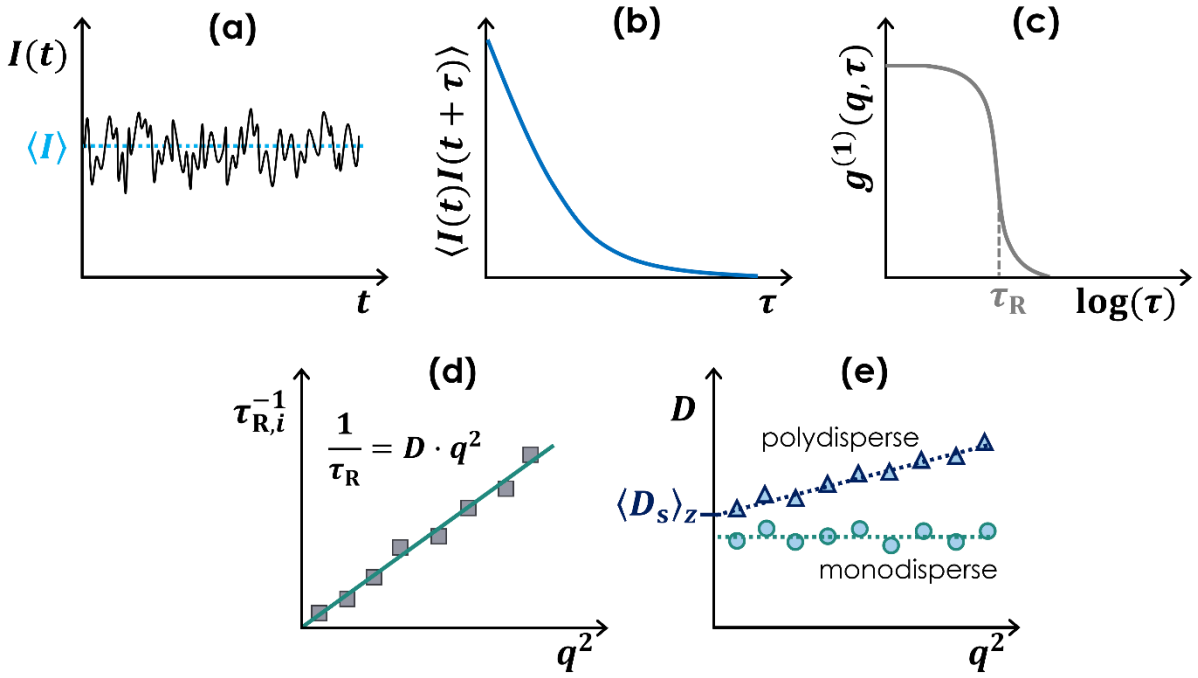

Figure 1. 10: Data acquisition, processing, and evaluation in dynamic light scattering. **(a)** Recorded time-dependent intensity fluctuations. **(b)** Intensity autocorrelation function as a function of correlation time, τ. **(c)** Semi-logarithmic plot of the amplitude correlation function derived from the intensity correlation function. The characteristic time, τ_R, corresponds to the decay of the amplitude correlation function to $1/e$ of its initial value. **(d)** If the characteristic time is plotted for different scattering angles, i.e. as a function of the scattering vector q, the diffusion coefficient, D, is obtained as the slope of a linear fit to the data points. **(e)** In case of monodisperse samples, an angle-independent diffusion coefficient is obtained. For polydisperse samples, a linear increase of the diffusion coefficient with increasing scattering vector can be observed. The "true" average diffusion coefficient, $\langle D_s \rangle_z$ is determined by extrapolating the data towards zero scattering vector.[65,67]

For the case of polydisperse samples containing several diffusing and scattering species, additional exponential terms must be added to **Equation 22**. Every species "i" then has a corresponding characteristic relaxation time $\tau_{R,i}$ and diffusion coefficient D_i.[65,67,69]

The received diffusion coefficient is only angle-independent for monodisperse spheres without interactions (see **Figure 1. 10e**). However, the case of no interactions is only present at very high dilution. The diffusion coefficient then corresponds to the self-diffusion coefficient. In contrast, in more concentrated solutions, interactions between the scattering particles can strongly influence their mobility. For polydisperse samples, however, an increase of the diffusion coefficient with scattering angle can be observed (see **Figure 1. 10e**). To receive the self-diffusion for this type of sample, an extrapolation towards zero scattering vector q, is carried out. This results in the z-average of the self-diffusion coefficient $\langle D_s \rangle_z$.[65,69]

Finally, from the self-diffusion coefficient, D_s, the hydrodynamic radius, R_H, can be determined according to the Stokes–Einstein equation with the temperature, T, and the solvent viscosity, η_s. For polydisperse samples, the hydrodynamic radius also corresponds to a z-average value $\langle R_H \rangle_z$.[55,57,62,65,67]

$$R_H = \frac{k_B T}{f} = \frac{k_B T}{6\pi\eta_s D_s} \tag{23}$$

The hydrodynamic radius reflects the radius of an equivalent sphere that diffuses ideally and experiences the same friction, f, upon diffusion as the scattering particle. Thus, the hydrodynamic radius does not correspond to the precise hydrodynamic radius of the scattering particle (unless it is a monodisperse sphere without interaction).[57,65,67]

Up to this point, light scattering from (polymer) solutions was considered. However, it is also possible to investigate **polymer networks** or **gels** using light scattering and thereby characterize their structural characteristics. If compared to a corresponding polymer solution at the same concentration, the scattering intensity of a gel is higher. This is due to the fact that in addition to dynamic thermal concentration fluctuations, δc_F, which are caused by Brownian molecular motion (fluctuation of the polymer chains between the crosslinking points), frozen concentration fluctuations, δc_C, due to an inhomogeneous distribution of crosslinking points also contribute to the scattering signal. How these contributions constitute the total concentration fluctuation, δc, is illustrated in **Figure 1. 11**.[70,71]

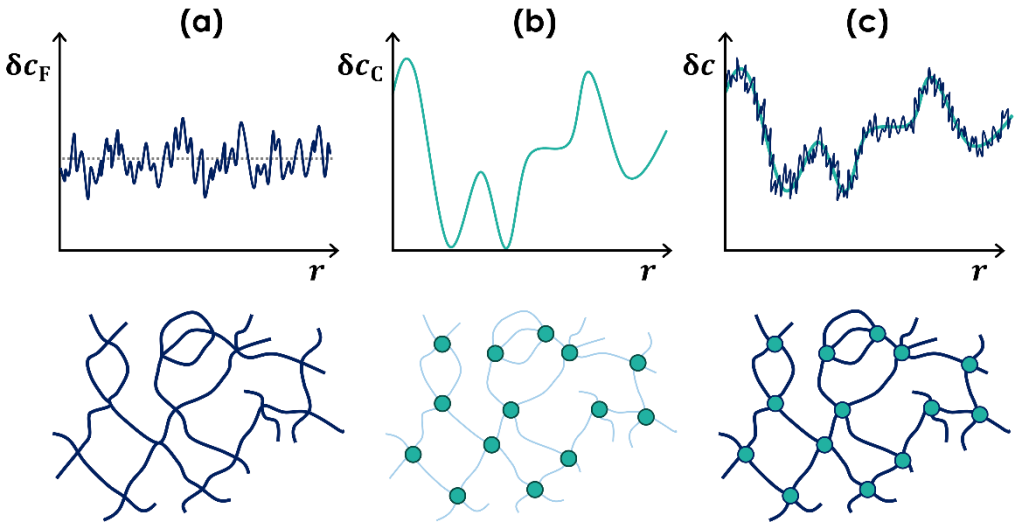

Figure 1. 11: Contributions to the position-dependent scattering of gels due to concentration fluctuations, which are composed of thermal fluctuations **(a)** and frozen inhomogeneities **(b)**. Their superposition constitutes the resulting overall concentration fluctuation **(c)**.[67,70,71]

Thus, the overall concentration fluctuation is a superposition of both types of concentration fluctuations and in analogy to the frozen concentration fluctuations dependent on the position, r, in the gel.[67,70,71]

$$\delta c(r) = \delta c_F(r) + \delta c_C(r) \tag{24}$$

Accordingly, the total position-dependent scattering intensity or Rayleigh ratio of the gel, R_{gel}, in static light scattering is composed of a fluid scattering contribution, R_F, arising from thermal concentration fluctuations, and excess scattering, R_{Ex}, resulting from frozen concentration fluctuations. The fluid scattering intensity thereby corresponds in good approximation to the scattering intensity of the uncrosslinked polymer solution of the same concentration. In dynamic light scattering, the scattering intensity of the gel, $I_{gel}(t)$, is analogously composed of the time-dependent fluctuating intensity, $I_F(t)$, due to the diffusive motion of polymer chain segments, and a constant scattering contribution, I_C, due to static inhomogeneities.[67,70,71]

$$R_{gel} = R_F + R_{Ex} \tag{25a}$$

$$I_{gel}(t) = I_F(t) + I_C \tag{25b}$$

Because of the position-dependent scattering intensity mentioned above, polymer gels are non-ergodic systems. This means that the time average of the scattering intensity is unequal to the ensemble average. Therefore, light scattering measurements on gels must be carried out at

several different positions in order to obtain adequate statistics. This is realized in the experimental setup by use of a rotating cuvette. In ergodic systems, e.g. dilute polymer solutions, on the other hand, the time average and ensemble average are identical.[67,70,71]

Commonly static and dynamic light scattering are measured simultaneously on gels. From the static measurements and the obtained excess scattering, the static correlation length Ξ can be calculated, which is a measure of the average distance over which spatial inhomogeneities (frozen concentration fluctuations) occur. From the dynamic measurement, the dynamic correlation length, ξ_H, is received, which is a measure of the distance of concentration correlation. In ideal polymer networks the dynamic correlation length can be regarded as the mesh size of the network, i.e. the distance between two crosslinking points.[67,70,71]

1.6. References

[1] C. K. Varnava, C. S. Patrickios, *Polymer* **2021**, *215*, 123322.

[2] "Hermann Staudinger", can be found under https://uni-freiburg.de/universitaet/universitaet-im-ueberblick/herausragende-leistungen/nobelpreis/hermann-staudinger/, **2023**.

[3] IUPAC: INTERNATIONAL UNION OF PURE AND APPLIED CHEMISTRY, "WHAT ARE POLYMERS?", can be found under https://iupac.org/polymer-edu/what-are-polymers/, **2023**.

[4] Y. Gu, J. Zhao, J. A. Johnson, *Angewandte Chemie (International ed. in English)* **2020**, *59*, 5022.

[5] W. H. Carothers, *Chem. Rev.* **1931**, *8*, 353.

[6] Nobel Prize Outreach AB, "The Nobel Prize in Chemistry 1953", can be found under https://www.nobelprize.org/prizes/chemistry/1953/summary/, **2023**.

[7] V. Gold (Ed.) *The IUPAC Compendium of Chemical Terminology*, International Union of Pure and Applied Chemistry (IUPAC), Research Triangle Park, NC, **2019**.

[8] a) H. Namazi, *BioImpacts: BI* **2017**, *7*, 73; b) *Encyclopedia of physical science and technology*, Academic Press, San Diego, **2002**; c) K. Naka in *Encyclopedia of polymeric nanomaterials. 3.V* (Eds.: S. e. Kobayashi, K. e. Mullen), Springer, Berlin, **2015**, pp. 1295–1300.

[9] M. D. Lechner, K. Gehrke, E. H. Nordmeier, *Makromolekulare Chemie. Ein Lehrbuch für Chemiker, Physiker, Materialwissenschaftler und Verfahrenstechniker*, Springer Berlin Heidelberg; Imprint: Springer Spektrum, Berlin, Heidelberg, **2014**.

[10] P. J. Flory, *Faraday Discuss. Chem. Soc.* **1974**, *57*, 7.

[11] M. Chelu, A. M. Musuc, *Gels (Basel, Switzerland)* **2023**, *9*.

[12] F. Horkay, J. F. Douglas in *ACS Symposium Series* (Eds.: F. Horkay, J. F. Douglas, E. Del Gado), American Chemical Society, Washington, DC, **2018**, pp. 1–13.

[13] C. S. Patrickios, *Macromolecular Symposia* **2010**, *291-292*, 1.

[14] R. Staňo, P. Košovan, A. Tagliabue, C. Holm, *Macromolecules* **2021**, *54*, 4769.

[15] Y. Gu, J. Zhao, J. A. Johnson, *Trends in Chemistry* **2019**, *1*, 318.

[16] S. Seiffert, *Polym. Chem.* **2017**, *8*, 4472.

[17] S. Nakagawa, N. Yoshie, *Polym. Chem.* **2022**, *13*, 2074.

[18] M. Rikkou-Kalourkoti, C. S. Patrickios, T. K. Georgiou in *Polymer Science: A Comprehensive Reference*, Elsevier, **2012**, pp. 293–308.

[19] G. Hild, *Progress in Polymer Science* **1998**, *23*, 1019.

[20] T. Sakai, T. Matsunaga, Y. Yamamoto, C. Ito, R. Yoshida, S. Suzuki, N. Sasaki, M. Shibayama, U. Chung, *Macromolecules* **2008**, *41*, 5379.

[21] T. Sakai, Y. Akagi, T. Matsunaga, M. Kurakazu, U. Chung, M. Shibayama, *Macromolecular rapid communications* **2010**, *31*, 1954.

[22] Y. Akagi, T. Matsunaga, M. Shibayama, U. Chung, T. Sakai, *Macromolecules* **2010**, *43*, 488.

[23] T. Sakai, *Physics of polymer gels*, Wiley- VCH Verlag, Weinheim, **2020**.

[24] M. Shibayama, X. Li, T. Sakai, *Ind. Eng. Chem. Res.* **2018**, *57*, 1121.

[25] M. Shibayama, X. Li, T. Sakai, *Colloid Polym Sci* **2019**, *297*, 1.

[26] Y. Akagi, J. P. Gong, U. Chung, T. Sakai, *Macromolecules* **2013**, *46*, 1035.

[27] D. E. Apostolides, C. S. Patrickios, T. Sakai, M. Guerre, G. Lopez, B. Améduri, V. Ladmiral, M. Simon, M. Gradzielski, D. Clemens et al., *Macromolecules* **2018**, *51*, 2476.

[28] C. Bunk, L. Löser, N. Fribiczer, H. Komber, L. Jakisch, R. Scholz, B. Voit, S. Seiffert, K. Saalwächter, M. Lang et al., *Macromolecules* **2022**, *55*, 6573.

[29] a) K. Nishinari in *Gels: Structures, Properties, and Functions*, Springer Berlin Heidelberg, Berlin, Heidelberg, **2009**, pp. 87–94; b) K. Almdal, J. Dyre, S. Hvidt, O. Kramer, *Polymer Gels and Networks* **1993**, *1*, 5.

[30] K. Kajiwara, Y. Osada, *Gels Handbook, Four-Volume Set*, Elsevier Science, Burlington, **2000**.

[31] Y. OSADA in *Gels Handbook*, Elsevier, **2001**, pp. 13–25.

[32] A. K. Nayak, B. Das in *Polymeric Gels*, Elsevier, **2018**, pp. 3–27.

[33] J. Jagur-Grodzinski, *Polymers for Advanced Techs* **2010**, *21*, 27.

[34] a) M. A. Kuzina, D. D. Kartsev, A. V. Stratonovich, P. A. Levkin, *Adv Funct Materials* **2023**, *33*; b) A. YAMAUCHI in *Gels Handbook*, Elsevier, **2001**, pp. 4–12; c) N. M. Sangeetha, U. Maitra, *Chemical Society reviews* **2005**, *34*, 821.

[35] a) M. WEBER, R. STADLER, *Polymer* **1988**, *29*, 1064; b) M. WEBER, R. STADLER, *Polymer* **1988**, *29*, 1071.

[36] D. Chen, J. P. Kennedy, A. J. Allen, *Journal of Macromolecular Science: Part A - Chemistry* **1988**, *25*, 389.

[37] C. S. Patrickios, K. Matyjaszewski, *Polymer International* **2021**, *70*, 10.

[38] L. Mespouille, J. L. Hedrick, P. Dubois, *Soft Matter* **2009**, *5*, 4878.

[39] C. S. Patrickios (Ed.) *Polymer Chemistry Series*, Royal Society of Chemistry, Cambridge, **2020**.

[40] G. Erdodi, J. P. Kennedy, *Progress in Polymer Science* **2006**, *31*, 1.

[41] C. S. Patrickios, T. K. Georgiou, *Current Opinion in Colloid & Interface Science* **2003**, *8*, 76.

[42] A. Dabbaghi, A. Ramazani, N. Farshchi, A. Rezaei, A. Bodaghi, S. Rezayati, *Journal of Industrial and Engineering Chemistry* **2021**, *101*, 307.

[43] F. Perin, A. Motta, D. Maniglio, *Materials science & engineering. C, Materials for biological applications* **2021**, *123*, 111952.

[44] S. A. Wilhelm, M. Maricanov, V. Brandt, F. Katzenberg, J. C. Tiller, *Polymer* **2022**, *242*, 124582.

[45] a) J. E. Mark, J. L. Sullivan, *The Journal of Chemical Physics* **1977**, *66*, 1006; b) G. Allen, P. L. Egerton, D. J. Walsh, *Polymer* **1976**, *17*, 65.

[46] Y. Gnanou, P. Lutz, P. Rempp, *Makromol. Chem.* **1988**, *189*, 2885.

[47] a) M. P. Lutolf, J. A. Hubbell, *Biomacromolecules* **2003**, *4*, 713; b) M. Vamvakaki, S. C. Hadjiyannakou, E. Loizidou, C. S. Patrickios, S. P. Armes, N. C. Billingham, *Chem. Mater.* **2001**, *13*, 4738; c) Y. Zheng, M. Micic, S. V. Mello, M. Mabrouki, F. M. Andreopoulos, V. Konka, S. M. Pham, R. M. Leblanc, *Macromolecules* **2002**, *35*, 5228; d) M. Kimura, Y. Nakagawa, N. Adachi, Y. Tatewaki, T. Fukawa, H. Shirai, *Chem. Lett.* **2009**, *38*, 382; e) J. A. Johnson, M. G. Finn, J. T. Koberstein, N. J. Turro, *Macromolecules* **2007**, *40*, 3589; f) B. D. Fairbanks, M. P. Schwartz, A. E. Halevi, C. R. Nuttelman, C. N. Bowman, K. S. Anseth, *Advanced materials (Deerfield Beach, Fla.)* **2009**, *21*, 5005.

[48] a) F. Lange, K. Schwenke, M. Kurakazu, Y. Akagi, U. Chung, M. Lang, J.-U. Sommer, T. Sakai, K. Saalwächter, *Macromolecules* **2011**, *44*, 9666; b) T. Matsunaga, T. Sakai, Y. Akagi, U. Chung, M. Shibayama, *Macromolecules* **2009**, *42*, 6245; c) T. Matsunaga, T. Sakai, Y. Akagi, U. Chung, M. Shibayama, *Macromolecules* **2009**, *42*, 1344; d) A. Sugimura, M. Asai, T. Matsunaga, Y. Akagi, T. Sakai, H. Noguchi, M. Shibayama, *Polym J* **2013**, *45*, 300.

[49] a) T. Hiroi, S. Kondo, T. Sakai, E. P. Gilbert, Y.-S. Han, T.-H. Kim, M. Shibayama, *Macromolecules* **2016**, *49*, 4940; b) S. Nakagawa, X. Li, H. Kamata, T. Sakai, E. P. Gilbert, M. Shibayama, *Macromolecules* **2017**, *50*, 3388; c) H. Kamata, U. Chung, M. Shibayama, T. Sakai, *Soft Matter* **2012**, *8*, 6876; d) M. Ohira, X. Li, C. I. Gupit, H. Kamata, T. Sakai, M. Shibayama, *Polymer* **2018**, *155*, 75; e) S. Nakagawa, X. Li, M. Shibayama, H. Kamata, T. Sakai, E. P. Gilbert, *Macromolecules* **2018**, *51*, 6645.

[50] H. C. Kolb, M. G. Finn, K. B. Sharpless, *Angew. Chem. Int. Ed.* **2001**, *40*, 2004.

[51] *Macromolecules* **2009**, *42*, 3827.

[52] P. L. Golas, K. Matyjaszewski, *Chemical Society reviews* **2010**, *39*, 1338.

[53] N. K. Devaraj, M. G. Finn, *Chem. Rev.* **2021**, *121*, 6697.

[54] NobelPrize.org, "The Nobel Prize in Chemistry 2022.", can be found under https://www.nobelprize.org/prizes/chemistry/2022/summary/.

[55] S. P. O. Danielsen, H. K. Beech, S. Wang, B. M. El-Zaatari, X. Wang, L. Sapir, T. Ouchi, Z. Wang, P. N. Johnson, Y. Hu et al., *Chem. Rev.* **2021**, *121*, 5042.

[56] S. Koltzenburg, M. Maskos, O. Nuyken, *Polymere: Synthese, Eigenschaften und Anwendungen*, Springer Berlin Heidelberg, Berlin, Heidelberg, **2014**.

[57] W. Burchard in *Branched polymers, Vol. 2* (Eds.: J. Roovers, W. Burchard), Springer Berlin Heidelberg, Berlin, Heidelberg, **1999**, pp. 113–194.

[58] H.-G. Elias, *Physikalische Strukturen und Eigenschaften*, **2001**.

[59] I. Teraoka, *Polymer solutions. An introduction to physical properties*, Wiley, New York, **2010**.

[60] G. Strobl, *The Physics of Polymers. Concepts for Understanding Their Structures and Behavior*, Springer-Verlag Berlin Heidelberg, Berlin, Heidelberg, **2007**.

[61] A. Eich, "Visko Fibel. Theorie und Praxis der Viskosimetrie mit Glas-Kapillarviskometern", can be found under https://www.xylemanalytics.com/File%20Library/Downloads/SIA_visko-Fibel_Deutsch.pdf, **2015**.

[62] M. Rubinstein, *Polymer Physics*, **2003**.

[63] M. Weissmüller, W. Burchard, *Acta Polymerica* **1997**, *48*, 571.

[64] K. Shida, K. Ohno, M. Kimura, Y. Kawazoe, Y. Nakamura, *Macromolecules* **1998**, *31*, 2343.

[65] W. Schärtl, *Light Scattering from Polymer Solutions and Nanoparticle Dispersions*, Springer, Berlin, Heidelberg, **2007**.

[66] T. Mezger, *The Rheology Handbook*, Vincentz Network, **2020**.

[67] S. Seiffert, *Physical Chemistry of Polymers*, De Gruyter, **2023**.

[68] C. Wrana, *Polymerphysik. Eine physikalische Beschreibung von Elastomeren und ihren anwendungsrelevanten Eigenschaften*, Springer Berlin Heidelberg, Berlin, **2014**.

[69] C. S. Johnson, D. A. Gabriel, *Laser light scattering*, Dover Publications, New York, **1994**.

[70] S. Seiffert, *Progress in Polymer Science* **2017**, *66*, 1.

[71] M. Shibayama, *Bulletin of the Chemical Society of Japan* **2006**, *79*, 1799.

2. MOTIVATION AND SCIENTIFIC GOAL

Amphiphilic polymer co-networks (APCN) consist of both, hydrophilic and hydrophobic building blocks, which makes their structure and properties dependent on the environmental conditions, such as solvent polarity. Especially, their environmentally sensitive permeability and viscoelasticity give rise to many potential applications such as membranes, drug delivery systems, tissue engineering, and in general biomedical applications. In the field of biomedical applications, many amphiphilic networks used consist at least in parts of poly(ethylene glycol) (PEG) or poly(ε-caprolactone) (PCL).

However, for a targeted design of APCNs for such and other applications, a rational understanding of the interplay between synthesis and environmental conditions, the resulting structure, and the related properties is essential. For this purpose of systematic exploration of structure–property relationships, model systems with a defined structure and almost no structural inhomogeneities are advantageous. Such model networks can be obtained with the tetra-PEG approach by hetero-complementary reaction of two hydrophilic poly(ethylene glycol) four-arm star polymers with different reactive end groups. The use of hetero-complementary reacting terminal groups prevents the formation of intramolecular loops and thus eliminates a significant part of undesirable microscopic defects. Networks prepared by this approach exhibit outstanding mechanical stability and homogeneity. Therefore, the adaption of this approach to amphiphilic systems seems promising for targeted structure-property relation studies on APCNs.

The above-mentioned synthesis strategy leads to permanent covalently crosslinked APCNs, which are only capable of correcting structural changes to a very limited extent, e.g. after adaptation to changing solvents. Thus, also reversible crosslinked networks based on star polymers are of special interest due to their ability to eliminate potential structural defects incorporated during preparation by reorganization. These reversible crosslinking points can consist of electrostatic interactions allowing for control of the bond strength through length and type of the ionic segments. In addition, switching between a gel state and a sol state can be possible by control of the pH value and usage of suitable polyelectrolyte or polyampholyte building blocks.

The present work is carried out in the framework of the research unit FOR2811 "Adaptive polymer gels with controlled network structure", whose overall objective is therefore to manufacture tailor-made amphiphilic polymer co-networks with near-ideal structure based on four-

armed star polymers that are either covalent-permanent or ionic-reversible crosslinked, and to comprehensively study the interplay of synthesis conditions, resulting structure and associated properties. The aim is to get a rational understanding of the interplay of network building block parameters (molecular weight; functionality; philie; mixing ratio), the resulting network structure (extent of crosslinking; elastically effective network strands; network connectivity and (in)homogeneity; modulus) and the corresponding phase morphology as a function of environmental conditions (temperature; solvent quality; pH). This interplay shall furthermore be investigated in different states of the network (as prepared; swollen; selectively swollen) and in bulk as well as at the surface. With this knowledge, specific functions for potential applications can be imprinted on the gels such as controlled substrate transport or release, volume change or mechanical strength.

How the subprojects (german: Teilprojekt (TP)) in the research unit FOR2811 act jointly to reach this goal is sketched in **Figure 2. 1** together with the respective network type (covalent-permanent or ionic-reversible) or the mainly used method to characterize the networks. Through close cooperation and feedback loops between theory (simulation) and experiment (synthesis; experimental), the subprojects TP1 to TP7 prepare the basis for the application oriented TP8.

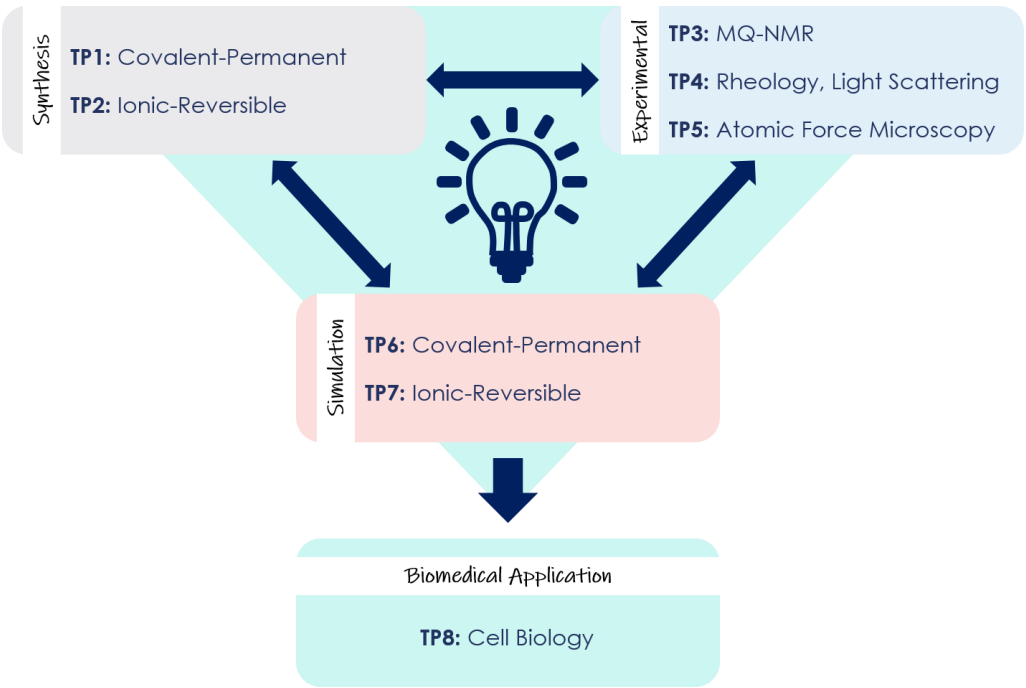

Figure 2. 1: Schematic representation of the subproject (german: Teilprojekt (TP)) interaction within the research unit FOR2811 divided into synthesis projects, experimental characterization projects and theoretical simulation projects. The subprojects are listed together with the respective network type or the most prominently used techniques for characterization. In addition, the cell compatibility and applicability of the networks for biomedical purposes is tested in TP8.

The present thesis represents the work of **TP4** and has the goal to bridge the respective synthesis projects (TP1, TP2) with the complementary theory projects (TP6, TP7), and to establish direct comparisons with the other experimental projects (TP3, TP5) in the field of structure-property relationships and their dependence on synthesis as well as environmental conditions. This translates into comprehensive investigation of the different network building blocks, the network formation process, and the final networks of both crosslinking types with the methods of viscometry, light scattering and rheology. Furthermore, in case of the permanent-covalent crosslinking, a characterization of the networks under different solvent conditions and in different states, i.e. in preparation state, swollen or selectively swollen, are of interest to identify the impact of the network building block architecture on the resulting network structure and properties. The amphiphilicity of the networks can be implemented by use of separate hydrophilic and hydrophobic building blocks as well as by direct use of amphiphilic building blocks (see **Figure 2. 2**). In the case of ionic-reversible crosslinking, the initial focus is on the synthesis and characterization of suitable ionic prepolymers (polyelectrolytes, polyampholytes) and the proof of the reversibility of this crosslinking type.

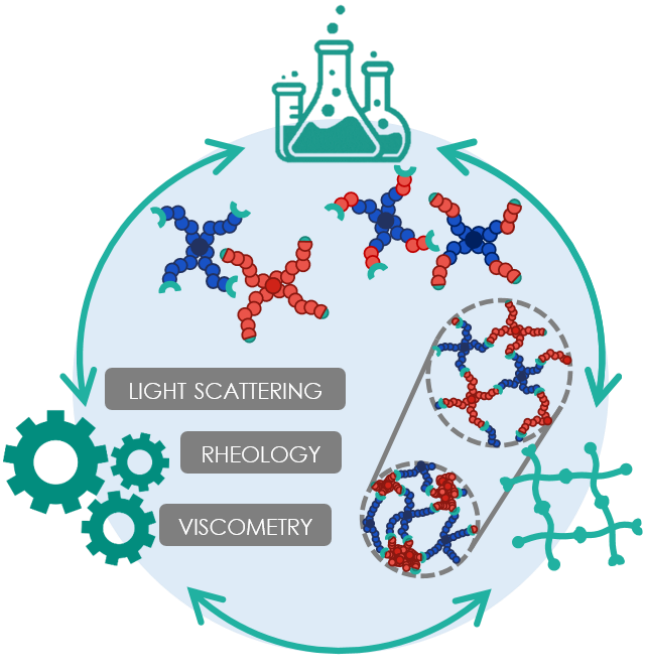

Figure 2. 2: Schematic representation of the scope of TP4 with regard to the permanent-covalent linkage of the building blocks. The aim is to gain a rational understanding of the relationship between the synthesis conditions and the building block architecture, the resulting structure and the corresponding properties. The tools for this are mainly the methods of viscometry, rheology and light scattering.

In this context, a first collaborative study addresses the fundamental aspects of synthesis, structure and properties in a common good solvent for amphiphilic polymer co-networks based on t-PEG and t-PCL. With the aim of obtaining model networks with a defined, homogeneous structure, a hetero-complementary coupling of the building blocks is required. This is realized by combining benzoxazinone-terminated t-PCL with amine-terminated t-PEG. The influence of the synthesis conditions (temperature, mixing ratio, solvent) on the structure and properties of the networks is probed, next to the characterization of the building blocks in solution and the gelation kinetics. The plausibility of the results is checked by a comparison with theoretical models and literature on previous model networks.

Although this first study considers fundamental issues, no information on the mechanical properties at equilibrium swelling and in general in a selective solvent, e.g. water, are provided. These aspects are addressed in a second collaborative study, which uses the complementary methods of rheology and atomic force microscopy to provide information on the mechanical properties over a wide range of length-scales and in both selective and non-selective solvent. Due to the hydrophobicity of t-PCL, a significant change in structure both in bulk and at the surface as well as in the mechanical properties is expected. The impact of the hydrophobic t-PCL is clarified by comparison with networks prepared solely from t-PEG but with the same benzoxazinone-based linking chemistry.

In the first two studies, separate hydrophilic and hydrophobic building blocks are used to form amphiphilic polymer networks. Another approach to such networks is to encode the amphiphilicity within the building block, e.g. by use of block copolymers with complementary end linking groups. This can also be applied to pre-structure the networks in the as-prepared state in order to implement specific structures and corresponding functions, e.g. transport properties for guest substances. Therefore, in a third collaborative study, block copolymers of four-armed t-PCL cores block extended with linear PEG, t-PCL-*b*-PEG, are synthesized and investigated concerning their solution behavior depending on the length of the PEG arms via DLS and TEM. In a rather good solvent for both types of polymer, single stars are expected. Whereas the formation of micellar structures is expected in water, which is only a good solvent for PEG, but a poor solvent for PCL. The length of the PEG arms can influence the stability of such micellar structures and may change the solution behavior.

A next step in exploring the potential of such amphiphilic block copolymers is to add hetero-complementary end groups and prepare networks by crosslinking. For this purpose, in a fourth collaborative study, networks composed of t-PEG-*b*-PCL block copolymers with

complementary benzoxazinone and amine linking end-groups are considered. Next to the building block themselves, the network formation as well as the swelling properties and the mechanics are examined. The networks are probed in two types of solvent, dimethyl sulfoxide and water to give a comprehensive overview on the structure and properties in a non-selective and a selective solvent.

Up to this point, only permanent-covalent crosslinked networks are subject of the investigation. However, ionic-reversible crosslinked networks are also of interest due to their ability to eliminate possible structural defects introduced during synthesis by reorganization and their potential for self-healing, which can be used in biomedical applications. Furthermore, the bond strength in such systems can be tuned by length and type of the ionic segments. To generate such networks, a first step is to synthesize and characterize suitable well-defined polyelectrolyte or polyampholyte building blocks based on four-armed star polymers.

In this context, a fifth study addresses the synthesis and pH-dependent solution behavior of t-PEG-*b*-PDha, i.e. a t-PEG core block extended with polydehydroalanine (PDha) segments. The ampholytic nature of polydehydroalanine causes the overall net charge and thus the solution behavior to be strongly dependent on the pH value. How the length of the PDha block and the molar mass of the PEG core influence this dependence will be probed by potentiometric titration, zeta potential measurements, dynamic light scattering and atomic force microscopy.

In a next step, this knowledge can be used to form ionic networks with a suitable counterpart, e.g. a strong negatively charged polyelectrolyte. To provide a first proof of concept and demonstrate the initial feasibility of the concept, purely hydrophilic gels are prepared in a first instance. The purely hydrophilic approach is also easier to implement in this early stage due to the high number of charges.

Thus, in a sixth study, ionically crosslinked gels are investigated by combining ionic block copolymers with a t-PEG core and attached poly carboxy betaine methacrylamide (PCBAMAA) or poly styrene sulfonate (PSSNa) segments, respectively. Styrene sulfonate is a strong electrolyte and therefore negatively charged over the entire pH-range investigated. Hence, the gel formation is dependent on the charge of the carboxy betaine species, which is positively charged at low pH and charge neutral at high pH. In consequence, a gel formation is expected at low pH and a sol state is expected at high pH. Switching the pH between low and high values, possibly enables switching between a gel and a sol state.

3. CHAPTER I: AMPHIPHILIC POLYMER CO-NETWORKS BASED ON PEG AND PCL

Amphiphilic Model Networks Based on PEG and PCL Tetra-Arm Star Polymers with Complementary Reactivity

[redacted] **N. Fribiczer**, [redacted]

Macromolecules, **2022**, 55, 15, 6573–6589; doi: 10.1021/acs.macromol.2c00693

The corresponding *Supporting Information* is included in **Appendix A.3**.

The results in this chapter were first published on August 1, 2022 and are adapted with permission from *Macromolecules*, **2022**, 55, 15, 6573–6589.

3.1. Specific Summary

Amphiphilic polymer co-networks consist of both, hydrophilic and hydrophobic building blocks, and swell independently in water as well as in organic solvents. Due to their amphiphilicity, they exhibit environmentally sensitive viscoelasticity and selective permeability, which makes them suitable candidates for applications as membranes and drug delivery systems among other biomedical applications. For all these applications control over the structure of the network is essential as the structure significantly determines the network properties. In this context, model networks with a defined starting structure are advantageous. Model networks are tailored infinite three-dimensional structures of covalently crosslinked polymers consisting of a defined number and length of monodisperse polymer strands connected by junction points of known and constant functionality. One way to such networks is the hetero-complementary reaction of star-polymers with different reactive end groups. The hetero-complementarity reduces the formation of microscopic defects and leads to enhanced mechanical stability and homogeneity. This concept can be adapted for amphiphilic networks to receive networks with a tailor-made structure and a high level of homogeneity.

For this purpose, 2-(4-nitrophenyl)-benzoxazinone terminated tetra-poly(caprolactone) (t-PCL) is hetero-complementary crosslinked with amino-terminated poly(ethylene glycol) (t-PEG) under different reaction conditions by varying solvent, concentration and temperature to form near-ideal amphiphilic polymer co-networks. The network building blocks are thoroughly characterized concerning their solution behavior in toluene, chloroform and tetrahydrofuran

using viscometry, dynamic light scattering (only in tetrahydrofuran due to insufficient contrast in toluene and chloroform) and the Flory–Huggins interaction parameter. Herein, the Flory–Huggins parameter is estimated for the used conditions combining literature data and the experimental viscometry results. All solvents are good solvents, but the solvent quality decreases in the order chloroform, toluene, and tetrahydrofuran and shows a temperature dependence especially for the t-PEG compound. Next to the characterization of the building blocks, the reaction kinetics during gel formation are examined with NMR spectroscopy and computer simulations. The results indicate a nearly homogeneous mixture in which the kinetics are only affected by local composition fluctuations after most of the star polymers are attached to the network. The local structure after gelation is characterized by an increased formation of double links between the same pair of star polymers compared to preceding work on pure hydrophilic star polymer networks prepared by the same crosslinking strategy but based on other end linking groups. Nevertheless, the networks possess a near model structure with a small defect fraction. The respective solvent quality of toluene, chloroform and tetrahydrofuran for the individual star polymer species is also reflected in the corresponding swelling capacities. Drying-reswelling-cycles reveal distinct post-crosslinking during the drying procedure resulting in a significant lower swelling degree after the first cycle. Rheological investigations of the as-prepared networks in toluene result in a similar power law behavior of modulus as related work, despite the modulus is a factor of 4 below the expectations from the phantom model.

The obtained results of this comprehensive study on amphiphilic co-networks based on t-PEG and t-PCL in co-solvents allow first deductions of structure–property relationships in such networks and provide a basis for further investigations in either a selective solvent or in the swollen state.

3.2. Author Contributions

[redacted]	Concept development, synthesis and optimization of network formation, analytical characterization of compounds, swelling experiments and paper writing.
[redacted]	MQ-NMR measurement and analysis.
Nora Fribiczer:	Viscometry, dynamic light scattering, and rheology measurements and analysis.
[redacted]	HR MAS and solution-state NMR measurements, on-line NMR kinetic studies.
[redacted]	Concept development and supervision of [redacted].
[redacted]	Literature research, calculation of Flory–Huggins parameters, computer simulations.
[redacted]	Supervision of [redacted] and manuscript correction.
[redacted]	Scientific supervision of [redacted] and manuscript correction.
[redacted]	Scientific supervision of [redacted] and manuscript correction.
[redacted]	Literature research, calculation of Flory–Huggins parameters, computer simulations, manuscript preparation and manuscript correction.
[redacted]	Concept development, scientific supervision of [redacted], and manuscript correction.

3.3. Acknowledgement

This work was carried out as part of the research collaboration ″Adaptive Polymer Gels with Model Network Structure″ (FOR2811) funded by the German Research Foundation (DFG), grant 397384169, and the individual grants 423514254, 423478088, 423435302, 423373052. The authors thank [redacted] for the opportunity to perform macromolecular structure analysis using size exclusion chromatography and [redacted] for performing these measurements.

3.4. Abstract

A new approach for the synthesis of model amphiphilic polymer co-networks (ACNs) based on a hetero-complementary coupling reaction of a 2-(4-nitrophenyl)-benzoxazinone terminated tetra-arm polycaprolactone star (tetra-PCL) with an amino-terminated tetra-arm polyethylene glycol star (tetra-PEG) is presented. The reaction conditions (solvent, concentration, and temperature) were varied widely. Reaction kinetics and gelation were analyzed with high-resolution NMR spectroscopy and computer simulations. The results agree with a nearly homogeneous mixture where local composition fluctuations affect kinetics only after most of the molecules are attached to the gel. Viscometry data, dynamic light scattering data, and literature data for the solubility parameters were combined to provide estimates for the Flory–Huggins interaction parameter of the two star polymers in toluene, chloroform, and THF as solvents. These estimates allow one to collapse equilibrium swelling data in different solvents on a universal curve. Multiple quantum NMR analysis shows an enhanced formation of double connections between the same pair of stars as compared to preceding work on tetra-PEG gels made by the same crosslinking strategy but with a different coupling reaction. Besides this last observation, the remaining results indicate that the networks possess a near model-like structure with only a small fraction of pending arms as the most relevant type of network defects.

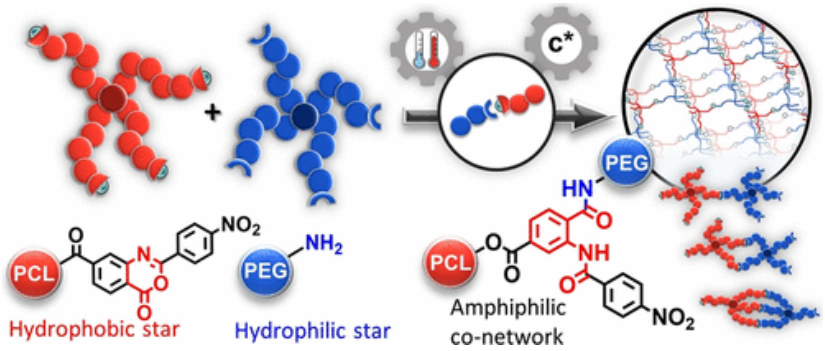

Scheme 3. 1: Schematic illustration of the reaction of benzoxazinone terminated PCL with amino terminated PEG to form an amphiphilic polymer co-network.

3.5. Introduction

Model amphiphilic polymer co-networks (ACNs) are tailor-made adaptive soft solids of covalently crosslinked polymers with both hydrophilic and hydrophobic units.[1–6] Based on their amphiphilicity, ACNs swell independently in water as well as in organic solvents.[7–9] The resulting environmentally sensitive viscoelasticity and selective permeability make them suitable for deliberately controlling the transport of molecules of different polarity through the swollen polymer network (gel).[6] The latter is exploited for soft contact lenses with extended wear time, the most common application of ACNs.[10–12] Further biomedical applications are (multi) stimuli-responsive functionalized ACN-based matrices or membranes especially for drug delivery devices[13–18] but also for tissue engineering[19] and bioartificial pancreas.[20] In addition, potential technological uses of ACNs are being explored as biocatalyst supports,[21] sensors,[22, 23] and polymer electrolytes for batteries.[8] The properties for all these and other applications are controlled by the polymer network structure, which in turn is strongly dependent on the formation process. A very good overview on the synthesis of ACNs is provided in the review by Erdodi and Kennedy.[6] A major concern of some authors cited there was to obtain networks with a defined structure. Although very promising results were achieved in some cases, the attained structures did not meet the criteria of a model network, which is characterized by a homogenous structure of defined length and number of monodisperse polymer strands connected together by junction points of known and constant functionality within an infinite three-dimensional net structure.[4, 24]

A seminal paper published by Sakai et al.[25] in 2008 showed one possible way to obtain hydrophilic star-polymer networks with a model network structure.[26] Their approach is based on an end-linking process through a hetero-complementary conversion of two four-arm polyethylene glycol stars (A_4- and B_4-type tetra-PEG) containing different reactive end groups. For star polymers with narrow polydispersity, the number of chain segments between the network junctions is well-fined. Furthermore, the hetero-complementary conversion of the terminal groups prevents arms of one star from reacting with each other. This eliminates the formation of a significant part of undesirable microscopic defects,[27] leading to a substantial enhancement of the elastic modulus of the networks when prepared at a low overlap number of the network strands.[28] Gels synthesized in this way are characterized by excellent mechanical stability and homogeneity.[29–31] While the structure of such gels is quite close to that of a model network, they still feature structural defects, like pending arms and double or multiple links between the star polymers, which are due to the statistical nature of the crosslinking process.[32] In particular, double links with adjacent stars (see **Scheme 3. 2**) can be detected and quantified by

low-field ^{1}H multiple-quantum nuclear magnetic resonance (MQ NMR) spectroscopy[33] and Monte Carlo simulations,[32] which provide detailed insight into the topology of the networks. In recent years, the synthesis and characterization of networks with well-defined structures have raised the understanding of their structure–property relations to a new level. In contrast, corresponding studies on amphiphilic co-networks have been performed only sporadically to date.[8, 9, 34, 35] With our contribution, we aim to advance the state of knowledge regarding structure–property relationships of model amphiphilic co-networks.

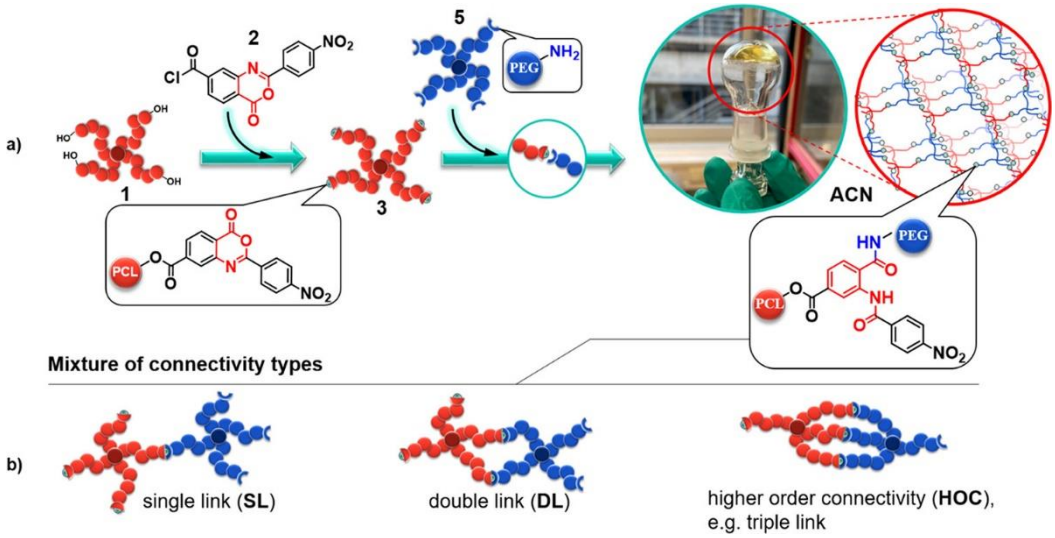

Scheme 3. 2: Synthesis of ACNs based on hydrophobic 2-(4-Nitrophenyl)-benzoxazinone-terminated PCL (**3**) and hydrophilic amino-terminated PEG (**5**) Tetra-arm star polymers: (**a**) Reaction scheme and (**b**) Connectivity types within the polymer network formed.

In analogy to the tetra-PEG gels, a key aspect in the synthesis of model ACNs is the hetero-complementary linkage of structurally defined hydrophilic and hydrophobic star polymers via their end groups. Typically, fast click reactions, such as azide–alkyne cycloaddition,[36] condensation reactions of amino groups with activated ester bonds,[9, 34] as well as the addition reaction of benzaldehyde and benzaacylhydrazide terminal groups,[8] have been used for the synthesis of A_2B_4- and A_4B_4-type ACNs. These reactions provide high conversions within a short time. While this may initially appear to be an advantage, it entails the risk that the components forming the network do not mix properly. As a result, additional defects and large-scale heterogeneities inducing shielding of reactive groups may occur. This problem has already been pointed out by Sakai et al.[37] in connection to the synthesis of tetra-PEG gels via the active ester method, where the rate of gelation was controlled by the pH value. Another influencing factor is a possible segregation of the chemically different building blocks during the ACN formation, which is also assumed to have an effect on network inhomogeneities. These aspects

have hardly been considered in previous works. To address this challenge of minimizing structural network defects, a homogeneous reaction mixture prior to gelation is essential, especially for systems based on components of different polarity. Accordingly, in addition to a hetero-complementary end group reaction with high conversion, a sufficiently slow and adjustable viscosity increase is of particular importance, i.e., a crosslinking reaction with an adjustable moderate reaction rate and a suitable nonselective solvent for both star polymers are desired.

In previous works, we used 2-phenylbenzoxazinone-based compounds to functionalize polymers with oxazinone groups.[38, 39] By the reaction of these oxazinone-functionalized polymers with amino group containing polymers, block and graft copolymers were obtained. As a proof of concept, we also synthesized A_2-B_4 hybrid networks by conversion of an oxazinone-terminated four-arm poly-ε-caprolactone star with a linear amino-terminated polypropylene glycol prepolymer.[40] A major advantage of the oxazinone-amine reaction is its controllable reactivity. By introducing electron-withdrawing substituents on the oxazinone group and varying the reaction temperature, the course of the reaction can be significantly influenced, offering great potential for the synthesis of well-defined ACNs.

Focusing on material properties and application but without addressing the network formation process and its influence on network defects, syntheses of highly biocompatible and biodegradable ACNs based on hydrophobic PCL and hydrophilic PEG have been reported several times in the literature.[41–43] ACNs with these components are also the subject of the present publication, but with special focus on the process of network formation. With the aim of obtaining networks with highly defined structures, the synthesis was carried out following the tetra-arm approach of Sakai et al.[25] In contrast to Sakai, in our method presented here, hydrophobic PCL and hydrophilic PEG tetra-arm stars were linked by the much slower 2-(4-nitrophenyl)-benzoxazinone/amine reaction in organic solvents similar to our earlier synthesis of A_2-B_4 hybrid networks.[40] In this approach, hydroxy-terminated star polymer tetra-PCL (**1**) was first reacted with 2-(4-nitrophenyl)-4-oxo-4H-benzo[d][1,3]oxazine-7-carboxylic acid chloride (**2**), resulting in 2-(4-nitrophenyl)-benzoxazinone-terminated tetra-PCL (**3**), which was crosslinked in different organic solvents with amino-terminated star polymer tetra-PEG (**5**) in a second step to give ACN gels (see **Scheme 3. 2**). The moderate rate of the crosslinking reaction allows the precursor star polymers to mix and diffuse and, moreover, the monitoring of this process by NMR spectroscopy and oscillatory shear rheology. Hagmann et al. previously analyzed the surface structure of thin films of these ACN gels using atomic force microscopy and compared this with their bulk structure.[44]

Our main concern is to show how the reaction conditions influence the course of the reaction and thus the microstructure and homogeneity of ACNs. In particular, we study the influence of the reaction conditions (solvent, concentration, and temperature) on the crosslinking process and the occurrence of associated network defects. The solvent quality of toluene, tetrahydrofuran, and chloroform as possible nonselective solvents is analyzed by using a combined approach of viscosity measurements and theoretical computations. Furthermore, the resulting environment-dependent viscoelasticity and swelling behavior of the gels prepared under different reaction conditions are investigated. We have also used large-scale computer simulations to model network formation under idealized conditions (perfect stars, all reactive groups reacted, perfect mixing of both components). Comparison with these data allows one to explore deviations from ideal reaction conditions and possible de-mixing effects.

3.6. Experimental Section

Materials

All chemicals and solvents (analytical grade) were obtained from Sigma-Aldrich and used as received unless differently mentioned. Hydroxy-terminated tetra-arm polyethylene glycol (tetra-PEG-OH) was obtained from JenKem Technology USA, purified by dialysis in water (ZelluTrans, Roth, 1000 g mol^{-1} molecular weight cutoff), and precipitated twice from THF in cold diethyl ether. The number-average molar mass (M_n) was determined by SEC-MALLS in water (M_n = 10 kg mol^{-1}, Đ = 1.02). ε-Caprolactone (ε -CL) was dried under reduced pressure over CaH_2 for at least 24 h, then purified by vacuum distillation and stored under nitrogen atmosphere. Tin(II)-2-ethylhexanoate ($Sn(oct)_2$) was purified by vacuum distillation and stored under nitrogen atmosphere. 2-(4-Nitrophenyl)-4-oxo-4H-benzo[*d*][1,3]oxazine-7-carboxylic acid chloride (**2**) was synthesized as described earlier.[40]

Synthesis of Functionalized Tetra-arm Star Polymers

2-(4-Nitrophenyl)-benzoxazinone-terminated Tetra-PCL (3)

Star polymer **3** was synthesized according to **Scheme 3. 3a** in two steps as previously reported.[40, 45] First, **1** was synthesized by ROMP of ε-CL using pentaerythritol as starter and $Sn(oct)_2$ as catalyst. The molar ratio of ε-CL/pentaerythritol/$Sn(oct)_2$ was adjusted to 87:1:0.1. Subsequently, the hydroxy terminal groups of **1** were converted with compound **2** to yield **3**. Under neutral conditions, the hydrolysis sensitivity of the benzoxazinone group is low. Nevertheless, compound **3** was stored and further processed under exclusion of moisture.

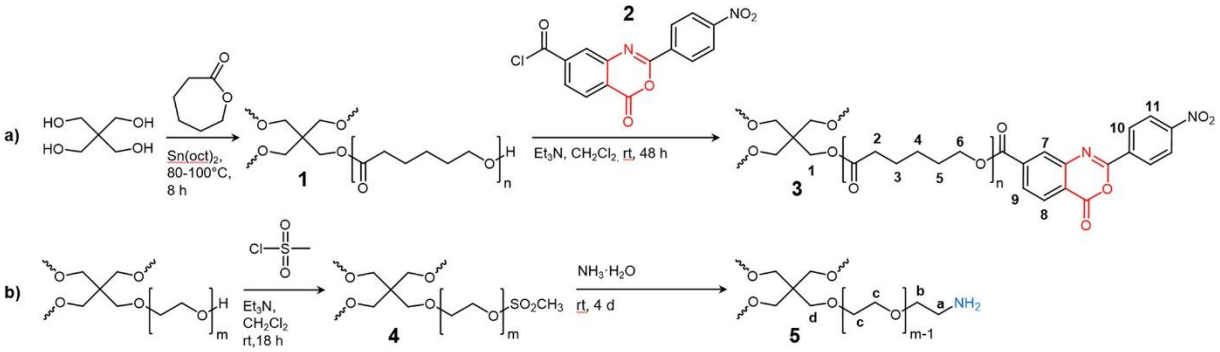

Scheme 3. 3: Synthesis of tetra-arm star polymers **3** and **5**.

^{1}H NMR (THF-d_8, 40 °C): δ 8.53 (d, 8.9 Hz; 10), 8.39 (d, 8.9 Hz; 11), 8.32 (d, 1.5 Hz; 7), 8.29 (d, 8.1 Hz; 8), 8.18 (dd, 8.1 Hz, 1.5 Hz; 9), 4.39 (t, 6.6 Hz; 6 next to OC(*O*)Ph), 4.12 (s; 1), 4.02 (t, 6.7 Hz; 6), 2.32 (t, 7.4 Hz; 4 next to core), 2.26 (t, 7.4 Hz; 2), 1.65–1.55 (3, 5), 1.38 ppm (m; 4), see also **Figures A.3. 1** and **A.3. 3c**. The complete ^{1}H and ^{13}C NMR characterization data (solvent: $CDCl_3$) of **3** are reported in a separate publication.[45]

Mesylate-Terminated Tetra-PEG (4)

Star polymer **4** was synthesized by adapting a previously reported procedure (see first step in **Scheme 3. 3b**).[46] Briefly, purified tetra-PEG-OH (10 g, 1 mmol) with a number-average molar mass of 10 kg mol^{-1} was dissolved in 50 mL of anhydrous CH_2Cl_2 under a nitrogen atmosphere. Then 8.5 mmol of triethylamine and 8 mmol of mesyl chloride were added to the solution and stirred overnight. After the reaction, the mixture was filtered to remove insoluble triethylamine hydrochloride, concentrated in vacuo, and poured into a 10-fold excess of cold diethyl ether. The precipitated star polymer **4** (9.1 g, 91%) was isolated by filtration and dried in vacuo at 40 °C.

^{1}H NMR ($CDCl_3$): δ 4.37 (t, 8H; SO_2OCH_2), 3.76 (m, 8H; $SO_2OCH_2CH_2$), 3.70–3.45 (CH_2CH_2), 3.41 (s; $CH_{2,core}$), 3.07 ppm (s, 12H; CH_3SO_2).

Amino-terminated Tetra-PEG (5)

Star polymer **5** was prepared as described earlier (see second step in **Scheme 3. 3b**).[46] Briefly, star polymer **4** (9 g, 0.9 mmol) was dissolved in 28% aqueous ammonia solution (100 mL). The reaction mixture was left to stir for 4 days at room temperature. The ammonia was allowed to evaporate overnight after NaOH (5 M) was added dropwise until the pH reached 13. The solution was dialyzed several times against deionized water for 24 h. The aqueous solution was

concentrated in vacuo, and the water was completely removed by lyophilization to give **5** (7.2 g, 80%).

^{1}H NMR (THF-d_8, 40 °C): δ 3.55 (s; c), 3.42 (br; b), 3.41 (s; d), 2.76 (br; a), 2.36 ppm (v br; NH_2 and water from solvent); see also **Figure A.3. 2**.

Synthesis of Amphiphilic Co-networks (CN)

A series of amphiphilic co-networks **CN** was synthesized by hetero-complementary reaction of the end groups of **3** and **5**.

For the synthesis, the polymer concentration, the temperature, and the solvents were varied. A sample overview is given in **Table 3. 1**.

First, stock solutions of **3** and **5** with different polymer volume factions (ϕ = 0.06, 0.18, and 0.30) were prepared. The ϕ values correspond roughly to 1, 3, and 5 times the overlap concentration c^* (70 mg mL^{-1}), which appears as the last part of the sample name (e.g. **CN1-1**, **CN1-3**, and **CN1-5** are synthesized at 1c^*, 3c^*, and 5c^*, respectively). For the synthesis, aliquots of the stock solutions were poured together at a certain temperature and allowed to react. After reaching the gel point (visual detection), the temperature was raised to the final reaction temperature until crosslinking was completed. To ensure equivalence of the reactive groups, ^{1}H NMR spectra of mixtures of the stock solutions were recorded. Based on the intensities of the end group signals, concentration differences of the reactive groups could be compensated by post-dosing of the deficiency component.

The synthesis of **CN2-1** in THF (ϕ = 0.06) is described in the following as an example: To start the crosslinking, 0.972 g of the stock solution of **5** was placed in a 5 mL reaction flask equipped with a flat stirrer using a 1 mL syringe. Then, 0.784 g of the stock solution of **3** was added, and the reaction flask was tightly closed. The reaction mixture was stirred at 25 °C until gelation was observed. After this, the reaction flask was placed in a preheated oil bath (40 °C) for 3 days.

^{1}H NMR (THF-d_8, 40 °C): δ 12.94 (br; PhN*H*CO), 9.49 (d, 1.3 Hz; 7′), 8.38 (d, 8.5 Hz; 10′), 8.33 (t; CH_2N*H*CO), 8.25 (d, 8.5 Hz; 11′), 8.88 (d, 8.3 Hz; 8′), 7.77 (dd, 8.3 Hz, 1.3 Hz; 9′), 4.34 (t, 6.5 Hz; 6 next to OC(*O*)Ph), 4.12 (s; 1), 4.02 (t, 6.7 Hz; 6), 3.67 (t; a′), 3.55 (b′, c), 3.42 (s; d), 2.32 (t, 7.4 Hz; 4 next to core), 2.26 (t, 7.4 Hz; 2), 1.65–1.55 (3, 5), 1.38 ppm (m; 4).

Table 3. 1: Sample overview.

sample[a]	solvent	ϕ_0 [b]	T_1 [c] (°C)	T_2 [d] (°C)	p [e]	Q_v [f]				w_{sol} [g] (%)	f_{defs} [h]
						1	**2**	**3**	**4**		
CN1-1	THF	0.06	25	25	0.98	20.9	13.2	10.4	10.2	8	-
CN2-1	THF	0.06	25	40	0.99	20.0	14.0	10.7	10.2	9	-
CN3-1	THF	0.06	25	60	0.99	19.6	15.2	11.6	10.2	9	-
CN1-3	THF	0.18	25	25	0.98	11.7	10.2	9.4	9.0	2	-
CN2-3	THF	0.18	25	40	0.99	11.4	10.7	9.5	8.8	4	-
CN3-3	THF	0.18	25	60	0.99	11.6	10.7	9.3	9.3	2	-
CN2-5	THF	0.30	25	40	0.84	9.2	8.7	8.2	7.8	1	-
CN3-5	THF	0.30	25	60	0.99	8.2	7.9	8.1	7.7	1	-
CN4-1	THF-d_8	0.06	40	80	-	20.0	14.0	13.6	-	-	9
CN5-1	THF-d_8	0.06	60	60	-	20.5	14.1	13.5	-	-	5
CN4-3	THF-d_8	0.18	40	80	-	15.1	13.6	13.6	-	-	2
CN5-3	THF-d_8	0.18	60	60	-	14.8	13.4	13.6	-	-	1
CN6-1	toluene-d_8	0.06	40	80	-	19.4	12.2	12.0	-	-	3
CN7-1	toluene-d_8	0.06	60	60	-	17.1	11.8	11.5	-	-	3
CN6-3	toluene-d_8	0.18	40	80	-	11.0	10.4	9.8	-	-	1
CN7-3	toluene-d_8	0.18	60	60	-	11.1	10.0	10.4	-	-	1
CN8-1	$CDCl_3$	0.06	40	80	-	28.5	22.1	20.6	-	-	28
CN9-1	$CDCl_3$	0.06	60	60	-	30.9	23.3	22.7	-	-	-
CN8-3	$CDCl_3$	0.18	40	80	-	23.6	21.9	21.3	-	-	0
CN9-3	$CDCl_3$	0.18	60	60	-	23.2	21.8	22.2	-	-	0
PEG-1[i]	D_2O	0.15	25	25	-	32.3	-	-	-	-	10
PEG-2	toluene-d_8	0.15	25	25	-	10.8	-	-	-	-	1

[a] The general sample code CN*x*-*y* of the co-networks denotes differences in solvent and temperature regime (same *x* means same solvent and temperature regime) and differences in concentrations (*y* = 1, 3, and 5 for 1*c**, 3*c**, and 5*c**, respec tively).

[b] Polymer volume fraction at preparation.

[c] Reaction temperature before reaching the gel point.

[d] Reaction temperature after reaching the gel point.

[e] Degree of conversion determined by ^{1}H HR MAS NMR spectroscopy after removal of the sol fraction, evaporation of the reaction solvent, and reswelling in D_2O.

[f] Gravimetrically determined equilibrium volume swelling degree (columns 1–4 refer to four consecutive measurements with intermediate drying steps).

[g] Sol fractions gravimetrically determined for **CN1** to **CN3**.

[h] Defect fractions determined by MQ NMR spectroscopy.

[i] Synthesized according to Sakai et al [25]

The data are related to the kinetics experiments and were determined from a low-conversion sample. The signals are significantly broadened at higher conversion and for the final networks (see **Figure A.3. 3a,b**). The assignments are in accordance with data reported in our recent study on soluble tetra-arm polymers containing the same structural motif.[45] A part of the analysis (rheology, NMR) requires a modified preparation that is explained in the corresponding sections below.

For comparison, PEG–PEG networks were synthesized by the Sakai active-ester linking chemistry in water[25] (**PEG-1**) and by conversion of **5** with oxazinone-terminated tetra-PEG in toluene (**PEG-2**). In each case, tetra-PEG-OH (M_n = 10 kg mol^{-1}) was used as the starting material for the syntheses.

Characterization

Size Exclusion Chromatography (SEC)

The number-average and weight-average molar masses (M_n and M_w) and the molar mass distribution (Đ) of the tetra-PCL-based star polymers **3a–c**, **5b**, and **5c** presented in **Table 3. 2** were determined using an isocratic HPLC pump (Agilent 1200) with an autosampler (Agilent Technologies, Santa Clara, CA) equipped with twofold detection (SEC-MALS/dRI). Details are described in the **Appendix A.3** Section 5.

Table 3. 2: Molecular Characteristics of different batches of Tetra-arm star polymers **3** and **5**.

	3a	**3b**	**3c**	**5a**	**5b**	**5c**
$M_{n,NMR}$[a] (kg mol^{-1})	11.1 ± 0.2	11.3 ± 0.2	10.5 ± 0.2	11.4 ± 0.2	10.8 ± 0.2	11.1 ± 0.2
$M_{n,SEC}$[b] (kg mol^{-1})	11.4 ± 0.2	11.7 ± 0.1	11.0 ± 0.1		10.4 ± 0.3	11.0 ± 0.1
$M_{w,SEC}$[b] (kg mol^{-1})	12.4 ± 0.2	12.6 ± 0.1	11.8 ± 0.0		10.6 ± 0.2	11.5 ± 0.3
Đ[b]	1.09 ± 0.01	1.07 ± 0.1	1.07		1.02 ± 0.01	1.05 ± 0.01

[a] Based on ^{1}H NMR end group analysis (see **Figure A.3. 1** and **A.3. 2** and comments).
[b] Based on SEC (MALS/dRI detection) in THF (**3a–c**) and water (**5a–c**).

Viscometry

Overlap concentrations c^* of star polymers **3** and **5** in THF, toluene, and chloroform were determined by capillary viscometry using eq 3.1, adopting the same convention as for linear polymers:[47]

$$[\eta] = \lim_{c \to 0} \frac{\eta_{sp}}{c} = \frac{1}{c^*} \tag{3.1}$$

where η_{sp} is the specific viscosity and [η] is the intrinsic viscosity of the solutions. Measurements were performed at 25 and 35 °C. The evaluation was carried out according to Schulz and Blaschke.[48] Details are described in SI (**Appendix A.3**) Section 6 (**Table A.3. 1**).

Dynamic Light Scattering (DLS)

The hydrodynamic radii R_h of compounds **3** and **5** in THF were determined by DLS measurements using the Stokes–Einstein equation:

$$R_h = \frac{k_B T}{6\pi\eta_s D} \tag{3.2}$$

where k_B is the Boltzmann constant, T the absolute temperature, η_s the viscosity of the solvent, and D the diffusion coefficient. The measurements were performed on a light scattering setup equipped with an ALV-SP125 goniometer, an ALV/LSE5004 multi tau correlator, a fiber optical ALV/High QE APD avalanche photodiode with pseudo-cross correlation, and a uniphase He/Ne laser (632.8 nm, Thorlabs Inc.). Details of the DLS analysis are described in **Appendix A.3**, Section 7. Results are presented in **Tables A.3. 2** and **A.3. 3** of the SI.

Equilibrium Swelling Experiments

Equilibrium volume swelling degrees Q_v were determined at room temperature. As-prepared co-networks (gel) were first placed in a large excess of the synthesis solvent for 48 h to remove the sol fraction.

Subsequently, the gels were separated from the swelling medium and weighted. After drying in a vacuum oven at 40 °C, the weight of the polymer (w_p) was determined, while the solvent weight in the swollen gel (w_s) is the weight loss of the sample during drying.

Q_v was determined as follows:

$$Q_v = 1 + \left(\frac{\rho_p}{\rho_s}\right)\left(\frac{w_s}{w_p}\right). \quad (3.3)$$

Here, ρ_s is the density of the used swelling solvent and ρ_p is the density of the polymers (1.13 g mL^{-1} as average for both PEG and PCL).[49] The procedure of swelling the samples to equilibrium followed by complete drying was repeated up to three times for all networks. As a result, equilibrium degrees of swelling (Q_{v1}, Q_{v2}, etc.) were measured, where the index counts the number of the swelling experiment.

Rheology

Rheological measurements were performed on an Anton Paar modular compact rheometer of type MCR 302 (Anton Paar, Graz, Austria) equipped with a plate–plate geometry of type PP25 with a plate diameter of 25 mm. A Peltier plate was used to control the temperature, and a solvent trap was used to prevent the evaporation of the solvent. Gels were prepared from homogenized equimolar mixtures of stock solutions of **3** and **5** in a mold fitting exactly the dimension of the probe geometry. The mixture was allowed to react overnight at room temperature. Frequency sweeps were carried out at a shear deformation of γ = 1% and in the range of ω = 1–100 rad s^{-1}. Storage moduli averaged over the full frequency range are shown in SI (**Appendix A.3**) Section 8 (**Table A.3. 4**).

High-Resolution Solution NMR Spectroscopy

^{1}H NMR spectra (500.13 MHz) were recorded on an Avance III 500 spectrometer (Bruker Biospin). $CDCl_3$ ($\delta(^1H)$ = 7.26 ppm) and THF-d_8 ($\delta(^1H)$ = 1.72 ppm) were used as the solvent, lock, and internal standard. The sample temperature was kept constant (30 ± 0.5) °C, unless otherwise specified, using a BVT-3000 unit.

The reaction kinetics of the co-network formation was followed by *in situ* ^{1}H NMR spectroscopy in THF-d_8 at ϕ = 0.06 and T = 25, 40, and 60 °C, respectively. For the measurements, stock solutions of **3** and **5** were prepared and combined with an equimolar ratio of reactive groups in a 5 mm NMR tube using a glass syringe and a precision balance. The tube was then sealed with a rubber septum, shaken sufficiently, and immediately placed in the preheated NMR probe. After reaching the reaction temperature within approximately 5 min, the measurements were started. Sixteen scans with an acquisition time of 1.93 s and a delay time of 10 s were

collected, resulting in a total experiment time of 191 s for each measurement. The normalized intensities of the signals at 9.5 ppm ($H_{7'}$ of **CN**) and 8.53 ppm (H_{10} of **3**) were used to calculate the conversion $p = I(H_{7'})/[I(H_{7'}) + 0.5\ I(H_{10})]$ of the crosslinking reaction. Inversion-recovery T_1 measurements on **3** and on a **CN** in THF-d_8 at 40 °C give T_1 values of 3.0 s for H_{10} and 3.4 s for $H_{7'}$. Thus, with an interval between the 90° ^{1}H pulses of ∼12 s, an equal and almost complete T_1 relaxation (97 vs 98%) of both protons occurs. Errors result mainly from the signal overlaps that occur at higher conversions since the network formation leads to significant line broadening.

High-Resolution (HR) MAS NMR Spectroscopy

The measurements were performed on an Avance III 500 NMR spectrometer with a Bruker HR MAS probe using a ZrO_2 rotor (4 mm outer diameter) with a PTFE insert (50 µL insert volume). For the measurements, the insert was filled with the dried co-networks (∼2 mg). After addition of $CDCl_3$ (∼50 µL) and a swelling time of 30 min, the spectra were recorded at 30 °C with a rotation frequency (ν_r) of 4650 Hz. Under these conditions, a minimal overlap of signals and spinning sidebands was observed. The conversion was determined from the integral intensities of a signal of the reacted benzoxazinone group ($H_{7'}$ of **CN**; 9.5 ppm) and of the nonreacted benzoxazinone group (H_{10} of **3**; 8.53 ppm) as described for the kinetics experiments.

MQ NMR Spectroscopy

Static proton solid-state NMR experiments for the quantification of connectivities and isotropic fraction are based upon the existence of motion-averaged residual dipolar couplings (RDCs) among the protons, which are nonzero for network chains that are fixed at their ends. At low overlap of the network strands (the entanglement-free limit), the magnitudes of the measured RDCs reflect roughly the elastic contribution of the respective chains and their connectivities (see **Scheme 3. 2**).[50, 51] Experiments were carried out on a Bruker mq20 MiniSpec with the specifications mentioned in the SI (**Appendix A.3**). The experiment provides two signal functions as a function of a double-quantum pulse sequence duration (DQ evolution time τ_{DQ}): the DQ intensity buildup (I_{DQ}) reflecting the magnitude of the RDCs and a reference intensity (I_{ref}). The sum of these two signals, referred to as summed multiple-quantum intensity ($I_{MQ} = I_{DQ} + I_{ref}$), corresponds to a full dipolar echo and is used to quantify and thus compensate for transverse relaxation effects (long-time signal loss). These data were evaluated similar to Lange et al.,[33] except for some relevant procedural differences that will be explained below.

Comparable data analysis was also applied on other tetra-arm star polymer systems.[52, 53] Typically, three types of connectivities can be distinguished differing sufficiently in their RDC as shown in **Scheme 3. 2** (SL, DL, and HOCs). This three-component fit was assumed to be a proper modeling choice for our system since the chemical and steric differences between PEG and PCL chains are small (see **Table A.3. 3**) and because all elastic strands contain a PCL and a PEG block that are under the same tension. Both types of macromonomers are dominated by trains of CH_2 groups, justifying the assumption that the measured RDCs of the different macromonomers are similar. Therefore, we will stick to the model of the three Abragam-like (A.-l.) functions representing one connectivity fraction each, as proposed in ref [54].

Further, the equality of the RDCs of PEG and PCL subchains was qualitatively confirmed in preliminary chemical shift resolved RDC measurements using the POST-C7 sequence.[55] Details will be reported elsewhere. As shown exemplarily in **Figure 3. 1a**, the proposed three-component fit well reproduces all features in both signals.

In contrast to Lange et al.,[33] we refrain from a global optimization algorithm and instead propose another simultaneous fitting procedure of I_{MQ} and I_{DQ} data. We decided to minimize the summed normalized root-mean-squared error (nRMSE) of both functions using a self-written MatLab 2018b script where the total RMSE was minimized using the MatLab fmincon algorithm for constrained, nonlinear optimization procedures. We follow a grid-search based procedure that replaces the global optimization procedure by Lange et al.[33]

The most relevant parameter, being the fraction of single links f_{SL}, is fixed, and the fit is carried out with one fixed parameter, automatically stabilizing the whole procedure. Afterward, the f_{SL} parameter is incremented by a small step Δf_{SL} (here $\Delta f_{SL} = 0.01 = 1\%$), and the fit is evaluated again. This is done over the whole range of expected a1-values (here: between 0.1 and 0.9). The total RMSE is plotted (see **Figure 3. 1b,c**), and the minimum is detected and is taken as the best-fit result. The stability of the fit was tested by using randomly determined starting parameters within a physically meaningful range. The presented error bars (confidence boundaries) were chosen such that the corresponding curves present suitable envelopes for the data up to a 30% increase of the nRMSE minimum value. Since the minimum is taken as the reference value, error bars for the presented data are not symmetric and represent the range of possible values. We stress that the error bars describe a possible *systematic* error (possible fitting bias, e.g., arising from the fact that a single A.-l. function may not be a perfect approximation to a signal fraction), which means that trends in the best-fit results for different samples are meaningful even if they are smaller than this systematic variation range.

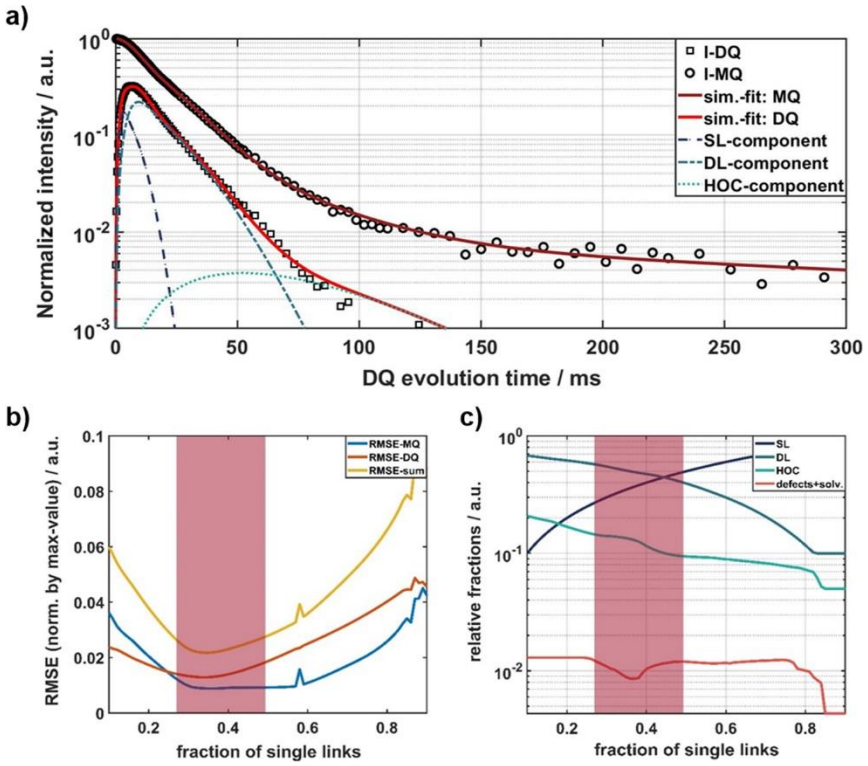

Figure 3. 1: (a) Exemplary fit of MQ NMR data of sample **CN6-3**, (b) RMSE minimum, and (c) dependence of relative connectivity fractions corresponding to the respective fixed SL fraction value.

Other sources of errors, e.g., rf-pulse miscalibration or ambiguities in the distinction of different connectivities, are not (or in the latter case only partially) included into the error bars. The fitting ambiguity between DL and HOC is circumvented by evaluating mostly the better defined single-link fraction and comparing it to the sum of other connectivities. Connectivity distributions of ACNs investigated are summarized in SI (**Appendix A.3**) Section 9 (**Table A.3. 5**).

Computer Simulations

Stoichiometric solutions of two different tetra-arm star polymers were equilibrated using a GPU-Version[56, 57] of the bond-fluctuation model.[58] The number of Kuhn segments per star arm in the simulations[59] was chosen to be roughly comparable with the experiments based upon literature data for the properties of Kuhn segments of PEG and PCL (see **Table A.3. 3**).[60, 61] After equilibration of the sample, reactivity of the end groups was turned on, and reactions were possible only upon collision of two different reactive groups mimicking the hetero-complementary coupling of the stars in the experiments; see ref [32] for more details. Reaction kinetics was followed for 10 independent samples at five different concentrations between approximately 1 and 4 times the overlap concentration of the star polymers (for more details,

see SI (**Appendix A.3**) Section 12). Gelation was detected by analyzing molecular weight distributions as described recently.[61] In a subsequent simulation, a series of gels prepared at a broader range of concentrations were swollen to equilibrium, and the equilibrium degree of swelling was determined from the average polymer volume fraction inside the swollen gel. More details on the simulations with a particular focus on equilibrium swelling properties and the residual bond orientations are available in ref [63].

3.7. Results and Discussion

Synthesis and Characterization of Tetra-arm Star Polymers 3 and 5 and Analysis of Their Interactions with Solvents

The hydrophobic tetra-PCL-based **3** was prepared as shown in **Scheme 3. 3a**. Starting from pentaerythritol, ε-CL was polymerized by ROP with $Sn(oct)_2$ as catalyst to give tetra-PCL-OH (**1**). The molar mass of **1** (10 kg mol^{-1}, ~2.5 kg mol^{-1} per arm) was adjusted by the molar ratio of pentaerythritol/ε-CL (1:87). As shown by NMR spectroscopy,[40, 45] the following esterification of the hydroxy terminal groups of **1** with compound **2** proceeded quantitatively. The NMR investigations also showed that **1** contained a small number of unreacted hydroxy groups on the pentaerythritol core (≤6% three-arm stars).[45] During esterification with **2**, these hydroxy groups are also converted, resulting in an average end group functionality of $f \geq 3.8$ (conversion $p \geq 95\%$) in tetra-PCL **3**.

The hydrophilic tetra-PEG-based **5** was synthesized using commercially available monodisperse tetra-PEG-OH with a molar mass of 10 kg mol^{-1}. After the removal of low molecular weight fractions, the terminal hydroxy groups of tetra-PEG-OH were reacted first with mesyl chloride to give **4** and then with ammonia to yield amino-terminated tetra-PEG **5** (see **Scheme 3. 3b**). Comparison of the ^{1}H NMR spectra of **1** and **3** as well as tetra-PEG-OH **4** and **5** showed that the respective end group modification occurred quantitatively. The molar masses of **3** and **5** (see **Table 3. 2**) were determined by ^{1}H NMR end group analysis (see **Figures A.3. 1 and A.3. 2**) and SEC. There is a very good correlation between the number-average molar masses determined by NMR spectroscopy and SEC.

Due to the large amount of material required for the network syntheses, three batches with similar molar masses were synthesized for the hydrophobic (**3a–c**) as well as for the hydrophilic component (**5a–c**). The deviations of the molar masses between the individual batches are small, indicating a very good reproducibility of the synthesis. In addition, all samples are

characterized by narrow molar mass distributions, which are an essential prerequisite for the synthesis of model networks. Due to the very good agreement of the molecular parameters of the individual batches, in the following, no explicit reference to the respective batches used for further characterization and network synthesis will be made.

To ensure the formation of homogeneous networks, a sufficiently high star polymer concentration in the reaction mixture and good polymer–solvent interactions are essential. In other words, poor solubility or even phase separation must be avoided. Key parameters in this context are the Flory–Huggins interaction parameters χ between the polymers and the solvents and the overlap concentration c^* of the star polymers in solution. The experimental data for χ in the literature (see **Table 3. 3**) are not really consistent and were measured mainly at temperatures around 100 °C outside of our temperature window for synthesis and analysis. If this is not the case like in ref [64], the data were computed from swelling measurements and thus may contain a dependence on the model for elasticity and swelling.

Theoretical estimates for the interaction parameter can be made using the Hildebrand–Scott solubility parameter,[65] the Hansen method for the solubility parameters,[66,67] or the Tian–Munk model,[68] whereby the latter is the most general approach, allowing also for negative interaction parameters as measured for chloroform. In SI (**Appendix A.3**) Section 10, we have compiled the original data regarding the corresponding solubility parameters, and we provide a brief description how the interaction parameters were computed. The results of these computations are summarized in **Table 3. 3**.

When comparing with our viscosity data for dilute solutions of compounds **3** and **5** at different temperatures and in different solvents (see **Figure 3. 2a**), only the Tian–Munk interaction parameter χ_{TM} (see **Table 3. 3**) allows us to put all measured overlap concentrations of a given polymer in the correct order. Moreover, χ_{TM} shows the best agreement with the published experimental data when assuming better solubility at elevated temperatures, as indicated by the viscosity data. Therefore, we use χ_{TM} as the starting point to develop below an improved estimate χ_{η} that reproduces accurately the ratio of the measured intrinsic viscosities of both compounds, allowing for a quantitative comparison of data measured in different solvents.

Table 3. 3: Flory–Huggins interaction parameter χ of PEG and PCL in different solvents.

χ[a]	Toluene	THF	Chloroform	Reference
χ PEG	0.26 (100 °C)	0.30 (100 °C)	-0.55 (100 °C)	67
χ PEG[b]	0.54 - 0.47 (85 - 105 °C)	-	-1.00 to -0.86 (85 - 105 °C)	68
χ PEG	-	0.38	-	62
χ_η PEG[c]	0.38	0.41	-1.61	this work
χ_{HS} PEG[d]	0.57	0.45	0.43	this work (SI)
$\chi_{\alpha=0.6}$ PEG[d]	0.56	0.14	0.25	this work (SI)
χ_{TM} PEG[d]	0.30	0.38	-1.04	this work (SI)
χ PCL	0.08 (100 °C)	0.13 (100 °C)	-0.40 to -0.22 (100 - 120 °C)	67
χ PCL	-0.01 - 0.07 (70 - 140 °C)	-	-	69
χ_η PCL[c]	-0.05	0.07	-0.54	this work
χ_{HS} PCL[d]	0.53	0.42	0.41	this work (SI)
$\chi_{\alpha=0.6}$ PCL[d]	0.41	0.16	0.12	this work (SI)
χ_{TM} PCl[d]	0.09	0.18	-0.71	this work (SI)

[a] Data refer to 25 °C if no explicit temperature is noted.

[b] For M_n = 10 kg mol^{-1}.

[c] Based on viscosity data.

[d] Computed in this work using the Hildebrand–Scott approach[65,69] (χ_{HS}), the Tian–Munk model[68] (χ_{TM}), or the Hansen approach[66,67] for α = 0.6 ($\chi_{\alpha=0.6}$) as described in the SI (**Appendix A.3**).

As all solvents are good solvents according to χ_{TM}, we start with computing the square radius of gyration, R_g^2, of the star polymers in the particular good solvent:

$$R_g^2 \approx b^2(1-2\chi_{TM})^{2\nu-1}\frac{1}{(2\nu+1)(2\nu+2)}\left(3-\frac{2}{f}\right)\left(\frac{N}{f}\right)^{2\nu} \quad (3.4)$$

This equation combines relations for the size of linear chains in good solvents[5, 72] with the dependence of R_g^2 on the number of star arms, *f*. Above, ν = 0.5876 is the Flory exponent,[73] while the Kuhn length *b* and the number of Kuhn segments per star polymer, *N*, are

given in **Table A.3. 3**. In this table, we compiled literature data for geometric parameters of the polymer, from which *b* and *N* were computed.

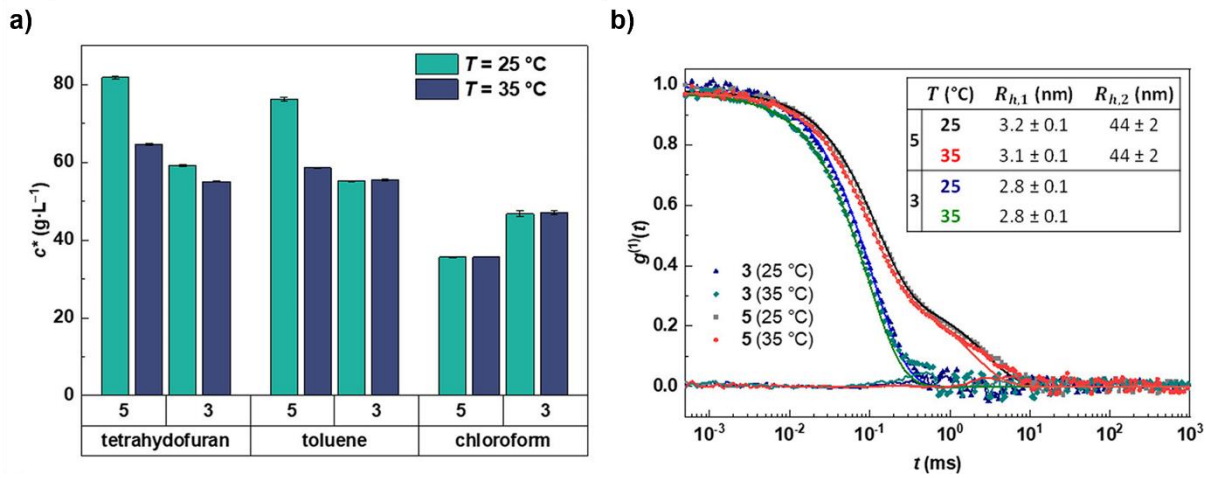

Figure 3. 2: (a) Overlap concentrations *c** of star polymers **3** and **5** determined by viscometry in tetrahydrofuran, toluene, and chloroform at 25 and 35 °C. (b) Hydrodynamic radii R_h and DLS autocorrelation functions (rectangles) with respective fit (solid lines) and corresponding residual fluctuations around zero for THF solutions (c = 30 g L^{-1}) of PEG star polymer **5** at 25 (brown) and 35 °C (red) and PCL star polymer **3** at 25 (blue) and 35 °C (green) measured at a scattering angle of 30°. Corresponding fit parameters are summarized in **Table A.3. 1**.

Numerical results[74] for the ratio between the radius of gyration and the hydrodynamic radius R_h of self-avoiding walks are close to 1.58. A numerical test in the dilute regime using our simulation model for star polymers with a number of Kuhn segments comparable to the experiments provides 1.57. Experimental data lead to a ratio R_g/R_h that is typically smaller by 10–20% as compared to these numerical data,[47] mainly due to the assumptions made for computing R_h. Therefore, we use $R_g/R_h \approx 1.35 \pm 0.08$ to estimate R_h. These results are combined with the viscosity data to compute the ratio

$$z = \frac{M_w[\eta]}{N_A R_h R_g^2} \tag{3.5}$$

Here, N_A is Avogadro's constant. For linear chains, $z \approx 7$ is a constant in good solvent.[5] The corresponding z of star polymers is not known but can be expected to be larger since the increased compactness of the molecules overcompensates the poorer draining of the solvent and the shift of the universal constant for viscosity with increasing f. [75, 76] We have computed z for all combinations between the polymers and the solvents of our study and obtained $z = 9.1 \pm 0.6$ when using χ_{TM}. Repeating this analysis with other estimates for the interaction

parameter produces a significantly larger scatter for *z*, supporting our observation that χ_{TM} fits best to the experimental data.

Assuming that *z* is a constant for a fixed $f = 4$ and not only for the linear case $f = 2$, we invert the above computation starting from $z = 9.1$ and convert the viscosity data into experimentally based estimates for the interaction parameter χ_η. These estimates are also listed in **Table 3. 3** and have a high correlation with the experimental data for χ. The above procedure minimizes errors for individual interaction parameters but cannot remove all errors on an absolute scale. The main benefit of the above approach is that χ_η is correct on a relative scale (within the error of the viscosity measurements) such that we can compare experimental data for different solvents with high accuracy.

A quantitative test of the above computations is possible with dynamic light scattering (DLS) since the hydrodynamic radius can be measured by this method. The DLS correlation functions of **3** and **5** in THF at 25 and 35 °C are depicted in **Figure 3. 2b**. The data of **5** show two distinct relaxation modes, indicating the formation of aggregates. This was accounted for by considering two independent decays for the data analysis; see SI (**Appendix A.3**) Section 7 for a detailed description. The key result of this analysis is the hydrodynamic radius of both compounds (the data of **5** also contain an estimate for the cluster size) that is provided in the inset of **Figure 3. 2b**. Using χ_η and the computation of R_g and R_h above provides $R_h = 2.8 \pm 0.2$ nm for compound **3** in perfect agreement with the DLS data. The same computation for compound **5** leads to a significantly smaller $R_h = 2.4 \pm 0.2$ nm, reproducing the trend of the viscosity measurements, while the DLS data refer to an enlarged estimate for R_h. Apparently, the dynamics of individual stars interferes here with the dynamics of the clusters. However, the physical origin for the clustering is not clear and might be related to the differences in the oxygens between both polymers, which seem to be essential for the significant difference in the interaction parameter.

Altogether, the agreement for compound **3** strongly supports our analysis, suggesting that there are no large collective shifts to be expected on an absolute scale for our set of interaction parameters. Furthermore, a concentration of 70 g L^{-1} is sufficient for all three solvents to ensure overlap of the star polymers. Therefore, this concentration is generally used as a benchmark for networks prepared at or above the overlap concentration c^*.

Synthesis, Kinetics, and Gelation of Amphiphilic Co-networks $CN_{25,\ 40,\ 60}$

To investigate the gelation kinetics of the crosslinking reaction between **3** and **5** according to **Scheme 3. 4**, time-dependent *in situ* ^{1}H NMR measurements of the reacting mixtures were carried out at 25, 40, and 60 °C in THF-d_8 at a concentration of 70 g L^{-1}. In the following, these networks will be referred to as **CN_{25}**, **CN_{40}**, and **CN_{60}**. For each measurement, corresponding volume fractions of two stock solutions of the star polymers **3** and **5** were poured into an NMR tube and brought to the desired reaction temperature within ~5 min. The reaction was equimolar with respect to the reacting terminal groups. Selected spectra recorded during the reaction at 40 °C are shown in **Figure 3. 3a**. For clarity, only the region of aromatic protons is shown. The intensities of the signals at 9.5 ppm ($H_{7'}$ of **CN**) and at 8.54 ppm (H_{10} of **3**) were used to calculate the conversion p of the crosslinking reaction (see also **Figure A.3. 3**). The signal assignment is based on the spectra of the corresponding star block copolymers, as described separately.[45]

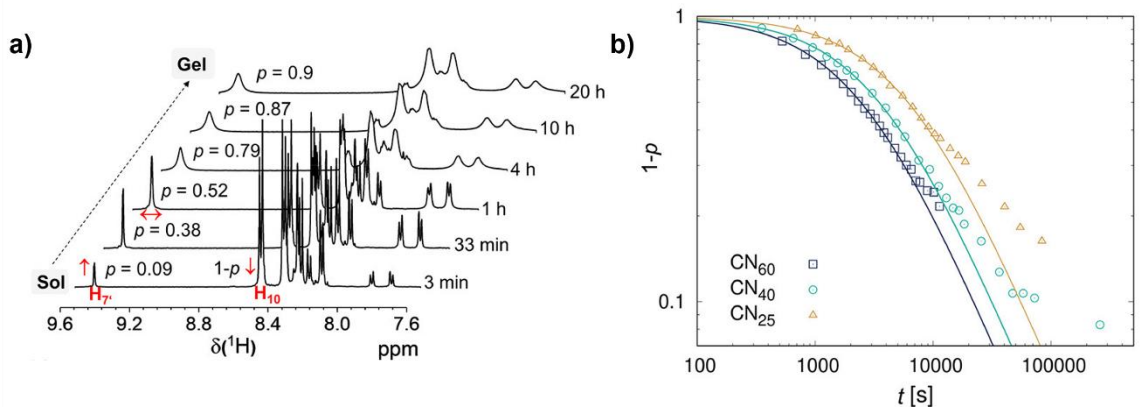

Figure 3. 3: NMR spectroscopic monitoring of the crosslinking reaction between **3** and **5** in THF-d_8 at a concentration of 70 g L^{-1} (~ c*): (**a**) time-dependent ^{1}H NMR spectra (region of aromatic protons) recorded during the network formation of **CN_{40}** at 40 °C and (**b**) (1 – p)–time curves calculated from the signal intensities of $H_{7'}$ and H_{10} at three different temperatures (**$CN_{25,\ 40,\ 60}$**).

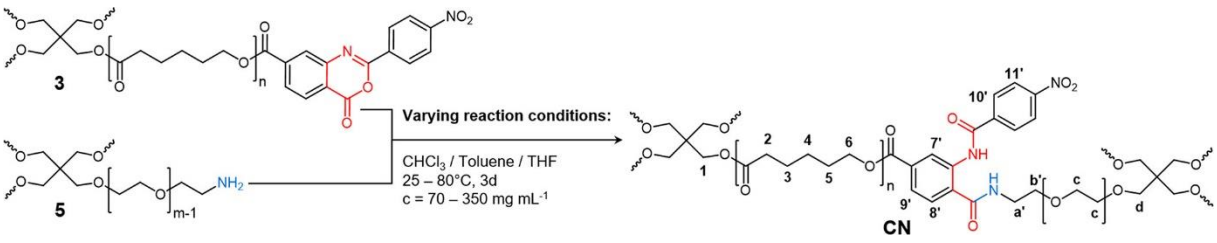

Scheme 3. 4: Synthesis of amphiphilic co-networks (**CN**).

In **Figure 3. 3a**, the $H_{7'}$ signal of the formed benzamide group appears already after 3 min, indicating that the reaction begins immediately after the solutions are poured together. However, the reaction is of intermediate rate and could be well followed up to the conversion of $p \sim 0.9$ for **CN40** and $p \sim 0.8$ for **CN25** and **CN60**. Continuing the reaction outside the spectrometer reveals that complete conversion could not be achieved under the given reaction conditions even after a total reaction time of 3 days. The respective conversion–time curves for **CN25, 40, 60** are shown in **Figure 3. 3b**.

For a more detailed analysis of kinetics, we consider that the reactive groups are stoichiometrically balanced, $[3]_0 = [5]_0$. In this case, kinetics can be written as

$$\frac{d[3]}{dt} = -k[3][5] = -k[3]^2 \tag{3.6}$$

with the solution

$$\frac{[3]}{[3]_0} = \frac{1}{1 + k[3]_0 t} = 1 - p. \tag{3.7}$$

Here, t is the reaction time, k the reaction constant, and [3] and [5] are the concentrations of the two reactive groups of the star polymers **3** and **5** at time t. p is the conversion of the reactive groups, and $[3]_0$ is the initial concentration of the reactive groups.

A simple evaluation of an assumed second-order reaction with equimolar reactants **3** and **5** is possible with the plot of 1/[3] vs t. The plots show a very good linear dependence up to conversions of ~60% (see **Figure A.3. 5**), confirming that the reaction of the terminal groups of **3** and **5** follows over a wide range the kinetics of a second-order reaction (see **Table 3. 4**). In a second approach, the data on the reaction kinetics were analyzed in two steps. First, the low time limit of the ratio of the concentrations $[3]/[3]_0$ of the reactive groups was fit to a modified form of **Equation 3.7** in the form of

$$\frac{[3]}{[3]_0} = 1 - p = \frac{1}{1 + k[3]_0(t + t_0)} \tag{8}$$

for the low t data with $p < 0.4$ to determine an effective time offset t_0. This offset accounts for sample handling and temperature equilibration in the NMR spectrometer in the initial period. For the three graphs in **Figure 3. 3b**, we have shifted each data set along the time axis by the corresponding t_0 and plotted against **Equation 3.7**. Up to $p \sim 0.6$, the reactions closely follow the predicted ideal reaction kinetics.

Using the obtained *k* values at temperatures of 25, 40, and 60 °C from **Table 3. 4**, the Arrhenius activation energy E_a of 21.8 ± 0.9 kJ mol^{-1} was determined. The corresponding ln *k* vs 1/*T* plot and the associated calculation of E_a are shown in SI (**Appendix A.3**) in Section 11 (**Figure A.3. 6**). A significant slowdown of kinetics is visible at higher conversions. This observation is equivalent to the behavior of the simulation data shown in SI (**Appendix A.3**) Section 12. Such a slowdown in a recombination reaction of two species at stoichiometric conditions is a signature of composition fluctuations.[77, 78] These become stationary after gelation as the star polymers are rapidly incorporated into the gel (see **Figure A.3. 7**). Therefore, the slowdown also is a measure of the quality of the mixture. The onset of this process occurs at almost the same conversion as in the perfect mixtures of the simulations, indicating near-perfect mixing conditions in the experiment. Regarding the NMR spectra in **Figure 3. 3a**, it is noticeable that the signal widths increase significantly with increasing crosslinking. This is caused by the reduced mobility of the segments in the network.

Table 3. 4: Reaction kinetics and gel point determination by *In Situ* NMR spectroscopy.

T (°C)	$[3]_0$, $[5]_0$ [a] (10^{-2} mol L^{-1})	k [b] (L mol^{-1} s^{-1})	t_c [c] (min)	p_c [d]	Δp [e]
25	1.22	0.013 (0.013)	73	0.42	0.09
40	1.22	0.024 (0.023)	46	0.44	0.11
60	1.22	0.034 (0.032)	31	0.43	0.10

[a] Concentration of the reactive groups; corresponds to an overall concentration of star polymers of 70 g L^{-1}.
[b] Reaction constant; values in brackets are based on the plot shown in **Figure A.3. 5**.
[c] Gelation time.
[d] Conversion at gel point.
[e] Delay of the gel point conversion according to eq 3.10.

For gel point determination, the time change of the line width at half height ($w_{1/2}$) of the signal $H_{7'}$ was determined and converted to the effective transverse relaxation time T_2^* (see **Figure 3. 4**). The time axis was also corrected here by t_0. Gelation can be traced by a sudden drop in T_2^* from a nearly constant level prior to gelation.[79]

Subsequently, the resulting gelation times t_c in **Table 3. 4** were determined from the intersection of the horizontal lines with linear fits to the steepest descents of the data shown in **Figure 3. 4** (note the logarithmic time axis).

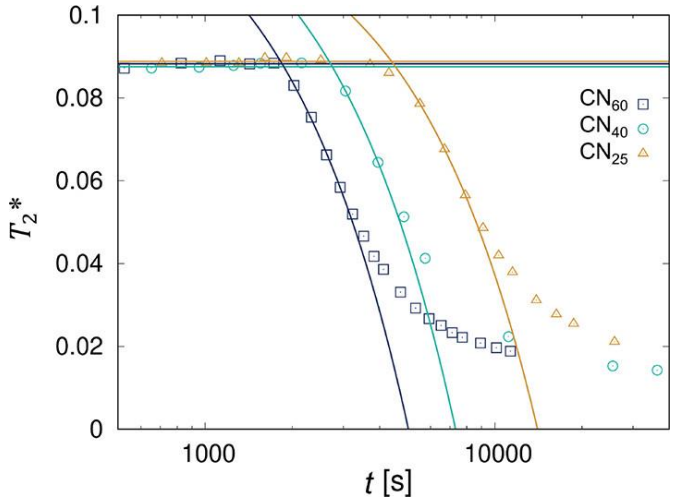

Figure 3. 4: NMR gel point analysis of the sol–gel transition during the **CN** network formation. T_2* relaxation time was determined from the linewidth at half height, $w_{1/2}$ (Hz), of signal $H_{7'}$ according $T_2^* = 1/\pi w_{1/2}$.

The gelation times refer to conversions at the gel point p_c according to

$$p_c = \frac{k[3]_0 t_c}{1 + k[3]_0 t_c} \tag{3.9}$$

The delay of the gel point conversion is thus computed from

$$\Delta p = p_c - p_{c,id} = \frac{k[3]_0 t_c}{1 + k[3]_0 t_c} - \frac{1}{f - 1} \tag{3.10}$$

where $p_{c,\,id}$ is the conversion at the ideal gel point for functionality $f = 4$. All results of this analysis are summarized in **Table 3. 4**. For comparison, the gel point of the simulations at c^* is located at a conversion of $p = 0.44 \pm 0.01$, which agrees within error with the experiments at all temperatures. This agreement shows that experiments and simulations were conducted at roughly the same overlap number of the star polymers since the delay of the gel point is a universal function of the junction functionality and the overlap of the network strands.[62]

Characterization of Amphiphilic Co-Networks

A series of ACNs were synthesized by equimolar conversion of star polymers **3** and **5** (see sample overview in **Table 3. 1**). For the synthesis, corresponding aliquots of the stock solutions of **3** and **5** were poured together. The solvent, temperature, and polymer concentration were varied. After completion of the crosslinking reaction (~3 days), equilibrium volume swelling degrees Q_v of the co-networks were determined gravimetrically (see **Figure 3. 5**). Swelling experiments were repeated three to four times for each sample (Q_{v1}, Q_{v2}, etc.), where all swelling experiments were followed by a period of complete drying of the samples prior to the next swelling experiment.

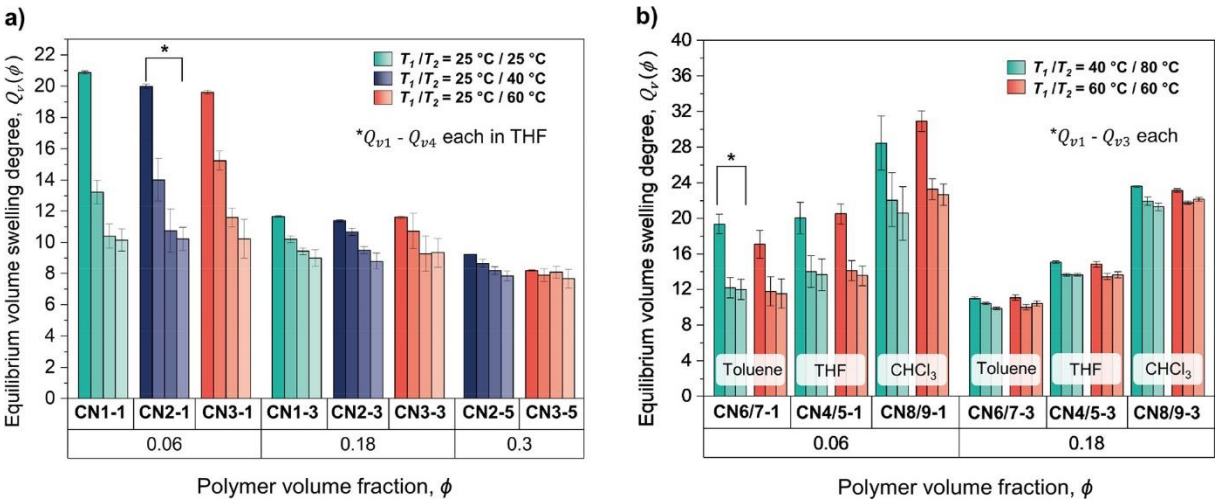

Figure 3. 5: Equilibrium volume swelling degrees Q_v of ACNs synthesized under different reaction conditions (T, ϕ_0, and solvent) and swollen with the same solvent. The columns for a given sample correspond to three to four consecutive swelling–drying cycles (Q_{v1}–Q_{v4}) from left to right, where the swelling starts from the preparation state. Different colors represent varying synthesis temperatures (T_1 = pre-gel point, T_2 = post-gel point). (**a**) Co-networks synthesized in THF and (**b**) co-networks synthesized in toluene-d_8, THF-d_8, and $CDCl_3$, respectively.

Figure 3. 5a shows equilibrium swelling degrees Q_v of samples synthesized in THF, while deuterated solvents (toluene-d_8, THF-d_8, $CDCl_3$) were used for the syntheses of the samples in **Figure 3. 5b**. The use of deuterated solvents enabled additional MQ-NMR studies on the gels obtained. However, we have to keep in mind that, in some cases, deuterated solvents may develop interactions significantly different from the protonated counterpart.[80] For the swelling experiments, the corresponding nondeuterated solvents were used. Both diagrams show that swelling from the preparation state (Q_{v1}) without intermediate drying delivers the highest swelling ratios. The reason for this is related to the slowdown of the reaction kinetics discussed in the preceding section: random diffusion of both compounds leads to a spontaneous formation and decay of local composition fluctuations during the concourse of the reactions. When most

of the star polymers are attached to the gel, these composition fluctuations become static and turn into a distribution of local domains with varying stoichiometric imbalance. The kinetics in these domains comes to a stop once reactive groups of the minority component are consumed, driving a continuous slowdown of the reaction.

The subsequent equilibrium swelling of the samples after crosslinking reduces the overlap between the molecules preventing complete reactions; drying causes the opposite effect: the overlap number of the star polymers grows[5] $\propto\phi^{1/(6\nu-2)}$, bringing previously separated end groups of star polymers in contact allowing for additional reactions. In other words, the evaporation of the solvent increases the polymer concentration and thus the concentration of reacting groups, resulting in higher conversions after drying. This effect is particularly pronounced for samples synthesized at low polymer concentration ($\phi_0 = 0.06$) since the low ϕ_0 at preparation causes a slower kinetics and a lower maximum *p*, which is most increased by post-reaction due to a larger change in the overlap number upon drying compared to $\phi_0 = 0.18$ and $\phi_0 = 0.30$. The decreasing swelling degrees Q_v with repeated measurements also show that the linkages formed during the reaction are stable under the given conditions. Otherwise, an increase in the Q_v values would be expected.

Apparently, the composition fluctuations of the co-networks of **Figure 3. 5a** exceed the stochastic composition fluctuations of the perfectly mixed co-networks in the simulations even though kinetics did not indicate a large discrepancy. This can be judged from the comparatively large sol fractions (see **Table 3. 1**) in the experiments; see **Figure A.3. 7** in the SI for data around *c** and ref [27] for simulation data at different concentrations (note the different definition of *c**). The reason for this difference is not clear at the moment and will be explored by additional computer simulations.

The swelling experiments also show that the synthesis temperature and thus reaction kinetics have no significant influence on the network properties. Regarding the influence of the solvents (see **Figure 3. 5b**), it is noticeable that synthesis and swelling in chloroform result in distinctly larger Q_v values. *A priori*, it is not clear whether this results from a different solvent quality or from differences in the network structure. However, this point can be clarified by plotting all Q_{v1} data and swelling data of the simulations in a universal plot where solvent quality and differences in *N* cancel out; see **Figure 3. 6**.

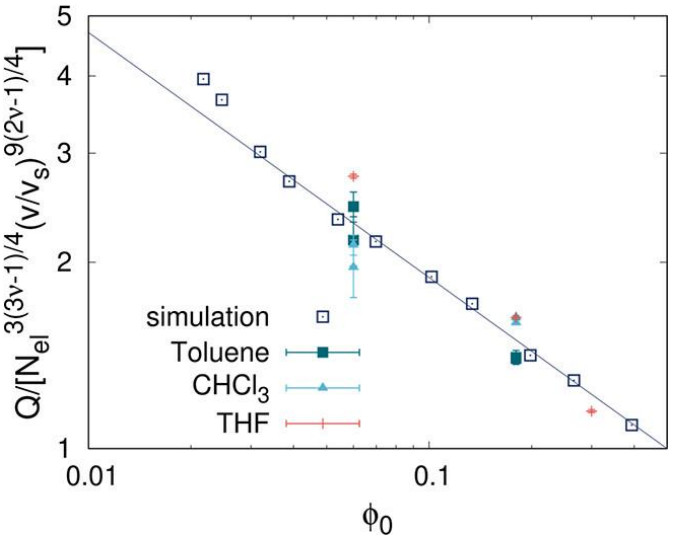

Figure 3. 6: Equilibrium degree of swelling (first swelling) in the experiment and the simulations. The line is a power law fit to $\phi_0^{-0.40 \pm 0.01}$ to the simulation data for $\phi_0 > 0.03$. Multiple experimental data points at the same ϕ_0 refer to different temperature programs. The statistical error of the simulation data is comparable to the symbol size.

This universal plot is obtained as follows. For the experimental data, we convert χ_η into an estimate for the excluded volume

$$\mathrm{v} = \left(1 - 2\chi_\eta\right)\mathrm{v}_s \tag{3.11}$$

where v_s is the unit volume of the Flory–Huggins lattice that is set by the solvent molecules. In our co-networks, roughly half of the polymer is PEG and the other half PCL. Thus, we expect a sample average interaction parameter in a common nonselective solvent that is roughly the average of the corresponding χ_η estimates. This leads to a v/v_s of 0.67, 0.52, and 3.15 for toluene, THF, and chloroform, respectively. A crossover between the semi-dilute good-solvent regime and the concentrated regime is expected around $\phi^{**} \approx v/v_s$.[5] Since all networks were prepared and swell below ϕ^{**}, all experiments refer to swelling in the good-solvent regime for both polymer components.

In the simulations, the excluded volume per monomer can be counted directly.[81] Exactly eight lattice sites are blocked per monomer for the implicit solvent that fills the rest of the lattice leading to an excluded volume parameter for chain swelling of $8/b^3$ where $b \approx 2.73$, while at low concentrations, N refers to the number of independent segments of the self-avoiding walk. This provides $v/v_s \approx 0.39$ for the simulation data that all refer to swelling in the good-solvent limit.

For swelling in the good-solvent regime, scaling models[5, 82] predict the entanglement-free limit:

$$Q \approx N^{3(3\upsilon-1)/4}\phi_0^{-1/4}(\mathrm{v}/\mathrm{v_s})^{9(2\upsilon-1)/4} \tag{3.12}$$

leading directly to the universal plot in **Figure 3. 6**. Flory-type mean-field models[83, 84] arrive at nearly the same scaling as a function of *N* but with a different scaling as a function of ϕ_0:

$$Q \propto N^{3/5}\phi_0^{-2/5}. \tag{3.13}$$

The data in **Figure 3. 6** roughly collapse on a single line, supporting our analysis of the interaction parameters. Note that we have enforced a conversion of exactly $p = 0.95$ in the simulations that serves as a benchmark for the experimental systems. Accordingly, the experimental data are not far from conversions around $p \approx 0.95$. We further conclude that the large swelling in $CHCl_3$ results from the solvent quality and not from a lower conversion.

The exponent for ϕ_0 in **Figure 3. 6** is in remarkable agreement with the mean field model prediction; however, this point has to be considered with care. It is expected that entanglements cause a stronger concentration dependence of the equilibrium degree of swelling as can be judged from swelling data on Olympic gels[85] $\propto\phi_0^{-0.72}$ and theoretical predictions up to $\propto\phi_0^{-1}$.[81] Network defects have a strong impact on the scaling of equilibrium swelling data.[83, 86] In particular, preparation of model networks at low ϕ_0 enhances the formation of network defects leading to a stronger dependence on ϕ_0. Such nonidealities are minimized by our network architecture. Nevertheless, we observe a somewhat stronger effective power law dependence of modulus on ϕ_0 as expected theoretically; see below. This leads in effect to a stronger dependence of Q on ϕ_0 as predicted by the scaling model assuming an ideal network structure. Exponents of −0.71 and −0.75 were reported[87] for model PDMS networks made of strands below the entanglement molecular weight or an exponent of −0.4 for gelatin gels.[88] For the data of Gnanou et al.[89] excluding the networks with a sol fraction beyond 10% (see Tables 30 and 31 in ref [4]), one obtains exponents of −0.52 and −0.92 for the short and the long polymers, respectively. A simulation study reported exponents increasing from −0.25 to −0.55 with increasing length of still quite short chains.[90] In contrast to this, we found only a very weak increase of the exponent for increasing *N*.[63] Altogether, the dependence on ϕ_0 has not been settled yet, but this open question could be advanced by using network architectures as ours that are less susceptible to network defects.

For the networks synthesized in THF (**CN1–1** to **CN3–5**), the degree of conversion *p* was determined by ^{1}H NMR end group analysis of spectra obtained by HR MAS NMR spectroscopy. This technique provides well-resolved NMR spectra for swollen **CN** samples (see **Figure A.3. 4**). For the measurements, the as-prepared gels were dried and re-swollen in $CDCl_3$ directly in the rotor insert. The state of the networks during these measurements is comparable to that during the second swelling experiment (Q_{v2}). It should be mentioned here that, for preparation-related reasons, measurement of the co-networks directly after synthesis has not yet been possible for the determination of conversion *p*. The calculation of *p* followed the procedure reported for the kinetics experiments and gave conversions $p \geq 0.98$ (see **Table 3. 1**) for the investigated co-networks, with the exception of **CN2–5** (probably due to insufficient mixing before gelation). These measurements confirm that after the removal of the sol fraction by Q_{v1} and subsequent evaporation of the synthesis solvent, virtually all benzoxazinone groups were converted to benzamide groups.

Oscillatory shear rheology was used to investigate the viscoelastic behavior of the co-networks synthesized overnight at concentrations ranging from *c** to 5*c** in a mold at room temperature. The data of all measurements are summarized in **Table A.3. 4**. **Figure 3. 7** shows the typical rheological frequency sweep of a permanently crosslinked polymer gel with an elastic plateau of the storage modulus $G'(\omega)$ that dominates over the loss modulus $G''(\omega)$ for all concentrations. The loss modulus G'' is more than 2 orders of magnitude smaller and develops a weak frequency dependence at low frequencies and concentrations, indicating minor contact problems like a marginal slip of the sample inside the rheometer. The onset of the relaxation of network defects is visible at larger concentrations and frequencies.

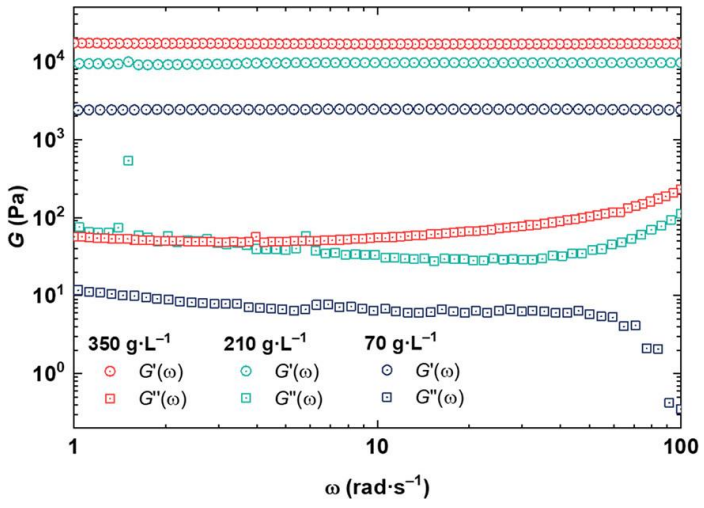

Figure 3. 7: Oscillatory shear-rheology of amphiphilic polymer gels based on star polymers **3** and **5** gelated in a mold at *c** (70 g L^{-1}, blue), 3*c** (210 g L^{-1}, green), and 5*c** (350 g L^{-1}, red) in toluene at preparation conditions.

For a quantitative test of our data, we consider that PEG and PCL stars have molar masses of 10.7 and 11.8 kg mol^{-1}, respectively, and the average density of the polymers[49] in the dry networks is around 1.13 g mL^{-1}. Two stars of this type in a co-network produce four network strands if all reactive groups are connected, leading to a molar mass around $M_{el} \approx 5.6$ kg mol^{-1} per network strand. The entanglement molar mass M_e in melts of PEG is around[68, 91] 2 kg mol^{-1} and does not exceed 3 kg mol^{-1} for PCL melts.[92, 93] The plateau modulus of entangled melts[94, 95] is $\propto \phi_0^{7/3}$, and there is $\phi_0 \leq 1/3$ for all of our samples. Thus, the about two to three entanglements per network strand in melts reduce to an entanglement contribution to modulus of the order of $kT/4$ per network strand for the largest ϕ_0, so that they become negligible for $\phi_0 \approx \phi^*$. Therefore, we use the phantom model prediction:[5]

$$G_{ph} \approx \phi_0 \left(1 - \frac{2}{f}\right) \frac{\rho RT}{M_{el}} \tag{3.14}$$

leading to $G_{ph}/\phi_0 \approx 252$ kPa for a quick quantitative test of the rheology data. A power law fit of the rheology data of **Table A.3. 4** in the SI is in accord with $G_{ph} \approx \phi_0^{1.22 \pm 0.05} \cdot 64$ kPa, with an extrapolated amplitude at $\phi_0 = 1$ almost a factor of 4 below the expectations. The exponent for ϕ_0 is somewhat larger than unity similar to a related work,[96] indicating corrections due to entanglements for the largest ϕ_0 and a growing impact of a decreasing conversion and formation of finite loops[51, 97] toward small ϕ_0. Rheology during gelation indicates qualitatively that kinetics might be somewhat slower in toluene than in THF (a quantitative discussion of these results is omitted here due to the solvent evaporation observed in these measurements). Nevertheless, we expect a conversion of at least 0.8 for our samples when reacted overnight, which suffices to explain a drop in modulus only up to 40%. Moreover, for our particular network architecture, the small corrections due to finite loops above the overlap threshold are too small to close the gap to the measurements. In a closely related work,[8] amphiphilic co-networks were synthesized using the same molecular architecture, similar molar masses of the star polymers, and a similar range of ϕ_0 with a quicker kinetics than in our study. The modulus in this study remains about a factor of 3 below the phantom estimate, which is not much different from our observations. The origin for this discrepancy is not understood at the moment.

One of the main concerns of this work was to find out how the reaction conditions affect the microstructure and homogeneity of the ACNs. Using the MQ experiment described in the *Experimental Section*, we analyzed samples synthesized under different conditions (**CN1-1** to **CN9-3**) in terms of their connectivities (see **Scheme 3. 2**), isotropic (defect) frac-

tions, and related average RDCs. We refrain from discussing the results of the sample series **CN1** to **CN3** in detail, which were dried after gelation and were subject to post-curing (see **Figure 3. 5**). However, the connectivities of these samples are summarized in the SI (see **Table A.3. 5**).

First, we investigated differences between networks synthesized by our method (**PEG-2** and **CN5-3**) with networks synthesized according to Sakai et al.[25] (**PEG-1**). In addition to the different linkage mechanisms, it should be noted that the synthesis according to our method was carried out in the less polar solvent (toluene-d_8 versus D_2O). The polymer concentrations during the syntheses were comparable (~3c*, with neglectable small variations; see **Table 3. 1**), but our oxazinone terminated tetra-stars are not compatible with water-based gel synthesis, precluding the corresponding control experiment.

In **Figure 3. 8**, it can be seen that the SL fraction of the gels synthesized by our method (**PEG-2** and also **CN5-3**) is significantly lower (13–19%) than for of the gel synthesized according to Sakai (**PEG-1**). This in fact applies to all co-networks mentioned in this work (see **Table A.3. 5**). In comparison to earlier studies on Sakai's tetra-PEG networks, this deviation is even more pronounced.[33] There, the SL fraction (> 60%) is close to the value expected for a randomly linked network. The dominance of the double links over the single links in our networks is surprising. Possible reasons for this are discussed below. Interestingly, we also find considerably lower HOC fractions and larger RDC values in our gels, which cannot be explained yet. It is assumed that the deviations may arise from the different linking chemistry or from the overall PEG star conformation in the different less polar solvents used for the syntheses.

For further investigation on factors influencing the microstructure of our amphiphilic PEG–PCL co-networks, sample series with different parameter variations (see **Table 3. 1**) were synthesized for checking the influence of (i) the network composition (PEG–PCL co-network vs PEG–PEG network with benzoxazinone/amino end groups), (ii) the solvent, and (iii) the temperature programs during synthesis. Aspect (i) is also addressed in **Figure 3. 8**, whereas **Figure 3. 9** shows the rest of the results.

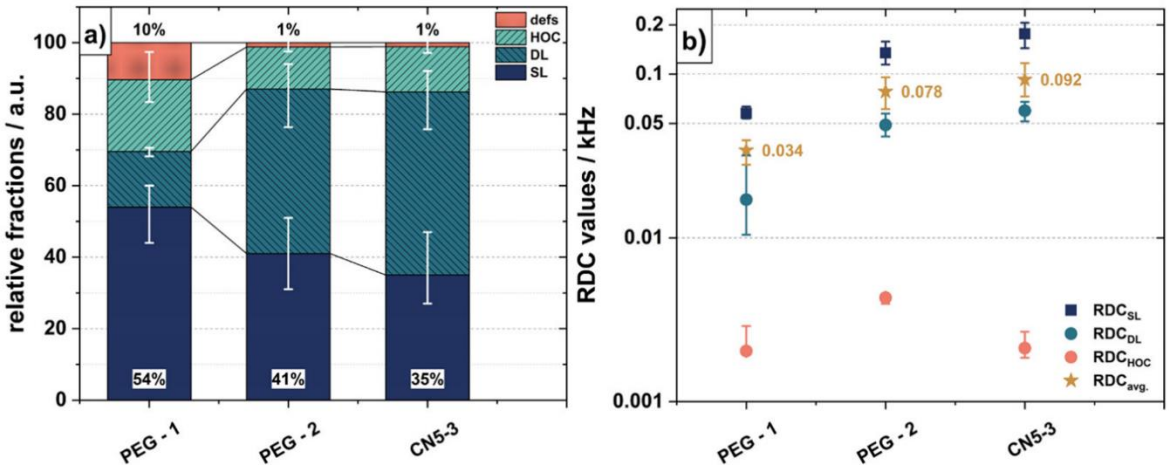

Figure 3. 8: (**a**) Comparison of different connectivity fractions obtained for different networks. **PEG-1** was synthesized in water according to Sakai et al., [25] whereas **PEG-2** and **CN5-3** were synthesized in toluene according to our method. Note that the significant increase in the apparent defect fraction for the Sakai network arises mainly from HDO, which arises from moisture-related water uptake. (**b**) Corresponding RDC values and the fraction-weighted average RDC of the presented samples and connectivity fractions.

(i) The most fundamental difference between our networks and a PEG–PEG gel is the fact that we have stars made of different polymers. The interaction parameters in **Table 3. 3** show that no miscibility problems should arise related to the polymers. Moreover, for **PEG-2**, synthesized by the oxazinone coupling reaction referred to above, the same qualitative trend of a decreased SL fraction (in comparison to the data by Lange et al.[33] was found (see **Figure 3. 8**), ruling out the polymers as the source of this discrepancy. Still, we find a slight quantitative increase in the estimated fraction of single links from 35 to 41% on going from ACN to the homo-PEG gel, although the actual polymer fraction upon synthesis was even slightly lower for the latter. We want to remind here that although this trend is within the shown error bars, the error bars are to be seen as systematic deviations arising from a slight unambiguity in the used fit function, meaning that if the upper boundary is chosen for the PEG–PCL network, it also has to be chosen for the PEG–PEG network (see *Experimental Section* and **Figure 3. 1**).

(ii) To investigate the solvent influence on the connectivities, three solvents with different polarity were used in the synthesis (THF-d_8, toluene-d_8, and $CDCl_3$). Unexpectedly, no significant difference between all three solvents either in the overall connectivity distribution or in the RDC values was found (see **Figure 3. 9**). Regardless of the choice of solvent, the SL fraction is well below the expectations. This indicates that the biased connectivity distribution cannot be attributed to different polarities of the solvents and

therefore not to slightly different hydrodynamic radii R_h or overlap concentrations c^* of the tetra-stars.

(iii) The last possibly relevant structure-determining parameter is the reaction temperature. From the theoretical point of view, it was expected that at lower reaction temperatures and so at lower reaction rates, the forming network would be able to relax better, resulting in higher homogeneity. However, at low temperatures, differences in the affinity of the two tetra-stars to the solvents used may become more pronounced, resulting in a larger difference in the respective c^* values. This may have a negative impact on the network structure. To gain a better insight on the temperature effect on the connectivity distribution, the temperature before and after the gel point was varied. Two different temperature protocols were applied (40 °C pre- and 80 °C post-gel temperature vs 60 °C during the whole synthesis). Again, the results (see **Figure 3. 9**) show that the temperature has a negligible effect on the connectivity distribution.

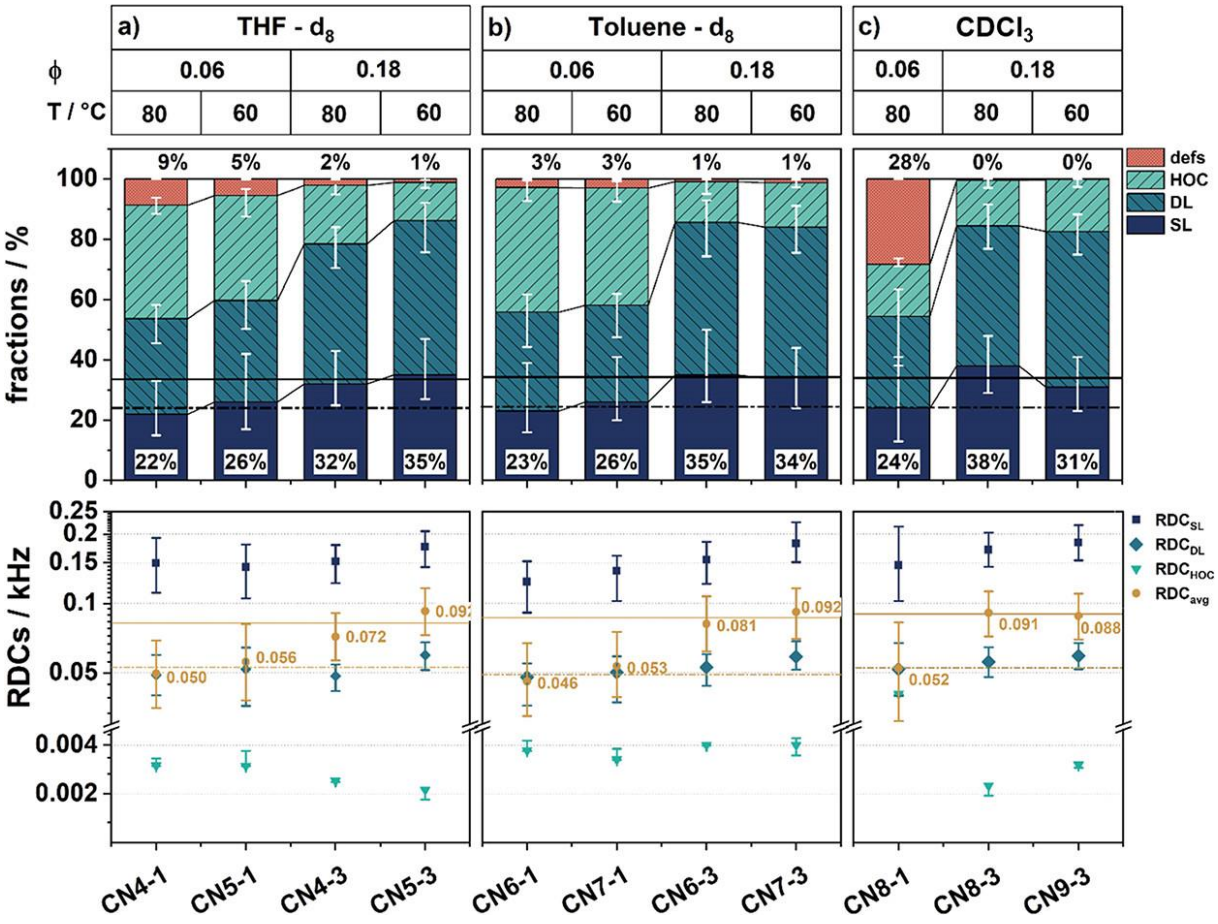

Figure 3. 9: Connectivities and RCS values of ACNs synthesized in (**a**) THF-d_8, (**b**) toluene-d_8, and (**c**) $CDCl_3$. The syntheses were carried out at two different concentrations (ϕ = 0.06 and 0.18), and two different temperature programs were applied (pre- and post-gel temperature = 60/60 °C and 40/80 °C, respectively). The reaction conditions are indicated above the diagrams. Only the highest reaction temperature is given (60 and 80 °C).

A noticeable influence on the connectivity distribution seems to be exerted by the concentration of the stars. In the networks synthesized at higher concentrations (~3*c**, ϕ_0 = 0.18), the SL fraction tends to be higher, while the HOC fraction and the fraction of defects (defs) appear to be even lower. This trend is even more evident in sample **CN3-5** (see SI, **Table A.3. 5**), which was synthesized at ~5*c** but at a slightly different temperature program (25 °C pre- and 60 °C post-gel temperature). For this network, the highest SL fraction (~52%) was found, which is very close to the value of the **PEG-1** network synthesized according to Sakai et al.[25] (54%, see **Figure 3. 8**). For this sample, the lowest Q_v value was found (see **Figure 3. 7a).**

Overall, the MQ studies show that for our networks the influence of the reaction conditions on the microstructure is small. Apart from the obvious influence of concentration (the higher above *c**, the more single links), the reaction solvents and temperature do not affect the micro-structure significantly. Rather, it can be concluded that the synthesis presented here is already in an optimized state, covering a variety of different conditions with reliable and reproducible outcome. Yet, the reason for the differences compared to the water-based hydrogels from Sakai et al.[25] is still unclear.

A nontrivial aspect to consider could be specific interactions of the end groups of the tetra-stars used by us. In contrast to the Sakai gels, one tetra-star possesses aromatic oxazinone terminal groups, which may be assumed to interact with each other or with the linking groups formed during the synthesis by favorable van der Waals or π–π interactions. The polar nitro substituent on the oxazinone group could further enhance specific interactions. The resulting increase in the local concentration of oxazinone groups could promote a formation of double links.

Still, it should be stressed that all data sets can be well fitted with the assumed three-component model for the polymer connectivities, which, despite the somewhat biased connectivity fractions, indicate that the overall network has a model-like network structure with the expected well-defined crosslink distribution. Alternative modeling procedures that include distributions for RDC values and fractions of connectivities do not provide an equally good fit, as can be seen already by the prominent peak in the 7–15 ms regime of the I_{DQ} curves.

3.8. Conclusions

The method presented here for the preparation of ACNs by hetero-complementary linkage of oxazinone- and amino-terminated tetra-arm stars has proved to be extremely robust with respect to the synthesis conditions applied. Regardless of widely varying reaction parameters (T, ϕ, and solvent), the networks obtained differed only slightly with respect to their properties.

Kinetic studies of the crosslinking reaction performed by *in situ* NMR measurements allowed the reaction to be followed in time and confirm a second-order reaction up to conversions of about 60%. Based on the changing signal widths of certain NMR signals, gel points could be determined.

The overlap concentrations of both tetra-arm stars in THF, toluene, and $CHCl_3$ were determined by viscometry. We have computed estimates for the interaction parameters using the Hildebrand–Scott approach,[65] the Hansen approach,[66, 67] and the model of Tian and Munk.[68] The latter provides the best agreement with the viscometry data. We have combined our viscosity measurements with the Tian–Munk estimate to obtain an improved estimate that correctly considers relative differences between the solvents used. These improved estimates seem to be reasonable approximations of the interaction parameters since we can collapse all experimental and simulation data on equilibrium swelling in a universal plot. Furthermore, quantitative agreement was obtained between the hydrodynamic radii determined by DLS in different solvents when the interaction parameters determined according to our estimation were applied.

Rheological characterization of the as-prepared gels leads to the same qualitative trends as reported for other hetero-complementary coupled networks of star polymers.[8] Modulus data on a quantitative basis are clearly below the expectations and in the range of recent experiments on comparable co-network gels.[8]

The equilibrium swelling degrees show a power law dependence on the polymer volume fraction at preparation, $\phi_0^{-0.40 \pm 0.01}$. This dependence is in between the scaling limits of entanglement-free networks and entanglement dominated systems and is only coincidentally close to the classical prediction.[63]

An essential aspect of the work was to find out what influence the reaction conditions have on the network microstructure. For this purpose, MQ NMR investigations were carried out that provided information on occurring connectivities (see **Scheme 3. 2**) and possible network defects. We observe significant differences to previously studied tetra-PEG networks regarding

the frequency of double links. These differences cannot be explained by different interactions between polymers and solvents but could be related to specific interaction of the linking groups in the network. To verify this, additional investigations are intended that include alternative linking reactions for which such interactions are varied systematically.

3.9. References

[1] Rikkou-Kalourkoti, M.; Patrickios, C. S.; Georgiou, T. K. 6.08 - Model Networks and Functional Conetworks. In *Polymer Science: A Comprehensive Reference*: Matyjaszewski, K.; Möller, M., Eds.; Elsevier: Amsterdam, 2012; Vol. 6, pp. 293– 308.

[2] Patrickios, C. S.; Georgiou, T. K. Covalent amphiphilic polymer networks. *Curr. Opin. Colloid Interface Sci.* **2003**, *8*, 76– 85, DOI: 10.1016/S1359-0294(03)00005-0

[3] Hernández-Ortiz, J. C.; Vivaldo-Lima, E. Crosslinking. In *Handbook of polymer synthesis, characterization, and processing*; John Wiley & Sons: Mexico, 2013; Vol. 1, pp. 187– 204.

[4] Hild, G. Model networks based on 'endlinking' processes: synthesis, structure and properties. *Prog. Polym. Sci.* **1998**, *23*, 1019– 1149, DOI: 10.1016/S00796700(97)00055 -5

[5] Rubinstein, M.; Colby, R. H. *Polymer physics*; Oxford University Press: New York, 2003; Vol. 23.

[6] Erdodi, G.; Kennedy, J. P. Amphiphilic conetworks: Definition, synthesis, appli-cations. *Prog. Polym. Sci.* **2006**, *31*, 1– 18, DOI:10.1016/j.progpolymsci.2005.11.001

[7] Yamamoto, K.; Ito, E.; Mori, Y. SAXS and SANS Studies on the Phase-Separated Network Structure of Amphiphilic Copolymer Composed of Poly(dimethyl siloxane) and Poly(N,N-dimethyl acrylamide) Gels Swollen in Water and a Water/Methanol Mixture. *Macromol. Symp.* **2019**, *385*, 1800181, DOI: 10.1002/masy.201800181

[8] Apostolides, D. E.; Patrickios, C. S.; Sakai, T.; Guerre, M.; Lopez, G.; Améduri, B.; Ladmiral, V.; Simon, M.; Gradzielski, M.; Clemens, D.; Krumm, C.; Tiller, J. C.; Ernould, B.; Gohy, J.-F. Near-Model Amphiphilic Polymer Conetworks Based on Four-Arm Stars of Poly(vinylidene fluoride) and Poly(ethylene glycol): Synthesis and Characterization. *Macromolecules* **2018**, *51*, 2476– 2488, DOI: 10.1021/acs.macromol.7b02475

[9] Hiroi, T.; Kondo, S.; Sakai, T.; Gilbert, E. P.; Han, Y. S.; Kim, T. H.; Shibayama, M. Fabrication and Structural Characterization of Module-Assembled Amphiphilic Conetwork Gels. *Macromolecules* **2016**, *49*, 4940– 4947, DOI: 10.1021/

acs.macromol.6b00842

[10] Künzler, J.; Ozark, R. Methacrylate-capped fluoro side chain siloxanes: Synthesis, characterization, and their use in the design of oxygen-permeable hydrogels. *J. Appl. Polym. Sci.* **1997**, *65*, 1081– 1089, DOI: 10.1002/(SICI)1097-4628(19970808)65:6<1081::AID-APP3>3.0.CO;2-G

[11] Nicolson, P. C.; Vogt, J. Soft contact lens polymers: an evolution. *Biomaterials* **2001**, *22*, 3273– 3283, DOI: 10.1016/S0142-9612(01)00165-X

[12] Friends, G. D.; Kunzler, J. F.; Ozark, R. M. Recent advances in the design of polymers for contact lenses. *Macromol. Symp.* **1995**, *98*, 619– 631, DOI: 10.1002/masy.19950980153

[13] Iván, B.; Kennedy, J. P.; Mackey, P. W., Amphiphilic Networks. In *Polymeric Drugs and Drug Delivery Systems*; ACS, 1991, Vol. 469, 203– 212, DOI: 10.1021/bk-1991-0469.ch019 .

[14] Kennedy, J. P.; Fenyvesi, G.; Levy, R. P.; Rosenthal, K. S. Amphiphilic membranes with controlled mesh dimensions for insulin delivery. *Macromol. Symp.* **2001**, *172*, 56– 66, DOI: 10.1002/1521-3900(200107)172:1<56::AIDMASY56>3.0.CO;2-D

[15] Kennedy, J. P.; Rosenthal, K. S.; Kashibhatla, B. Two generations of synthetic membranes for biological/medical applications. *Des. Monomers Polym.* **2004**, *7*, 485– 494, DOI: 10.1163/1568555042474112

[16] Lin, C.; Gitsov, I. Preparation and Characterization of Novel Amphiphilic Hydrogels with Covalently Attached Drugs and Fluorescent Markers. *Macromolecules* **2010**, *43*, 10017– 10030, DOI: 10.1021/ma102044n

[17] Schöller, K.; Küpfer, S.; Baumann, L.; Hoyer, P. M.; De Courten, D.; Rossi, R. M.; Vetushka, A.; Wolf, M.; Bruns, N.; Scherer, L. J. From Membrane to Skin: Aqueous Permeation Control Through Light-Responsive Amphiphilic Polymer Co-Networks. *Adv. Funct. Mater.* **2014**, *24*, 5194– 5201, DOI: 10.1002/adfm.201400671

[18] Grossen, P.; Witzigmann, D.; Sieber, S.; Huwyler, J. PEG-PCL-based nanomedicines: A biodegradable drug delivery system and its application. *J. Controlled Release* **2017**, *260*, 46– 60, DOI: 10.1016/j.jconrel.2017.05.028

[19] Ozcelik, B.; Brown, K. D.; Blencowe, A.; Ladewig, K.; Stevens, G. W.; Scheerlinck, J.-P. Y.; Abberton, K.; Daniell, M.; Qiao, G. G. Biodegradable and Biocompatible Poly(Ethylene Glycol)-based Hydrogel Films for the Regeneration of Corneal Endothelium. *Adv. Healthcare Mater.* **2014**, *3*, 1496– 1507, DOI: 10.1002/adhm.201400045

[20] Guzman, G.; Nugay, T.; Nugay, I.; Nugay, N.; Kennedy, J.; Cakmak, M. High strength bimodal amphiphilic conetworks for immunoisolation membranes: synthesis, characterization, and properties. *Macromolecules* **2015**, *48*, 6251– 6262, DOI: 10.1021/ acs.macromol.5b01343

[21] Sittko, I.; Kremser, K.; Roth, M.; Kuehne, S.; Stuhr, S.; Tiller, J. C. Amphiphilic polymer conetworks with defined nanostructure and tailored swelling behavior for exploring the activation of an entrapped lipase in organic solvents. *Polymer* **2015**, *64*, 122– 129, DOI: 10.1016/j.polymer.2015.03.038

[22] Huang, C.-S.; Jakubowski, K.; Ulrich, S.; Yakunin, S.; Clerc, M.; Toncelli, C.; Rossi, R. M.; Kovalenko, M. V.; Boesel, L. F. Nano-domains assisted energy transfer in amphiphilic polymer conetworks for wearable luminescent solar concentrators. *Nano Energy* **2020**, *76*, 105039 DOI: 10.1016/j.nanoen.2020.105039

[23] Ulrich, S.; Osypova, A.; Panzarasa, G.; Rossi, R. M.; Bruns, N.; Boesel, L. F. Pyranine-Modified Amphiphilic Polymer Conetworks as Fluorescent Ratiometric pH Sensors. *Macromol. Rapid Commun.* **2019**, *40*, 1900360, DOI: 10.1002/marc.201900360

[24] Lang, M. Cyclic Structures in Polymer Model Networks. *Macromol. Symp.* **2019**, *385*, 1800168, DOI: 10.1002/masy.201800168

[25] Sakai, T.; Matsunaga, T.; Yamamoto, Y.; Ito, C.; Yoshida, R.; Suzuki, S.; Sasaki, N.; Shibayama, M.; Chung, U. I. Design and Fabrication of a High-Strength Hydrogel with Ideally Homogeneous Network Structure from Tetrahedron-like Macromonomers. *Macromolecules* **2008**, *41*, 5379– 5384, DOI: 10.1021/ma800476x

[26] Nakagawa, S.; Yoshie, N. Star polymer networks: a toolbox for cross-linked polymers with controlled structure. *Polym. Chem.* **2022**, *13*, 2074– 2107, DOI: 10.1039/ D1PY01547H

[27] Lang, M.; Schwenke, K.; Sommer, J. U. Short Cyclic Structures in Polymer Model Networks: A Test of Mean Field Approximation by Monte Carlo Simulations. *Macromolecules* **2012**, *45*, 4886– 4895, DOI: 10.1021/ma300317z

[28] Lang, M. Elasticity of phantom model networks with cyclic defects. *ACS Macro Lett.* **2018**, *7*, 536– 539, DOI: 10.1021/acsmacrolett.8b00020

[29] Matsunaga, T.; Sakai, T.; Akagi, Y.; Chung, U.-I.; Shibayama, M. Structure Characterization of Tetra-PEG Gel by Small-Angle Neutron Scattering. *Macromolecules* **2009**, *42*, 1344– 1351, DOI: 10.1021/ma802280n

[30] Matsunaga, T.; Sakai, T.; Akagi, Y.; Chung, U.-I.; Shibayama, M. SANS and SLS studies on tetra-arm PEG gels in as-prepared and swollen states. *Macromolecules* **2009**, *42*, 6245– 6252, DOI: 10.1021/ma901013q

[31] Hiroi, T.; Ohl, M.; Sakai, T.; Shibayama, M. Multiscale dynamics of inhomogeneity-free polymer gels. *Macromolecules* **2014**, *47*, 763– 770, DOI: 10.1021/ma402439v

[32] Schwenke, K.; Lang, M.; Sommer, J. U. On the Structure of Star-Polymer Networks. *Macromolecules* **2011**, *44*, 9464– 9472, DOI: 10.1021/ma202022q

[33] Lange, F.; Schwenke, K.; Kurakazu, M.; Akagi, Y.; Chung, U.-I.; Lang, M.; Sommer, J. U.; Sakai, T.; Saalwächter, K. Connectivity and Structural Defects in Model Hydrogels: A Combined Proton NMR and Monte Carlo Simulation Study. *Macromolecules* **2011**, *44*, 9666– 9674, DOI: 10.1021/ma201847v

[34] Kamata, H.; Akagi, Y.; Kayasuga-Kariya, Y.; Chung, U.; Sakai, T. ″Nonswellable″ Hydrogel Without Mechanical Hysteresis. *Science* **2014**, *343*, 873– 875, DOI: 10.1126/science.1247811

[35] Nakagawa, S.; Li, X.; Kamata, H.; Sakai, T.; Gilbert, E. P.; Shibayama, M. Microscopic Structure of the ″Nonswellable″ Thermoresponsive Amphiphilic Conetwork. *Macromolecules* **2017**, *50*, 3388– 3395, DOI:10.1021/acs.macromol.7b00486

[36] Truong, V.; Blakey, I.; Whittaker, A. K. Hydrophilic and amphiphilic polyethylene glycol-based hydrogels with tunable degradability prepared by "click" chemistry. *Biomacromolecules* **2012**, *13*, 4012– 4021, DOI: 10.1021/bm3012924

[37] Kurakazu, M.; Katashima, T.; Chijiishi, M.; Nishi, K.; Akagi, Y.; Matsunaga, T.; Shibayama, M.; Chung, U.-I.; Sakai, T. Evaluation of Gelation Kinetics of Tetra-PEG Gel. *Macromolecules* **2010**, *43*, 3935– 3940, DOI: 10.1021/ma100176f

[38] Jakisch, L.; Komber, H.; Böhme, F. Introduction of a New Coupling Agent for Selective Coupling of Hydroxy and Amino Group-Containing Polymers. *Macromol. Mater. Eng.* **2007**, *292*, 557– 570, DOI: 10.1002/mame.200700005

[39] Zhang, H.; Jakisch, L.; Komber, H.; Voit, B.; Böhme, F. Synthesis of multifunctional coupling agents and their selective reactions with hydroxy and amino groups in the melt. *Tetrahedron* **2013**, *69*, 3656– 3663, DOI: 10.1016/j.tet.2013.03.024

[40] Jakisch, L.; Garaleh, M.; Schäfer, M.; Mordvinkin, A.; Saalwächter, K.; Böhme, F. Synthesis and Structural NMR Characterization of Novel PPG/PCL Conetworks Based upon Heterocomplementary Coupling Reactions. *Macromol. Chem.Phys.* **2018**, *219*, 1700327, DOI: 10.1002/macp.201700327

[41] Wang, H.; Qin, A.; Li, X.; Zhao, X.; Liu, D.; He, C. Biocompatible Amphiphilic Conetwork Based on Crosslinked Star Copolymers: A Potential Drug Carrier. *J. Polym. Sci., Part A: Polym. Chem.* **2015**, *53*, 2537– 2545, DOI: 10.1002/pola.27721

[42] Zare, Y.; Dabbaghi, A.; Rahmani, S. Increasing the hydrophilicity of star-shaped amphiphilic co-networks by using of PEG and dendritic s-PCL cross-linkers. *Polym. Adv. Technol.* **2019**, 2790– 2801, DOI: 10.1002/pat.4711

[43] Yuan, Y.; Zhang, A.-K.; Ling, J.; Yin, L.-H.; Chen, Y.; Fu, G.-D. Well-defined biodegradable amphiphilic conetworks. *Soft Matter* **2013**, *9*, 6309– 6318, DOI:10.1039/ c3sm27853k

[44] Hagmann, K.; Bunk, C.; Böhme, F.; von Klitzing, R. Amphiphilic Polymer Conetwork Gel Films Based on Tetra-Poly(ethylene Glycol) and Tetra-Poly(ε-Caprolactone). *Polymers* **2022**, *14*, 2555, DOI: 10.3390/polym14132555

[45] Bunk, C.; Komber, H.; Lang, M.; Fribiczer, N.; Geisler, M.; Formanek, P.; Jakisch, L.; Seiffert, S.; Voit, B.; Böhme, F. Amphiphilic tetra-PCL-b-PEG star block copolymers using benzoxazinone-based linking groups. *Polym. Chem.*, **2023**,14, 1965-1977 DOI: 10.1039/D3PY00078H

[46] Ishii, S.; Kokubo, H.; Hashimoto, K.; Imaizumi, S.; Watanabe, M. Tetra-PEG network containing ionic liquid synthesized via Michael addition reaction and its application to polymer actuator. *Macromolecules* **2017**, *50*, 2906– 2915, DOI: 10.1021/ acs.macromol.6b02750

[47] Burchard, W. Solution properties of branched macromolecules. In *Branched polymers II*; Springer, 1999, 113– 194, DOI: 10.1007/3-540-49780-3_3 .

[48] Schulz, G. V.; Blaschke, F. Eine Gleichung zur Berechnung der Viscositätszahl für sehr kleine Konzentrationen, [Molekulargewichtsbestimmungen an makromolekularen Stoffen, IX]. *J. Prakt. Chem.* **1941**, *158*, 130– 135, DOI: 10.1002/prac.19411580112

[49] *Average Density of amorphous polymers*; http://polymerdatabase.com/polymer%20physics/Polymer%20Density.html

[50] Lang, M. Monomer fluctuations and the distribution of residual bond orientations in polymer networks. *Macromolecules* **2013**, *46*, 9782– 9797, DOI: 10.1021/ma402013b

[51] Lang, M. On the elasticity of polymer model networks containing finite loops. *Macromolecules* **2019**, *52*, 6266– 6273, DOI: 10.1021/acs.macromol.9b00996

[52] Ahmadi, M.; Löser, L.; Fischer, K.; Saalwächter, K.; Seiffert, S. Connectivity Defects and Collective Assemblies in Model Metallo-Supramolecular Dual-Network Hydrogels. *Macromol. Chem. Phys.* **2020**, *221*, 1900400, DOI: 10.1002/macp.201900400

[53] Nicolella, P.; Koziol, M. F.; Löser, L.; Saalwächter, K.; Ahmadi, M.; Seiffert, S. Defect-controlled softness, diffusive permeability, and mesh-topology of metallo-supramolecular hydrogels. *Soft Matter* **2022**, 1071, DOI: 10.1039/D1SM01456K

[54] Chassé, W.; Valentín, J. L.; Genesky, G. D.; Cohen, C.; Saalwächter, K. Precise dipolar coupling constant distribution analysis in proton multiple-quantum NMR of elastomers. *J. Chem. Phys.* **2011**, *134*, 044907, DOI: 10.1063/1.3534856

[55] Hohwy, M.; Jakobsen, H. J.; Eden, M.; Levitt, M. H.; Nielsen, N. C. Broadband dipolar recoupling in the nuclear magnetic resonance of rotating solids: A compensated C7 pulse sequence. *J. Chem. Phys.* **1998**, *108*, 2686– 2694, DOI: 10.1063/1.475661

[56] Müller, T.; Wengenmayr, M.; Dockhorn, R.; Knespel, M., *LeMonADE-project/LeMon-ADE-GPU: Release v1.2* ; 2021, DOI: 10.5281/zenodo.5513487 .

[57] Müller, T.; Wengenmayr, M.; Dockhorn, R.; Rabbel, H.; Knespel, M.; Checkervarty, A.; Sinapius, V.; Guo, H., Werner, M., *LeMonADE-project/LeMonADE: LeMonADE v2.2.2* ; 2021, DOI: 10.5281/zenodo.5061542 .

[58] Carmesin, I.; Kremer, K. The bond fluctuation method: a new effective algorithm for the dynamics of polymers in all spatial dimensions. *Macromolecules* **1988**, *21*, 2819– 2823, DOI: 10.1021/ma00187a030

[59] Wittmer, J. P.; Beckrich, P.; Meyer, H.; Cavallo, A.; Johner, A.; Baschnagel, J. Intramolecular long-range correlations in polymer melts: The segmental size distribution and its moments. *Phys. Rev. E.* **2007**, *76*, 011803, DOI: 10.1103/PhysRevE.76.011803

[60] Gerstl, C.; Schneider, G. J.; Pyckhout-Hintzen, W.; Allgaier, J.; Willbold, S.; Hofmann, D.; Disko, U.; Frielinghaus, H.; Richter, D. Chain conformation of poly (alkylene oxide) s studied by small-angle neutron scattering. *Macromolecules* **2011**, *44*, 6077– 6084, DOI: 10.1021/ma201288a

[61] Lee, H.; Venable, R. M.; MacKerell, A. D., Jr.; Pastor, R. W. Molecular dynamics studies of polyethylene oxide and polyethylene glycol: hydrodynamic radius and shape anisotropy. *Biophys. J.* **2008**, *95*, 1590– 1599, DOI: 10.1529/biophysj.108.133025

[62] Lang, M.; Müller, T. Analysis of the Gel Point of Polymer Model Networks by Computer Simulations. *Macromolecules* **2020**, *53*, 498– 512, DOI: 10.1021/acs.macromol.9b02217

[63] Lang, M.; Scholz, R.; Löser, L.; Bunk, C.; Fribiczer, N.; Seiffert, S.; Böhme, F.; Saalwächter, K. Swelling and residual bond orientations of polymer model gels: the entanglement free limit. *Macromolecules* **2022**, DOI: 10.1021/acs.macromol.2c00589

[64] Rebello, N. J.; Beech, H. K.; Olsen, B. D. Adding the Effect of Topological Defects to the Flory–Rehner and Bray–Merrill Swelling Theories. *ACS Macro Lett.* **2021**, *10*, 531– 537, DOI: 10.1021/acsmacrolett.0c00909

[65] Hildebrand, J. H.; Scott, R. L. *The solubility of nonelectrolytes*; Dover Publications: New York, 1964.

[66] Hansen, C. M. *Hansen solubility parameters: a user's handbook;* 2 ed.; CRC Press: Boca Raton, 2007.

[67] Hansen, C. M. *The three dimensional solubility parameter*; Danish Technical: Copenhagen, 1967, 14.

[68] Tian, M.; Munk, P. Intermolecular contact interactions and their temperature dependence. *J. Solution Chem.* **1995**, *24*, 267– 284, DOI: 10.1007/BF00979194

[69] Mark, J. E. *Physical properties of polymers handbook*; Springer, 2007, Vol. 1076, DOI: 10.1007/978-0-387-69002-5.

[70] Adamska, K.; Voelkel, A. Hansen solubility parameters for polyethylene glycols by inverse gas chromatography. *J. Chromatogr. A* **2006**, *1132*, 260– 267, DOI:10.1016/ j.chroma.2006.07.066

[71] Sarac, A.; Şakar, D.; Cankurtaran, O.; Karaman, F. Y. The ratio of crystallinity and thermodynamical interactions of polycaprolactone with some aliphatic esters and aromatic solvents by inverse gas chromatography. *Polym. Bull.* **2005**, *53*, 349– 357, DOI: 10.1007/s00289-005-0340-2

[72] Hammouda, B. SANS from homogeneous polymer mixtures: A unified overview. In *Polymer Characteristics*; Springer, 1993; 87– 133, DOI: 10.1007/BFb0025862.

[73] Clisby, N. Accurate estimate of the critical exponent ν for self-avoiding walks via a fast implementation of the pivot algorithm. *Phys. Rev. Lett.* **2010**, *104*, 055702 DOI: 10.1103/PhysRevLett.104.055702

[74] Clisby, N.; Dünweg, B. High-precision estimate of the hydrodynamic radius for self-avoiding walks. *Phys. Rev. E* **2016**, *94*, 052102, DOI: 10.1103/PhysRevE.94.052102

[75] Weissmüller, M.; Burchard, W. Viscosity of fractions from end-linked polystyrene star macromolecules. *Acta Polym.* **1997**, *48*, 571– 578, DOI: 10.1002/actp.1997.010481207

[76] Shida, K.; Ohno, K.; Kimura, M.; Kawazoe, Y.; Nakamura, Y. Dimensional and hydrodynamic factors for flexible star polymers in the good solvent limit. *Macromolecules* **1998**, *31*, 2343– 2348, DOI: 10.1021/ma971312y

[77] Ovchinnikov, A. A.; Zeldovich, Y. B. Role of density fluctuations in bimolecular reaction kinetics. *Chem. Phys.* **1978**, *28*, 215– 218, DOI: 10.1016/0301-0104(78)85052-6

[78] Kang, K.; Redner, S. Scaling approach for the kinetics of recombination processes. *Phys. Rev. Lett.* **1984**, *52*, 955, DOI: 10.1103/PhysRevLett.52.955

[79] Saalwächter, K.; Gottlieb, M.; Liu, R.; Oppermann, W. Gelation as studied by proton multiple-quantum NMR. *Macromolecules* **2007**, *40*, 1555– 1561, DOI: 10.1021/ma062776b

[80] Yuan, G.; Hammouda, B. Solvent and polymer H/D isotope effects on miscibility in Poly (ethylene oxide)/Ethanol system. *Polymer* **2019**, *166*, 178– 183, DOI: 10.1016/j.polymer.2019.01.063

[81] Lang, M.; Rubinstein, M.; Sommer, J.-U. Conformations of a long polymer in a melt of shorter chains: Generalizations of the Flory theorem. *ACS Macro Lett.* **2015**, *4*, 177– 181, DOI: 10.1021/mz500777r

[82] Obukhov, S. P.; Rubinstein, M.; Colby, R. H. Network modulus and superelasticity. *Macromolecules* **1994**, *27*, 3191– 3198, DOI: 10.1021/ma00090a012

[83] Bastide, J.; Picot, C.; Candau, S. Some comments on the swelling of polymeric networks in relation to their structure. *J. Macromol. Sci., Part B: Phys.* **1981**, *19*, 13– 34, DOI: 10.1080/00222348108212840

[84] Flory, P. J. *Principles of polymer chemistry*; Cornell University Press, 1953.

[85] Lang, M.; Fischer, J.; Werner, M.; Sommer, J.-U. Swelling of Olympic gels. *Phys. Rev. Lett.* **2014**, *112*, 238001, DOI: 10.1103/PhysRevLett.112.238001

[86] Lang, M.; John, A.; Sommer, J.-U. Model simulations on network formation and swelling as obtained from cross-linking co-polymerization reactions. *Polymer* **2016**, *82*, 138– 155, DOI: 10.1016/j.polymer.2015.10.061

[87] Candau, S.; Peters, A.; Herz, J. Experimental evidence for trapped chain entanglements: their influence on macroscopic behaviour of networks. *Polymer* **1981**, *22*, 1504– 1510, DOI: 10.1016/0032-3861(81)90320-7

[88] Klepko, V. V.; Mel'nichenko, Y. B. Kinetics and equilibrium swelling of gelatine gels. *Polymer* **1995**, *36*, 5057– 5059, DOI: 10.1016/0032-3861(96)81636-3

[89] Gnanou, Y.; Hild, G.; Rempp, P. Molecular structure and elastic behavior of poly (ethylene oxide) networks swollen to equilibrium. *Macromolecules* **1987**, *20*, 1662– 1671, DOI: 10.1021/ma00173a037

[90] Chen, Z.; Cohen, C.; Escobedo, F. A. Monte Carlo simulation of the effect of entanglements on the swelling and deformation behavior of end-linked polymeric networks. *Macromolecules* **2002**, *35*, 3296– 3305, DOI: 10.1021/ma012048i

[91] Niedzwiedz, K.; Wischnewski, A.; Pyckhout-Hintzen, W.; Allgaier, J.; Richter, D.; Faraone, A. Chain dynamics and viscoelastic properties of poly (ethylene oxide). *Macromolecules* **2008**, *41*, 4866– 4872, DOI: 10.1021/ma800446n

[92] Gimenez, J.; Cassagnau, P.; Michel, A. Bulk polymerization of ε-caprolactone: Rheological predictive laws. *J. Rheol.* **2000**, *44*, 527– 547, DOI: 10.1122/1.551099

[93] Sangroniz, L.; Barbieri, F.; Cavallo, D.; Santamaria, A.; Alamo, R. G.; Müller, A. J. Rheology of self-nucleated poly (ε-caprolactone) melts. *Eur. Polym. J.* **2018**, *99*, 495– 503, DOI: 10.1016/j.eurpolymj.2018.01.009

[94] Adam, M.; Delsanti, M. Viscosity and longest relaxation time of semi-dilute polymer solutions. I. Good solvent. *J. Phys.* **1983**, *44*, 1185– 1193, DOI: 10.1051/jphys: 0198300440100118500

[95] Colby, R. H.; Fetters, L. J.; Funk, W. G.; Graessley, W. W. Effects of concentration and thermodynamic interaction on the viscoelastic properties of polymer solutions. *Macromolecules* **1991**, *24*, 3873– 3882, DOI: 10.1021/ma00013a021

[96] Akagi, Y.; Matsunaga, T.; Shibayama, M.; Chung, U.-i.; Sakai, T. Evaluation of topological defects in tetra-PEG gels. *Macromolecules* **2010**, *43*, 488– 493, DOI: 10.1021/ma9019009

[97] Zhong, M.; Wang, R.; Kawamoto, K.; Olsen, B. D.; Johnson, J. A. Quantifying the impact of molecular defects on polymer network elasticity. *Science* **2016**, *353*, 1264– 1268, DOI: 10.1126/science.aag0184

4. CHAPTER II: MECHANICS IN THE SWOLLEN STATE

Impact of Swelling on Macroscopic and Nanoscopic Mechanical Properties of Amphiphilic Polymer Co-Networks in Non-Selective and Selective Solvents

N. Fribiczer, [redacted]

Macromol. Chem. Phys., **2023**, 2300389, doi:10.1002/macp.202300389

The corresponding *Supporting Information* is included in **Appendix A.4**.

The results in this chapter were first published on December 5, 2023 and are adapted with permission from *Macromol. Chem. Phys.*, **2023**, 2300389.

4.1. Specific Summary

In the last chapter, amphiphilic polymer co-networks composed of t-PEG and t-PCL were comprehensively studied with respect to the interplay of synthesis conditions, resulting network connectivities and swelling properties next to a characterization of the network building blocks and the network formation kinetics. Additionally, first rheological studies in the preparation state were shown. However, no mechanical data in the fully swollen state were presented, neither in a non-selective solvent nor in a selective solvent. This is detrimental, as investigations in the selective solvent water might be of particular interest for potential (biomedical) applications.

For this reason, co-networks of t-PEG and t-PCL at equilibrium swelling are investigated in both the non-selective solvent toluene and the selective solvent water by the complementary methods of shear rheology and atomic force microscopy (AFM). This approach provides a characterization on different length-scales next to information on the mechanics in bulk and at the surface. Furthermore, it enables identification of possible heterogeneities at the micro- and nanoscopic level as well as potential microphase separation effects at the surface. The networks are synthesized in the non-selective solvent toluene at different temperatures and concentrations and subsequently swollen to equilibrium, dried, and either reswollen in toluene to identify the impact of drying or swollen in the selective solvent water. It was found in earlier studies (see *Chapter I*) that drying of the networks at higher temperatures (> 40 °C) leads to a noticeable amount of post-crosslinking, reducing the swelling degree after drying. Thus, a different drying

process is carried out at room temperature over a longer period of time, which proves to have a negligible effect on both swelling and mechanics.

The PEG-PCL networks show a concentration dependent swelling degree in toluene which follows an apparent scaling law and is in accord with previous findings; in water, in contrast, a constant swelling degree of three is observed. The latter finding can be attributed to counteracting swelling and shrinking tendencies which balance each other due to a 50:50 mixture of hydrophilic and hydrophobic components. This microphase separation in water can be visualized at the surface by atomic force microscopy revealing nearly spherical PCL domains in the size range of 20 nm. Despite this microphase separation, similar moduli are obtained with rheology and AFM in both solvents.

An apparent scaling law of modulus with polymer volume fraction is found, which is in accord with previous findings of such networks in a non-selective solvent. In the selective solvent water, however, a rather linear scaling is found due to the concentration independent swelling. The amphiphilic networks are further compared with pure hydrophilic PEG-PEG networks of the same crosslinking chemistry to identify the impact of the amphiphilicity on the swelling ability and the mechanical performance. Moreover, the mesh size of the networks is estimated using the plateau modulus to evaluate the possible permeability for guest substances.

This study marks a further step towards rationally understanding the interplay between synthesis conditions, the resulting structure and corresponding properties and using this knowledge for the targeted design of functional materials. To further explore the potential of these amphiphilic networks for applications, the swelling and mechanics, as well as the permeability can be tuned by changing the ratio as well as the molecular weight of the hydrophilic and hydrophobic building blocks. More detailed information on the structure can be gained by light scattering experiments and information on the permeability are accessible via FRAP investigations using different sizes of fluorescent tracer. Both methods can also provide complementary data on the mesh size.

4.2. Author Contributions

Nora Fribiczer:	Concept development, rheology measurements, swelling experiments, evaluation of data and comparison with literature, manuscript preparation and correction.
[redacted]	Atomic force microscopy measurements and evaluation.
[redacted]	Synthesis of network components.
[redacted]	Scientific supervision of [redacted] and manuscript correction.
[redacted]	Scientific supervision of [redacted] and manuscript correction.
[redacted]	Scientific supervision and manuscript correction.

4.3. Acknowledgement

The authors thank the German Research Foundation (DFG) for funding within the Research Unit FOR2811 „Adaptive Polymer Gels with Model Network Structure“ under grant No. 397384169 along with grants 423373052 (TP4), 423768931 (TP5), and 423514254 (TP1).

4.4. Abstract

Amphiphilic polymer gels show environmentally sensitive mechanical properties depending on the solvent polarity, which makes them useful for applications in soft contact lenses, membranes, drug delivery systems, and tissue engineering. To rationally design the material properties for such applications, a sound knowledge about the mechanical properties at different solvency states is necessary. To acquire such knowledge, amphiphilic networks are prepared by hetero-complementary coupling of amine-terminated tetra-poly(ethylene glycol) with 2-(4-nitrophenyl)-benzoxazinone terminated tetra-poly(ε-caprolactone). The mechanical properties are investigated on different length-scales and under non-selective and selective solvent conditions using shear rheology and atomic force microscopy. The swelling as well as the modulus in good solvent are in accord with scaling laws found for other four-arm star-shaped polymer networks and theoretical predictions. The swelling in selective solvent reveals a concentration-independent volume swelling degree and a nearly linear scaling of the modulus with concentration. The surface topography probed by atomic force microscopy reveals microphase-separated structures in the range of 20 nm. Similar modulus values are obtained for bulk films in water using the complementary methods of atomic force microscopy and rheology. The data are compared with pure hydrophilic networks to identify the effect of amphiphilicity on the material properties.

4.5. Introduction

Amphiphilic polymer co-networks (APCNs) are composed of both hydrophilic and hydrophobic parts that independently swell in water and organic solvents.[1] The swollen networks show environmentally sensitive viscoelasticity and selective permeability, allowing the transport of hydrophilic and hydrophobic substances to be controlled. For this reason, APCNs are most commonly used in soft contact lenses[2, 3] and are excellent candidates for use as membranes,[4] drug delivery systems,[5, 6, 7] and in tissue engineering.[7, 8] Among others, amphiphilic networks consisting in part of poly(ethylene glycol) (PEG) or poly(ε-caprolactone) (PCL), have been described in many research articles focusing on biomedical applications.[5, 9]

To enable targeted materials design for these and other applications, a profound knowledge of the interplay between structural changes and resulting properties under different environmental and network-preparation conditions is essential. To investigate such structure-property relations, model networks with a defined starting structure are advantageous. A powerful approach to obtain such model networks was popularized by Sakai et al.[10] utilizing hetero-complementary coupling of tetra-poly(ethylene glycol) (t-PEG) star polymers to obtain model networks with minimal network defects.[11, 12] The hetero-complementary coupling based on click-chemistry prevents the formation of intramolecular loops and leads to a nearly homogeneous structure, as confirmed by Lange et al.[13] with NMR and Monte-Carlo simulations.[11, 14] Despite the presence of pending arms and double links with adjacent star polymers, networks synthesized by this procedure show outstanding homogeneity and enhanced mechanical properties.[10, 12, 15]

This model-network-approach was also extended to amphiphilic networks. Hiroi et al.[16] combined t-PEG with linear poly(dimethyl siloxane) (PDMS) to form an amphiphilic network, which showed microphase-separation in water. The microphase-separated structure varied with the polymer volume fraction of PDMS from core-shell to lamellar morphologies. Nakagawa et al.[17] studied the structure of thermos-responsive networks prepared from tetra-poly(ethyl glycidyl ether-co-methyl glycidyl ether) (t-PEMGE) and t-PEG with neutron scattering and showed that the swelling degree of the network can be tuned by the network composition. Apostolides et al.[18] utilized hydrophilic t-PEG with hydrophobic tetra-poly(vinylidene fluoride) (t-PVDF) to form near-model amphiphilic co-networks. The swelling degree was found to be dependent on solvent quality, and characterization of the networks in the selective solvent water revealed the formation of hydrophobic clusters. Selective solvent here means that the solvent is a good one for the hydrophilic part and a bad one for the hydrophobic part of the network. An

informative overview of the development in the field of amphiphilic polymer networks is given in a book by Patrickios.[2]

In 2022, Bunk et al.[19] presented the synthesis of a t-PEG and tetra-poly(ε-caprolactone) (t-PCL) based APCN in the non-selective solvents tetrahydrofuran, toluene, and chloroform, i.e., good solvents for both star polymer types. Despite the hetero-complementary coupling reaction, a notable amount of double links was found in the networks, which was attributed to possible specific interactions of the aromatic oxazinone terminal groups promoting the formation of double links. The double link fraction decreased with increasing polymer volume fraction. Nevertheless, an overall model-like network structure was stated due to the good agreement with a three-component fit of the data, which was used in previous work on t-PEG networks. First rheological investigations at preparation conditions were presented and connected to NMR-studies as well as theoretical calculations by Lang et al.[20] The overall scaling of the modulus with polymer volume fraction was found to be in accord with previous findings for t-PEG gels,[21] although the modulus was nearly a factor of 4 below the expectations from the phantom network model.[19, 20] Furthermore, gel films based on the system of Bunk et al.[19] were studied by atomic force microscopy (AFM).[22] The preparation method of the films was recognized to distinctly influence the elastic moduli found. Thin films prepared by spin coating showed a ten-fold higher modulus in the selective solvent water and nearly a four-fold higher modulus in the non-selective solvent toluene compared to films obtained through bulk synthesis. This finding was explained by the drying process during spin coating, which induces the proceeding reaction of the network components resulting in crosslinking of different network levels. This leads to an overall tighter network that exhibits a lower degree of swelling and higher elastic moduli.

However, up to now, no systematic characterization of the mechanical properties on different length scales, i.e. from macroscopic over microscopic to nanoscopic scales at the swelling equilibrium was presented, neither in a non-selective solvent nor in the selective solvent water. This is detrimental, as data in water are of particular interest for potential applications.

In this work, we aim to close this gap by investigating the impact of different synthesis and environmental conditions on the mechanical properties by shear rheology and atomic force microscopy. These complementary methods provide a characterization on different length-scales to identify possible heterogeneities at the micro- and nanoscopic level and potential micro- and nanophase-separation effects at the surface. The PEG-PCL networks studied correspond to those described by Bunk et al.[19] and are based on star polymers with 10 kg mol^{-1} each. Our

aim is to extend this previous work by investigating the swollen gel state and to gain interesting insights by comparing them with PEG-PEG networks also based on star polymers with 10 kg mol^{-1} each. The networks are synthesized in the non-selective solvent toluene at different temperatures and concentrations, subsequently swollen to equilibrium, dried, and transferred either back to toluene to identify the impact of drying or to the selective solvent water. The PEG-PEG networks are used to show the influence of the hydrophobic PCL part on the swelling capacity and the mechanical properties. Furthermore, swelling degree and mechanical properties are compared with predictions from theoretical models to demonstrate consistency with previous work on these systems and in general networks based on the t-PEG approach.

4.6. Results and Discussion

Network formation

Prior to the study of swollen gels, the network formation of PEG-PCL gels is studied by shear rheology in toluene and compared with NMR studies in d_8-THF.[19] For this purpose, stock solutions of the star polymers are prepared at the respective concentrations, mixed in stochiometric ratio and applied onto the rheometer, which is preheated to the synthesis temperature. The gelation is investigated at 25 °C, 40 °C, and 60 °C. The network formation takes place according to **Figure 4. 1** by hetero-complementary coupling of benzoxazinone functionalized t-PCL with amino functionalized t-PEG. The overlap concentration c^* of the polymers was determined in previous work [19] and a concentration of 70 g L^{-1} was chosen to ensure overlap of both type of star polymers. Since this work uses the same polymeric system, we adapt this and analyze networks synthesized in the concentration range c = 70; 140; 210; 280; 350 g L^{-1} corresponding to roughly 1–5c^*. The corresponding polymer volume fractions at preparation, ϕ_0, range from ϕ_0 = 0.06–0.3. The network formation in this work is solely carried out in toluene.

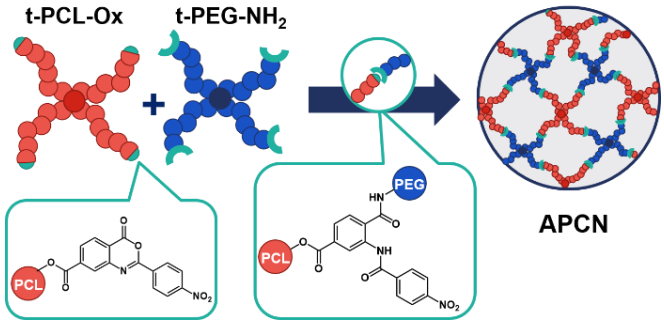

Figure 4. 1: Schematic reaction of t-PCL-Ox with t-PEG-NH_2 to form an APCN.

The received gel points are summarized in **Figure 4. 2a** and are estimated as the crossover of storage (G') and loss modulus (G'') during the course of gelation (see **Figure 4. 2b**). Values with the suffix NMR are based on NMR spectroscopic monitoring of the crosslinking reaction (with permission from ref. [19]). The gel point shifts to shorter timescales with increasing concentration and temperature, which is in line with expectations. Compared to the data from NMR studies in d_8-THF, the rheological gel point is shifted on the time scale by a factor of 1.1–1.5 to longer times. This discrepancy between the gel point from NMR and rheology decreases with increasing synthesis temperature. This can be attributed to the choice of solvent: Bunk et al.[19] already stated that the kinetics are slower in toluene than in THF. Also, a different methodology is used, and the intersection of storage and loss modulus represents only an upper estimate of the network formation time.[23] Nonetheless, the gel points of both methods and solvents are in semi-quantitative agreement and in the same order of magnitude.

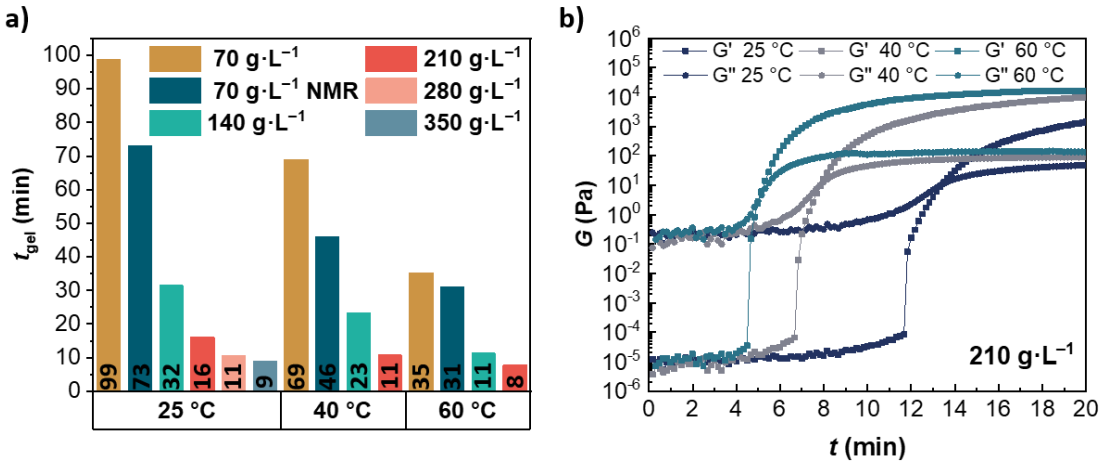

Figure 4. 2: a: Plot of the time at the gel point against the synthesis temperature of PEG-PCL networks at different synthesis concentrations in toluene. The data marked with NMR were reproduced with permission from Bunk et al.[19] **b:** Exemplary plot of the recorded time sweeps for gelation at 210 g L^{-1} and 25 °C (dark blue), 40 °C (gray) and 60 °C (light blue) in toluene.

Swelling Properties

Non-selective Solvent

In the following, we consider the influence of preparation conditions on the swelling degree of PEG-PCL and PEG-PEG networks in the non-selective solvent toluene. Throughout this work, we solely consider the volume swelling degree defined as $Q = 1 + \left(\frac{\rho_p}{\rho_s}\right)\left(\frac{w_s}{w_p}\right)$ with the density of the polymer and the solvent (ρ_p and ρ_s), the weight of the polymer (w_p), and the weight of the solvent (w_s). Generally, the networks are prepared in toluene and subsequently swollen to equilibrium without any drying. Afterwards, the networks are dried and reswollen in the respective solvent. For distinguishing the swelling degree before and after drying, the designations „Q_1“ and „Q_2“ are used accordingly. All PEG-PEG networks discussed in this publication are prepared at 25 °C.

The swelling degrees of PEG-PCL networks prepared at 25 °C and 60 °C range from around 8 to 18 depending on polymer volume fraction (see **Figure 4. 3**). The networks prepared at elevated temperatures tend to have a slightly lower degree of swelling for low polymer volume fractions. However, at high polymer volume fractions, the values equalize. One possible explanation is that toluene evaporated during the network preparation, thereby increasing the polymer concentration and the concentration of reacting groups. Previously separated end groups are brought into contact, resulting in higher conversions and increased overlap between the molecules. At the same time, reactivity increases at elevated temperature. Nevertheless, the influence of the synthesis temperature on the degree of swelling is small. In accordance with our data, Bunk et al.[19] reported a degree of swelling of about 17–19 at ϕ_0 = 0.06 and 11 at ϕ_0 = 0.18 in toluene-d_8. This gives evidence that the used preparation and swelling procedure is consistent with the original method.

The respective degree of swelling of PEG-PEG networks in toluene prepared at 25 °C range from 7 to 13 depending on the polymer volume fraction at preparation (see **Figure 4. 3**). The lower degree of swelling can be attributed to the poorer solvent quality of toluene for PEG compared to PCL. This aspect was already discussed in the publication of Bunk et al.[19] based on viscosity data and the Flory-Huggins interaction parameter.

Figure 4. 3 further shows that the plot of the average equilibrium degree of swelling, Q_1, against the polymer volume fraction at preparation, ϕ_0, follows an apparent scaling law of $Q_1 \sim \phi_0^{-\alpha}$ with α = 0.45 ± 0.01 for PEG-PCL prepared at 25 °C and α = 0.40 ± 0.01 prepared at 60 °C as well as α = 0.43 ± 0.01 for PEG-PEG networks. These exponents are in agreement with

previous data[19] and corresponding simulations of swelling in the good-solvent regime.[20] The simulations were performed for a conversion of 95%, so the gels prepared in this experimental study must be close to this conversion. Furthermore, they follow the expectations of a scaling with $\alpha = 2/5 = 0.4$ from mean field model predictions.[24] Discrete values of the degree of swelling are noted in **Table A.4. 1** of the Supporting Information (**Appendix A.4**).

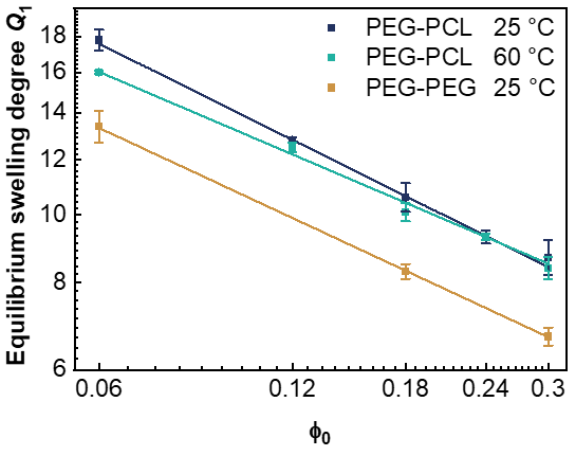

Figure 4. 3: Average equilibrium swelling degree, Q_1, in toluene as a function of polymer volume fraction at preparation. The data follow an apparent scaling law of $Q_1 \sim \phi_0^{-\alpha}$ for all three systems, the PEG-PCL networks synthesized at 25 °C (dark blue) and 60 °C (cyan) as well as the PEG-PEG networks prepared at 25 °C (gold).

Effect of Drying

To transfer the networks from the non-selective solvent in which they are prepared to the selective solvent, drying and reswelling is a common procedure. In this section, the influence of the drying procedure on the swelling ability of the networks is investigated as drying can increase the conversion via post-crosslinking, thus reducing the swelling capacity.

The investigated PEG-PCL gels are synthesized in toluene and dried at room temperature for five days to remove toluene. Subsequently, the networks are reswollen in toluene and the recovered swelling degree ($Q_2/Q_1 \cdot 100\%$) is calculated. **Figure 4. 4** shows the recovered swelling degree for gels synthesized at 25 °C and 60 °C as well as for different polymer volume fractions. The results show that with the moderate way of removing the solvent, the swelling behavior of the networks hardly changes. Although the reaction conditions have an effect on the swelling behavior of the networks at low polymer volume fractions, the influence on the recovery swelling degrees is only small (see **Figure 4. 3**). For all networks, the second swelling in toluene almost restores the initial value, indicating that the drying procedure used does not change the network structure much. In contrast, drying at higher temperatures leads to significant changes,

as evidenced by the sample synthesized at a concentration of ϕ_0 = 0.06 and dried at 60 °C. Here, reswelling in toluene achieves only 55% of the initial swelling degree. This effect of drying at elevated temperatures (40 °C) was also shown by Bunk et al.[19] for up to three drying and reswelling cycles in tetrahydrofuran, toluene, and chloroform. The effect was particularly pronounced after the first drying and reswelling cycle and at low polymer volume fractions. Only 63–68% of the initial swelling degree was recovered in toluene at ϕ_0 = 0.06. At higher volume fractions of ϕ_0 = 0.18 about 90–95% recovery was observed. This shows that the relative number of free reaction groups is higher at low polymer content which leads to stronger additional crosslinking after the first drying. Apparently, post-reactions take place during drying at higher temperatures, resulting in increased network density. Nevertheless, the solvent evaporation rate has an impact on the gel structure especially during synthesis, which becomes for instance important during preparation of thin gel films (i.e. high surface/volume ratio). Hagmann et al.[22] prepared either thin films by spin coating or dried their films at 60°C. In both cases, rapid evaporation of the solvents led to noticeable post-crosslinking, resulting in high elastic moduli. In contrast to this, we show that drying of the gels at room temperature over a longer period of time has a negligible effect on the swelling capacity especially at higher polymer volume fractions. Therefore, it is justified to compare the swelling degrees Q_1 in toluene with Q_2 in water for the PEG-PEG networks. The suitability of the presented drying procedure at room temperature is further proven by rheological measurements and comparison of the storage modulus in toluene before and after drying. The exact values of **Figure 4. 4** are included in **Table A.4.2**.

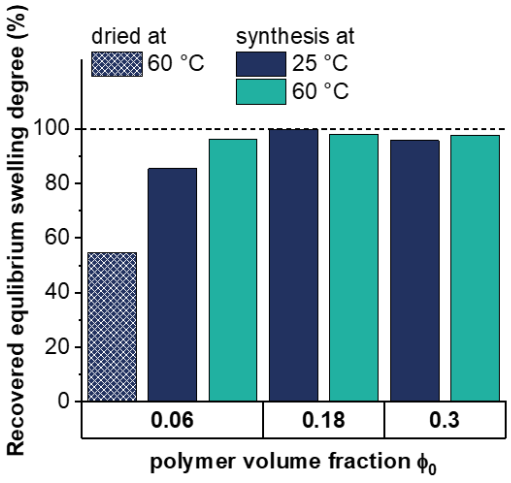

Figure 4. 4: Recovered swelling degrees ((Q_2/Q_1)·100%) of PEG-PCL networks synthesized at 25 °C (dark blue) and 60 °C (cyan) after respective drying procedure and reswelling in toluene. Unless stated otherwise, the gels were dried at 25 °C for five days.

Selective Solvent

After studying the swelling of the networks in a non-selective solvent and the impact of the drying procedure, swelling in the selective solvent water is investigated, which is of particular interest due to potential applications. The networks are prepared in toluene, dried at room temperature for five days, and reswollen to equilibrium in water. The swelling degrees in water determined after drying are referred to as Q_2.

While the gels are highly swollen and transparent in toluene, they exhibit lower swelling and a cloudy appearance in water (see **Figure A.4. 1** and **A.4. 2**). This indicates clustering or colloidal behavior of the PCL star polymers due to their hydrophobicity. AFM tapping mode images of the swollen APCNs are taken to get an idea of the surface structure in toluene and the extent of microphase separation in water (see **Figure 4. 5**). In water, the microphase-separated structure essentially resembles nearly spherical domains, which could be visualized at the surface by phase imaging in AFM (see **Figure 4. 5**). The size of these domains at the surface is 20 ± 5 nm, giving evidence of the clustering of several PCL-stars. A similar average distance of roughly 19 nm between the microphase-separated domains and a radius of the domains of roughly 5–6 nm was also found in SAXS experiments on bulk gels by Löser et al., representing the aggregation of 17–25 PCL star polymers.[25] The study furthermore confirms that the PCL clusters are nearly PEG free and adapt an ellipsoidal shape. Such small length-scales are close to the resolution limit of the AFM measurements carried out in this study, since the curvature radius of the AFM tips is roughly 8 nm for imaging in tapping mode and 30 nm for determining mechanical properties through indentation measurements, respectively. Nevertheless, it is quite remarkable to find the same type of phase separation on the same length-scale through various methods such as SAXS and AFM. Deviations in size and shape may be attributed to differences in the analysis of bulk and surface structure.

In toluene, in contrast, no underlying structure can be detected in the AFM phase image (see **Figure 4. 5**). This is consistent with the expectation, as both star-types swell in the non-selective solvent, resulting in homogeneously swollen networks on the investigated length-scale. These findings are also confirmed by height images, which show a smooth surface in toluene and a significantly rougher surface in water. The height images are provided in **Figure A.4. 3** in the Supporting Information (**Appendix A.4**).

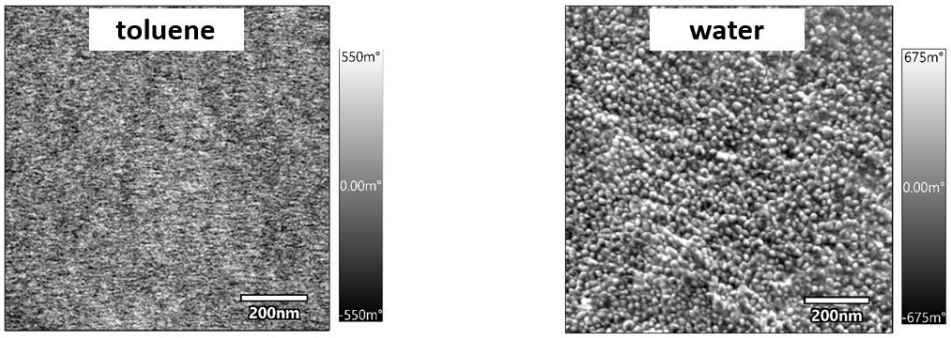

Figure 4. 5: Surface topography of PEG-PCL gels measured with AFM in tapping mode. The phase images of the networks swollen in toluene (non-selective solvent, and non-dried) and water (selective solvent; after drying and reswelling) are displayed. In toluene, no surface structure is noticeable; in water, in turn, microphase-separation is visible in the form of nearly spherical structures covering the entire surface.

The respective swelling degrees of PEG-PCL and PEG-PEG networks in water are displayed in **Figure 4. 6**. The PEG-PCL networks show a degree of swelling statistically scattering around 3, independent of the initial polymer volume fraction at preparation and the synthesis temperature (see **Figure 4. 6a**; discrete values are included in **Table A.4.3**). The significantly lower values compared to swelling in toluene can be explained by the selective swelling behavior of the respective polymers PEG and PCL in water. Whereas the hydrophilic PEG tends to swell in water, the hydrophobic PCL shows the opposite tendency to contract and repel the water. Due to the 50:50 mixture in all networks investigated, these opposite tendencies of swelling and shrinking seem to balance out, resulting in a swelling degree of three. That might explain why the swelling degree of PEG-PCL gels does not depend on the polymer content.

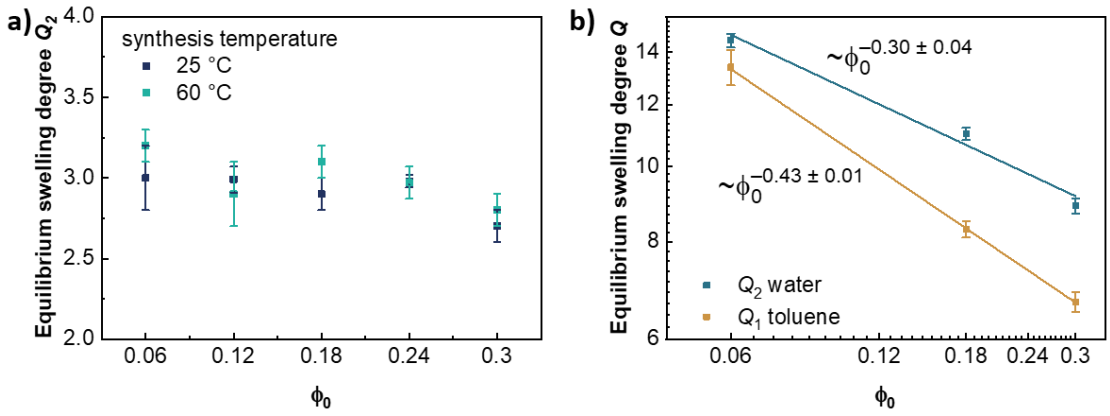

Figure 4. 6: Equilibrium swelling degree as a function of polymer volume fraction at preparation. **a**: PEG-PCL gels in water synthesized at 25 °C (dark blue) and 60 °C (cyan). **b**: PEG-PEG networks in water (blue) and toluene (gold) synthesized at 25 °C. Since the gels were synthesized in toluene they were dried before studying them in water.

Considering the swelling degree in water and the network composition (50:50 mixture of the star polymers), the found nearly spherical shape in **Figure 4. 5** can possibly be explained by the phase separation behavior of block copolymers, although they have a higher degree of freedom compared to the network. It is known from block copolymers in bulk that spherical structures are obtained at low volume fractions of one of the blocks.[26] In our case, a degree of swelling of 3 roughly translates to a total polymer volume fraction of 0.3.[27] As only half of the polymer fraction consists of PCL stars, the polymer volume fraction of PCL is about 0.15. Such small fractions of one species are assigned to the aforementioned spherical structures.[26, 28]

In contrast to the PEG-PCL networks, which have a cloudy appearance in water, the PEG-PEG gels remain transparent (see **Figure A.4. 1**). They exhibit a higher swelling degree ranging from 9 to 14.5 depending on the initial polymer volume fraction (see **Figure 4. 6b**). Hence, the swelling ratio of PEG-PEG gels is much higher than that of PEG-PCL gels. This is plausible because water is a better solvent for PEG than for PCL. The PEG-PEG networks also show a degree of swelling that is 1.1–1.3 times higher in water than in toluene. Both water and toluene are in general good solvents for PEG, but the higher swelling degree in water indicates a slightly better solvent quality.

The solvent quality is often discussed in terms of the Flory–Huggins interaction parameter χ, which quantifies the interaction energies between the polymer and the solvent. Another important parameter in this context is the overlap concentration c^*, which is inversely proportional to the intrinsic viscosity $[\eta]$.[29] In turn, the intrinsic viscosity is a measure of the increase in viscosity caused by the polymer and gives an indication on the expansion of the polymer in solution. The Flory–Huggins parameter of linear PEG in water is about 0.43[30] and that of t-PEG-NH_2 was determined to be 0.465–0.495[31] depending on the molar mass. In toluene, a value of χ = 0.38 was computed for t-PEG-NH_2 with 10 kg mol^{-1} from experimental viscosity data at 25 °C using the Tian–Munk model.[19, 32] Based on this estimate, toluene would be the better solvent for PEG, but the swelling results indicate the opposite trend. Therefore, the overlap concentration or its reciprocal, the intrinsic viscosity, is used as a further measure of solvent quality. The overlap concentration in toluene of amine terminated t-PEG at 25 °C is c^* = 76.2 ± 0.5 g L^{-1} [19] corresponding to an intrinsic viscosity of $[\eta]$ = 0.01312 L g^{-1}. The value in water was determined in this work to be c^* = 60 ± 2 g L^{-1} corresponding to $[\eta]$ = 0.01680 L g^{-1} and agrees very well with the overlap concentration of 60 g L^{-1} determined by Sakai et al.[10] for the formation of t-PEG networks in aqueous buffer solution. According to

these data, PEG is more expanded, i.e., swollen, in water than in toluene. Therefore, a lower polymer concentration is required to achieve space filling.

To validate the viscosity results, they are related to the value for linear PEG chains of the same molar mass. The ratio of the intrinsic viscosity of the star polymers to that of corresponding linear polymers is called the contraction factor, which indicates that star polymers are more compact and have a lower radius of gyration than their linear analogues at the same molar mass.[33] The contraction factor describes this decrease in intrinsic viscosity due to the more compact architecture and is defined as $g_\eta = [\eta]_b/[\eta]_l$ with intrinsic viscosity of the branched four-armed star polymer, $[\eta]_b$, and the intrinsic viscosity of the linear polymer $[\eta]_l$. For four-armed star polymers in a good solvent contraction factors of g_η = 0.68–0.74 [33, 34] are found. In this work, we calculated a ratio of g_η= 0.68 using $[\eta]_l$ = 0.02486 L g^{-1} for linear PEG (10 kg mol^{-1})[35] and the experimentally found value of $[\eta]_b$ = 0.01680 L g^{-1} for t-PEG-NH_2 (10.8 kg mol^{-1}). This agrees quite well with the literature data despite the difference in molar mass and the change in end-group chemistry from hydroxy to amine end groups. In conclusion, based on the experimental viscosity data, water is the better solvent for PEG at the experimental conditions used.

Just like in toluene, the swelling degree of the PEG-PEG gels in water shows a dependency on the initial polymer volume fraction according to the apparent scaling law $Q_2 \sim \phi_0^{-\alpha}$ (see **Figure 4. 6b**). The exponent of the apparent scaling law $Q_2 \sim \phi_0^{-\alpha}$ is 0.30 ± 0.04 and consequently lower than in toluene. As both toluene and water are rather good solvents for PEG, we would expect a similar exponent. The swelling degree in water was determined after drying of the gels in between for the solvent exchange from toluene to water. This might have induced some post-crosslinking reaction, leading to higher conversion and thus lower achievable swelling degree. This effect is more pronounced at lower polymer volume fractions, which results in the observed lower exponent. An additional point to keep in mind is the connection of the PEG-PEG networks by an aromatic linking group, which could affect the swelling capacity of the gels in water by clustering.

The data of the PEG-PEG gels confirm the assumption made above that the low swelling degree of PEG-PCL networks in water is mainly due to the hydrophobicity of the PCL moieties. The possible additional shrinkage tendency due to the aromatic linking group should be negligible in contrast to the shrinking induced by PCL, as the PEG-PEG gels swell more in water than in the less polar solvent toluene.

Mechanical Properties

All shear rheological and AFM measurements in this chapter were performed at equilibrium swelling and at 25 °C, if not stated otherwise.

Effect of Drying on Mechanics

In a first step, the drying procedure is verified by comparing the storage moduli of the gels swollen in toluene before and after drying. Storage moduli of toluene-swollen gels before (G_1') and after the drying procedure (G_2') as determined by rheology are summarized in **Figure 4. 7**. The gels are again prepared in toluene, dried at room temperature for five days, and subsequently reswollen in toluene.

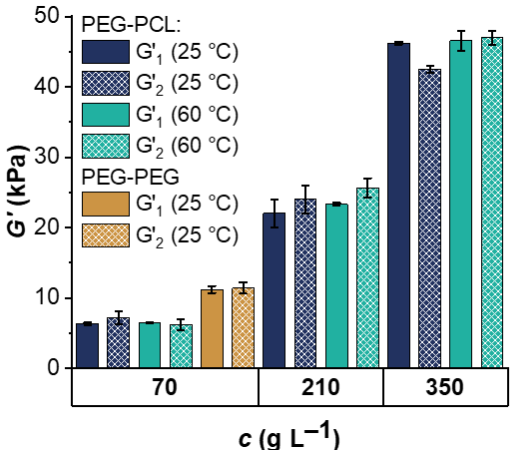

Figure 4. 7: Rheology measurements in toluene: Storage modulus of PEG-PCL (dark blue: synthesis at 25 °C; and cyan: synthesis at 60 °C) and PEG-PEG networks (gold: synthesis at 25 °C) at swelling equilibrium in toluene before drying, G_1' (plane bars), and after drying for five days at room temperature, G_2' (hatched bars).

For both PEG-PCL and PEG-PEG networks, the storage moduli after the drying are slightly higher, but within the margin of the error. This is in accord with the previous findings for the swelling degree, which were also not significantly influenced by the chosen drying procedure. Again, the values are independent of the chosen preparation temperature. Therefore, we conclude that this moderate drying procedure does not lead to a distinct increase in conversion due to the slow drying and is suitable for the transfer from non-selective to selective solvent.

Furthermore, it is obvious from **Figure 4. 7** that the PEG-PEG gels show a higher storage modulus compared to the PEG-PCL ones prepared at the same concentration. This is reasonable, as we observed lower swelling degrees of the PEG-PEG gels in toluene (compare **Figure 4. 3**).

Non-selective solvent

In a second step, the storage moduli and scaling behavior of PEG-PCL and PEG-PEG gels are discussed. The gels are prepared in toluene, subsequently swollen to equilibrium and investigated via shear rheology and AFM.

From shear rheology, the shear storage modulus G' as well as the shear loss modulus G'' are received directly on a macroscopic length-scale. Whereas in AFM, the elastic modulus E is obtained by static indentation measurements. As our networks are essentially elastic, we assume for the elastic storage modulus $E' \approx E$. Colloidal probes (µm-sized) are used to obtain elastic information on a larger scale, while nanoindentation with a sharp AFM-tip is performed to obtain information on very small length-scales. Respective histograms of the received elastic moduli in both types of solvent are included in **Figure A.4. 4**.

Comparison of both methods is feasible by converting the elastic storage modulus E' to shear storage modulus G' using the relation $G' = \frac{E'}{2(1+\mu)}$ with the Poisson ratio μ.[23, 27] According to literature, a Poisson ratio of μ = 0.5 applies to incompressible materials, whereas Poisson ratios down to μ = 0.25 are found for materials under deformation and in contact with excess solvent, which are also described in theoretical work.[36, 37, 38] In contrast, an increase in Poisson ratio was found for networks in contact with air under deformation (μ > 0.5).[36] For swollen gels, values between these extremes, namely 0.25 < μ < 0.5, are found.[38, 39] For t-PEG gels, however, it was found for biaxial deformation that the Poisson ratio is well approximated with μ = 0.5,[40] which was also stated in other work comparing Young's modulus with shear modulus.[41] Furthermore, using μ = 0.5 or μ = 0.25 to convert the elastic modulus to shear modulus results in a factor of 1.2 lower or higher values, respectively. This factor is within the margin of error of the transformed AFM results (see **Table A.4. 4**). Therefore, and for consistency with the AFM evaluation (see *Experimental Section*), μ = 0.5 is used.

Table 4. 1 summarizes the shear modulus of toluene-swollen and non-dried PEG-PCL gels received by rheology and converted from AFM measurements with a Poisson's ratio of 0.5 for measurements with tip (tip radius ≈ 8 nm) and colloidal probes with a radius of 3.3 µm (CP33).

Table 4. 1: Storage modulus of PEG-PCL networks swollen in toluene converted with a Poisson's ratio of μ = 0.5 from AFM measurements with tip (radius ≈ 8 nm) and colloidal probe (CP33: radius 3.3 μm) as well as storage modulus directly from rheological measurements. The error of the converted modulus corresponds to the percentage error of the original data.

c [1] ($g \cdot L^{-1}$)	G_1' (kPa) from AFM		G_1'(kPa) from rheology	
	Tip [2]	CP33 [2]	25 °C [3]	60 °C [3]
70	9 ± 3	8 ± 1	6.3 ± 0.2	6.5 ± 0.1
140	25 ± 4	15 ± 3	13.91 ± 0.09	15.3 ± 0.2
210	31 ± 16	20 ± 6	22 ± 2	23.3 ± 0.2
280	43 ± 20	25 ± 7	34 ± 1	34.9 ± 0.3
350	79 ± 14	35 ± 7	46.2 ± 0.2	47 ± 1

[1] Concentration at preparation; [2] Synthesis at 60 °C; [3] Synthesis temperature.

Both the microscopic and macroscopic derived shear moduli are approximately equal for the PEG-PCL networks swollen in toluene (see also **Figure 4. 8**). The values obtained with the sharp tip are shifted to slightly higher values compared to the colloidal probes and the rheology measurements, especially at high initial polymer concentration. This shift could be due to the fact that the tip geometry of the manufacturer is not exactly known and may also vary among the individual tips. To clarify this, studying the exact tip shapes via electron microscopy would be necessary. In addition, evaporation of the solvent may have occurred during the changing of the tips and sample handling, which in turn leads to harder networks. Finally, the networks are not completely ideal regarding their connectivity, as shown in earlier studies by MQ-NMR[19] which may influence the modulus on these small length-scales. The overall agreement between AFM for both indenter geometries and rheology is somewhat expected since the networks are swollen in a co-solvent for both polymer types and the surface topography does not reveal any underlying structure. Consequently, the results substantiate the picture of a homogeneous swollen network.

In analogy to the swelling degree in the previous section, the storage modulus follows an apparent scaling law $G_1' \sim \phi_0^{-\alpha}$ as a function of initial polymer volume fraction. **Figure 4. 8** shows the storage modulus, G_1', of the PEG-PCL networks included in **Table 4. 1** in toluene as a function of concentration at network preparation.

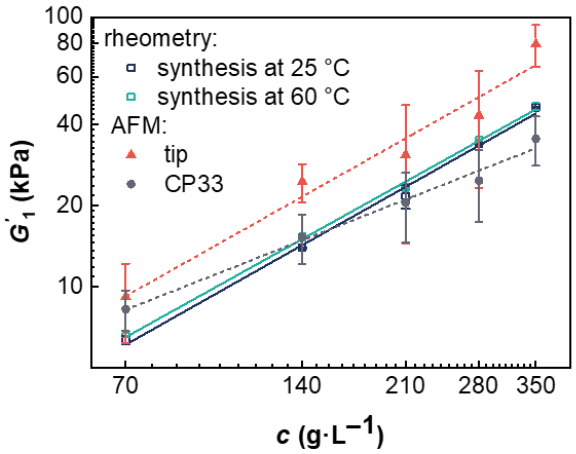

Figure 4. 8: Storage modulus from AFM (full symbols) and rheology (open symbols) of PEG-PCL networks swollen in toluene. Rheology measurements were conducted on gels synthesized at 25 °C (dark blue) and 60 °C (cyan). AFM measurements were performed on gels synthesized at 60 °C using a sharp tip (red triangles) or colloidal probe CP33 (grey circles).

The storage moduli obtained from rheology show exponents of 1.23 ± 0.05 and 1.21 ± 0.03 for the networks prepared at 25 °C and 60 °C, respectively. The modulus converted from AFM measurements with tip follows an analogue scaling with an exponent of 1.2 ± 0.1. The results with colloidal probes scale with a nearly linear exponent of 0.86 ± 0.06. Small deviations between the methodologies are to be expected since delamination of network gel films on a macroscopic scale occurred during AFM measurements. Evaporation of solvent during sample handling contributes to sample inhomogeneities. To counteract delamination, gel films were immobilized on silicon substrates as described previously,[22] however, after some time, sample deformation still occurred and complicated the measurements independent of indenter geometry. A similar log–log slope of roughly 1.3 was found in related work on t-PEG gels in the preparation state based on precursors of 10 kg mol^{-1} [21, 42] as well as in biaxial deformation of t-PEG gels based on 20 kg mol^{-1} precursors.[40] Additionally, the scaling with an exponent of 1.22 ± 0.05 was found for the PEG-PCL networks in toluene in the preparation state.[19] The exponent higher than 1 can be attributed to the following reasons: The conversion at low concentrations is somewhat lower than at high concentrations. At higher concentrations, there are fewer connectivity defects, especially double links, which reduce the modulus, and above the overlap concentration, additional effects due to entanglements may play a role.

The PEG-PEG networks, instead, show a shallower and nearly linear scaling with an exponent of 0.94 ± 0.08 (see **Figure 4. 9a**, absolute values of modulus in **Table 4. 4**). Nevertheless, the scaling with an exponent near one in case of the PEG-PEG networks is also reasonable as the modulus is proportional to the concentration of the elastically active network strands which in turn is proportional to polymer concentration. The different scaling due to the change from amphiphilic to hydrophilic networks might be attributed to a change in the factors named above. Furthermore, a higher fraction of single links was found for pure PEG-PEG networks, than for PEG-PCL networks at the overlap concentration, i.e., fewer defects result in a higher modulus.[19] Likewise, the t-PEG-Ox macromonomers show a different conformation and expansion in toluene during synthesis than their PCL analogues, which may influence the resulting gel structure. Similarly, the onset of entanglements may shift and influence the modulus. Which one of the mentioned effects is finally responsible for the shift in scaling cannot be explained yet.

In summary, it was shown that absolute numbers of modulus in toluene are comparable for rheology and AFM measurements on bulk films. The modulus in this work is three times higher compared with the modulus in the preparation state of Bunk et al.,[19] despite measurement at equilibrium swelling. This is attributed to the significantly longer reaction time in this work and the resulting higher conversion, since the same scaling is seen in both cases.

To consider the efficiency of crosslinking, the number density of elastically active network strands ν is caluclated from the experimental results, ν_{exp}, and compared to the theoretical, ideally achievable value, ν_{theo}. The experimental number density of elastically active network strands can be calculated from modulus data $\nu_{\mathrm{exp}} = \frac{G'}{0.5RT}$ and the theoretical value can be calculated from the polymer concentration at network formation under consideration of the decrease in concentration due to swelling.[18, 23, 43] The resulting number densities for both network types (synthesis at 25 °C) based on the rheological measurements are summarized in **Table 4. 2**. The values received from the AFM measurements are included in **Table A.4. 5** as they show qualitatively the same trend and are in the same order of magnitude. Furthermore, in AFM, the swelling of the gels is affected by the attachment of the networks to the silicon substrate, i.e., the concentration decrease cannot be determined accurately for calculation of the theoretical expected value. Therefore, the same theoretical values included in **Table 4. 2** were taken as a reference for the AFM results in **Table A.4. 5**.

Table 4. 2: Comparison of experimentally found and theoretically calculated elastically effect chains, ν_{exp} and ν_{theo}, based on the phantom network model prediction for PEG-PCL and PEG-PEG networks in toluene at 25 °C.

	PEG-PCL			**PEG-PEG**		
c (g ·L^{-1})	ν_{exp} (mmol·L^{-1})	ν_{theo} (mmol·L^{-1})	ν_{exp}/ν_{theo}	ν_{exp} (mmol·L^{-1})	ν_{theo} (mmol·L^{-1})	ν_{exp}/ν_{theo}
70	5.1	12.2	0.4	9.0	15.4	0.6
140	11.2	18.0	0.6			
210	17.5	22.9	0.8	22.8	27.7	0.8
280	27.4	27.4	1.0			
350	37.3	30.8	1.2	42.0	37.9	1.1

Table 4. 2 illustrates, that the crosslinking efficiency increases with concentration and reaches the maximal efficiency at four times the overlap concentration (280 g L^{-1}). This is in line with MQ-NMR studies[19] of the connectivities of such networks, revealing that the fraction of single links increases with increasing concentration, while higher order connectivities and defects decrease. The PEG-PEG networks show a slightly higher crosslinking efficiency at low concentrations compared to the PEG-PCL networks, which is also expected based on the aforementioned investigations. The ratio higher than one at 350 g L^{-1} could be the result of occurring entanglements and an accompanying increase in modulus. A further check for plausibility of the results is performed later on by comparison with the modulus from the phantom network model.

Selective Solvent

Investigation of the mechanical properties in the selective solvent water are of special interest, due to possible applications in this medium. All samples presented in this chapter are prepared in toluene, dried according to the drying procedure described above and reswollen in water to equilibrium. **Table 4.3** summarizes the shear moduli of PEG-PCL networks in water from rheology and those calculated from AFM measurements with a Poisson ratio of 0.5. The total values are 7–10 times higher compared to toluene, which is a result of the lower swelling degree due to the collapse of the hydrophobic PCL parts of the network. The total values are of the same order of magnitude for both methods, AFM and rheology, and independent of the indenter geometry used in AFM and the preparation temperatures of the networks. The error of the AFM data is significantly larger due to the rough surface and the macroscopic distortion of the sample that occurred specifically after drying and reswelling of the sample. Sample distortion is not so

critical in rheology because small discs are measured and a plate-plate geometry is used, which automatically flattened the gels to fit in the gap. In the AFM measurements, however, the distortion is on the length-scale investigated. This effect becomes more severe the higher the concentration. Therefore, measurements of 280 g L^{-1} and 350 g L^{-1} is not possible using the AFM methodology. Additionally, the fit of the force-distance-curves is dependent on the fit-depth, indicating non-Hertzian elastic behavior of the gel film in water. All force distance curves are fitted to an indentation depth of 100 nm to obtain comparable results throughout all experiments. We attribute this non-Hertzian elastic behavior to the microphase-separated surface structure of dense PCL clusters composed of several tens of PCL star polymers surrounded by expanded PEG polymers.[25]

Table 4. 3: Storage modulus of PEG-PCL networks swollen in water from AFM measurements with tip (radius ≈ 8 nm) and colloidal probe (CP33: 3.3 µm) converted with a Poisson's ratio of µ = 0.5 as well as storage modulus directly from rheological measurements. The error of the converted modulus corresponds to the percentage error of the original data.

c [1] (g ·L^{-1})	G_2' (kPa) from AFM		G_2' (kPa) from rheology	
	tip	CP33	25 °C [2]	60 °C [2]
70	77 ± 17	63 ± 14	67.5 ± 0.5	65 ± 2
140	106 ± 27	119 ± 22	143 ± 3	137 ± 3
210	176 ± 70	164 ± 28	181 ± 5	186 ± 8
280	–	–	248 ± 8	230 ± 10
350	–	–	290 ± 10	299 ± 3

[1] Concentration at preparation; [2] Synthesis temperature.

Due to the found microphase-separated structure in water (see **Figure 4. 4**), differences in local modulus from AFM and macroscopic modulus in rheology would have been expected, as especially the AFM tip size is a similar size regime as the observed domains at the surface. This expected differences in water cannot be found in the experiment. This might be due to the circumstance that the AFM nanoindenter tip with a curvature radius of roughly 8 nm may not be sharp enough to properly observe local differences in modulus. Also, we assume that the indentation process (with an indentation depth of more than 100 nm) occurs by pushing hard PCL spheres through a soft, swollen PEG network. This process is independent of the precise starting point. In both cases, a rather averaged modulus is measured.

In analogy to the storage modulus in toluene, an apparent scaling law of modulus with polymer volume fraction $G_2' \sim \phi_0^{-\beta}$ can be observed. **Figure 4. 9** shows this dependency at swelling equilibrium in water as a function of concentration at network preparation for both PEG-PEG (a) and PEG-PCL (b) networks.

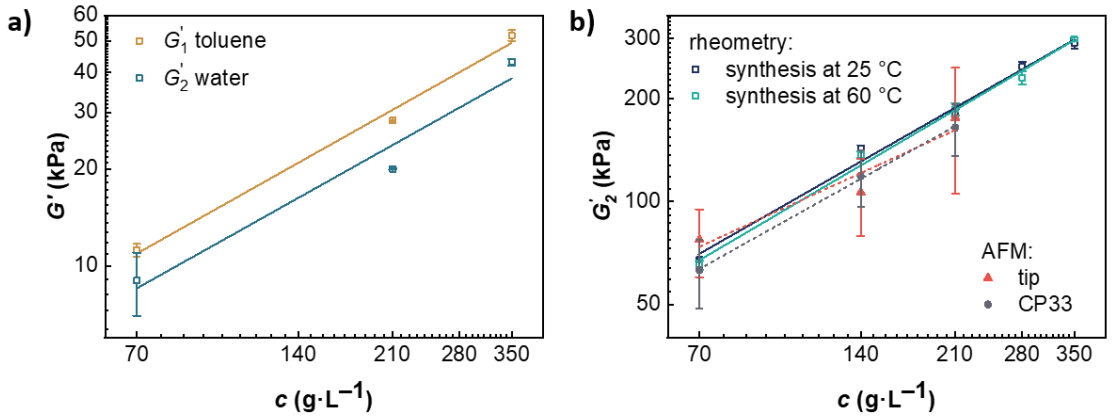

Figure 4. 9: Storage modulus at equilibrium swelling obtained by rheology (open symbols) and converted from AFM (full symbols) **a**: PEG-PEG gels in toluene (gold) and water (light blue) synthesized at 25 °C. **b**: PEG-PCL gels in water obtained by AFM with tip (red triangles) and colloidal probe (grey circles) for a synthesis temperature of 60 °C and by rheology (open rectangles) for synthesis temperatures of 25 °C (dark blue) and 60 °C (cyan).

The exponent is found to be 0.90 ± 0.05 and 0.92 ± 0.04 for PEG-PCL networks prepared at 25 °C and 60 °C studied by rheology. An analogue scaling with exponents of 0.7 ± 0.2 and 0.88 ± 0.03 is found for the samples studied by AFM with tip and colloidal probe. The scaling is nearly linear, which is reasonable as the modulus is proportional to the effective elastically active network strands, which are in turn proportional to the polymer concentration. Due to the concentration-independent swelling degree of 3 in water, the polymer concentration decreases by about one third at each concentration due to swelling. However, since this is the same for all concentrations, the increase in concentration is still linear. Therefore, the concentration of the effective elastically active network strands also increases linearly and thus also the modulus.

The PEG-PEG networks also show a comparable scaling with an exponent of 0.9 ± 0.2, which is in accord with the exponent in toluene of 0.94 ± 0.08 and again nearly linear (absolute values of modulus are included in **Table 4. 4**). This is reasonable, as both solvents are non-selective solvents for PEG and a similar scaling is to be expected.

Comparison with phantom model and mesh size estimation

To compare our results with theory, we relate them to the expectation from the phantom network model. The phantom modulus in the investigated systems can be described as follows[19, 23, 27, 44]

$$G_{\mathrm{ph}} \approx \phi_0 \left(1 - \frac{2}{f}\right) \frac{\rho RT}{M_{\mathrm{el}}} \qquad (1)$$

This yields $G_{\mathrm{ph}}/\phi_0 \approx 253.5$ kPa for PEG-PCL and $GG_{\mathrm{ph}}/\phi_0 \approx 240.4$ kPa for PEG-PEG with a functionality f = 4, the density of the dry network being ρ =1.13 g mL^{-1} [45] on average, the universal gas constant R, the temperature T = 298.15 K, and the molar mass per network strand of $M_{\mathrm{el}} \approx 5.5$ kg mol^{-1} in case of the PEG-PCL networks and $M_{\mathrm{el}} \approx 5.8$ kg mol^{-1} in case of PEG-PEG networks, respectively. With the respective polymer volume fractions at preparation ϕ_0, the expected modulus can be estimated as $G_{\mathrm{ph}} \approx \phi_0 \cdot 253.5$ kPa or respectively $G_{\mathrm{ph}} \approx \phi_0 \cdot 240.4$ kPa. The resulting moduli are summarized in **Table 4. 4**. We again use the rheology data for comparison as the corresponding errors are small compared to the AFM results. The comparison with the experimentally determined values in **Table 4. 1** shows that the phantom modulus is always higher than the experimental value. This can be explained by the assumptions of the model system, in which ideal crosslinking of the polymers is presupposed. However, this is not the case for the present systems due to a non-negligible amount of double links and other connectivity defects, as shown in previous work.[19] The discrepancy between phantom modulus and experimental modulus decreases for the PEG-PCL systems with increasing concentration, which can be attributed to the stronger dependence of modulus on polymer volume fraction than the linear dependency predicted by the phantom network model. This is due to the fact that at low concentrations there is lower conversion and a higher fraction of connectivity defects, whereas at high concentrations there is more ideal crosslinking with less connectivity defects. Additionally, at high concentrations, entanglements can further increase the modulus. The ratio of phantom to experimental modulus for the PEG-PEG networks in both solvents is lower compared with the PEG-PCL networks and does not decrease with concentration but is rather constant. Here, the scaling with modulus was nearly linear as applied in the phantom model prediction. The lower ratio can be attributed to the slightly higher fraction of single links in these type of networks compared to their amphiphilic analogues and the resulting more ideal network structure.[19]

Table 4. 4: Calculated phantom modulus, G_{ph}, of PEG-PCL and PEG-PEG networks as well as the experimentally received modulus, G_{exp}, of the PEG-PEG networks in water and toluene. The ratio of phantom modulus and experimentally obtained modulus was calculated for the networks prepared at 25 °C. The index "tol" represents toluene and the index "water" represents water.

c [1] ($\mathrm{g \cdot L^{-1}}$)	PEG-PCL		PEG-PEG				
	G_{ph} (kPa)	$G_{\mathrm{ph}}/G_{\mathrm{exp}}^{\mathrm{tol}}$	G_{ph} (kPa)	$G_{\mathrm{exp}}^{\mathrm{tol}}$ (kPa)	$G_{\mathrm{ph}}/G_{\mathrm{exp}}^{\mathrm{tol}}$	$G_{\mathrm{exp}}^{\mathrm{water}}$ (kPa)	$G_{\mathrm{ph}}/G_{\mathrm{exp}}^{\mathrm{water}}$
70	15.2	2.4	14.4	11.2 ± 0.5	1.3	9 ± 2	1.6
140	30.4	2.2	28.9				
210	45.6	2.1	43.3	28.3 ± 0.1	1.5	20.03 ± 0.09	2.2
280	60.8	1.8	57.7				
350	76.1	1.7	72.1	52 ± 2	1.4	43 ± 1	1.7

[1] Concentration at preparation.

Overall, the experimentally found values are a factor of maximum 2.4 below the expectation from the phantom network model. This is within reasonable limits, since the networks do not resemble the ideally connected network assumed in the model due to connectivity defects. Furthermore, the experimental system might behave differently compared to the assumptions in the phantom model. Likewise, this is an improvement compared with previous data of PEG-PCL networks in the preparation state[19] and related work based on t-PEG and t-PVDF[18] which reported values a factor of 4 and a factor of 3 below the phantom model expectation, respectively.

Finally, to get an idea about the permeability of the networks for possible guest substances, the mesh size ξ of the networks in the respective solvents can be estimated at T = 298.15 K from the plateau modulus G_{p} in rheology, which corresponds to the experimental found storage modulus G', and the Avogadro-constant N_{A} as follows[27, 46]

$$\xi = \left(\frac{RT}{G' N_A}\right)^{1/3} \tag{2}$$

Figure 4. 10 illustrates that the mesh size decreases with increasing concentration and when switching from non-selective solvent toluene to the selective solvent water. Furthermore, the mesh sizes of the amphiphilic PEG-PCL and the hydrophilic PEG-PEG networks show similar values in the non-selective solvents. This is to be expected, due to the same architecture of the

networks, which consist of four-armed star polymers, and the similar molar masses of the building blocks. The trend of the lower swelling of PEG-PEG networks in toluene is also represented here by a slightly lower mesh size.

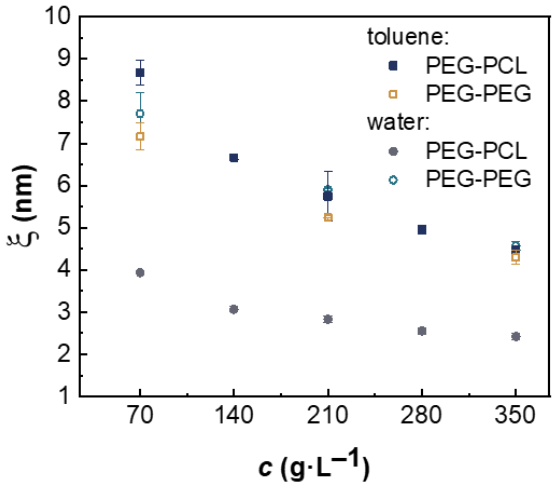

Figure 4. 10: Mesh size as a function of preparation concentration for PEG-PCL (full symbols) and PEG-PEG (open symbols) networks prepared at 25 °C in toluene (dark blue, gold) and water (grey and light blue).

From a complementary study on the same polymeric system, the mesh size can be roughly estimated from the correlation length in SAXS at the overlap concentration in d_8-toluene, resulting in 4.9 nm and 4.7 nm for PEG-PCL and PEG-PEG networks, respectively.[25] This is consistent with the trend of smaller mesh size of the PEG-PEG networks compared with the PEG-PCL networks obtained in this work. In addition, the values are in the same order of magnitude, despite different methodologies being used.

4.7. Conclusion

In this study, amphiphilic polymer co-networks are prepared by hetero-complementary crosslinking of oxazinone-terminated t-PCL and amino-terminated t-PEG and investigated regarding their environmental sensitive mechanics by AFM and shear rheology. In addition, they are compared to pure hydrophilic PEG-PEG networks with the same crosslinking chemistry.

As expected, the gelation reaction becomes faster with increasing concentration and temperature. However, the gel points are shifted to longer timescales compared to previous NMR results in d_8-tetrahydrofuran[19] which is attributed to slower kinetics in toluene and the rheology result as an upper estimate of the gel point.

The equilibrium swelling in the non-selective solvent reveals a concentration dependent swelling degree which follows an apparent scaling law in accord with previous findings and mean field model predictions. [19, 20, 24] In contrast, the swelling in the selective solvent is constant at a swelling degree of 3, due to a balance in the opposing swelling and shrinking tendencies of the 50:50 mixture of hydrophilic and hydrophobic building blocks. For solvent exchange, a gentle drying procedure at room temperature turns out to be suitable.

The modulus of gels is demonstrated at different length scales by AFM and rheology, interestingly, showing moduli in the same order of magnitude. This substantiates the picture of homogeneously swollen gels in the non-selective solvent and is further supported by the homogeneous surface structure observed with AFM measurements. For the selective solvent, however, this finding is rather unexpected, since a spherical nano-phase separation can be observed at the surface. Further investigations need to be performed to clarify the role of indenter size and geometry on nanomechanical properties as well as the mechanism by which hard PCL spheres are pushed through the swollen PEG network.

An apparent scaling law of modulus with polymer volume fraction is found. The scaling of the PEG-PCL networks is in accord with previous findings of such networks in a good solvent.[19, 21, 40, 42] However, in water, the scaling is rather linear due to the concentration independent swelling. Such a nearly linear scaling is also found for the PEG-PEG networks in both solvents together with similar mechanical properties.

With this, we demonstrate the precise control of synthesis conditions leading to homogeneous gel networks with defined mechanical properties. This marks a further step towards rationally understanding the interplay between synthesis conditions, the resulting structure and corresponding properties and using this knowledge for the targeted design of functional materials.

4.8. Experimental

Materials

Toluene (≥ 99.5%) was purchased from Fisher Chemical. Milli-Q water was produced in an in-house Milli-Q-system from Merck.

Synthesis of amino-terminated tetra-poly(ethylene glycol) (t-PEG-NH_2) and 2-(4-Nitrophenyl)-benzoxazinone-terminated tetra-poly(ε-caprolactone) (t-PCL-Ox)

The synthesis procedure of the tetra-arm star polymers was developed and described by Bunk et al.[19] In general, t-PEG-NH_2 is prepared from t-PEG-OH in a two step synthesis. First, the mesylate-terminated t-PEG is formed using triethylamine and mesylchloride, which is then converted into the amine-terminated PEG with ammonia. The product is characterized by a narrow molar mass distribution (Đ = 1.02 –1.05) and a molar mass of about 10.8 ± 0.2 kg mol^{-1}. t-PCL-Ox is again synthesized in two steps: First, t-PCL-OH is prepared in a ring opening polymerization starting from pentaerythritol. Esterification of t-PCL-OH with 2-(4-Nitrophenyl)-4-oxo-4H-benzo[d][1,3]oxazine-7-carboxylic acid chloride, yields t-PCL-Ox with an oxazinone terminal group as coupling agent. This product in turn is characterized by a narrow molar mass distribution (Đ = 1.07–1.09) and a molar mass of about 11.3 ± 0.2 kg mol^{-1}.

Preparation, drying and swelling of amphiphilic co-networks for rheology

Stock solutions of t-PEG-NH_2 and t-PCL-Ox at the respective concentrations were prepared in toluene and mixed in equimolar ratio related to the reactive terminal groups. We used concentrations ranging from 70–350 g L^{-1}, corresponding roughly to one to five times the overlap concentration c^*. The mixture was homogenized, poured into a teflon mold, sealed with a plug, and allowed to react at a constant temperature of 25 °C or 60 °C for 3 days. The reaction of t-PEG-NH_2 with t-PCL-Ox takes place according to **Figure 4. 1**. The resulting gels were detached from the mold and put into an excess of toluene for two days to reach the swelling equilibrium. The swollen networks were weighed directly after the swelling procedure to determine the equilibrium volume swelling degree Q as follows

$$Q = 1 + \left(\frac{\rho_p}{\rho_s}\right)\left(\frac{w_s}{w_p}\right)$$

Here, ρ_p and ρ_s are the density of the polymer and the solvent used, w_p is the weight of the polymer, i.e., the dry network, and w_s is the weight of the solvent, i.e. the difference of swollen to dried weight. The average density of PEG and PCL is 1.13 g mL^{-1}.[45]

Unless stated otherwise, solvent exchange to a new solvent was carried out via the dry state. For this purpose, the gels were dried at 25 °C at normal pressure for five days to remove the solvent. Subsequently, they were swollen in an excess of the respective new solvent for two days to reach swelling equilibrium.

Preparation of PEG-PEG networks

Stock solutions of t-PEG-NH_2 and t-PEG-Ox at 70 g L^{-1}, 210 g L^{-1}, and 350 g L^{-1} were prepared in toluene and mixed in equimolar ratio related to the reactive terminal groups. The preparation, swelling, and drying procedure is described in detail above. All PEG-PEG networks were prepared at 25 °C. t-PEG-Ox with a molar mass of about 12.5 ± 0.2 kg mol^{-1} was prepared starting from t-PEG-OH according to the procedure described above for synthesis of t-PCL-Ox.

Rheology

Rheological measurements were carried out with an Anton Paar modular compact rheometer of type MCR302 (Anton Paar, Graz, Austria) equipped with a plate–plate geometry of type PP25 or PP08 with a plate diameter of 25 mm or 8 mm, respectively. A Peltier plate was used to control the temperature and a solvent trap was utilized to prevent solvent evaporation. The time sweeps for gel point determination were conducted at a constant frequency of ω = 6 rad s^{-1} and a deformation amplitude of γ = 1%. Frequency sweeps were carried out at a shear deformation of γ = 0.2% and in the range of ω = 0.1–100 rad s^{-1}.

Viscometry

The intrinsic viscosity [η] of t-PEG-NH_2 in Milli-Q water at 25 °C was determined using an Micro-Ubbelohde Viscometer of Type 537 10/I and the Schulz-Blaschke extrapolation method.[24] The overlap concentration c^* was calculated from the intrinsic viscosity as $c^* = 1/[\eta]$ adapting the same convention as for linear polymers.[47]

Preparation of APCN gel films for atomic force microscopy

Additionally, gel samples were prepared for AFM characterization by adding 100 µL of equimolar PEG-PCL polymer mixtures onto amino-functionalized silicon wafers (1x1 cm) (Siegert Wafer, Aachen, Germany), for each concentration respectively, resulting in the formation of a gel film. As described previously,[22] APCN gel films were immobilized on the silicon targets which mostly prevents detachment of the sample during the measurements after

the addition of excess solvent. Samples were kept in an air-tight container with calculated toluene headspace at 60 °C overnight to complete the reaction. After the completion of the reaction, excess toluene was added to each sample to reach equilibrium swelling degree. For measurements in water, samples were exposed to ambient conditions overnight allowing for the evaporation of toluene. Samples were then reswollen in water for one day and kept in excess solvent until measurement.

Atomic Force Microscopy

PEG-PCL gels were characterized with atomic force microscopy (AFM). AFM measurements were carried out at room temperature on the MFP3D SA and Cypher (Asylum Research/Oxford Instruments, Wiesbaden, Germany). All measurements were performed in a closed environment with samples in excess solvent and sufficient solvent headspace to prevent solvent evaporation during the measurements. Surface topographies of PEG-PCL gel films were obtained in tapping mode using the cantilevers AC240TSA (70 kHz, 2 N m^{-1}, 7 nm tip radius) or BL-AC40TSA (110 kHz, 0.09 N m^{-1}, 8 nm tip radius) (Oxford, Instruments, Wiesbaden, Germany). Additionally, static indentation measurements were carried out to obtain information about the elastic behavior of gel networks. To investigate different length-scales, cantilevers of different geometries were used. For small scale measurements, the cantilevers CSC38/No Al (10 kHz, 0.03 N m^{-1}) with a tip radius of 8 nm were used. For larger scale measurements, the tipless cantilevers CSC37/tipless/No Al (20 kHz, 0.3 N m^{-1}) and CSC38 tipless/No Al (10 kHz, 0.03 N m^{-1}) with glued and sintered colloidal probes (radius 3.3 μm) were used. All cantilevers used for indentation experiments were fabricated by MikroMasch and purchased from NanoAndMore (Wetzlar, Germany). Elastic moduli were obtained by recording force maps for tip and colloidal probe measurements on random sample locations to obtain average values and their standard deviations. Force curves were fitted up to an indentation depth of 100 nm using the Hertz model, assuming a Poisson ratio of 0.5. All obtained values were extracted from the AFM in-built software features of IGOR 6.38801 (16.05.191, Asylum research, Santa Barbara, CA, USA).

4.9. References

[1] G. Erdodi, J. P. Kennedy, *Progress in Polymer Science*. **2006**, 31, 1; b) C. S. Patrickios, T. K. Georgiou, *Current Opinion in Colloid & Interface Science*. **2003**, 8, 76;

[2] C. S. Patrickios, Ed., Amphiphilic Polymer Co-networks, Cambridge, Royal Society of Chemistry. **2020**.

[3] a) Z. Mutlu, S. Shams Es-Haghi, M. Cakmak, *Advanced healthcare materials*. **2019**, 8, e1801390; b) P. C. Nicolson, J. Vogt, *Biomaterials*. **2001**, 22, 3273;

[4] a) K. Schöller, S. Küpfer, L. Baumann, P. M. Hoyer, D. de Courten, R. M. Rossi, A. Vetushka, M. Wolf, N. Bruns, L. J. Scherer, *Adv. Funct. Mater*. **2014**, 24, 5194; b) J. Tobis, L. Boch, Y. Thomann, J. C. Tiller, *Journal of Membrane Science*. **2011**, 372, 219; c) G. Erdodi, J. P. Kennedy, *J. Polym. Sci. A Polym. Chem*. **2005**, 43, 4965;

[5] P. Grossen, D. Witzigmann, S. Sieber, J. Huwyler, *Journal of controlled release : official journal of the Controlled Release Society*. **2017**, 260, 46.

[6] a) Y.-Y. Liu, Y.-H. Shao, J. Lü, *Biomaterials.* **2006**, 27, 4016; b) L. Bromberg, M. Temchenko, T. A. Hatton, *Langmuir : the ACS journal of surfaces and colloids*. **2002**, 18, 4944; c) M. L. Adams, A. Lavasanifar, G. S. Kwon, *Journal of pharmaceutical sciences*. **2003**, 92, 1343;

[7] G. Lin, L. Cosimbescu, N. J. Karin, A. Gutowska, B. J. Tarasevich, *Journal of materials chemistry. B*. **2013**, 1, 1249.

[8] a) H. Wang, Q. Li, J. Yang, J. Guo, X. Ren, Y. Feng, W. Zhang, *Journal of materials chemistry. B*. **2017**, 5, 1408; b) R. Murphy, D. P. Walsh, C. A. Hamilton, S.-A. Cryan, M. in Het Panhuis, A. Heise, *Biomacromolecules*. **2018**, 19, 2691;

[9] a) F. Perin, A. Motta, D. Maniglio, *Materials science & engineering. C, Materials for biological applications*. **2021**, 123, 111952; b) A. Dabbaghi, A. Ramazani, N. Farshchi, A. Rezaei, A. Bodaghi, S. Rezayati, *Journal of Industrial and Engineering Chemistry*. **2021**, 101, 307; c) M. Shibayama, X. Li, T. Sakai, *Ind. Eng. Chem. Res*. **2018**, 57, 1121;

[10] T. Sakai, T. Matsunaga, Y. Yamamoto, C. Ito, R. Yoshida, S. Suzuki, N. Sasaki, M. Shibayama, U. Chung, *Macromolecules*. **2008**, 41, 5379.

[11] Y. Gu, J. Zhao, J. A. Johnson, *Angewandte Chemie (International ed. in English)*. **2020**, 59, 5022.

[12] M. Shibayama, X. Li, T. Sakai, *Colloid Polym Sci*. **2019**, 297, 1.

[13] F. Lange, K. Schwenke, M. Kurakazu, Y. Akagi, U. Chung, M. Lang, J.-U. Sommer, T. Sakai, K. Saalwächter, *Macromolecules*. **2011**, 44, 9666.

[14] S. Nakagawa, N. Yoshie, *Polym. Chem*. **2022**, 13, 2074.

[15] a) T. Sakai, Y. Akagi, T. Matsunaga, M. Kurakazu, U. Chung, M. Shibayama, *Macromolecular rapid communications*. **2010**, 31, 1954; b) T. Sakai, *Reactive and Functional Polymers.* **2013**, 73, 898;

[16] T. Hiroi, S. Kondo, T. Sakai, E. P. Gilbert, Y.-S. Han, T.-H. Kim, M. Shibayama, *Macromolecules*. **2016**, 49, 4940.

[17] S. Nakagawa, X. Li, M. Shibayama, H. Kamata, T. Sakai, E. P. Gilbert, *Macromolecules*. **2018**, 51, 6645.

[18] D. E. Apostolides, C. S. Patrickios, T. Sakai, M. Guerre, G. Lopez, B. Améduri, V. Ladmiral, M. Simon, M. Gradzielski, D. Clemens, C. Krumm, J. C. Tiller, B. Ernould, J.-F. Gohy, *Macromolecule*s. **2018**, 51, 2476.

[19] C. Bunk, L. Löser, N. Fribiczer, H. Komber, L. Jakisch, R. Scholz, B. Voit, S. Seiffert, K. Saalwächter, M. Lang, F. Böhme, *Macromolecules*. **2022**, 55, 6573.

[20] M. Lang, R. Scholz, L. Löser, C. Bunk, N. Fribiczer, S. Seiffert, F. Böhme, K. Saalwächter, *Macromolecules*. **2022**, 55, 5997.

[21] Y. Akagi, T. Matsunaga, M. Shibayama, U. Chung, T. Sakai, *Macromolecules*. **2010**, 43, 488.

[22] K. Hagmann, C. Bunk, F. Böhme, R. von Klitzing, *Polymers*. **2022**, 14.

[23] S. P. O. Danielsen, H. K. Beech, S. Wang, B. M. El-Zaatari, X. Wang, L. Sapir, T. Ouchi, Z. Wang, P. N. Johnson, Y. Hu, D. J. Lundberg, G. Stoychev, S. L. Craig, J. A. Johnson, J. A. Kalow, B. D. Olsen, M. Rubinstein, *Chemical reviews*. **2021**, 121, 5042.

[24] J. Bastide, C. Picot, S. Candau, *Journal of Macromolecular Science, Part B*. **1981**, 19, 13.

[25] L. Löser, C. Bunk, R. Scholz, M. Lang, F. Böhme, K. Saalwächter, *Macromolecules*, **2024**, 57, 3, 940–954

[26] Y. Mai, A. Eisenberg, *Chemical Society reviews*. **2012**, 41, 5969.

[27] M. Rubinstein, R. H. Colby, *Polymer physics*, 1st edition, Oxford, Oxford Univ. Press. **2003**.

[28] a) F. S. Bates, G. H. Fredrickson, *Annual review of physical chemistry*. **1990**, 41, 525; b) F. S. Bates, G. H. Fredrickson, *Physics Today*. **1999**, 52, 32;

[29] W. Burchard, "Solution Properties of Branched Macromolecules", in *Branched Polymers II.* Springer Berlin Heidelberg, Berlin, Heidelberg. **1999**, p. 113 ff.

[30] E. W. Merrill, K. A. Dennison, C. Sung, *Biomaterials.* **1993**, 14, 1117.

[31] T. Matsunaga, T. Sakai, Y. Akagi, U. Chung, M. Shibayama, *Macromolecules.* **2009**, 42, 6245.

[32] M. Tian, P. Munk, *J Solution Chem*. **1995**, 24, 267.

[33] M. Weissmüller, W. Burchard, *Acta Polym*. **1997**, 48, 571.

[34] K. Shida, K. Ohno, M. Kimura, Y. Kawazoe, Y. Nakamura, *Macromolecules.* **1998**, 31, 2343.

[35] S. Kirinčič, C. Klofutar, *Fluid Phase Equilibria*. **1999**, 155, 311.

[36] R. H. Pritchard, E. M. Terentjev, *Polymer*. **2013**, 54, 6954.

[37] a) R. H. Pritchard, P. Lava, D. Debruyne, E. M. Terentjev, *Soft Matter*. **2013,** 9, 6037; b) A. Konda, K. Urayama, T. Takigawa, *Macromolecules*. **2011**, 44, 3000; c) E. Geissler, A. M. Hecht, *Macromolecules*. **1980**, 13, 1276; d) N. Bouklas, R. Huang, *Soft Matter*. **2012**, 8, 8194;

[38] K. Urayama, T. Takigawa, T. Masuda, *Macromolecules*. **1993**, 26, 3092.

[39] a) J. Yoon, S. Cai, Z. Suo, R. C. Hayward, *Soft Matter*. **2010**, 6, 6004; b) F. Di Lorenzo, J. Hellwig, R. von Klitzing, S. Seiffert, *ACS macro letters*. **2015**, 4, 698;

[40] T. Katashima, K. Urayama, U. Chung, T. Sakai, *Soft Matter*. **2012**, 8, 8217.

[41] T. Matsunaga, T. Sakai, Y. Akagi, U. Chung, M. Shibayama, *Macromolecules*. **2009**, 42, 1344.

[42] T. Sakai, M. Kurakazu, Y. Akagi, M. Shibayama, U. Chung, *Soft Matter*. **2012**, 8, 2730.

[43] B. Lindemann, U. P. Schröder, W. Oppermann, *Macromolecules*. **1997**, 30, 4073.

[44] Y. Akagi, T. Katashima, Y. Katsumoto, K. Fujii, T. Matsunaga, U. Chung, M. Shibayama, T. Sakai, *Macromolecules*. **2011**, 44, 5817.

[45] Chemical Retrieval on the Web (CROW), *Polymer database: Average density of amorphous polymers*.http://polymerdatabase.com/polymer%20physics/Polymer%20Density.html. (accessed: April 2023).

[46] a) P. Nicolella, M. F. Koziol, L. Löser, K. Saalwächter, M. Ahmadi, S. Seiffert, *Soft Matter.* **2022**, 18, 1071; b) J. Wang, V. M. Ugaz, *Electrophoresis.* **2006**, 27, 3349; c) Y. Tsuji, X. Li, M. Shibayama, *Gels (Basel, Switzerland).* **2018**, 4;

[47] G. V. Schulz, F. Blaschke, *J. Prakt. Chem*. **1941**, 158, 130.

5. CHAPTER III: AMPHIPHILIC STAR BLOCK COPOLYMERS

Amphiphilic tetra-PCL-*b*-PEG star block copolymers using benzoxazinone-based linking groups

[redacted] **N. Fribiczer**, [redacted]

Polym. Chem., **2023**,14, 1965-1977, doi: 10.1039/D3PY00078H

The corresponding *Supporting Information* is included in **Appendix A.5**.

The results in this chapter were first published on March 29, 2023 and are adapted with permission from *Polym. Chem.*, 2023, 14, 1965-1977.

5.1. Specific Summary

The first two studies presented in this work give a comprehensive overview of the interplay between synthesis and environmental conditions and the resulting properties of amphiphilic polymer co-networks based on separate hydrophilic and hydrophobic building blocks, namely t-PEG and t-PCL. In general, the properties of such networks are crucially dependent on their structure both in a non-selective and in a selective solvent.

Therefore, amphiphilic block copolymers can be used to pre-structure the networks in order to specifically generate structure and corresponding function. This is of particular interest regarding required transport properties for biomedical applications. Amphiphilic star block copolymers are also in general well-suited for biomedical applications due to their tendency to form self-assembling micelles, vesicles, or gels. Moreover, micelles formed by star polymers show an increased stability compared to their linear counterparts.

To get first insights in the solution behavior of such four-armed amphiphilic star block copolymers, two well-defined copolymers with a poly(ε-caprolactone) (ε-CL) core and PEG arms with different length are prepared by the hetero-complementary linking reaction used in the first two studies. First, hydroxyl terminated PCL is synthesized by a ring opening polymerization, followed by end group esterification with a benzoxazinone coupling agent and attachment of linear amino-terminated PEG to obtain tetra-PCL-*b*-PEG. The study of the solution behavior by DLS in ethyl acetate and dichloromethane, common good solvents for both blocks, identifies single star polymers. In acetone, in contrast, single stars as well as clusters are obtained, the size of which increases with increasing polymer concentration. This is found for both sample types

independent of the PEG block length. In water, however, DLS and TEM measurements reveal that micellar structures with a hydrodynamic radius of about 20 nm are formed in the sample with longer PEG arms. Furthermore, a slow morphology change of spherical micelles to long cylindrical micelles is observed by TEM after one week. In contrast, the star polymer with short PEG arms forms a cloudy suspension in water without the formation of a precipitate, indicating structures in the range of the wavelength of visible light or larger.

A next step in exploring the potential of these amphiphilic block copolymers is to synthesize the copolymers with hetero-complementary end groups and prepare networks by crosslinking. Further studies can then investigate the ability of the pre-structured networks to introduce certain functionality, e.g. the directed transport of guest substances for biomedical applications.

5.2. Author Contributions

[redacted]	Polymer synthesis, synthesis optimization, NMR evaluation, manuscript preparation and correction.
[redacted]	NMR measurement and analysis, and manuscript correction.
[redacted]	DLS analysis, TEM image analysis and interpretation, manuscript preparation and correction.
Nora Fribiczer:	DLS measurement and DLS analysis.
[redacted]	MALDI-TOF MS measurements.
[redacted]	TEM and Cryo-TEM measurement and analysis.
[redacted]	Preparation of alkylester and benzoxazinone substituted pentaerythrit mixtures.
[redacted]	Scientific Supervision of [redacted] and manuscript correction.
[redacted]	Supervision of [redacted] and manuscript correction.
[redacted]	Concept development, scientific supervision of [redacted], and manuscript correction.

5.3. Acknowledgement

This work was performed within the collaborative research project "Adaptive polymer gels with model network structure" (FOR2811), funded by the German Research Foundation (DFG), grant numbers 397384169, 423514254, 423478088 and 423373052. We thank [redacted] for SEC measurements. Differential scanning calorimetry experiments were performed by [redacted] and ATR-FTIR spectroscopy measurements were done by [redacted].

5.4. Abstract

In this study, two well-defined amphiphilic tetra-arm star block copolymers with a poly(ε-caprolactone) (ε-CL) core and poly(ethylene glycol) (PEG) arms with different length (800 g mol^{-1} and 2100 g mol^{-1}) were prepared by a hetero-complementary linking reaction and studied in detail. A pentaerythritol core was used as an initiator for the ring-opening polymerization (ROP) of ε-CL, generating a hydroxy-terminated tetra-arm star polymer (tetra-PCL–OH) with controlled molar mass (M_n ~ 10 kg mol^{-1}) and low dispersity ($Đ$ < 1.1). After end group esterification with 2-(4-nitrophenyl)-4-oxo-4*H*-benzo[*d*][1,3]oxazine-7-carboxylic acid chloride, linear hydrophilic PEG was attached to the respective tetra-PCL to obtain tetra-PCL-*b*-PEG star block copolymers. The behavior of the two amphiphilic block copolymers was studied in water by a combination of variable-temperature ^{1}H NMR spectroscopy, DLS, DSC and TEM measurements. In the case of longer PEG arms, spherical micelles form at elevated temperatures and remain stable at room temperature over days. Transmission electron microscopy indicates a possible slow morphology change of spherical micelles into long cylindrical micelles after one week. Suspensions of the star block copolymers with the short PEG arms in water remain cloudy, in contrast to the star block copolymers with long arms.

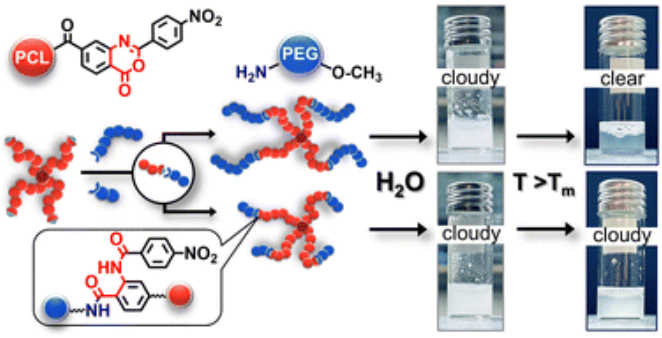

Scheme 5. 1: Schematic representation of the synthesis of tetra-PCL-*b*-PEG star block copolymers and their solution behavior in water.

5.5. Introduction

Star block copolymers consist of chemically distinct polymer segments (AB-type arms or A-type and B-type arms) connected by a central branching point called the core.[1, 2] They represent an attractive class of branched polymers which differ distinctly from their linear analogs in terms of a reduced hydrodynamic volume, lower dispersity ($Đ$), and high functionality with the same synthesis strategy, molar mass and composition.[2–5] There are two main strategies for producing this type of polymer: "arm-first" and "core-first" where either the block-copolymer arms or the central homopolymer star are synthesized first. For the latter strategy, one considers in general that the second block of the arms is polymerized in a subsequent step, while the "grafting-onto" variant of the core-first strategy describes the subsequent attachment of independently functionalized and synthesized polymers, *e.g.* by "click" chemistry or Steglich esterification.[2, 6–10] This last approach allows designing star block copolymers with the highest structural control. Star block copolymers with both hydrophilic and hydrophobic components, such as poly(ethylene glycol) (PEG), the most widely used biocompatible polymer for biological applications, and poly(ε-caprolactone) (PCL), a biodegradable and non-toxic industrial polyester, have proven to be useful materials for biomedical applications.[11–14] This is due to the amphiphilic nature of PCL-*b*-PEG copolymers, manifested in their tendency to form self-assembling micelles, vesicles, or gels.[3, 15–21]

Micelles prepared from PCL-*b*-PEG star block copolymers were frequently studied (see **Table A.5. 3**), since the micelle stability of stars is increased over their linear counterparts.[3, 16] As shown in **Table A.5. 3**, all strategies have been used to prepare a broad variety of star polymers with different cores and functionalities providing molar masses from 10 kg mol^{-1} to beyond 200 kg mol^{-1}. High molecular weight stars with PCL as the outer block ("tail") first form micelles and then may gel upon increasing polymer volume fraction in water,[16] while stars with PEG tails do not gel upon micro-phase separation in water. A crucial point of these materials is that both polymers crystallize at similar temperatures, such that structure formation may depend on solvent quality or additional details of the sample preparation.[22] This difficulty is partially visible in the micellization data summarized in SI **Tables A.5. 3** and **A.5. 4** where significant changes in micelle size or critical micelle concentration were observed for copolymers of similar architecture, molar mass and composition. Our interest in tetra-PCL-*b*-PEG micelles stems from investigations on model amphiphilic conetworks based on tetra-arm PEG and PCL star polymers.[23–25] Here, soluble amphiphilic star block copolymers containing the same building blocks are needed to structure the material prior to network formation.

In the present work, such star block copolymers were synthesized in a similar manner as the co-networks by grafting amino-terminated linear PEGs of different molar mass onto benzoxazinone-terminated tetra-arm PCL (see **Scheme 5. 2**). By using the bi-functional benzoxazinone-based coupling agent **2**, which reacts hetero-complementarily with hydroxy and amino groups under mild conditions without any by-products,[26–28] uniform star block copolymers can be prepared. Particular attention was paid to the defined structure of the tetra-PCL–OH core **1**, its quantitative benzoxazinone functionalization (**3**), and their subsequent complete reaction with amino-terminated PEG **5** to form uniform tetra-PCL-*b*-PEG star block copolymers **6**. Furthermore, the influence of PEG chain length on the behavior of the star block copolymers in aqueous medium and on the formation and stability of micellar structures was studied in detail.

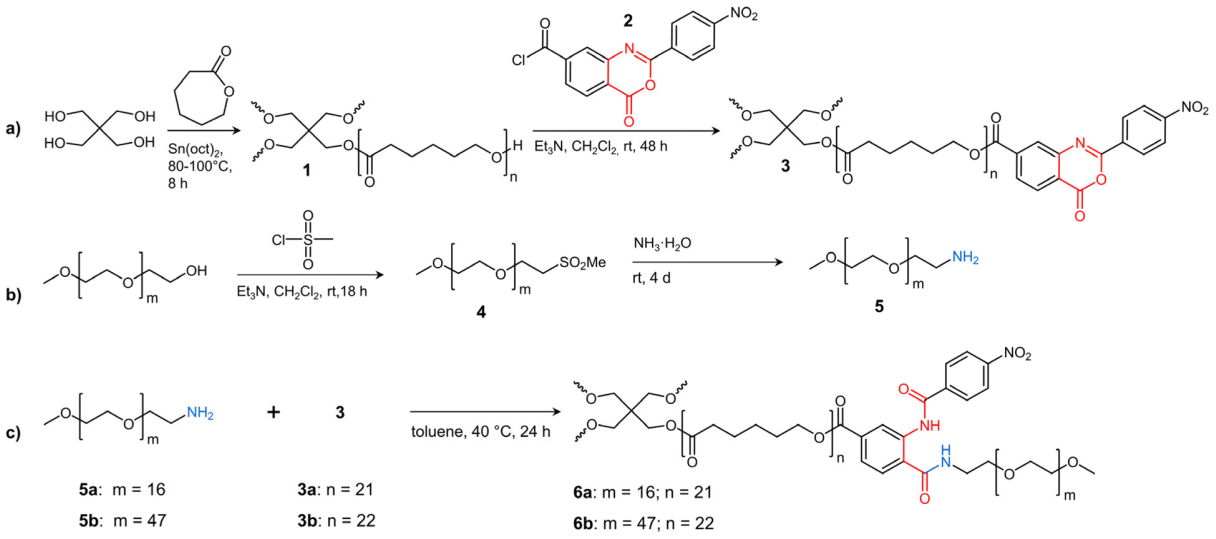

Scheme 5. 2: Synthesis of **(a)** 2-(4-nitrophenyl)-benzoxazinone-terminated tetra-PCL star polymer **3**, **(b)** MeO–PEG–NH_2 **5**, and **(c)** amphiphilic tetra-PCL-*b*-PEG star block copolymer **6**.

5.6. Experimental Section

Materials

All chemicals and solvents (analytical grade) were obtained from Sigma-Aldrich and used as received unless otherwise specified. Methoxy poly(ethylene glycol) (MeO–PEG–OH) (M_n = 2100 g mol^{-1}) was obtained from JenKem Technology (USA) and precipitated twice from THF in cold diethyl ether. Mono-amino-terminated MeO–PEG (MeO–PEG–NH_2, **5a**, M_n = 822 g mol^{-1}) was obtained from Iris Biotech (Germany). ε-Caprolactone (ε-CL) was dried under reduced pressure over CaH_2 for at least 12 hours, then purified by vacuum distillation and stored under nitrogen atmosphere. Tin(ii)-2-ethylhexanoate ($Sn(oct)_2$) was purified by vacuum distillation and stored under nitrogen atmosphere. 2-(4-Nitrophenyl)-4-oxo-4*H*-benzo[*d*][1,3]oxazine-7-carboxylic acid chloride **2** was synthesized as described earlier.[27–29]

Synthetic procedures

Tetra-PCL–OH (1)

Following Jakisch et al., two batches (**a**, **b**) of **1** were prepared by bulk polymerization of ε-CL with pentaerythritol as initiator using $Sn(oct)_2$ as catalyst.[26] The target M_n of 10 kg mol^{-1} was adjusted by the ε-CL : $Sn(oct)_2$: pentaerythritol molar ratio of 87 : 0.1 : 1. The synthesis was carried out as follows: first, 136 mg of pentaerythritol and 9.92 g of ε-CL were added to a Schlenk flask at room temperature under nitrogen. The dispersion was stirred at 120 °C for 30 min to obtain a homogeneous mixture. The reaction mixture was cooled to 80 °C and the polymerization was started by injecting the catalyst ($Sn(oct)_2$, 0.2 mL of 0.5 M dry toluene solution) under nitrogen. After 2 h, the reaction temperature was increased to 100 °C for another 6 h. Then, the very viscous reaction mixture was cooled to room temperature to stop the bulk polymerization. The polymer was purified by precipitation from a concentrated CH_2Cl_2 solution into a 10-fold amount of cold methanol. After filtration and drying in vacuum, a powdery product of **1** was obtained.

^{1}H NMR ($CDCl_3$): δ 4.11 (s; C$H_{2,core}$), 4.06 (t, 6.7 Hz; CH_2OC(O)), 3.65 (t, 6.5 Hz; CH_2OH), 2.30 (t, 7.6 Hz; CH_2C(O)O), 1.7–1.6 (CH_2CH_2CH_2), 1.38 ppm (m; CH_2CH_2CH_2).

^{13}C NMR ($CDCl_3$): δ 173.3 (*C*=O), 172.7 (*C*=O next to core), 64.0 (*C*H_2OC(O)), 62.4 (*C*H_2OH), 61.9 (*C*$H_{2,core}$), 41.9 (*C*$_{core}$), 34.0 (*C*H_2C(O)O), 32.2 (*C*H_2CH_2OH), 28.2 (*C*H_2CH_2OC(O)), 25.4 (*C*H_2CH_2C(O)O), 24.4 ppm (CH$_2$*C*H$_2$CH$_2$).

2-(4-Nitrophenyl)-benzoxazinone-terminated tetra-PCL (3)

Compound **3** was prepared as described earlier[26] by conversion of **1** with 2-(4-nitrophenyl)-4-oxo-4*H*-benzo[*d*][1,3]oxazine-7-carboxylic acid chloride **2** (**Scheme 5. 2a**). An amount of 0.5 mmol of **1** was dissolved in dry CH_2Cl_2 (30 mL). Then, 4.5 mmol (0.62 mL) of triethylamine and 4 mmol of previously dissolved **2** in dry CH_2Cl_2 (15 mL) were slowly added to the solution at room temperature under nitrogen using a syringe. The reaction mixture was stirred for 48 h, the insoluble salt (triethylammonium chloride) was removed by filtration and **3** was obtained by precipitation in cold methanol. **3** was prepared in two batches (**a**, **b**) used for the synthesis of **6a** and **6b**.

^{1}H NMR ($CDCl_3$): δ 8.52 (d, 8.8 Hz; 19), 8.39 (s; 11), 8.38 (d, 8.8 Hz; 20), 8.34 (d, 8.2 Hz; 14), 8.20 (d, 8.2 Hz; 15), 4.41 (t, 6.7 Hz; 8 next to C_9), 4.10 (s; 2), 4.06 (t, 6.7 Hz; 8), 2.35 (t, 7.4 Hz; 4 next to C_9), 2.30 (t, 7.4 Hz; 4), 1.85 (m; 7 next to C_9), 1.73 (m; 5 next to C_9), 1.7–1.6 (5, 7), 1.52 (m; 6 next to C_9), 1.38 ppm (m; 6).

^{13}C NMR ($CDCl_3$): δ 173.4 (3), 172.8 (3 next to core), 164.7 (9), 158.0 (16), 155.6 (17), 150.3 (21), 146.3 (12), 138.1 (10), 135.5 (18), 129.4 (15), 129.3 (19), 129.0 (14), 128.9 (11), 123.9 (20), 120.0 (13), 65.8 (8 next to C_9), 64.1 (8), 61.9 (2), 42.0 (1), 34.1 (4), 28.3 (7), 25.5 (5), 24.5 ppm (6).

MeO–PEG–NH_2 (5b)

Compound **5b** was synthesized in two steps by adapting a previously reported procedure (**Scheme 5. 2b**).[30] In the first step, MeO–PEG–OH (M_n = 2100 g mol^{-1}, m = 47) was converted with mesylchloride to MeO–PEG–OMs intermediate (**4**). The resulting mesyl groups were subsequently converted into amino groups by reaction with aqueous ammonia. Briefly, an amount of 1 mmol of MeO–PEG–OH, 8.5 mmol of triethylamine and 8 mmol of mesylchloride were dissolved in anhydrous CH_2Cl_2 (50.0 mL) and stirred overnight. The solution was filtered and the solvent was evaporated. The polymer was dissolved in THF and poured into a large excess of cold diethyl ether. The precipitated white solid of **4** was isolated by filtration and dried under vacuum at 40 °C. The purified **4** with terminal mesyl groups was dissolved in 28 wt% aqueous ammonia solution (100 mL). The reaction mixture was left with stirring for 5 days at room temperature. The ammonia was allowed to evaporate over night after NaOH (5 M) was added dropwise until the pH reached 13. After the product was extracted 3 times with CH_2Cl_2 and washed with saturated sodium chloride solution, drying over anhydrous $MgSO_4$ followed. The

crude product was precipitated into a 10-fold amount of cold diethyl ether. The precipitate was filtered and dried under vacuum at 40 °C.

^{1}H NMR ($CDCl_3$): δ 3.62 (s; c), 3.48 (m; b), 3.35 (s; d), 2.84 (t, 5.3 Hz; a), 1.8 ppm (v br; NH_2).

^{13}C NMR ($CDCl_3$): δ 73.3 (b), 71.5, 70.5, 70.2 (all c), 58.9 (d), 41.7 ppm (a).

Tetra-PCL-*b*-PEG star block copolymer (6)

Star block copolymer **6a** and **6b** with two PEG blocks of different lengths were prepared by the hetero-complementary amine–benzoxazinone reaction of **3** with **5** in toluene (**Scheme 5. 2c**). As an example, the synthesis of **6b** was carried out as follows: an amount of 0.1 mmol of **3a** was dissolved in anhydrous toluene (10 mL). Then, 0.45 mmol of **5b** were added to the solution and stirred 24 h under nitrogen at 40 °C. The solvent was removed by evaporation and the obtained slightly yellowish powder was dispersed in water. The residue of **5b** was then extracted from the solid by centrifugation at 20 °C for 20 minutes at 20 400*g*. The supernatant was then removed, fresh water added, and centrifuged again. This procedure was carried out 4 times. The purified powder was then freeze-dried to give **6b**.

^{1}H NMR (**6b**, $CDCl_3$). δ 12.62 (s; Ph–N*H*–CO–Ph), 9.41 (s; 11), 8.36 (d, 8.8 Hz; 20), 8.21 (d, 8.8 Hz; 19), 7.82 (d, 8.2 Hz; 15), 7.75 (d, 8.2 Hz; 14), 7.36 (t, 5.4 Hz; CH_2–N*H*–CO–Ph), 4.41 (t, 6.7 Hz; 8 next to C_9), 4.10 (s; 2), 4.05 (t, 6.7 Hz; 8), 3.70–3.50 (a, b, c), 3.37 (s; d), 2.34 (t, 7.4 Hz; 4 next to C_9), 2.30 (t, 7.4 Hz; 4), 1.83 (m; 7 next to C_9), 1.72 (m; 5 next to C_9), 1.7–1.6 (5, 7), 1.50 (m; 6 next to C_9), 1.38 ppm (m; 6).

^{13}C NMR (**6b**, $CDCl_3$): δ 173.2 (3), 172.5 (3 next to core), 168.3 (16), 165.3 (9), 163.0 (17), 149.6 (21), 140.0 (18), 139.5 (12), 133.9 (10), 128.4 (19), 127.3 (14), 124.0 (15), 123.7 (20), 123.2 (13), 121.8 (11), 71.7 (*c* next to C_d), 70.5–69.0 (b, c), 65.1 (8 next to C9), 63.8 (8), 61.7 (2), 58.7 (d), 41.8 (1), 39.9 (a), 33.9 (4), 28.1 (7), 25.3 (5), 24.3 ppm (6).

Model reaction with pentaerythritol

As model compounds for NMR signal assignments, mixtures of alkyl ester- and benzoxazinone-substituted pentaerythritol (**7**, **8**) were obtained by subsequent reaction of pentaerythritol with lauryl chloride and compound **2** (**Scheme 5. 3**). First, an excess of pentaerythritol was reacted in a non-stoichiometric ratio with lauryl chloride in presence of triethylamine as acid scavenger overnight at room temperature in THF. The precipitate was filtered off, the product was washed several times with water and dried under vacuum to give **7** consisting of a mixture

of partially (A_3B, A_2B_2, AB_3) and completely (B_4) esterified pentaerythritol. Subsequently, the mixture **7** was reacted with a twofold excess of compound **2** in presence of triethylamine in THF. After stirring the reaction mixture over night, the insoluble salt was removed by filtration and the crude product mixture **8** (C_3B, C_2B_2, CB_3 and B_4) was purified by precipitation into a 10-fold amount of cold methanol. The precipitate was filtered and dried under vacuum at 40 °C.

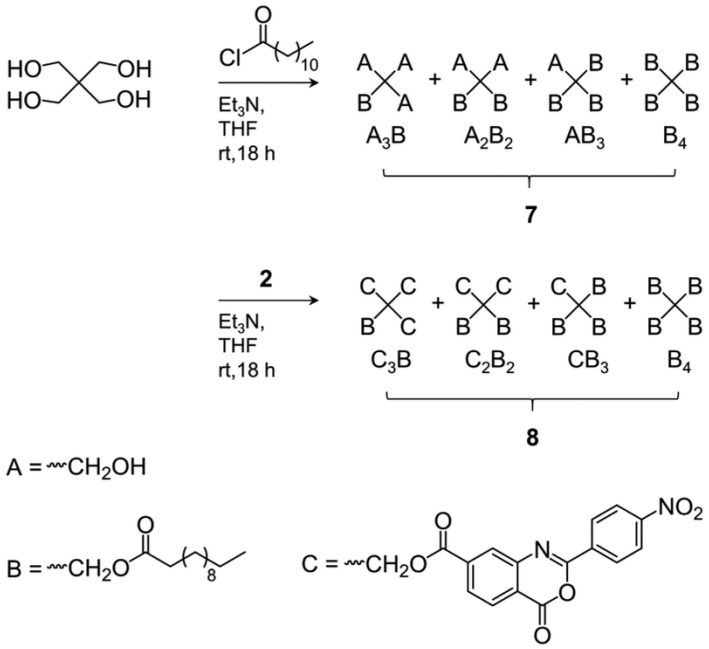

Scheme 5. 3: Synthesis of alkyl ester- (**7**) and benzoxazinone/alkyl ester-substituted (**8**) pentaerythritol mixtures as model compounds for NMR signal assignments.

Methods

NMR spectroscopy

^{1}H (500.13 MHz) and ^{13}C (125.76 MHz) NMR spectra were recorded using an Avance III 500 spectrometer (Bruker Biospin). $CDCl_3$ ($\delta(^1H)$ = 7.26 ppm; $\delta(^{13}C)$ = 77.0 ppm) and D_2O ($\delta(^1H)$ = 4.79 ppm) were used as solvent, lock, and internal standard. Sample temperature was kept constant at 30 °C ± 0.5 K unless otherwise specified. For temperature dependent measurements, powdered **6** was finely dispersed in D_2O and immediately transferred in tubes to the spectrometer for the measurements. The sedimentation during the measurements was slow and was assumed not to influence the results. The spectra were referenced on the $H_{5,7}$ signal of PCL ($\delta(^1H)$ = 1.55 ppm).

MD-SEC

Multidetection-hyphenated size exclusion chromatography (MD-SEC) of **1**, **3**, **6a** and **6b** was performed in THF with a flow rate of 1 mL min^{-1} using an Agilent degasser, an isocratic pump and an autosampler (series 1100/1200). Star polymers **1** and **3** were separated with 2× Agilent SEC columns PLgel MIXED-C. Star block copolymers **6a** and **6b** were separated with coupled Shodex SEC columns KF-802 and KF-803. The detection system downstream was comprised of a Wyatt multiangle light scattering detector (MALS) HELEOS® II, a viscometric detector Viscostar® III and a differential refractometer Optilab® T-rEX. The refractive index increment of the samples **3** and **6a**, **6b** in THF was determined in batch to d*n*/d*c* = 0.0957 ± 0.0016 mL g^{-1}. For **1**, a d*n*/d*c* = 0.072 ± 0.003 mL g^{-1} was used as reported in the literature for PCL in THF.[31,32] MD-SEC of **5a** and **5b** was performed using an aqueous solution containing 0.01 M NaH_2PO_4 (pH = 7) and 0.2 M $NaPO_3$ as eluent with two aquagel-OH MIXED-H columns (Agilent Technologies, USA) by using a dRI detector K-2301 (Knauer, DE) and a MALS-detector MiniDAWN TREOS II (Wyatt Technologies, USA).

MALDI-TOF mass spectrometry

Matrix-assisted laser desorption/ionization time-of-flight mass spectrometry (MALDI-TOF MS) of all samples was done with an Autoflex Speed MALDI-TOF spectrometer from Bruker Daltonics GmbH, equipped with a pulsed Nd:YAG laser (355 nm, 1 kHz). A mixture of *trans*-2-[3-(4-*tert*-butylphenyl)-2-methyl-2-propenylidene]-malononitrile (DCTB) and potassium acetate were used as matrix and ion adductor, respectively. For the measurements, 1.6 µL sample solution in THF (2 g L^{-1}), 8 µL of DCTB matrix solution in THF (10 g L^{-1}), and 0.8 µL of potassium acetate solution in ethanol (1 g L^{-1}) were mixed and drop-casted on the target plate. TOF-calibration was performed using PEG reference standards.

ATR-FTIR spectroscopy

FTIR spectra of **3** and **6b** were obtained using a Vertex 80v FTIR spectrometer (Bruker) with a Golden Gate Diamond ATR unit (SPECAC) and an MCT detector. Each spectrum was recorded with 100 scans and a resolution of 4 cm^{-1}. The spectra were baseline corrected and normalized to the band intensity of the C–O asymmetric stretching vibration of PCL at 1240 cm^{-1}.

DLS

Dynamic light scattering (DLS) measurements of **6a** and **6b** were performed at 20 °C and at concentrations of 0.025 to 1 g L^{-1} in water, 2.5 to 20 g L^{-1} in acetone, 5 and 10 g L^{-1} in ethyl acetate and 10 g L^{-1} in dichloromethane using cylindrical quartz-glass cuvettes and a light scattering setup equipped with an ALV-SP125 goniometer, an ALV/LSE5004 multi tau correlator at a fiber optical ALV/High QE APD avalanche photodiode with pseudo-cross correlation and a He/Ne laser (632.8 nm, Thorlabs Inc.). The solutions were filtered prior to the measurements. The solutions in the organic solvents were used after dissolution with stirring overnight at room temperature. In contrast, the water solutions of **6b** were brought to 70 °C to completely dissolve them and then cooled back to 20 °C.

DSC

DSC experiments of **1**, **6a** and **6b** were performed with a DSC Q2000 and DSC 2500 (TA Instruments, USA). Melting and crystallization experiments were performed in water under nitrogen at a sample concentration of 20 g L^{-1} with heating and cooling rates of 10 and 5 K min^{-1}, respectively. Sample suspensions (~5 mg) were weighed in Tzero-Al-hermetic pans (hermetically sealed; pressure stable up to 3 bar) and equilibrated at 10 °C for a period of 5 min. For analysis of the first and second heating, samples were heated from 10 °C to 80 °C, cooled to 10 °C, held for 30 minutes, and then reheated to 80 °C.

TEM

TEM images of **6b** were recorded with a Libra120 (Carl Zeiss Microsopy GmbH, Oberkochen, Germany) operated at 120 kV. Images were recorded in bright field at small defocus to improve the contrast. For the measurement, 2 µL of sample solution were dripped on copper grids coated with a formvar/carbon foil. After a waiting time t (between 2 seconds and 10 minutes), the sample was blotted with filter paper to remove excess specimen not adsorbed on the grid. Afterwards, 2 µL stain solution (either 2 wt% uranyl acetate in water (UCA), or 2 wt% phosphotungstic acid in water (PTA)) were dripped on the grid and excess stain solution was blotted with a filter paper after one minute. All TEM images were taken within 48 hours after preparation of the sample solutions.

Cryo-TEM

Cryo-TEM images of **6b** were acquired using the same equipment as for the TEM measurements. 2 μL of sample solution were dropped on the holey grids (Qunatifoil type R2/2), blotted with filter paper after 5 seconds, and rapidly frozen in liquid ethane at −178 °C using a Leica GP (Grid Plunging) device (Leica Microsystems GmbH, Wetzlar, Germany). All images were recorded in bright field at −172 °C. The measurements were conducted one week after preparation of the sample solutions.

5.7. Results and Discussion

Synthesis and structural analysis

The synthesis of amphiphilic tetra-PCL-*b*-PEG star block copolymers **6a** and **6b** is shown in **Scheme 5. 2**. First, tetra-PCL–OH **1** was synthesized by ROP of ε-CL using pentaerythritol as initiator and $Sn(oct)_2$ as catalyst, followed by terminal group functionalization with 2-(4-nitrophenyl)-benzoxazinone-based compound **2** by esterification to give **3**. Subsequently, the 2-(4-nitrophenyl)-benzoxazinone end groups of **3** were reacted with MeO–PEG–NH_2 (**5**) of different lengths (m = 16 and 47). The synthesis results are summarized in **Table 5. 1**, and the ^{1}H NMR spectra of **3**, **5b**, and **6b** are shown in **Figure 5. 1**. The desired M_n of **1** (~10 kg mol^{-1}), which forms the hydrophobic core of **6a** and **6b**, was controlled by the molar ratio of ε-CL to pentaerythritol. $M_{n,NMR}$ values of 9.3 kg mol^{-1} and 9.7 kg mol^{-1} determined by ^{1}H NMR end group analysis (see SI **Figure A.5. 3**) agree very well with the targeted value (**Table 5. 1**). Functionalization of the terminal hydroxy groups of **1** was carried out with an excess of **2** in solution. The conversion of the terminal CH_2OH group, characterized by the methylene signal at 3.64 ppm in the ^{1}H NMR spectrum of **3** (see **Figure 5. 1c**), was ≥95%.

The M_n values of **3** shown in **Table 5. 1** increased slightly compared to **1**. The somewhat reduced dispersity is probably caused by the purification steps performed after functionalization. The results clearly show that no degradation of the tetra-PCL star occurred during the modification. **Figure 5. 1b** depicts the ^{1}H NMR spectrum of MeO–PEG–NH_2 (**5b**). Absence of the methyl signal of the mesyl group at 3.08 ppm indicates a high amino functionalization of **5b**, which is calculated to be about 90% based on the intensities of the methyl ether (3.35 ppm) and the CH_2NH_2 (2.84 ppm) signals.

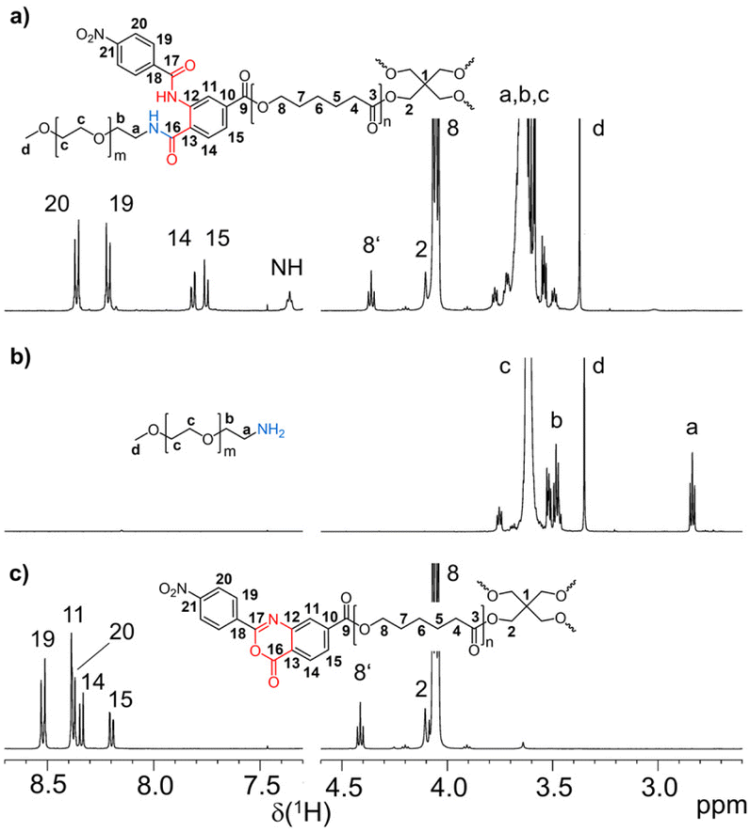

Figure 5. 1: ^{1}H NMR spectra (regions) of **(a)** tetra-PCL-*b*-PEG star block copolymer **6b**, **(b)** MeO–PEG–NH_2**5b**, and **(c)** benzoxazinone-terminated tetra-PCL star polymer **3** (solvent: $CDCl_3$).

Table 5. 1: Molecular characterization of **1a**, **1b**, **3a**, **3b**, **5a**, **5b**, **6a**, and **6b** by NMR spectroscopy, MALDI-TOF MS and MD-SEC measurements.

Poly-mer	$P_{n,NMR}$ [a] ($Ø P_{n,arms}$ = ¼ P_n)	$M_{n,NMR}$ [a] (kg mol^{-1})	$M_{n,SEC}$ (kg mol^{-1})	$M_{n,MALDI-TOF}$ (kg mol^{-1})	$M_{w,SEC}$ (kg mol^{-1})	$M_{w,MALDI-TOF}$ (kg mol^{-1})	$Đ_{SEC}$	$Đ_{MALDI-TOF}$
1a	80 ± 2	9.3 ± 0.2	8.7 ± 0.6	8.6 ± 0.2	9.5 ± 0.6	8.93 ± 0.16	1.09 ± 0.3	1.04
1b	84 ± 2	9.7 ± 0.2	10.8 ± 0.6	8.9 ± 0.2	11.8 ± 0.6	9.62 ± 0.11	1.09 ± 0.2	1.09
3a	84 ± 2	10.9 ± 0.3	9.6 ± 0.7	9.7 ± 0.1	10.0 ± 0.5	10.3 ± 0.2	1.04 ± 0.3	1.06
3b	88 ± 2	11.3 ± 0.3	10.7 ± 0.5	9.5 ± 0.3	11.4 ± 0.4	9.9 ± 0.3	1.07 ± 0.2	1.04
5a	16	0.765	-	0.785	-	0.825	-	1.05
5b	47 ± 1	2.1 ± 0.1	2.1 ± 0.1	2.01 ± 0.02	2.3 ± 0.1	2.04 ± 0.02	1.06	1.02
6a	-	13.5 ± 0.3	13.9 ± 0.6	11.6 ± 0.7	15.5 ± 0.5	12.2 ± 0.7	1.11 ± 0.04	1.05
6b	-	19.3 ± 0.4	17.6 ± 0.6	16.2 ± 0.6	17.9 ± 0.6	17.1 ± 0.7	1.03 ± 0.04	1.06

[a] Based on ^{1}H NMR end group analysis (see SI **Figure A.5. 3, A.5. 5, A.5 .7** and comments), P_n is the degree of polymerization (number of polymer units per star).

A further issue is the perfectness of the tetra-PCL star structure. Mixtures of differently substituted pentaerythritol (**7**, **8**) were obtained by sequential conversion of pentaerythritol with lauryl chloride and compound **2** (**Scheme 5. 3**). The components of these mixtures serve as model compounds for NMR spectroscopic analysis. Detailed signal assignments are given in the SI (**Appendix A.5**) Chapter 6 and 7. It was found that the ^{1}H NMR spectrum of tetra-PCL–OH **1** is less suitable for quantifying structural defects caused by incomplete conversion of the pentaerythritol core. However, the different substitution patterns of the core can be well distinguished in the ^{1}H NMR spectrum of compound **3**. This becomes clear by comparison with the spectrum of mixture **8** (see Fig. 5.2). The signals of the species with only three PCL arms (**CB_3**) could be identified (~6 mol%), while lower degrees of substitution (**C_2B_2**, **C_3B**) could hardly be detected and are estimated to be <1 mol%. In the ^{1}H NMR spectrum of **6b** (see **Figure 5. 1a**), the signals of the benzoxazinone terminal groups disappeared completely whereas new signals could be assigned to the newly formed linking benzamide group between the PCL core and the PEG arms. Since all benzoxazinone signals disappear in the spectrum of **6b**, it can be assumed that the benzoxazinone groups on the core also participate in the reaction with amino-terminated **5b**.

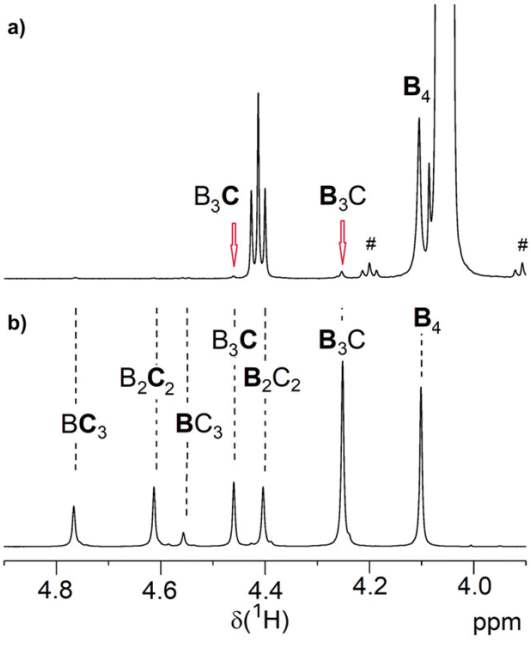

Figure 5. 2: Region of the ^{1}H NMR spectrum of (a) benzoxazinone-terminated star **3a** and (b) the corresponding benzoxazinone/alkyl ester-substituted compound mixture **8** (solvent: $CDCl_3$). The abbreviations are explained in **Scheme 5. 3** and symbol # marks ^{13}C satellite signals.

The FTIR spectra of **3** and **6b** shown in **Figure 5. 3** also confirm the complete conversion of the terminal benzoxazinone groups. In the spectrum of **3**, the carbonyl stretching band and the C=N stretching band of the benzoxazinone group are clearly visible at 1772 and 1616 cm^{-1}, respectively. After reaction with the amino-terminated PEG **5b**, these bands disappear completely in the spectrum of **6b**. Instead, amide I (carbonyl stretching band at 1648 cm^{-1}) and amide II (N–H deformation band at 1582 cm^{-1}) bands are visible, which can be attributed to the newly formed benzamide linking group.

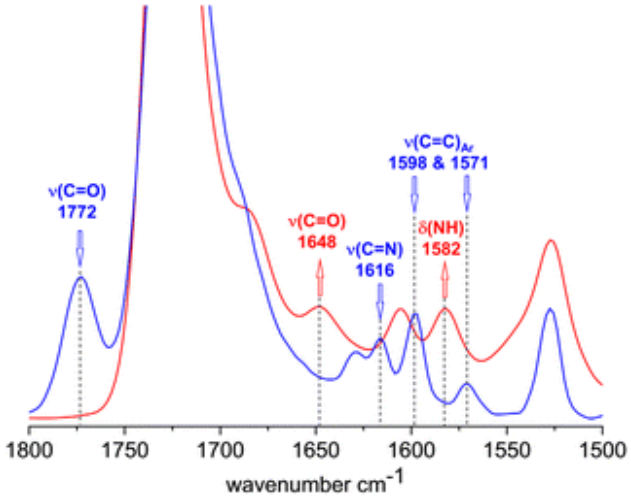

Figure 5. 3: FTIR spectra of **3** (blue) and **6b** (red) in the region of unreacted and reacted benzoxazinone group.

MALDI-TOF mass spectra of **1**, **3**, **6a** and **6b** are shown in **Figure 5. 4**. To exclude mass discrimination effects, the results from the MALDI-TOF analysis were validated by measurements in linear and reflector TOF mode as well as by MD-SEC. Due to an identified slight mass discrimination for **6a**, the average molar masses of **6a**, **6b** were determined from mass spectra measured in linear TOF mode (see **Appendix A.5** Chapter 9).

The spectra of tetra-PCL-star polymers **1** and **3** are well resolved and allow conclusions about the molecular architecture. This high resolution is not found in the spectra of the star block copolymers **6a** and **6b** since linking of two polymers with different repeating units usually smears out the discrete signals of the individual polymers. In the spectra of **1** and **3**, the distance between two main peaks corresponds very well to the molar mass of one repeating unit of PCL (M_n = 114.1 g mol^{-1}). The observed peak shift $\Delta m/z$ = 1177.3 between **1** and **3** (see **Figure 5. 4a**) indicates an attachment of four 2-(4-nitrophenyl)-benzoxazinone terminal units per molecule. A small, but significantly resolved trace impurity (see Fig. 5.4b) of $\Delta m/z$ = 294.7 may refer to a superimposition of fractions with lower number of modified terminal units

($\Delta m/z$ = 294.7 $[M + K]^+$, one unit and $\Delta m/z$ = 867.2 $[M + Na]^+$, three units). For a detailed assignment of trace impurities found by MALDI-TOF MS, see **Appendix A.5** Chapter 9.

The insignificantly low intensity of the mass peaks coming from trace impurities compared to the strongly dominating ones of the main fractions agrees with the findings by ^{1}H NMR spectroscopy and confirms an almost complete termination of the tetra-PCL star polymer **3** with oxazinone groups.

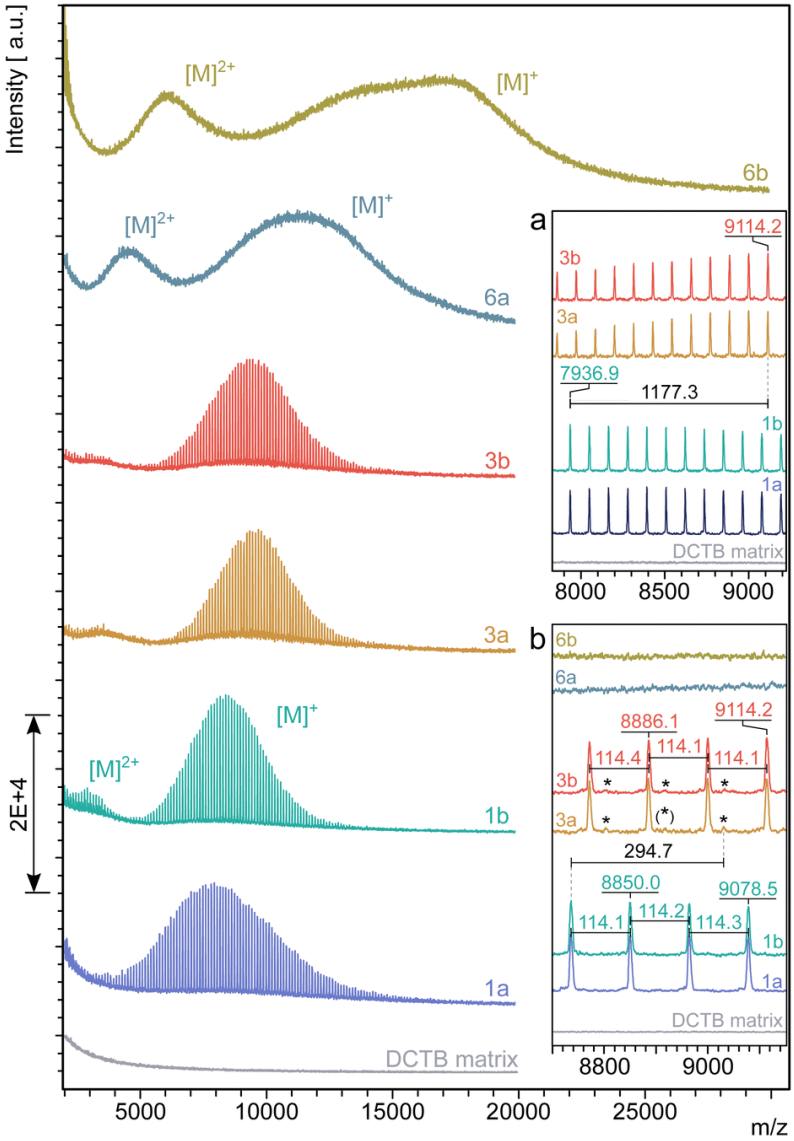

Figure 5. 4: Molar mass distribution determined by MALDI-TOF mass spectrometry of the star polymers **1**, **3**, **6a** and **6b** in THF with a shift in the discrete molecule masses between **1** and **3** of their main fractions by $\Delta m/z$ = 1177.3 (inset **a**) and the mass differences in between the discrete molecule masses $\Delta m/z$ = 114 (inset **b**). The most significant trace impurity found of $\Delta m/z$ = 294.7 between **1** and **3** is assigned by an asterisk.

The molar mass measurements confirm the narrow dispersity of the samples even after the third modification step (**Table 5. 1**). There is a clear shift to higher molar masses from **1** to **3** and especially to **6a** and **6b**. The MALDI-TOF MS based molar masses tend to be slightly smaller than those determined by NMR spectroscopy and MD-SEC, but in principle show the same trend.

These results, together with the FTIR spectroscopy, MD-SEC and NMR spectroscopy measurements, show that the hetero-complementary conversion between **3** and **5** proceeded quantitatively and that the resulting star block copolymers **6a** and **6b** are characterized by high molecular uniformity.

Amphiphilic behavior in selective solvent

PCL-*b*-PEG copolymers are inherently amphiphilic because water is a selective solvent for the hydrophilic PEG block. In water, these polymers tend to form micelles,[3, 15–20] whereby the micelle geometry is controlled in first instance by the volume fraction of the soluble block [33] with only small changes for a low functionality as 4 (number of arms). Since both PEG and PCL have a density close to 1.13 g cm^{-3}, the PEG volume fraction of **6a** and **6b** are approximately 23% and 44%, respectively. For linear PEG-*b*-PCL block copolymers, precipitate was found in one work below 12% PEG fraction.[34] Vesicles with sizes ranging from 60 nm to 10 μm were found[35] for compositions between 9% and 36% PEG.[34–37] Cylindrical micelles with a length up to 20 microns may form between 13% and 55% PEG.[19, 34, 35, 37–39] Also, a lamellar phase was observed for 11% to 16% PEG[19] that could be an intermediate state of vesicle formation. The different particulate structures mentioned above overlap significantly, which complicates the analysis and a discussion of these solutions in addition to possible transitions between different morphologies that can be driven by crystallization[40] and possible concentration dependencies of the observed morphologies.[41] Similar to the linear block copolymers, we expect that sample **6a** may form a broad variety of different morphologies. This complicates a quantitative analysis of particle size by DLS. For block copolymers with a composition comparable to **6b**, most of the above-mentioned works report only spherical micelles; only sometimes [38, 39] cylindrical micelles are detected, see also **Table A.5. 4** in the Appendix.

The solubility of the tetra-PCL-*b*-PEG star block copolymers **6a** and **6b** in water was investigated at room temperature and at 80 °C. For this purpose, both polymers were suspended in water at a concentration of 10 mg mL^{-1} at room temperature (see **Figure 5. 5**, left). After heating to 80 °C, a clear solution of **6b** was obtained within 5 minutes (see **Figure 5. 5**, right),

which remained stable when cooled back to room temperature. In contrast, **6a** remained cloudy over the entire temperature range without the formation of a precipitate (see **Figure 5. 5**, right). Both observations agree with the formation of spherical micelles in the low nm range for **6b** and the formation of micelles with a size comparable to the wavelength of light or larger for **6a**. The equilibrium melting temperature was estimated to be close to 64 °C[42, 43] for PCL and around 70 °C [42–45] for PEG. Crystallization temperatures up to 49 °C[46, 47] and around 40 °C[48, 49] were reported for PCL and PEG, respectively. Thus, thermal treatment at 80 °C melts crystalline portions of both polymers, which is a mandatory step for dissolving the star block copolymers. Phase separated PCL domains may crystallize upon cooling back to room temperature. To gain a better insight into the solution and self-assembly behavior of tetra-PCL-*b*-PEG star block copolymers in water, DSC, (cryo-)TEM, DLS, and ^{1}H NMR measurements were performed on aqueous dispersions of **6a** and **6b**.

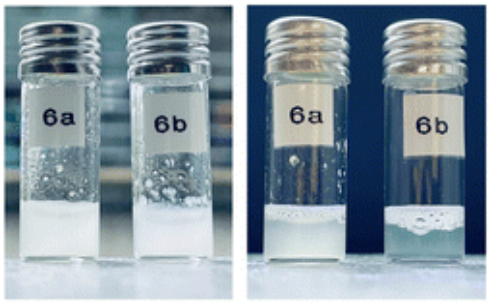

Figure 5. 5: Suspensions of **6a** and **6b** in water at room temperature (left) and after 5 min of heating to 80 °C and subsequent cooling to room temperature (right).

Thermal behavior in water

DSC measurements were performed on the star block copolymers **6a** and **6b** as well as on the star polymer **1** suspended in water. The DSC heating and cooling runs are shown in **Figure 5. 6**, and the results are summarized in **Table 5. 2**. We take the peak position of the heat flow as rough estimates for the melting and crystallization temperature, if a peak can be observed. In the first heating run of the dispersion of **1**, a distinct melting transition is visible at about 52 °C. During cooling, crystallization appears close to 30 °C. In the second heating run, the melting is slightly shifted to lower temperatures (T_m = 46 °C), indicating a smaller stem length of the crystals. At the end of the synthesis, specimen **1** was precipitated from a concentrated CH_2Cl_2 solution into a 10-fold amount of cold methanol followed by filtration and drying in vacuum. This process determines the geometry of the PCL crystals prior to the first heating run,

while the melting temperature of the second heating run is related to the stem length of the crystalline PCL domains in water.

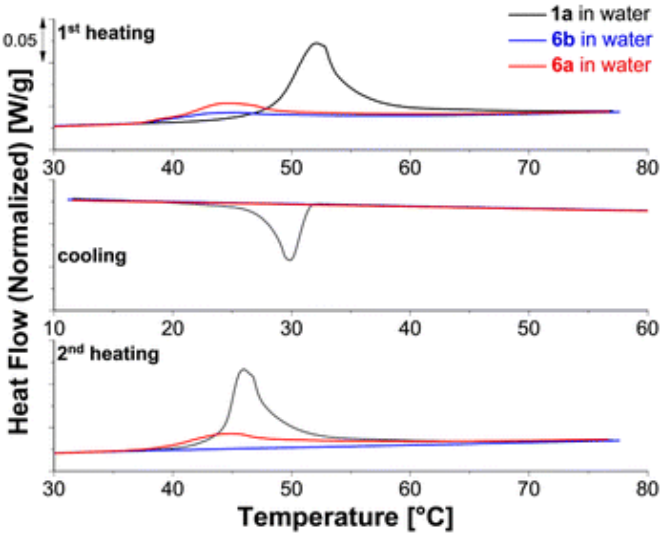

Figure 5. 6: DSC thermograms of **1a** (black), **6a** (red) and **6b** (blue) in water.

Table 5. 2: Thermal behavior of **1a**, **6a** and **6b** in water.

Polymer	1st heating run T_m a)(°C)	cooling run T_c b) (°C)	2nd heating run T_m a) (°C)
1a	52.1	29.9	46
6a	45	-	45
6b	45	-	-

[a] Melting temperature. [b] Crystallization temperature.

Compared to **1**, the melting transitions of the star block copolymers **6a** and **6b** appear in the first heating run at lower temperature (T_m = 45 °C). This difference results in part from the different treatment of the specimens at the end of the synthesis: **6a** and **6b** are purified in water followed by freeze-drying. Thus, the crystal geometry is here affected by the micelle geometry that is established during this process. During cooling, no crystallization is visible for either copolymer. The second heating scan, recorded after 30 minutes of isothermal annealing at 10 °C, shows a melting peak only for the sample with the shorter PEG block (**6a**). For explaining this difference, we consider the visible appearance of the samples and the morphologies reported in literature, see SI **Table A.5. 4**. Based on this information, we expect mainly small spherical micelles for **6b** and larger structures possibly cylindrical micelles or vesicles for **6a**.

Semi-crystalline vesicles and cylindrical micelles of PCL-*b*-PEG copolymers with a similar composition as **6a** and **6b** were analyzed previously.[34] Crystallization of vesicles was possible at room temperature, while significant crystallization of cylindrical micelles occurred only significantly below 0 °C. Our observations, therefore, hint towards a significant volume fraction of vesicles in aqueous suspensions of **6a**.

Micelle morphology: TEM and cryo-TEM

Optical techniques like TEM and cryo-TEM provide direct access to the morphology of the micelles. However, TEM requires staining and adsorption of the micelles on a substrate, which may impact the morphology of the micelles[50] or their tendency to crystallize. Cryo-TEM shows typically only the phase separated portion of the micelles. A combination of both allows to check morphological changes and to gain information about the dissolved part of the micelles. **Figure 5. 7** shows two typical TEM micrographs where **6b** was stained with PTA (left) or with UAC (right). Our general observation is that PTA leads to a larger tendency of spherical micelles (a) to aggregate. Flat structures parallel to the surface develop (c) or might be initiated by cylindrical micelles that tend to appear in bundles (b). For UAC stained samples, adsorbed micelles tend to combine in larger structures, the onset of spherulitic structures is possible, and some larger flat objects with a round geometry form (d). This figure contrasts with the cryo-TEM results of **Figure 5. 8** where we observe a large abundance of spherical micelles and only some cylindrical ones.

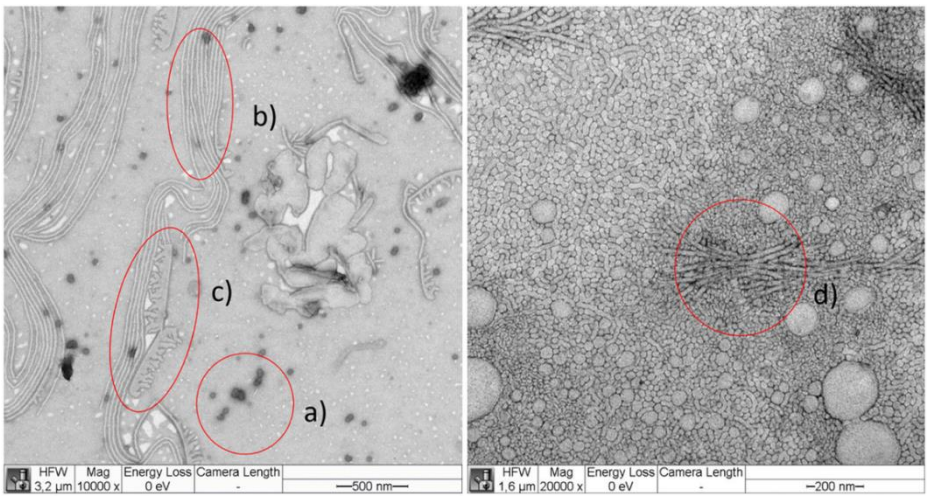

Figure 5. 7: TEM micrograph of **6b** adsorbed within 10 seconds from 1 g L^{-1} solution in water stained with PTA (left) and adsorbed within 10 seconds from 10 g L^{-1} solution in water stained with UAC (right). PTA enters predominantly the PEG corona. Thus, spherical micelles are grey objects with a darker boundary (**a**), cylindrical micelles as double grey lines (**b**), while flat surface structures have average grey color with a darker line as boundary (**c**). UAC stained objects show a similar appearance as PTA stained objects with characteristic super structures (**d**).

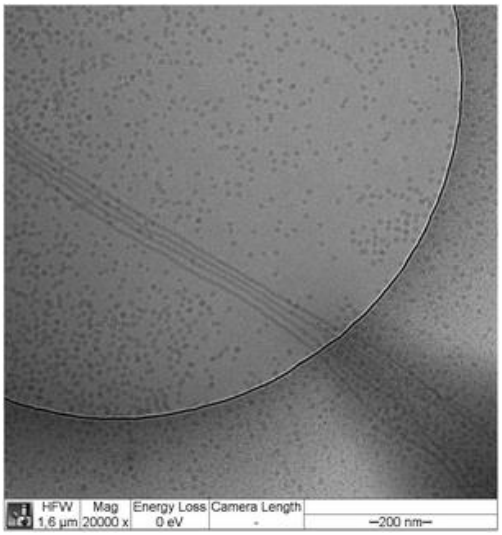

Figure 5. 8: Cryo-TEM image of a rapidly frozen 10 g L^{-1} solution of **6b**.

We argue that the structures that are visible on the TEM images but do not appear on the cryo-TEM images are most likely surface initiated with additional dependence on the particular stain. The common structure observed in all images are spherical and cylindrical micelles. The diameters of the spherical micelles were determined by manual measurement of typically 30 micelles using the Fiji software. The results are summarized in **Table 5. 3**. Our data agree with literature data on linear block copolymers that are equivalent to a single arm of our star block copolymers. For instance, the PCL_{24}–PEG_{44} blocks similar to star arms produce 21.7 ± 5.9 nm sized spherical micelles[19] (stained with PTA and prepared using a different protocol) in quantitative agreement with our work (see **Table 5. 3**).

Table 5. 3: Size of spherical micelles of **2b** in water determined by TEM with PTA or UAC as stain or by cryo-TEM.

method	**particle size (nm)**		
	(0.1 g L^{-1}) [a)]	**(1 g L^{-1}) [a)]**	**(10 g L^{-1}) [a)]**
TEM (PTA)	28 ± 8	30 ± 5	38 ± 17
TEM (UAC)	25 ± 5	29 ± 5	24 ± 4
Cryo-TEM		15 ± 3	16 ± 3

[a] Concentration of the sample solution.

The diameter of the cylindrical micelles in cryo-TEM was 12 ± 2 nm in 10 g L^{-1} samples and 13.5 ± 0.7 nm in 1 g L^{-1} samples. With UCA, a cylindrical micelle thickness of 21 ± 3 nm was measured in samples adsorbed from 1 g L^{-1} solution.

We now attempt to correlate the above measurements. Let us assume that the PEG corona of the micelles is not visible in the cryo-TEM images and that the stain does not penetrate the PCL domain. Since PEG is about half of the molar mass of **6b**, dry adsorbed undeformed spherical micelles in TEM should have a size approximately $2^{1/3}$ times larger than the PCL core, i.e. about 20 nm, which is below the size given in **Table 5. 3**. In the dry adsorbed state, the PEG tails are still swollen by the stain and may develop conformations that are either collapsed due to drying or significantly stretched, when the PEG with the stain inside tends to spread over the substrate. To understand which of these effects is more relevant, we consider Flory's characteristic ratio C_∞ of PEG that ranges roughly from 4 to 7[51] in literature with rotational isomeric state computations around $C_\infty = 5$.[52] For a root mean square bond length of 1.46 nm,[53] this latter estimate corresponds to a Kuhn segment size of about 8.8 Å with a Kuhn molar mass of 107 g mol^{-1}. The 2100 g mol^{-1} PEG tails of the star arms consist, therefore, of approximately 20 Kuhn segments. Assuming random walk conformations of the PEG tails as lower bound for the thickness of a PEG corona in non-stretched conformations, we estimate that this layer is at least 4 nm thick and the micelles should appear of at least 23 nm size in TEM. Fully stretched chain conformations on the substrate would lead to a layer of about 17 nm thickness leading to a maximum size of 50 nm in the adsorbed state. Our data lie in between these limits and are in accordance with a weakly stretched PEG corona in the dry adsorbed state or alternatively, a weak penetration of the stain into the PCL domain.

PCL in the crystalline state adopts almost planar zig-zag conformations deviating slightly from the fully extended form[54] with a fiber axis of 1.705 nm corresponding to two chemical monomers. Thus, a cylindrical micelle diameter of 12 ± 2 nm refers to about 13 monomers in nearly fully extended conformations. The PCL cores of **6b** contain approximately 21 monomers per arm. Thus, the diameter of the cylindrical micelle is presumably a one-folded crystal with about 11 monomers in nearly fully extended conformation. A micelle core of about 15–16 nm is almost midway between a one-folded crystal or a fully extended conformation of PCL arms, and thus, not in accord with an expected crystalline morphology.[43] Since also DSC did not show crystallization of **6b**, we conclude that the spherical micelles at room temperature consist of an amorphous PCL core.

A crystalline tetra-PCL star with $M_n \sim 10$ kg mol^{-1} and a density around 1.2 g cm^{-3},[54] occupies a volume of about 14 nm^3. A sphere with a diameter of 15–16 nm and a volume of order 2000 nm^3 provides space for roughly 140 such tetra-PCL star cores and about 1.4 nm^2 surface area per PEG tail. In comparison, thinner cylindrical micelles with 12–13 nm diameter provide only about 1.2 nm^2 per PEG tail. A similar ratio is obtained when considering amorphous PCL.

This reduction refers to an energetic barrier for forming cylindrical micelles as long as the PEG remains dissolved and amorphous, indicating that spherical micelles are at least meta-stable. This barrier can be overcome, for instance, by significant changes of the solvent quality, by adjusting temperature, or when surface adsorption or favorable interactions with some solutes increase the PEG concentration locally, since the solvent quality of water decreases with the PEG volume fraction.[55, 56] This may explain the lower frequency of cylindrical micelles and short precursors of these in the cryo-TEM images despite of the longer storage time of the solution prior to the measurement (7 days) as compared to the micrographs with UCA and PTA stain (up to 2 days). In consequence, we expect that solutions of **6b** immediately after heating beyond the melting temperature develop a dominant portion of spherical micelles but will not exhibit a significant portion of cylindrical micelles.

Samples **6a** in comparison to **6b** contain shorter PEG tails which stabilize these samples less against morphological changes that might be induced by contact with a surface, staining, or due to temperature changes during sample preparation. Since morphological changes were already a serious issue for **6b**, we omitted a similar analysis of **6a**.

Particle size analysis by DLS

DLS studies were first performed in different organic solvents with the aim of identifying good solvents for both PEG and PCL. Prior to the measurements, we scanned literature to identify possible solvents, see **Appendix A.5** Section 10, **Table A.5. 5.** Tetrahydrofuran, toluene and chloroform were analyzed in our preceding paper.[23] In the present work, we employ acetone, ethyl acetate, and dichloromethane at different concentrations between 2.5 and 20 g L^{-1}. The R_H values of **6b** determined from the DLS measurements are summarized in the SI **Table A.5. 1**. The distribution of R_H is monodisperse in dichloromethane and ethyl acetate. At 10 g L^{-1}, we obtain 3.8 ± 0.3 nm and 4.3 ± 0.1 nm, respectively. For comparison, an estimate of R_H by computing R_g with C_∞ = 5 and a Kuhn segment size of about 9 Å for PCL[32] and the parameters for PEG mentioned above yields R_H = 3.4 when using R_g/R_H = 1.05 for experimental data.[57] Therefore, these solvents are presumably good solvents for the polymers. Surprisingly, our data indicate that ethyl acetate is the better solvent for the copolymer, which contrasts the trend expected from literature data, see **Appendix A.5**, Section 10, **Table A.5. 1**. In acetone, the data fit is best when a bidisperse particle distribution is assumed, see **Figure A.5. 1**. The fast mode yields a hydrodynamic radius of R_H = 3.0–3.6 nm for **6a** and R_H = 3.6–4.2 nm for **6b** depending on the concentration. The latter is in good agreement with the hydrodynamic radius in dichloromethane and ethyl acetate indicating dissolved single star block copolymers

in the sample. The reduced size of **6a** compared to **6b** reflects the lower molar mass of this compound.

The slow mode refers to a hydrodynamic radius that increases with concentration between 14–23 nm and 18–34 nm in the case of **6a** and **6b**, respectively, see **Table A.5. 1**. Such a behavior is typically attributed to the formation of aggregates or clusters. The nature of these clusters, however, remains unclear: literature data for the solvent quality of acetone regarding both PEG and PCL is scattered around the theta condition, see **Table A.5. 5**. Furthermore, the relative amplitude of the fast component in **Table A.5. 1**. does not strongly decay with concentration as one expects for micelle formation or other forms of associations where increasing concentrations favors associations.

For analyzing **6b** in water, samples were prepared at 20 g L^{-1}, heated up to 70 °C and cooled back to room temperature. Afterwards, the solution was diluted stepwise to a lowest concentration of 0.025 g L^{-1}. All measurements were conducted within 6 h after preparation starting from the largest concentration. In all samples, monodisperse clusters with a hydrodynamic radius of 20–22 nm are observed, see **Table A.5. 1**. The size of the dried adsorbed stained micelles in TEM is about 10 to 15 nm less than the particle diameter measured by DLS, which is reasonable when considering the swelling of the densely grafted PEG tails in water, a possible weak penetration of the stain into the PCL, and additional corrections like a weak dispersity of the PEG tails. Up to the end of our measurement time of 6 h, we detect no significant traces of larger species like cylindrical micelles of sample **6b** in water.

Temperature-dependent ^{1}H NMR measurements in water

Variable temperature (VT) ^{1}H NMR measurements were performed on suspensions of star block copolymers **6a** and **6b** in D_2O to investigate the influence of the different PEG block length at constant PCL core size on the molecular dynamics (see **Figure 5. 9** and **Figure A.5. 19** and **A.5. 20**). The standard high-resolution NMR measurements performed here require sufficient mobility of the structural units accompanied with long T_2 relaxation times to detect the corresponding NMR signals. This qualitative study is based on the detection of mobility changes during heating from 30 to 80 °C. For both samples, the PCL signals are collapsed at 30 °C, and only for **6b** a broadened ^{1}H NMR signal at ~3.65 ppm indicates PEG mobility. With increasing temperature, the changes for both samples are quite different. From ~45 °C, broad signals appear for both the PCL and PEG moiety of **6a** that steadily increase in intensity with further increase in temperature but remain broad (see **Figure 5. 9b** and **Figure A.5. 19**). For **6b**,

a steep increase in intensity of all signals is observed in the narrow temperature range from ~35 °C to ~45 °C with only minor changes at higher temperatures (see **Figure 5. 9a** and **Figure A.5. 20**). Spectra recorded at 40 °C over a period of one hour are identical and indicate a steady state at a given temperature (see **Figure A.5. 21**). Within this temperature range the turbid sample becomes clear and remains so, while the sample of **6a** remains turbid over the whole range studied. The behavior of the two samples also differs when they are cooled back to 30 °C (see **Figure 5. 9c** and **d**). For **6a**, the signals start to broaden with cooling and after keeping the sample at 30 °C for one hour, the residual signals disappear (see **Figure 5. 9d** and **Figure A.5. 19**). Comparison with the spectrum of the initial sample at 30 °C (see **Figure 5. 9b**) shows that the sample has returned to its original state. A comparable behavior is observed for a dispersion of the unmodified and water-insoluble PCL core **1b** (see **Figure A.5. 22**). The spectrum of **6b** after cooling to 30 °C (see **Figure 5. 9c**) resembles almost the high-temperature spectrum and remains unchanged within 24 hours. The PCL/PEG ratio determined for **6b** from the ^{1}H NMR spectra at 80 °C and at 30 °C (24 h) matches the ratio determined in $CDCl_3$ as a good solvent. Also, for **6a** the PCL/PEG ratio at 80 °C is very similar to that of the $CDCl_3$ solution.

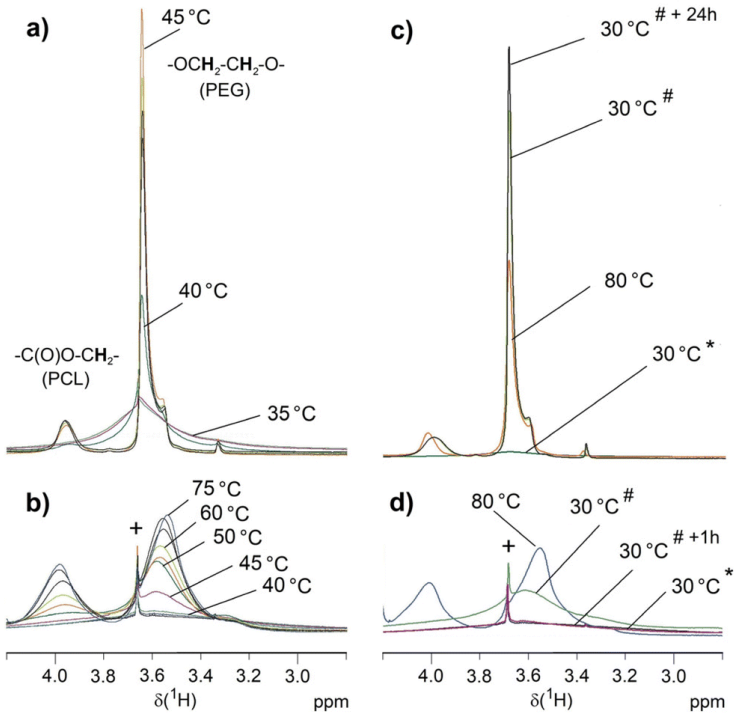

Figure 5. 9: VT ^{1}H NMR measurements on **6b** (**a** and **c**) and **6a** (**b** and **d**) in D_2O (suspension of 5 g L^{-1}). Only selected temperatures are indicated. The complete series are depicted in the SI **Fig. A.5. 19** and **A.5. 20**. Besides the initial spectra at 30 °C (*), (**c**) and (**d**) show additional spectra recorded after cooling down the samples to 30 °C (#) and after keeping the sample for one hour (**6a**) or 24 hours (**6b**) at 30 °C (*+1 h, *+24 h). Symbol + marks the signal of a trace of unreacted **5** that is the only compound dissolved at 30 °C.

The findings of these VT ^{1}H NMR experiments correspond to the results of crystallization studies in water by DSC and to the DLS results. The PCL phase of the dispersed samples prior to the first heating is a rigid phase and therefore the spectrum is silent for these signals. The PEG chains are also immobile and only the outermost PEG sphere of **6b** seems to show a mobility sufficient to detect a signal. At the melting range of the PCL core (T_m ~ 45 °C, see **Table 5. 3**) the corresponding signals appear for both star block copolymers, which is associated with increased mobility. This is confirmed by a reference experiment on the water-insoluble PCL core **1a** that also shows resolved signals above T_m. The PEG chains become also more mobile but only for **6b** the PEG signal is narrow with a hump probably indicating a still ordered PEG portion. For **6b**, micellar structures form in this process, which have high stability. This agrees with the DLS measurements that after heating the sample to 70 °C and subsequent cooling prove stable micellar structures with hydrodynamic radii of about 20 nm at 25 °C for **6b**. PCL recrystallization is suppressed in the micellar structures and the ^{1}H NMR signals of PCL remain unchanged after cooling. The two blocks are mobile enough in their entirety in these micellar structures to be quantitatively detected by solution-state NMR techniques as confirmed by the PCL/PEG ratio, which is consistent with that of the $CDCl_3$ solution. The linking groups between both blocks result in well-resolved signals in accordance to the mobility of both blocks. For **6a**, the mobility of the short PEG chains seems to be hindered by the larger PCL fraction as indicated by the rather broad signal also at 85 °C. However, the mobility in both blocks is sufficient to largely reflect the PCL/PEG ratio from the $CDCl_3$ solution in the signal integrals and also the signals of the linking groups can be detected. Different to **6b**, the increased mobility within the particles during heating does not result in the formation of small micellar structures with a size below the wavelength of visible light in the aqueous environment. Below T_m of PCL, re-formation of a largely immobilized structure occurs, leading to signal collapse for both PCL and PEG in these high-resolution NMR measurements.

In conclusion, these straightforward ^{1}H NMR experiments on suspensions in D_2O allow a qualitative evaluation of melting and recrystallization as well as micellar structure formation for these tetra-PCL-*b*-PEG star block copolymers as demonstrated here for the influence of different PEG chain lengths. The increase in mobility with temperature should be due to both melting PCL structures and solvation of the hydrophilic PEG chains. The formation of small cylindrical micelles or spheres requires a sufficiently high content of the hydrophilic PEG as obviously realized for **6b** but not for **6a**.

5.8. Conclusion

In this work, a combination of "core fist" and "grafting-onto" approach was presented to prepare two uniform tetra-PCL-*b*-PEG star block copolymers with PCL cores of the same size but with PEG arms of different lengths. The synthesis was carried out by reacting a benzoxazinone-terminated tetra-PCL star with amino-terminated linear PEG. The polymers are characterized by a high degree of uniformity, which can be attributed to the use of structurally uniform starting components and to the quantitative conversion of the reacting end groups. Comprehensive studies of the synthesized star polymers by NMR and ATR-FTIR spectroscopy confirmed the quantitative conversion of the benzoxazinone-terminated tetra-PCL star polymer with the amino-terminated linear PEG chains. The expected molar masses as well as their uniformity were confirmed by MD-SEC measurements and MALDI-TOF MS. In addition, DSC, DLS and ^{1}H NMR measurements in the selective solvent water provided insights into the amphiphilic character. After heating suspensions of the star block copolymers in water above the melting point of PCL (T_m = 45 °C), only the star block copolymer with m = 47 repeating units of PEG and n = 22 repeating units of PCL per arm formed a clear solution with spherical micellar structures in a wide concentration range. The suspension of the star block copolymer with m = 16 and n = 21 in water remained cloudy after heating above T_m. Here large structures form, presumably vesicles that allow recrystallization of the PCL cores upon cooling. DLS measurements of aqueous solutions of the larger star polymer within 6 hours after preparation indicate no formation of cylindrical vesicles. Cryo-TEM images show the formation of some cylindrical micelles after 6 days. This indicates that the spherical micelles are likely a metastable state where the samples lock in during cooling. The studies show that the length of the PEG chains can be used to tune size, stability, and crystallinity of micelles made of star block copolymers in water.

With regard to the self-assembly behavior of the star block copolymers, the question arises as to the influence of the relatively large benzoxazinone linker group. In particular, the strong electron-withdrawing effect of the nitro group suggests the formation of strong dipole–dipole interactions at this structural unit. This type of interaction is also thought to occur in the synthesis of related amphiphilic networks and to be responsible for specific deviations in the network connectivities.[23] This is the subject of further investigation using various spectroscopic methods directed at the specific interactions of these groups with each other and with the solvents used. In the case of the star polymers studied here, it is expected that in polar solvents such as water the dipole–dipole interactions are suppressed, so that the remaining hydrophobic interactions of the linker groups predominate. The extent to which this influences

the association behavior of the star block copolymers in water or other solvents cannot be conclusively clarified from the present studies. Comparative studies with alternative linker groups are planned for this purpose.

5.9. References

[1] Y. Zhang , T. Guan , G. Han , T. Guo and W. Zhang , *Macromolecules*, 2019, **52** , 718 –728.

[2] A. S. R. Oliveira , P. V. Mendonça , S. Simões , A. C. Serra and J. F. J. Coelho , *J. Polym. Sci.*, 2021, **59** , 211 –229.

[3] P. Dong , X. Wang , Y. Gu , Y. Wang , Y. Wang , C. Gong , F. Luo , G. Guo , X. Zhao , Y. Wei and Z. Qian , *Colloids Surf., A*, 2010, **358** , 128 –134.

[4] K. Ishizu and S. Uchida , *Prog. Polym. Sci.*, 1999, **24** , 1439 –1480.

[5] W. Burchard *Branched polymers II* , Springer, 1999, 113–194.

[6] A. J. Inglis , P. Pierrat , T. Muller , S. Bräse and C. Barner-Kowollik , *Soft Matter*, 2010, **6** , 82 –84.

[7] A. M. Bhayo, R. Abdul-Karim, S. G. Musharraf and M. I. Malik, *RSC Adv.*, 2018, **8** , 28569 –28580.

[8] T. Öztürk, A. Kiliçlioğlu, B. Savaş and B. Hazer, *J. Macromol. Sci., Part A: Pure Appl.Chem.*, 2018, **55**, 588 –594.

[9] A. Imdad, K. Faheem, R. Sana, P. Samina, A. Shakil, S. Muhammad Raza and M. Muhammad Imran, *React. Funct. Polym.*, 2020, **150**, 104553.

[10] X. Yan, J. Li and T. Ren, *RSC Adv.*, 2018, **8**, 29464 –29475.

[11] Ö. Gökçe Kocabay and O. İsmail, *Int. J. Polym. Mater. Polym. Biomater.*, 2021, **70**, 328 –337.

[12] A. Behl, V. S. Parmar, S. Malhotra, and A. K. Chhillar, *Polymer*, 2020, **207**, 122901.

[13] H. Chunyan, C. Zhuo, W. Shengjie, H. Yanfeng, W. Hai, S. Hongfan, K. Deling, L. Xigang, W. Chun, Z. Linhua and Z. Dunwan, *Chin. Chem. Lett.*, 2017, **28**, 1905 –1909.

[14] K. S. Shalaby, M. E. Soliman, G. Bonacucina, M. Cespi , G. F. Palmieri , O. A. Sammour , A. A. El Shamy , L. Illum and L. Casettari , *Pharm. Res.*, 2016, **33** , 2010 –2024.

[15] C. Lu, S.-R. Guo, Y. Zhang and M. Yin, *Polym. Int.*, 2006, **55**, 694 –700.

[16] C. Lu, L. Liu, S.-R. Guo, Y. Zhang, Z. Li and J. Gu , *Eur. Polym. J.*, 2007, **43**, 1857 –1865.

[17] S. Guo and Y. Zhang, *J. Polym. Sci., Part B: Polym. Phys.*, 2008, **46**, 1412 –1418.

[18] Z.-X. Du, J.-T. Xu and Z.-Q. Fan, *Macromol. Rapid Commun.*, 2008, **29**, 467 –471.

[19] Z.-X. Du, J.-T. Xu and Z.-Q. Fan, *Macromolecules*, 2007, **40** , 7633 –7637.

[20] J. J. Crassous, P. Schurtenberger, M. Ballauff and A. M. Mihut, *Polymer*, 2015, **62**, A1 – A13.

[21] M. Alami-Milani, P. Zakeri-Milani, H. Valizadeh, R. Salehi and M. Jelvehgari, *Iran. J. Basic Med. Sci.*, 2018, **21**, 153.

[22] N. Brigham, C. Nardi, A. Carandang, K. Allen and R. M. Van Horn, *Macromolecules*, 2017, **50**, 8996 –9007.

[23] C. Bunk, L. Löser, N. Fribiczer, H. Komber, L. Jakisch, R. Scholz, B. Voit, S. Seiffert, K. Saalwächter, M. Lang and F. Böhme, *Macromolecules*, 2022, **55**, 6573 –6589.

[24] M. Lang, R. Scholz, L. Löser, C. Bunk, N. Fribiczer, S. Seiffert, F. Böhme and K. Saalwächter, *Macromolecules*, 2022, **55**, 5997 –6014.

[25] K. Hagmann, C. Bunk, F. Böhme and R. von Klitzing, *Polymers*, 2022, **14** , 2555.

[26] L. Jakisch, M. Garaleh, M. Schäfer, A. Mordvinkin, K. Saalwächter and F. Böhme, *Macromol. Chem. Phys.*, 2018, **219**, 1700327.

[27] H. Zhang, L. Jakisch, H. Komber, B. Voit and F. Böhme, *Tetrahedron*, 2013, **69**, 3656 – 3663.

[28] L. Jakisch, H. Komber and F. Böhme, *Macromol. Mater. Eng.*, 2007, **292**, 557 –570.

[29] L. Jakisch, H. Komber and F. Böhme, *J. Polym. Sci., Part A: Polym. Chem.*, 2003, **41**, 655 –667.

[30] S. Ishii, H. Kokubo, K. Hashimoto, S. Imaizumi and M. Watanabe, *Macromolecules*, 2017, **50**, 2906 –2915.

[31] K. A. Barrera-Rivera, R. Vera-Graziano, E. López-Sánchez and A. Martinez-Richa, *J. Polym. Res.*, 2015, **22**, 1 –8.

[32] Y. Huang, Z. Xu, Y. Huang, D. Ma, J. Yang and J. W. Mays, *Int. J. Polym. Anal. Charact.*, 2003, **8**, 383 –394.

[33] S. Jain and F. S. Bates, *Science*, 2003, **300**, 460 –464.

[34] K. Rajagopal, A. Mahmud, D. A. Christian, J. D. Pajerowski, A. E. Brown, S. M. Loverde and D. E. Discher, *Macromolecules*, 2010, **43**, 9736 –9746.

[35] J. A. Zupancich, F. S. Bates and M. A. Hillmyer, *Macromolecules*, 2006, **39**, 4286 – 4288.

[36] P. P. Ghoroghchian, G. Li, D. H. Levine, K. P. Davis, F. S. Bates, D. A. Hammer and M. J. Therien, *Macromolecules*, 2006, **39**, 1673.

[37] J. Zhou, R. Ni and Y. Chau, *RSC Adv.*, 2017, **7**, 17997 –18000.

[38] Y. Geng and D. E. Discher, *J. Am. Chem. Soc.*, 2005, **127**, 12780 –12781.

[39] J.-X. Yang, B. Fan, J.-H. Li, J.-T. Xu, B.-Y. Du and Z.-Q. Fan, *Macromolecules*, 2016, **49**, 367 –372.

[40] A. M. Mihut, J. J. Crassous , H. Schmalz , M. Drechsler and M. Ballauff , *Soft Matter*, 2012, **8** , 3163 –3173.

[41] N. Fairley, B. Hoang and C. Allen, *Biomacromolecules*, 2008, **9**, 2283 –2291.

[42] B. Bogdanov, A. Vidts , E. Schacht and H. Berghmans , *Macromolecules*, 1999, **32** , 726 –731.

[43] B. Wunderlich *Macromolecular physics volume 3 Crystal Melting*, Academic Press, New York, 2012.

[44] C. P. Buckley and A. J. Kovacs, *Colloid Polym. Sci.*, 1976, **254**, 695 –715.

[45] C. Luo, W. Chen and Y. Gao, *Polym. Sci., Ser. A*, 2016, **58**, 196 –205.

[46] P. M. Remiro, M. M. Cortazar, M. E. Calahorra and M. M. Calafel, *Macromol. Chem. Phys.*, 2001, **202**, 1077 –1088.

[47] R. De Juana and M. Cortazar, *Macromolecules*, 1993, **26**, 1170 –1176.

[48] B. Bogdanov, A. Vidts, A. Van Den Buicke, R. Verbeeck and E. Schacht, *Polymer*, 1998, **39**, 1631 –1636.

[49] P. C. Ashman and C. Booth, *Polymer*, 1975, **16**, 889 —896.

[50] P. K. Kilpatrick, W. G. Miller and Y. Talmon, *J. Colloid Interface Sci.*, 1985, **107**, 146 –158.

[51] G. D. Smith, D. Y. Yoon, R. L. Jaffe, R. H. Colby, R. Krishnamoorti and L. J. Fetters, *Macromolecules*, 1996, **29**, 3462 –3469.

[52] G. D. Smith, D. Y. Yoon and R. L. Jaffe, *Macromolecules*, 1993, **26**, 5213 –5218.

[53] H. Lee, R. M. Venable, A. D. MacKerell and R. W. Pastor, *Biophys. J.*, 2008, **95**, 1590 –1599.

[54] Y. Chatani, Y. Okita, H. Tadokoro and Y. Yamashita, *Polym. J.*, 1970, **1**, 555 –562.

[55] L. Huang and K. Nishinari, *J. Polym. Sci., Part B: Polym. Phys.*, 2001, **39**, 496 –506.

[56] W. D. Mkandawire and S. T. Milner, *Macromolecules*, 2021, **54**, 3613 –3619.

[57] M. Rubinstein and R. H. Colby, *Polymer physics*, Oxford university press, New York, 2003

6. CHAPTER IV: NETWORKS FROM AMPHIPHILIC STAR BLOCK COPOLYMERS

Amphiphilic Polymer Co-Networks Based on Cross-linked tetra-PEG-*b*-PCL Star Block Copolymers

[redacted] **N. Fribiczer**, [redacted]

Polymer, **2024**, *required reviews completed* (status: 07.03.2024; initial submission: 11.01.2024)

The corresponding *Supporting Information* is included in **Appendix A.6**.

The results in this chapter were adapted with permission from the authors.

6.1. Specific Summary

In the last chapters, networks composed of separate four-armed t-PEG and t-PCL building blocks were characterized in detail and first insights into the solution behavior of amphiphilic star block copolymers, namely t-PCL-*b*-PEG, were given. This chapter now focuses on networks based on crosslinked amphiphilic block copolymers. However, instead of using the already known t-PCL-*b*-PEG polymers for network formation, the reverse t-PEG-*b*-PCL block copolymers are synthesized. Those are chosen due to the synthetically less complex end group modification compared to the previously investigated ones.

In general, it is well-known that a rational design of regular patterns or certain morphologies is possible for block copolymers by a suitable choice of the polymer blocks, polymer architecture, and the solvent. An orientation of these patterns can be achieved by deformation or shearing of the material, or by incorporating lamellar morphologies. These concepts could be applied to amphiphilic block copolymers to possibly enable the controlled and directed transport of guest substances. Again, model networks are a powerful tool to get a rational understanding of the underlying processes due to the separate control over key material parameters. In this chapter, a further building block is added to the exploration of structure-property relationships of amphiphilic polymer co-networks and their use for the targeted design of applications by investigation of networks comprised of star-shaped t-PEG-*b*-PCL block copolymers.

The star-shaped block copolymers are synthesized starting from hydroxyl-terminated t-PEG (t-PEG-OH). The PCL block is added in a ring-opening polymerization of ε-caprolactone, in which the t-PEG-OH serves as an initiator. The end groups are subsequently converted to amine

or benzoxazinone functionalities, which corresponds to the hetero-complementary crosslinking chemistry from the previous *Chapters I* and *II*. In contrast to these earlier studies, gelation is carried out in DMSO, as gelation in the previously used solvents takes an unexpectedly long time and is therefore not feasible. One problem that arises from the use of DMSO is its highly hygroscopic nature, which affects all measurements in which the material is in contact with air and therefore air moisture. This must therefore be considered when discussing the measurement results.

The gelation reaction in DMSO is monitored by rheology and reveals a two-step mechanism at temperatures < 60 °C. At temperatures ≥ 60 °C, a one-step gelation is observed. The second process is attributed to the actual crosslinking, whereas the first process reflects the association of prolonged PCL segments after initial reaction of the star polymers. This association is further promoted by the benzoxazinone linking groups, which, according to viscosity measurements, reduce the solubility of the star polymers. In addition, the mechanics of the final networks are characterized in DMSO in the as-prepared state and at equilibrium swelling in water. The modulus in water is several times higher than in DMSO accompanied by a highly opaque appearance. The swelling of the networks in different solvents is investigated and decreasing degrees of swelling are found in the order chloroform, toluene and DMSO, water, and methyl tert-butyl ether (MTBE). Finally, the connectivity of the networks is investigated by multiple quantum NMR. The fraction of single and double links is similar to the fractions of networks consisting of separate t-PEG and t-PCL building blocks (see *Chapter I*) for concentrations at and above the overlap concentration. Furthermore, the defect fractions are very low at 1–7% and increase with decreasing concentration.

Further studies on the network structure and morphology in water or other appropriately selective solvents (only good solvent for the hydrophobic or hydrophilic part and poor solvent for the other part) are required to take the step towards a possible material design. The hygroscopic nature of DMSO is discussed here as a problem during measurements but could also be used in the future to drive structural changes over time through water uptake. In addition, studies on the permeability of the material for guest substances of different philie can contribute to the understanding of possible transport functions.

6.2. Author Contributions

[redacted]	Concept development, synthesis optimization, swelling experiment evaluation, and manuscript preparation and correction.
Nora Fribiczer:	Viscometry and rheology measurements and evaluation, determination of swelling degree in DMSO and water.
[redacted]	MQ NMR spectroscopy and analysis.
[redacted]	MALDI-TOF MS measurements.
[redacted]	Supervision of [redacted] and manuscript correction.
[redacted]	Scientific supervision of [redacted] and manuscript correction.
[redacted]	Scientific supervision of [redacted] and manuscript correction.
[redacted]	Scientific supervision and manuscript correction.
[redacted]	Concept development, scientific supervision and manuscript correction.

6.3. Acknowledgement

This work was supported by the German Research Foundation (DFG) and carried out as part of the Research Unit FOR-2811, grant 397384169, and the individual grants 423514254, 423478088, 423435302, 423373052. [redacted] thanks [redacted] for performing the syntheses. The Authors thank [redacted] kindly for recording all HR NMR spectra.

6.4. Abstract

A new class of AB_4-type amphiphilic polymer co-networks (ACN) was prepared by hetero-complementary 2-(4-nitrophenyl)-benzoxazinone/amine end group crosslinking chemistry in dimethyl sulfoxide (DMSO). For this purpose, a well-defined star block copolymer (tetra-PEG-*b*-PCL) consisting of a hydrophilic tetra-arm PEG core (M_n ~ 5 kg·mol^{-1}) and hydrophobic PCL wings with a total molar mass of M_n ~ 10 kg·mol^{-1} was synthesized by ring-opening polymerization (ROP). This tetra-PEG-*b*-PCL star block copolymer was functionalized either with 2-(4-nitrophenyl)-benzoxazinone or with amino terminal groups. The ACN synthesis was carried out by conversion of these two star block copolymers. The overlap concentration of c^* ~ 76 g·L^{-1} determined by viscosity measurements of both stars showed no significant temperature dependence. The network syntheses carried out at different concentrations (0.5 c^* to 2.5 c^*) resulted in conversion degrees in the range of $p \approx 95$ % or higher as detected by HR MAS NMR spectroscopy. As in previous work on the synthesis of A_4B_4 networks using the same crosslinking chemistry, deviations from the expected network structure (increased proportion of double links between two stars) were detected also here by multi quantum NMR spectroscopy. The expected environmentally sensitive behavior of the ACNs was confirmed in terms of their equilibrium swelling in solvents of different quality to PEG and PCL. The scaling of the swelling and viscoelasticity data as a function of preparation concentration showed deviations from the expectations of a perfectly crosslinked star polymer network. Finally, a two-step gelation process was observed by rheology at 30 °C in DMSO, which is related to associations between the 2-(4-nitrophenyl)-benzoxazinone groups surrounded by PCL blocks that become apparent on the time scale of rheology when the molar mass is increased as a result of crosslinking.

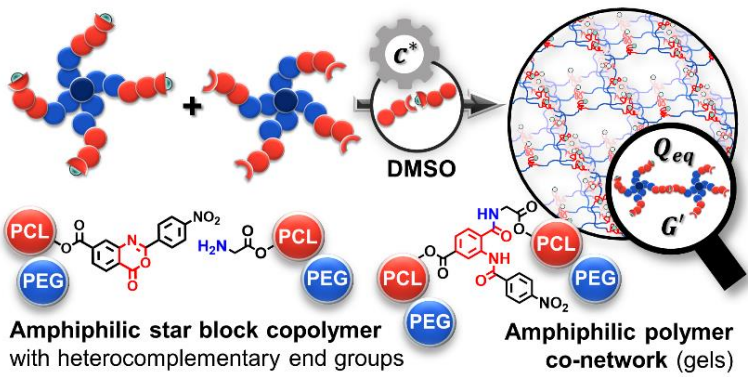

Scheme 6. 1: Schematic representation of network formation from amphiphilic star block copolymers and corresponding properties of the resulting gel.

6.5. Introduction

Amphiphilic polymer co-networks (ACNs) and gels provide elastic matrices that allow for a co-continuous transport of hydrophilic and hydrophobic solutes depending on the thermodynamic state of the sample.[1, 2] When exposed to a selective solvent of a particular philicity, the poorly soluble polymer separates on the nanoscale forming irregular domains that depend on the local composition of both polymer components and the structure of the network. For block copolymer melts and solutions, it is well established that regular patterns can be designed by a suitable choice of the polymer blocks, the polymer architecture, and the solvent.[3-5] These patterns can be guided into a particular direction, for instance, by shearing the polymer domains.[6, 7] Similarly, in networks made of different components, a long-range orientational order can be imposed by sample deformation.[8] When applied to amphiphilic gels or networks made from different polymer blocks, these concepts can be used to design new materials with oriented domains that can be prepared or switched on demand[9] leading eventually to a controllable transport of different classes of solutes in different directions. However, for a basic understanding of these processes, model samples are needed that allow a separate control of the key material parameters.

In recent years, we have developed a platform of such model networks based upon the hetero-complementary coupling reaction[10-12] of amine- and 2-(4-nitrophenyl)-benzoxazinone-terminated network components. The hetero-complementary strategy has the advantage of avoiding network defects like pending loops that become abundant in the vicinity of the overlap concentration.[13, 14] In consequence, model networks can be prepared with a low variation in the connectivity of the branching units over a broad range of concentrations,[15, 16] which is highly favorable for a concise test of basic physical concepts. In the synthesis of ACNs based on hydrophilic tetra-PEG and hydrophobic tetra-PCL stars, this 2-(4-nitrophenyl)-benzoxazinone/amine reaction has been well established.[10, 15, 17-19] Nevertheless, it should be noted that the linkage of purely hydrophilic and hydrophobic components as described in Ref. [10] may be accompanied by separation processes that can strongly affect the final structure of the network (see also *Chapter I* of this thesis). This is especially important if the solvent used in the synthesis provides a different solvent quality for the two components. In order to better understand the structure-forming processes, star block copolymers are used in this work in which both components are already included. Specifically, these are two batches of tetra-arm star block copolymers consisting each of a PEG core and PCL wings differing only in their end groups (2-(4-nitrophenyl)- benzoxazinone and amine, respectively). Apart from the end groups,

the structural parameters of both stars are equal. Therefore, their solubilities should hardly differ. The synthesis of the star block copolymers, the corresponding ACN formation in dimethyl sulfoxide (DMSO), and their possible connectivity motifs between the same pair of stars are illustrated in **Scheme 6. 2**.

Since linear block copolymers with a similar molar mass as our block-stars are soluble in DMSO,[20] another goal of this work is to test whether or not DMSO allows to suppress associations between the linking groups during crosslinking that perturbed an experimental analysis of the different network connectivities in preceding work.[10] We expect that our results impact further development of switchable amphiphilic model systems with a controlled transport of solutes of different philicity.

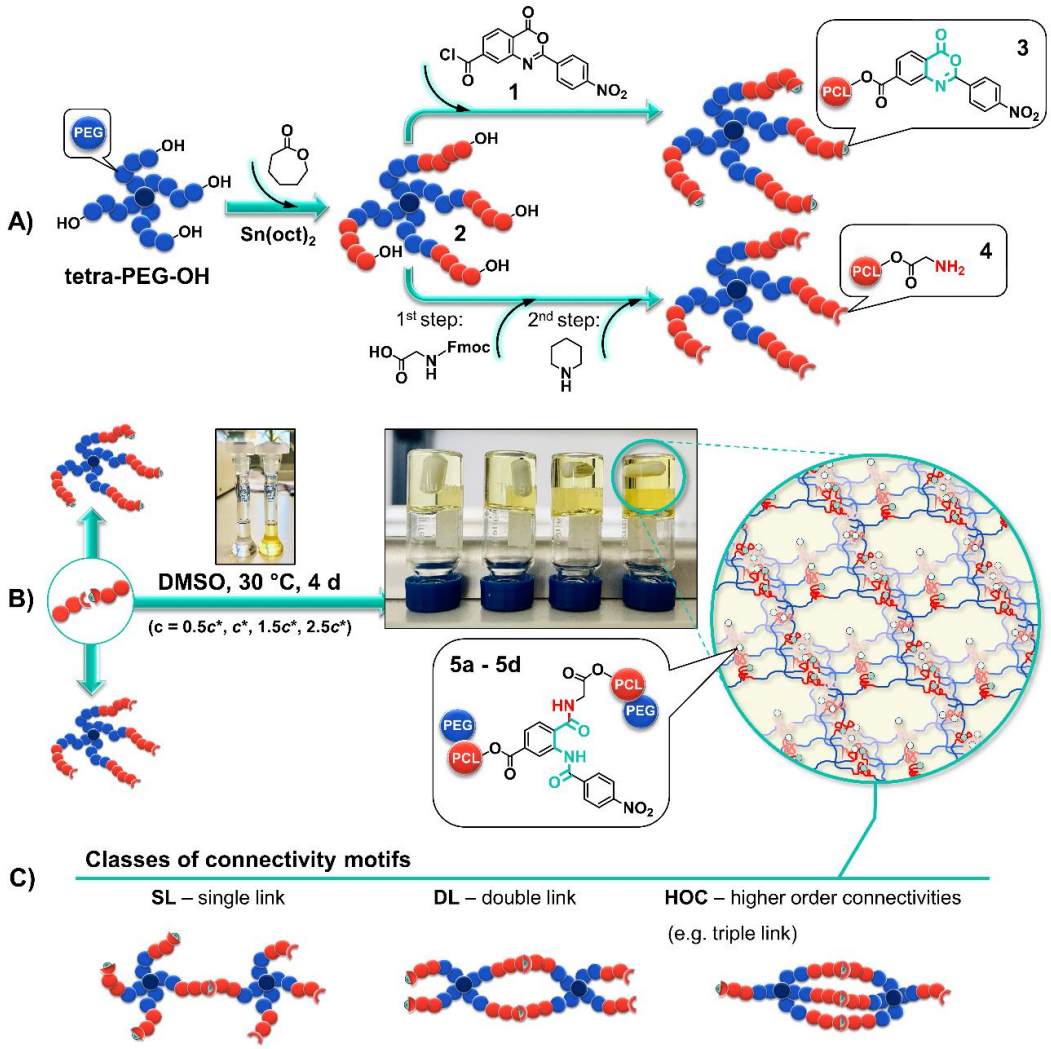

Scheme 6. 2: A) Synthesis of hydroxy-terminated tetra-PEG-*b*-PCL star block copolymer **2**, 2-(4-nitrophenyl)-benzoxazinone-terminated tetra-PEG-*b*-PCL star block copolymer **3**, amino-terminated tetra-PEG-*b*-PCL star block copolymer **4**, and their hetero-complementary reaction **B)** to obtain amphiphilic polymer co-networks **5a - 5d** with different classes of possible connectivity motifs **C)**.

6.6. Experimental

Materials

Hydroxy-terminated poly(ethylene glycol) star polymer (**tetra-PEG-OH**) was purchased from JenKem Technology, USA. Prior to use, **tetra-PEG-OH** was first dialyzed against water (ZelluTrans, Roth, dialysis membrane *MWCO* 1000) and subsequently precipitated twice from THF in cold diethyl ether. The number-average molar mass (M_n) and the dispersity ($Đ$) were determined via MALDI-TOF MS (M_n = 5.2 kg mol^{-1}, $Đ$ = 1.01). The number-average degree of polymerization (P_n) of 116 was determined by ^{1}H NMR spectroscopy, corresponding to an M_n of 5.2 kg mol^{-1}. ε-Caprolactone (ε-CL, 97 %, Sigma-Aldrich) was dried with calcium hydride (CaH_2) for 24 h, then distilled under vacuum and stored under nitrogen atmosphere. Stannous octoate ($Sn(oct)_2$, 98.0 %, Sigma-Aldrich) was purified by vacuum distillation and kept under nitrogen atmosphere. N-alpha-(9-fluorenylmethyloxycarbonyl)-glycine (**Fmoc-Gly-OH**, ≥ 99.0 %) was obtained from Merck KGaA (Novabiochem®), Germany, and used as supplied. Deuterated dimethyl sulfoxide (DMSO-d_6, 99.80 % D, Eurisotop, Germany), dimethyl sulfoxide (DMSO, 99.9 %, Acros Organics), tert-butyl methyl ether (MTBE, 99 %, Alfa Aesar), tetrahydrofuran (THF, 99.6 %, Acros Organics), N, N'-dimethylformamide (DMF, (≥ 99.8 %, VWR chemicals) chloroform (≥ 99.8 %, Fisher Chemicals), diethyl ether (≥ 99.5 %, stabilized, Th. Geyer (CHEMSOLUTE®)), piperidine (≥ 99.0 %, Iris Biotech GmbH), N, N′-dicyclohexylcarbodiimide (DCC, > 97.0 %, TCI chemicals), triethylamine (≥ 99.5 %, Sigma-Aldrich), and 4-dimethylaminopyridine (DMAP, ≥ 99.8 %, Sigma-Aldrich) were used without further purification. The synthesis of 2-(4-nitrophenyl)-4-oxo-4H-benzo[d][1,3]oxazine-7-carboxylic acid chloride (**1**) has been described earlier.[11]

Synthesis and Functionalization of tetra-PEG-b-PCL Star Block Copolymers

Hydroxy-terminated tetra-PEG-b-PCL star block copolymer (2).

To obtain star block copolymer **2**, ring-opening polymerization (ROP) of ε-CL initiated by **tetra-PEG-OH** with $Sn(oct)_2$ as catalyst was performed according to our previous publications (see **Scheme 6. 2A**).[10, 11] A typical ROP, **tetra-PEG-OH** (1 eq., 30 g, 5.77 mmol) with a number-average molar mass of 5.2 kg mol^{-1} was dissolved in 31.2 mL ε-CL (46 eq., 30.3 g, 0.265 mol) for 20 min at 80 °C. Subsequently, the polymerization was started by adding $Sn(oct)_2$ (0.05 eq., 0.57 mL of 0.5 M solution in toluene) under a continuous flow of nitrogen. After stirring for 2 h at 80 °C, the temperature was increased to 100 °C for another 3.5 h. The polymerization was stopped by cooling to room temperature and the product was then isolated

by precipitation in cold diethyl ether. After washing the product vigorously with fresh diethyl ether, filtering through a filter funnel, and drying *in vacuo* at 40 °C overnight, tetra-PEG_{116}-*b*-PCL_{44} star block copolymer **2** was obtained as a white powder. Yield: 58 g (96 %).

^{1}H NMR (DMSO-d_6): δ 4.30 (t, 5.1 Hz; 11), 4.11 (t, 4.7 Hz; 4*), 3.98 (t, 6.4 Hz; 10), 3.51 (s; 3, 4), 3.40 – 3.34 (m; 10*), 3.29 (s; 2), 2.27 (t, 7.1 Hz; 6), 1.60 - 1.45 (m; 7, 9), 1.30 ppm (m; 8). The determination of the block ratio by ^{1}H NMR spectroscopy, the corresponding chemical structures, and the proton signal assignments are reported in the SI (**Figure A.6. 1 and A.6. 2b**).

2-(4-Nitrophenyl)-benzoxazinone-terminated tetra-PEG-b-PCL star block copolymer (3).

Star block copolymer **3** was synthesized by attaching 2-(4-nitrophenyl)-4-oxo-4H-benzo[d][1,3]oxazine-7-carboxylic acid chloride (**1**) (8 eq., 5.13 g, 15.54 mmol) to the hydroxyl terminal groups of star block copolymer **2** (1 eq., 20 g, 1.94 mmol) in the presence of triethyl-amine (8 eq., 1.57 g, 15.54 mmol) (**Scheme 6. 2A**). Yield: 19 g (85 %). Details of the reaction are reported elsewhere.[10-12]

^{1}H NMR (DMSO-d_6): δ 8.50 – 8.39 (m; 21, 22), 8.32 (d, 8.1 Hz; 13), 8.20 (s; 16), 8.15 (d, 8.1 Hz; 12), 4.35 (t, 6.1 Hz; 10*), 4.11 (m; 4*), 3.98 (m; 10), 3.51 (s; 3, 4), 3.29 (s; 2), 2.26 (m; 6), 1.53 (m; 7, 9), 1.29 ppm (m; 8). The corresponding chemical structures and the proton signal assignments are given in the SI (**Figure A.6. 2c**).

Amino-terminated tetra-PEG-b-PCL star block copolymer (4).

Star block copolymer **4** was synthesized according to **Scheme 6. 2A** in two steps. First, the hydroxyl terminal groups of star block copolymer **2** were esterified with N-alpha-(9-fluorenyl-methyloxycarbonyl)-glycine (**Fmoc-Gly-OH**) by the Steglich method,[21, 22] after which the α-amino group was deprotected by piperidine. A representative experiment is described as follows: Star block copolymer **2** (1 eq., 30.0 g, 2.91 mmol) was dissolved in 150 mL of a mix-ture of DCM and DMF (2:1). After cooling the solution to 0 °C, **Fmoc-Gly-OH** (8 eq., 6.9 g, 23.30 mmol) and DMAP (0.4 eq., 142.2 mg, 1.16 mmol) were added and the mixture was stirred at 0 °C under nitrogen for 30 min. To activate the carboxyl group of **Fmoc-Gly-OH**, 40 mL of a previously prepared solution of DCC (7 eq., 4.2 g, 20.37 mmol) in DCM and DMF (as above 2:1) was added dropwise under nitrogen. The mixture was stirred at 0 °C for 1 h and at room temperature for another 23 h. Then, precipitated dicyclohexylurea was removed by filtration first at room temperature and then at –20 °C. Subsequently, the filtrate was concentrated *in*

vacuo and precipitated in cold diethyl ether. After washing the product with fresh diethyl ether, filtering, and drying *in vacuo* at 35 °C overnight, the precipitation was performed one more time. The corresponding chemical structure and the proton signal assignments of the intermediate Fmoc-glycine-terminated tetra-PEG-*b*-PCL star block copolymer are given in the SI (**Figure A.6. 3b**). To deprotect the α-amino group, the intermediate was dissolved in 100 mL of a piperidine/DMF mixture (20% v/v). The mixture was stirred at room temperature for 1 h, filtered off, and the filtrate was precipitated in cold n-hexane. N-hexane was decanted, and the waxy residue was dissolved in 40 mL DCM and precipitated in cold diethyl ether. In a final step, the precipitate was separated by filtration, washed several times with fresh diethyl ether and dried overnight at 30 °C *in vacuo*. The resulting star block copolymer **4** was obtained as a white powder. Yield: 14 g (47 %).

^{1}H NMR (DMSO-d_6): δ 4.11 (t, 4.8 Hz; 4*), 4.02 (m; 10*), 3.98 (t, 6.6 Hz; 10), 3.51 (s; 3, 4), 3.32 (s; 2), 3.25 (s; a), 2.27 (t, 7.1 Hz; 6), 1.60 - 1.49 (m; 7, 9), 1.3 ppm (m; 8). The corresponding chemical structures and the proton signal assignments in the respective 1D and 2D ^{1}H NMR spectra are provided in the SI (**Figure A.6. 3a and A.6. 4**).

Synthesis of Amphiphilic Polymer Co-networks (5a - 5d)

5a – **5d** were synthesized by mixing DMSO stock solutions of the two star block copolymers **3** and **4** with an equimolar ratio of reactive end groups at different preparation concentrations (c_{prep} = 38, 76, 114 and 190 g·L^{-1}) (see **Scheme 6. 3**). The *c* values represent 0.5, 1, 1.5 and 2.5 times the overlap concentration *c** (76 g·L^{-1}) assigned to sample designations **5a**, **5b**, **5c**, and **5d**, respectively. The synthesis of a representative network (**5a**) was performed as follows: 0.478 g of the DMSO solution of **3** (38 g·L^{-1}) was transferred to a 2-mL glass vial (Agilent) equipped with magnetic stirrer using a 1-mL syringe. Subsequently, 0.440 g of the DMSO solution of **4** with the same concentration was added. The vial was closed and the reaction mixture was stirred at 30 °C until gelation. To keep humidity out during the reaction time, the gel was placed in a preheated desiccator with silica gel and all together in a drying oven for four days at 30 °C.

^{1}H NMR (DMSO-d_6): δ 12.40 (s; ArN*H*CO), 9.5 (br; CH_2N*H*CO), 9.19 (br; 16'), 8.42 (br; 22'), 8.15 (br; 21'), 8.00 (br; 13'), 7.82 (br; 12'), 4.32 (br; 10*'), 4.11 (s; 4*), 4.08 (br; a'), 3.97 (br; 10), 3.50 (s; 3, 4), 2.26 (br; 6), 1.54 (br; 7, 9), 1.30 ppm (br; 8). The proton signal assignments of ACN **5a** are shown in **Figure 6. 2A**.

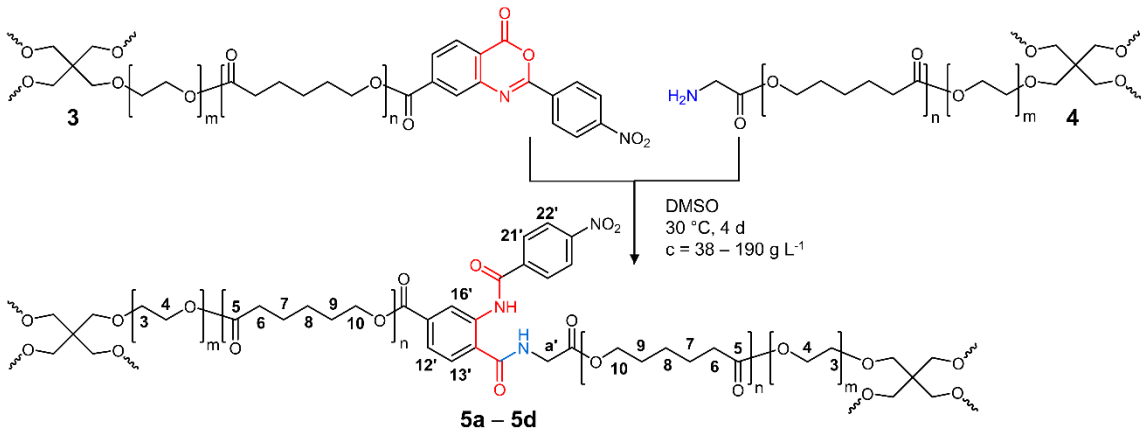

Scheme 6. 3: Synthesis of amphiphilic polymer co-networks (**5a** – **5d**).

Characterization

MALDI-TOF mass spectroscopy

Matrix-assisted laser desorption/ionization time-of-flight mass spectra (MALDI-TOF MS) of star polymers **tetra-PEG-OH**, **2**, **3** and **4** were recorded in linear positive TOF mode with a Bruker Autoflex Speed MALDI-TOF/TOF spectrometer, equipped with a Smartbeam-II Nd:YAG laser (355 nm, 1 kHz). A combination of trans-2-[3-(4-tert-butylphenyl)-2-methyl-2-propenylidene]-malononitrile (DCTB) and potassium acetate was selected as matrix and ion adductor, respectively. For a MALDI-TOF MS experiment, 8 µL of DCTB matrix solution in THF (10 g·L^{-1}), 1.6 µL polymer solution in THF (2 g·L^{-1}), and 0.8 µL of potassium acetate solution in ethanol (1 g·L^{-1}) were mixed and dropped onto the target plate. TOF-calibration was performed using PEG reference standards between 1 and 10 kDa by PSS Polymer Standards Service GmbH, Germany.

Viscometry

A capillary viscometer of micro-Ubbelohde type I was used to determine the overlap concentrations c^* of star block copolymers **3** and **4** in DMSO at 30 °C and 45 °C. Temperature was held constant by a water bath. Stock solutions of the respective polymers were prepared and diluted to c = 15, 12, 9, 6, and 3 g·L^{-1} and kept at constant temperature for 10 minutes prior to the measurement. The specific viscosity η_{sp} was calculated from the time t that a defined volume of the polymer solution needs to flow through the capillary and the corresponding time t_s for the pure solvent (1).

$$\eta_{\mathrm{sp}} = \frac{\eta - \eta_s}{\eta_{\mathrm{s}}} \approx \frac{t - t_{\mathrm{s}}}{t_s} \tag{1}$$

The reduced viscosity η_{red} is then calculated as

$$\eta_{\mathrm{red}} = \frac{\eta_{\mathrm{sp}}}{c} \tag{2}$$

The intrinsic viscosity $[\eta]$ is defined as[23]

$$[\eta] = \lim_{c \to 0} \frac{\eta_{\mathrm{sp}}}{c} = \frac{1}{c^*} \tag{3}$$

and was extrapolated according to the method of Schulz–Blaschke.[24]

$$\frac{\eta_{\mathrm{sp}}}{c} = [\eta] + k_{\mathrm{SB}}[\eta]\eta_{\mathrm{sp}} \tag{4}$$

Volume Swelling Degree (Q_v)

Q_v values of ACNs were determined in DMSO, H_2O, MTBE, $CHCl_3$, and toluene at room temperature directly after preparation (Q_{v1}) and after subsequent freeze-drying (Q_{v2}). For this purpose, all ACNs were first left to equilibrate in DMSO for two days. The ACNs were then stored in the respective solvent for another four days without prior drying. After equilibration was completed, the ACNs were weighed (Q_{v1}), freeze-dried *in vacuo*, weighed (dry weight), and placed again in the previously used fresh swelling medium for four days (Q_{v2}). The resulting gravimetrically determined equilibrium volume swelling degrees Q_v were calculated according to our previously published procedure.[10, 11]

High-Resolution Solution NMR spectroscopy

^{1}H NMR spectra (500.13 MHz) were recorded on an Avance III 500 spectrometer (Bruker Bio-spin). DMSO-d_6 ($\delta(^1H)$ = 2.50 ppm) and $CDCl_3$ ($\delta(^1H)$ = 7.26 ppm) were used as solvent, lock, and internal standard. Sample temperature was controlled to be constant (30 ± 0.5 °C) using a BVT-3000 instrument unless otherwise noted.

High-Resolution (HR) MAS NMR Spectroscopy

^{1}H HR-MAS NMR spectra of **5a** – **5d** were measured in a Bruker HR MAS probe with a ZrO_2 rotor (4 mm outer diameter) and a PTFE insert (50 µL insert volume) using an Avance III 500 NMR spectrometer. For the experiments, the insert was filled with the ACNs swollen in DMSO-d_6. The spectra were recorded at 30 °C with a rotation frequency (ν_r) of 4650 Hz. The reaction efficiency p was determined from the normalized integral intensities of a signal of the reacted 2-(4-nitrophenyl)-benzoxazinone group (*H*13' of **5a** – **5d**; 8.00 ppm) and of the non-reacted 2-(4-nitrophenyl)-benzoxazinone group (*H*13 of **3**; 8.32 ppm) marked in **Figure 6. 2**, following our previously published report.[10]

MQ NMR Spectroscopy

Static proton solid-state MQ-NMR experiments were used to quantify connectivity motifs and fraction of defects in a set of as-prepared ACNs (**5a** – **5d**). In crosslinked polymeric materials, a non-zero dipolar coupling between neighboring protons (the so-called residual dipolar coupling RDC) survives at long times, since network elasticity prevents an isotropic averaging of the segment orientations. The specific value of these RDCs depends on intrinsic properties such as chain length and type of repeating unit, but also on the forces from the connected chains that hold the chain in place. All studied samples were synthesized in 2-mL Agilent vials according to the synthesis protocol described above. Vials were kept immersed in a drying agent to minimize hydration effects of the DMSO-d_6 due to air humidity. All experiments were performed on a Bruker MiniSpec mq20 with a magnetic field of B_0 = 0.47 T (= proton Larmor frequency of 20 MHz). Temperature was regulated using a BVT-3000 unit and kept stable at T = 25 °C ± 1 °C. Pulse lengths were calibrated between 1.5 and 2.0 µs for 90° pulses and between 3.5 and 4.0 µs for 180° pulses. Measurements were performed using the Baum-Pines sequence[25] with incremented delays in-between the pulses up to a total DQ excitation time of several hundreds of ms. The recycle delay between two subsequent scans was set to 2.0 s, which ensures a full build-up of the polymer backbone magnetization, while partially filtering-out undesired magnetization arising from non-perfectly deuterated DMSO. Due to the low number of isotropic defects (< 7 % for all samples), a separation of sol content and proton-containing solvent using additional relaxation experiments (analogous to e.g.[26]) is not feasible, as the error of this procedure is on the order of the value itself. Therefore, measured defect components are always to be interpreted as a sum of sol, pending chains, and proton-containing solvent. The

obtained data are analyzed using Python 3.10 and Lmfit 1.0.3[27] with the procedures analogous to Ref. [10].

As in previous work on networks with the same architecture,[10, 16, 26, 28] a set of three classes of connectivity motifs (SL – single link, DL – double link, HOC – higher order connectivities, see **Scheme 6. 2C**) with distinct orientational degrees of freedom is assumed.[1] Each of these motifs are associated with a set of parameters (a_i, D^i_{res}, T^i_2), where a_i is its relative proton-weighted fraction, D^i_{res} is its dipolar coupling value and T^i_2, the corresponding transversal relaxation rate of the moiety. The experiment itself delivers a set of two related curves, being a relaxation-only signal (I_{ref}) and a so-called MQ build-up curve (I_{DQ}). Both curves were fitted simultaneously using the equations derived in Ref. [16] with the result of having a proton-weighted quantification of the occurrences of each moiety with a distinct mobility (a_i), as well as a rough measure of their orientational degree of freedom (D^i_{res}). Specific details on the latter are discussed in more depth in Ref. [15]. This result allows basic, but unique judgement on the structural composition and connectivity motifs of each of the gels in dependence on the synthesis parameters.

Rheology

Rheological measurements were conducted by oscillatory shear measurements on an Anton Paar modular compact rheometer of type MCR 302 (Anton Paar, Graz, Austria) equipped with a plate-plate geometry of type PP25 (diameter: 25 mm) or PP8 (diameter: 8 mm) and a solvent trap. The solvent trap was equipped with a drying agent to reduce a possible water uptake of DMSO from air. A Peltier plate was used for temperature control. ACNs were prepared in a sealed Teflon form surrounded by a drying agent according to the synthesis protocol described above at c = 38, 76, 114 and 190 g·L^{-1}. The viscoelastic behavior was studied both on the fully reacted ACNs **5a** – **5d** (five days at 30 °C) and during their gelation process as a function of time in the temperature range 30–80 °C. The measurements of full-reacted ACNs were performed immediately after preparation in DMSO and then at equilibrium volume swelling degree (Q_v) in water (five days of swelling). After swelling, samples were cut to fit into the PP8. Frequency sweeps were conducted with a shear amplitude of γ = 0.5 % and in the range of ω = 1–100 rad·s^{-1}.

[1] A special aspect of our network architecture is the suppression of pending loops and all other cyclic structures that are made of an odd number of network strands.[13, 14] This leads to a clearer separation of the RDC of double links from the remaining signal of the elastic part of the network, see e.g. the green data set in Figure 3 of Ref. [41]. After elimination of the RDC of all odd i_{min} in this Figure, the difference between the RDC at $i_{min} = 2$ (the double links) and the remaining $i_{min} \geq 4$ becomes more than a factor of two and thus, these signals can be discerned. For more conceptual insights, the reader is referred to Ref. [47].

6.7. Results and Discussion

In this study, amphiphilic star block copolymers were prepared which already contain both components (PCL, PEG) in one star, see **Scheme 6. 4B**. This complements our previous work on A_4B_4-type ACNs, where hydrophobic PCL and hydrophilic PEG tetra-arm star polymers served as building blocks,[10, 15, 17] see **Scheme 6. 4A**. The current synthesis strategy allows to encode the amphiphilic character in the precursor polymers. This guarantees the miscibility of the components on the length scale of individual stars, while the physics of block copolymers can be utilized to structure the material on demand prior to gelation.

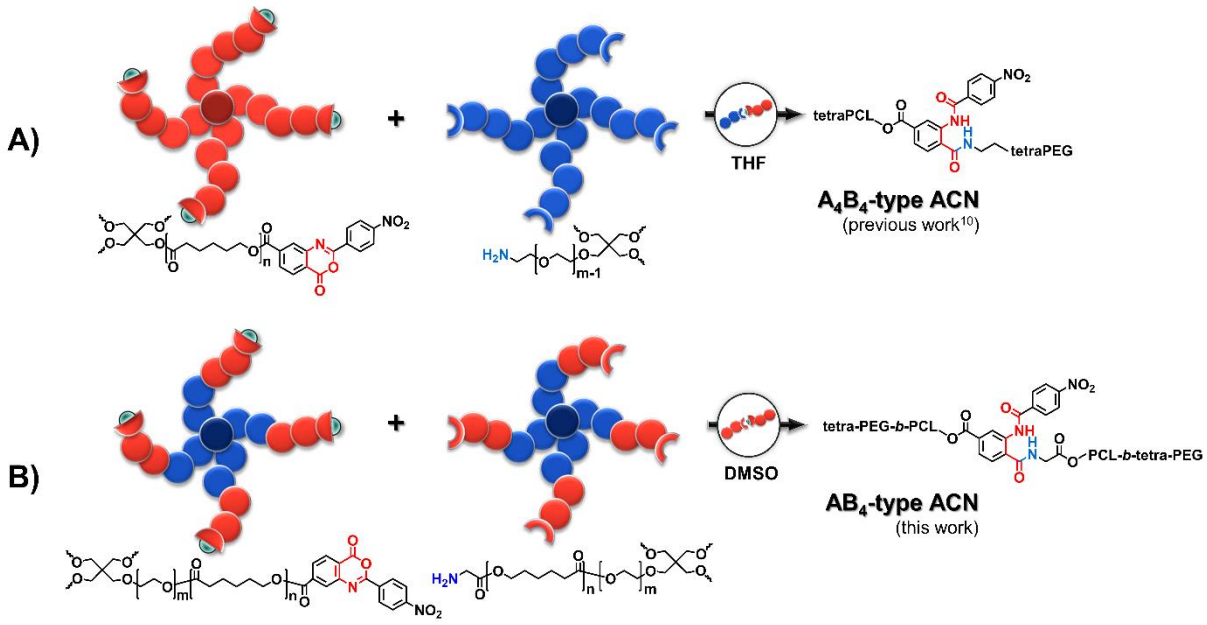

Scheme 6. 4: Comparison of two synthesis strategies for the formation of ACNs with model structure from **A)** homo-PEG and -PCL star polymers as described in our previous work[10] and **B)** PEG-*b*-PCL star polymers of the present work.

In the following, we first explain the synthesis strategy and structural analysis of 2-(4-nitrophenyl)-benzoxazinone- and amino-terminated tetra-PEG-*b*-PCL star block copolymers, **3** and **4**, respectively. This also includes the determination of the overlap concentration c^* of **3** and **4**, and the understanding between the polymer blocks (PEG, PCL) in the synthesis solvent DMSO (interaction parameters). The results are summarized in **Table 6. 1** and **6. 2**. Then, the formation of ACNs by hetero-complementary reaction of **3** and **4** and analysis of the co-networks **5** by HR MAS (high- resolution magic-angle-spinning) and MQ (multiple quantum) NMR spectroscopy in DMSO as well as swelling experiments in different solvents are described. Finally, both the solvent-dependent viscoelastic behavior of ACNs and their

temperature- and concentration-dependent gelation process determined by rheological studies are discussed. The results are summarized in **Table 6. 3** and **6. 4**.

Synthesis and Structural Analysis of tetra-PEG-b-PCL Star Block Copolymers 3 and 4

The synthesis steps of star block copolymer **3** and **4** shown in **Scheme 6. 2A** were monitored by NMR spectroscopy and MALDI-TOF MS. Initially, hydroxy-terminated star block copolymer **2** was prepared by ROP of ε-caprolactone (ε-CL) according to the "core-first" approach with **tetra-PEG-OH** as the initiating core. With this synthesis strategy, monodisperse tetra-PEG$_{116}$-*b*-PCL$_{44}$ star block copolymer **2** with the targeted number of ε-CL repeating units per arm (n = 11, see **Table 6. 1**) was achieved as determined by ^{1}H NMR end group analysis (see SI **Figure A.6. 1**). SI **Figure A.6. 2b** depicts the ^{1}H NMR spectrum of star polymer **2**. Absence of the hydroxy signal *H*5 at 4.52 ppm indicates a quantitative esterification of the PEG hydroxy groups. To introduce the above-mentioned terminal groups, the hydroxy groups of **2** were then modified with **Fmoc-Gly-OH** and 2-(4-nitrophenyl)-benzoxazinone-based compound **1**, respectively. By comparing the stacked ^{1}H NMR spectra of **2** and **3** in SI **Figure A.6. 2** and of **2** and **4** in SI **Figure A.6. 3**, the complete disappearance of the proton signal *H*11 at 4.30 ppm of **2** demonstrated a quantitative conversion of the hydroxy groups to the respective end groups. Furthermore, the Fmoc group was successfully cleaved, as indicated by the absence of proton signals in the aromatic region of **4** at 7.32 – 7.89 ppm (see SI **Figure A.6. 3a**).

MALDI-TOF mass spectra of **tetra-PEG-OH, 2**, **3** and **4** were measured to determine the molar masses of the stars (by the mass to charge ratio) and their relative differences (see SI **Figure A.6. 5**). Between the mass peak apexes of **1** and **2**, a relative difference of m/z ≈ 4700 was observed, corresponding to a relative difference in number average molar mass of 4.9 ± 0.2 kDa which agrees to the total number of PCL repeating units per tetra-PEG-core found by solution NMR spectroscopy. Star block copolymer **3** showed a relative difference between the peak apexes of m/z ≈ 1100 to its predecessor **2**, which corresponds to the molar mass of the four oxazinone terminal groups. The relative increase in m/z of star block copolymer **4** to its precursor **2** (between peak apexes) of about m/z 1050 is significantly higher than expected. For the conversion of hydroxy groups to amino groups (see **Scheme 6. 2**), an increase in molar mass of 228 g·mol^{-1} is expected. The distinctly higher increase in molar mass can be explained by chemical adduction of molecules of the MALDI-matrix DCTB to free terminal amino groups, as reported earlier.[29] This effect indicates indirectly the existence of free terminal amino groups, but it was not further investigated since it is beyond the scope of this work.

Table 6. 1: Molecular characteristics of star polymers **1**, **2**, **3**, and **4**.

Star polymer	m_{PEG} [a]	n_{PCL} [a]	w_{PEG} [b] (%)	w_{PCL} [b] (%)	M_n [c] kg mol^{-1}	M_n [d] kg mol^{-1}	$Đ$ [d]	$c^*_{30\,°C}$ [e] (g L^{-1})	$c^*_{45\,°C}$ [e] (g L^{-1})
PEG	29	-	97.4	-	5.2 ± 0.1	5.2 ± 0.1	1.01	-	-
2	29	11	49.8	48.9	10.3 ± 0.2	10.1 ± 0.6	1.04	-	-
3	29	11	44.6	43.9	11.4 ± 0.2	10.5 ± 0.7	1.04	74.2 ± 0.4	76.2 ± 0.9
4	29	11	48.7	47.9	10.5 ± 0.2	11.4 ± 0.7	1.03	77.2 ± 0.3	77.9 ± 0.4

[a] Number of monomer units of the PEG block and the PCL block per arm, respectively, based on ^{1}H NMR spectroscopic analysis (see SI Fig. S1 and comments).

[b] Proportions of the core and the end groups were also taken into account in the calculation.

[c] Determined by ^{1}H NMR spectroscopy.

[d] Determined by MALDI-TOF MS, $Đ$ = Dispersity (M_w / M_n).

[e] Overlap concentration determined by viscometry with Schulz-Blaschke regression model in DMSO (see **Figure 6. 1**).

For understanding the behavior of the star block-copolymers in solution, the interaction between the polymer blocks and DMSO needs to be understood. **Table 6. 2** contains an estimate for the interaction parameters of PEG and PCL with DMSO based upon literature data on the solubility parameters[30, 31] and the Hansen approach[31].

Table 6. 2: Hansen estimates of the interaction parameter χ based upon different data[30, 31]for the solubility parameters. The calculation and all parameters are described in **Section A.6.7** of the SI.

X estimates of DMSO for	25 °C	80 °C	Ref.
PEG	0.11	0.09	[30]
PEG	0.33	0.28	[31]
PCL	0.43	0.42	[30]
PCL	0.60	0.58	[31]

The computations and the key parameters used are summarized in **Section A.6. 7** of the supporting information (**Appendix A.6**). **Table 6. 2** indicates a significant dependence of χ on the available data for the solubility parameters. Therefore, we compare with other literature data for testing the quality of the interaction parameter estimates. According to Qin and Wu[32], 80 kDa PCL does not dissolve in DMSO at room temperature, but it dissolves at 80 °C. Since the molar mass of the PCL is rather large and the temperature dependence of the interactions between DMSO is expected to be weak, see **Table 6. 2**, this indicates that the parameters of Ref. [31] for PCL agree better with the experiment. Thus, DMSO is presumably a weakly poor solvent for PCL. DMSO is a strongly hygroscopic solvent and it absorbs significant amounts

of water from air during typical times where experiments are conducted.[33] Since water is a non-solvent for PCL, this effect develops a significant impact on the solubility of the PCL over time. This point is even utilized for the spinning process of PCL fibers from a solvent mixture containing DMSO: humidity of the surrounding air is the control parameter for the microstructure and the porosity of the resulting PCL fibers.[34, 35] We were not aware of this complication when designing our experiments. Instead, we expected from Ref. [36] that our star block-copolymers should simply be soluble in DMSO, which is apparently not the general case, in particular, when a contact between solvent and air cannot be avoided entirely and when long measurement times are involved (e.g. rheology during crosslinking, frequency sweeps for rheology, etc. ...). The corresponding data are discussed in the following sections with particular care. The experiments in the preceding sections, on the other hand, were conducted under conditions where an impact of humidity can be safely ignored.

The investigations with NMR spectroscopy and MALDI-TOF MS show that star block copolymers **3** and **4** are characterized by a high molecular uniformity and functionality, which is a prerequisite for the synthesis of model networks. Another important aspect is the knowledge of the overlap concentrations c^* of the stars, since only above this concentration, homogeneous space-filling networks can be expected. The overlap concentration can be estimated from the intrinsic viscosity $[\eta]$,[2, 17] see equation (3). The intrinsic viscosity and the overlap concentration of a polymer depend on temperature and the solvent quality.[37] For tetra-PEG- and tetra-PCL-stars, overlap concentrations c^* in different solvents were analyzed in our previous publication.[10] In the present study, dilution series of the star block copolymers **3** and **4** in DMSO were used to determine $[\eta]$ at 30 and 45 °C following the protocol of preceding work.[10] According to the Schulz-Blaschke equation (4), $[\eta]$ values for **3** and **4** were obtained by linear extrapolation of the reduced viscosities η_{red} to the zero specific viscosity η_{sp} (see **Figure 6. 1**). The resulting estimates for the overlap concentration c^* are shown in **Table 6. 1**. These results indicate that the quality of DMSO for star polymers **3** and **4** decreases with increasing temperature in contrast to the expectation, see **Table 6. 2**. Apparently, the higher humidity provided by the water bath at 45 °C causes already a somewhat lower solubility of the star blocks in DMSO inside the viscosimeter. Thus, the data at 30 °C provide effectively an upper bound for the overlap concentration at zero humidity. This point is also evident from the Schulz-Blaschke constants as determined from the slope of the data. These refer to a solvent quality in the range of theta to slightly poor solvent conditions,[38] while a net solvent quality between good and theta can be expected from **Table 6. 2**. Since polymers **3** and **4** differ only in their end-groups, the larger slope of the data for **3** indicates a comparatively lower solubility of

the oxazinone end-groups in DMSO. But as the intrinsic viscosity is not largely modified, the solubility appears to be still good enough to prevent an aggregation of **3**.

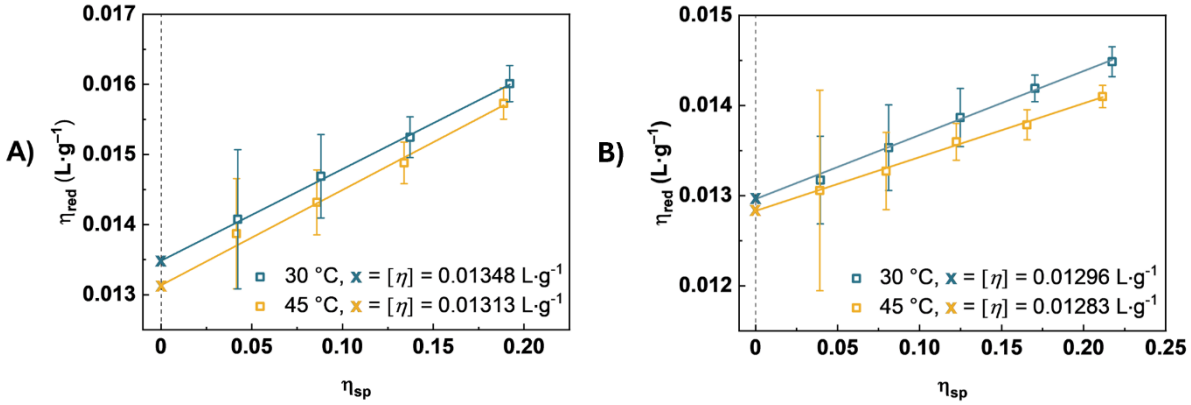

Figure 6. 1: Schulz-Blaschke plots of star polymer **3** (**A**) and **4** (**B**) in DMSO measured at T = 30 and 45 °C.[24]

Synthesis and Structural Analysis of ACNs 5a – 5d

The syntheses were carried out in solution (gels) by hetero-complementary coupling of star block copolymers **3** and **4** at equimolar ratio of the terminal groups and varying preparation concentration c_{prep} (see **Table 6. 3**) within four days at 30 °C. DMSO was chosen as a solvent because both star block copolymers are soluble in it.[36] In addition, DMSO has a high boiling point of 189 °C, which prevents evaporation of the solvent during rheological measurement. Toluene as a potential solvent also meets the above conditions, but surprisingly, no gelation was observed in this solvent within 24 h. In DMSO, gelation was observed within one hour after mixing the stoichiometric stock solutions and continued for a total of 4 days to generate the highest possible conversion. The characteristic parameters of the networks synthesized at different c_{prep} are summarized in **Table 6. 3**. The sample designations **5a** – **5d** reflect the different preparation conditions of the ACNs. For different analytical methods, several samples with the same designation were prepared, for instance, when observing gelation in situ in the rheometer. Since the applied network synthesis was shown to be highly reproducible,[10] we expect comparable results for samples with the same preparation conditions.

First, the degree of conversion p was determined by ^{1}H HR MAS NMR spectroscopy of the sol-extracted ACNs **5a** – **5d** swollen in DMSO-d_6 as described previously.[10, 12] It is noteworthy that the synthesis was performed in DMSO-d_6 and that the samples were not dried before measurements to avoid possible post reactions.

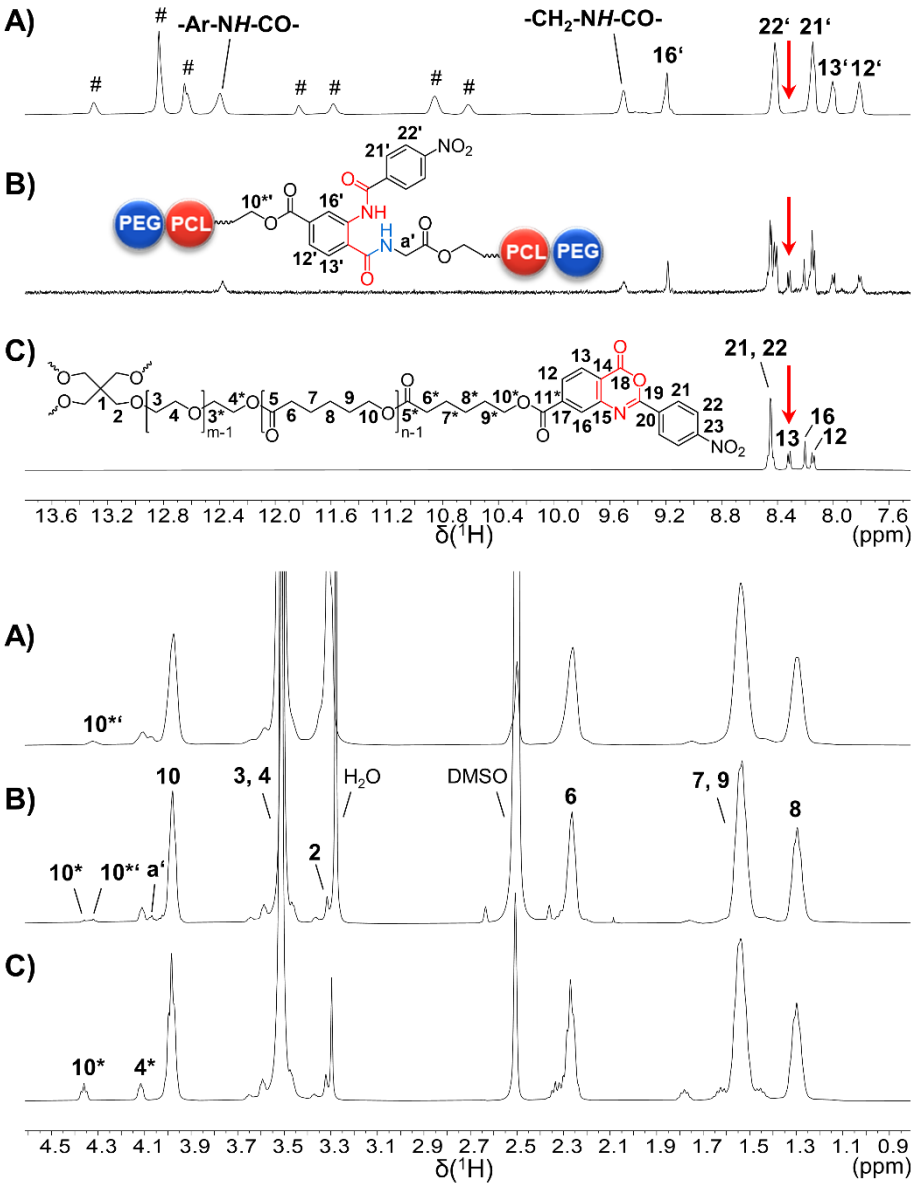

Figure 6. 2: ^{1}H NMR spectra (regions) in DMSO-d_6 at 30 °C of **A) 5a** measured with a HR MAS NMR probe at equilibrium swelling, **B)** during reaction after 45 min at a 2-(4-nitrophenyl)-benzoxazinone conversion of ~50% and **C)** of star block copolymer **3**. The red arrow indicates unreacted 2-(4-nitrophenyl)-benzoxazinone groups (*H*13), which have almost completely disappeared in **A)**. Symbol # denotes spinning side bands of the intense aliphatic signals.

Figure 6. 2 shows the ^{1}H NMR spectra of **3** (A), a mixture of **3** and **4** after 45 min of crosslinking (B), and ACN **5a** after 4 days of crosslinking (C) at 30 °C DMSO-d_6. Decisive for the determination of the degree of conversion are the terminal group signals, the intensity of which disappear during the reaction. Accordingly, the proton signals *H*13 of star polymer **3** and *H*13' of the resulting ACN **5a** were used to calculate *p* of **5a** – **5d**. It is clearly visible that the *H*13 signal of the 2-(4-nitrophenyl)-benzoxazinone terminal groups in **Figure 6. 2c** disappeared almost completely in **Figure 6. 2a** (red arrow). Instead, new signals appear that

can be assigned to the newly formed benzamide linkage between the PCL blocks in the network (e.g. *H*13'). The resulting values of p in **Table 6.3** are distinctly higher than in classical tetra-PEG gels[39] and comparable to our preceding work.[10] Due to the broadened shape of signal *H*13 caused by an extreme shortening of T_2 at the sol-gel transition,[10] the p values even tended to be underestimated.

Another major concern was to investigate the topological microstructure of the ACNs. In our previous publication,[10] the static low-field ^{1}H MQ NMR spectroscopy has proved to be a powerful tool to quantify structural heterogeneities (e. g. sol fraction) as well as the chain connectivities of ACNs based on tetra-PEG and tetra-PCL synthesized in a similar manner as described here. Comparable studies were performed on ACNs **5a - 5d** swollen in DMSO-d_6. The results are summarized in **Table 6. 3** (defect fractions f_{def}), **Figure 6. 3** (connectivity fractions), see also **SI Section A.6. 5 Table A.6. 1**.

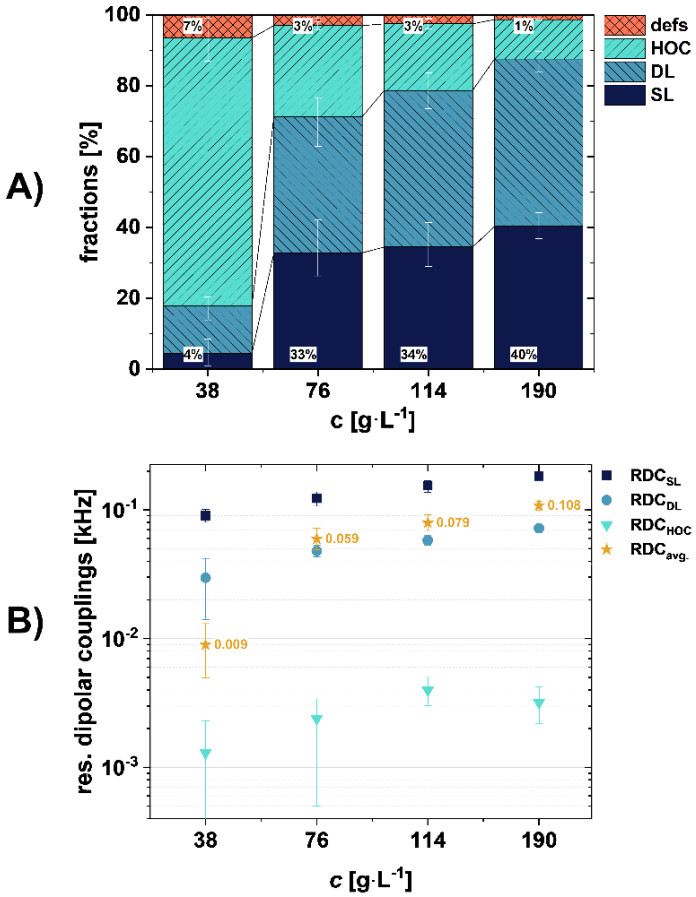

Figure 6. 3: Connectivity fractions **(A)** and RCS value **(B)** of ACN **5a** – **5d** synthesized at different concentrations (76 g·L^{-1} ~ c^*) in DMSO-d_6. (SL – single link, DL – double link, HOC – higher order connectivities, defs – isotropic defects).

The defect fraction includes unbound chains and dangling chain ends in the network. The results are in accord with the data on conversion and show a concentration dependence that results from the smaller number of suitable reaction partners for the hetero-complementary coupling with decreasing concentration. The connectivity fraction indicates how many arms of a star are connected to a neighboring star, illustrated in **Scheme 6. 2C**. One distinguishes between single links (SL), double links (DL) and higher order connectivities (HOC). In a perfect network, only single links would occur. However, due to the statistical course of the crosslinking reaction, the formation of DL and HOC cannot be prevented. Examples for the connectivity distribution of single and double links in homogeneous model networks made of star polymers are given in the literature.[13, 16]

Table 6. 3: Characteristic structural parameters of the synthesized ACNs **5a** – **5d** based on the crosslinking of star block copolymers **3** and **4** in DMSO at 30 °C.

ACN	c_{prep} (g·L^{-1})	c_{prep}/c^*	ϕ_0	p [a]	f_{def} [b]
5a	38	0.5	0.034	≥0.90	0.07
5b	76	1	0.068	≥0.95	0.03
5c	114	1.5	0.102	≥0.95	0.03
5d	190	2.5	0.170	≥0.95	0.01

[a] Degree of conversion p determined by ^{1}H HR MAS NMR spectroscopy after removal of the sol fraction and swollen in DMSO-d_6.

[b] Isotropic defect fraction determined by ^{1}H MQ NMR spectroscopy.

For ACNs **5a** – **5d**, we find the expected trend of a decreasing isotropic defect fraction (from 7% at c_{prep} = 0.5c^* to 1% at c_{prep} = 2.5c^*) that is accompanied by a consistently increasing fraction of single links (SL) (4% at c_{prep} = 0.5c^* to 40 % at c_{prep} = 2.5c^*), as well as a strongly-increasing average residual dipolar coupling (RDC) (9 Hz at c_{prep} = 0.5c^* to 109 Hz at c_{prep} = 2.5c^*) see **Table A.6. 1** in the SI. The decrease in isotropic defect fraction with increasing c_{prep} is roughly in agreement with the data on conversion (see **Table 6. 3**). While the general behavior aligns well with our previous work, we find the specific values at c_{prep} = 0.5c^* rather unexpected, as these suggest that this sample contains nearly no single links and only a rather small number of double links. We note, that at c_{prep} = 0.5c^* the distinction between components of unique RDCs is barely possible due to a high fraction of low orientations that are typically assigned to more complex structures, defects, or double links.

There are two possibilities how an enhanced portion of low orientation can arise inside our networks. First, the viscosity measurements showed a significantly larger Schulz-Blaschke constant for compound **3** as compared to **4** indicating a poor solubility of the 2-(4nitrophenyl)-benzoxazinone terminal group in DMSO. Possible associations of terminal groups attached to the same star lead to an apparent double link between star center and the location of the association. In effect, the analysis of the NMR data will overestimate the amount of double links and more complex associations mostly at the expense of single links. Second, a clear distinction between single and double links requires that the networks are far from the gelation threshold. Otherwise, there will be a significant portion of star polymers that connect in effect only two other stars introducing longer strands with correspondingly lower orientation. Such structures will be misinterpreted then as double links, more complex structures or even defects.

In order to understand, which of these processes is more relevant for interpreting the experimental data, we compare with the simulation data of Ref. [15] providing estimates for the amount of double links in comparable systems without associations. For comparison, data were chosen near 0.5*c** at a slightly higher conversion of $p = 0.95$ as compared to the experiment. The reason for this choice is that samples at low concentrations are closer to the critical concentration for gelation where the length of virtual chains modeling the elasticity of the surrounding network diverges, and consequently, different motifs become indistinguishable. For more certainty, we analyzed the network structure to determine single links (SL), double links (DL), higher order connectivities (HOC), and elastically inactive defects. For these different kinds of connections, the distributions of the vector order parameters are shown in **Figure 6. 4**.

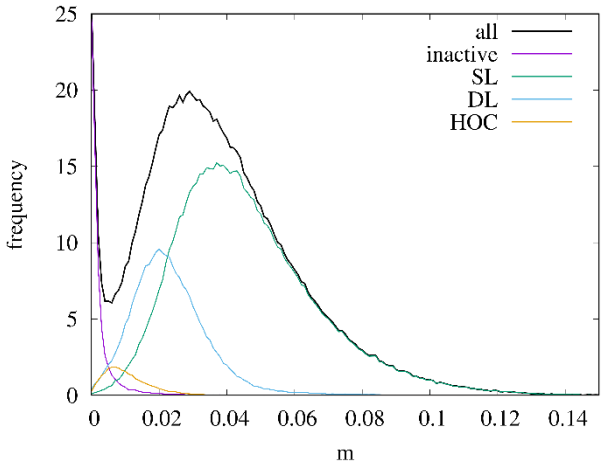

Figure 6. 4: Distribution of the vector order parameters of different connectivity types at 0.5*c** as determined from computer simulations. The weight fractions of single links (SL), double links (DL), higher order connectivities (HOC), and elastically inactive defects are 68.2%, 23.2%, 2.4%, and 6.2%, respectively. Data were computed from the network with N = 43 described in preceding work.[15]

The simulation data in **Figure 6. 4** show that higher order connectivities play no role at 0.5*c** and thus, for all samples of our study. This leaves only possible associations on the time scale of the NMR experiments as explanation for the experimental data. The vector order parameter is proportional to the RDC that is measured in the experiments, see Ref. [40] for more details.

At the lowest concentration, the simulation data show that the peak positions of the different contributions differ by a factor of two in the RDCs, which is on the edge of being separable in the experiment, see Ref. [16]. The RDC is proportional to the elastic contribution per strand in the entanglement free limit. For a double link inside an otherwise perfect network, a ratio of 8:3 between SL and DL is, expected theoretically, which is found in good approximation in the experiment and in simulations at larger concentrations.[16, 41] At $c_{prep} > 0.5c^*$, the SL fractions are consistently below the data of the simulation (> 60 % SL fraction), while being on-par with the values for the amphiphilic copolymer networks characterized in our previous work. In combination with the large Schulz-Blaschke constant of compound **3** (which differs from compound **4** only in the terminal group), we have now high confidence that a possible association of the 2-(4-nitrophenyl)-benzoxazinone terminal group in **3** is perturbing the assignment of single and double links.

Swelling Properties of ACNs 5a - 5d

Equilibrium volume swelling degrees Q_v of ACNs **5a** – **5d** were investigated in solvents of different quality with respect to PEG and PCL (see **Figure 6. 5**). In **Figure 6. 5A**, Q_v was determined both directly after synthesis without drying the samples ($Q_{\mathrm{v}1}$) and after freeze-drying with subsequent swelling ($Q_{\mathrm{v}2}$). In the first case, the data at and above the overlap threshold are described by a power-law $Q \sim \phi_0^\gamma$ with an exponent $\gamma = -0.76 \pm 0.05$ which disagrees with our previous work[15] and the predictions by Flory-style mean-field scaling models[42, 43] for swelling in a good-solvent. In particular, for the samples synthesized near *c** ($\phi_0 = 0.068$) and especially below *c**, an increase of the equilibrium swelling degree is observed as compared to our preceding work[10], which indicates a somewhat lower extent of reactions or an additional enhancement of double links that contribute less to the shear modulus.[41] The larger concentration of not yet reacted end groups upon drying enhances the formation of additional bonds in a different state of strain.[10, 14] In consequence, a large drop in the equilibrium degree of swelling is observed after the first drying step. This has already been observed in our previous studies on ACNs based on tetra-PEG and tetra-PCL.[10]

To demonstrate the amphiphilic nature of the networks, swelling tests in solvents of different polarity were performed on five batches of ACN **5c** synthesized at 1.5*c**. The results are shown in **Figure 6. 5B**. Here, the measurements refer to an analysis both directly after synthesis in DMSO with swelling in the respective solvent (Q_{v1}) and after freeze-drying with subsequent swelling (Q_{v2}) as described in the *Experimental Section*. The largest Q_v was observed in $CHCl_3$, which can be attributed to good solvent quality for both PEG and PCL. The equilibrium degree of the first swelling in chloroform is comparable with our expectations based upon Ref. [10] indicating a similar reaction efficiency in DMSO as in chloroform. The lowest Q_v was observed in H_2O (close to a theta solvent for most concentrations of PEG and a non-solvent for PCL)[44] and MTBE (poor solvent for both). From the bar chart in **Figure 6. 5B**, it can also be seen that **5c** shows similar swelling degrees in DMSO and toluene. In this case, toluene is the better solvent for PCL,[10] while these roles are reversed for DMSO. In addition, due to the structural similarity, toluene is suspected to contribute to the solvation of the benzamide groups by π-π interactions, which is similar to our discussion of linker associations in DMSO. Thus, the agreement in the average degree of swelling in DMSO and toluene is not in conflict with our RDC data.

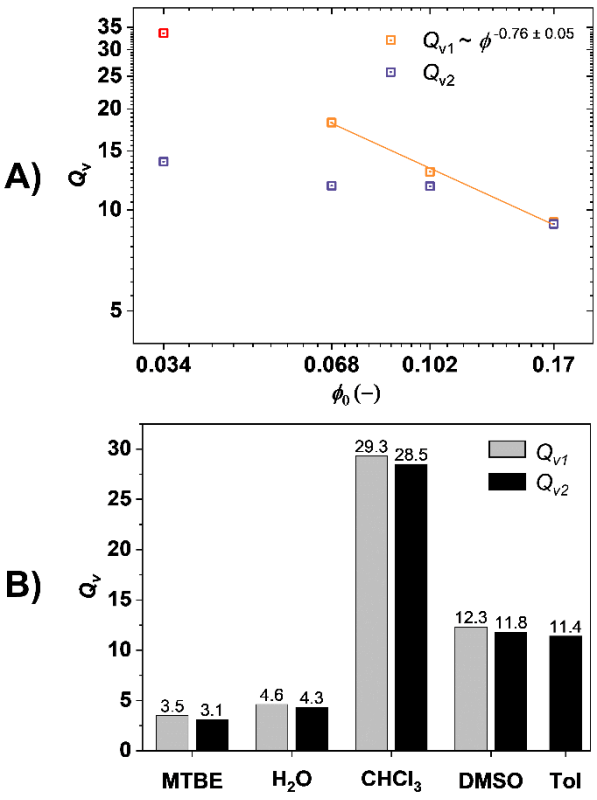

Figure 6. 5: Equilibrium volume degree of swelling Q_v (Q_{v1} directly measured after preparation with and Q_{v2} measured after freeze-drying and re-swelling) **A)** as a function of polymer volume fractions at preparation state ϕ_0 in DMSO with a power-law fit $Q \sim \phi_0^{\gamma}$ at $\phi_0 \geq 0.068$ and **B)** of **5c** in dimethyl sulfoxide (DMSO), toluene (Tol), methyl-tert-butyl ether (MTBE), chloroform ($CHCl_3$), and H_2O.

Viscoelastic Behavior of ACNs 5a – 5d

In the following, the results of oscillatory shear rheological measurements of **5a** – **5d** in the as-prepared state in DMSO, at swelling equilibrium in H_2O, and during the gelation process of star polymer **3** and **4** at different gel preparation conditions are discussed. The measurements on as-prepared samples were performed after a reaction time of five days in DMSO. Details about the sample preparation are described in the *Experimental Section*. Additionally, measurements were made on samples swollen in water. The elastic contributions of the storage moduli *G*' and their corresponding swelling degrees in equilibrium Q_{v1} are listed in **Table 6. 4**.

Table 6. 4: Storage moduli and equilibrium swelling degrees in DMSO and H_2O of ACNs **5a** – **5d** synthesized in DMSO at 30 °C.

ACN	ϕ_0	G' [a] (kPa)		Q_{v1}	
		DMSO	H_2O	DMSO	H_2O
5a	0.034	0.69 ± 0.02	29.00 ± 1.07	33.6	10.2
5b	0.068	5.18 ± 0.24	72.65 ± 0.93	18.2	6.2
5c	0.102	9.74 ± 0.41	105.3 ± 4.35	13.0	4.9
5d	0.170	29.87 ± 1.39	152.3 ± 1.67	9.2	3.8

[a] Storage moduli in DMSO (as-prepared state) and in H_2O at equilibrium swelling at T = 25 °C.

An example of an as-prepared gel sample as well as the rheological frequency sweeps of **5a** – **5d** in DMSO are shown in **Figure 6. 6**. In all cases, a dominance of the elastic behavior ($G' > G''$) is observed, which is typical for the plateau regime of a polymer network that is stable on the time scale of the experiment. When repeating the frequency sweeps, sometimes, a small drift of the data was observed as a function of time (not shown). Moreover, a sample left overnight in the rheometer turned opaque indicating a slow water uptake from air during the measurements despite of using a solvent trap equipped with a drying agent. A reduced solvent quality for PCL due to the presence of water induces smaller equilibrium strand sizes and ultimately a micro-phase separation, both enhancing the modulus of the samples. Therefore, our modulus data provide only an upper bound for the data in a water free sample. As compared to our preceding paper,[10] the modulus at c^* is about twice as large while this difference grows to a factor of about 3 at $3c^*$. The remarkable point is that the equilibrium degree of swelling does not follow this trend see **Figure 6. 5B** of the present work (toluene and DMSO produce equivalent results, i.e. equivalent net interaction parameters) and Figure 5 of Ref. [10] (the interpolated (to $1.5c^*$) equilibrium degree of the second swelling in toluene is around 11 and equivalent to the data in **Figure 6. 5B**).

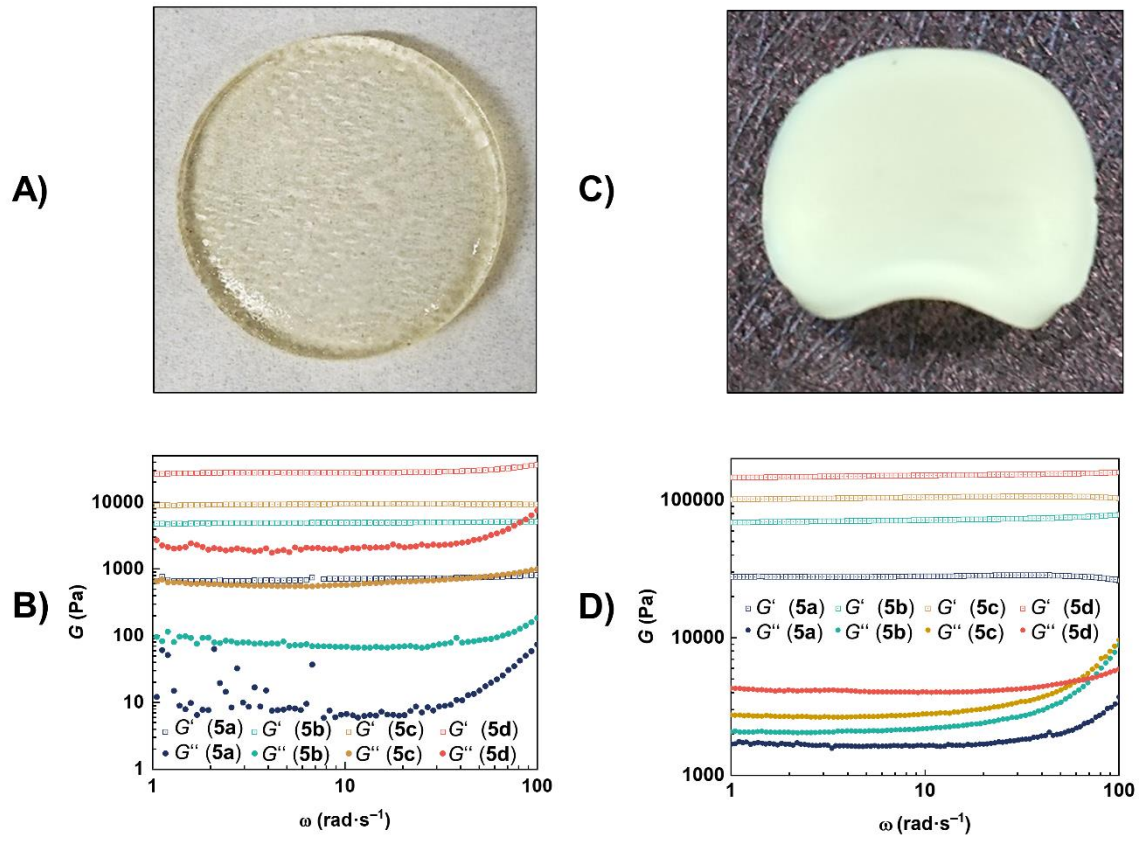

Figure 6. 6: A) Appearance of an as-prepared gel sample, **B)** rheological frequency sweeps of **5a** – **5d** in DMSO at preparation conditions, **C)** Appearance of a gel sample after exchange of DMSO with water, **D)** rheological frequency sweeps of **5a** – **5d** in H_2O at swelling equilibrium.

A better insight into this puzzling situation is obtained when analyzing the time-dependent rheological measurements performed during crosslinking under the same reaction conditions as described in **Table 6. 3**. The respective time evolution curves of *G′* are shown in **Figure 6. 7**, see also **SI Section A.6. 6 Table A.6**. **2**. We observe a two-step increase of the storage modulus at low temperatures, while at larger temperatures, there is only a one step increase. In the latter case, the single process must describe the gelation of the samples. According to the temperature dependence of the processes, the second process at lower temperatures in **Figure 6. 7B** refers to crosslinking, while an explanation of the nature of the additional first process requires further tests. First, rheological measurements of pure solutions of **3** and **4** do not reproduce the effect. Thus, the effect arises only as the consequence of the crosslinking reactions. Crosslinking glues two PCL sections together. We argue that the longer PCL sections after crosslinking associate in the DMSO solution. This association is probably enhanced by the coupling terminal 2-(4-nitrophenyl)-benzoxazinone group itself that lowers the solubility of the star polymers, see section *viscosity measurements*. This hypothesis is the same as used to explain the MQ-NMR data and it allows to remove all other conflicting observations:

First, it is well established[45, 46] that the concentration of the associated groups grows with concentration. Thus, we can expect an enhancement of modulus at preparation conditions that grows with concentration through additional contributions from sticky chain sections. Second, reversible networks do not resist swelling in the limit of very long times. Thus, we expect no impact on the equilibrium degree of swelling beyond a concentration dependent renormalization of the net interactions between the polymers and the solvent. The renormalized interactions lead to a stronger concentration dependence of the equilibrium degree of swelling as observed in **Figure 6. 5a**. Taking both points together, permanent networks with sticky chain sections can develop a higher modulus at preparation conditions even though the equilibrium degree of swelling is nearly identical to a permanent network without such sticky chain sections.

The time dependent rheology data on *G'* provides additional interesting insights. The disappearance of the first gelation process does not indicate a complete disappearance of all the associations. It only shows that there are too little associations to drive the system through gelation prior to the gelation of the permanent network structure itself. Moreover, the stability of the associations must exceed 1 second at the measurement temperature, if the second process is visible. The frequency sweeps show that the associations are stable over 1 s at 30 °C while NMR indicates stable associations up to 1 ms at 80 °C. Both are not in conflict with each other and allow for a rearrangement of the associations on the time scale of the swelling experiments (days).

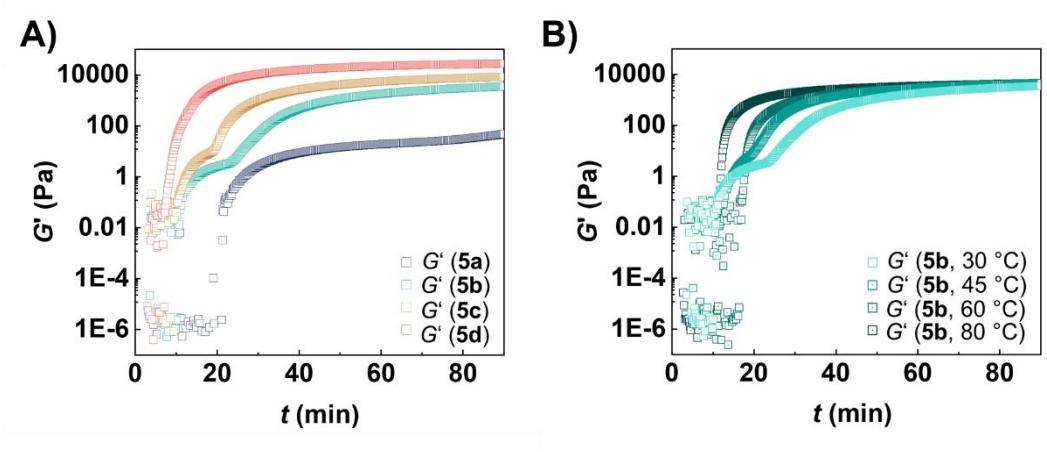

Figure 6. 7: In situ measurements of the storage modulus as a function of time during gelation for **A)** samples **5a** to **5d** at different polymer volume fractions, see **Table 6.3**, and **B)** sample **5b** at different temperatures from 30 to 80 °C.

After preparation, gels **5a - 5d** were swollen to equilibrium in excess H_2O without an intermediate drying step. The gels appear white due to a micro-phase separation of the hydrophobic polymer domains inside the network (see **Figure 6. 6C**). The equilibrium degree of swelling of these samples was determined gravimetrically and is summarized in **Table 6. 4**. The equilibrium degree of swelling of samples **5b - 5d** prepared at and above the overlap threshold scales as $Q \sim \phi_0^{\gamma}$ with $\gamma = -0.53 \pm 0.03$. The elastic modulus of these samples is several times higher in comparison to the modulus in DMSO. For a first glimpse on the physics of this process, let us consider the ratio of the modulus of a homogeneous network before and after a change in sample volume. For this modulus ratio, the following dependence on the polymer volume fraction is expected[38] in good ($\nu = 0.588$) and theta ($\nu = 1/2$) solvent $G(\varphi)/G(\varphi_0) \approx (\varphi/\varphi_0)^{1/3+(2\nu-1)/(3\nu-1)}$, when swelling from a preparation state to a swelling equilibrium with $\phi < \phi_0$. For our samples, however, a change in interactions and chain conformations drives the system to a swelling equilibrium characterized by $\phi > \phi_0$. Our rheology–data for samples **5b - 5d** prepared at and above *c** are in accord with an exponent of 2.2 ± 0.5 for the modulus ratio. Here, the network elasticity has to work against the osmotic pressure of the sample and additional constraints arising from the interphase between swollen and phase separated polymers. The new equilibrium degree of swelling reflects the sum of all these constraints on the free energy. The osmotic pressure in homogeneous samples in good and theta solvents scales[38] as $\Pi \approx \phi^{3\nu/(3\nu-1)}$, which is not largely different from the observed increase in modulus. This observation could be useful for developing a model for the elasticity of amphiphilic gels in a selective solvent.

6.8. Conclusion

Following our earlier work on the synthesis of ACNs based on tetra-PEG and tetra-PCL stars,[10] we synthesized networks in which the hydrophobic and hydrophilic components were already contained in all individual stars. The latter is the major difference to the preceding work allowing for a possible structuring of the networks in a block copolymer morphology prior to the synthesis. As in the preceding paper, the hetero-complementary 2-(4-nitrophenyl)-benzoxazinone/amine reaction has proved to be very effective to link the star polymers. Apart from the resulting differences in the arrangement of the polymer blocks, the new ACNs do not differ from the ACNs in Ref. [10] in terms of linking group, degree of polymerization of the network strands, and the volume fraction of the amphiphilic and hydrophilic components. Since

the two block stars **4** and **5** are structurally identical except for their end groups, the small difference in their solubility can be attributed to the end groups. A synthesis in toluene did not produce networks within 24 hours, therefore, DMSO was used as a solvent. The strong hygroscopic nature of DMSO is problematic when contact to humidity cannot be avoided completely, e.g. when analyzing network formation by rheology in situ, since the slightly poor solvent quality of DMSO is continuously reduced with increasing water uptake of DMSO.

The results show that the conversion of the end groups is comparable or somewhat below (for low concentrations) to the data of our previous work.[10] The different philicity of the stars compared to Ref. [10] appears to additionally impact the synthesis in addition to the impact of the aromatic terminal and linker groups. The rheological investigations show a two-stage increase in viscosity during the synthesis, while solutions of the stars with only the 2-(4-nitrophenyl)-benzoxazinone group do not develop associations that are stable on the time scale of the experiment. Thus, the extension of the PCL block via the crosslinking reaction contributes significantly to the assumed associations of the 2-(4-nitrophenyl)-benzoxazinone groups. This contribution was lacking for the networks of Ref. [10] due to a different solvent and different architecture of the stars. However, for both sets of networks, an unexpectedly high apparent content of double links is determined by MQ NMR. In this regard, we cannot discriminate whether this high fraction of double links refers to true double links or just apparent double links via associations and to which extent the amount of true double links is enhanced by associations during crosslinking process. Associations are being reduced with decreasing concentration, i.e. during swelling. Therefore, associations play a lesser role at equilibrium swelling. On the contrary, associations enhance the modulus in the preparation state. Therefore, it is not necessarily a contradiction to observe a similar equilibrium degree of swelling for networks that develop a larger modulus (on the time scale of the rheology) at preparation conditions, since the extra contribution of the associations to modulus is largely reduced at the low concentrations at swelling equilibrium.

6.9. References

[1] G. Erdodi and J. P. Kennedy, *Prog. Polym. Sci.*, 2006, **31**, 1-18.

[2] Z. Mutlu, S. Shams Es-haghi and M. Cakmak, *Adv. Healthc. Mater.*, 2019, **8**, 1801390.

[3] N. Hampu and M. A. Hillmyer, *ACS Macro Lett.*, 2020, **9**, 382-388.

[4] F. S. Bates and G. H. Fredrickson, *Annu. Rev. Phys. Chem.*, 1990, **41**, 525-557.

[5] D. G. Tsalikis, M. Ciobanu, C. S. Patrickios and Y. Higuchi, *Macromolecules*, 2023, DOI: 10.1021/acs.macromol.3c01392.

[6] L. S. Shagolsem, T. Kreer, A. Galuschko and J.-U. Sommer, *J. Chem. Phys.*, 2016, **145**.

[7] K. A. Koppi, M. Tirrell, F. S. Bates, K. Almdal and R. H. Colby, *J. Phys. II France*, 1992, **2**, 1941-1959.

[8] S. Panyukov and M. Rubinstein, *Macromolecules*, 1996, **29**, 8220-8230.

[9] N. Hampu and M. A. Hillmyer, *Macromolecules*, 2020, **53**, 7691-7704.

[10] C. Bunk, L. Löser, N. Fribiczer, H. Komber, L. Jakisch, R. Scholz, B. Voit, S. Seiffert, K. Saalwächter, M. Lang and F. Böhme, *Macromolecules*, 2022, **55**, 6573-6589.

[11] L. Jakisch, M. Garaleh, M. Schäfer, A. Mordvinkin, K. Saalwächter and F. Böhme, *Macromol. Chem. Phys.*, 2018, **219**, 1700327.

[12] C. Bunk, H. Komber, M. Lang, N. Fribiczer, M. Geisler, P. Formanek, L. Jakisch, S. Seiffert, B. Voit and F. Böhme, *Polym. Chem.*, 2023, DOI: 10.1039/D3PY00078H.

[13] M. Lang, K. Schwenke and J. U. Sommer, *Macromolecules*, 2012, **45**, 4886-4895.

[14] K. Schwenke, M. Lang and J. U. Sommer, *Macromolecules*, 2011, **44**, 9464-9472.

[15] M. Lang, R. Scholz, L. Löser, C. Bunk, N. Fribiczer, S. Seiffert, F. Böhme and K. Saalwächter, *Macromolecules*, 2022, **55**, 5997-6014.

[16] F. Lange, K. Schwenke, M. Kurakazu, Y. Akagi, U. I. Chung, M. Lang, J. U. Sommer, T. Sakai and K. Saalwachter, *Macromolecules*, 2011, **44**, 9666-9674.

[17] K. Hagmann, C. Bunk, F. Böhme and R. von Klitzing, *Polymers*, 2022, **14**, 2555.

[18] L. Löser, C. Bunk, R. Scholz, M. Lang, F. Böhme and K. Saalwächter, *submitted to Macromolecules*, 2023.

[19] N. Fribiczer, K. Hagmann, C. Bunk, F. Böhme, R. von Klitzing and S. Seiffert, *submitted to Macromol. Chem. Phys.*, 2023.

[20] C. Saldías, Á. Leiva, S. Bonardd, C. Quezada, S. Saldías, M. Pino and D. Radic', *React. Funct. Polym.*, 2015, **96**, 78-88.

[21] B. Neises and W. Steglich, *Angew. Chem. Int. Ed. Engl.*, 1978, **17**, 522-524.

[22] G. Höfle, W. Steglich and H. Vorbrüggen, *Angew. Chem. Int. Ed. Engl.*, 1978, **17**, 569-583.

[23] W. Burchard, in *Branched polymers II*, Springer, 1999, pp. 113-194.

[24] v. G. Schulz and F. Blaschke, *J. Prakt. Chem.*, 1941, **158**, 130-135.

[25] J. Baum, M. Munowitz, A. N. Garroway and A. Pines, *J. Chem. Phys.*, 1985, **83**, 2015-2025.

[26] M. Ahmadi, L. Löser, K. Fischer, K. Saalwächter and S. Seiffert, *Macromol. Chem. Phys.*, 2020, **221**, 1900400.

[27] R. O. M. Newville, A. Nelson, A. Ingargiola, T. Stensitzki, D. Allan, A. Fox, F. Carter, M., Ray Osborn, D. P. lneuhaus, S. Weigand, G. C. Deil, Mark, Allan L. R. Hansen, G. Pasquevich, *Journal*, 2021, DOI: 10.5281/zenodo.5570790.

[28] P. Nicolella, M. F. Koziol, L. Löser, K. Saalwächter, M. Ahmadi and S. Seiffert, *Soft Matter*, 2022, **18**, 1071-1081.

[29] X. Lou, B. F. M. de Waal, J. L. J. van Dongen, J. A. J. M. Vekemans and E. W. Meijer, *J. Mass Spectrom.*, 2010, **45**, 1195-1202.

[30] A. Alanazi, S. Alshehri, M. Altamimi and F. Shakeel, *J. Mol. Liq.*, 2020, **299**, 112211.

[31] C. M. Hansen, *Hansen solubility parameters: a user's handbook*, CRC Press, Boca Raton, 2 edn., 2007.

[32] X. Qin and D. Wu, *J. Therm. Anal. Calorim.*, 2012, **107**, 1007-1013.

[33] R. Ellson, R. Stearns, M. Mutz, C. Brown, B. Browning, D. Harris, S. Qureshi, J. Shieh and D. Wold, *Comb. Chem. High Throughput Screen.*, 2005, **8**, 489-498.

[34] M. Şimşek, *J. Mater. Res.*, 2020, **35**, 332-342.

[35] C. Ramos, G.-M. Lanno, I. Laidmäe, A. Meos, R. Härmas and K. Kogermann, *Int. J. Polym. Mater.*, 2021, **70**, 880-892.

[36] S. César, L. Ángel, B. Sebastián, Q. Caterina, S. Soledad, P. Maximiliano and R. Deodato, *React. Funct. Polym.*, 2015, **96**, 78-88.

[37] T. Alfrey, A. Bartovics and H. Mark, *J. Am. Chem. Soc.*, 1942, **64**, 1557-1560.

[38] M. Rubinstein and R. H. Colby, *Polymer physics*, Oxford university press, New York, 2003.

[39] M. Kurakazu, T. Katashima, M. Chijiishi, K. Nishi, Y. Akagi, T. Matsunaga, M. Shibayama, U.-i. Chung and T. Sakai, *Macromolecules*, 2010, **43**, 3935-3940.

[40] M. Lang, *Macromolecules*, 2013, **46**, 9782-9797.

[41] M. Lang, *ACS Macro Lett.*, 2018, **7**, 536-539.

[42] J. Bastide, C. Picot and S. Candau, *J. Macromol. Sci. Phys.*, 1981, **19**, 13-34.

[43] P. J. Flory, *Principles of polymer chemistry*, Cornell university press, 1953.

[44] M. A. Woodruff and D. W. Hutmacher, *Prog. Polym. Sci.*, 2010, **35**, 1217-1256.

[45] A. N. Semenov and M. Rubinstein, *Macromolecules*, 1998, **31**, 1373-1385.

[46] K. S. Kumar and M. Lang, *Macromolecules*, 2023, **56**, 7166-7183.

[47] K. Saalwächter, in *Modern Magnetic Resonance*, ed. G. A. Webb, Springer International Publishing, Cham, 2017, pp. 1-28.

7. CHAPTER V: TAILOR-MADE IONIC FOUR-ARM STAR BLOCK COPOLYMERS

Double hydrophilic poly(ethylene glycol)-*block*-poly(dehydroalanine) four-arm star block co-polymers: synthesis and solution behavior

[redacted] **N. Fribiczer**, [redacted]

Polym. Chem., **2022**, 13, 4298–4308, doi: 10.1039/D2PY00579D

The corresponding *Supporting Information* is included in **Appendix A.7**.

7.1. Specific Summary

Next to the covalent amphiphilic star polymer networks in the previous chapters, ionic reversible networks are of interest due to their enhanced dynamics and potential elimination of structural defects induced during preparation by reorganization. The use of electrostatic interactions as crosslinking points allows for control of the bond strength through length and type of the ionic segments. Suitable candidates for such ionic segments are either weak polyelectrolytes such as polymethacrylic acid or polyampholytes such as polydehyroalanine. The bond strength is then tunable by the pH value controlling the overall net charge of the segments and thus, the attractive and repulsive interactions.

The first step to create such ionic reversible networks is the synthesis of suitable polyelectrolyte building blocks and the characterization of their pH-dependent solution behavior. The goal is to create well-defined network building blocks based on four-arm star polymers with attached ionic segments by block extension of the arms.

For this purpose, hydrophilic star-shaped block copolymers based on a PEG core block extended with different block length of ampholytic polydehydroalanine (PDha) are prepared. Next to variation of the ampholytic block from 6–7 over 20 to 41 units, also the molar mass of the PEG core is modified using 5, 10, and 20 kg mol^{-1} tetra-arm star PEG. Due to the ampholytic nature of the PDha, the solution properties are markedly influenced by the pH value. Above a pH of 7, the overall net charge of PDha is negative, whereas the isoelectric point is reached around a pH of 3 and below a pH of 2, the overall net charge is positive. Therefore, significant

aggregation around the isoelectric point is expected. The solution and aggregation behavior at different pH-values is investigated by DLS, AFM, potentiometric titration, and zeta potential measurements. The DLS results indicate an increasing aggregation tendency with decreasing pH and increasing PDha segment length, whereas the PEG core size has only minor influence. The AFM results substantiate these findings by identifying aggregates in the same size range as the DLS experiments. Due to the drying procedure before AFM investigations, all aggregate sizes are shifted to slightly smaller length-scales. These investigations show that even short stickers of 6–7 units of PDha have a considerable influence and increase the aggregation tendency at low pH values with aggregate sizes beyond 1 µm.

Overall, this study illustrates how the structure of polyelectrolytes depends on the pH value and how the block length of the ionic segments influences the aggregation behavior. In a next step, this knowledge about the net-charge at different pH can be used to form ionic networks with a suitable counterpart.

7.2. Author Contributions

[redacted]	Concept development, polymer synthesis, polymer characterization, titrations and zeta potential measurements, manuscript preparation and correction.
Nora Fribiczer:	DLS measurements and evaluation, manuscript preparation and manuscript correction.
[redacted]	Concept development, manuscript preparation and correction.
[redacted]	AFM measurements and evaluation, manuscript preparation and correction.
[redacted]	Scientific Supervision of [redacted] and manuscript correction.
[redacted]	Concept development, scientific supervision and manuscript correction.

7.3. Acknowledgement

This work was performed within the research unit FOR2811, funded by the German Research Foundation (DFG, TP02 and TP04, grant 423435431). [redacted]. are grateful for financial support from the DFG (Germany's Excellence Strategy—EXC 2051—project-ID 390713860, "Balance of the Microverse") and the Carl-Zeiss-Foundation ("Durchbrüche" – Intelligente Substrate). The authors further acknowledge [redacted] for SEC analysis, [redacted] for scientific discussions, and the NMR department at Friedrich-Schiller-University Jena for their continuous support.

7.4. Abstract

Star-shaped block copolymers are of interest as versatile and highly functional polymeric building blocks and show interesting solution properties or self-assembly. Herein, we report the synthesis of novel, double hydrophilic four-arm star-shaped block copolymers, based on different poly(ethylene glycol) cores (PEG) and short blocks ("stickers") of polydehydroalanine (PDha). As PDha is a polyampholyte we were mainly interested in the pH-dependent solution behavior, which we characterize by dynamic light scattering (DLS), atomic force microscopy (AFM), potentiometric titration, and zeta potential measurements. Our main interest was to elucidate how the presence of a short (6–7 units) or intermediate (up to 41 units) PDha segment influences the solution properties of such double hydrophilic block copolymers depending on the solution pH. As we can show, even short "stickers" show a profound influence and lead to increasing aggregation tendency at low pH values, as demonstrated by DLS and AFM experiments with aggregate sizes beyond 1 µm.

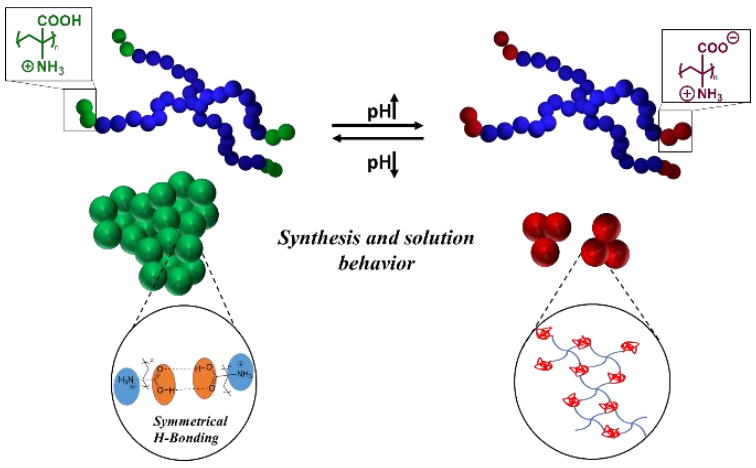

Figure 7. 1: Schematic representation of the pH-dependent solution behavior of t-PEG-*b*-PDha.

7.5. Introduction

Double hydrophilic copolymers (DHCs) are defined by consisting of two distinct hydrophilic blocks of different chemical nature.[1] Nowadays the material class of DHCs has a broad application range starting from drug carriers to gene delivery, as sensors, nanoreactors, or for the synthesis of multifunctional hybrid materials. This wide range of applications can be explained by the possibility of precisely modifying the composition and topology of the underlying polymers.[2] After Stille *et al.* published their work on the first linear double hydrophilic copolymer (DHC) in 1972,[3] this polymer class was significantly extended, not only by using a broad variety of monomers but also in terms of various topologies, ranging from linear block copolymers, brushes, or macrocycles to well-defined star-shaped examples.[2, 4, 5] Based on these architectural differences, the polymer properties differ significantly, and thus new possible applications can be explored. For example, compared to linear double hydrophilic block copolymers (DHBC), star-shaped block copolymers show a higher density of functional groups, increased loading capacities, and lower aggregation numbers.[6] Furthermore, the behavior of polymers in solution especially with regard to viscosity and solubility is also influenced by the topology.[6, 7] Star-shaped double hydrophilic copolymers are in comparison to their linear counterparts a rather unknown field of polymer chemistry as this architecture brings unique difficulties in its synthesis. In general, they are synthesized *via* controlled radical polymerization techniques (CRP), but side reactions such as star-star coupling, or the temporally unequal or only proportional initiation of adjacent arms need to be avoided. The CRP methods mainly include nitroxide mediated polymerization (NMP), atom transfer radical polymerization (ATRP), or reversible addition fragmentation polymerization (RAFT).[8, 9] In 2019 Hawker *et al.* reported on minimizing star-star coupling in Cu(0)-mediated controlled radical polymerizations. They synthesized different star-shaped homo and block copolymers using a variety of acrylates resulting in conversions up to 95%, dispersities (*Đ)* below 1.2, and investigated critical factors like the influence of arm length, the number of arms, or the monomer side chain used.[10] Later in 2020 Lin *et al.* reported star-shaped double hydrophilic copolymers containing pH-responsive blocks describing the synthesis and the dual pH-responsive behavior of star-shaped poly(4-vinyl pyridine)-*block*-poly(acrylic acid) (P4VP-*b*-PAA) diblock copolymers. According to their results, full protonation of both groups occurs under acidic conditions leading to a cationic polymer species and good water solubility. Consequently, at high pH values deprotonation of the acidic group leads to an anionic species. In between those extremes, at pH 5-8, aggregation of the polymers occurs due to the presence of both, positive and negative charges and, thus, the formation of complexes.[11] In principle, many recent examples focus on

the increase of conversion or the suppression of side reactions. However, no, or only little attention was paid to the number of repeating units actually required to influence solution properties of star-shaped (block) copolymers.

In this work, we present the synthesis of well-defined double hydrophilic poly(ethylene glycol)-*block*-polydehydroalanine $[PEG_x\text{-}b\text{-}PDha_y]_4$ star-shaped block copolymers with either short (6-7 repeat units) or longer arms (~ 40 repeat units) for the ampholytic segment. While PEG offers high-water solubility, PDha as weak polyampholyte is either positively charged, negatively charged, or zwitterionic depending on the solution pH value and, with that, our aim was to study the influence of short charged segments on the solution behavior of such materials.[12] As both oppositely charged moieties are carried in the same monomer unit, PDha can further be defined as polyzwitterion.[13] In 2013 Günther *et al.* compared free radical polymerization with NMP for the polymerization of *tert*-butoxycarbonylaminomethyl acrylate (*t*BAMA) and investigated afterwards the deprotection reaction of P*t*BAMA to obtain PDha.[14] Furthermore, in 2016 Billing *et al.* reported on the synthesis of homo and diblock copolymers containing P*t*BAMA segments *via* ATRP using a bromide ester-based PEG macroinitiator.[15] Later in 2017, the deprotection of these materials could be shown but, due to the harsh deprotection conditions, it was not possible to obtain PEG-*b*-PDha due to cleavage of the ester linkage between both blocks.[16] We could later overcome this obstacle by the use of a more hydrolysis stable amide-based macroinitiator for the block extension of linear PEG with *t*BAMA and the successful deprotection to PEG-*b*-PDha, thereby avoiding cleavage of the second block.[17] We now extend this to star-shaped block copolymers and as the resulting $[PEG_x\text{-}b\text{-}PDha_y]_4$ block copolymers provide both, amino and carboxylic acid groups in the PDha segment, these materials are of interest for either reversible physical crosslinking due to electrostatic interactions with an oppositely charged counterpart under basic or acidic conditions or the amino group can be used for permanent crosslinking due to covalent linkage using either epoxides or *aza*-michael acceptors. This has been shown for a range of PDha-based graft copolymers which used either benzyl glycidyl ether (BGE), 1,2-epoxy octane (EOct), nonafluoropentyloxirane (NFPO), poly(ethylene glycol)glycidyl lauryl glycidyl ether (PEO-LGE), acrylonitrile (ACN)[18], NiPAAm[19], phosphonic acid,[20] or epoxy-functionalized PEG[21] for grafting reactions. The herein shown synthetic strategy allows the addition of 6-7 repeating units of PDha at each arm, yielding star-shaped block copolymers with defined and short charged end groups. Further to the synthesis of $[PEG_x\text{-}b\text{-}PDha_{6\text{-}7}]_4$ star-shaped block copolymers with $Đ$ of < 1.10, we also show that block extensions with higher conversions of up to 41% adding more than 40 repeating

units of P*t*BAMA at each arm are possible, yielding well-defined star-shaped block copolymers with longer polyampholytic segments.

7.6. Experimental Part

Materials

Methanesulfonyl chloride (≥ 99.7%) alpha-Bromoisobutyryl bromide (98%), Cu(I) bromide (99.999%), Cu(I) chloride (99.99%), Cu(II) bromide (99%), Cu(II) chloride (99%) and Cu(0) powder (99,999%) were purchased from Sigma-Aldrich. TFA (≥ 99.9%) was purchased from Roth, triethylamine (≥ 99.0%) from CHEMSOLUTE® and *N*-(*tert*-butoxycarbonyl)-L-serinmethylester (98%) from Carbolution Chemicals, LiOH monohydrate (56% LiOH) from acros organics, all $[PEG_x\text{-}NH_2]_4$ species from JenKem Technology. Cu(I)X was purified by stirring in glacial acetic acid overnight and rinsing with methanol before drying *in vacuo*. All other reagents were used as received.

Analytic Methods

Nuclear magnetic resonance (NMR) spectroscopy

^{1}H-NMR and ^{13}C measurements were performed on a Bruker AC 300 MHz using $CDCl_3$ or D_2O/NaOD as solvent.

Size exclusion chromatography (SEC)

SEC traces were measured in DMSO on a Jasco instrument using DMSO + 0.5% LiBr as solvent at a flow rate of 0.5 mL/min at 65 °C and a Pullulan calibration. The setup contains PSS NOVEMA 3000 Angström / 300 Angström columns, an RI-930 detector, as well as a PU-980 pump.

Measurements using DMAc + 0.21 wt.% LiCl as eluent were carried out using an Agilent 1200 Infinity system equipped with a G1310A Pump, a G1362A AS autosampler, and three consecutive PSS SDV, 5 µm, 8 × 300 mm columns. DMAc was used at a flow rate of 1 mL/min. The column oven was set to 30 °C, and signals were detected using a G1315D DAD and a G1362A RID detector. The system was calibrated using PEG/PEO (238 to 969000 g/mol) or PMMA (400 to 2200000 g/mol).

Dynamic Light Scattering (DLS)

DLS measurements were performed on solutions at c = 0.2 mg mL^{-1} at scattering angles of 30°–150° using a light scattering setup equipped with an ALV-SP125 goniometer, an ALV/LSE5004 multi tau correlator, a fiber optical ALV/High QE APD avalanche photodiode with pseudo-cross correlation (ALV-Laservertriebsgesellschaft mbH, Langen, Germany) and a uniphase He/Ne laser (632.8 nm, Thorlabs Inc). The temperature was controlled by a Huber Pilot One thermostat (Peter Huber Kältemaschinenbau AG, Offenburg, Germany) and kept at 25 °C. The solutions were filtered with a Millex LCR filter (0.45 µm; 13 mm) at pH = 13, a Millex glass fiber filter (1 µm; 25 mm) at pH = 5, and a Millex LS filter (5 µm; 25 mm) at pH = 3 to account for the respective aggregation tendency. The samples were filtered in a dust-free laminar flow box prior to the measurement to obtain dust free polymer solutions. The samples for DLS were prepared by dissolution of the respective polymer in 0.1 M NaOH over-night at room temperature on a shaking plate and titration to the desired pH using 0.5 M, 0.2 M and 0.1 M HCl. Details on the DLS analysis are given in the SI (**Appendix A.7**).

Titrations

pH titrations were carried out using an OMNIS Advanced Titrator (Deutsche METROHM Prozessanalytik GmbH & Co. KG, Filderstadt, Germany) equipped with a magnetic stirrer, a Pt1000 temperature sensor, and a dosing module. For pH detection, either an ECOTRODE plus pH-glass electrode, or a BIOTRODE was used. The polymers were dissolved in 0.1 M NaOH resulting in a 0.2 mg mL^{-1} solution with a pH between 12 and 13 and subsequently titrated with 0.1 M HCl at a dosing rate of 0.01 mL min^{-1}. For sample taking the titration was paused at the desired pH value and afterward continued.

Zeta potential measurements

Zeta potentials were measured on a ZetaSizer Nano ZS from Malvern *via* M3-PALS technique with a laser beam at 633 nm. The detection angle was 13°. The electrophoretic mobilities (u) were converted into ζ-potentials *via* the Smoluchowski equation,[22] where η denotes the viscosity and ε the permittivity of the solution.

Atomic force microscopy (AFM)

AFM measurements were conducted on a NT-MDT Integra system in tapping mode. Commercially available cantilevers (NSC35, Anfatec instruments AG) were used to investigate the morphology of aggregates. Polymer films were spin-coated at 2000 rpm on piranha cleaned silicon substrates at room temperature. Images were acquired at a scan speed of 1.5 Hz and were analyzed with the Gwyddion software package.

Fourier-transform infrared spectroscopy (FTIR)

IR measurements were carried out on a Perkin Elmer Frontier FTIR spectrometer equipped with a Specac Golden Gate ATR accessory (with high temperature diamond top plate and temperature controller).

Synthesis of *t*BAMA

N-(*Tert*-butoxy carbonyl)-*D*-serine methyl ester (10 g, 45.6 mmol) was dissolved in dichloromethane (200 mL). Methane sulfonyl chloride (Ms-Cl, 6 mL, 77.5 mmol) was then added to this solution under vigorous stirring. The reaction mixture was cooled to 0 °C before triethylamine (TEA, 23 mL, 165.9 mmol) was added dropwise. The solution was stirred at 0 °C for 1 h, and then for a further 2 h at room temperature. The reaction mixture was then washed with a potassium bisulfate solution (1%) to neutrality. The organic phase was dried over Na_2SO_4, filtered, and the solvent removed under reduced pressure. The product was further purified *via* column chromatography with silica gel (*n*-hexane:ethyl acetate = 8/2 (v/v)). The product was then dried under reduced pressure to obtain a colorless oil with a yield of 87% (8 g, 39 mmol).

^{1}H-NMR (300 MHz, $CDCl_3$, δ): 7.00 (s, 1 H, -NH), 6.13 (s, 1 H, -C-CH_2-), 5.70 (s, 1 H -C-CH_2-), 3.8 (s, 3 H, -O-CH_3), 1.46 (s, 9 H, -COO-C-$(CH_3)_3$) ppm. The ^{13}C-NMR spectrum can be found in the supporting information (**Figure A.7. 1**).

Synthesis of [PEG-amide-Br]$_4$

α-Bromoisobutyryl bromide (1.28 mL, 11.85 mmol) was added dropwise to a solution of $[PEO_{55}$-$NH_2]_4$ (3 g, 3 mmol) and trimethylamine (TEA, 1.68 mL, 2.5 mmol) in DCM (120 mL) at 0 °C. Afterwards, the solution was stirred for 72 h at room temperature. The resulting solvent mixture was extracted once each with saturated sodium bicarbonate, deionized water, and saturated brine. The organic phase was dried over $MgSO_4$. After evaporation of the DCM, the

concentrated solution was precipitated twice into cold diethyl ether. The white precipitate was dried under vacuum (2 g, 1.9 mmol, 62% yield).

^{1}H-NMR (300 MHz, $CDCl_3$, δ): 3.9-3.5 (m, backbone), 1.94 (s, 24 H, -C- $(CH_3)_2$Br) ppm.

^{13}C-NMR (300 MHz, CDCl3, δ): 32.47 (-C-$(CH_3)_2$), 40.10 (-C-$(CH_3)_2$), 45.51 (carbon core), 62.51 (core-CH_2-), 62.58 (-O-CH_2-CH_2-), 70.56 (-O-CH_2-CH_2-), 171.97 (-C=O). The ^{13}C-NMR spectrum can be found in **Figure A.7. 2**.

Synthesis of [PEG$_{55}$-*b*-P*t*BAMA$_6$]$_4$ *via* ATRP

For a typical synthesis of [PEG$_{55}$-*b*-P*t*BAMA$_6$]$_4$, *t*BAMA (5.64 g, 200 eq, 28.2 mmol; or 50 eq each arm), d*N*bpy (458.84 mg, 8 eq, 1.12 mmol) and [PEG$_{55}$-amide-Br]$_4$ (800 mg, 1 eq, 0.14 mmol) were dissolved in 1.5 mL dioxane/DMF (v/v) = 10/20 and deoxygenated using four consecutive freeze-pump-thaw cycles. Afterward, CuCl (34.7 mg, 4 eq, 0.35 mmol) was added under inert conditions to the still frozen reaction mixture followed by four cycles changing between vacuum and argon before the polymerization mixture was allowed to warm up and set to 60 °C. The polymerization was carried out at 60 °C for 24 h. The reaction was then terminated by cooling in liquid nitrogen followed by the addition of methanol. After removal of the residual copper using a neutral AlOx column, the solvent was removed by freeze-drying at the Schlenk line for a few hours. The residue was dissolved in DCM and precipitated three times into cooled *n*-hexane. The desired block copolymer was isolated by the removal of the leftover solvent under reduced pressure as a white powder.

^{1}H-NMR (300 MHz, $CDCl_3$, δ): 6.36-4.75 (m, -NH (residue)), 3.96-3.33 (PEG-backbone + methyl ester), 3.38-1.78 (P*t*BAMA backbone), 1.63-1.05 (C-$(CH_3)_3$).

^{13}C-NMR (300 MHz, CDCl3, δ): See SET-LRP

Synthesis of [PEG$_{27}$-*b*-P*t*BAMA$_{41}$]$_4$ *via* SET-LRP

For a typical synthesis of [PEG$_{27}$-*b*-P*t*BAMA$_{41}$]$_4$, *t*BAMA (2822 mg, 14 mmol, 400 equivalents), TPMA (81.5 mg, 280 µmol, 8 equivalents), Copper(II) Chloride (1.88 mg, 14 µmol, 0.4 equivalents), [PEG$_{27}$-amide-Br]$_4$ (200 mg, 35 µmol, 1 equivalent) were dissolved in 22.5 mL *iso*-propanol and deoxygenated using four consecutive freeze-pump-thaw cycles. Afterward, Cu(0) (8.91 mg, 140 µmol, 4 equivalents) was added under inert conditions to the still frozen reaction mixture followed by four cycles changing between vacuum and argon before the polymerization mixture was allowed to warm up. The polymerization was carried out at room

temperature (23 °C) for 48 h. The reaction was then terminated by cooling in liquid nitrogen followed by precipitation into cold *n*-hexane. The residue was dissolved in dioxane and passed over a neutral AlOx column to remove the leftover copper species. The desired block copolymer was isolated by the removal of the leftover solvent under reduced pressure as a white powder.

^{1}H-NMR (300 MHz, $CDCl_3$, δ): 6.36-4.75 (m, -NH (residue)), 3.96-3.33 (PEG-backbone + methyl ester), 3.38-1.78 (P*t*BAMA backbone), 1.63-1.05 (C-$(CH_3)_3$).

^{13}C-NMR (300 MHz, CDCl3, δ): 28.54 ($(Me)_3$-O-**C**=O), 32.47 (-C-$(CH_3)_2$), 40.10 (-C-$(CH_3)_2$), 41.45 (**Me**-O-C=O), 45.51 (carbon core), 51.90 (P*t*BAMA backbone), 60.03 (P*t*BAMA backbone),67.05 (core-CH_2-), 70.05 (-O-CH_2-CH_2-), 70.57 ((**Me**)$_3$-O-C=O), (105.15 (Leftover monomer)), (131.26 (Leftover monomer)), 153.89 ($(Me)_3$-O-**C**=O),164.44 (Me-O-**C**=O), 171.97 (-NH-**C**=O). The ^{13}C-NMR spectrum can be found in **Figure A.7. 3.**

Deprotection of [PEG$_{27}$-*b*-P*t*BAMA]$_4$ to [PEG-*b*-PDha]$_4$

[PEG_{27}-*b*-P*t*$BAMA_6$]$_4$ (600 mg) was dissolved in TFA (25 eq.) and stirred for 10 h at 50 °C. Afterward, the reaction mixture was neutralized and dialyzed against water for 3 days with 3 solvent exchanges per day. Afterward, the resulting dispersion was freeze-dried and washed with *n*-hexane. The polymer was obtained as slightly pinkish powder (yield: 50%).

^{1}H-NMR (300 MHz, $CDCl_3$, δ): 3.81-3.30 (s, (PEG-backbone), 2.70-1.82 (m, PDha-backbone).

7.7. Results and Discussion

Synthesis of [PEG$_x$-b-PtBAMA$_y$]$_4$ star-shaped block copolymers

Herein we report the synthesis of four-arm star-shaped double hydrophilic block copolymers based on different PEG core sizes (5,000 g/mol – [PEG$_{27}$-amide-Br]$_4$, 10,000 g/mol – [PEG$_{56}$-amide-Br]$_4$, and 20,000 g/mol – [PEG$_{112}$-amide-Br]$_4$). These were modified as ATRP macroinitiators and, subsequently, block extension with different lengths of *t*BAMA was carried out. Afterwards, deprotection resulted in the formation of [PEG$_x$-*b*-PDha$_y$]$_4$ block copolymers featuring PDha segments of different length (**Scheme 7. 1**).

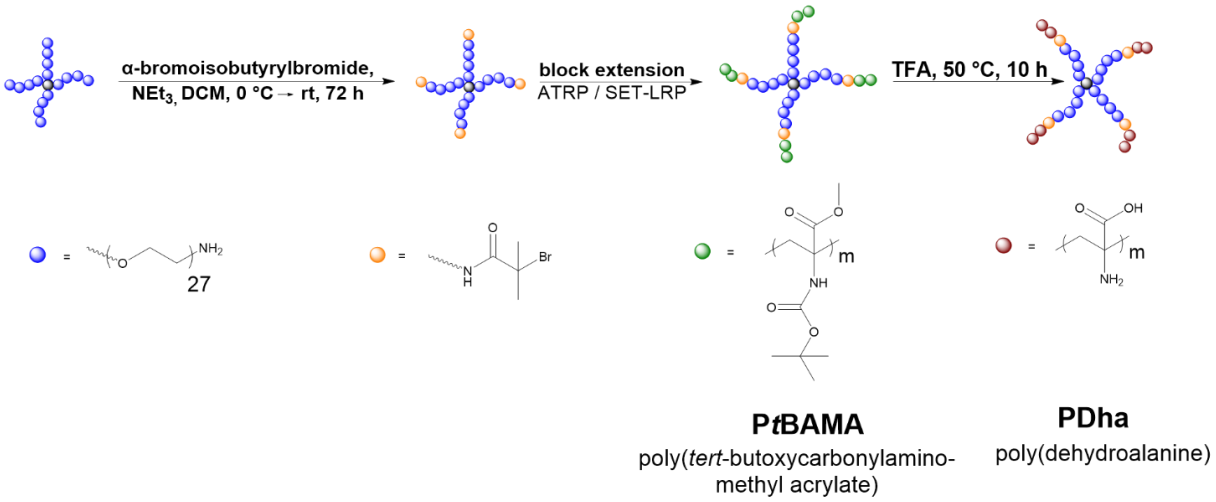

Scheme 7. 1: Synthetic route for the synthesis of double hydrophilic [PEG-*b*-PDha]$_4$ star block copolymers.

Starting from different core sizes of [PEG-NH$_2$]$_4$, *α*-Bromoisobutyryl bromide was used for end group modification of all four arms, achieving amide-based macroinitiators for atom transfer radical polymerization (ATRP) and single electron transfer living radical polymerization (SET-LRP). As the deprotection of *t*BAMA is performed under acidic conditions, an amide macroinitiator was chosen. This functionality leads to higher stability towards hydrolysis in comparison to typically reported ester counterparts. This concept was already successfully used for linear block copolymers.[17] ^{1}H-NMR spectroscopy shows a quantitative modification of the amines when the corresponding methyl groups are compared to the PEG backbone (**Figure A.7. 4**). Furthermore, the conversion of [PEG$_{27}$-NH$_2$]$_4$ to the [PEG$_{27}$-amide-Br]$_4$ macroinitiator was monitored *via* FTIR spectroscopy showing that the C=O vibration at 1670 cm^{-1} and the -NH vibration at 1523 cm^{-1} appear with the introduction of the bromine-terminated end-group (**Figure A.7. 5**).

We will first describe the choice of starting conditions for the block extension *via* ATRP. Afterwards, optimal conditions for the addition of 6-7 repeating units of *t*BAMA *via* ATRP are shown, followed by an increase of conversion to 40% resulting in well-defined [PEG_{27}-*b*-P*t*$BAMA_{41}$]$_4$ *via* SET-LRP. Finally, conditions for the deprotection of P*t*BAMA in a one-pot reaction are shown. For the ATRP, optimization of different parameters like the amount of deactivator species, type of copper species, solvent, concentration, temperature, and choices of ligand on *Đ* and conversion are detailed in the supporting information (**Figures A.7. 6–A.7. 9** and **Tables A.7. 1 – A.7. 5**). The choice of ligands used was based on their activity (k_{ATRP}) according to literature values.[23] Here, mainly two ligands with different activity were compared: [(2-pyridyl)methyl]amine (TPMA) showing higher k_{ATRP} and 4,4'-di-5-nonyl-2,2'-bipyridine (dNbpy) showing lower k_{ATRP} considering the activation determined by Robert *et al.* in 2000.[24] Furthermore, dNbpy was already tested for linear block copolymers, resulting in slow conversion and *Đ* < 1.4, which rendered dNbpy a promising candidate for our work.[17] Hence, dNbpy will in the following be used for the addition of short segments *via* ATRP while TPMA is used for higher conversions and longer PDha chains *via* SET-LRP. Regarding temperature, we choose 60 °C according to previous experience.[17]

Towards short PtBAMA segments

Table 7. 1 sums up the successful block extension of [PEG-amide-Br]$_4$ adding 6 repeating units *t*BAMA at each arm without significant changes in *Đ* if compared to the macroinitiator. This was achieved using ratios of *t*BAMA:dNbpy:CuCl:macroinitiator = 200:8:4:1 with a concentration of 0.63 mmol mL^{-1} for 4 h at 60 °C using a dioxane:DMF ratio of 1:2. Additionally, no deactivator species was added for this reaction, since already enough control over the reaction can be expected due to the use of dNbpy as ligand. As the first reaction starting from [PEG_{27}-amide-Br]$_4$ was sufficient, this ratio was transferred to comparative experiments starting from the macroinitiators with higher molecular weight. In both cases, the reaction could be successfully transferred to different core sizes (**Table 7. 1**). **Figure 7. 2** shows the corresponding SEC traces (**Figure 7. 2A**) and each in comparison to the respective macroinitiator (**Figure 7. 2B – C**).

Table 7. 1: Reaction conditions used to synthesize $[PEG_x\text{-}b\text{-}PtBAMA_{6\text{-}7}]_4$ *via* ATRP starting from different PEG core sizes. Corresponding polymer properties are characterized by SEC and ^{1}H-NMR spectroscopy.

Entry	[I]	DPn PEG/ arm	[Cu(I)Cl]	[*t*BAMA]	[dNbpy]	T [°C]	DPn, P*t*BAMA/arm[b]	M_n [g/mol][a]	[*Đ*][a]
1	1	27	4	200	8	60	**6**	15,000	**1.09**
2	1	56	4	200	8	60	**6**	22,200	**1.06**
3	1	112	4	200	8	60	**7**	36,800	**1.09**

[a] Determined by SEC (eluent: DMAc/LiCl [99.79/0.21], PMMA calibration) and by [b] ^{1}H-NMR spectroscopy. All reactions use a monomer concentration= 0.63 mmol/mL (ratio: dioxane/DMF=1:2).

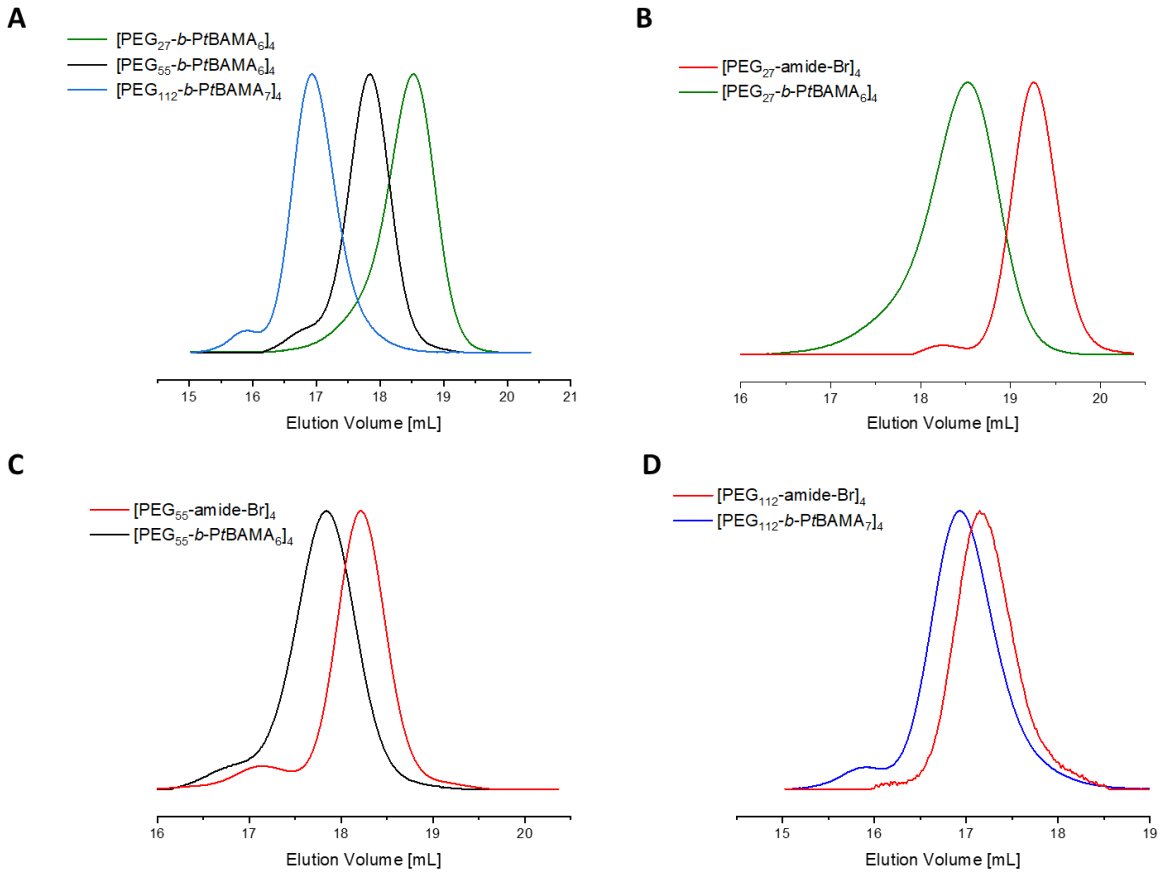

Figure 7. 2: A: Comparison of different $[PEG_x\text{-b-}PtBAMA_{6\text{-}7}]_4$ species (eluent: DMAc/LiCl [99.79/0.21]); **B** SEC elution traces (eluent: DMAc/LiCl [99.79/0.21]) showing $[PEG_{27}\text{-b-}PtBAMA_6]_4$ and the corresponding $[PEG_{27}\text{-amide-Br}]_4$ macroinitiator used. **C:** SEC-traces (eluent: DMAc/LiCl [99.79/0.21]) showing $[PEG_{55}\text{-b-}PtBAMA_6]_4$ and the corresponding $[PEG_{55}\text{-amide-Br}]_4$ macroinitiator used. **D:** SEC-traces (eluent: DMAc/LiCl [99.79/0.21]) showing $[PEG_{112}\text{-b-}PtBAMA_7]_4$ and the corresponding $[PEG_{112}\text{-amide-Br}]_4$ macroinitiator used.

In summary, all three star-shaped block copolymer species show *Đ* of 1.06-1.09 being comparable to the respective macroinitiators and show parallel shifts in SEC towards higher molecular weight, hinting towards no or little leftover macroinitiator. Additionally, all the block

copolymers were synthesized on a gram scale starting from 800 mg of macroinitiator. We explain the observed shoulder visible at both, macroinitiator and the corresponding star-shaped block copolymer due to impurities of the pentaerythritol-core with dipentaerythritol, resulting in additional $[PEG\text{-}NH_2]_6$ next to $[PEG\text{-}NH_2]_4$. Attempts to purify the starting material used or the resulting block copolymers resulting were so far unsuccessful.

Towards increasing conversion

The use of different solvents (**Table 7. 2**) reveals that the conversion can be drastically increased if alcohols are used as solvent (ethanol < iso-propanol < 1-octanol). Alcohols as solvents are well known to promote the disproportionation of Cu(I)X into Cu(0) and Cu(II)X which is a crucial step in SET-LRP.[25] Additionally, more recent work of avoiding star-star coupling reactions shows that Cu(0) mediated controlled radical polymerization combines high-end group fidelity with fewer star-star coupling reactions observed.[10,26-28] After several optimizations steps comparing different alcohol species as solvent using SET-LRP (see **Appendix A.7**) and ATRP, monomodal size distributions for conversions of more than 40% could be achieved, leading up to 41 repeating units of P*t*BAMA at each arm and a corresponding *Đ* of < 1.4 (**Figure A.7. 8 and A.7. 9**).

Table 7. 2: Reaction conditions used to synthesize $[PEG_{27}\text{-}b\text{-}PtBAMA_y]_4$ *via* SET-LRP, showing the influence of solvent used. The corresponding block copolymer characteristics were determined by SEC and ^{1}H-NMR spectroscopy.

Entry	[I]	[Cu(0)]	[Cu(II)Cl]	[*t*BAMA]	[L]	T [°C]	DPn,NMR /arm	M_n [g/mol]	[*Đ*]	Reaction time
1	1	4	0.8	400	8	RT	41	27,800	1.37	48 h
2	1	4	0.4	400	8	RT	70	69,400	2.49	24 h

[a] Determined by SEC (eluent: DMAc/LiCl [99.79/0.21], PMMA calibration) and by [b] ^{1}H-NMR spectroscopy. All reactions use a monomer concentration = 0.63 mmol/mL and either *iso*-propanol (entry 1) or 1-octanol (entry 2) as solvent.

Based on the synthetic conditions established above, a small set of 5 different star-shaped block copolymers were chosen for subsequent deprotection. The samples differ either in the length of the PEG chains ($[PEG_{27}\text{-}b\text{-}PDha_6]_4$, $[PEG_{55}\text{-}b\text{-}PDha_6]_4$ and $[PEG_{112}\text{-}b\text{-}PDha_7]_4$) or the length of the P*t*BAMA block was varied ($[PEG_{27}\text{-}b\text{-}PDha_6]_4$, $[PEG_{27}\text{-}b\text{-}PDha_{20}]_4$ or $[PEG_{27}\text{-}b\text{-}PDha_{41}]_4$).

One-pot deprotection of PtBAMA to PDha

As already shown in **Scheme 7. 1**, for the one-pot deprotection of P*t*BAMA neat TFA is used at 50 °C to obtain $[PEG_x\text{-}b\text{-}PDha_y]_4$. **Figure 7. 3** shows the quantitative deprotection of the ester group and additionally the deprotection of > 95% of the boc group after 10 h reaction time. The signal of the ester group is overlapping with the PEG backbone when $CDCl_3$ is used as NMR-solvent. However, after deprotection of the boc group the leftover ester signal shifts towards lower ppm when a mixture of D_2O/NaOD is used, which allows determining the quantitative cleavage of the ester group.

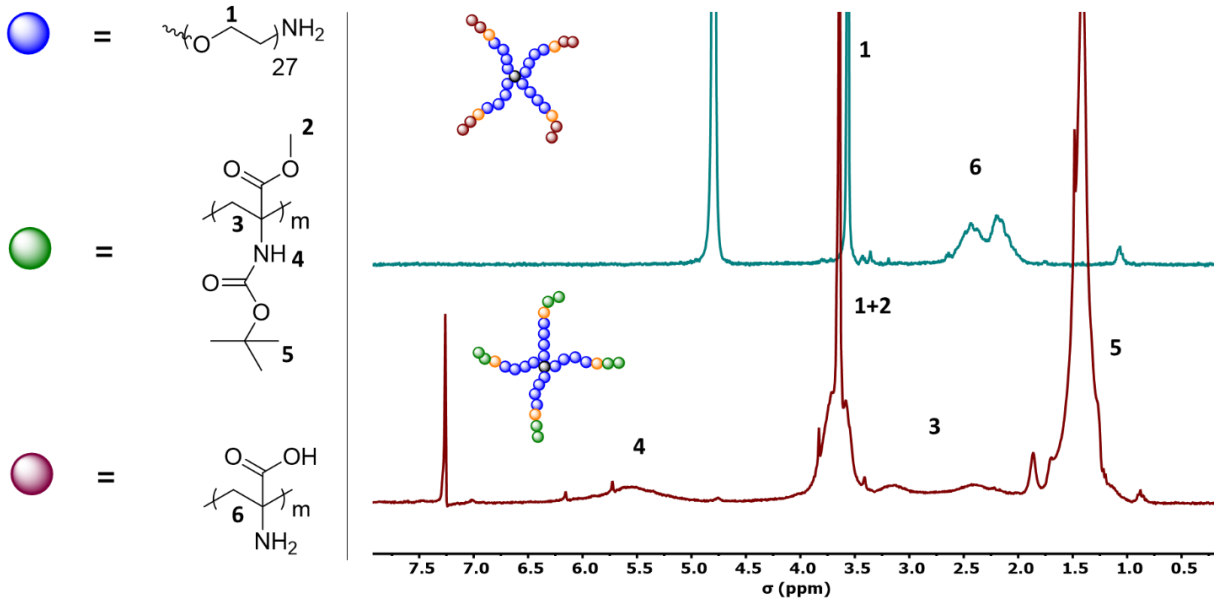

Figure 7. 3: ^{1}H-NMR spectroscopy measurements of $[PEG_x\text{-b-}PtBAMA_y]_4$ (red trace, measured in $CDCl_3$) and $[PEG_x\text{-b-}PDha_y]_4$. (blue trace, measured in D_2O/NaOD).

As the star-shaped block copolymers after deprotection show limited solubility in all solvents except DMSO and water, both were used as potential solvents for SEC measurements. Unfortunately, in both cases either column interactions or uneven baselines prevented a meaningful evaluation of the obtained data. To assess the stability of the amide linkage between both blocks during the deprotection reaction we used ^{1}H-NMR spectroscopy. For that, the $[PEG_{55}\text{-amide-Br}]_4$ macroinitiator of higher molecular weight was stirred in a large excess of neat TFA at 50 °C for 10 h and, after workup, the ratio between PEG backbone and amide was compared, resulting in a cleavage of < 10% (**Figure A.7. 10**). Additionally, all star-shaped block copolymers after deprotection showed signal for both segments in NMR spectroscopy.

Solution behavior of [PEG-b-PDha$_x$]$_4$

Since [PEG$_x$-*b*-PDha$_y$]$_4$ is a double hydrophilic star-shaped block copolymer carrying polyzwitterions as the second block, the polymers were dissolved in 0.1 M NaOH and their solution behavior at different pH values was characterized *via* potentiometric titrations, ζ-potential measurements, DLS and additionally AFM measurements after immobilization on silicon substrates. **Figure 7. 4A** shows the potentiometric titration of [PEG$_{27}$-*b*-PDha$_6$]$_4$ dissolved in 0.1 M NaOH (c = 0.2 mg mL^{-1}) which was afterwards titrated with 0.1 M HCl. For the corresponding ζ-potential measurements the titration was stopped at the desired pH values and samples were taken before the titration was continued. **Figure 7. 4C** shows the mean values of a triple determination for each of these corresponding samples.

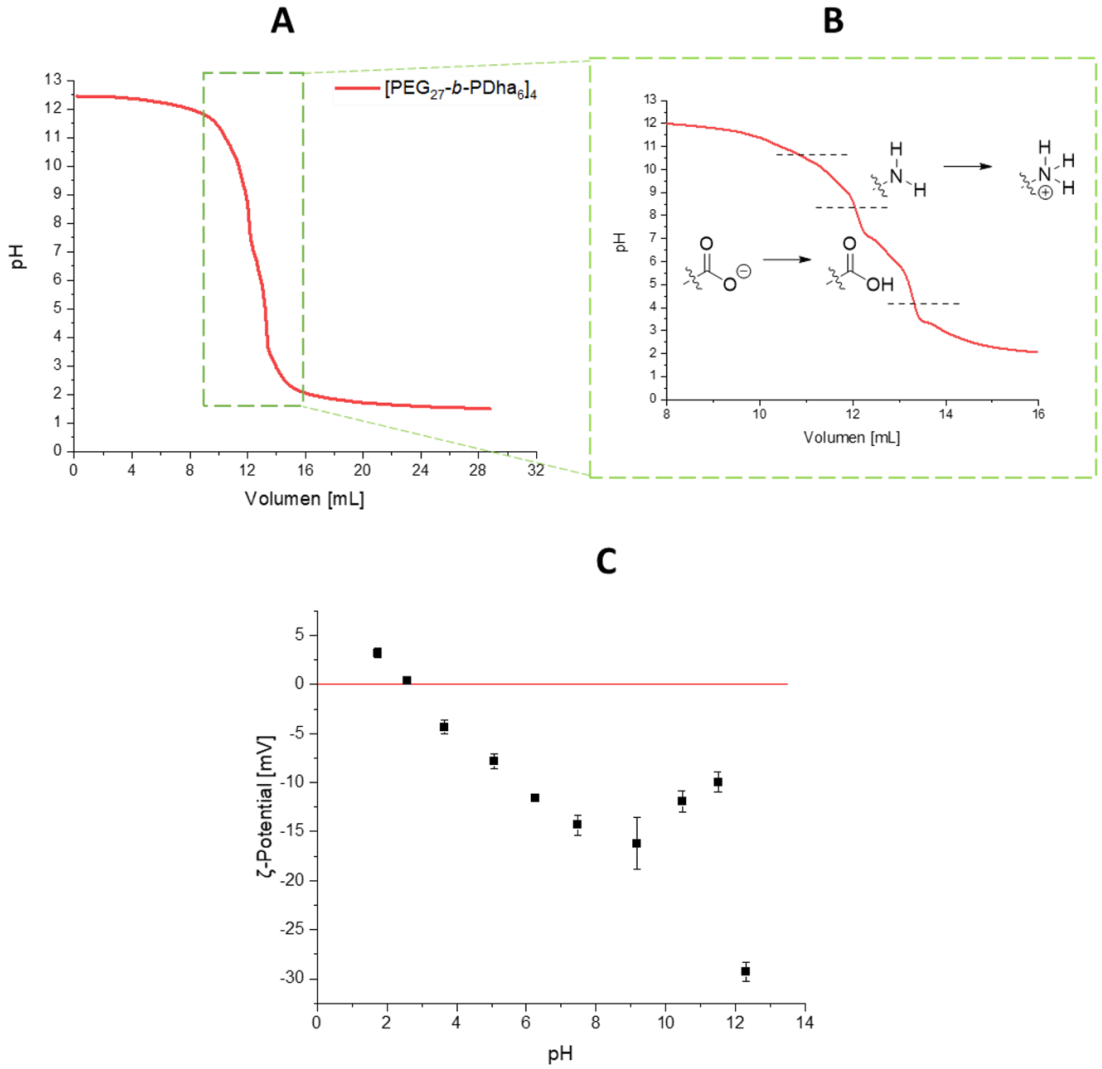

Figure 7. 4: A Potentiometric titration of [PEG$_{27}$-b-PDha$_6$]$_4$ dissolved in 0.1 M NaOH at a concentration of 0.2 mg/mL and titrated with 0.1 M HCl; **B** Zoom of **Figure 7. 4A** in the range of 8-16 mL; **C** ζ-Potential of [PEG$_{27}$-b-PDha$_6$]$_4$ at different pH values determined by titration (**Figure A.7. 11**: Titration and ζ-Potential of [PEG$_{27}$-b-PDha$_{41}$]$_4$).

Starting around pH 12.5 the first titration steps until pH 11 correspond mainly to the neutralization of excess NaOH. Afterward, from pH 11 to pH 7 the stepwise protonation of the -NH_2 groups of the PDha segment can be observed, being in accordance with earlier work on PDha homopolymers where a pK_B of 9.2 for the -NH_2 groups was determined.[14] Within this pH range the star-shaped block copolymer shows a negative net charge, which we further support with the negative ζ-potential measurements (**Figure 7. 4C**). However, in literature typical pK_A values of comparable –COOH groups of alanine are reported around a pK_A of 2.35,[29-32] fitting to our measurements. Due to that at pH values of 6 and below the protonation of the $–COO^–$ groups of the PDha block should increase, leading to charge neutrality at the isoelectric point and afterwards a positive net charge due to protonation of the –COOH groups and the presence of positively charged $–NH_3^+$ moieties. The potentiometric titration shows clearly a second equivalence point around pH = 3–4 corresponding to the pK_A of the carboxylic acid groups, while the ζ-potential measurements detect the isoelectric point between pH = 2 and pH = 4 and an overall positive charge below pH = 2. With that both, the potentiometric titration and the corresponding ζ-potential measurements describe the same trend for the charge inversion of the PDha segments. The differences can be tentatively explained due to the influence of the PEG core which might influence the overall charge of the star-shaped block copolymers.[33]

At higher concentrations of 20 mg mL^{-1}, lower pH values then pH = 7 lead to aggregation observable by turbidity and finally precipitation of the star-shaped block copolymer at pH values lower than 4. In case of lower concentrations (0.2 mg mL^{-1}), no precipitation was observed.

Additionally, both experiments were carried out using $[PEG_{27}$-*b*-$PDha_{41}]_4$, showing comparable results and with that no or nearly no changes in characterization when the ratio of PEG to PDha per arm is significantly altered (**Figure A.7. 11**). However, for further investigation next to potentiometric titrations and ζ-Potential measurements dynamic light scattering measurements and atomic force microscopy at the same concentrations will be discussed, showing the expected aggregation behavior which at higher concentrations leads to the observed precipitation.

Dynamic light scattering was used to gain insight into pH-dependent solution behavior of the star-shaped block copolymers. Sample preparation was carried out by dissolution at pH = 13 at 0.2 mg mL^{-1} or 0.4 mg mL^{-1} respectively in case of pH = 3 and pH = 5, followed by titration (see below). Please note that comparably large aggregates were formed at pH = 3 after titration, thus measurements had to be conducted directly after titration and a 5 µm filter had to be used to account for large aggregates. **Figure 7. 5A** shows the normalized correlation functions of

$[PEG_{27}$-*b*-$PDha_6]_4$ and $[PEG_{27}$-*b*-$PDha_{41}]_4$ at c = 0.2 mg mL^{-1}. From this graph, it is already evident, that the decay times are shifted to higher values at pH = 3 if compared to pH = 13, indicating slower diffusion and correspondingly higher hydrodynamic radii. Additionally, the raw data fluctuates strongly around the baseline, indicating higher order aggregates. It is also apparent that the decay curve for $[PEG_{27}$-*b*-$PDha_{41}]_4$ content drops off later at pH = 3, resulting in larger aggregates. However, at pH = 13, both samples show comparable decay times and with this comparable solution behavior.

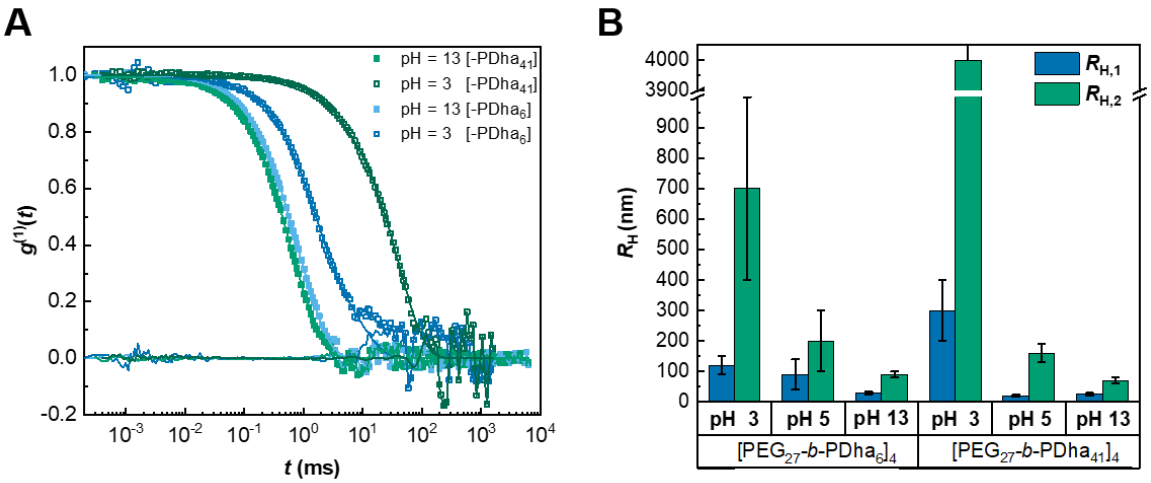

Figure 7. 5: A Normalized autocorrelation functions (rectangles) at a scattering angle of 90° of $[PEG_{27}$-b-$PDha]_4$ (blue) and $[PEG_{27}$-b-$PDha_{41}]_4$ (green) at a concentration of c = 0.2 mg mL^{-1} and at pH values of pH = 3 (open symbols) and pH = 13 (full symbols) together with their respective fit functions (solid lines) and the corresponding residuum fluctuating around zero. **B** Received hydrodynamic radii from the DLS measurements at 90°. The error bars were chosen to be large enough to capture the full distribution of radii.

These qualitative results are confirmed in **Figure 7. 5B**, which summarizes the hydrodynamic radii of $[PEG_{27}$-*b*-$PDha_6]_4$ and $[PEG_{27}$-*b*-$PDha_{41}]_4$ from the DLS measurements at pH values of 3, 5, and 13. For all measurements, a biexponential fit of the data was used to account for the size distribution of the aggregates, resulting in two hydrodynamic radii. The smaller hydrodynamic radius is assigned to $R_{H,1}$ and the larger to $R_{H,2}$. Details of the hydrodynamic radius calculation and the fitting procedure are given in the SI (**Appendix A.7**). In general, the hydrodynamic radii increase with decreasing pH value, as the repulsive interactions from –COO$^-$ groups start to vanish at pH = 5 due to their protonation and the isoelectric point is reached at around pH = 3. Besides decreasing electrostatic repulsion, we also assume that increasing inter- and intra-molecular hydrogen bond formation occurs at lower pH values, further increasing the tendency to form aggregates. In case of $[PEG_{27}$-*b*-$PDha_{41}]_4$ this increase is more pronounced ranging from tens of nanometer, (70 ± 10) nm, at pH = 13 to (160 ± 30) nm at

pH = 5 to a few micrometer, (4 ± 1) µm, at pH = 3 for $R_{H,2}$. In case of [PEG$_{27}$-*b*-PDha$_6$]$_4$ the increase of $R_{H,2}$ ranges only from (90 ± 10) nm at pH = 13 to a few hundred nanometers, (700 ± 300) nm, at pH = 3. This stronger aggregation tendency for [PEG$_{27}$-*b*-PDha$_{41}$]$_4$ in comparison to [PEG$_{27}$-*b*-PDha$_6$]$_4$ can be attributed to the increased DP of the PDha segments, leading to stronger attraction, either due to hydrogen bonding or to chain collapse of the outer blocks. Comparing the complete set of materials varying in PDha-content ([PEG$_{27}$-*b*-PDha$_6$]$_4$; [PEG$_{27}$-*b*-PDha$_{20}$]$_4$; [PEG$_{27}$-*b*-PDha$_{41}$]$_4$) as well as in core size ([PEG$_{55}$-*b*-PDha$_6$]$_4$; [PEG$_{112}$-*b*-PDha$_7$]$_4$) at c = 0.2 mg/mL and a scattering angle of 90°, the found hydrodynamic radii at pH = 13 and pH = 5 are of the same order of magnitude at the respective pH value. We receive radii of approximately $R_{H,1}$ = 20–30 nm and $R_{H,2}$ = 60–90 nm at pH = 13, and $R_{H,1}$ = 20–90 nm and $R_{H,2}$ = 100–250 nm at pH = 5 indicating comparable solubility and solution behavior independent of core size or length of the polyampholytic block. The higher radii at lower pH can be attributed to the partial protonation of the –COOH groups which results in lower repulsion between the stars and allows for higher aggregation numbers. At the lowest pH, however, the hydrodynamic radii vary widely, but the overall aggregation tendency increases with decreasing core size as well as with increasing PDha content. The results at a scattering angle of 90° and at the different pH values are summarized in **Table A.7. 6.**

Moreover, we also examined the aggregates formed by [PEG$_{27}$-*b*-P*t*BAMA$_6$]$_4$ by AFM. The films of the copolymer solutions at pH = 3 and pH = 13 at a concentration of 0.2 mg mL^{-1} were deposited on silicon wafers by spin coating. **Figure 7. 6** shows representative AFM images of aggregates formed at pH = 3 (**Figure 7. 6A**) and pH = 13 (**Figure 7. 6D**). At pH = 3, the lateral sizes of the aggregates is distinctly larger (≈ 800 nm–1.7 µm) compared to pH = 13 (≈ 40 nm–200 nm), which is in agreement with the results obtained from DLS experiments. The overall sizes are slightly lower, presumably due to drying during sample preparation. With further increase of the solution concentration to 1 mg mL^{-1}, larger aggregates were observed (**Figure A.7. 12**). Additionally, the size of the aggregates increases if the PDha block lengths is increased in case of [PEG$_{27}$-*b*-PDha$_{41}$]$_4$ (**Figure A.7. 13**). We explain the formation of larger aggregates at lower pH values due to the increasing formation of H-bonds within the PDha segments as well as an overall decreased solubility in aqueous media, as also discussed above and illustrated in **Figure 7. 7**. Overall, a similar trend for the solution behavior of [PEG-*b*-PDha]$_4$ star-shaped block copolymers is observed: decreasing solubility at lower pH due to the pH-responsive PDha segments. It seems that even short PDha block lengths of 6-7 repeat units per arm are sufficient to significantly influence the solution behavior of the materials, depending on pH.

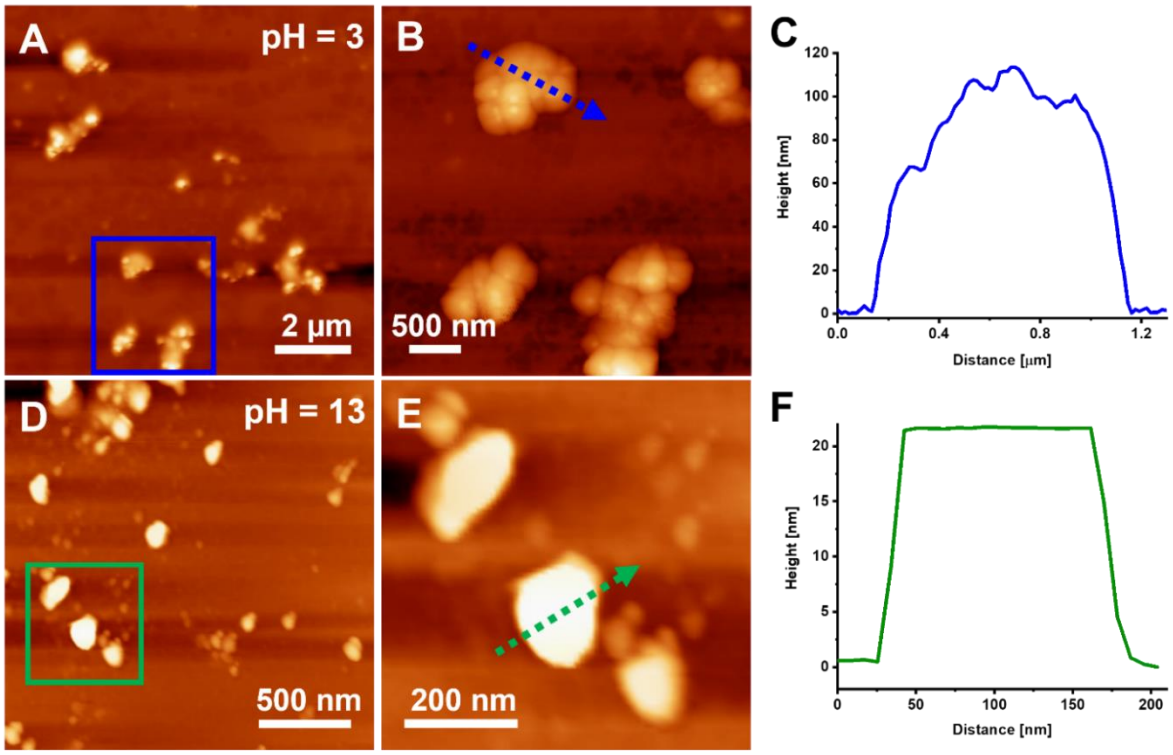

Figure 7. 6: A and **D** AFM height images showing the aggregates of $[PEG_{27}$-*b*-$PDha_6]_4$ at pH = 3 and pH = 13 at a concentration of 0.2 mg mL^{-1} respectively. **B** Zoomed in AFM height image for the region marked by the blue box in A. **C** Cross-sectional height profile along the blue dashed line shown in B. **E** Zoomed in AFM height image for the region marked by the green box in D. **F** Cross-sectional height profile along the green dashed line shown in E.

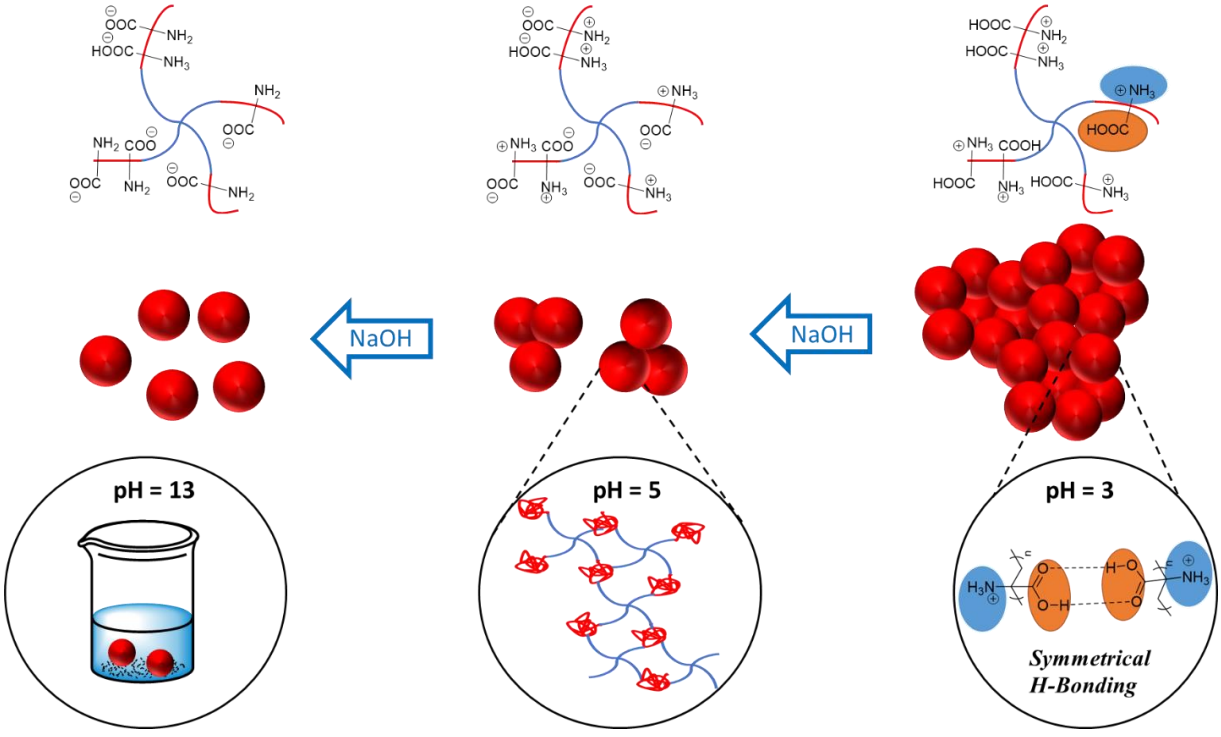

Figure 7. 7: Schematic depiction of the expected aggregation behavior of $[PEG_{27}$-b-$PDha_y]_4$.

We further explain the smaller aggregates present at pH = 5 with a partial collapse of the PDha segments, being closer to the isoelectric point and the absence of electrostatic stabilization leads to agglomeration of the star block copolymers as illustrated in **Figure 7. 7** (middle part). At pH 13 the aggregates observed are smaller if compared to pH = 5 and pH = 3. There are several examples in the literature demonstrating the aggregation of double hydrophilic block copolymers in water, such as Ke et al.[34], describing the formation of loose aggregates of poly(ethylene glycol)-*block*-poly(*N*,*N*-dimethylacrylamide) (PEG-*b*-PDMA). Another case uses stimuli-responsive poly(ethylene oxide)-*block*-poly(*N*-isopropylacrylamide) (PEO-*b*-PNIPAM) block or graft copolymers in water and also included theoretical descriptions.[35, 36]

7.8. Conclusion

We have demonstrated the synthesis of well-defined star-shaped $[PEG_x$-*b*-P*t*$BAMA_y]_4$ based on different core sizes of $[PEG\text{-amide-Br}]_4$ macroinitiators of either 5,000 g/mol, 10,000 g/mol, or 20,000 g/mol. Afterward, we additionally showed that with a change from ATRP to SET-LRP it is possible to change from the addition of only 6-7 P*t*BAMA units per arm (ATRP) to longer chains of up to 41 repeat units (SET-LRP) in a well-controlled manner. For all block copolymers, deprotection towards PDha was possible in a one-pot reaction using TFA and the resulting double hydrophilic block copolymers revealed interesting solution properties, which resulted in an increased aggregation tendency at low pH values, as indicated by a combination of DLS, AFM, potentiometric titrations, and ζ-Potential measurements.

Based on the results presented herein, we will utilize the pH-dependent solution characteristics of such materials for their use in hydrogels as charged stickers to induce reversible crosslinking, as already investigated from a theoretical point of view.[37] On the other hand, longer PDha blocks will allow for subsequent modification towards multi-functional materials and their use in sensing based on post-polymerization modification of the highly functionalized PDha part. [19]

7.9. References

[1] H. Cölfen, *Macromol. Rapid Commun.*, 2001, **22**, 219-252.

[2] A. Nabiyan, J. B. Max and F. H. Schacher, *Chem. Soc. Rev.*, 2022.

[3] M. Kamachi, M. Kurihara and J. Stille, *Macromolecules*, 1972, **5**, 161-167.

[4] J. N. Kizhakkedathu, K. R. Kumar, D. Goodman and D. E. Brooks, *Polymer*, 2004, **45**, 7471-7489.

[5] Z. Ge, Y. Zhou, J. Xu, H. Liu, D. Chen and S. Liu, *J. Am. Chem. Soc.*, 2009, **131**, 1628-1629.

[6] A. Skandalis and S. Pispas, *J. Polym. Sci., Part A: Polym. Chem.*, 2019, **57**, 1771-1783.

[7] L. Wang, Z. Li, P. Huang, Z. He and W. Ding, *Colloid. Polym. Sci.*, 2018, **296**, 1787-1794.

[8] S. Angot, K. S. Murthy, D. Taton and Y. Gnanou, *Macromolecules*, 2000, **33**, 7261-7274.

[9] G. Cheng, A. Böker, M. Zhang, G. Krausch and A. H. Müller, *Macromolecules*, 2001, **34**, 6883-6888.

[10] B. G. van Ravensteijn, R. Bou Zerdan, M. E. Helgeson and C. J. Hawker, *Macromolecules*, 2018, **52**, 601-609.

[11] Y.-W. Harn, Y. He, Z. Wang, Y. Chen, S. Liang, Z. Li, Q. Li, L. Zhu and Z. Lin, *Macromolecules*, 2020, **53**, 8286-8295.

[12] P. Theato, *Angew. Chem.*, 2007, **119**, 4480-4483.

[13] A. B. Lowe and C. L. McCormick, *Chem. Rev.*, 2002, **102**, 4177-4190.

[14] U. Günther, L. V. Sigolaeva, D. V. Pergushov and F. H. Schacher, *Macromol. Chem. Phys.*, 2013, **214**, 2202-2212.

[15] M. Billing and F. H. Schacher, *Macromolecules*, 2016, **49**, 3696-3705.

[16] M. Billing, G. Festag, P. Bellstedt and F. H. Schacher, *Polymer Chemistry*, 2017, **8**, 936-945.

[17] J. B. Max, P. J. Mons, J. C. Tom and F. H. Schacher, *Macromol. Chem. Phys.*, 2020, **221**, 1900383.

[18] J. Max, D. Pergushov, L. Sigolaeva and F. Schacher, *Polymer Chemistry*, 2019, **10**, 3006-3019.

[19] J. B. Max, A. Nabiyan, J. Eichhorn and F. H. Schacher, *Macromol. Rapid Commun.*, 2021, **42**, 2000671.

[20] A. Nabiyan, J. B. Max, C. Neumann, M. Heiland, A. Turchanin, C. Streb and F. H. Schacher, *Eur. J. Chem.*, 2021, **27**, 16924-16929.

[21] J. Max, K. Kowalczuk, M. Köhler, C. Neumann, F. Pielenz, L. Sigolaeva, D. Pergushov, A. Turchanin, F. Langenhorst and F. Schacher, *Macromolecules*, 2020, **53**, 4511-4523.

[22] P. Leroy, C. Tournassat, O. Bernard, N. Devau and M. Azaroual, *J. Colloid Interface Sci.*, 2015, **451**, 21-39.

[23] W. Tang, N. V. Tsarevsky and K. Matyjaszewski, *J. Am. Chem. Soc.*, 2006, **128**, 1598-1604.

[24] F. Zeng, Y. Shen, S. Zhu and R. Pelton, *Macromolecules*, 2000, **33**, 1628-1635.

[25] V. Percec, T. Guliashvili, J. S. Ladislaw, A. Wistrand, A. Stjerndahl, M. J. Sienkowska, M. J. Monteiro and S. Sahoo, *J. Am. Chem. Soc.*, 2006, **128**, 14156-14165.

[26] C. Boyer, A. Atme, C. Waldron, A. Anastasaki, P. Wilson, P. B. Zetterlund, D. Haddleton and M. R. Whittaker, *Polymer Chemistry*, 2013, **4**, 106-112.

[27] C. Boyer, A. Derveaux, P. B. Zetterlund and M. R. Whittaker, *Polymer Chemistry*, 2012, **3**, 117-123.

[28] C. Waldron, A. Anastasaki, R. McHale, P. Wilson, Z. Li, T. Smith and D. M. Haddleton, *Polymer Chemistry*, 2014, **5**, 892-898.

[29] M.-K. Chun, C.-S. Cho and H.-K. Choi, *J. Controlled Release*, 2002, **81**, 327-334.

[30] B. N. Dickhaus and R. Priefer, 2016.

[31] R. Dong, M. Lindau and C. K. Ober, *Langmuir*, 2009, **25**, 4774-4779.

[32] W. Guo and N. Hu, *Biophys. Chem.*, 2007, **129**, 163-171.

[33] M. J. Barthel, A. C. Rinkenauer, M. Wagner, U. Mansfeld, S. Hoeppener, J. A. Czaplewska, M. Gottschaldt, A. Träger, F. H. Schacher and U. S. Schubert, *Biomacromolecules*, 2014, **15**, 2426-2439.

[34] F. Ke, X. Mo, R. Yang, Y. Wang and D. Liang, *Macromolecules*, 2009, **42**, 5339-5344.

[35] I. V. Berlinova, P. V. Iliev, N. G. Vladimirov and C. P. Novakov, *Journal of Polymer Science Part A: Polymer Chemistry*, 2007, **45**, 4720-4732.

[36] J. Wu, Z. Wang, Y. Yin, R. Jiang, B. Li and A.-C. Shi, *Macromolecules*, 2015, **48**, 8897-8906.

[37] A. Tagliabue, J. Landsgesell, M. Mella and C. Holm, *Soft Matter*, 2021, **17**, 1574-1588.

8. CHAPTER VI: FROM IONIC BLOCK COPOLYMERS TO REVERSIBLE HYDROGELS

Electrostatically triggered hydrogel formation based on star-shaped polyampholytic block copolymers: a combined experimental and theoretical approach

[redacted] **N. Fribiczer**, [redacted]

Macromolecules, **2024,** *under review* (status: 07.03.2024; initial submission: 18.01.2024)

The corresponding *Supporting Information* is included in **Appendix A.8**.

The results in this chapter were adapted with permission from the authors.

8.1. Specific Summary

In general, two oppositely charged polyelectrolytes are required to form a network based on electrostatic interactions. By use of charged four-armed block copolymers, the strength of the bond can be adjusted by the length of the ionic block and the type of ionic species. To incorporate pH-dependent reversibility, one polyelectrolyte can be replaced by a polyampholyte, which allows the overall charge to be reversed by changing the pH value. This in turn enables a possible switch between a gel state and a sol state under suitable conditions.

Such a (one time) reversible network formation is presented in the following publication. In order to provide a better insight into the personal contribution to the following study as well as the path to this type of network chemistry and the obstacles on the way there, a brief recapitulation of the preliminary investigations is given below. The structures of the monomers used are shown in **Scheme 8. 1** for a better understanding and overview.

In the last chapter (*Chapter V*), the synthesis of star-shaped block copolymers was described, which consist of a four-armed PEG core block extended with multiple ampholytic polydehydroalanin segments at each arm. As a counterpart to form a potential reversible network, t-PEG block extended by poly (styrene sulfonic acid) natrium salt (PSSNa, **1**) was chosen as a permanently negative charged strong polyelectrolyte. Unfortunately, no gel formation on practical relevant timescales could be observed neither optical nor by rheology.

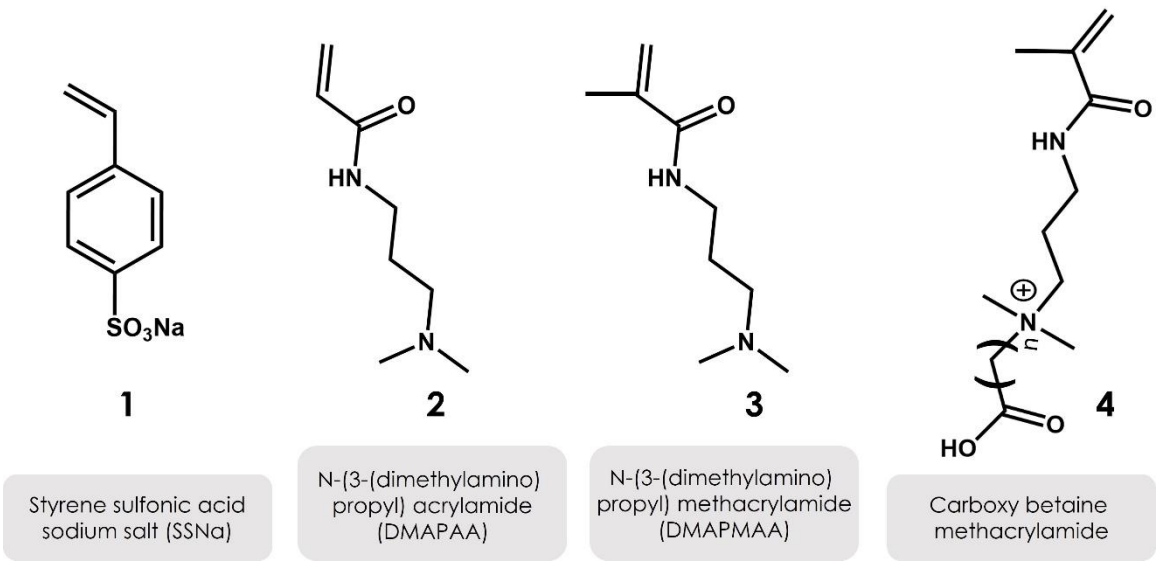

Scheme 8. 1: Representation of the monomers used for the block extension of the four-armed PEG core. The carboxy betaine methacrylamide was used with different linker length (n) between the quaternized nitrogen and the carboxylic acid group.

Therefore, poly (N-(3-(dimethyl amino) propyl) acrylamide) (DMAPAA, **2**) was investigated as ionic block together with PSSNa regarding a potential gel formation. By quaternization of the terminal amino group, a permanent positive charge was incorporated. It was found that the type of quaternization agent (methyl iodide or ethyl bromide) as well as the presence of the counterions has a significant effect on the mechanical stability (see **Figure 8. 1a**). Despite positive optical flip vial tests, only a highly viscous liquid-like material could be detected by rheology measurements over a wide range of frequencies. First promising results were obtained by a change from the acrylamide to the methacrylamide (DMAPMAA, **3**) species in combination with **1** (see **Figure 8. 1b**). With this system, a dominating storage modulus was found in rheology at suitable environmental conditions and thus a gel formation. Nevertheless, only a gel state was obtainable.

After all these initial and preliminary tests, changing the ion block to a carboxy betaine species (**4**) led to the desired presence of a sol and a gel state depending on the pH conditions. In three preliminary experiments, the most promising betaine species was determined with respect to the betaine block length (sticker length), the length of the aliphatic chain between the amine and the terminal carboxyl group (linker length) as well the concentration regime for the sol-gel transition (see **Figure 8. 1c** and **d**). It was found that a concentration of 5–10 wt% together with a block length of about 100 units of each betaine and PSSNa is suitable and that a longer linker length of about 6 CH_2 units results in the most stable gels. Experiments with shorter ionic blocks did not lead to improved gel formation, nor did the use of shorter linker lengths.

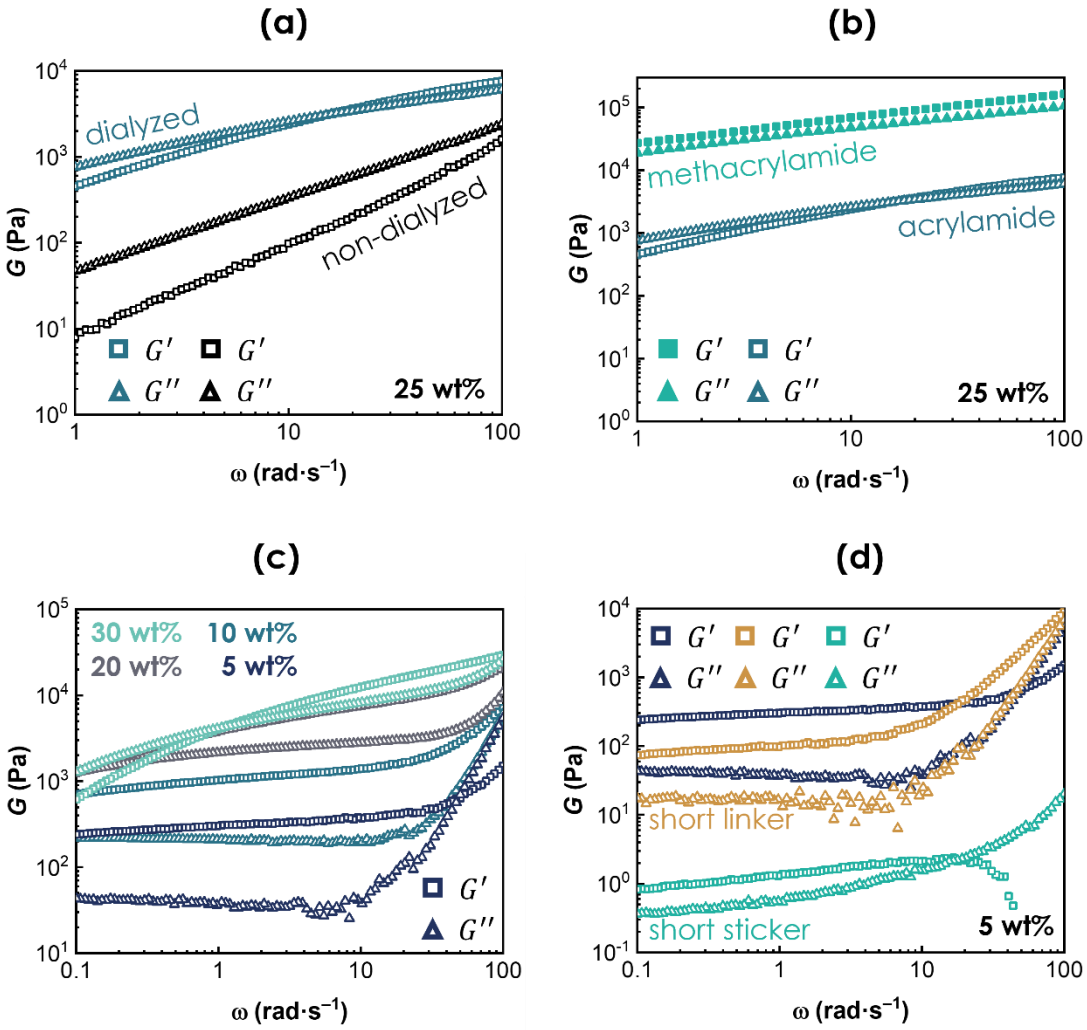

Figure 8. 1: Selection of some important preliminary rheological experiments at pH ≈ 4 of charge-balanced mixtures of t-PEG (M = 5 kg mol^{-1}) block extended each with **(a) 1** and **2 (**quaternized with methyl iodide as quaternization agent) with around 70 ionic units per arm at a concentration of 25 wt% in a non-dialyzed (black) and a dialyzed (light blue) state. The influence of the quaternization agent is not shown here. **(b) 1** and **2** (light blue, corresponds to **a**) as well as **1** and **3** (cyan) with around 80 ionic units per arm at a polymer concentration of 25 wt%. Both **2** and **3** are quaternized with methyl iodide as quaternization agent. **(c) 1** and **4** with around 100 ionic units per arm at different polymer concentrations of 30 wt% (light cyan), 20 wt% (grey), 10 wt% (light blue), and 5 wt% (dark blue). **(d) 1** and **4** at a concentration of 5 wt% with around 100 units per arm and a linker length of 6 CH_2-groups (dark blue; corresponds to **c**) as well as with short linkers of only 3 CH_2-groups (gold), and with around 60 units per arm (short sticker) and a linker length of 6 CH_2-groups (cyan).

Based on these optimizations, a final system with a block length of 100 ionic units each, a linker length of 5 CH_2-groups and a concentration range of 0.5–10 wt% was designed. This final system is presented and characterized in the following publication.

The synthesis of the star-shaped block copolymers is described, starting from amino-terminated PEG and addition of either PSSNa or PDMAPMAA by reversible-deactivation radical polymerization (RDRP). The carboxy betaine methacrylamide is then obtained by post-polymerization functionalization with a suitable quaternization agent. The carboxylic group of the betaines can

be either negatively (deprotonated) or neutrally (protonated) charged depending on the pH value. In addition, the quaternary nitrogen exhibits an ever-present positive charge. The PSSNa is a strong electrolyte and thus negatively charged in the entire investigated pH range. If both polymers are mixed under charge-balanced conditions, hydrogel formation is to be expected at a low pH value and a liquid-like material at a neutral to high pH value.

This hydrogel formation at low pH (pH = 3) is actually observed in the experiment. Sulfuric acid, phosphoric acid and hydrochloric acid are tested and hydrogels with the highest modulus are obtained with sulfuric acid, which is therefor used for all other investigations. The mechanical characteristics are probed by rheology at pH = 3 and pH = 13 for different polymer concentrations between 0.5–10 wt%. At low pH a hydrogel formation is obtained at all concentrations, which is in line with the expectations. However, at high pH a liquid-like material is only found for concentrations $\leq$ 2 wt%, higher concentrations remain solid-like. The high concentration regime exceeds the overlap concentration of around 2 wt% and thus a transient network is formed due to overlapping chain segments.

To enable reversibility of the gel formation, the liquid-like state must be attainable. Therefore, only concentrations below 2 wt% are considered. The reversibility of the gel formation is investigated by switching from pH = 3 to pH = 13. After reaching basic conditions, a liquid-like material is observed as expected. The change back to acidic conditions does not lead to a solid-like material. The material remains liquid-like due to the high salt concentration in the system. However, at least a one-time change between the gel and sol state is possible. The underlying mechanisms and interactions are further explored with simulation techniques, which reveal that both partial functionalization and charge regulation upon interaction of betaine and sulfonate species increase the net charge in the betaine chains. This increases the pH window of electrostatic attraction between the two polymer species and thus extends the solid-like regime towards basic conditions.

This provides the basis for further investigations of these materials with regard to their reversibility and the influence of polymer and salt concentration. In addition, optimization of the functionalization can help to shorten the pH range of the stable gels and thus enable multiple switching due to lower salt concentrations. In addition, the influence of the base used can be investigated in a similar way to the acid test. Moreover, other combinations of polyionic materials can be tested at concentrations below the overlap concentrations regarding reversible hydrogel formation.

8.2. Author Contributions

[redacted]	Concept development, polymer synthesis, polymer characterization, titrations and zeta potential measurements, synthesis and characterization of hydrogels, manuscript preparation and correction.
[redacted]	Concept development, MD/MC simulations and evaluation, manuscript preparation and correction.
[redacted]	Concept development, rheology measurements and evaluation, manuscript preparation and correction.
Nora Fribiczer:	Preliminary rheology measurements and evaluation, concept development, rheology measurements and evaluation, manuscript preparation and correction.
[redacted]	Concept development for simulations, MD/MC simulations and evaluation.
[redacted]	Concept development for simulations, scientific supervision of [redacted] and manuscript correction.
[redacted]	Scientific supervision of [redacted] and [redacted] and manuscript correction.
[redacted]	Concept development, scientific supervision and manuscript correction.

8.3. Acknowledgement

The authors thank the German Research Foundation (DFG) for funding within the Research Unit FOR2811 „Adaptive Polymer Gels with Model Network Structure“ under grant No. 423791428 along with grants 423435431 (TP2), 423373052 (TP4), and 423435431 / 397384169 (TP7). The authors acknowledge [redacted] for SEC analysis and the NMR department at Friedrich-Schiller-University Jena for their continuous support.

8.4. Abstract

Herein, we describe the synthesis and properties of reversibly electrostatically crosslinked hydrogels based on star-shaped block copolymers. We synthesized two different star-shaped block copolymers based on 4-arm poly(ethylene glycol) (PEG) with oppositely charged second blocks: PEG-*block*-poly(styrene sulfonic acid) $[PEG_{27}$-*b*-$PSSNa_{100}]_4$ and PEG-*block*-poly(carboxy betaine methacrylamide) $[PEG_{27}$-*b*-$PCBAMAAm_{108}]_4$ using reversible-deactivation radical polymerization techniques starting from $[PEG_{27}$-amide-$Br]_4$ macroinitiators. At total polymer concentrations below 4 weight percent of both, the betaine and sulfonate species with about 100 charged units per arm, we observe the formation of either a liquid-like or a gel-like state depending on the pH value. Oscillatory shear-rheology experiments are performed to investigate the influence of polymer concentration, the type of counterion, or salt concentration on the hydrogel formation and the type of betaine to successfully form hydrogels. In addition, the pH-dependent switching from the gel to the sol state is investigated. Using molecular simulation techniques, we rationalize our experimental findings.

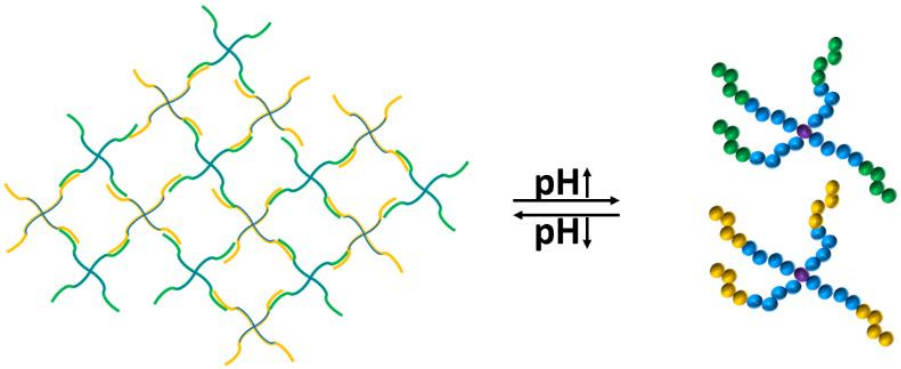

Scheme 8. 2: Schematic representation of the pH-dependent behavior of ionic block copolymers between a gel state and a sol state.

8.5. Introduction

In the early 1950s, Wichterle and Lim proposed their idea of designing a new biologically and chemically stable material that exhibits shape stability whilst being soft like the surrounding tissue, additionally having a high permeability to water-soluble nutrients and metabolites.[1] Later on, in 1953 Lim published the synthesis of copolymers based on 2-hydroxyethyl methacrylate (HEMA) and ethylene dimethacrylate (EDMA), the first synthetic material corresponding to that idea, which we nowadays consider a hydrogel.[2] With the invention of this first hydrogel both, Wichterle and Lim reported their first exact material definition in 1960 and defined a hydrogel as a water-swollen polymeric material that maintains a distinct three-dimensional structure.[2] Due to their high-water content and depending on their potential bio-compatibility, research in this area highly increased. Today there are numerous application fields of many different hydrogel materials, reaching from soft contact lenses over wound care materials to diapers or the field of implants. All hydrogel materials can be classified into different subgroups depending on whether they are natural or synthetic gels, the presence of pores, or the nature of the network itself, but mostly they are distinguished by the nature of their cross-linking, i.e. whether they are chemical or physical gels. [1] By changing parameters such as the type of monomers used and the topology and combination of the resulting polymers, different scientific and industrial problems can be addressed and solved. In 2008, Sakai *et al.* described well-defined and homogeneous networks by combining two symmetrical tetrahedron-like macromonomers of the same molecular weight and size where each macromonomer has four reactive end groups.[3] This work was followed by different examples of chemically crosslinked networks based on star-shaped polymers, reaching from non-reversible examples using Michael-type thiol–ene,[4–6] amidation reactions,[7–9] radical-mediated thiol-ene, [10, 11] Cu-catalyzed alkyne–azide cycloaddition (CuAAC)[12–14] over strain-promoted alkyne-azide cycloadditions (SPAAC)[14] and thiol-halide chemistry[15, 16] to reversible networks. For example, the latter allowed repairing defects formed during the initial reaction and were based on diels-alder chemistry (DA),[17] boronic acid-diol condensation reactions,[18] hydrazide-carbonyl condensation, [19, 20] or reversible cycloaddition reactions ([2 + 2] / [4 + 4]).[21–24] Chemical crosslinks are used in most of the reported systems due to their higher robustness compared to physical crosslinks. Nevertheless, there are a few reports on physically crosslinked hydrogels in that field *via* either H-bonding[25] or host-guest complexation chemistry.[26]

The library of physically crosslinked hydrogels can be extended if the topology is changed from star-shaped polymers to linear examples. In general, these use ionic interactions and the formation of coacervates,[27–29] thermo-responsive behavior,[30] crystallization,[31, 32] or hydrogen

bonding.[33–36] Additionally, due to the nature of physical crosslinks, it is expected that these systems can exhibit self-healing as already shown by Libin Liu *et al.* for a series of zwitterionic polymer hydrogels.[37]

To the best of our knowledge, there is so far no system described that shows the formation of hydrogels merely due to electrostatic interactions based on star-shaped block copolymers. In our work, we first discuss the synthesis of different four-arm star-shaped block copolymers based on [PEG_{27}-amide-Br]$_4$ *via* reversible-deactivation radical polymerization techniques with either sulfonated styrene or dimethylamino propyl methacrylamide in a well-defined manner. Afterwards, we describe the quaternization and successful betaine formation of the dimethyl amino propyl (meth)acrylamide units.

However, the combination of both the betaine species and the sulfonate species with about 100 charged units per arm ([PEG_{27}-*b*-$PSSNa_{100}$]$_4$ and [PEG_{27}-*b*-$PCBAMAAm_{108}$]$_4$) at charge-balanced mixing conditions of low amounts of polymer (below 4 wt%) depending on the pH value results in a liquid-like material (pH = 13) or a hydrogel (pH = 3). Due to the pH-responsive behavior of the acidic group of the betaine, which is protonated at low pH and deprotonated at high pH values, network formation occurs close to pH = 3, resulting in stronger networks whilst with a pH below 3 no network formation occurs due to precipitation of the star-shaped block copolymer. However, at pH ≥ 13, the carboxy group of the betaine species is fully deprotonated resulting in disturbed network formation, an altered charge balance, and with that a liquid appearance (and no network formation), when mixed with the sulfonate species. Furthermore, we characterize the pH-dependent behavior of mixtures with different concentrations *via* rheology and the influence of different counterions on the network strength by varying the acids used for hydrogel formation at low pH values. We further explore the influence of the pK_a value of the carboxylic acid group of the betaine by varying the linker length between both charges present in the [PEG_{27}-*b*-$PCBAMAAm_{108}$]$_4$ building blocks. Finally, we show that the hydrogel formation can be reversed by changing to high pH for an already-formed hydrogel, resulting in dissolution of the network structure. Formation and stability of the networks are described using hybrid MD/MC simulations using the simulation software package LAMMPS.[38] Please note that some literature examples suggest that the presence of negatively charged sulfonates could make the ionizable groups on betaines adopt their charge in order to enable electrostatic attraction between the two polymers.[39–42] However, the simulation of more than one chain, in our case the simulation of 4 arm star-shaped block copolymers remains challenging. We herein discuss the first simulations on this topic providing suitable explanations for the network formation and dissolution based on different pH values.

8.6. Results and Discussion

Our general idea was to find a material combination for the reversible formation of hydrogels based on star-shaped block copolymers of opposite charge. Therefore, two different kinds of star-shaped block copolymers were synthesized by block extension of PEG-based macroinitiators. We targeted $[PEG_{27}$-*b*-$PSSNa_{100}]_4$ as polyanionic species and PEG-*block*-poly(dimethyl aminopropyl meth acrylamide) ($[PEG_{27}$-*b*-$PDMAPMAAm_{108}]_4$) as charge-tunable building block, where in the latter case post-polymerization functionalization was carried out using ethyl 6-chlorohexanoate or shorter alkyl chains. The term "linker" is defined in the following as the spacer between the two charges in the polybetaine structure. The ester was afterwards deprotected under basic conditions to achieve the desired betaines, revealing strong shifts in the pK_a values of the carboxyl groups depending on the linker length, where longer alkyl chains resulted in higher pK_a values.[43] **Scheme 8. 3** illustrates the synthesis of the desired star-shaped block copolymers and **Scheme 8. 4** the expected reversible hydrogel formation.

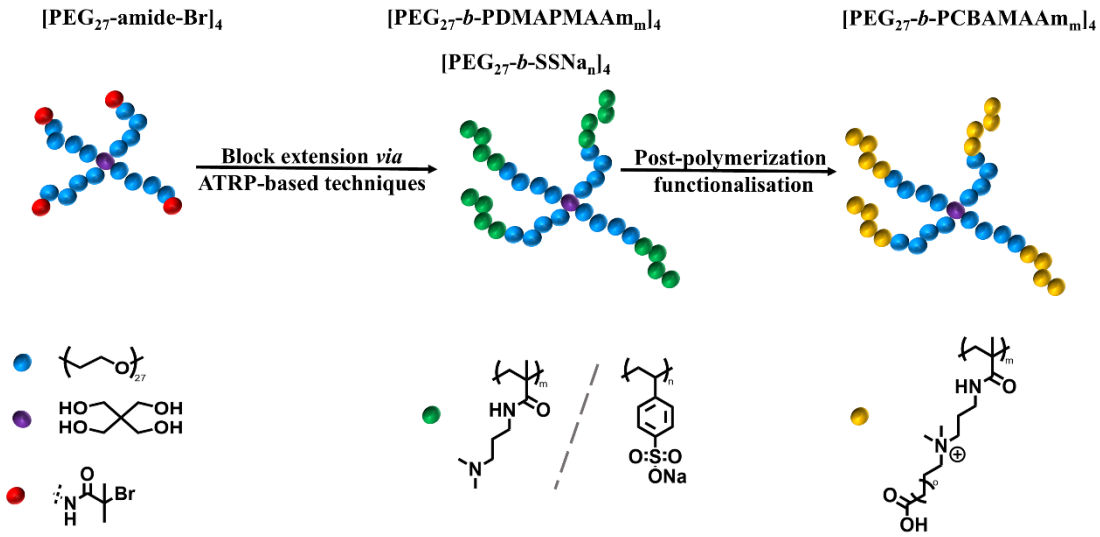

Scheme 8. 3: Synthesis of $[PEG_{27}$-b-$PDMAPMAAm_{108}]_4$ and $[PEG_{27}$-b-$PSSNa_{100}]_4$ via reversible-deactivation radical polymerization (RDRP) techniques, followed by subsequent post-polymerization modification of $[PEG_{27}$-b-$PDMAPMAAm_{108}]_4$ towards $[PEG_{27}$-b-$PCBAMAAm_{108}]_4$ star-shaped block copolymers.

Upon changes in pH value, the carboxylic group of the betaines should be either negatively charged or protonated. If both polymers, $[PEG_{27}$-*b*-$PSSNa_{100}]_4$ and $[PEG_{27}$-*b*-$PCBAMAAm_{108}]_4$, are mixed under charge balanced conditions in aqueous media, hydrogel formation is expected at lower pH (pH = 3) and absence of network formation at basic conditions (pH ≥ 13), as illustrated in **Scheme 8. 4**.

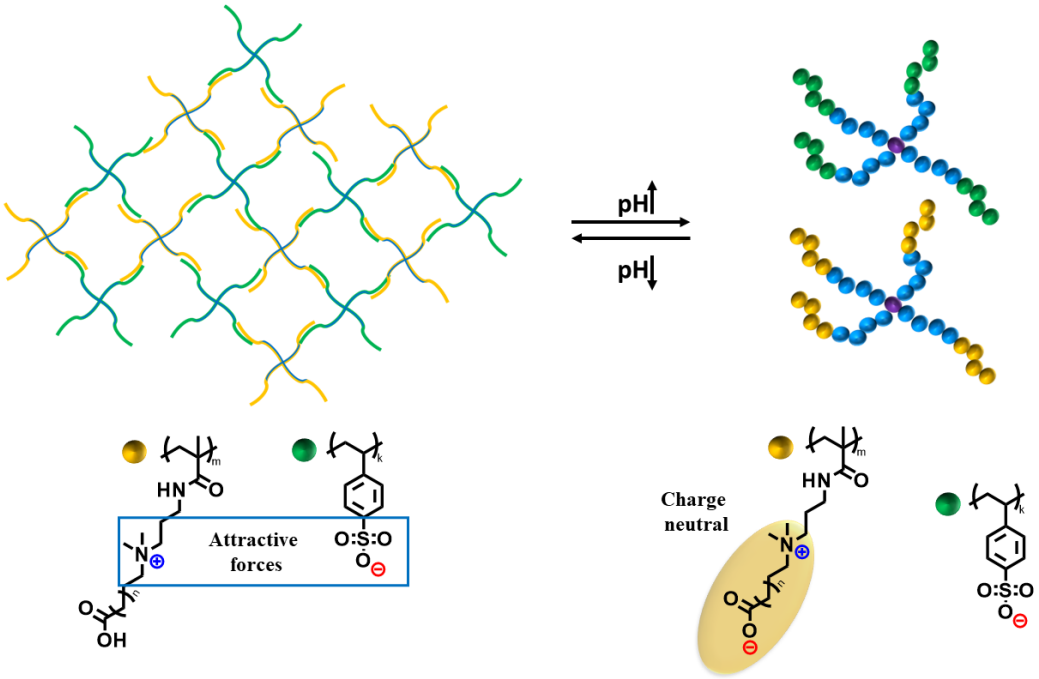

Scheme 8. 4: Illustration of the expected reversible hydrogel formation mechanism between [PEG_{27}-b-PCBA-$MAAm_{108}$]$_4$ and [PEG_{27}-b-$PSSNa_{100}$]$_4$.

Synthesis and characterization of star-shaped block copolymers

All star-shaped block copolymers were synthesized using reversible-deactivation radical polymerization (RDRP) techniques. Therefore, the [PEG-amide-Br]$_4$ macroinitiator (also termed "CORE" – see below) was synthesized *via* end group modification reaction of [PEG_{27}-NH_2]$_4$ (5,000 g/mol) with *α*-bromoisobutyryl bromide. In case of block extension with SSNa a [PEG_{27}-amide-Br]$_4$ concentration of 2.3 µmol/mL (water: iso-propanol = 1:1) and a molar ratio of SSNa:bpy:CuCl:[PEG_{27}-amide-Br]$_4$ = 800:8:4:1 was used for the polymerization reaction. After 15 h of reaction time at 23 °C, SEC showed a broad shift towards lower elution volumes (**Figure 8. 2C**) with a corresponding $Đ$ of 1.30 and M_n of 122 kg/mol (4-arm PEG calibration), whilst the corresponding ^{1}H-NMR spectrum reveals a successful addition of 400 repeating units SSNa per star and 100 units per arm respectively (**Figure 8. 2A**). Zeta potential measurements demonstrate that [PEG_{27}-*b*-$PSSNa_{100}$]$_4$ is negatively charged between pH = 1.4 and 10 (**Figure 8. 2E**). However, the negative charge reduces drastically at around pH = 1.4 as we assume to be closer to the pK_a value of PSSNa based on reported values for linear samples between 1.22 and 1.50,[44] depending on block length and polymer concentration. Thus, a pH value of 3 was chosen for hydrogel formation, to ensure that negligible protonation of the sulfonate occurs. Additionally, a ^{13}C NMR can be found in the SI (**Appendix A.8**; **Figure A.8. 2**).

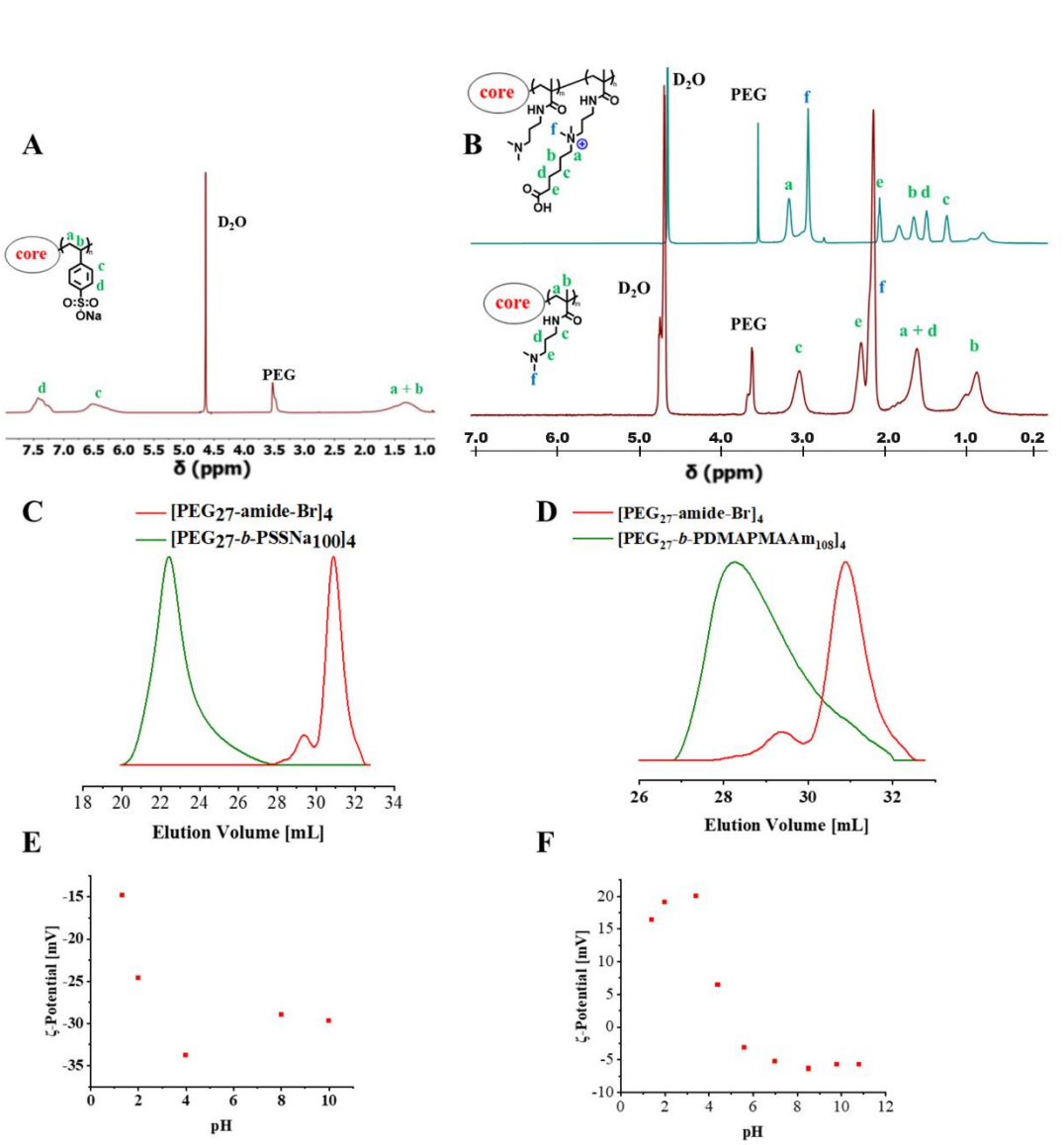

Figure 8. 2: A: ^{1}H-NMR spectroscopy measurements (D_2O) of $[PEG_{27}\text{-b-}PSSNa_{100}]_4$, **B:** ^{1}H-NMR spectroscopy measurements (D_2O) of $[PEG_{27}\text{-b-}PDMAPMAAm_{108}]_4$ and $[PEG_{27}\text{-b-}(PDMAPMAA_{26}\text{-g-}PCBAMAAm_{82})_{108}]_4$, **C:** SEC traces of block extension of $[PEG_{27}\text{-amide-Br}]_4$ with SSNa (eluent: DMSO\LiCl [99.79/0.21], 4-arm PEG calibration), **D:** SEC traces of block extension of $[PEG_{27}\text{-amide-Br}]_4$ with DMAPMAAm (eluent: DMSO\LiCl [99.79/0.21], 4-arm PEG calibration), **E:** Zeta potential measurements of $[PEG_{27}\text{-b-}PSSNa_{100}]_4$ at different pH values, **F:** Zeta potential measurements of $[PEG_{27}\text{-b-}(PDMAPMAAm_{26}\text{-g-}PCBAMAAm_{82})_{108}]_4$ at different pH values.

In case of block extension with DMAPMAAm an initiator concentration of 2.3 µmol/mL (water: iso-propanol = 1:5) and a molar ratio of DMAPMAAm:HMTETA:Cu(0):$CuCl_2$:Initiator = 800:8:2:0.8:1 resulted after 10 h reaction time at room temperature in a conversion of 54%, adding 108 repeating units of DMAPMAAm per arm. **Figures 8. 2B** and **D** show the corresponding analytics proving the successful block extension *via* ^{1}H spectroscopy and SEC measurements. The SEC traces reveal a typical shift to lower elution volumes when compared to the $[PEG_{27}\text{-amide-Br}]_4$ macroinitiator, additionally revealing a dispersity of 1.18 and a

M_n of 11,400 g/mol when compared to the 4-arm PEG standard. We assume the tailing towards higher elution volumes to originate from interactions with the column material.

However, additionally, **Figure 8. 2B** is showing the analytics corresponding to the post-polymerization functionalization reaction of $[PEG_{27}$-*b*-$PDMAPMAAm_{108}]_4$ resulting in $[PEG_{27}$-*b*-$(PDMAPMAA_{26}$-*g*-$PCBAMAAm_{82})_{108}]_4$. For the post-polymerization functionalization $[PEG_{27}$-*b*-$PDMAPMAAm_{108}]_4$ was modified using a ratio of DMAPMAAm:6-chlorohexanoate of 1:1.5, resulting in $[PEG_{27}$-*b*-$(PDMAPMAAm_{26}$-*g*-PCBAMAAm-$ester_{82})_{108}]_4$ (75% conversion). The limitation in the conversion can be explained due to steric hindrance. The ester is afterwards deprotected under basic conditions resulting in $[PEG_{27}$-*b*-$(PDMAPMAA_{26}$-*g*-$PCBAMAAm_{82})_{108}]_4$. **Figure 8. 2B** shows both, the ^{1}H-NMR of the successful block extension and the ^{1}H-NMR of successful post-polymerization functionalization reaction. Additionally, the betaine is characterized *via* potentiometric titration and zeta potential measurements. The zeta potential measurements in **Figure 8. 2F** reveal net zero charge around pH 4–6 where we expect the pK_a of the carboxylic acid group. Nevertheless, at higher pH, the overall charge is shifted to slightly negative values which is a known phenomenon for PEG-based materials.[45] Additionally, the ^{13}C NMR can be found in the SI (**Appendix A.8**; **Figure A.8. 3**).

Hydrogel formation

The following hydrogel formation experiments are based on three pre-experiments.

1.) The final block length was adjusted to the above-described block lengths of about ~100 charges per arm of each star-shaped block copolymer. Lower number of charges per arm did not result in a hydrogel as defined by rheology. We propose that the term 'gel' should be limited to systems, which fulfil the following phenomenological characteristics: (a) they consist of two or more components one of which is a liquid, present in substantial quantity and (b) they are soft, solid, or solid-like materials. We further propose a definition of the solid-like characteristics of gels in terms of the dynamic mechanical properties, a storage modulus, G', which exhibits a pronounced plateau extending to times at least of the order of seconds and a loss modulus, G'', which is considerably lower than the storage modulus in the plateau region.[46]

2.) H_2SO_{4aq} and NaOHaq are used to adjust the pH value. The influence of counterions for the low pH regime in terms of hydrogel strength is determined by the choice of acid can be described as H_2SO_4 > H_3PO_4 > HCl (**Figure A.8. 4**).

3.) The linker length of the betaine is adjusted to 5 CH_2 groups between the quarternized nitrogen and the carboxylic acid group. The work by Zhang *et. al* shows that the linker group at the betaine directly influences the pK_a value of the corresponding acid group, with longer linkers resulting in higher pK_a values.[43] Considering the pK_a values for different betaine homopolymers and monomers the estimated pK_a for 5 CH_2 groups used as linker should be around 5.12 in water at room temperature.[43] **Figure A.8. 1** in the SI (**Appendix A.8**) shows oscillatory shear-rheology measurements of the system at $pH = 3$ using different linker lengths. The linker length of 5 is chosen for the final experiments as it shows the highest mechanical resilience.

All following hydrogel formation experiments have in common, that the two star-shaped polymer species $[PEG_{27}$-*b*-$PCBAMAAm_{108}]_4$ and $[PEG_{27}$-*b*-$PSSNa_{100}]_4$ are mixed near the charge balance. The charge balance is calculated corresponding to the expected charges at $pH = 3$ using H_2SO_{4aq} to adjust the pH at lower values. The charge balance conditions are chosen because at this point the Coulomb attraction outweighs the repulsion for neutral polyampholytes.[47, 48]

Figure 8. 3 shows oscillatory shear-rheology data describing the influence of the polymer concentrations used for hydrogel formation varied from 0.5 wt% up to 10 wt% and probed at $pH = 3$ and $pH = 13$. At $pH = 3$ the carboxylic acid group of the betaine is protonated, resulting in network formation. At $pH = 13$, however, deprotonation of the carboxylic acid group leads to a change in the overall charge balance and destabilization of the network (**Scheme 8. 4**), resulting in a viscous liquid (**Figure 8. 3**). The highest storage moduli can be achieved with either 1 wt% or 10 wt% of star-shaped block copolymer at $pH = 3$. At $pH = 13$ viscous liquids are expected, which is observed for polymer concentrations of 0.5 wt%, 1 wt%, or 2 wt%. However, if higher polymer concentrations are used (4 wt% and 10 wt%), network formation is indicated by rheology ($G' > G''$). We assume that for polymer concentrations above 2 wt%, the overlap concentration (c^*) is exceeded, resulting in the formation of a physical gel due to chain overlapping. Therefore, the overlap concentrations of both polymer species $[PEG_{27}$-*b*-$PDMAPMAAm_{108}]_4$ (c^* = 39.7 ± 0.2 g·L^{-1}) and $[PEG_{27}$-*b*-$PSSNa_{100}]_4$ (c^* = 21.5 ± 0.5 g·L^{-1}) were calculated based on the specific viscosity η_{sp} determined using a capillary viscometer of micro-Ubbelohde type I (for the exact calculation: see the supporting information **Table A.8. 1** and above). However, as both values fit to our explanation, we consider the use of concentrations higher than 2 wt% not suitable for the pH reversible formation of hydrogels at this point.

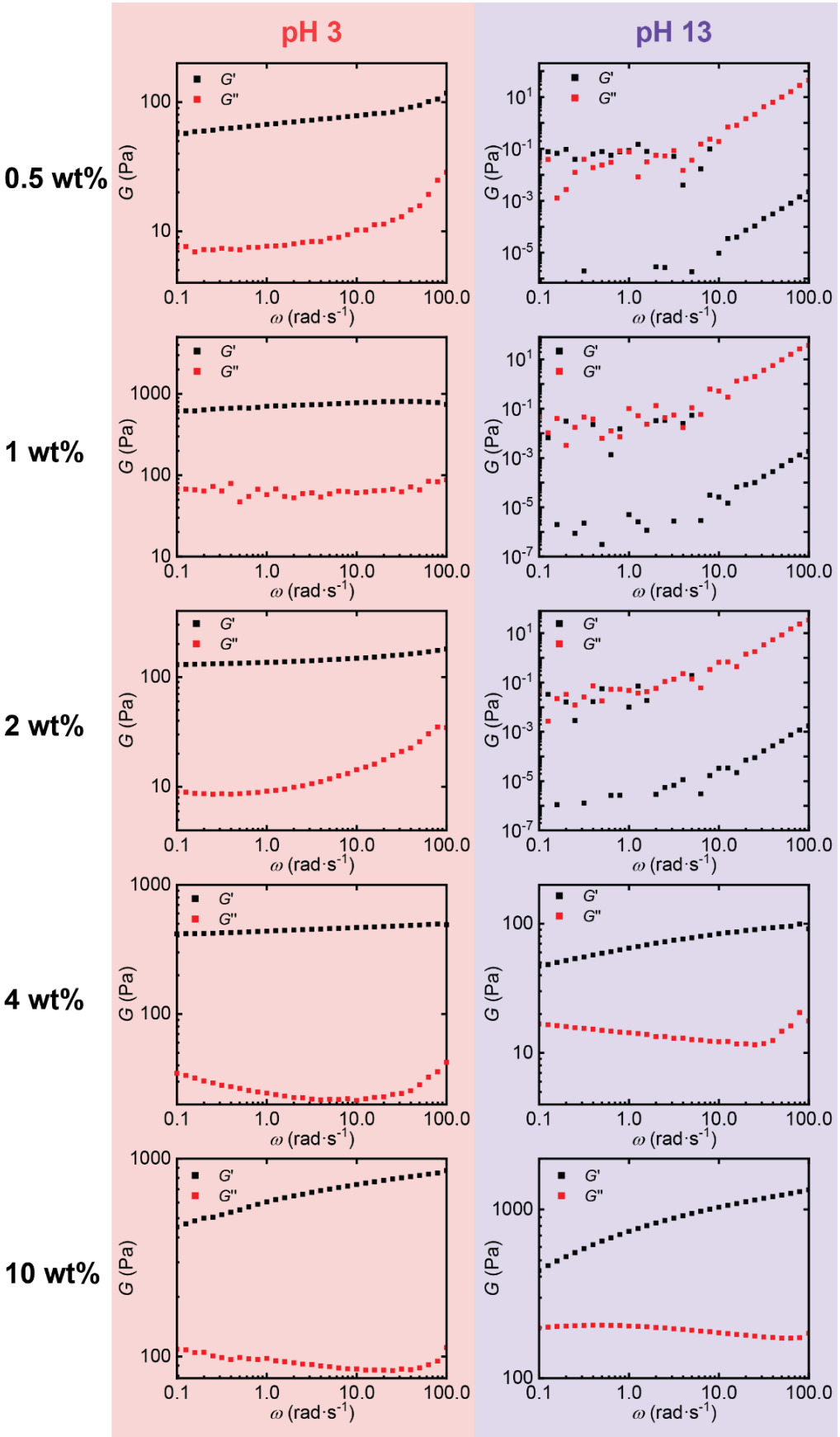

Figure 8. 3: Oscillatory shear-rheology of gels at varying concentrations ranging from 0.5 wt% to 10 wt% at pH 3 and pH 13.

Reversible hydrogel formation

Next to the influence of concentration and pH, the ability of the system to reversibly switch between hydrogel and viscous liquid is of interest. Using a gel synthesized at a concentration of 2 wt% at pH = 3 we switched to a 1 wt% viscous liquid at pH = 13 *via* the addition of concentrated $NaOH_{aq}$. Both samples, before and after the pH switch are investigated *via* oscillatory shear-rheology. **Figure 8. 4** shows the corresponding rheology measurements. The measurement at pH = 3 (left) shows the expected result o $G' > G''$, as does the measurement at pH = 13 (right), which gives the expected change to $G' < G''$. A change back to pH = 3 did not result in the reformation of the network, presumably due to the increased salt concentration weakening the attractive electrostatic forces between both polymer species. The inverse attempts to start at pH = 13 and switch to pH = 3 were also not successful. However, it is noteworthy that the addition of 0.05 M NaCl to a network formed at pH = 7 has a comparable effect.

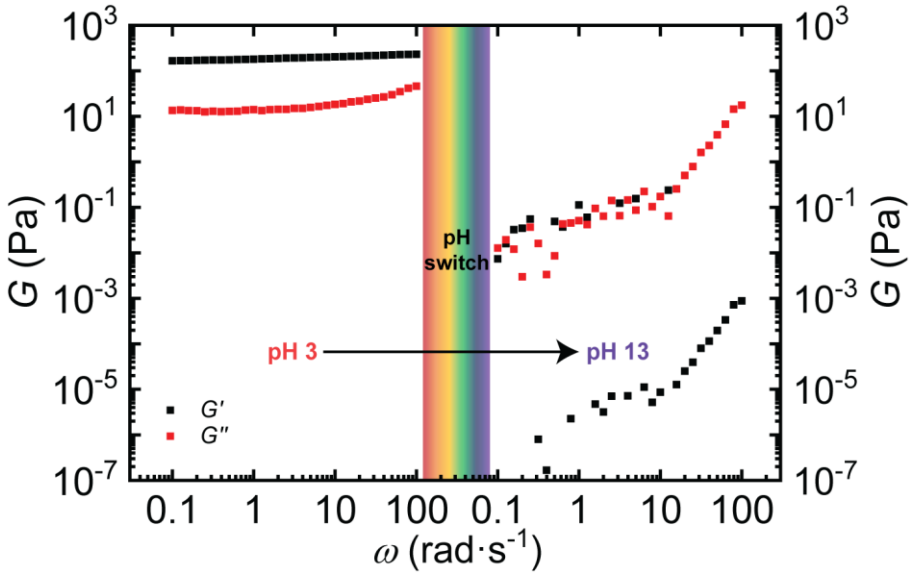

Figure 8. 4: Oscillatory shear-rheology of a gel synthesized at a concentration of 2 wt% at pH = 3 and then switched to pH = 13 leading to a viscous liquid with a concentration of 1 wt%. * Please note that this Figure consists of two individual plots (left = before switching; and right = after switching).

Nevertheless, we expected that the obstacle of high salt concentrations for the switching can be overcome if smaller pH changes can be utilized for the successful shift between liquid and solid, which is why pH changes between pH = 3 to pH = 13 for (in steps of ΔpH = 1) a 1 wt% gel were also investigated (**Figure A.8. 5**). The corresponding shear rheology reveals that at all pH values from pH = 3 to pH = 12, G' is dominating G'' and at least pH = 13 is necessary to result in network dissolution. This is rather unexpected as we would expect the formed networks

to disassemble at a pH value close to the estimated pK_a = 5.0 of the carboxylic acid groups.[49] The solid line in **Figure 8. 5** shows that, in the ideal case, the functionalized betaines should feature a positive net charge at $pH = 3$, when only the amine groups are protonated. As the pH value increases, the carboxylate groups are dissociated to about 50 % at $pH = 5$, and the net charge approaches zero at $pH = 6$. At the same time, the solid line in **Figure 8. 5** shows that if only 75% of the amine groups are functionalized, the remaining primary amine groups (ammonium at pH < pK_a) get deprotonated at $pH = 9$, leading to a scenario where a net zero charge is reached around $pH = 10$. In that way, the partial functionalization (~ 75%, see above) leads to the assumption that the hydrogels should start to disassemble at pH values above 10, which is different if compared to our experimental observations.

To get more insight into the underlying mechanism and interactions, we also performed molecular simulations using a coarse-grained model of a polyanion with a fixed charge, interacting with a polyampholyte with variable, pH-dependent charge, as illustrated in **Figure 8. 5** in the simulation model and method part. Because simulating a system of star-shaped block copolymers with comparable size as in the experiments is difficult to realize, we focused on the interaction between just two arms of length $N = 20$ instead of $N = 100$ (with N = number of charges) used in the experiments. The simulation results (data points) in **Figure 8. 5** show that the fully functionalized betaine in the bulk, i.e. at $r = 17.5$ nm from the sulfonate, has a significantly lower net charge than predicted by the ideal model. In the bulk, the net charge starts at about 0.3 e per monomer at $pH = 4$ and drops to zero at $pH = 6$. On the contrary, the net charge of the same polymer in the complex with sulfonate, i.e. at r = 1 nm from the sulfonate, is much higher than predicted by the ideal model. It starts at about 0.8 at pH = 4, decreases slower than in the ideal case, and reaches zero around $pH = 8$. The distances representing the "bulk" and the "complex" have been chosen arbitrarily. However, **Figure A.8. 6** reveals that the charge in the bulk is constant across a broad range of distances whereas the charge at small distances slightly varies. Therefore, the trend as a function of pH remains robust, although the actual value of the charge may slightly differ, depending on the chosen distance. By comparing the charge on the polymer in the bulk and in the complex with the sulfonate, we observe that it is always higher in the complex, making the electrostatic interaction with the polyanion more favorable. Nonetheless, this charge regulation upon complexation with sulfonate results in a favorable electrostatic interaction only up to $pH = 8$. At $pH > 8$, the net charge on the fully functionalized betaine is effectively zero both in the bulk and in the complex, so it cannot explain the experimentally observed stable gels up to $pH = 12$.

The preceding discussion revealed that both partial functionalization of betaines and charge regulation upon their interaction with sulfonates should increase the net charge in the betaine chains and thereby increase the pH window of their electrostatic attraction to sulfonates. In **Figure 8. 5** we show that also in the case of 75% functionalized betaine the net charge in the complex is higher than in the bulk. However, owing to the 25% of non-functionalized primary amines, the positive net charge about 0.25 e per monomer persists in the complex up to pH = 10, although in the bulk it becomes almost zero already at $\mathrm{pH} = 9$. Thus, the partial functionalization, in combination with charge regulation, might explain why the electrostatic interaction between the betaines and sulfonates is favorable at much higher pH values than originally anticipated.

To quantify the effect of charge regulation on the complexation, we used the simulations to compute the potential of mean force (PMF) as a function of the distance between the two chains. The PMF represents the free energy of interaction between these chains, averaged over various chain conformations, ionization states and positions of small ions. In the supporting information, **Figure A.8. 6**, we show that the PMF as a function of separation between the chains exhibits a global minimum at small separations at all pH values, except $\mathrm{pH} = 12$. The free energy of interaction between the chains can be assessed based on the depth of this minimum, $\Delta\mathrm{F} = \min(\,\mathrm{PMF(r)}\,)$ where we set PMF = 0 at large separations. In **Figure 8. 5** we plot this free energy of interaction as a function of the pH. For both, fully functionalized and partly functionalized betaine chains, we observe that at $\mathrm{pH} = 4$ the attraction is rather strong, $\Delta\mathrm{F} \sim -80\ k_\mathrm{B}T$ per chain. For the fully functionalized betaine chains, the F steadily increases as the pH is increasing, until it becomes almost zero at $\mathrm{pH} > 9$. On the contrary, the F for the partly functionalized betaine exhibits a very slow increase at $\Delta\mathrm{F} \sim -40\ k_\mathrm{B}T$ per chain between $\mathrm{pH} = 6$ and $\mathrm{pH} = 9$. This plateau in the free energy correlates with the plateau in the net charge of the partly functionalized betaine in complex with the sulfonate, observed in **Figure A.8. 6**. At $\mathrm{pH} > 9$, the free energy increases more steeply again, until it reaches zero at $\mathrm{pH} = 11$. Thus, the remaining 25% of net charge of the partly functionalized betaines allows them to retain about 50% of the maximum free energy of interaction with the anionic sulfonates. This attraction persists over a broad pH window, up to $\mathrm{pH} = 10$, which is not only much higher than the pK_a of the carboxylate groups, but also higher than the pK_a of the primary amine. Furthermore, the chains in our simulations were about 5 times shorter than in the experiments, and complexes observed in the experiments might involve more than one pair of chains. Therefore, we can reasonably expect that the free energy of interaction in the experimental system is at least $-200\ k_\mathrm{B}T$ per chain at intermediate pH values, instead of $-40\ k_\mathrm{B}T$ per chain in the simulations.

To get a better feeling of this interaction strength, this value could be compared to the energy of a single hydrogen bond, which is about –10 k_BT.[50] Thus, –200 k_BT would correspond to about 20 hydrogen bonds, which should be sufficient to form a stable gel. Due to the long-range nature of electrostatic interactions, the free energy of interaction should increase faster than proportional to the chain length, so the attraction should be even stronger than this conservative estimate. For the same reasons, the pH window of favorable interactions should be larger in the experimental system than in our simulations. Therefore, we can conclude that our simulation model explains why the partly functionalized betaines form gels with the sulfonates up to unexpectedly high pH values.

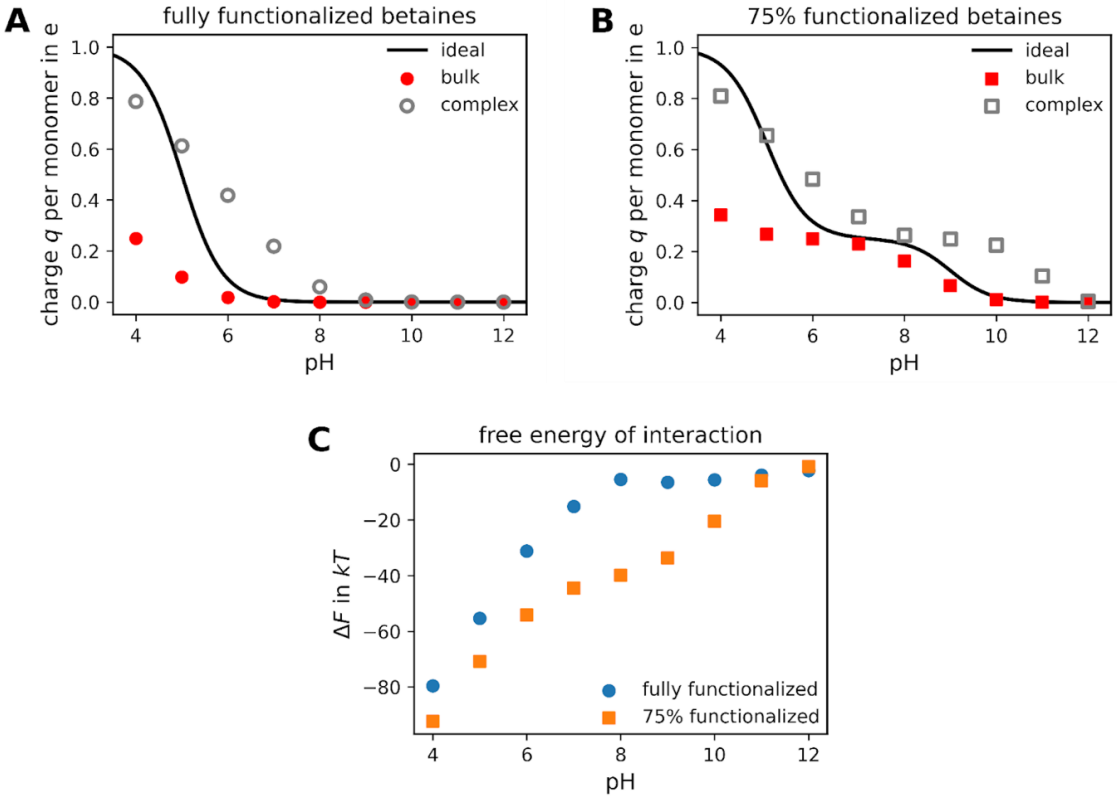

Figure 8. 5: Panels **A, B**: Net charge per monomer, calculated using the Henderson-Hasselbalch equation (solid line), assuming ideal behavior of the functional groups with $pKa = 5.0$ (carboxylate) and $pKa = 9.0$ (amine). Data points represent the charge computed from the simulations for the betaine chains in the bulk, and in the complex with the sulfonate chains. Panel A shows the data for fully functionalized betaines, panel B shows the same data for 75% functionalization, obtained from simulations of chains with $N = 20$ monomers. Panel **C**: Free energy of interaction per chain, corresponding to the interaction of a sulfonated polyanion and functionalized betaines.

8.7. Conclusion

We herein presented the synthesis of 4-arm star-shaped [PEG_{27}-*b*-$PSSNa_{100}$]$_4$ and [PEG_{27}-*b*-$PDMAPMAAm_{108}$]$_4$ block copolymers *via* reversible-deactivation radical polymerization techniques starting from [PEG_{27}-amide-Br]$_4$ macroinitiators. Subsequent post-polymerization functionalization reactions of [PEG_{27}-*b*-$PDMAPMAAm_{108}$]$_4$ resulted in a pH-responsive betaine species, [PEG_{27}-*b*-$PCBAMAAm_{108}$]$_4$. The corresponding pK_a value of the acid group of the betaine could be adjusted by the linker length. Both species, [PEG_{27}-*b*-$PSSNa_{100}$]$_4$ and [PEG_{27}-*b*-$PCBAMAAm_{108}$]$_4$ were afterwards mixed at different pH values and concentrations at charged-balanced conditions to form reversibly electrostatically crosslinked hydrogels. The resulting material was characterized *via* oscillatory shear-rheology, indicating a pH-dependent formation of either networks at $\mathrm{pH} = 3$ or viscous liquids at $\mathrm{pH} = 13$ if amounts of ≤ 2 wt% are used. Additionally, we could demonstrate that switching from at $\mathrm{pH} = 3$ to $\mathrm{pH} = 13$ results in a dissolution of the hydrogel. Due to rather high salt concentrations multiple switching cycles at this point are not possible. However, if pH values between $\mathrm{pH} = 3$ and $\mathrm{pH} = 12$ are used, network formation was observed by shear rheology with G' dominating G'' but at least $\mathrm{pH} = 13$ was necessary to result in full disassembly of the network. This was rather unexpected,[49] but could be tentatively explained by hybrid MD/MC simulations, which revealed that the partly functionalized betaines form gels with the sulfonates up to unexpectedly high pH values. To avoid network formation at higher pH values future experiments should focus on the quantitative functionalization of the PDMAPMAAm, as well as on approaches where a pH switch could possibly be performed without increasing the ionic strength. We assume that several switching cycles are possible in this way, which makes such materials very interesting for the directed transport of charged guest molecules. In addition, the question of how the history of such a material influences the degree of order can be addressed with such materials.

8.8. Experimental

Materials

α-Bromoisobutyryl bromide (98%), Cu(I) chloride (99.99%), Cu(II) chloride (99%), Cu(0) powder (99,999%), Ethyl 4-bromobutyrate (95%), Ethyl 6-bromobutyrate (95%), Iodmethane (99%), 1,1,4,7,10,10-Hexamethyltriethylentetramin (97%), 2,2´-Bipyridyl (99%), Bromoethane (98%) and N-[3-(Dimethylamino)-propyl]-methacrylamide (99%) were purchased from Sigma-Aldrich (Darmstadt, Germany). $[PEG_{27}\text{-}NH_2]_4$ was purchased from JenKem Technology (Plano, USA). *N*-[3-(Dimethylamino)-propyl]-acrylamid (97%) was purchased from TCI chemicals (Eschborn, Germany). Styrene-4-sulfonic acid sodium salt was purchased from Alfa Aesar (Karlsruhe, Germany) and Chloroacetic acid was purchased from Merck (Darmstadt, Germany). Cu(I)X was purified by stirring in glacial acetic acid overnight and rinsing with methanol before drying *in vacuo*. All other reagents were used as received.

Analytic Methods

Nuclear magnetic resonance (NMR) spectroscopy

^{1}H-NMR and ^{13}C measurements were performed on a Bruker AC 300 MHz using $CDCl_3$, DMSO or D_2O as solvent. The spectra were referenced by using the residual signal of the deuterated solvent.

Size exclusion chromatography (SEC)

Water SEC: For aqueous SEC measurements, a Jasco system was applied equipped with a DG-2080-53 degasser, a PU-980 pump, a RI-2031 Plus refractive index detector and a column set of PSS NOVEMA-MAX 30/1000/1000 Å. Measurements were performed at 30 °C with a flow rate of 1 ml min-1. Aqueous 0.3% TFA/ 0.1 M NaCl solution (pH < 2) was used as eluent. The system was calibrated using poly(2 vinylpyridine) (600-1,000,000 g mol^{-1}) standards.

DMSO SEC: An Agilent 1260 Infinity II system equipped with a 1260 IsoPump (G7110B), a 1260 ALS (G1329B) autosampler and three consecutive PSS GRAM analytical, 10 µm, 8x300 mm columns (guard/100/3000/3000 Å) was used for SEC measurements. DMSO + 0.21 wt.% LiCl was used as an eluent at a flow rate of 1 mL min^{-1}. The column oven (TCC6500) was set to 70 °C and signals were detected using a 1260 VWD (G7114A) and a 1260 RID (G7162A) detector. The system was calibrated using PSS PEG/PEO (238 to 969 000 g·mol^{-1}) standards.

Rheology

Rheological measurements were performed on an Anton Paar MCR 302 modular compact rheometer equipped with a cone-plate geometry of type CP25 with a diameter of 25 mm and a cone angle of 1°. A Peltier plate was used to keep the temperature constant at 20 °C, and a solvent trap was used to prevent the evaporation of water. Frequency sweeps were performed in the range of 100 to 0.1 rad/s with a shear strain of $\gamma = 0.4\%$. All samples were prepared by adding an aqueous solution of the desired pH to the already premixed sulfonate and betaine components. After mixing the gels were allowed to equilibrate for 72 h.

Titrations

pH titrations were carried out on an OMNIS Advanced Titrator (Deutsche METROHM Prozessanalytik GmbH & Co. KG, Filderstadt, Germany) equipped with a magnetic stirrer, a Pt1000 temperature sensor, and a dosing module. For pH detection, either an ECOTRODE plus pH-glass electrode, or a BIOTRODE was used. The polymers were dissolved in 0.1 M NaOH resulting in a 0.2 mg mL^{-1} solution with a pH between 12 and 13 and subsequently titrated with 0.1 M HCl at a dosing rate of 0.01 mL min^{-1}. For sample taking the titration was paused at the desired pH value and afterward continued.

Zeta potential measurements

Zeta potential measurements the zeta potentials were measured on a ZetaSizer Nano ZS from Malvern *via* M3-PALS technique with a laser beam at 633 nm. The detection angle was 13°. The electrophoretic mobilities (u) were converted into ζ-potentials *via* the Smoluchowski equation[51] where η denotes the viscosity and ε the permittivity of the solution.

Differential scanning calorimetry

The differential scanning calorimetry (DSC) measurements were performed on a DSC 204 F1 Phoenix from Netzsch under a nitrogen atmosphere with a heating rate of 10 K/min. The thermal gravimetric analysis (TGA) was carried under nitrogen using a Netzsch TG 209F1.

Synthesis of [PEG-Amide-Br]$_4$

[PEG-Amide-Br]$_4$ was synthesized as described elsewhere.[52] α-Bromoisobutyryl bromide (1.48 mL, 12. 85 mmol) was added dropwise to a solution of [PEO_{55}-NH_2]$_4$ (3 g, 3 mmol) and trimethylamine (TEA, 1.68 mL, 12 mmol) in DCM (120 mL) at 0 °C. Afterward, the solution was stirred for 72 h at room temperature. The resulting solvent mixture was extracted once each with saturated sodium bicarbonate, deionized water, and saturated saline solution. The organic phase was dried over $MgSO_4$. After evaporation of the DCM, the concentrated solution was precipitated twice into cold diethyl ether. The white precipitate was dried under vacuum (2 g, 1.9 mmol, 62 % yield).

^{1}H-NMR (300 MHz, $CDCl_3$, δ): 3.9-3.5 (m, backbone), 1.94 (s, 24 H, -C- $(CH_3)_2$Br) ppm.

Synthesis of [PEG_{27}-*b*-$PSSNa_y$]$_4$ *via* ATRP

For a typical synthesis of [PEG_{27}-*b*-$PSSNa_{100}$]$_4$, SSNa (5.78 g, 800 eq, 28 mmol), bpy (43.84 mg, 8 eq, 0.28 mmol), and [PEG_{27}amide-Br]$_4$ (200 mg, 1 eq, 35 µmol) were dissolved in 15 mL H_2O/*iso*-propanole (v/v) = 1/1 and deoxygenated using four consecutive freeze-pump-thaw cycles. Afterward, CuCl (14.13 mg, 4 eq, 0.14 mmol) was added under inert conditions to the still frozen reaction mixture followed by four cycles changing between vacuum and argon before the polymerization mixture was allowed to defreeze and set to 23 °C. The polymerization was carried out at 23 °C for 15 h. The reaction was then terminated by cooling in liquid nitrogen followed by opening the reaction vessel to achieve ambient conditions. After removal of the residual copper using a silica column, the leftover monomer was removed *via* dialyses against water (3 days with 3 exchanges per day). Finally, the solvent was removed by freeze-drying to achieve a white/slightly pink solid.

^{1}H-NMR (300 MHz, D_2O, δ): 7.6-7.1 (m, aromate), 6.7-6.0 (m, aromate), 3.5-3.3 (m, PEG-backbone), 2.0-0.9 (m, sulfonate-backbone) ppm.

^{13}C-NMR (300 MHz, D_2O, δ): PSSNA: 150.8-148.2 (m, aromate: PSSNA backbone-**C**-$(CH)_2$), 141.2-138.1 (m, aromate: sulfonate-**C**-$(CH)_2$), 130.0-126.7 (m, aromate: PSSNA backbone-C-(**C**H)$_2$), 126.4-123.7 (m, aromate: sulfonate-C-(**C**H)$_2$), 45.1-38.7 (m, PSSNa backbone), **PEG**: 70.3-68.4 (m, PEG backbone) ppm.

Synthesis of [PEG$_{55}$-*b*-PDMAPMAAm$_{108}$]$_4$ *via* Cu(0) mediated reversible-deactivation radical polymerization techniques

For a typical synthesis of [PEG$_{27}$-*b*-PDMAPMAAm$_{108}$]$_4$, DMAPMAAm (972 mg, 800 eq, 5.6 mmol), HMTETA (13.2 µL, 8 eq, 56 µmol), $CuCl_2$ (0.8 mg, 0.8 eq, 5.6 µmol) and [PEG$_{27}$-amide-Br]$_4$ (40 mg, 1 eq, 7 µmol) were dissolved in 3 mL H_2O/*iso*-propanole (v/v) = 1/5 and deoxygenated using four consecutive freeze-pump-thaw cycles. Afterward, Cu(0) (1.8 mg, 2 eq, 14 µmol) was added under inert conditions to the still frozen reaction mixture followed by four cycles changing between vacuum and argon before the polymerization mixture was allowed to defreeze and set to 23 °C. The polymerization was carried out at 23 °C for 10 h. The reaction was then terminated by cooling in liquid nitrogen followed by opening the reaction vessel to achieve ambient conditions. After removal of the residual copper using a neutral Alox column, the leftover monomer was removed *via* dialyses against water (3 days with 3 exchanges per day). Finally, the solvent was removed by freeze-drying to achieve a white solid.

^{1}H-NMR (300 MHz, D_2O, δ): 3.8-3.5 (m, PEG), 3.3–2.8 (m, amide-C**H$_2$**-CH_2-), 2.5-2.0 (m, -C**H$_2$**-N-(C**H$_3$**)$_2$, 1.9-1.4 (m, backbone + amide-CH_2-C**H$_2$**-), 1.2-0.6 (m, -C-C**H$_3$**), ppm.

Synthesis of [PEG$_{27}$-*b*-PCBAMAAm$_{108}$]$_4$

The modification of [PEG$_{55}$-*b*-PDMAPMAAm$_{108}$]$_4$ involves a quaternization-hydrolysis method as already reported by McCornick and others for carboxybetaine monomers.[53, 54] In our case, 400 mg of [PEG$_{27}$-*b*-PDMAPMAAm$_{108}$]$_4$ were dissolved in 20 mL of ACN and 6.5 mL ethyl 6-bromobutyrate was added dropwise to the reaction mixture. The reaction was proceeding over 96 h at 50 °C. The resulting polymer was obtained after dialyses against water (3 days with 3 exchanges per day), followed by freeze-drying. Afterward, the resulting CBMA-ester was deprotected by mixing 400 mg ester (30 mmol) with 35 mmol NaOH and 4 mL water into a 10 mL flask. The reaction mixture was set to 50 °C to react for 24 h. Afterward, the pH of the resulting reaction mixture was set to pH = 7 and purified *via* dialyses against water (3 days with 3 exchanges per day). The final product was obtained as white solid after removal of the solvent by freeze-drying.

^{1}H-NMR (300 MHz, D_2O, δ): 3.6-3.5 (m, PEG backbone), 3.2-3.0 (m, -N-(CH_3)$_2$-C**H$_2$**- and -amide-C**H$_2$**-), 3.0-2.8 (m, -N-(C**H$_3$**)$_2$-CH_2- and amide-CH_2- CH_2-C**H$_2$**-), 2.1-2.0 (m, -C**H$_2$**-COOH), 1.9-1.7 (m, amide-CH_2-C**H$_2$**-), 1.7-1.5 (m, -N-(CH_3)$_2$-CH_2-C**H$_2$**-), 1.5-1.4 (m, -C**H$_2$**-CH_2-COOH), 1.3-1.1 (m, -C**H$_2$**-CH_2-CH_2-COOH), 1.0-0.6 (m, betaine backbone + methyl).

^{13}C-NMR (300 MHz, D_2O, δ): 181.0 (-**C**OOH), 178.8 (**C**ONH-CH_2-), 69.5 (PEG backbone), 64.1 (-N-$(CH_3)_2$-**C**H_2-), 61.6 (-**C**H_2-N-$(CH_3)_2$-), 50.6 (-N-(**C**$H_3)_2$-), 45.1 (CH_3-**C**), 42.6 (CONH-**C**H_2-), 37.3 (Betaine backbone + -**C**H_2-COOH), 25.4 (-**C**H_2-CH_2-CH_2-COOH), 25.2 (**C**H_3-C), 22.2-19.5 (-N-$(CH_3)_2$- CH_2- **C**H_2- CH_2- **C**H_2-), 18.8-15.7 (CONH-CH_2- **C**H_2-) ppm.

Simulation Model and Method

Coarse-Grained Model

We performed computer simulations using a generic bead-spring polymer model, derived from the Kremer-Grest model.[55] While simulating a solution of star polymers is feasible for small stars and has been done in the past, [42, 56] the charged blocks of the star polymers considered in this study are too large for this approach. Thus, to gain at least some understanding of the system, we focused on the interaction between just the charged blocks of two arms of the different stars of opposite charge, leveraging free energy methods to obtain information about their association behavior. Similar approaches have been previously used to study polyelectrolyte complexation. [57]

In our coarse-grained model, the excluded volume interactions between the particles (monomers and small ions alike) were described by the WCA potential,[58]

$$V_{\mathrm{WCA}} = 4\varepsilon\left(\left(\frac{\sigma}{r}\right)^{12} - \left(\frac{\sigma}{r}\right)^{6}\right)\theta\left(\sigma 2^{\frac{1}{6}} - r\right),$$

where θ is the Heaviside step function. The bead diameter was set to a value of $\sigma = 0.355$ nm and the energy scale had a value of $\varepsilon = k_{\mathrm{B}}T$. Due to the purely repulsive nature of the WCA potential, monomer-specific interactions such as hydrophobicity were not considered in our model. To represent the covalent bonds between monomers, we used the FENE potential,[55]

$$V_{\mathrm{FENE}} = -\frac{k\Delta r_{\mathrm{max}}{}^{2}}{2}\ln\left(1 - \left(\frac{r}{\Delta r_{\mathrm{max}}}\right)^{2}\right)$$

with a maximum bond extension of $\Delta r_{\mathrm{max}} = 1.5\,\sigma$ and a spring constant of $k = \frac{30\,k_{\mathrm{B}}T}{\sigma^2}$. In combination with the WCA interaction, these parameters correspond to an average equilibrium bond length of 0.96 σ. Electrostatic interactions between charges were modeled using the full Coulomb potential,

$$V_{\text{Coulomb}} = \frac{z_i \, z_j \, k_{\text{B}} T \lambda_{\text{B}}}{r}$$

with a Bjerrum length of $\lambda_{\text{B}} = 2\,\sigma = 0.71$ nm, corresponding to water at room temperature, accounting implicitly for the dielectric properties of the solvent. In the simulations, we employed the P³M method[59] with a relative error of 10^{-4} to compute the long-range electrostatic energies and forces.[60, 61]

Using the described approach, we built up the molecular geometry of the considered polymers in the following way. The employed mapping between coarse-grained beads and the different functional groups is shown in **Figure 8. 6**. In all cases, we used a degree of polymerization of $\mathrm{N} = 20$. For the sulfonate chain, each monomer was represented by a neutral backbone monomer and a negatively charged residue that represented the sulfonate group (**Figure 8. 6 (a)**). Because in the considered range of pH-values the charge regulation of the sulfonate group can be neglected, the respective charge was fixed in the simulation model. For the carboxybetaine chain, we had to distinguish between the fully functionalized case and the case of 75 % functionalization. The functionalized monomers consisted of a neutral backbone particle, a positively charged amine, a neutral spacer and a pH-responsive residue that represented the carboxylic group (**Figure 8. 6 (b)**). Using experimental data for monomeric carboxybetaine molecules, we estimated a value of pK_a = 5.0 for the carboxylic group.[62] In case of non-functionalized monomers, only the neutral backbone monomer as well as a pH-responsive tertiary amine were present (**Figure 8. 6 (c)**). The pK_a = 9.0 for this group was estimated from experimental data as well.[49, 63] **Figure 8. 6 (e)** shows the chain architecture of the carboxybetaine chains for the fully functionalized case and the case of 75 % functionalization. In the case of a non-fully functionalized carboxybetaine chain, we uniformly distributed 5 non-functionalized monomers along the chain.

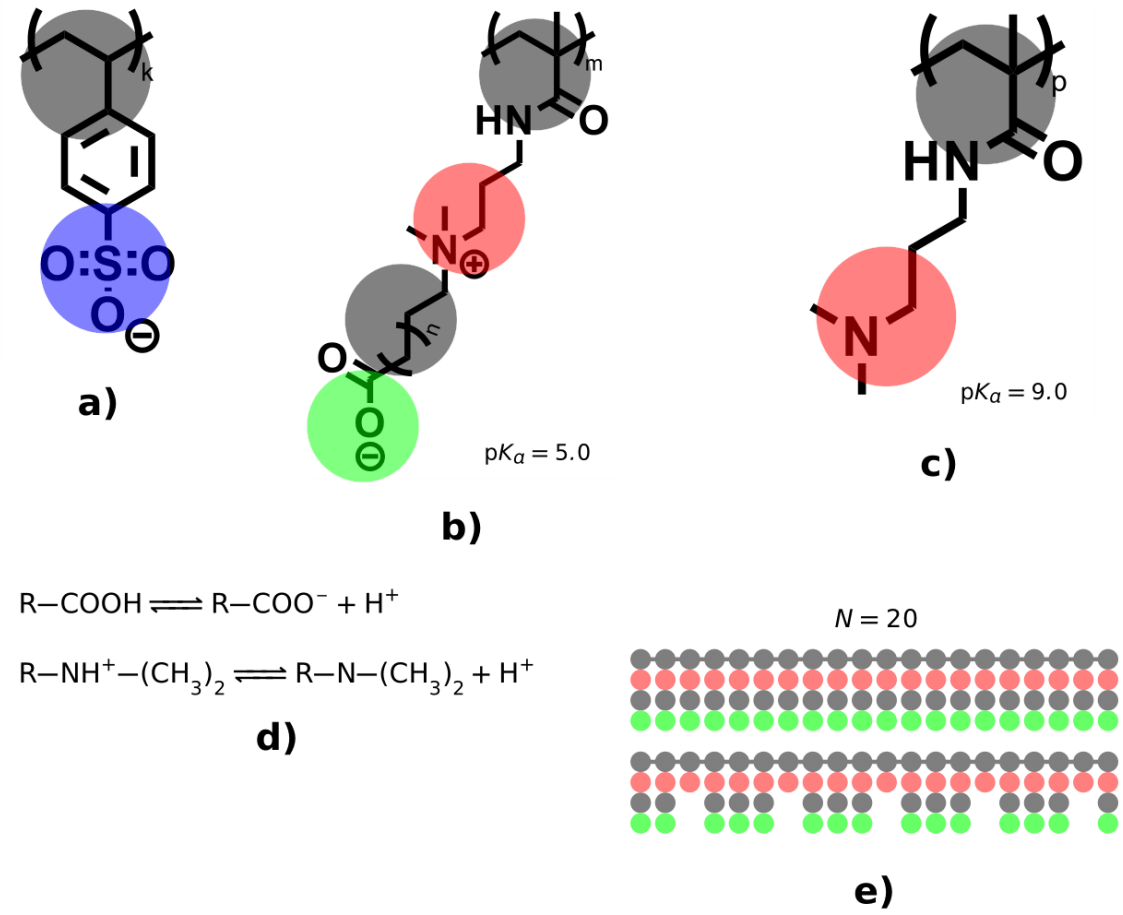

Figure 8. 6: Schematic representation of the coarse-grained mapping employed in this study. **(a)**: The sulfonate chain is represented by a neutral backbone with negatively charged side groups. **(b)**: The carboxybetaine chain is represented by a neutral backbone with side groups that consist of a positively charged bead, a neutral spacer and a pH-responsive acid group (carboxyl). **(c)**: In the non-functionalized case, the neutral spacer and the carboxylic group are not present. **(d)**: Chemical reactions that take place in the various functional groups. **(e)**: Schematic representation of the chain architecture in the fully functionalized case (top) and the case of 75% functionalization (bottom).

Simulation Methodology

We performed hybrid MD/MC simulations using the simulation software package LAMMPS.[38] To sample different polymer conformations, we used Langevin dynamics. In our simulations, we used a friction coefficient of $\gamma = 1.0\,\tau^{-1}$ and an integration time step of $\Delta t = 0.01\tau$, where $\tau = \sqrt{m\sigma^2/k_{\mathrm{B}}T}$ is the Lennard-Jones time scale. In order to take into account the varying ionization states of the weak polyelectrolyte chains, we used the grand-reaction method by Landsgesell *et al.*[64] in the formulation of Curk *et al.*[65] In this method, the chemical equilibria of the various pH-responsive groups are taken into account *via* the reaction-ensemble Monte-Carlo method.[66, 67] Furthermore, the system is grand-canonically coupled to a reservoir at a fixed pH and salt concentration. In our simulations, we set the reservoir salt

concentration to a value of $c_{NaCl} = 10^{-4}$ M and varied the pH-value. Using the Debye-Hueckel mean-field theory, we verified that the chosen box sizes were large enough in order to avoid spurious self-interactions between the chains and their periodic images.

Since we were interested in the potential of mean force (PMF) between the centers of mass of the chains, the grand-reaction method had to be combined with an enhanced sampling approach. In order to obtain the PMF, we used the adaptive biasing force method (ABF),[68–71] implemented in the Colvars library.[72] To obtain the PMF in an efficient manner, we subdivided the considered range of distances [0 σ, 50 σ] into 5 smaller windows of size 10 σ each ("stratification strategy",[70]), allowing for a trivial parallelization by running a separate simulation for each window. In order to apply the ABF, the windows were divided into bins of length 0.5 σ. To ensure that the stratification did not hinder the ergodic sampling of the phase space,[70] we verified a-posteriori that the obtained mean force was continuous across the window boundaries (see **Figure A.8. 7**).

The simulations were performed using the following protocol. After an equilibration procedure consisting of 10^7 integration and 10^7 reaction steps, we performed a production run consisting of 2×10^8 integration and 2×10^8 reaction steps. In order to circumvent non-equilibrium effects, which can appear due to large initial fluctuations of the mean force when the number of samples is small, we did not apply the full biasing force from the start of the production run. Rather, the biasing force was only applied after a certain number of samples had been collected. More specifically, the applied biasing force in a given bin was set to zero if less than $N_{samples} = 250$ samples had been accumulated for that bin, while the full force was applied for $N_{samples} > 500$. In between these two limits, the applied biasing force was scaled by a factor of $2N_{samples}/500 - 1$, i.e. following a linear ramp.

8.9. References

[1] Kopeček, J.; Yang, J., Hydrogels as smart biomaterials. *Polymer international* **2007,** *56* (9), 1078-1098.

[2] Wichterle, O.; Lim, D., Hydrophilic gels for biological use. *Nature* **1960,** *185* (4706), 117-118.

[3] Sakai, T.; Matsunaga, T.; Yamamoto, Y.; Ito, C.; Yoshida, R.; Suzuki, S.; Sasaki, N.; Shibayama, M.; Chung, U.-i., Design and fabrication of a high-strength hydrogel with ideally homogeneous network structure from tetrahedron-like macromonomers. *Macromolecules* **2008,** *41* (14), 5379-5384.

[4] Lutolf, M.; Hubbell, J., Synthesis and physicochemical characterization of end-linked poly (ethylene glycol)-co-peptide hydrogels formed by Michael-type addition. *Biomacromolecules* **2003,** *4* (3), 713-722.

[5] Darling, N. J.; Hung, Y.-S.; Sharma, S.; Segura, T., Controlling the kinetics of thiol-maleimide Michael-type addition gelation kinetics for the generation of homogenous poly (ethylene glycol) hydrogels. *Biomaterials* **2016,** *101*, 199-206.

[6] Macdougall, L. J.; Truong, V. X.; Dove, A. P., Efficient in situ nucleophilic thiol-yne click chemistry for the synthesis of strong hydrogel materials with tunable properties. *ACS Macro Letters* **2017,** *6* (2), 93-97.

[7] Akagi, Y.; Matsunaga, T.; Shibayama, M.; Chung, U.-i.; Sakai, T., Evaluation of topological defects in tetra-PEG gels. *Macromolecules* **2010,** *43* (1), 488-493.

[8] Akagi, Y.; Gong, J. P.; Chung, U.-i.; Sakai, T., Transition between phantom and affine network model observed in polymer gels with controlled network structure. *Macromolecules* **2013,** *46* (3), 1035-1040.

[9] Akagi, Y.; Sakurai, H.; Gong, J. P.; Chung, U.-i.; Sakai, T., Fracture energy of polymer gels with controlled network structures. *The Journal of chemical physics* **2013,** *139* (14), 144905.

[10] Brown, T. E.; Carberry, B. J.; Worrell, B. T.; Dudaryeva, O. Y.; McBride, M. K.; Bowman, C. N.; Anseth, K. S., Photopolymerized dynamic hydrogels with tunable viscoelastic properties through thioester exchange. *Biomaterials* **2018,** *178*, 496-503.

[11] Fairbanks, B. D.; Schwartz, M. P.; Halevi, A. E.; Nuttelman, C. R.; Bowman, C. N.; Anseth, K. S., A versatile synthetic extracellular matrix mimic via thiol-norbornene photopolymerization. *Advanced materials* **2009,** *21* (48), 5005-5010.

[12] Wang, S.; Beech, H. K.; Bowser, B. H.; Kouznetsova, T. B.; Olsen, B. D.; Rubinstein, M.; Craig, S. L., Mechanism Dictates Mechanics: A Molecular Substituent Effect in the

Macroscopic Fracture of a Covalent Polymer Network. *Journal of the American Chemical Society* **2021,** *143* (10), 3714-3718.

[13] Oshima, K.; Fujimoto, T.; Minami, E.; Mitsukami, Y., Model polyelectrolyte gels synthesized by end-linking of tetra-arm polymers with click chemistry: synthesis and mechanical properties. *Macromolecules* **2014,** *47* (21), 7573-7580.

[14] Oshima, K.; Mitsukami, Y., Anionic amphiphilic model conetworks synthesized by end-linking of tetra-arm copolymers. *Polymer* **2016,** *100*, 134-142.

[15] Truong, V. X.; Donderwinkel, I.; Frith, J. E., Bioorthogonal hydrogels by thiol–halide click crosslinking with fast gelation time and tunable stability in aqueous media. *Journal of Polymer Science Part A: Polymer Chemistry* **2019,** *57* (18), 1872-1876.

[16] Huang, X.; Nakagawa, S.; Li, X.; Shibayama, M.; Yoshie, N., A simple and versatile method for the construction of nearly ideal polymer networks. *Angewandte Chemie International Edition* **2020,** *59* (24), 9646-9652.

[17] Defize, T.; Riva, R.; Raquez, J. M.; Dubois, P.; Jérôme, C.; Alexandre, M., Thermoreversibly crosslinked Poly (ε-caprolactone) as recyclable shape-memory polymer network. *Macromolecular Rapid Communications* **2011,** *32* (16), 1264-1269.

[18] He, L.; Fullenkamp, D. E.; Rivera, J. G.; Messersmith, P. B., pH responsive self-healing hydrogels formed by boronate–catechol complexation. *Chemical Communications* **2011,** *47* (26), 7497-7499.

[19] Apostolides, D. E.; Patrickios, C. S.; Sakai, T.; Guerre, M.; Lopez, G. r.; Améduri, B.; Ladmiral, V.; Simon, M.; Gradzielski, M.; Clemens, D., Near-model amphiphilic polymer conetworks based on four-arm stars of poly (vinylidene fluoride) and poly (ethylene glycol): synthesis and characterization. *Macromolecules* **2018,** *51* (7), 2476-2488.

[20] Apostolides, D. E.; Sakai, T.; Patrickios, C. S., Dynamic covalent star poly (ethylene glycol) model hydrogels: A new platform for mechanically robust, multifunctional materials. *Macromolecules* **2017,** *50* (5), 2155-2164.

[21] Truong, V. X.; Li, F.; Forsythe, J. S., Versatile bioorthogonal hydrogel platform by catalyst-free visible light initiated photodimerization of anthracene. *ACS Macro Letters* **2017,** *6* (7), 657-662.

[22] Truong, V. X.; Li, F.; Ercole, F.; Forsythe, J. S., Wavelength-selective coupling and decoupling of polymer chains via reversible [2+ 2] photocycloaddition of styrylpyrene for construction of cytocompatible photodynamic hydrogels. *ACS Macro Letters* **2018,** *7* (4), 464-469.

[23] Honda, S.; Tanaka, N.; Toyota, T., Synthesis of star-shaped poly (n-butyl acrylate) oligomers with coumarin end groups and their networks for a UV-tunable viscoelastic material. *Journal of Polymer Science Part A: Polymer Chemistry* **2018,** *56* (1), 9-15.

[24] Kalayci, K.; Frisch, H.; Barner-Kowollik, C.; Truong, V. X., Wavelength-dependent stiffening of hydrogel matrices via redshifted [2+ 2] photocycloadditions. *Advanced Functional Materials* **2020,** *30* (15), 1908171.

[25] Tan, H.; Xiao, C.; Sun, J.; Xiong, D.; Hu, X., Biological self-assembly of injectable hydrogel as cell scaffold via specific nucleobase pairing. *Chemical Communications* **2012,** *48* (83), 10289-10291.

[26] Chen, H.; Zhang, J.; Yu, W.; Cao, Y.; Cao, Z.; Tan, Y., Control Viscoelasticity of Polymer Networks with Crosslinks of Superposed Fast and Slow Dynamics. *Angewandte Chemie International Edition* **2021,** *60* (41), 22332-22338.

[27] Sun, T. L.; Kurokawa, T.; Kuroda, S.; Ihsan, A. B.; Akasaki, T.; Sato, K.; Haque, M.; Nakajima, T.; Gong, J. P., Physical hydrogels composed of polyampholytes demonstrate high toughness and viscoelasticity. *Nature materials* **2013,** *12* (10), 932-937.

[28] Mabesoone, M. F.; Gopez, J. D.; Paulus, I. E.; Klinger, D., Tunable biohybrid hydrogels from coacervation of hyaluronic acid and PEO-based block copolymers. *Journal of Polymer Science* **2020,** *58* (9), 1276-1287.

[29] Dong, P.; Cui, K.; Xu, F.; Jiang, T.; Ma, Z., Synthesis of new ionic crosslinked polymer hydrogel combining polystyrene and poly (4-vinyl pyridine) and its self-healing through a reshuffling reaction of the trithiocarbonate moiety under irradiation of ultraviolet light. *Polymer International* **2018,** *67* (7), 868-873.

[30] Fu, W.; Zhao, B., Thermoreversible physically crosslinked hydrogels from UCST-type thermosensitive ABA linear triblock copolymers. *Polymer Chemistry* **2016,** *7* (45), 6980-6991.

[31] Gupta, S.; Webster, T. J.; Sinha, A., Evolution of PVA gels prepared without crosslinking agents as a cell adhesive surface. *Journal of Materials Science: Materials in Medicine* **2011,** *22* (7), 1763-1772.

[32] Pan, S.; Xia, M.; Li, H.; Jiang, X.; He, P.; Sun, Z.; Zhang, Y., Transparent, high-strength, stretchable, sensitive and anti-freezing poly (vinyl alcohol) ionic hydrogel strain sensors for human motion monitoring. *Journal of Materials Chemistry C* **2020,** *8* (8), 2827-2837.

[33] Boucard, N.; Viton, C.; Domard, A., New aspects of the formation of physical hydrogels of chitosan in a hydroalcoholic medium. *Biomacromolecules* **2005,** *6* (6), 3227-3237.

[34] Berger, J.; Reist, M.; Mayer, J. M.; Felt, O.; Gurny, R., Structure and interactions in chitosan hydrogels formed by complexation or aggregation for biomedical applications. *European journal of pharmaceutics and biopharmaceutics* **2004,** *57* (1), 35-52.

[35] Takigami, M.; Amada, H.; Nagasawa, N.; Yagi, T.; Kasahara, T.; Takigami, S.; Tamada, M., Preparation and properties of CMC gel. *Transactions of the Materials Research Society of Japan* **2007,** *32* (3), 713-716.

[36] Wang, C.; Liu, Y.; Qu, X.; Shi, B.; Zheng, Q.; Lin, X.; Chao, S.; Wang, C.; Zhou, J.; Sun, Y., Ultra-Stretchable and Fast Self-Healing Ionic Hydrogel in Cryogenic Environments for Artificial Nerve Fiber. *Advanced Materials* **2022,** *34* (16), 2105416.

[37] Yang, J.; Du, Y.; Li, X.; Qiao, C.; Jiang, H.; Zheng, J.; Lin, C.; Liu, L., Fatigue-Resistant, Notch-Insensitive Zwitterionic Polymer Hydrogels with High Self-Healing Ability. *Chempluschem* **2020,** *85* (9), 2158-2165.

[38] Thompson, A. P.; Aktulga, H. M.; Berger, R.; Bolintineanu, D. S.; Brown, W. M.; Crozier, P. S.; in't Veld, P. J.; Kohlmeyer, A.; Moore, S. G.; Nguyen, T. D., LAMMPS-a flexible simulation tool for particle-based materials modeling at the atomic, meso, and continuum scales. *Computer Physics Communications* **2022,** *271*, 108171.

[39] Pineda, S.; Staňo, R.; Murmiliuk, A.; Blanco, P.; Montes, P.; Tošner, Z.; Groborz, O.; Pánek, J.; Hrubý, M.; Štepánek, M., Charge regulation triggers condensation of short oligopeptides to polyelectrolytes. **2023**.

[40] Murmiliuk, A.; Košovan, P.; Janata, M.; Procházka, K.; Uhlík, F.; Štěpánek, M., Local pH and Effective p K of a Polyelectrolyte Chain: Two Names for One Quantity? *ACS Macro Letters* **2018,** *7* (10), 1243-1247.

[41] Lunkad, R.; Murmiliuk, A.; Tošner, Z.; Štěpánek, M.; Košovan, P., Role of p KA in Charge Regulation and Conformation of Various Peptide Sequences. *Polymers* **2021,** *13* (2), 214.

[42] Staňo, R.; Košovan, P.; Tagliabue, A.; Holm, C., Electrostatically cross-linked reversible gels—effects of pH and ionic strength. *Macromolecules* **2021,** *54* (10), 4769-4781.

[43] Zhang, Z.; Vaisocherová, H.; Cheng, G.; Yang, W.; Xue, H.; Jiang, S., Nonfouling behavior of polycarboxybetaine-grafted surfaces: structural and environmental effects. *Biomacromolecules* **2008,** *9* (10), 2686-2692.

[44] Dickhaus, B. N.; Priefer, R., Determination of polyelectrolyte pKa values using surface-to-air tension measurements. *Colloids and Surfaces A: Physicochemical and Engineering Aspects* **2016,** *488*, 15-19.

[45] Barthel, M. J.; Rinkenauer, A. C.; Wagner, M.; Mansfeld, U.; Hoeppener, S.; Czaplewska, J. A.; Gottschaldt, M.; Träger, A.; Schacher, F. H.; Schubert, U. S., Small but powerful: co-assembly of polyether-based triblock terpolymers into sub-30 nm micelles and synergistic effects on cellular interactions. *Biomacromolecules* **2014,** *15* (7), 2426-2439.

[46] Almdal, K.; Dyre, J.; Hvidt, S.; Kramer, O., Towards a phenomenological definition of the term 'gel'. *Polymer gels and networks* **1993,** *1* (1), 5-17.

[47] Higgs, P. G.; Joanny, J. F., Theory of polyampholyte solutions. *The Journal of chemical physics* **1991,** *94* (2), 1543-1554.

[48] Kudaibergenov, S. E., Recent advances in the study of synthetic polyampholytes in solutions. *Polymer Latexes-Epoxide Resins-Polyampholytes* **1999**, 115-197.

[49] van de Wetering, P.; Moret, E. E.; Schuurmans-Nieuwenbroek, N. M.; van Steenbergen, M. J.; Hennink, W. E., Structure− activity relationships of water-soluble cationic methacrylate/methacrylamide polymers for nonviral gene delivery. *Bioconjugate chemistry* **1999,** *10* (4), 589-597.

[50] Atkins, P.; De Paula, J.; Keeler, J., *Atkins' physical chemistry*. Oxford university press: 2023.

[51] Leroy, P.; Tournassat, C.; Bernard, O.; Devau, N.; Azaroual, M., The electrophoretic mobility of montmorillonite. Zeta potential and surface conductivity effects. *Journal of Colloid and Interface science* **2015,** *451*, 21-39.

[52] Mons, P. J.; Fribiczer, N.; Kowalczuk, K.; Poudel, P.; Seiffert, S.; Schacher, F. H., Double hydrophilic poly (ethylene glycol)-block-poly (dehydroalanine) four-arm star block copolymers: synthesis and solution behavior. *Polym. Chem.* **2022,** *13* (29), 4298-4308.

[53] Weng, X.-D.; Bao, X.-J.; Jiang, H.-D.; Chen, L.; Ji, Y.-L.; An, Q.-F.; Gao, C.-J., pH-responsive nanofiltration membranes containing carboxybetaine with tunable ion selectivity for charge-based separations. *Journal of Membrane Science* **2016,** *520*, 294-302.

[54] Lowe, A. B.; McCormick, C. L., Synthesis and Solution Properties of Zwitterionic Polymers. *Chemical Reviews* **2002,** *102* (11), 4177-4190.

[55] Grest, G. S.; Kremer, K., Molecular dynamics simulation for polymers in the presence of a heat bath. *Physical Review A* **1986,** *33* (5), 3628.

[56] Tagliabue, A.; Landsgesell, J.; Mella, M.; Holm, C., Can oppositely charged polyelectrolyte stars form a gel? A simulational study. *Soft Matter* **2021,** *17* (6), 1574-1588.

[57] Rathee, V. S.; Sidky, H.; Sikora, B. J.; Whitmer, J. K., Role of associative charging in the entropy–energy balance of polyelectrolyte complexes. *Journal of the American Chemical Society* **2018,** *140* (45), 15319-15328.

[58] Weeks, J. D.; Chandler, D.; Andersen, H. C., Role of repulsive forces in determining the equilibrium structure of simple liquids. *The Journal of chemical physics* **1971,** *54* (12), 5237-5247.

[59] Hockney, R. W.; Eastwood, J. W., *Computer simulation using particles*. crc Press: 2021.

[60] Deserno, M.; Holm, C., How to mesh up Ewald sums. I. A theoretical and numerical comparison of various particle mesh routines. *The Journal of chemical physics* **1998,** *109* (18), 7678-7693.

[61] Deserno, M.; Holm, C., How to mesh up Ewald sums. II. An accurate error estimate for the particle–particle–particle-mesh algorithm. *The Journal of chemical physics* **1998,** *109* (18), 7694-7701.

[62] Weers, J. G.; Rathman, J. F.; Axe, F. U.; Crichlow, C. A.; Foland, L. D.; Scheuing, D. R.; Wiersema, R. J.; Zielske, A. G., Effect of the intramolecular charge separation distance on the solution properties of betaines and sulfobetaines. *Langmuir* **1991,** *7* (5), 854-867.

[63] Shahrbabaki, Z.; Oveissi, F.; Farajikhah, S.; Ghasemian, M. B.; Jansen-van Vuuren, R. D.; Jessop, P. G.; Yun, J.; Dehghani, F.; Naficy, S., Electrical Response of Poly (N-[3-(dimethylamino) Propyl] Methacrylamide) to CO2 at a Long Exposure Period. *ACS omega* **2022,** *7* (26), 22232-22243.

[64] Landsgesell, J.; Hebbeker, P.; Rud, O.; Lunkad, R.; Košovan, P.; Holm, C., Grand-reaction method for simulations of ionization equilibria coupled to ion partitioning. *Macromolecules* **2020,** *53* (8), 3007-3020.

[65] Curk, T.; Yuan, J.; Luijten, E., Accelerated simulation method for charge regulation effects. *The Journal of Chemical Physics* **2022,** *156* (4).

[66] Smith, W.; Triska, B., The reaction ensemble method for the computer simulation of chemical and phase equilibria. I. Theory and basic examples. *The Journal of chemical physics* **1994,** *100* (4), 3019-3027.

[67] Johnson, J. K.; Panagiotopoulos, A. Z.; Gubbins, K. E., Reactive canonical Monte Carlo: a new simulation technique for reacting or associating fluids. *Molecular Physics* **1994,** *81* (3), 717-733.

[68] Hénin, J.; Chipot, C., Overcoming free energy barriers using unconstrained molecular dynamics simulations. *The Journal of chemical physics* **2004,** *121* (7), 2904-2914.

[69] Darve, E.; Rodríguez-Gómez, D.; Pohorille, A., Adaptive biasing force method for scalar and vector free energy calculations. *The Journal of chemical physics* **2008,** *128* (14).

[70] Comer, J.; Gumbart, J. C.; Hénin, J.; Lelièvre, T.; Pohorille, A.; Chipot, C., The adaptive biasing force method: Everything you always wanted to know but were afraid to ask. *The Journal of Physical Chemistry B* **2015,** *119* (3), 1129-1151.

[71] Henin, J.; Fiorin, G.; Chipot, C.; Klein, M. L., Exploring multidimensional free energy landscapes using time-dependent biases on collective variables. *Journal of chemical theory and computation* **2010,** *6* (1), 35-47.

[72] Fiorin, G.; Klein, M. L.; Hénin, J., Using collective variables to drive molecular dynamics simulations. *Molecular Physics* **2013,** *111* (22-23), 3345-3362.

9. CONCLUSIONS AND OUTLOOK

In this thesis, the interplay of synthesis and environmental conditions on the resulting structure and corresponding properties of (amphiphilic) model networks comprised of covalently or ionically crosslinked tetra-functional polymers was investigated in a collaborative fashion within the framework of the research unit FOR2811.

This model-like character is achieved for the covalent-permanent networks by hetero-complementary crosslinking of four-armed star polymers, which significantly reduces the formation of microscopic defects and thus leads to homogeneous networks with a defined structure.

The first four studies (*Chapter I–IV*) deal with covalent-permanent amphiphilic networks, which are prepared by the aforementioned hetero-complementary crosslinking. For this purpose, the polymer end groups are modified with a benzoxazinone linking group or an amine functionalization. In the first instance, networks of separate hydrophilic (t-PEG) and hydrophobic (t-PCL) four-armed star polymers are thoroughly investigated, starting with the synthesis and characterization of the building blocks, continuing with the network formation kinetics on to the network connectivity, the swelling properties and the rheological behavior at preparation conditions. As an extension of this first comprehensive study, the swelling and mechanics under different solvent conditions and on different length scales are investigated using rheology and atomic force microscopy. The use of the latter technique also provides insights into the surface structure at different solvent qualities and reveals a microphase-separation in the selective solvent.

In these studies, amphiphilicity is introduced by separate hydrophilic and hydrophobic building blocks. Another way to generate amphiphilicity is the direct use of amphiphilic building blocks, in this case amphiphilic four-armed star block copolymers composed of both PEG and PCL. Hence, the synthesis and solution behavior of t-PCL-*b*-PEG block copolymers with different PEG-block length in various solvents is described in a third study in order to create a knowledge base for further investigations. The solvent quality of different solvents is estimated with literature data and probed with dynamic light scattering. The formation of micellar structures in water is detected with both dynamic light scattering and TEM.

In a final study on this topic, four-armed star block copolymers with hetero-complementary end groups are synthesized and linked to form a network. Due to the better feasibility of end group

modification in the synthesis, t-PEG-*b*-PCL block copolymers are used for this purpose. First, the solution behavior of the building blocks is discussed together with the solvent quality of several solvents. In a next step, the network formation at different concentrations and temperatures is examined. Interestingly and unexpectedly, no network formation is observed in toluene, which was used in previous studies as a common solvent for the networks consisting of t-PEG and t-PCL. As an alternative solvent, DMSO is chosen, in which a two-step crosslinking mechanism is found. The final networks are further characterized in terms of their connectivity, their swelling ability, and their mechanics in the as-prepared state and at equilibrium swelling. The results are further compared to previous studies on networks consisting of separate t-PEG and t-PCL building blocks. A further complication arises due to the highly hygroscopic nature of DMSO and the ever-present air humidity. As water is a poor solvent for PCL, the overall quality of the solvent reduces upon water uptake. This requires a differentiated discussion of the conducted experiments.

In summary, a profound knowledge of the interplay of synthesis and environmental conditions, the resulting structure and the associated properties of covalent-permanent amphiphilic conetworks has been gained. The influence of the building block architecture and composition is investigated by using separate hydrophilic and hydrophobic components and combining them to form an amphiphilic star block copolymer. In addition, the influence of the synthesis conditions on the resulting network structure and properties, such as swelling and mechanics, is examined in detail. Furthermore, the influence of environmental conditions such as solvent quality is tested in the as-prepared and swollen state. In order to further enrich this database and take the step towards rational material design, experiments on the selective permeability of the networks would be advantageous, particularly with regard to the release of drugs or the transport of guest substances in general. Such investigations can be carried out on a macroscopic level or with the aid of suitable microscopy or NMR techniques. Further investigations of the network structure by combined static and dynamic light scattering could also provide valuable information on the (in)homogeneity of the networks.

The two final studies (*Chapters V & VI*) are dedicated to the reversible ionic linkage of purely hydrophilic networks based on tetra-functional block copolymers. First, a possible ampholytic building block based on a t-PEG core and attached poly dehydroalanine (PDha) segments, t-PEG-*b*-PDha, is designed and characterized with regard to the pH-dependent solution behavior and the influence of the building block architecture on the aggregation tendency. While the molecular weight of the PEG core has a negligible effect, the length of the charged

block contributes significantly to the aggregation behavior. Even short PDha block lengths can lead to considerable aggregation in the corresponding pH range.

In a final study, gels are prepared by electrostatic crosslinking of four-arm star block copolymers with a PEG core and attached polycarboxybetaine methacrylamide (PCBAMAA) or polystyrene sulfonate (PSSNa) segments. This system is chosen due to unsuccessful gel formation experiments with t-PEG-*b*-PDha from the previous study. The selected system does not only form a gel at suitable conditions (concentration, pH), but can also be reversibly switched from gel to sol state. However, this switching has so far only been realized in one direction and only once per gel. A critical factor when switching the pH value is the additional amount of salt introduced into the system, which leads to precipitation of the polymers. In order to increase the number of possible sol-gel transitions, systems with a smaller pH gap between the sol and gel state can be considered. Due to the smaller pH gap, less salt is introduced into the system upon a pH change, which may result in increased reversibility.

So far, only purely hydrophilic networks with electrostatic crosslinking have been considered. Therefore, the introduction of amphiphilicity could be a next step, together with further research into the properties of the produced gels and the optimization of the reversible sol-gel transition. In analogy to the covalent-permanent networks, findings on the permeability of the gels for charged molecules and the identification of possible ion channels are of interest. In addition, further knowledge about the structure of the physical gel can contribute to a better understanding of the underlying processes.

In conclusion, a knowledge base on covalent-permanent or ionic-reversible star polymer networks based on four-armed star polymers and block copolymers has been created. By further variation of parameters like the molecular weight of the building blocks, the mixing ratio of hydrophilic and hydrophobic segments, and the stoichiometry and answering open questions, an even more comprehensive understanding of the underlying mechanisms can be obtained. In addition, a combination of covalent-permanent and ionic-reversible approach or the incorporation of e.g. thermoresponsive segments may be used to introduce certain functions and properties into the networks. On the other hand, the targeted incorporation of defects by using a non-stochiometric mixing ratio can open up new areas of application. However, the studies carried out so far provide a solid basis to do so.

10. FURTHER PROJECTS

This chapter contains some further collaborative projects in which the methods of light scattering and rheology are used to complement the respective study. The first subchapter includes two projects dealing with theoretical or structural aspects, respectively, of amphiphilic polymer co-networks based on t-PEG and t-PCL, as described in *Chapter I and II*. The second subchapter examines amphiphilic random or block copolymers based on poly(ethylene glycol) and oleyl glycidyl ether. Whereas the third subchapter contains three projects located in the area of biomaterials, investigating different approaches to photocrosslink and bioprint decellularized extracellular matrices to form natural tissue mimics. The latter projects bridge the gap between polymer science and biomaterials, demonstrating how universal the method of rheology is and how diversely it can be applied.

10.1 Further Studies on APCNs based on PEG and PCL

Amphiphilic polymer co-networks consisting of t-PEG and t-PCL are characterized in *Chapter I and II* in terms of their building blocks, network structure, mechanics and swelling. To extend these studies, a first collaborative project compares these experimental data with theoretical calculations and predictions, focusing on the swelling of the networks at different solvent conditions. In a second project, the network formation and the structure of the networks in a common good solvent for both building blocks is explored with light scattering, which provides insights into possible inhomogeneities and complements the structure picture drawn from *Chapter I and II*. Comparison with purely hydrophilic networks prepared by the same crosslinking chemistry give insights into the role of amphiphilicity on the network formation and the final network structure.

Swelling and Residual Bond Orientations of Polymer Model Gels: The Entanglement-Free Limit

[redacted], **N. Fribiczer**, [redacted]

Macromolecules, **2022**, 55, 14, 5997–6014, doi: 10.1021/acs.macromol.2c00589

Personal Contributions: Rheology measurements.

Abstract:

We investigate the swelling of polymer model networks prepared at different polymer volume fractions and in solvents of different quality. We extend the existing theory to describe residual bond orientations (the vector and the tensor order parameters) for theta, good, and athermal solvents and put these relations in context with modulus at preparation conditions and the equilibrium degree of swelling. We find good agreement with the assumption of affine swelling for the weakly entangled networks of our study. The same scaling relations (up to numerical coefficients) are obtained for the vector order parameter, m, and the tensor order parameter, S, as a function of the preparation conditions, network structure, the equilibrium degree of swelling, Q, and the modulus at swelling equilibrium, G. We obtain $m \propto Q^{-2}$ and $G \propto m^{3/2}$ for swelling in theta solvents and $m \propto Q^{-1.08}$ with $G \propto m^{2.14}$ in the good-solvent regime, in both cases independent of preparation conditions. Modulus and residual bond orientation are related by $G \propto \phi_0 m$ and $G \propto \phi_0^{1.23} m$ as a function of the preparation polymer volume fraction ϕ_0 for theta solvents and good solvents, respectively. Computer simulations and experimental data for the good-solvent regime show good agreement with the predictions.

Light Scattering on Amphiphilic Polymer Co-Networks based on t-PEG and t-PCL

N. Fribiczer*, [redacted]
*These authors contributed equally.

Manuscript in preparation

Personal Contributions: Concept development; Static and dynamic light scattering on amphiphilic polymer co-networks; Manuscript preparation.

Abstract:

Amphiphilic polymer co-networks consist of both hydrophilic and hydrophobic building blocks and swell independently in water and in organic solvents. Their properties show a delicate dependency on the solvent polarity, such as environmentally sensitive viscoelasticity and selective permeability. This makes them promising candidates for the use in drug delivery systems as well as for membranes and other biomedical applications. To truly exploit their potential for this and other applications, the interplay between microscopic network structure and resulting macroscopic properties has to be understood. The network structure may feature local connectivity defects next to network inhomogeneities and possible microphase separation on even larger scales. To explore these structures imparted during network synthesis, simultaneous dynamic and static light scattering is conducted during network formation and on as-prepared gels in a common good solvent for both building block types. Comparison with pure hydrophilic networks based on the same crosslinking approach and chemistry can give insights into the role of amphiphilicity on the resulting network structure.

10.2 Dynamic Light Scattering on other Amphiphilic Block Copolymers

In *Chapter III* the technique of dynamic light scattering is used to characterize t-PCL-*b*-PEG block copolymers with different PEG block length in solution. In analogy, dynamic light scattering is applied in the following project to study the solution behavior of amphiphilic copolymers based on monomethoxy poly(ethylene glycol) and oleyl glycidyl building blocks combined either in a statistical copolymer or in block copolymers.

Polymers of Biobased Oleyl Glycidyl Ether: Insights into Copolymerization with Ethylene Oxide, Postmodification, Thermal Properties, and Micellization Behavior

[redacted], **N. Fribiczer**, [redacted]

Manuscript in preparation

Personal Contributions: Dynamic light scattering measurements and evaluation.

Abstract:

Biobased monomers offer a potentially sustainable alternative to those derived from depleting fossil resources. Fatty alcohols represent a linear aliphatic motive and are abundant in several oleiferous plants in nature. Oleyl glycidyl ether (OlGE) is a highly hydrophobic monomer synthe-sized from a fatty alcohol and epichlorohydrin. When combined with hydrophilic monomethoxy poly(ethylene glycol) (mPEG) macroinitiators (M_n = 2 000 and 5 000 g/mol), well-defined, highly amphiphilic AB block copolymers are obtained via anionic ring-opening polymerization ($Đ \leq 1.08$). An investigation of the statistical copolymerization kinetics of the apolar OlGE and ethylene oxide (EO) was conducted by in situ ^{1}H NMR spectroscopy, revealing an almost ideally random copolymerization with slightly favored incorporation of EO (r_{EO} = 1.27, r_{OlGE} = 0.78). Both statistical and block co-polymers were investigated regarding their behavior in aqueous solution. Critical micelle concentration (CMC) measurements demonstrated low CMCs ranging from 73.4 to 23.8 mg/L when employing fluorometric analysis. Dynamic light scattering and transmission electron microscopy (TEM) indicate the formation of larger aggregates such as spherical to elongated micellar aggregates for most copolymers. Thermal properties were investigated using differential scanning calorimetry. The block copolymers featured two distinct melting temperatures (T_ms). Besides a melting transition of mPEG around 65 °C, the second T_m is attributed to the crystallization of the cis-alkenyl side chain of

OlGE. Varying degrees of side chain hydrogenation of the POlGE homopolymer allowed tailoring of the T_m within the range of –23.2 to 51.9 °C. The thiol-ene click reaction allows functionalization of the unsaturated side chains, e.g. to balance hydrophobicity. This work not merely highlights the prospect of novel surfactants, but it also emphasizes the potential for developing drug delivery systems featuring temperature-controlled release.

10.3 Decellularized extracellular matrix systems for vat 3D bioprinting

Three-dimensional bioprinting is a widely used technique for producing tissues that mimic their natural counterparts and, ideally, provide a tissue-like environment for cell encapsulation. The vat photopolymerization 3D printing technique requires photosensitive bioresins, which necessitates additional modification of the resin with photocrosslinkable components. The following three publications examine decellularized extracellular matrices (dECM) modified with either methacrylate (-MA), glycidyl methacrylate (-GMA), or norbornene (-NB) groups as a basis for 3D bioprinting along with a full characterization of the dECM in terms of biochemical, mechanical, and biophysical properties. In the course of these studies, the crosslinking reaction was initiated with UV light and monitored by rheology, since knowledge of the reaction kinetics is essential for the use of the respective dECM in the printing process.

Bioactive photocrosslinkable resin solely based on refined decellularized small intestine submucosa for vat photopolymerization of in vitro tissue mimics

[redacted], **N. Fribiczer**, [redacted]

Additive Manufacturing, **2023**, 64, 103439, doi: 10.1016/j.addma.2023.103439

Personal Contributions: Methodology; Investigation of crosslinking by rheology with UV light curing system.

Abstract:

Three-dimensionally (3D) printed tissue mimics are unique in vitro platforms for studying human pathophysiology in a more physiologically relevant manner compared to oversimplified 2D cell cultures and complex animal models. However, their 3D printing requires an availability of materials that at the same time show a high level of biomimicry and also have a suitable viscosity profile and crosslinking kinetics for the desired printing technique. We developed a new biomimetic material for vat photopolymerization by solubilizing and functionalizing porcine small intestine submucosa (dSIS) into photocrosslinkable dSIS methacryloyl (dSIS-MA) and by subsequently formulating it into a bioactive 3D printing resin. The concentration of 1.5 wt% of dSIS-MA yielded desired viscosity and photocrosslinking kinetics, and the 3D printing of the resin resulted in fully transparent and highly swelling dSIS-MA hydrogels with a stiffness resembling native intestinal tissue. The new dSIS-MA resin was successfully 3D printed into acellular intestine-mimicking scaffolds that desirably guided the seeded human intestinal cells to grow along the 3D villi mimics. Human small intestinal organoid-derived undifferentiated primary cells grew to confluency on the dSIS-MA hydrogels and formed continuous tight junctions, thereby demonstrating the suitability of the 3D printing material for growing intestinal epithelium mimics. Furthermore, a small fraction of the human primary intestinal cells produced mucin 5AC, demonstrating early differentiation of these cells on the dSIS-MA hydrogels. The excellent cell compatibility of the dSIS-MA material combined with its high printability and biomimicry indicated that this new resin can be a great help in modelling and reproducing native tissue architectures where enhanced physiological relevancy is desired.

Chemistry matters: A side-by-side comparison of two chemically distinct methacryloylated dECM bioresins for vat photopolymerization

[redacted], **N. Fribiczer**, [redacted]

Biomaterials Advances, **2024**, *required reviews completed*
(status 07.03.2024; initial submission: 07.02.2024)

Personal Contributions: Investigation of crosslinking by rheology with UV light curing system; manuscript correction.

Abstract:

Decellularized extracellular matrix (dECM) is an excellent natural source for 3D bioprinting materials due to its inherent cell compatibility. In vat photopolymerization, the use of dECM-based bioresins is just emerging, and extensive research is needed to fully exploit their potential. In this study, two distinct methacryloyl-functionalized, photocrosslinkable dECM-based bioresin were prepared from digested porcine liver dECM through functionalization with glycidyl methacrylate (GMA) or conventional methacrylic anhydride (MA) under mild conditions for systematic comparison. Although, the chemical modifications did not significantly affect the structural integrity of the dECM proteins, mammalian cells encapsulated in the respective hydrogels performed differently in long-term culture. In either case photocrosslinking during 3D (bio)printing resulted in transparent, highly swollen, and soft hydrogels with good shape fidelity, excellent biomimetic properties, and tunable mechanical properties (~ 0.2–2.5 kPa). Interestingly, at a similar degree of functionalization (DOF ~ 81.5–83.5%), the dECM-GMA resin showed faster photocrosslinking kinetics in photorheology resulting in lower final stiffness, and faster enzymatic biodegradation compared to the dECM-MA gels, yet comparable network homogeneity as accessed via Brillouin imaging. While human hepatic HepaRG cells exhibited comparable cell viability directly after 3D bioprinting within both materials, cell proliferation and spreading were clearly enhanced in the softer dECM-GMA hydrogels at a comparable degree of crosslinking. These differences in stiffness, biodegradation, and cell proliferation were attributed to the additional hydrophilicity introduced to dECM via methacryloylation through GMA compared to MA. Due to its excellent printability and cytocompatibility, the functional porcine liver dECM-GMA biomaterial enables the advanced biofabrication of soft 3D tissue analogs using vat photopolymerization-based bioprinting.

Precision Photoclick Hydrogel Formation: From Norbornene-Functionalized Liver dECM towards Physicochemical Mimicry of Native Liver Tissue for Advanced Tissue Engineering

[redacted], **N. Fribiczer**, [redacted]

Manuscript in preparation

Personal Contributions: Investigation of crosslinking by rheology with UV light curing system.

Abstract:

Photoreactive hydrogels derived from decellularized extracellular matrix (dECM) exhibit substantial promise in liver tissue engineering, owing to their distinctive bioactive components, soft elastic properties and porous structural characteristics. In this study, we propose an innovative photoclick hydrogel platform employing an orthogonal thiol-ene reaction. This reaction is set up between solubilized and norbornene-functionalized liver dECM and thiol-terminated polyethylene glycol (PEG). The establishment of light-induced network formation is demonstrated through a layered approach facilitated by a vat 3D printer on the reacting thiol-ene mixture, incorporating a photoinitiator. With the overarching goal of developing hydrogel scaffolds that physicochemically mimic native liver tissue, our approach seeks to transcend the limitations inherent in traditional methods. This precise and reproducible methodology for hydrogel formation aims to establish scaffolds that not only emulate the physicochemical characteristics of the native liver tissue but also offer enhanced controllability and reproducibility. Our study provides a comprehensive characterization of the thiol-ene mixtures encompassing biochemical, biophysical, and biological evaluations that systematically elucidate the performance and potential applications of the proposed photoclick hydrogel platform in liver tissue engineering.

PUBLICATIONS

I. *Swelling and Residual Bond Orientations of Polymer Model Gels: The Entanglement-Free Limit*
[redacted], N. Fribiczer, [redacted], *Macromolecules*, **2022**, 55, 14, 5997–6014.

II. *Double hydrophilic poly(ethylene glycol)-block-poly(dehydroalanine) four-arm star block copolymers: synthesis and solution behavior*
[redacted], N. Fribiczer, [redacted], *Polymer Chemistry*, **2022**, 13, 4298–4308.

III. *Amphiphilic Model Networks Based on PEG and PCL Tetra-arm Star Polymers with Complementary Reactivity*.
[redacted], N. Fribiczer, [redacted], *Macromolecules*, **2022**, 55, 15, 6573–6589.

IV. *Bioactive photocrosslinkable resin solely based on refined decellularized small intestine submucosa for vat photopolymerization of in vitro tissue mimics*
[redacted], N. Fribiczer, [redacted], *Additive Manufacturing*, **2023**, 64, 103439.

V. *Amphiphilic tetra-PCL-b-PEG star block copolymers using benzoxazinone-based linking groups*
[redacted], N. Fribiczer, [redacted], *Polymer Chemistry*, **2023**, 14, 1965–1977.

VI. *Impact of Swelling on Macroscopic and Nanoscopic Mechanical Properties of Amphiphilic Polymer Co-Networks in Non-Selective and Selective Solvents*
N. Fribiczer, [redacted], *Macromolecular Chemistry and Physics*, **2023**, 2300389

VII. *Amphiphilic Polymer Co-Networks Based on Cross-linked tetra-PEG-b-PCL Star Block Copolymers*

[redacted], N. Fribiczer, [redacted], *Polymer*, **2024**, *under review*

VIII. *Electrostatically triggered hydrogel formation based on star-shaped polyampholytic block copolymers: a combined experimental and theoretical approach*

[redacted], N. Fribiczer, [redacted], *Macromolecules*, **2024**, *under review*

IX. *Chemistry matters: A side-by-side comparison of two chemically distinct methacryloylated dECM bioresins for vat photopolymerization*

[redacted], N. Fribiczer, [redacted], *Biomaterials Advances*, **2024**, *under review*

CONFERENCE CONTRIBUTIONS

I. *Microscopic and macroscopic mechanical properties of amphiphilic model co-networks*

N. Fribiczer, [redacted]

Oral presentation at the virtual DPG-meeting "SKM 2021", 27.09. – 01.10.2021

II. *Mechanical Properties of amphiphilic model co-networks under various solvent conditions*

N. Fribiczer, [redacted]

Oral presentation at the Polymer Networks Group - PNG 2022 in Rome, 12.06 –16.06.2022

LIST OF ABBREVIATIONS

3D	three-dimensional
ABF	adaptive biasing force method
ACN/APCN	amphiphilic polymer co-network
AFM	atomic force microscopy
ATR	attenuated total reflection
ATRP	atom transfer radical polymerization
bpy	bipyridyl
CL	caprolactone
CP33	colloidal probe with a radius of 3.3 μm
CRP	controlled radical polymerization
CuAAC	Copper catalyzed alkine-azide cycloaddition
DA	Diels-Alder
DCC	*N,N′*-dicyclohexylcarbodiimide
DCM	dichloromethane
DCTB	trans-2-[3-(4-tert-butylphenyl)-2-methyl-2-propenylidene]-malononitrile
dECM	decellularized extracellular matrix
defs	defects
DHBC	double hydrophilic block copolymers
DHC	double hydrophilic copolymers
DL	double link
DLS	dynamic light scattering
DMAc	dimethylacetamide
DMAP	dimethylaminopyridine
DMF	dimethylformamide
DMSO	dimethyl sulfoxide
DQ	double-quantum
DSC	differential scanning calorimetry
ECM	extracellular matrix
EDMA	ethylene dimethacrylate
Fmoc	fluorenylmethoxycarbonyl
FTIR	Fourier-transform infrared spectroscopy
Gly	glycine
GMA	glycidyl methacrylate

HEMA	2-hydroxyethyl methacrylate
HMTETA	hexamethyltriamin
HOC	higher order connectivities
HOC	higher order connectivities
HR MAS NMR	high-resolution magic angle spinning nuclear magnetic resonance
MA	methacrylate
MALDI-TOF	matrix-assisted laser desorption/ionization time-of-flight
MALS	multi angle light scattering
MC simulation	Monte-Carlo simulation
MD simulation	molecular dynamics simulation
MD-SEC	multidetection-hyphenated size exclusion chromatography
MQ-NMR	multiple-quantum nuclear magnetic resonance
MS	mass spectroscopy
MTBE	methyl-tert-butyl ether
NB	norbornene
NMP	nitroxide mediated polymerization
NMR	nuclear magnetic resonance
PCBAMAA	poly(carboxy betaine methacrylamide)
PCL	poly(caprolactone)
PDha	poly(dehydroalanine)
PDMAPAA	poly dimethyl aminopropyl acrylamide
PDMAPMAA	poly dimethyl aminopropyl methacrylamide
PDMS	poly(dimethyl siloxane)
PEG	poly(ethylene glycol)
PEMGE	poly(ethyl glycidyl ether-co-methyl glycidyl ether)
PMF	potential of mean force
PMMA	poly methyl methacrylate
PP08	plate-plate geometry with a diameter of 8 mm
PP25	plate-plate geometry with a diameter of 25 mm
PSSNa	poly(styrene sulfonic acid)sodium salt; poly(styrene sulfonate)
PTA	phosphotungstic acid
PVDF	poly(vinyliden fluoride)
RAFT	radical atom
RDC	residual dipolar coupling
RDRP	reversible-deactivation radical polymerization

RMSE	root-mean-squared error
ROMP	ring-opening metathese polymerization
ROP	ring-opening polymerization
SAXS	small-angle x-ray scattering
SEC	size exclusion chromatography
SET-LRP	single-electron transfer-living radical polymerization
SI	supporting information
SIS	small intestine submucosa
SL	single link
SLS	static light scattering
SPAAC	strain-promoted alkyne-azide cycladdition
tBAMA	tert-butoxycarbonylaminomethyl acrylate
TEM	transmission electron microscopy
THF	tetrahydrofuran
Tol	toluene
UAC	uranyl acetate
UV	ultraviolet
VT-NMR	variable temperature nuclear magnetic resonance

LIST OF SYMBOLS

a	mobility	G_{ph}	phantom modulus
A_2	second virial coefficient	$g^{(1)}(q,\tau)$	amplitude correlation function
α	polarizability	$g^{(2)}(q,\tau)$	intensity correlation function
B	magnetic field	g_η	contraction factor
c	concentration	γ	deformation/strain
c^*	overlap concentration	H	enthalpy
χ	Flory-Huggins interaction parameter	I	intensity
C_∞	characteristic ratio	k	reaction constant
D	diffusion coefficient	K	optical constant
D_{res}	residual dipolar coupling	k_B	Boltzmann constant
δ	shift	k_H	Huggins constant
	solubility parameter	k_{SB}	Schulz-Blaschke constant
δ_x	x:TM Tian-Munk x:HS Hildebrandt-Scott x:H Hansen	λ	wavelength
		M	molar mass
$Đ$	dispersity	m	mass
E	elastic modulus	M_e / M_{ent}	entanglement molar mass
E_a	activation energy	M_{el}	molar mass per network strand
E_i	electric field of incident light	M_n	number average molar mass
ε	permittivity	M_w	weight average molar mass
η	viscosity	μ	Poisson ratio
η_{red}	reduced viscosity	μ_{ind}	induced dipole moment
η_{sp}	specific viscosity	n	refractive index
$[\eta]$	intrinsic viscosity	N	number of monomers
f	functionality	N_A	Avogadro constant
F	free energy	ν	frequency
f_{def}	defect fraction	ν_{eff}	concentration of effective elastically active network strands
f_{SL}	fraction of single links	ν as exponent	Flory exponent
f_{DL}	fraction of double links	ω	angular frequency
G	shear modulus	p	conversion
G^*	complex shear modulus	P_n	degree of polymerization
G'	storage modulus	ϕ	volume fraction
G''	loss modulus	ϕ_0	volume fraction at preparation

$\boldsymbol{\Pi}$	osmotic pressure	$\boldsymbol{t}$	time
$\boldsymbol{q}$	scattering vector	$\boldsymbol{\tau}$	correlation time
$\boldsymbol{Q}$	swelling degree	$\boldsymbol{\tau_0}$	terminal relaxation time
$\boldsymbol{Q_V}$	volume swelling degree	$\boldsymbol{\tau_R}$	characteristic relaxation time
$\boldsymbol{r}$	distance	$\boldsymbol{T_c}$	crystallization temperature
$\boldsymbol{R}$	gas constant	$\boldsymbol{\vartheta}$	angle between scattering plane and dipole axis
$\boldsymbol{R_g}$	radius of gyration	$\boldsymbol{\theta}$	scattering angle
$\boldsymbol{R_H}$	hydrodynamic radius	$\boldsymbol{T_m}$	melting temperature
$\boldsymbol{R_\theta}$	Rayleigh ratio	$\boldsymbol{u}$	electrophoretic mobility
$\boldsymbol{RR_{standard}}$	absolute Rayleigh ratio of standard	$\boldsymbol{v}$	volume
$\boldsymbol{\rho}$	density	$\boldsymbol{w}$	weight
$\boldsymbol{S}$	tensor order parameter	$\boldsymbol{\xi}$	mesh size
$\boldsymbol{\sigma}$	stress	$\boldsymbol{z}$	charge
$\boldsymbol{T}$	temperature	$\boldsymbol{\zeta}$	Zeta potential

APPENDIX

A.3. Supporting Information Chapter I

A.3.1. ^{1}H NMR spectroscopic investigation of star polymer 3

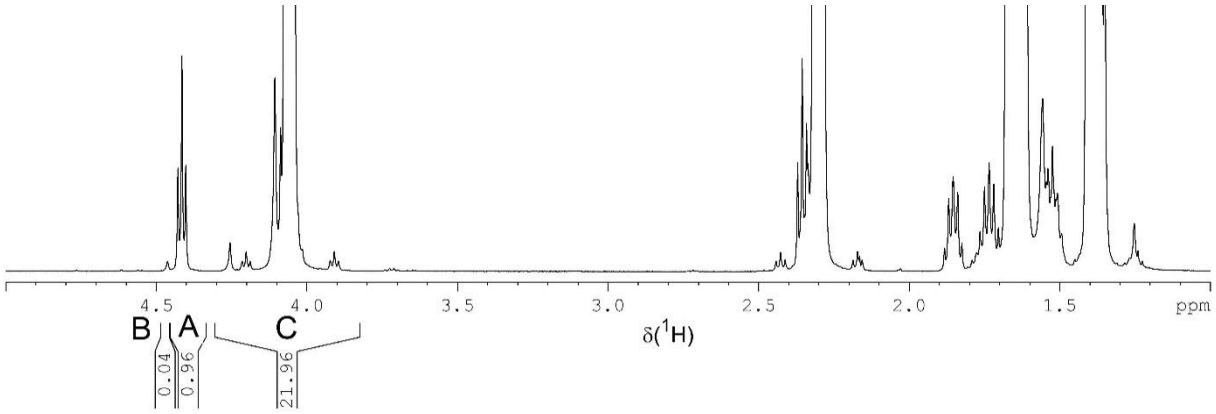

Figure A.3. 1*:* ^{1}H NMR spectrum of **3b** (region of aliphatic protons; CDCl3) with integral regions used for the calculation of the number-average molar mass $M_{n,NMR}$ for **3a – 3c** according the following comments.

*Calculation of the molar mass (exemplary for **3b**):*

- Integral A (I_A): terminal C**H**$_2$OBenzOx protons of PCL arms. Intensity is equal to intensity of C**H**$_2$O-PCL protons of core.
- Integral B (I_B): unreacted C**H**$_2$BenzOx protons of core (“defects”).
- Integral C (I_C): C**H**$_2$OC(O) protons of (n-1) PCL units and C**H**$_2$O-PCL of core.
- Content of BenzOx-reacted OCH_2 groups of core (“defects”, mainly tri arm structures):
  $= I_B / (I_A + I_B) = 4$ %
- Number of CL units per core unit:
  $n = 0.5 * I_C / 0.125 * (I_A + I_B) = 11 / 0.125 = 88$ (estimated error: ± 2%)
- Number-average molar mass by NMR end group method
  $M_{n,NMR} = n * M_{n,CL} + M_{n,core} + 4 * M_{n,BenzOx} = 88 * 114$ g mol^{-1}+ 136 g mol^{-1} + 4 *295 g mol^{-1} = 11.300 g mol^{-1} (± 200 g mol^{-1}).

A.3.2. [1]NMR spectroscopic investigation of star polymer 5

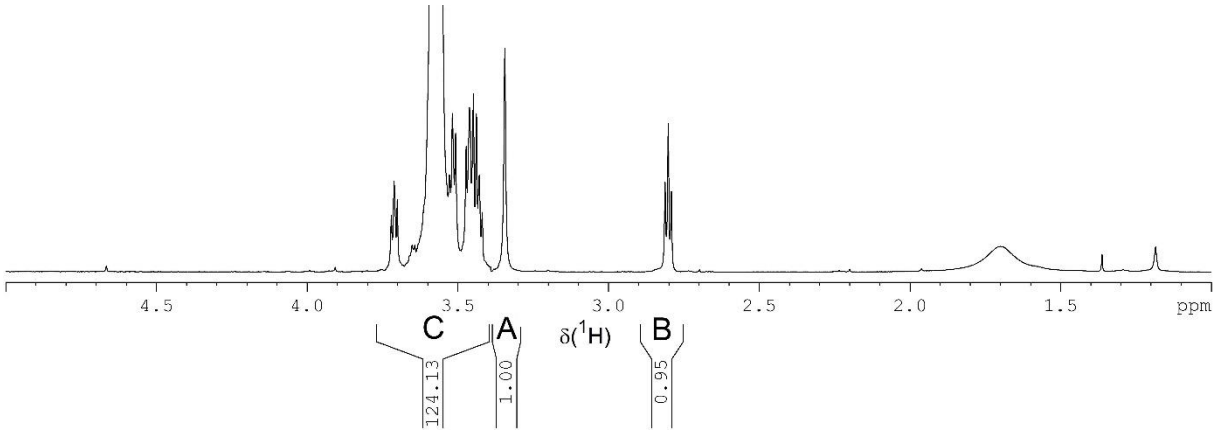

Figure A.3. 2: ^{1}H NMR spectrum of **5b** (region of aliphatic protons; CDCl3) with integral regions used for the calculation of the number-average molar mass $M_{n,NMR}$ for **5a – 5c** according the following comments.

*Calculation of the molar mass (exemplary for **5b**):*

- Integral A (I_A): C**H**$_2$O-PEG protons of core.
- Integral B (I_B): C**H**$_2$NH$_2$ protons of terminal unit of PEG arms
- Integral C (I_C): OC**H**$_2$C**H**$_2$O protons of (n-1) PEG units and OC**H**$_2$CH$_2$NH$_2$ protons of terminal unit of PEG arms.
- Number of CH_2CH_2O units per core unit:
  $n = 0.25 * (I_B + I_C) / 0.125 * I_A = 31 / 0.125 = 248$ (estimated error: ± 2%)
- Number-average molar mass by NMR end group method
  $M_{n,NMR} = n * M_{n,CH2CH2O} + M_{n,core} = 248 * 44$ g mol^{-1} + 136 g mol^{-1} = 10.800 g mol^{-1} (± 200 g mol^{-1})

A.3.3. ^{1}H NMR spectroscopic monitoring of network formation (signal assignments)

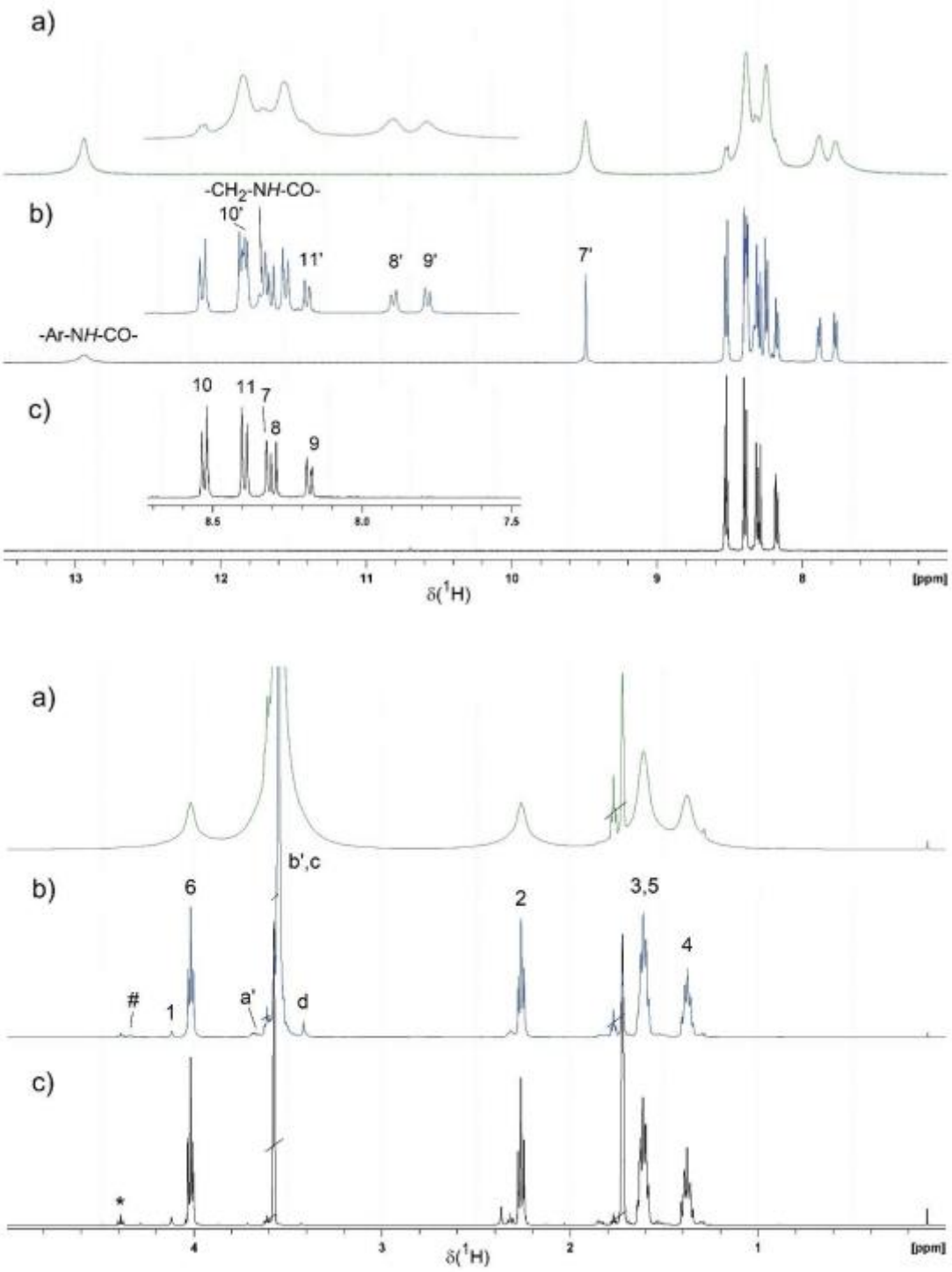

Figure A.3. 3: ^{1}H NMR spectra (regions) of **a)** a **CN** at a benzoxazinone conversion of 90 %, **b)** during a **CN** synthesis at a benzoxazinone conversion of 46 %, and **c)** of **3a** (all in THF-d8 at 40 °C). The OCH_2 signal of H_6 next to the benzoxazinone group is marked with * and after reaction with #. The assignment refers to the structures in **Scheme 3.2** in the main text.

A.3.4. HR MAS NMR spectroscopy of CN3-3

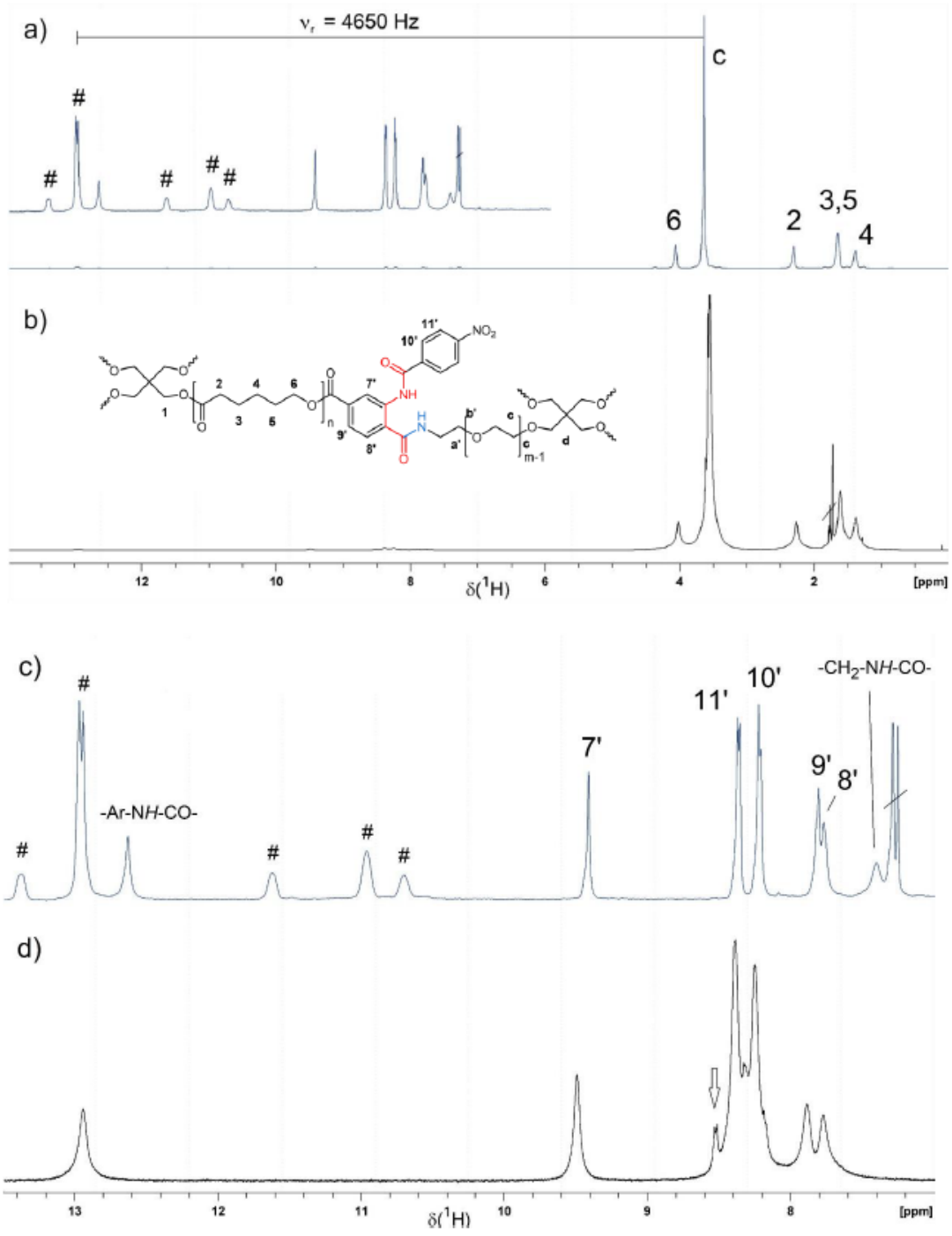

Figure A.3. 4*:* ^{1}H NMR spectra of **(a,c) CN3-3** swollen in CDCl3 and measured with a HR MAS NMR probe and **(b, d)** a **CN** at a benzoxazinone conversion of 90 % measured in a 5 mm NMR tube during a kinetics experiment (THF-d_8). Symbol # marks spinning side bands of the intense aliphatic signals appearing in a distance of n_r = 4650 Hz from the main signals. The arrow in **(d)** points to a signal of residual benzoxazinone groups (H_{10}) that disappeared for fully reacted **CN3-3**.

A.3.5. Size Exclusion Chromatography (SEC)

For the measurements of **3a-c**, two MIXED-C columns (300 x 7.5 mm, 5 µm, Agilent Technologies, USA) were connected in series. Detection was set up as follows: a DAWN® HELEOS II multi angle light scattering (MALS) detector (Wyatt Technology, USA, 18 photodiodes at multiple measurement angles, λ = 663 nm) and a differential refractive index (dRI) detector Optilab® T-rEX (Wyatt Technology, USA, equipped with a 512 photodiode array and λ = 663 nm). The eluent was THF (stabilized with 0.025 % butylated hydroxytoluene) with a flow rate of 1 mL/min. SEC characterization of **5b** and **5c** was performed using an aqueous solution containing 0.01 M NaH2PO4 (pH = 7) and 0.2 M NaPO3 as eluent at a flow rate of 1 ml min^{-1} with two aquagel-OH MIXED-H columns (250 x 4.6 mm, 8 µm, Agilent Technologies, USA). Molar mass determinations were performed by using a dRI detector K2301 (Knauer, DE) and a MALS-detector MiniDAWN TREOS II (Wyatt Technologies, USA).

A.3.6. Viscosimetry

A capillary viscometer of micro-Ubbelohde type I was used to determine η_{sp}. The capillary was sequentially precleaned with peroxomonosulfuric acid, hydrochloric acid, sodium hydroxide, water and acetone. Stock solutions of the respective polymers were prepared and diluted to 18, 15, 12, 9, 6, and 3 g L^{-1}. Measurements were performed at 25 and 35 °C. The capillary was rinsed with the respective solution and kept at constant temperature for 15 minutes prior to the measurement. At least ten data points were collected for each concentration. The specific viscosity η_{sp} was calculated from the time t that a defined volume of the polymer solution needs to flow through the capillary and the corresponding time t_s for the pure solvent.

$$\eta_{sp} = \frac{\eta - \eta_s}{\eta_s} \approx \frac{t - t_s}{t_s}. \quad (1)$$

The intrinsic viscosity [η] is defined as

$$[\eta] = \lim_{c \to 0} \frac{\eta_{sp}}{c} \quad (2)$$

And was extrapolated according to the method of Schulz–Blaschke.[1]

$$\frac{\eta_{sp}}{c} = [\eta] + k_{SB}[\eta]\eta_{sp} \quad (3)$$

The Schulz–Blaschke constant k_{SB} provides qualitative information on the solvent quality (lower k_{SB} refers typically to better solvent quality). All results of this analysis are summarized in **Table A.3.1**. The data shows that chloroform is the best solvent for both compounds, while compound **5** develops a significant temperature dependence in both THF and toluene.

Table A.3. 1: Overlap concentrations and Schulz–Blaschke constants from viscosity measurements for compounds **3** and **5.** The error for c^* is estimated from the error propagation as $\Delta c^* = \frac{1}{[\eta]^2} \cdot \Delta[\eta]$.

solvent	T **(°C)**	**3**		**5**	
		k_{SB}	c^* (g·L^{-1})	k_{SB}	c^* (g·L^{-1})
THF	25	0.41	59.2 ± 0.3	2.22	81.8 ± 0.3
	35	0.89	55.1 ± 0.1	0.42	64.6 ± 0.2
toluene	25	0.31	55.2 ± 0.1	1.65	76.2 ± 0.5
	35	0.29	55.4 ± 0.2	0.34	58.6 ± 0.1
$CDCl_3$	25	0.88	46.8 ± 0.7	0.37	35.6 ± 0.1
	35	0.86	47.1 ± 0.6	0.24	35.7 ± 0.1

A.3.7. Dynamic Light Scattering (DLS)

For all measurements, cylindrical quartz-glass cuvettes sequentially pre-cleaned with peroxomonosulfuric acid, aqua regia, sodium hydroxide, and water were used which were rinsed with hot acetone to remove dust prior to use. The temperature during the measurements was controlled by a Huber Pilot One thermostat (Peter Huber Kältemaschinenbau AG, Offenburg, Germany). Measurements were conducted at 25 and 35 °C and at a concentration of c = 30 g L^{-1}. The solutions of **5** were filtered with a Whatman Anotop (0.1 µm; 10 mm) and a Millex LG (0.2 µm; 13 mm) filter and the solutions of **3** with a Whatman Anotop (0.02 µm; 10 mm) and a Millex FG (0.2 µm; 13 mm) filter in a dust-free laminar flow box prior to the measurement to obtain dust free polymer solutions. The amplitude correlation functions $g^{(1)}(q,\tau)$ received from the DLS experiment were corrected for the baseline and normalized to unity. The data are displayed in **Figure 3 .2** of the manuscript and were fitted with an exponential function

$$g^{(1)}(q,\tau) = B \cdot \exp\left(-\frac{\tau}{\tau_{R,1}}\right) \quad (4)$$

in case of the tetra-PCL solutions and a biexponential function

$$g^{(1)}(q,\tau) = B \cdot \exp\left(-\frac{\tau}{\tau_{\mathrm{R},1}}\right) + (1-B) \cdot \exp\left(-\frac{\tau}{\tau_{\mathrm{R},2}}\right), \quad (5)$$

in case of the tetra-PEG solutions, where B is the amplitude of the fast process and $\tau_{\mathrm{R,i}}$ with i = 1, 2 is the characteristic relaxation time of the corresponding process.

The appearance of a second slow relaxation process for compound **5** indicates an apparent clustering in THF, which was already evident during the filtration process and required the use of a 0.1 µm syringe filter in contrast to a 0.02 µm filter for compound **3**. The diffusion coefficient

$$D = \left(\frac{1}{\tau_{\mathrm{R,i}} \cdot q^2}\right) \quad (6)$$

is extracted from the relaxation time using data at different scattering vectors q by plotting the inverse relaxation time against the square of the scattering vector q. The hydrodynamic radii are calculated using the Stokes-Einstein equation

$$R_h = \frac{k_{\mathrm{B}}T}{6\pi\eta_{\mathrm{s}}D} \quad (7)$$

with the Boltzmann constant k_{B}, the absolute temperature T, and the viscosity of the solvent η_{s}. The results of this analysis are summarized in **Table A.3. 2**.

Table A.3. 2: Fit parameters of the monoexponential and biexponential fits and extracted hydrodynamic radii of components **3** and **5** in THF at a scattering angle of 30° corresponding to **Figure 3. 2** of the manuscript.

Sample	$\boldsymbol{T}$ (°C)	**B**	$\boldsymbol{\tau_{\mathrm{R},1}}$ (ms)	$\boldsymbol{\tau_{\mathrm{R},2}}$ (ms)	$\boldsymbol{R_{\mathrm{h},1}}$ (nm)	$\boldsymbol{R_{\mathrm{h},2}}$ (nm)
3	25	1.0	0.11	-	2.8 ± 0.1	-
	35	1.0	0.10	-	2.8 ± 0.1	-
5	25	0.70	0.12	2.7	3.2 ± 0.1	44 ± 2
	35	0.68	0.10	1.8	3.1 ± 0.1	44 ± 2

Table A.3. 3: Geometric parameters of tetra-arm star polymers **3** and **5** used to calculate the radius of gyration.

poly-mer	C_∞ [a]	l (nm) [b]	b (m·10^{-10}) [c]	M_K (g·mol^{-1}) [d]	N [e]
PEG (**5**)	5[2]	0.146[3]	8.8	107	97
PCL (**3**)	5[4]	0.149[4]	9.0	118	98

[a] characteristic ratio
[b] root mean square of the bond length
[c] Kuhn length
[d] Kuhn molar mass
[e] number of Kuhn segments per star polymer

A.3.8. Rheology

With reference to the frequency sweep measurements on APCN-gels based on star polymers **5** and **3** shown in **Figure 3. 7** in the main text, storage moduli averaged over the full frequency range are shown **Table A.3. 4**.

Table A.3. 4: Average values of storage modulus over the full range of frequencies.

No.	c (g L^{-1})	G' (kPa)
1)	70	2.42 ± 0.01
2)	140	5.3 ± 0.1
3)	210	9.26 ± 0.09
4)	280	13.5 ± 0.2
5)	350	16.9 ± 0.1

A.3.9. MQ NMR Spectroscopy

Table A.3. 5: Overview of the connectivity distribution of all APCNs synthesized.

Sample	f_{SL} [a]	f_{DL} [b]	f_{HOC} [c]	f_{defs} [d]
	(%)			
CN1-1	-	-	-	-
CN2-1	-	-	-	-
CN3-1	24	65	10	01
CN1-3	39	51	9	1
CN2-3	39	49	11	1
CN3-3	36	52	10	2
CN2-5	-	-	-	-
CN3-5	52	39	8	1
CN4-1	22	32	38	9
CN5-1	26	34	35	5
CN4-3	32	47	19	2
CN5-3	35	51	13	1
CN6-1	23	33	41	3
CN7-1	26	32	39	3
CN6-3	35	51	13	1
CN7-3	34	50	15	1
CN8-1	24	31	17	28
CN9-1	-	-	-	-
CN8-3	38	46	15	0
CN9-3	31	52	17	0
PEG-PEG-1	54	16	20	10
PEG-PEG-2	41	46	12	1

a) fraction of single links
b) fraction of double links
c) fraction of higher order connectivities
d) defect and sol fraction

A.3.10. Calculation of interaction parameters from literature data

The Hildebrand-Scott solubility parameter for species $X = A, B$ is defined as[5,6]

$$\delta_X = \left(\frac{E_X}{v_X}\right)^{1/2} = \left(\frac{\Delta H_X - RT}{v_X}\right)^{1/2} \tag{8}$$

Here, R is the gas constant, T the absolute temperature, E_X is the energy of vapourization (cohesive energy), v_X the molar volume, and ΔH_X the enthalpy change of species X upon evaporization. For non-polar systems, a comparison of the solubility parameters provides a first estimate for the (enthalpic part) of the Flory interaction parameter

$$\chi_H \approx \frac{v_A}{RT}(\delta_B - \delta_B)^2 \tag{9}$$

where v_A is the molar volume of the solvent that establishes the unit volume of the FloryHuggins lattice in the dilute limit (the index B is used below for the polymers). Often, a correction is added on top of the enthalpic contribution[5] that is considered to be of entropic origin. Here, a constant between 0.3 and 0.4 is chosen (often 0.34) leading to the following estimate of the interaction parameter based upon the Hildebrand-Scott solubility parameters

$$\chi_{HS} \approx 0.34 + \frac{v_A}{RT}(\delta_A - \delta_B)^2. \tag{10}$$

Miscibility is expected if

$$\chi_{HS} < \chi_{crit} = 1/2. \tag{11}$$

For computation, the solubility parameters δ and the molar volumes v_A of **Table A.3. 6** were used

Table A.3. 6: Hansen solubility parameters in units of $MPa^{1/2}$ and molar volumes of the solvents

	δ_D	δ_P	δ_H	δ	v_A [cm^3 mol^{-1}]	**Refs.**
PEG	17	10	5	20.4	-	7-8
PCL	19.6	5	8.4	20.2	-	8
Toluene	18.0	1.4	2.0	18.1	106.8	8
Chloroform	17.8	3.1	5.7	18.7	80.7	8
THF	16.8	5.7	8.0	18.6	81.7	8
Water	15.5	16.0	42.3	47.8	18.0	8

Note that Ref. [8] contains multiple tables where parameters for the same compound are provided. These contain sometimes slightly different parameters (e.g. δ_H of toluene is either 18.0 or 18.3). In case of different parameters, we have chosen the parameter that appears most often.

The results of these computations are summarized in **Table 3. 3** of the main text. Hansen[8] introduced a generalization of the solubility parameter decomposing it into three different contributions related to dispersion forces, polar cohesive energy, and hydrogen bonding respectively,

$$\delta^2 = \delta_D^2 + \delta_P^2 + \delta_H^2. \tag{12}$$

Here, one computes first the solubility parameter distance

$$R_a^2 = 4(\delta_{DA} - \delta_{DB})^2 + (\delta_{PA} - \delta_{PB})^2 + (\delta_{HA} - \delta_{HB})^2 \tag{13}$$

for which the individual contributions are compared. As above, additional indices A and B refer to the different species. The coefficient of 4 was introduced in later works for convenience:[9] with this empirical parameter, all miscible materials appear roughly within a sphere when interpreting the above differences as differences along the three axes of a cartesian coordinate system. A connection to the Flory-Huggins interaction parameter χ is established by computing[10]

$$\chi_\alpha \approx \alpha \frac{v_A R_a^2}{4RT}, \tag{14}$$

which reduces to χ_{HS} in the absence of polar interactions and hydrogen bonding, if α = 1 as introduced originally by Hansen. Lindvig[10] analyzed a large number of solubilities and proposed that a coefficient of α = 0.6 leads to a better agreement with the Flory-Huggins parameter. Therefore, we have used α = 0.6 in combination with the solubility parameters of **Table A.3. 6**. The results of these computations are summarized in **Table 3. 3** of the main text. Tian and Munk[11] developed a refinement of the Hildebrand-Scott model that is somewhat similar to the Hansen approach. Here, the Flory interaction parameter is computed as

$$\chi_{TM} = \frac{\sigma_A v_A}{RT}[(\delta_{DA} - \delta_{DB})^2 + (\delta_{PA} - \delta_{PB})^2 + (\mathrm{A}_A - \mathrm{A}_B)(\mathrm{D}_A - \mathrm{D}_B)] \qquad (15)$$

where σ_A is a shape factor of the solvent, while hydrogen bonding is split into an acceptor A_X and a donor D_X contribution. We have compiled the relevant model parameters for our study from Ref. [11] in **Table A.3. 7**. The results of these computations are summarized in **Table 3. 3** of the main text.

Table A.3. 7: Tian-Munk solubility parameters in units of $\mathrm{MPa}^{1/2}$, shape factors and molar volumes of the solvent molecules (all data taken from Ref. [11] except of the molar volumes that were taken from Ref. [8])

	σ_A	δ_D	δ_P	A	D	v_A ($\mathrm{cm}^3\ \mathrm{mol}^{-1}$)
PEG	-	16.918	4.07	1.658	11.394	-
PCL	-	16.981	3.684	1.352	7.489	-
Toluene	1.220	16.204	3.327	1.218	0.860	106.8
Chloroform	1.365	15.685	3.989	4.000	0.761	80.7
THF	1.213	16.6	4.583	0.528	3.261	81.7

A.3.11. Reaction kinetics based on in situ ^{1}H NMR measurements

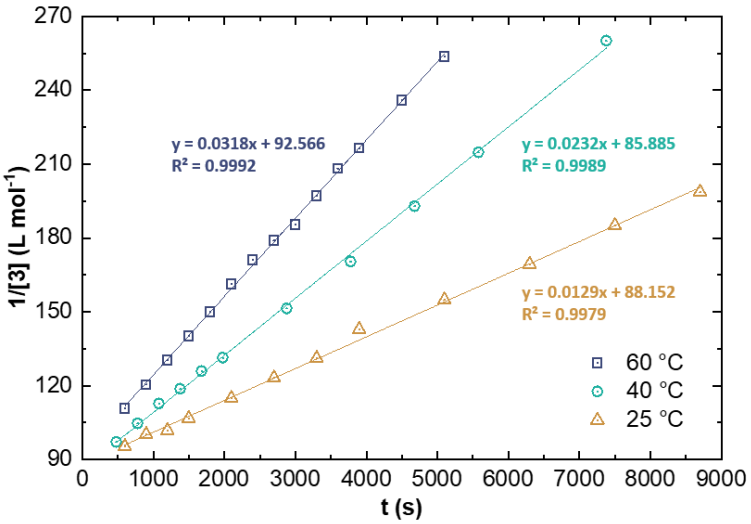

Figure A.3. 5: 1/[3] vs. *t* plot of kinetics data of the equimolar reaction of **3** and **5** in THF-d_8 at different temperatures. The first low conversion data point was not used because it is influenced by the necessary sample handling. This is also the reason that the curves do not cross the origin.

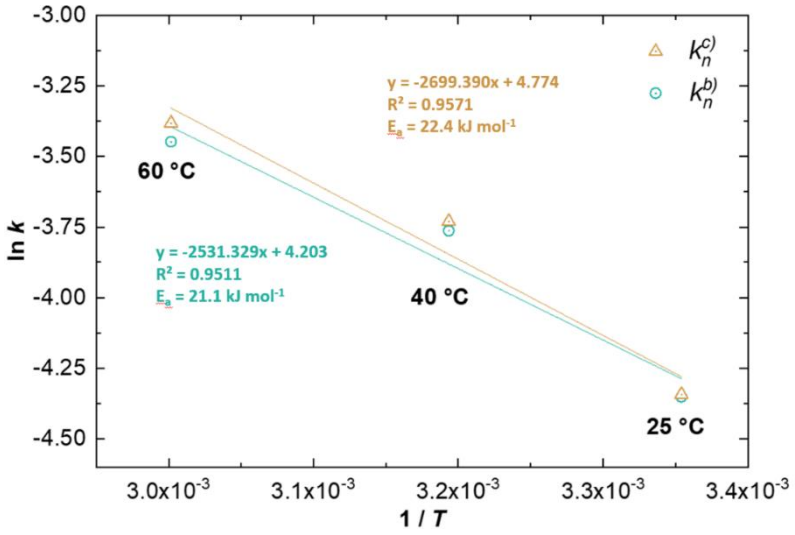

Figure A.3. 6: ln k vs. 1/T plot of kinetics data of the equimolar reaction of **3** and **5** in THF-d_8 at different temperatures. The rate constants $k_n^{c)}$ and $k_n^{b)}$ from **Table 3. 4** were used to determine the activation energies E_a.

Calculation of the activation energy E_a (exemplary for $k_n^{c)}$):

$$E_a = -(slope)8.314\,J\cdot mol^{-1} = -\frac{(-2699.390)(8.314)}{1000} = \mathbf{22.4\,kJ\cdot mol^{-1}}$$

A.3.12. Reaction kinetics in the simulations

One advantage of the computer simulations is that the degree of mixing can be controlled. A comparison with simulation data, therefore, can provide insight into quality of the mixture in an experiment. As benchmark for the experiments, we created "perfect" mixtures with a purely stochastic local composition of the two different star polymer types. Network formation of these perfect mixtures was simulated in the diffusion-controlled limit, since a reaction-controlled kinetics with reaction constants comparable to the experiment is not possible within reasonable simulation time. We have recorded the conversion, p, as a function of time t and the growth of the weight fraction of the largest cluster, w_{gel}, see **Figure A.3. 7**.

Diffusion controlled reactions of reactive groups attached to polymers refer to a compact exploration of space.[12] In case of Rouse dynamics of the reactive groups in melts, this leads to reaction kinetics that progresses with time t as t^{β} with β = 3/4. In semi-dilute solutions, one expects Zimm dynamics with mean square displacements $\propto t^{2/3}$ up to the relaxation time of a correlation volume that provide β = 1 within this time regime.

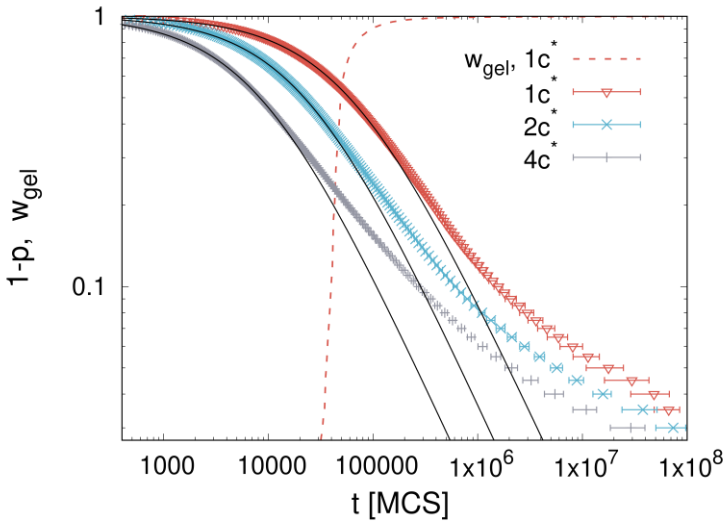

Figure A.3. 7: Reaction kinetics in the simulations with overlap concentrations in the range of c* to 4c*. Data are averages over 10 independent runs with same parameters. The weight fraction of the gel, w_{gel} for the samples at 1c* is included to demonstrate that kinetics departs from a homogeneous mixture after most of the stars are attached to the gel. The error of the kinetics data indicate the sample to sample variation in the time to reach a conversion of p.

Our Monte-Carlo simulations model no hydrodynamics, thus, dynamics is of Rouse type but must reflect swollen chains conformations up to the relaxation time of a correlation volume. For this particular case, we expect[13] mean square displacements $\propto t^{2\nu/(1-2\nu)}$ leading to $\beta = 3\nu/(1 + 2\nu) \approx 0.81$. In any of these cases, kinetics is governed by a dependence

$$\frac{[A]}{[A]_0} = \frac{1}{1 + k[A]_0 t^{\beta}}, \tag{16}$$

since the reaction scheme is ring-opening addition reaction of two different reactive groups in a stoichiometric mixture, see also the discussion in the main text. Here $[A]$ is the concentration of the compound at time t, $[A]_0$ is the initial concentration of the compound, and k is the reaction constant. We have fit this expression in **Figure A.3. 7** to the simulation data at low conversions, $p < 0.6$ and obtain a rather constant $\beta = 0.85 \pm .01$ for all samples not far from the expected $\beta \approx 0.81$. For higher conversions, $p \geq 0.6$, kinetics is delayed with respect to an ideal diffusion-controlled recombination process. This delay sets in at the time when most of the star polymers are attached to gel, see **Figure A.3. 7** where the weight fraction of gel is included for the samples with a concentration around $c*$ (data for w_{gel} at larger concentrations is shifted towards smaller times by the same factor as the reaction kinetics). If most stars are attached to gel, it is no more possible that diffusion can decay spontaneous composition fluctuations of the two types of star polymers in the sample - irrespective of whether kinetics is diffusion or reaction controlled. The data of the experiments depart from the ideal reaction kinetics of a perfectly mixed sample at nearly the same conversion. Therefore, we conclude that a nearly perfect mixing of the two compounds was reached in the experiments.

A.3.13. References

[1] Schulz, v. G.; Blaschke, F., Eine Gleichung zur Berechnung der Viscositätszahl für sehr kleine Konzentrationen,[Molekulargewichtsbestimmungen an makromolekularen Stoffen, IX]. *J. prakt. Chem.* **1941**, 158 (1-8), 130-135.

[2] Gerstl, C.; Schneider, G. J.; Pyckhout-Hintzen, W.; Allgaier, J. r.; Willbold, S.; Hofmann, D.; Disko, U.; Frielinghaus, H.; Richter, D., Chain conformation of poly (alkylene oxide) s studied by small-angle neutron scattering. *Macromolecules* **2011**, 44 (15), 6077-6084.

[3] Lee, H.; Venable, R. M.; MacKerell Jr, A. D.; Pastor, R. W., Molecular dynamics studies of polyethylene oxide and polyethylene glycol: hydrodynamic radius and shape anisotropy. *Biophys. J.* **2008**, 95 (4), 1590-1599.

[4] Huang, Y.; Xu, Z.; Huang, Y.; Ma, D.; Yang, J.; Mays, J. W., Characterization of poly (ε-Caprolactone) via size exclusion chromatography with online right-angle laser-light scattering and viscometric detectors. *Int. J. Polym. Anal. Charact*. **2003**, 8 (6), 383-394.

[5] Mark, J. E., *Physical properties of polymers handbook*. Springer: **2007**; Vol. 1076.

[6] Rubinstein, M.; Colby, R. H., *Polymer physics*. Oxford university press New York: **2003**; Vol. 23.

[7] https://www.hansen-solubility.com/contents/Inkjet_HSP_Chemstream.pdf.

[8] CM, H., *Hansen solubility parameters: a user's handbook*. Florida: CRC **2007**.

[9] Camacho, J.; Díez, E.; Díaz, I.; Ovejero, G., Hansen solubility parameter: From polyethylene and poly (vinyl acetate) homopolymers to ethylene–vinyl acetate copolymers. *Polym. Int.* **2017**, 66 (7), 1013-1020.

[10] Lindvig, T.; Michelsen, M. L.; Kontogeorgis, G. M., A Flory–Huggins model based on the Hansen solubility parameters. *Fluid Ph. Equilibria* **2002**, 203 (1-2), 247-260.

[11] Tian, M.; Munk, P., Intermolecular contact interactions and their temperature dependence. *J. Solut. Chem*. **1995**, 24 (3), 267-284. 19

[12] De Gennes, P., Kinetics of diffusion-controlled processes in dense polymer systems. I. Nonentangled regimes. *J. Chem. Phys*. **1982**, 76 (6), 3316-3321.

[13] Lang, M.; Werner, M.; Dockhorn, R.; Kreer, T., Arm retraction dynamics in dense polymer brushes. *Macromolecules* **2016**, 49 (14), 5190-5201.

A.4. Supporting Information Chapter II

A.4.1. Swelling properties – Non-selective solvent

Table A.4. 1: Equilibrium swelling degrees of PEG-PCL and PEG-PEG networks in toluene prepared at different concentrations and temperatures.

PEG-PCL			PEG-PEG	
c (g·L^{-1})	T (°C)[1]	Q_1[2]	T (°C)[1]	Q_1[2]
70	25	17.8 ± 0.6	25	13.4 ± 0.7
	60	16.0 ± 0.1		
140	25	12.8 ± 0.1		
	60	12.5 ± 0.2		
210	25	10.6 ± 0.5	25	8.3 ± 0.2
	60	10.1 ± 0.3		
280	25	9.3 ± 0.2		
	60	9.3 ± 0.1		
350	25	8.7 ± 0.5	25	6.7 ± 0.2
	60	8.4 ± 0.3		

[1] Synthesis temperature

[2] First swelling directly after synthesis without drying.

A.4.2. Swelling Properties – Effect of Drying

Table A.4. 2: Equilibrium swelling degrees of PEG-PCL networks in toluene before (Q_1) and after drying (Q_2). The drying was performed at room temperature for five days, if not stated otherwise.

c (g·L^{-1})	T (°C)[1]	Q_1	Q_2
70	25	17.58	9.60 [2]
	25	18.62	15.90
	60	16.00	15.40
210	25	10.94	10.93
	60	10.16	9.96
350	25	7.94	7.61
	60	8.40	8.21

[1] Synthesis temperature.

[2] Drying was performed at 60 °C.

A.4.3. Swelling Properties – Selective Solvent

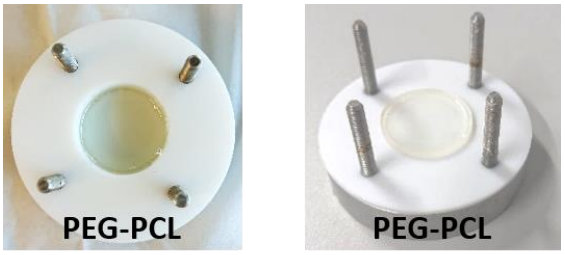

Figure A.4. 1: Pictures of PEG-PCL networks after preparation in toluene. This method of gelation in teflon molds was used for the rheology setup to obtain gels with the correct geometry. The gels were then swollen to equilibrium in excess toluene.

Figure A.4. 2: Pictures of a PEG-PEG network and a PEG-PCL network swollen in water. The transparent appearance of the PEG-PEG networks is due to the good solvent quality of water for PEG. In contrast, water is not a good solvent for PCL, resulting in contraction of PCL domains and a cloudy appearance.

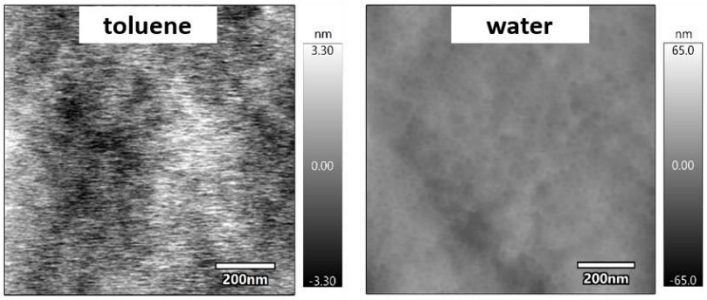

Figure A.4. 3: Height images measured with AFM in tapping mode of PEG-PCL networks swollen in either toluene or water. Whereas the gels show smooth surfaces in toluene without any noticeable structures, they show a rather rough surfaces in water. Further structural information is hidden in the surface roughness, but can be visualized via phase imaging.

Table A.4. 3: Equilibrium swelling degrees of PEG-PCL and PEG-PEG networks in water prepared at different concentrations and temperatures. The networks were prepared in toluene, dried at room temperature for five days and reswollen in water.

PEG-PCL			**PEG-PEG**	
c (g·L^{-1})	T (°C)[1]	Q_2	T (°C)[1]	Q_2
70	25	3.0 ± 0.2	25	14.5 ± 0.3
	60	3.2 ± 0.1		
140	25	2.99 ± 0.08		
	60	2.9 ± 0.2		
210	25	2.9 ± 0.1	25	11.0 ± 0.2
	60	3.1 ± 0.1		
280	25	2.98 ± 0.04		
	60	3.0 ± 0.1		
350	25	2.7 ± 0.1	25	8.9 ± 0.2
	60	2.8 ± 0.1		

[1] Synthesis temperature

A.4.4. Mechanical Properties – Non-selective solvent

Table A.4. 4: Storage modulus of PEG-PCL networks swollen in toluene (non-dried) converted with a Poisson's ratio of μ = 0.25 and μ = 0.5 from AFM measurements with tip (radius ≈ 8 nm) and colloidal probe (CP33: 3.3 µm) as well as storage modulus directly from rheological measurements. The error of the converted modulus corresponds to the percentage error of the original data.

c (g ·L^{-1})	G_1'(kPa)					
	μ = 0.25		μ = 0.5		rheology	
	tip	CP33	tip	CP33	25 °C	60 °C
70	11 ± 4	10 ± 2	9 ± 3	8 ± 1	6.3 ± 0.2	6.5 ± 0.1
140	29 ± 5	18 ± 4	25 ± 4	15 ± 3	13.91 ± 0.09	15.3 ± 0.2
210	37 ± 20	25 ± 7	31 ± 16	20 ± 6	22 ± 2	23.3 ± 0.2
280	52 ± 24	30 ± 9	43 ± 20	25 ± 7	34 ± 1	34.9 ± 0.3
350	95 ± 17	42 ± 9	79 ± 14	35 ± 7	46.2 ± 0.2	47 ± 1

Table A.4. 5: Comparison of experimentally found and theoretically calculated elastically effective network strands, ν_{exp} and ν_{theo}, based on the AFM measurements for PEG-PCL networks in toluene using a tip and colloidal probes.

c (g ·L^{-1})	ν_{theo} (mmol·L^{-1})	tip		CP33	
		ν_{exp} (mmol·L^{-1})	ν_{exp}/ν_{theo}	ν_{exp} (mmol·L^{-1})	ν_{exp}/ν_{theo}
70	12.2	7.4	0.6	6.6	0.5
140	18.0	19.8	1.1	12.3	0.7
210	22.9	24.9	1.1	16.5	0.7
280	27.4	34.8	1.3	19.9	0.7
350	30.8	64.1	2.1	28.6	0.9

A.4.5. Mechanical Properties – AFM histograms

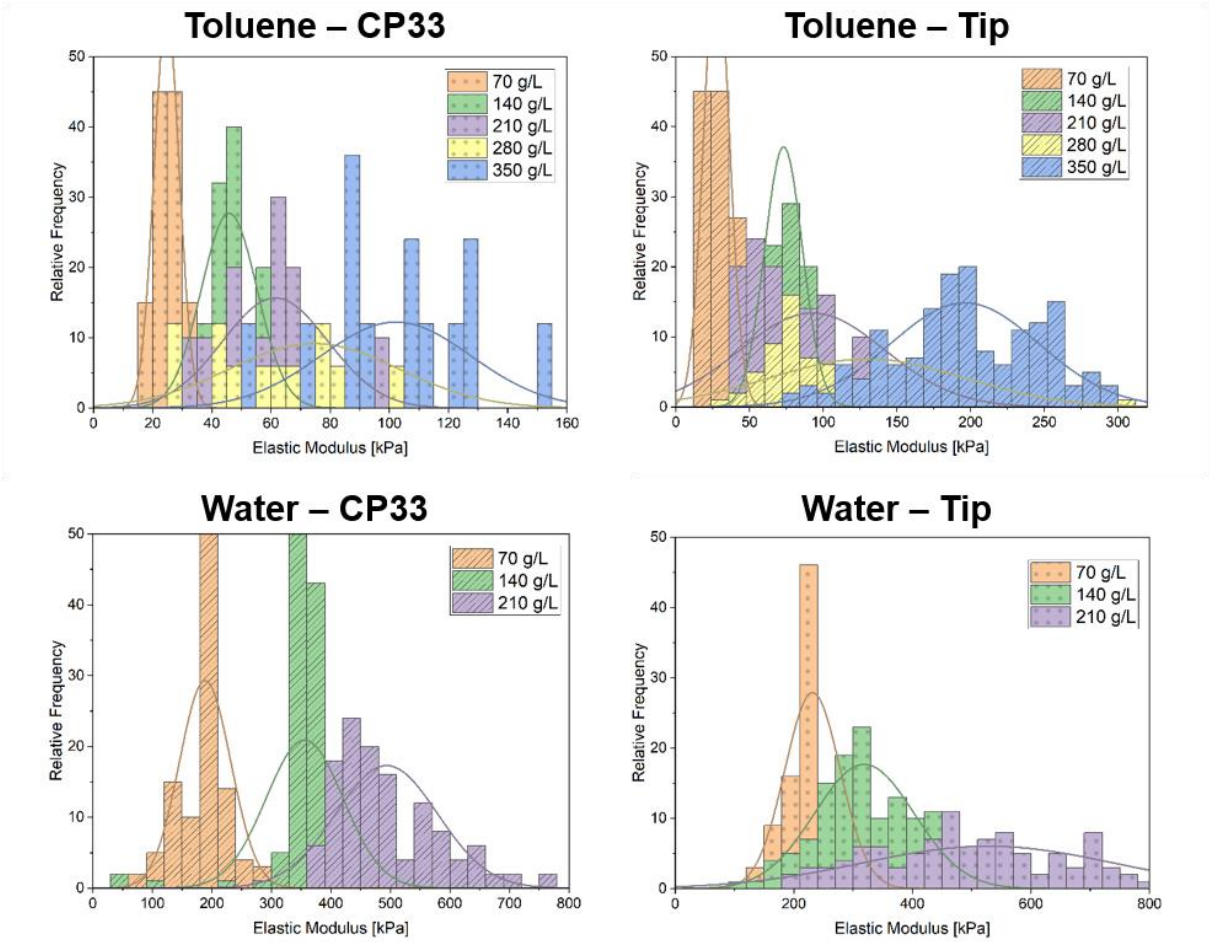

Figure A.4. 4: Elastic moduli of PEG-PCL networks swollen in toluene and water obtained from AFM measurements with colloidal probe (CP33: radius 3.3 µm) or tip (radius ≈ 8 nm). Elastic moduli are higher for gels that have been synthesized at higher network concentrations. Both tip and colloidal probe measurements demonstrate wider distributions of obtained moduli with increasing network concentrations. Gel networks swollen in water are stiffer than in toluene.

A.5. Supporting Information Chapter III

A.5.1. Dynamic Light Scattering (DLS)

The amplitude correlation functions $g^{(1)}(q,t)$ received from the DLS experiment for different scattering vectors q are fitted with monoexponential decay functions, $g^{(1)}(q,t) = A \cdot exp\left(\frac{-t}{\tau(q)}\right)$, for all solvents except of acetone. In the latter case, only a biexponential decay $g^{(1)}(q,t) = A \cdot exp\left(\frac{-t}{\tau_1(q)}\right) + B \cdot exp\left(\frac{-t}{\tau_2(q)}\right)$ provided a satisfying agreement with the data, see **Figure A.5. 1**. Here, A and B are the amplitudes, t is the time, and the characteristic relaxation times for a particular q are given by $\tau_i(q)$ with i = 1,2. For all samples analyzed, the quality of the data and the fit is comparable to the examples shown in **Figure A.5. 1**. The diffusion coefficient D is received as the slope from plotting $\tau_i(q)$ against q^2. The hydrodynamic radii are calculated using the Stokes-Einstein relation $R_H = \frac{k_B T}{6\pi\eta D}$, with the Boltzmann constant k_B, the absolute temperature T, and the viscosity of the solvent η. Reference values for the dynamic viscosity of the solvents at 20°C were taken from literature and are 0.437, 0.325, 0.452, and 1.003 (all in units of mPa·s) for dichloromethane[1], acetone[2], ethyl acetate[2], and water[3], respectively. Scattering vectors were computed for a given scattering angle using the wave length of 632.8 nm of the laser beam and literature data for the refractive index, which is 1.4244, 1.3588, 1.3724, and 1.3330 for the above solvents, respectively.[1, 4, 5]

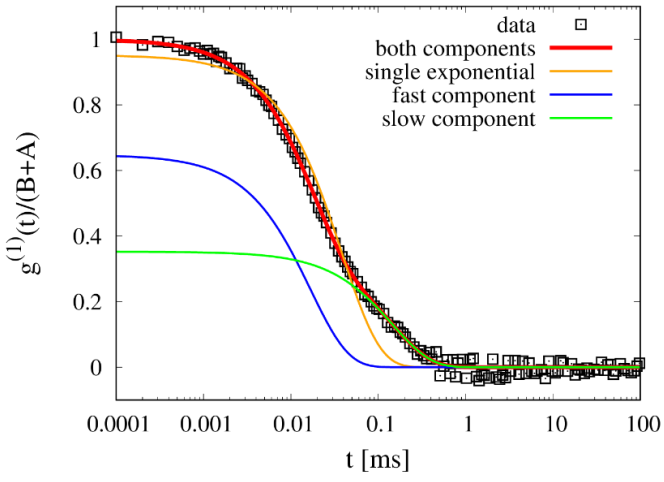

Figure A.5. 1: Amplitude correlation function of a 20 g L^{-1} solution of **6b** in acetone. Data were obtained at 90° scattering angle at a temperature of 20 °C and fit by a single and double exponential decay, where for the latter, the contributions of the slow and the fast component are shown.

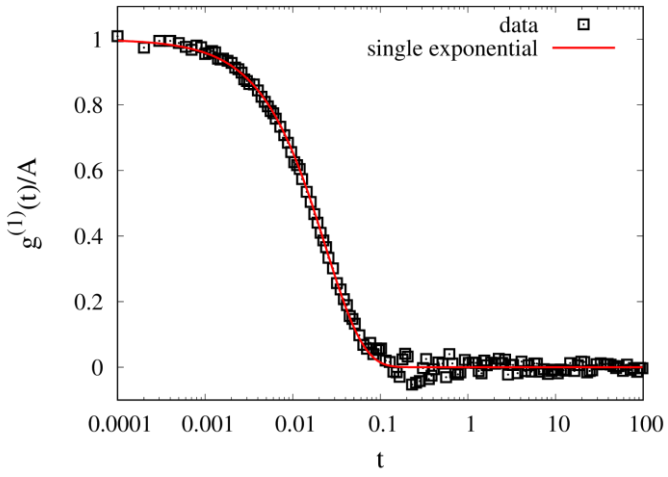

Figure A.5. 2: single exponential decay for 10 g L^{-1} solution of **6b** in ethyl acetate measured at a scattering angle of 90° and a temperature of 20 °C.

Table A.5. 1: Hydrodynamic radii of **6a** and **6b** in water and different organic solvents at 20 °C as a function of polymer concentration *c*. *F* is the relative amplitude of the fast component, $F = \frac{B}{A+B}$, in case of a bi-exponential fit. The error margins reflect the error of the numerical data regression. A more detailed discussion of systematic errors and the noise of the data provides no substantially larger errors.

polymer	solvent	*c* (g L^{-1})	F	$R_{H,1}$(nm)	$R_{H,2}$(nm)
6b	**water**	0.025		22.0 ± 0.5	–
		0.05		21.1 ± 0.3	–
		0.1		21.3 ± 0.3	–
		0.25		20.0 ± 0.1	–
		0.5		20.1 ± 0.1	–
		1		19.9 ± 0.2	–
	acetone	2.5	0.76	18.0 ± 1	3.5 ± 0.1
		5	0.69	21.8 ± 0.4	3.6 ± 0.1
		10	0.64	23.8 ± 0.4	3.7 ± 0.1
		20	0.62	34.8 ± 0.9	4.2 ± 0.1
	dichloromethane	10		3.8 ± 0.3	–
	ethyl acetate	5		4.2 ± 0.1	–
		10		4.3 ± 0.1	–
6a	**acetone**	2.5	0.59	14 ± 1	3.0 ± 0.2
		5	0.55	18.5 ± 0.9	3.2 ± 0.1
		10	0.59	21.5 ± 0.7	3.5 ± 0.1
		20	0.53	23.0 ± 0.4	3.6 ± 0.1

A.5.2. NMR Spectroscopic investigation of star polymer 1

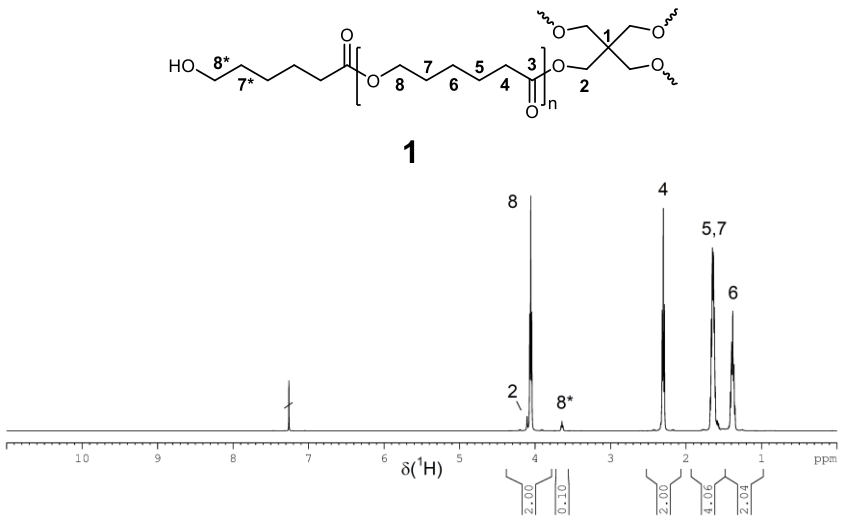

Figure A.5. 3: ^{1}H NMR spectrum of **1a** with integral regions used for calculation of the number-average molar mass $M_{n,NMR}$ for **1a** and **1b** as shown in the following notes (solvent: $CDCl_3$).

*Calculation of the molar mass (exemplary for **1a**):*

Average number of PCL units per PCL arm (n):

$n+1 = (0.5 \cdot (I_2 + I_8)) / (0.5 \cdot I_{8*}) = 1.00 / 0.05 = 20$ (estimated error: ± 2%)

Number-average molecular weight by NMR end group method:

$M_{n,NMR} = 4(n+1) \cdot M_{n,CL} + M_{n,core} = 80 \cdot 114 \text{ g mol}^{-1} + 136 \text{ g mol}^{-1}$

$= 9.300 \text{ g mol}^{-1} (\pm 200 \text{ g mol}^{-1})$

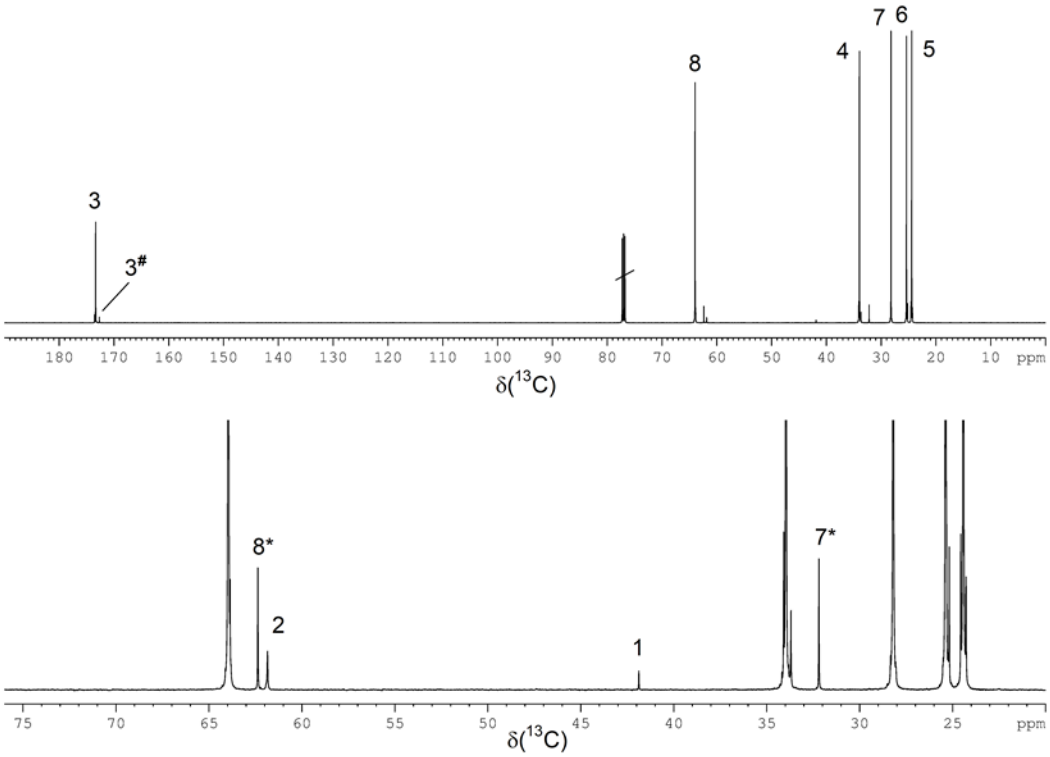

Figure A.5. 4: ^{13}C NMR spectrum of **1a** (solvent: $CDCl_3$). $3^{\#}$ is the carbonyl group next to the core.

A.5.3. NMR spectroscopic investigation of star polymer 3

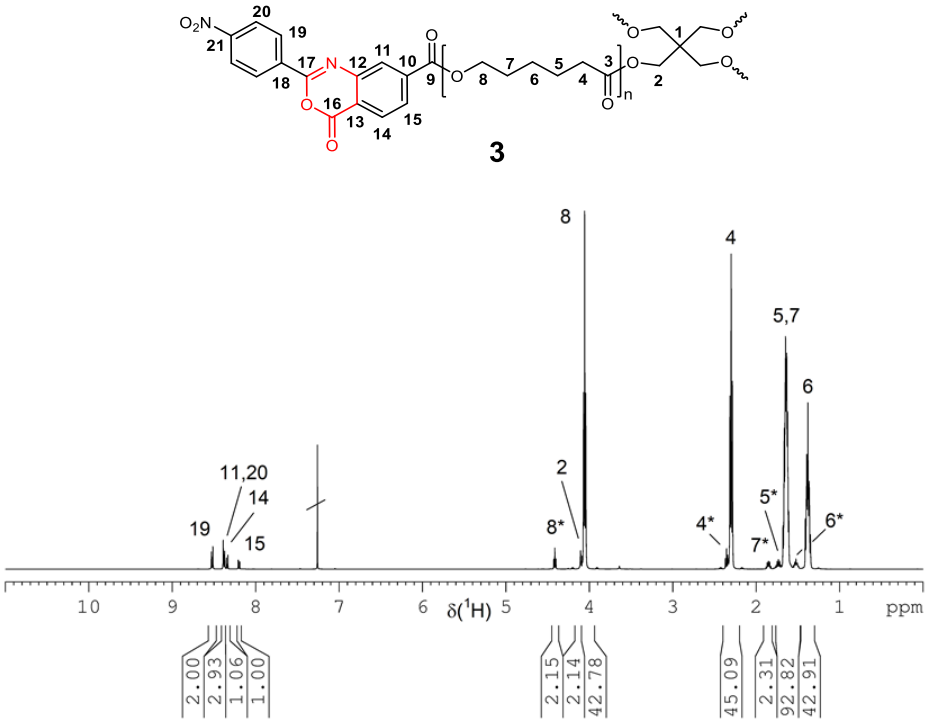

Figure A.5. 5: ^{1}H NMR spectrum of **3a** (solvent: $CDCl_3$). Symbol * indicates that the CL unit is bonded to the terminal oxazinone unit.

*Calculation of the molar mass (exemplary for **3a**):*

Average number of PCL units per PCL arm (n):

$n = (0.5 \cdot (I_2 + I_8)) \ / (0.5 \cdot I_{8*}) = 22.5 / 1.08 = 21$ (estimated error: ± 2%)

Number-average molecular weight by NMR end group method:

$M_{n,NMR} = 4n \cdot M_{n,CL} + M_{n,core} + 4 \cdot M_{n,BenzOx} = 84 \cdot 114 \text{ g mol}^{-1} + 136 \text{ g mol}^{-1} + 4 \cdot 295 \text{ g mol}^{-1}$ $= 10.900 \text{ g mol}^{-1}$ ($\pm 200 \text{ g mol}^{-1}$)

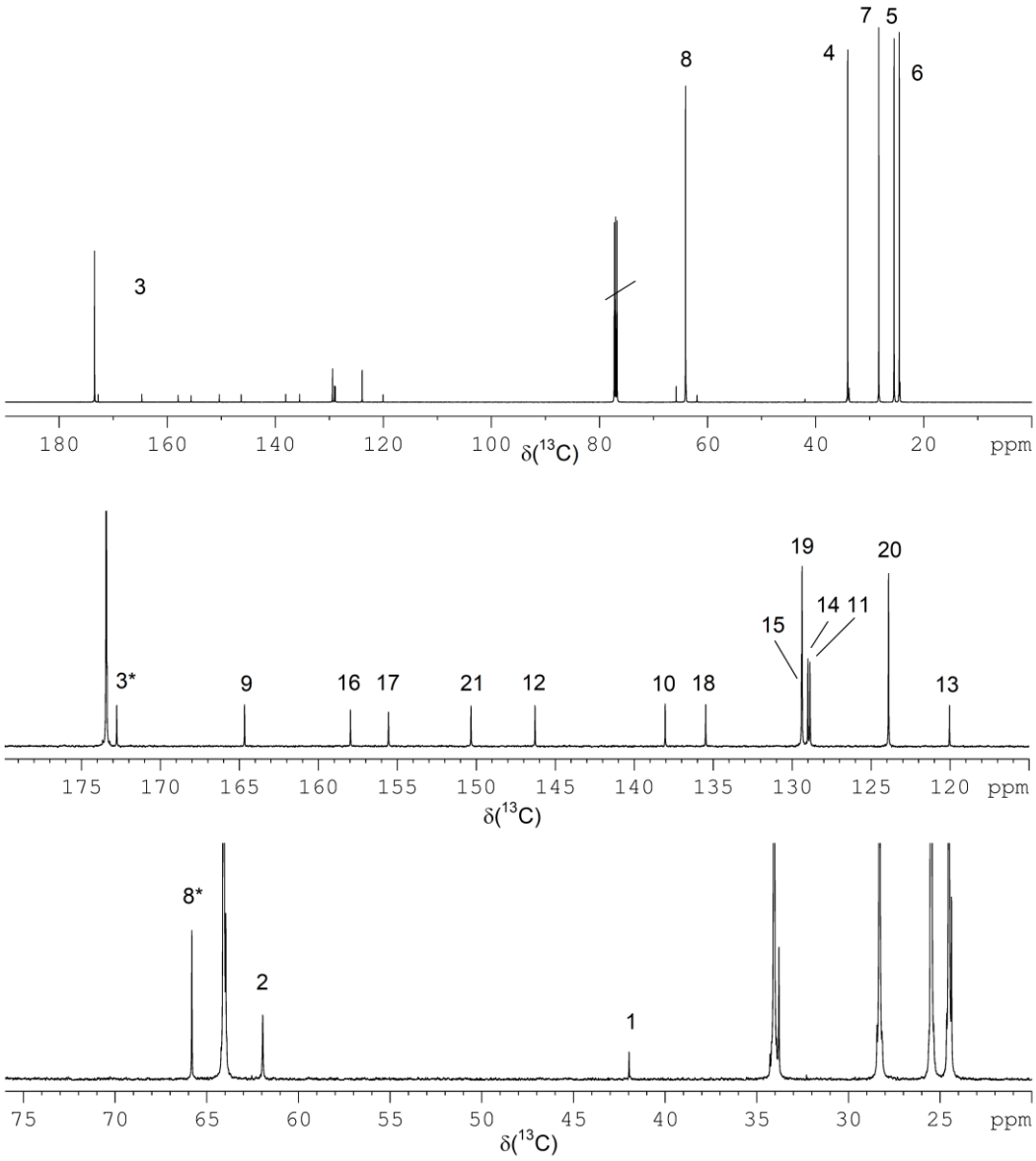

Figure A.5. 6: ^{13}C NMR spectrum of **3a** (solvent: $CDCl_3$). Symbol * indicates that the CL unit is bonded to the terminal oxazinone unit.

A.5.4. NMR spectroscopic investigation of polymer 5

*Calculation of the molar mass (exemplary for **5b**):*

Number of CH_2CH_2O units (m+1):

$m+1 = (0.25 \cdot (I_a + I_b + I_c)) \ / (\frac{1}{3} \cdot I_d) = 47$ (estimated error: ± 2%)

Number-average molecular weight by NMR end group method:

$M_{n,NMR} = m \cdot M_{n,CH2CH2O} + M_{n,CH3O} + M_{n,CH2CH2NH2} = 47 \cdot 44\ g\ mol^{-1} + 31\ g\ mol^{-1} = 2.100\ g\ mol^{-1}$ ($\pm 100\ g\ mol^{-1}$)

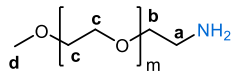

5

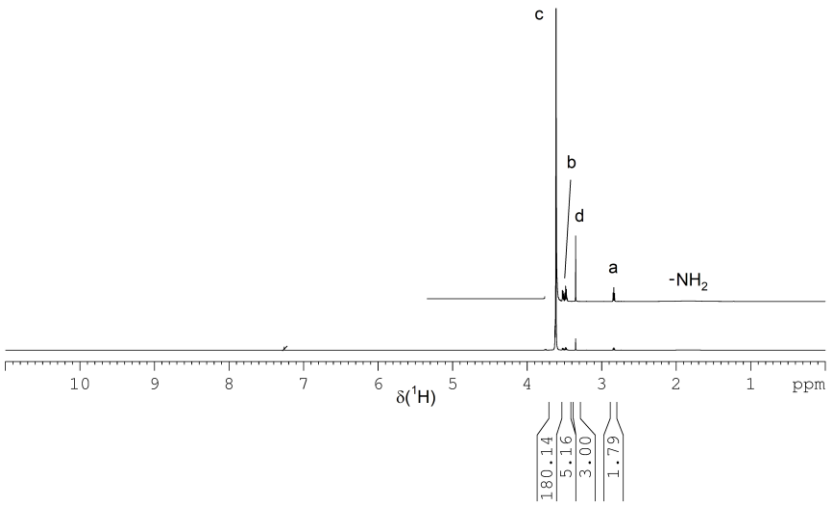

Figure A.5. 7: ^1H NMR spectrum of **5b** (solvent: $CDCl_3$).

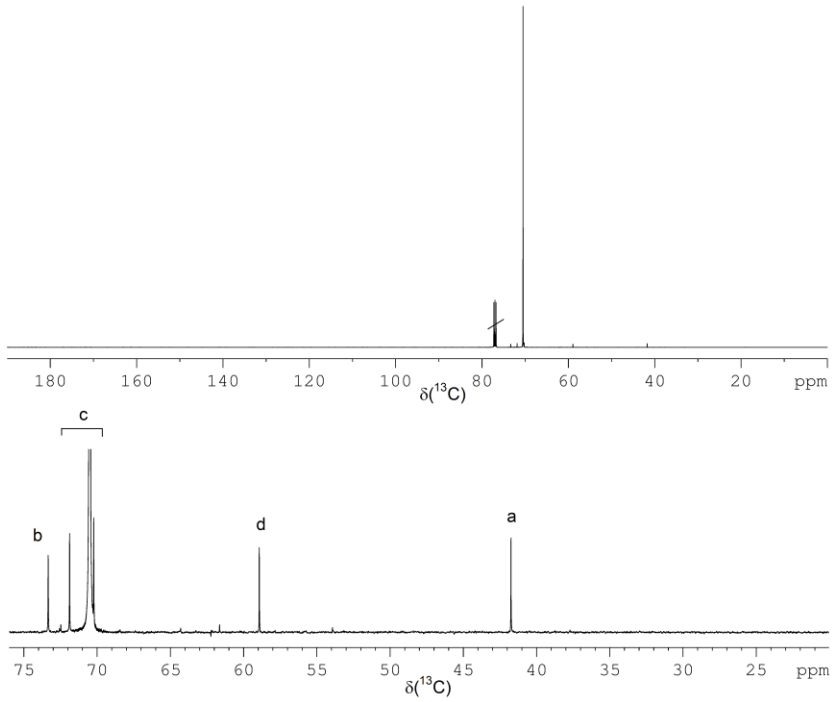

Figure A.5. 8: ^{13}C NMR spectrum of **5b** (solvent: $CDCl_3$).

A.5.5. NMR spectroscopic investigation of star block copolymer 6

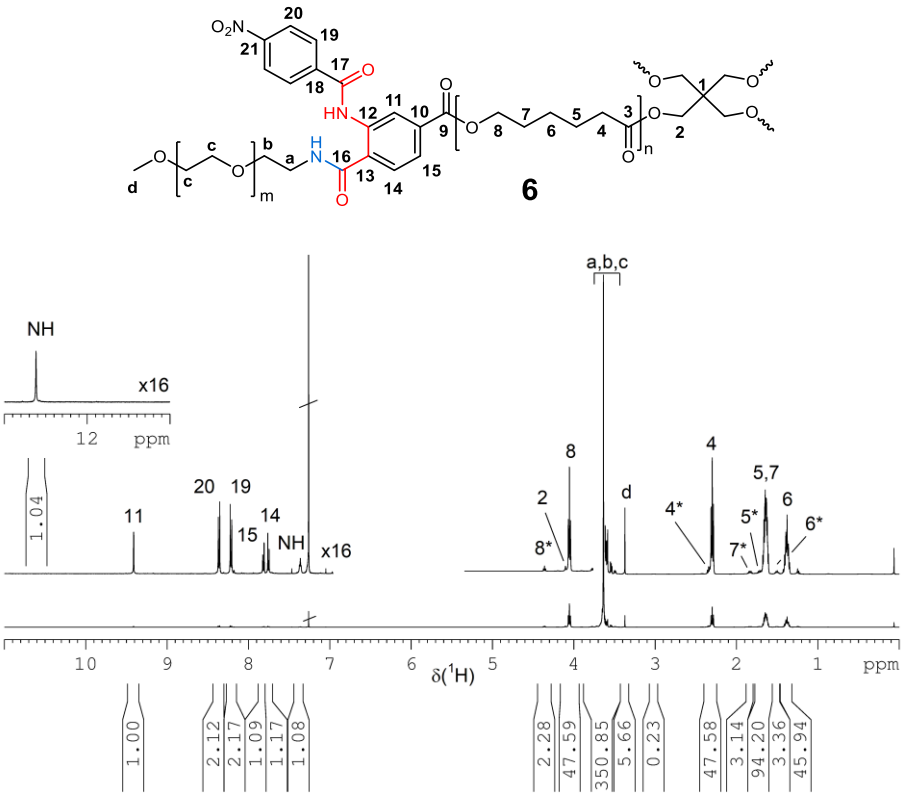

Figure A.5. 9: ^{1}H NMR spectrum of **6b** (solvent: $CDCl_3$). * indicates that the CL unit is bonded to the connecting unit.

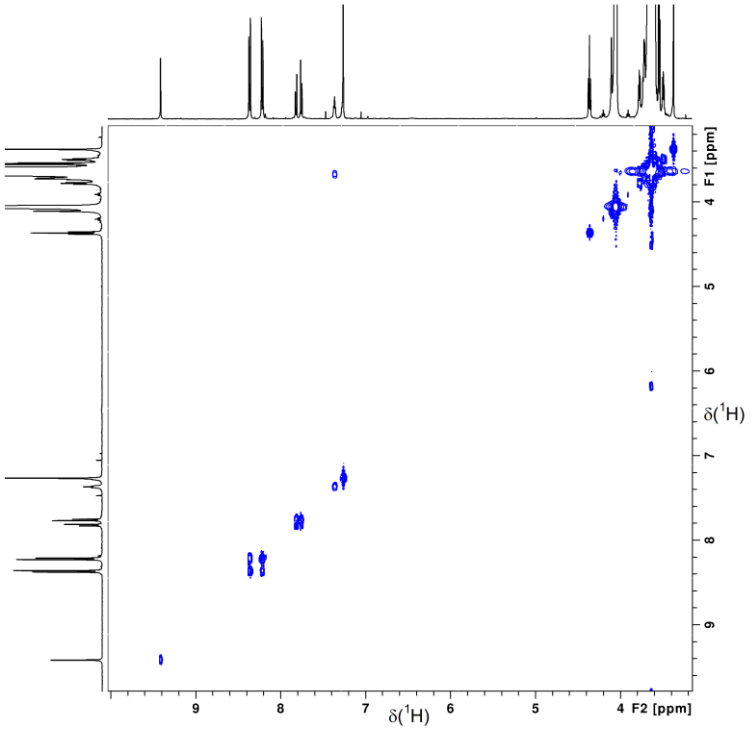

Figure A.5. 10: COSY spectrum (region) of 6b (solvent: CDCl3).

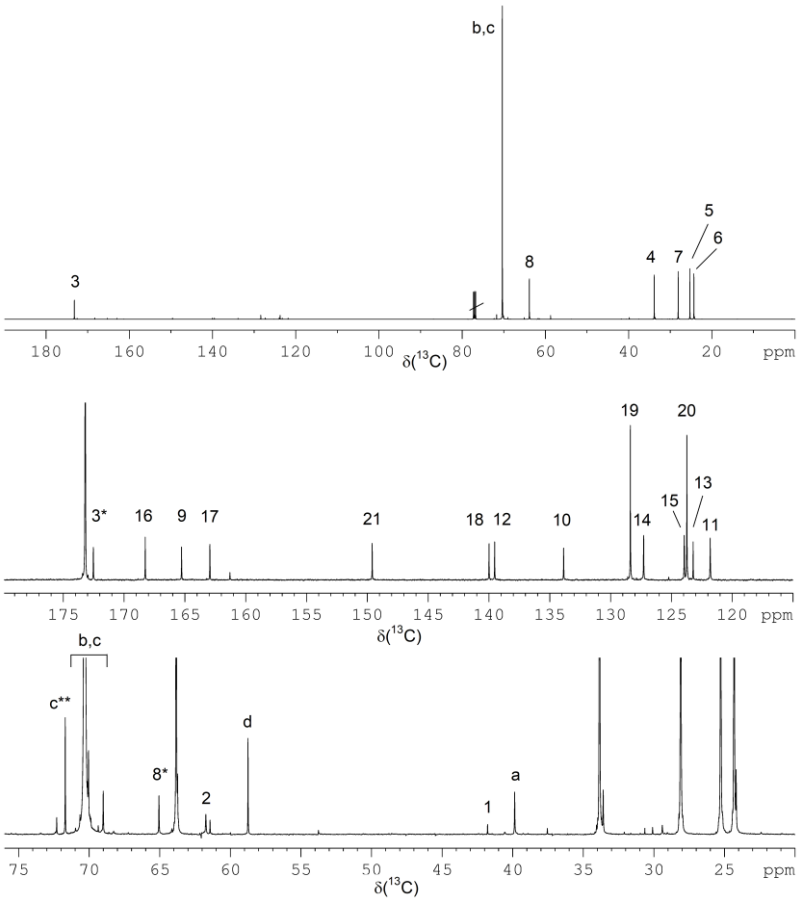

Figure A.5. 11: ^{13}C NMR spectrum of **6b** (solvent: $CDCl_3$). Symbol * indicates that the CL unit is bonded to the connecting unit and ** that the EG unit is bonded to connecting unit.

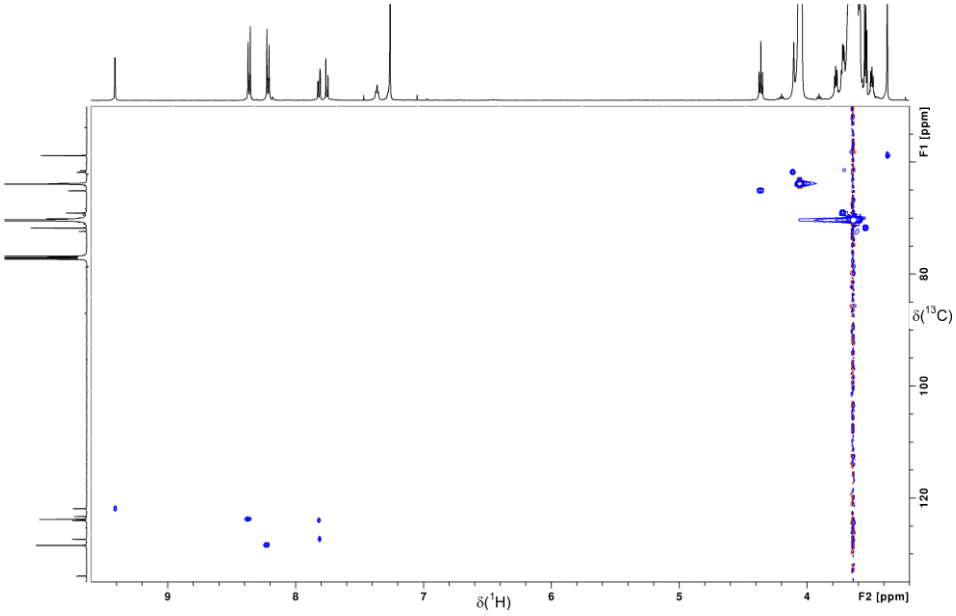

Figure A.5. 12: HSQC spectrum (region) of **6b** (solvent: $CDCl_3$).

A.5.6. NMR spectroscopic investigation of model compound 7

NMR spectra of partially (A_3B, A_2B_2, AB_3) and completely (B_4) esterified pentaerythrol with dodecanoate as ester moiety.

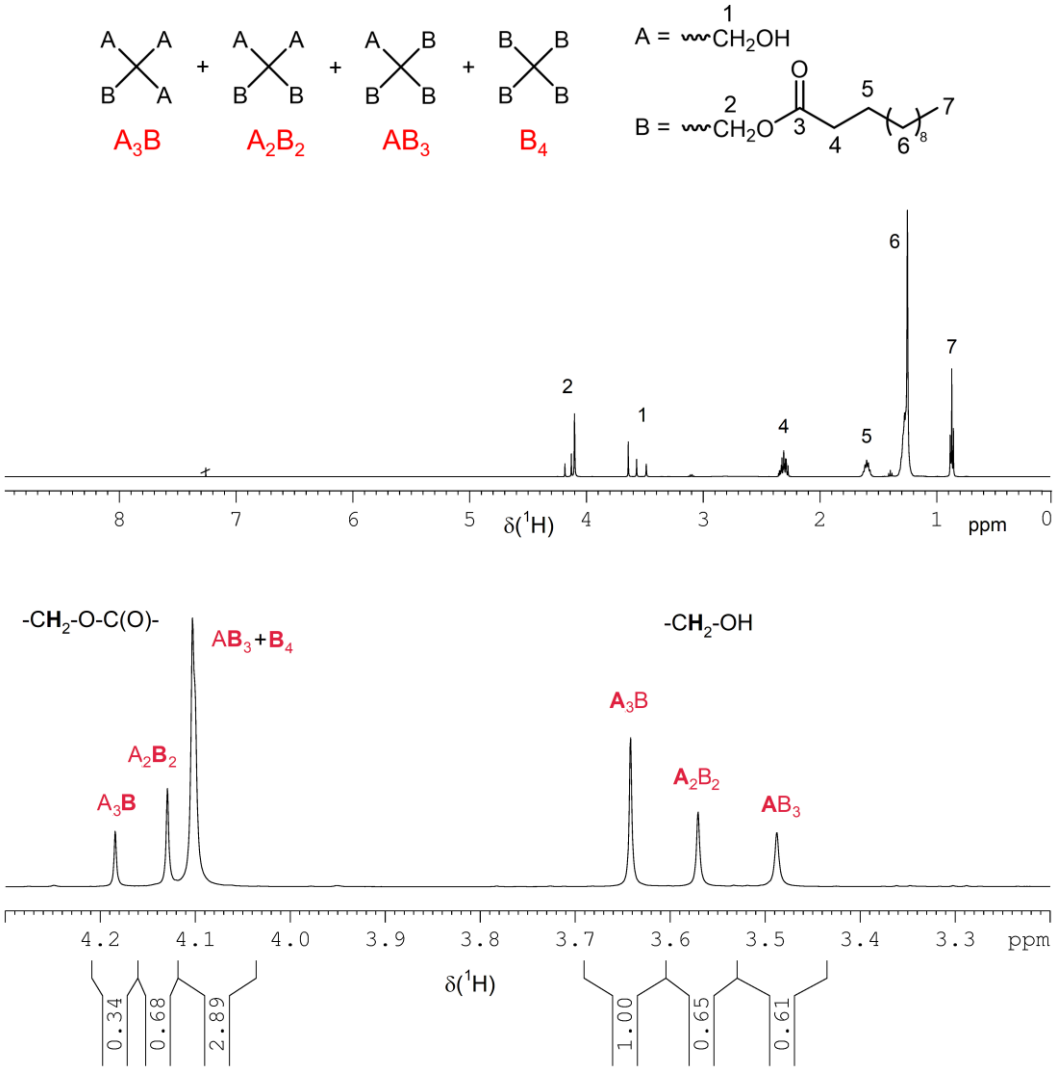

Figure A.5. 13: ^{1}H NMR spectrum (top) and enlarged region (bottom) of the mixture of **7** (A_3B – B_4) (solvent: $CDCl_3$).

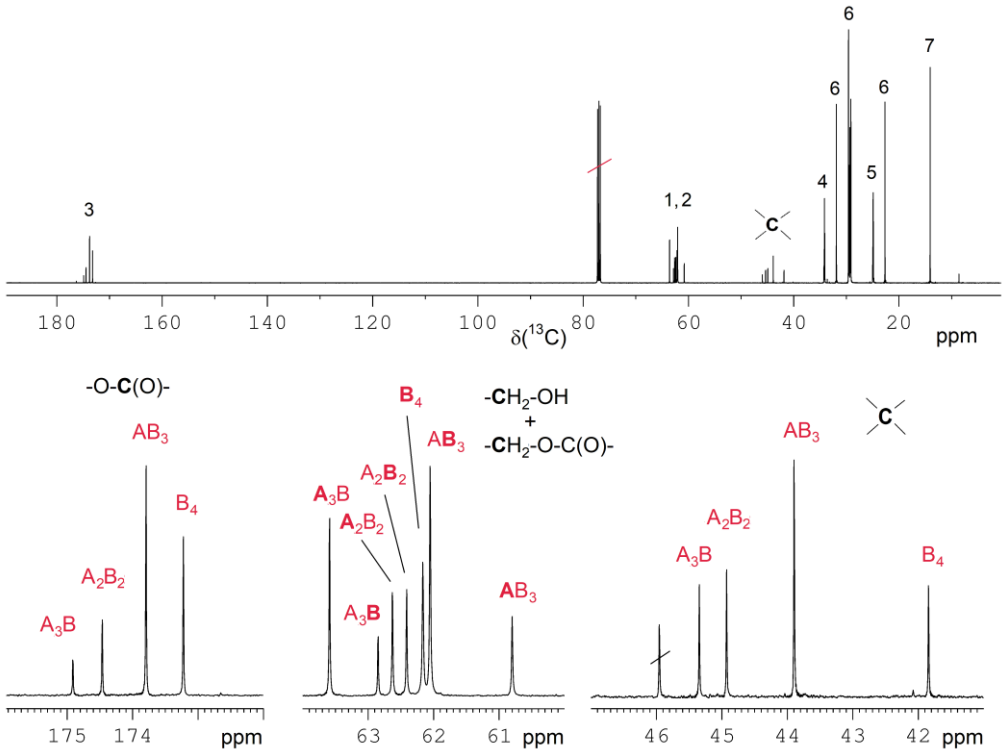

Figure A.5. 14: ^{13}C NMR spectrum (top) and enlarged regions (bottom) of the mixture of **7** (A_3B – B_4) (solvent: $CDCl_3$).

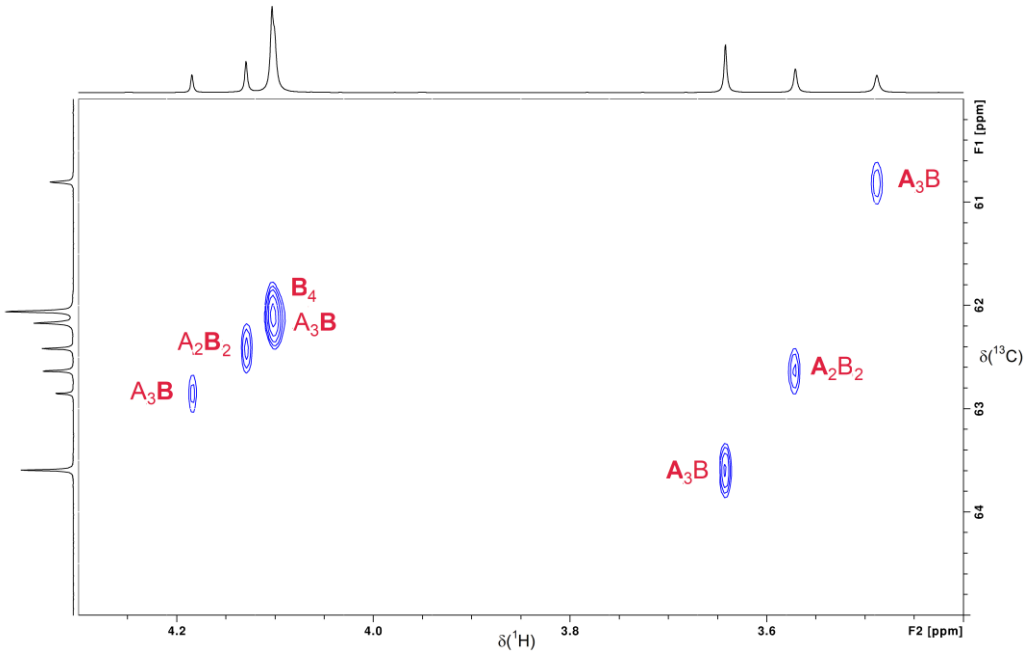

Figure A.5. 15: HSQC spectrum (region of $–CH_2OH$ and $–CH_2OR$ groups) of the mixture of **7** (A_3B – B_4) (solvent: $CDCl_3$).

A.5.7. NMR spectroscopic investigation of model compound 8

NMR spectra of partially (C_3B, C_2B_2, CB_3) and completely (B_4) esterified pentaerythrol with dodecanoate as ester moiety. Initially unreacted hydroxymethylene groups (A) are reacted to benzoxazinone end groups (C).

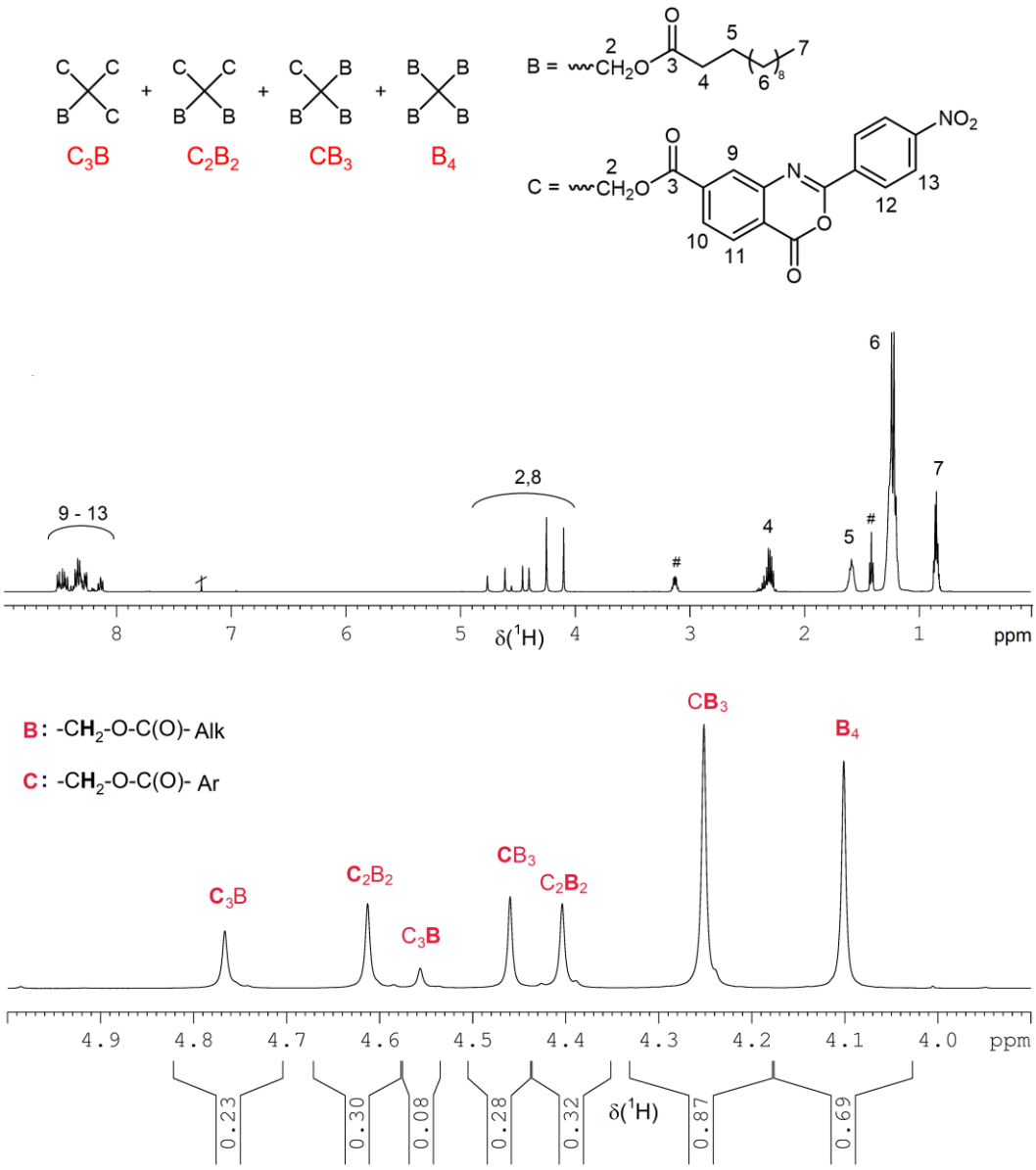

Figure A.5. 16: ^{1}H NMR spectrum (top) and enlarged region (bottom) of the mixture of **8** (C_3B – B_4) (solvent: $CDCl_3$).

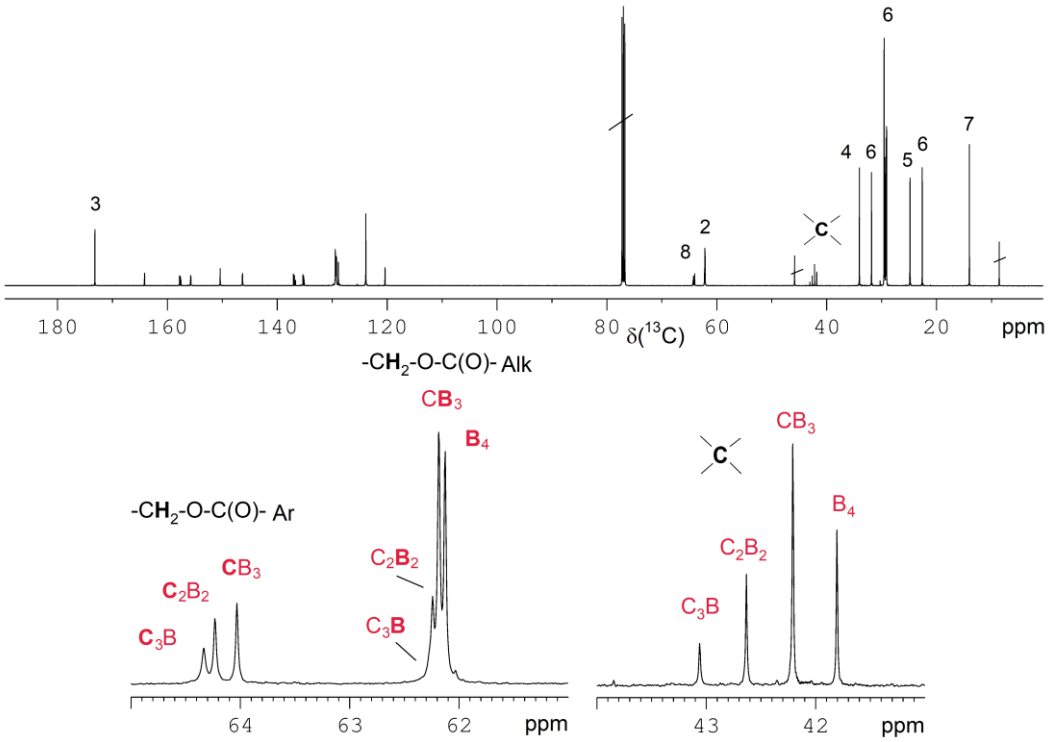

Figure A.5. 17: ^{13}C NMR spectrum (top) and enlarged regions (bottom) of the mixture of **8** (C_3B – B_4) (solvent: $CDCl_3$).

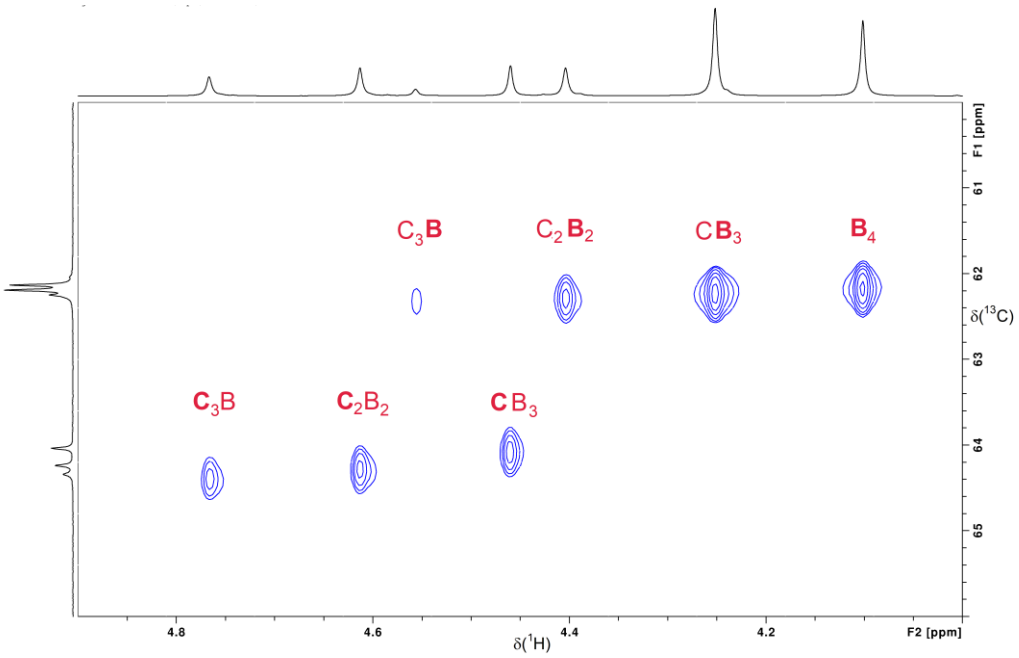

Figure A.5. 18: HSQC spectrum (region of –$CH_2OC(O)$Alk and –$CH_2OC(O)$Ar groups) of the mixture of **8** (C_3B – B_4) (solvent: $CDCl_3$).

A.5.8. Temperature-dependent ^{1}H NMR spectroscopic investigation of 6a and 6b in water

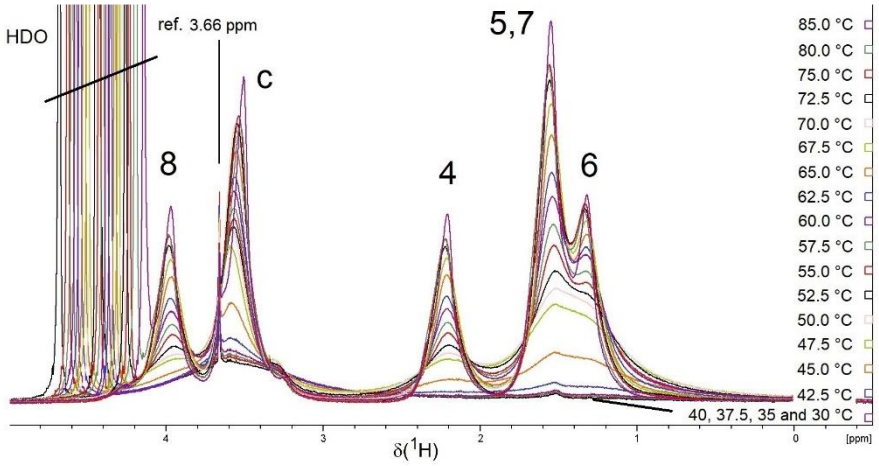

Figure A.5. 19a: Variable temperature (VT) ^{1}H NMR spectra (region) of a suspension of **6a** with short PEG chains in D_2O (5 g L^{-1}). The sample is turbid also at 85°C. The signal at 3.66 ppm is a trace of PEG not bonded to the core.

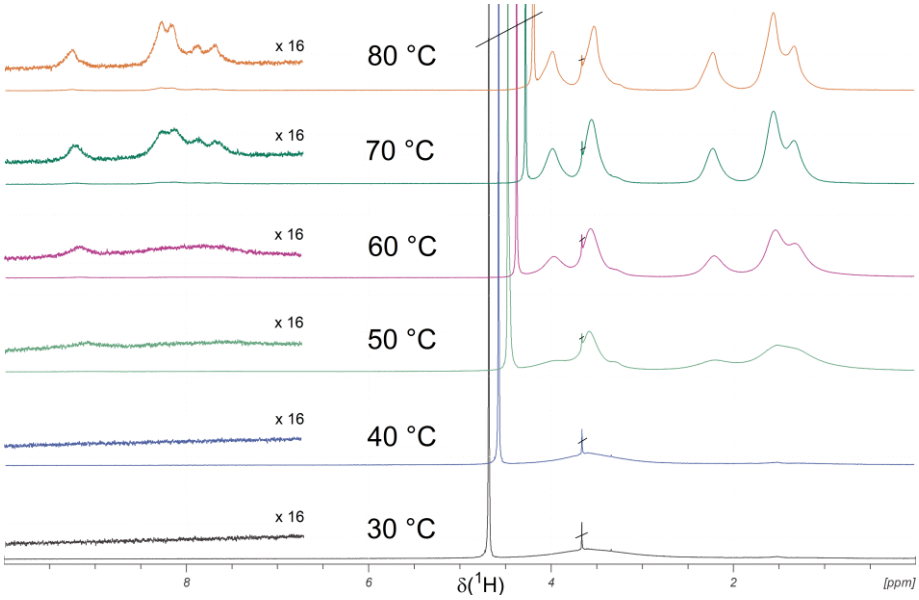

Figure A.5. 19b. Selected VT ^{1}H NMR spectra of a suspension of **6a** with short PEG chains in D_2O (5 g L^{-1}). The region of signals of the benzoxazinone-based linking group between PCL star and PEG arms is enlarged by a factor of 16.

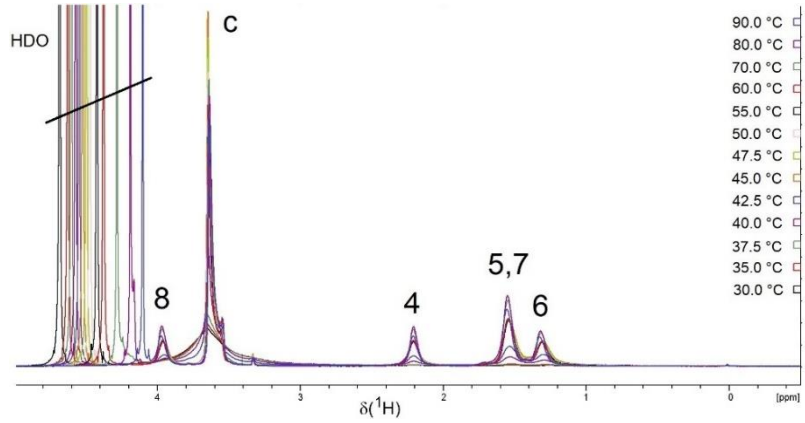

Figure A.5. 20a: VT ^{1}H NMR spectra (region) of a suspension of **6b** with long PEG chains in D_2O (5 g L^{-1}). The sample is clear at 90°C and very likely at lower temperatures. The magnification is lower compared to **Figure A.5. 19a.**

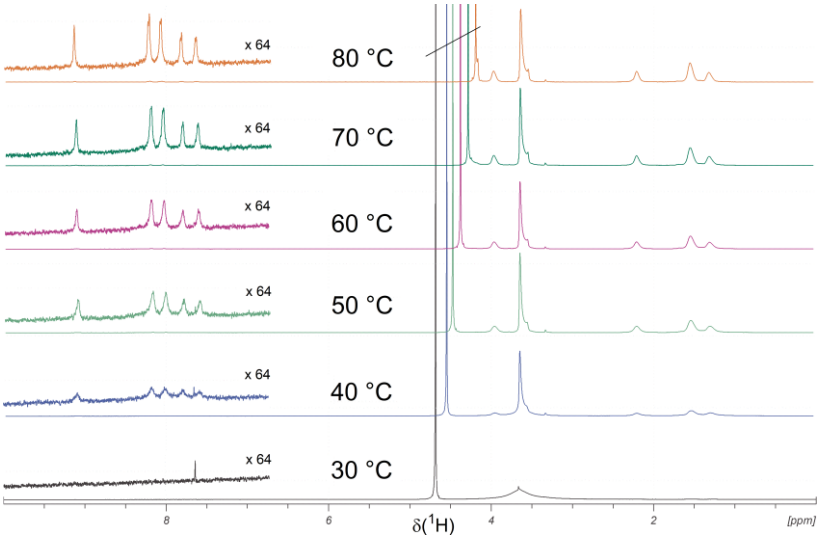

Figure A.5. 20b. Selected VT ^{1}H NMR spectra of a suspension of **6b** with long PEG chains in D_2O (5 g L^{-1}). The region of signals of the benzoxazinone-based linking group between PCL star and PEG arms is enlarged by a factor of 64.

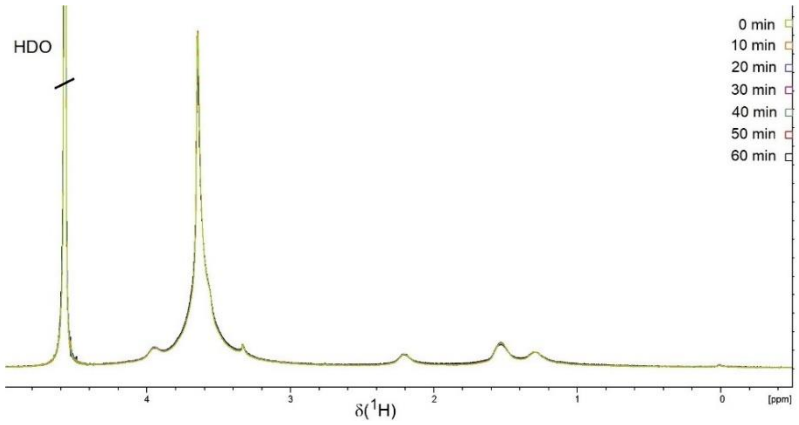

Figure A.5. 21: ^{1}H NMR spectra (region) of a suspension of **6b** (long PEG chains) in D_2O (5 g L^{-1}) recorded at 40 °C over a period of one hour. The spectra were recorded during the VT measurements depicted in **Figure A.5. 20** (heading period).

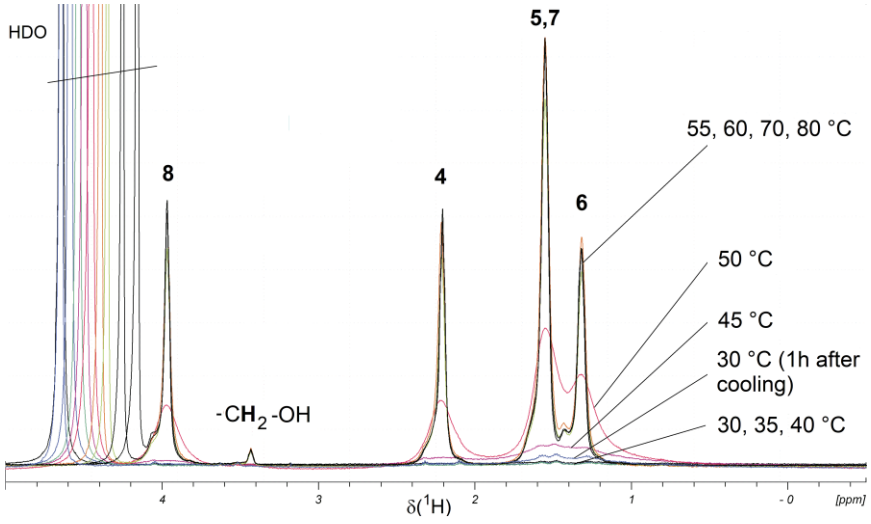

Figure A.5. 22: VT ^{1}H NMR spectra (region) of a suspension of **1a** in D_2O (5 g L^{-1}). The sample was turbid over the whole temperature range. Droplets were observed at T > 50°C.

A.5.9. Molar mass characterization of 1, 3, 5, 6 by MALDI-TOF and MD-SEC

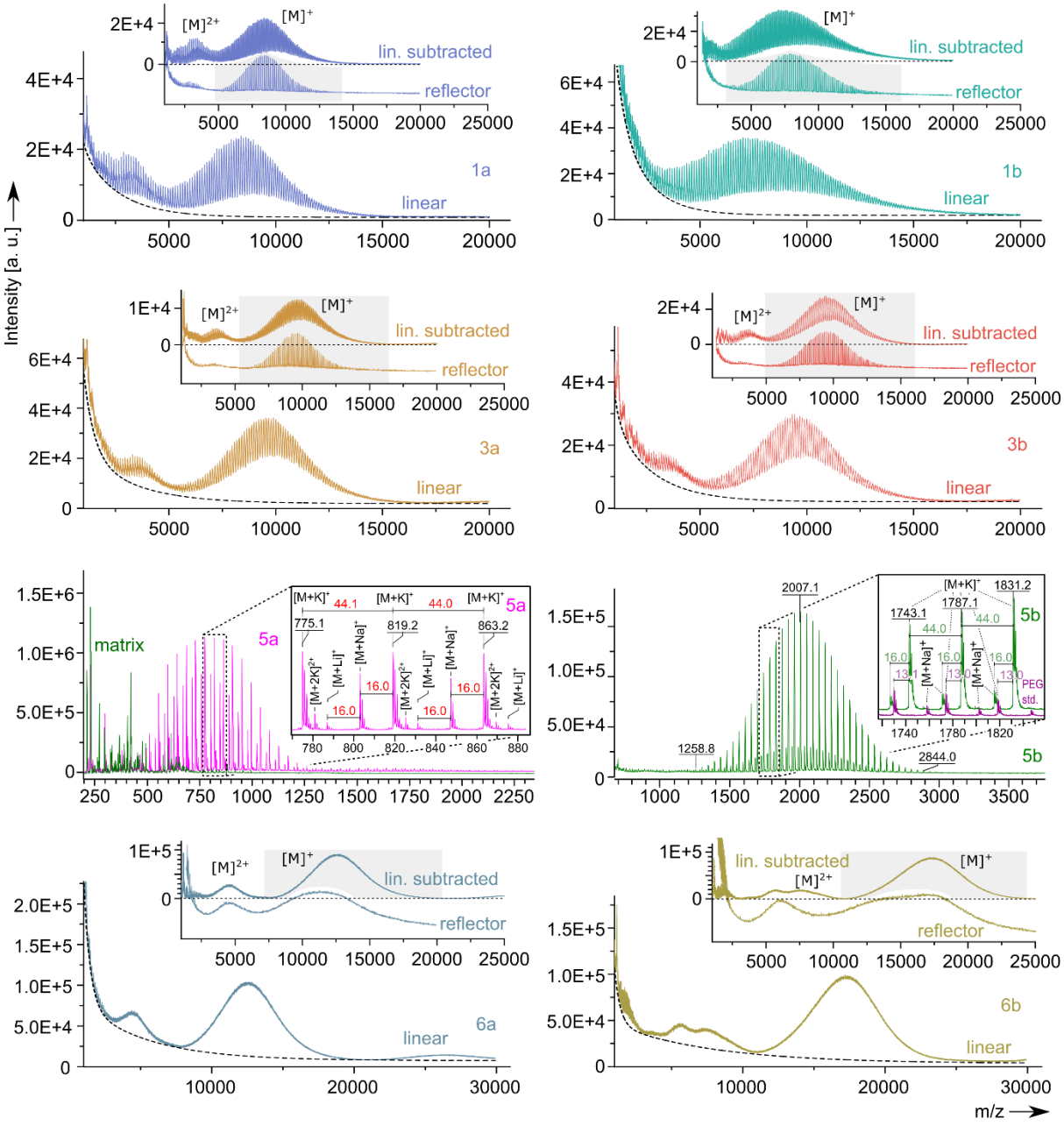

Figure A.5. 23: MALDI-TOF MS of **1a, 1b, 3a, 3b, 5a, 5b, 6a** and **6b** measured in linear and reflector TOF mode. For **5a, 5b**, masses below m/z 170 were suppressed by deflection. For all other samples, masses below m/z 700 were suppressed. Spectra of 6000 shots were accumulated each. Calibration and method verification were done with a hydroxy-terminated PEG MALDI-TOF calibration standard (PSS-mixkit) by PSS-Polymer Standards Service GmbH. Spectra recording and evaluation was done by using the software package Compass for flex series, Version 1.4. The dashed lines indicate the baseline being subtracted to yield a baseline-subtracted linear mode spectrum for molar mass average calculation. The molar mass averages reported in **Table 5. 1** of the main article were determined from the main fraction (single-charged adduct $[M]^+$) indicated by the marked grey zone. Assignments for 5a, 5b refer to the single-charged main potassium adduct $[M+K]^+$, the sodium adduct $[M+Na]^+$ with $\Delta m/z = -16$, the lithium adduct $[M+Li]^+$ with $\Delta m/z = -32$ or the double-charged adduct $[M+2K]^{2+}$, respectively.

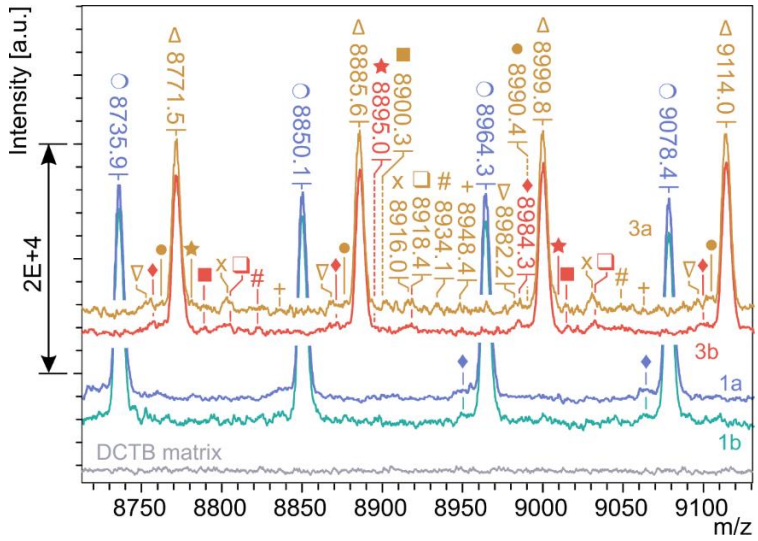

Figure A.5. 24: Trace impurity identification in MALDI-TOF mass spectra measured in reflector mode of **1** and **3**. The assigned mass traces are identified as reported in **Table A.5. 2**.

Table A.5. 2: Identified molecule mass traces found (barely resolved) in the MALDI-TOF mass spectra of **1** and **3**.

Symbol	m/z	$m/z_{theo.}$	Δm/z	$Δm/z_{theo.}$	Matched composition adducts
○	8964.3	8964.22	-	-	$[P\text{-}(PCL)_{77}H_4 + K]^+$
△	8999.8	8999.68	1177.3	1176.88	$[P\text{-}(PCL)_{67}(Bx\text{-}NO_2)_4 + K]^+$
♦	8984.3	8983.57	1161.4	1160.77	$[P\text{-}(PCL)_{67}(Bx\text{-}NO_2)_4 + Na]^+$
#	8934.1	8933.74	883.1	882.66	$[P\text{-}(PCL)_{69}(Bx\text{-}NO_2)_3H + K]^+$
❑	8918.4	8917.63	867.6	866.55	$[P\text{-}(PCL)_{69}(Bx\text{-}NO_2)_3H + Na]^+$
★	8895.0	8895.65	844.0	844.57	$[P\text{-}(PCL)_{69}(Bx\text{-}NO_2)_3H + H]^+$
▽	8982.2	8981.95	589.0	588.44	$[P\text{-}(PCL)_{72}(Bx\text{-}NO_2)_2H_2 + K]^+$
+	8948.4	8943.86	555.1	550.35	$[P\text{-}(PCL)_{72}(Bx\text{-}NO_2)_2H_2 + H]^+$
X	8916.0	8916.01	294.6	294.22	$[P\text{-}(PCL)_{74}(Bx\text{-}NO_2)H_3 + K]^+$
■	8900.3	8899.91	278.5	278.11	$[P\text{-}(PCL)_{74}(Bx\text{-}NO_2)H_3 + Na]^+$
●	8990.4	8992.07	254.5	256.13	$[P\text{-}(PCL)_{75}(Bx\text{-}NO_2)H_3 + H]^+$
♦	8948.7	8948.11	15.6	16.10	$[P\text{-}(PCL)_{77}H_4 + Na]^+$

Molecule composition declaration:

P- assigns the pentaetrythrit core unit

$(PCL)_x$ assigns the no. of poly(ε-caprolactone) repeating units in total

$(Bx\text{-}NO_2)_x$ assigns the no. of 2-(4-nitrophenyl)-benzoxazinone terminal units

$Δm/z$ and $Δm/z_{theo.}$refer to the actual and theoretical mass difference of the identified mass trace to the potassium adduct of a $P\text{-}(PCL)_{xx}H_4$ with equal total number of PCL repeating units.

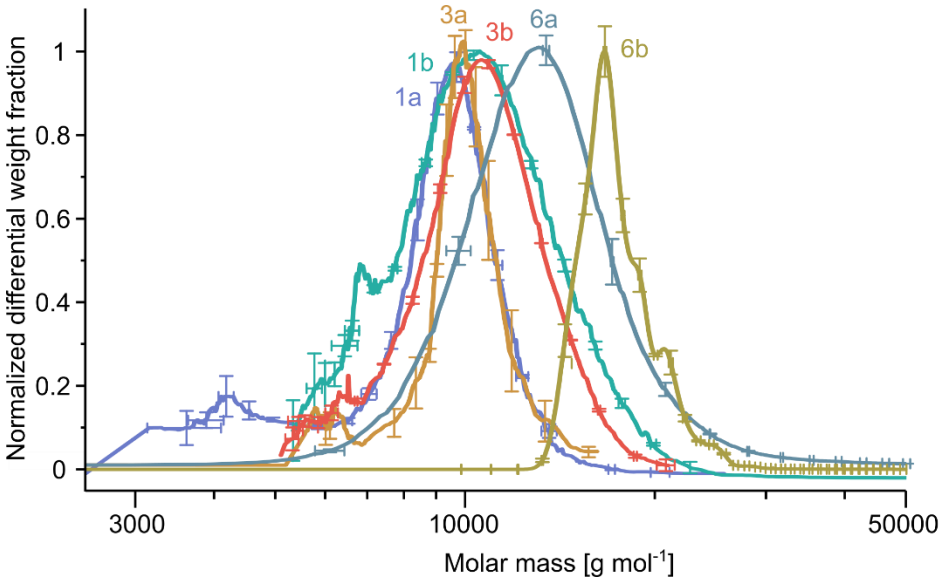

Figure A.5. 25: Differential molar mass distribution determined by MD-SEC of the star polymers **1**, **3**, **6a** and **6b** in THF. The corresponding molar mass averages are reported in **Table 5. 1** of the main article.

A.5.10. Relevant parameters for PCL-b-PEG block and star block copolymers (literature survey)

Table A.5. 3: Characteristics of *f* -arm PCL-b-PEG star block copolymers (references).

Ref.	f [a]	Core [b]	Tail [c]	Strategy [d]	M_n [e] [10^3 g mol^{-1}]	M_{PCL} [f] [10^3 g mol^{-1}]	M_{PEG} [f] [10^3 g mol^{-1}]	PDI [g]	CMC [h]	Size [i] [nm]	Type [j]
[6]	3, 4	B, P	PEG	**a**	29 - 40	4.7 - 5.1	5 - 5.2	1.17 - 1.32	8 - 22 g L^{-1}	115 - 129	-
[7]	4	C	PEG	**a**	28 - 55	1.9 - 8.6	5	1.23 - 1.34	80 - 322 μg L^{-1}	69 - 71	-
[8]	3, 4	n. i.	PCL	**c**	22 - 31	1.2 - 4.2	5 - 6	1.24 - 1.34	-	20 - 85	-
[9]	4	n. i.	PCL	**c**	24 - 31	1.1 - 2.8	5	1.28 - 1.34	32 - 320 μg L^{-1}	20 - 42	**s**
[10]	3, 4, 8	T, P, n.i.	PCL	**c**	31 - 43	2.6 - 7.3	1.3 - 3.1	1.04 - 1.24	-	-	-
[11]	8	n. i.	PCL	**c**	26 - 29	0.7 - 1.1	2.5	1.22 - 1.23	3 - 4.3 g L^{-1}	20 - 40	-
[12]	4	P	PEG	**c**	11 - 52	0.8 - 8.6	2 - 7.7	1.87 - 2.01	1.1 - 2.1 mg L^{-1}	-	-
[13]	3	T	PEG	**g**	25 - 81	5.1 - 10.3	2 - 4	1.16 - 1.23	1.1 mg L^{-1}	13 - 32	**s**
[14]	4	P	PEG	**g**	27	5.1	2	1.23	10 - 23 mg L^{-1}	45	**s**
[15]	4, 6	P, DP	PEG	**g**	11 - 59	2.3 - 5.5	4.9	1.08 - 1.19	0.43 - 2.1 mg L^{-1}	47 - 361	-
[16]	4→8 [k]	P	PEG	**g**	22 - ? [l]	1.7	1.1 - 2	1.5 - ?	16 - 79 μg L^{-1}	92 - 105	**s**
[17]	7	β-CD	PEG	**g**	26 - 51	1.2 - 5	1.1 - 2	1.1 ?	-	14 - 42	**s**
[18]	8	R	PEG	**g**	20 - 53 [m]	1.5 - 4.5 [m]	1 - 2	1.25 - 1.41	0.6 - 2.8 mg L^{-1}	16 - 33	**s**
[19]	16	D	PEG	**g**	131	3.1	5	1.02	3 mg L^{-1}	17/75 [n]	-
[20]	32	D	PEG	**g**	215	2.8	5	1.07	-	16/134 [n]	**s**

[a] Number of star arms

[b] Chemical structure of the core: B = 1,3,5-benzenetricarboxylic acid, P = pentaerythritol, DP = dipentaerythritol, C = chlorin, D = polyamidoamine dendrimer, T = tris(hydroxymethyl)propane, β-CD = per-2,3-acetyl-β-cyclodextrin, R = resorcinarene, n. i. = no information

[c] Polymer of the outer block

[d] Synthesis strategy: **a** = arm first, **c** = core first, **g** = grafting from

[e] Number average molar mass of the star in Dalton

[f] Number average molar mass of PCL and PEG blocks (one star arm), respectively in Dalton

[g] polydispersity index of the stars

[h] critical micellar concentration in water

[i] size of micelles in water

[j] type of micelles in water (**s** for spherical micelles)

[k] two outer PCL-PEG blocks were attached to each of four inner PCL chains

[l] unclear or missing information

[m] based on NMR data and PEG precursor weight

[n] bidisperse distributions

Table A.5. 4: Characteristics of PCL-b-PEG block copolymers (references).

Ref.	Analysis [a]	Type [b]	% PEO [c]	M_n [10^3 g mol^{-1}]	PDI	Ø [d] [nm]	↔ [e] [nm]
[21]	cryo-TEM	V	0.17 - 0.28	11.4 - 6.8	1.19 - 1.28	100 - 1000+	16 - 18
		C	0.2 - 0.28	9.6 - 5.2	1.2 - 1.28	18 - 21	50 - 1000+
		S	0.34 - 0.43	5.6 - 4.4	1.2 - 1.23	19 - 25	-
[22]	FM, SE	P	≥ 0.11 [h]	13.4 - 20.6	1.48 - 1.57	-	-
		V	0.13 - 0.36	4.1 - 34.6	1.42 - 1.6	~500 - ~5000 [i]	-
		C	0.13 - 0.25	7.9 - 15.5	1.42 - 1.6	-	1000-20000
		S [f]	0.28 - 0.65	1.5 - 19.9	1.23 - 1.6	-	-
[23]	cryo-TEM	C	0.42 - 0.55	≤ 4.77 | ≤ 11.5	≥ 1.19 | ≥ 1.3	11 | 29	10000+
		S	≥ 0.55	≤ 3.9 | ≤ 9.5	> 1.19 | > 1.3	~11 | ~29	-
[24]	FM	V	0.15	14	1.2	100 - 10000	22.5 ± 2.3
[25]	FR, TAN	V	0.09 - 0.25	8 - 21	1.32 - 1.52	60 - 260 [j]	~18 - 36
		S	0.09 - 0.25	8 - 21	1.32 - 1.52	-	-
[26]	TEM with PTA	S	0.15 - 67	4.8 - 32	1-08 - 1.19	10 - 40	-
		C	0.22	8.7	1.05	20	-
		L	0.11 - 0.16	12 - 18	1.09 - 1.10	20	-
[27]	TEM with UAC	S, C, L [g]	0.55	9.1	1.15	22 - 45	-
	cryo-TEM with UAC	C, unclear	0.55	9.1	1.15	24	-

[a] Analysis:

cryo-TEM … TEM of rapidly frozen samples, FM … flourescence microscopy,

SE … solvent evaporation method, FR … film rehydration method,

UAC … uranyl acetate, PTA … phosphotungstic acid.

[b] Types of particles:

S … spherical, C … cylindrical, V … vesicles, L … lamellar structures, P … precipitate.

[c] %PEO is the weight fraction of PEO (virtually identical to volume fraction of PEO) in the polymer.

[d] diameter of the micelles, cylinders, and vesicles.

[e] length of the cylindrical worms or the thickness of the vesicle wall. If cryo-TEM is used, only the dimensions of the PCL core can be analyzed**.**

[f] S6 of Ref. [22] shows spheres for the smallest polymers, which are not mentioned in Table S1 of Ref [22]**.**

[g] different morphologies were observed for different concentrations of the stock solution.

[h] calculated using Table S1 of the SI of Ref. [22].

[i] estimated from Figures in Ref. [22] as no quantitative analysis is performed; FR produces vesicles up to 40 μm.

[j] Vesicle diameter increases as a function of the temperature for the TAN method; highest stirring speed and concentrations of 1 mg mL^{-1} were used. Also, a significant dependence on the solvent used for the TAN method is recognized: precipitation from THF produces results comparable to FR, while DMSO, acetone, or methanol produce different results.

Table A.5. 5: Flory-Huggins interaction parameters χ between PEG or PCL and possible good solvents for both polymers (references).

	Ref.	Method [a]	T [K]	M_n / M_w [kg mol^{-1}]	Solvents [b]					
					THF	TO	AC	CHL	DCM	EA
PEG	[28]	IGC	303	0.4 / -	0.7	-	0.5	-0.4	-0.6	0.8
	[29]	IGC	298 [h]	- / 300	-	0.41	0.77	-	-	0.51
	[30]	GLC	343	10.7 / 11.5	-	0.29	-	-0.76	-	-
	[31] [c]	GLC	343	4000 / -	0.19	0.39	0.25	-	-	-
	[32]	theory [e]	298	- / -	0.38	0.30	0.54	-1.04	-	0.46
	[33]	mixed	373	- / -	0.30	0.26	0.47	-0.55	-0.51	0.39
	[34] [d]	IGC	358	35 / -	-	0.769	-	-0.683	-	-
	[35]	swelling	298	4.6 / 5.2	0.38	-	0.451	-	-	-
	[36]	viscosity [f]	298	11.4 / 12.4	0.41	0.38	-	-1.61	-	-
PCL	[32]	theory [e]	298	- / -	0.18	0.09	0.64	-0.71	-	0.36
	[33]	mixed	373	- / -	0.13	0.08	0.46	-0.4	-0.26	0.36
	[36]	viscosity [f]	298	10.4 / 10.6	-0.05	0.07	-	-0.54	-	-
	[37]	IGC	343	33 / -	-	-0.01	-	-	-	0.32
	[38]	IGC	343	33 / -	0.30	-	-	-	-	-
	[39]	IGC	343	- / -	0.13	0.06	0.55	-0.6	-	0.36
	[40]	visual [g]	298	14, 65 / -	s-p [i]	s-n [j]	p-n [k]	s	-	p-n [k]

[a] Inverse gas chromatography (IGC), gas-liquid chromatography (GLC), swelling refers to an analysis where the Flory-Rehner and Bray-Merill model were enriched by a discussion of network defects [41].

[b] Tetrahydrofuran (THF), toluene (TO), acetone (AC), chloroform (CHL), dichloromethane (DCM), ethyl acetate (EA).

[c] Original data were re-analyzed by Monique Galin and taken from Table 2 of Ref. [31].

[d] Only data for 10K PEG at lowest temperature is included in the table.

[e] theoretical estimate based upon the model of Tian and Munk [32]; parts of these data were published previously [36].

[f] viscosity data for ~11K star polymers was normalized by an average over the corresponding interaction estimates of Ref. [33] for PEG and PCL and refers to the dilute limit.

[g] PEG with 14K and 65K molar mass was dissolved in rather high concentrations (either 0.5 g or 2.5 g per 5 ml of solvent) and the solution was checked visually regarding dissolution of the polymer. The results were classified as soluble (s), partially soluble (p), and non-soluble (n).

[h] extrapolated from temperature range 343-363 K.

[i] 65K PEG at large concentrations was only partially soluble.

[j] 14K PEG was soluble, while 65K was partially soluble at low concentrations and non-soluble at high concentrations.

[k] 14K PEG was soluble, while 65K was not.

The interactions between PEG or PCL and the potential good solvents tetrahydrofuran (THF), toluene (TO) acetone (AC), chloroform (CHL), dichloromethane (DCM), and ethyl acetate (EA), were analyzed in several works based upon different methods, see Table. The scatter of the data stems in part from the method since the interaction parameters depend on polymer volume fraction [41] and measurement temperature T [42] (chromatographic data refers to the limit of high polymer volume fractions, swelling data is obtained in the semi-dilute regime, while viscosity data is collected in the dilute limit). End group corrections [43] were minimized by selecting the data for the largest polymers and temperature dependence was reduced by selecting measurement conditions closest to room temperature, if possible. Altogether, chloroform and dichloromethane are very good solvents for both polymers independent of the concentration range for all temperatures under investigation. THF and toluene are good solvents for PCL but may cross-over to theta or poor for PEG depending on experimental conditions. Ethyl acetate has somewhat poorer solvent quality than these for both polymers, while acetone is theta to poor for both polymers.

A.5.1. References

[1] M. Rossberg, W. Lendle, G. Pfleiderer, A. Tögel, T.R. Torkelson, K. K. Beutel, Chloromethanes. *Ullmann's Encyclopedia of Industrial Chemistry.* (2011). https://onlinelibrary.wiley.com/doi/epdf/10.1002/14356007.a06_233.pub3.

[2] Dortmund Data Bank; http://www.ddbst.com/en/EED/PCP/VIS_C4.php

[3] B. González, N. Calvar, E. Gómez, Á. Domínguez, *J. Chem. Thermodyn.* **39**, (2007) 1578-1588

[4] CRC Handbook of Chemistry and Physics, R. C. Weast, CRC Press Inc.,U.S.; 56th Revised edition (1975), ISBN: 978-0878194551

[5] CRC Handbook of Chemistry and Physics, W. M. Haynes (ed.) 94th Edition. CRC Press LLC, Boca Raton: FL 2013-2014, 3-250

[6] K. H. Kim, G. H. Cui, H. J. Lim, J. Huh, C.-H. Ahn, W. H. Jo, *Macromol. Chem. Phys.* **205** (2004) 1684-1692.

[7] C.-L. Peng, J.-J. Shieh, M.-H. Tsai, C.-C. Chang, P.-S. Lai, *Biomaterials* **29** (2008) 3599-3608.

[8] C. Lu, S.-R. Guo, Y-Zhang, M. Yin, *Polym Int.* **55** (2006) 694-700.

[9] C. Lu, L. Liu, S.-R. Guo, Y. Zhang, Z. Li, J. Gu, *Eur. Pol. J.* **43** (2007) 1857-1865.

[10] Y. K. Choi, Y. H. Bae, S. W. Kim, *Macromolecules* **31** (1998) 8766-8774.

[11] S. J. Buwalda, B. Nottelet, J. Coudane, Polymer Degradation and Stability 137 (2017) 173-183.

[12] M. Deng, Y. Chen, L. Piao, X. Zhang, Z. Dai, X. Jing, *J. Pol. Sci A* **42** (2004) 950-959.

[13] G. Jiang, H. Xu, *J. Appl. Pol. Sci.* **118** (2010) 1372-1379.

[14] F. Quaglia, L. Ostacolo, G. Nese, M. Canciello, G. de Rosa, F. Ungaro, R. Palumbo, M. Immacolata La Rotonda, G. Maglio, *J. Biomed. Mater. Res.* **87A** (2008) 563-574.

[15] H. J. Lim, H. Lee, K. H. Kim, J. Huh, C.-H. Ahn, J. W. Kim, *Colloid Polym. Sci.* **291** (2013) 1817-1827.

[16] S. Khoee, A. Kavand, F. H. Nasr, *Polym. Int.* **64** (2015) 1191-1201.

[17] P.-F. Gou, W.-P. Zhu, N. Xu, Z.-Q. Shen, *J. Pol. Sci. A* **46** (2008) 6455-6465.

[18] C. Gao, Y. Wang, W.-P. Zhu, Z.-Q. Shen, *Chin. J. Pol. Sci.* **32** (2014) 1431-1441.

[19] F. Wang, T. K. Bronich, A. V. Kabanov, R. D. Rauh, J. Roovers, *Bioconjugate Chem.* **16** (2005) 397-405.

[20] F. Wang, T. K. Bronich, A. V. Kabanov, R. D. Rauh, J. Roovers, *Bioconjugate Chem.* **19** (2008) 1423-1429.

[21] J. A: Zupancich, F. S. Bates, M. A. Hillmyer, *Macromolecules* **39** (2006) 4286-4288.

[22] K. Rajagopal, A. Mahmud, D. A. Christian, J. D. Pajerowski, A. E. X. Brown, S. M. Loverde, D. E. Discher, *Macromolecules* **43** (2010) 9736-9746.

[23] Y. Geng, D. E. Discher, *J. Am. Chem. Soc.* **127** (2005) 12780-12781.

[24] P. P. Ghoroghchian, G. Li, D. H. Levine, K. P. Davis, F. S. Bates, D. A. Hammer, M. J. Therien, *Macromolecules* **39** (2006) 1673-1675.

[25] J. Zhou, R. Ni, Y. Chau, *RSC Advances* **7** (2017) 17997-18000.

[26] Z.-X. Du, J.-T. Xu, Z.-Q. Fan, *Macromolecules* **40** (2007) 7633-7637.

[27] N. Fairley, B. Hoang, C. Allen, *Biomacromolecules* **9** (2008) 2283-2291.

[28] F. Sesigur, D. S. Dasdan, O. Yazici, F. Cakar, O. Cankurtaran, F. Karaman, *Optoelectr. Adv. Mater. Rapid Commun.* **10** (2016) 97-101.

[29] M. J. Fernandez-Berridi, T. F. Otero, G. M. Guzman, J. M. Elorza, *Polymer* **23** (1982) 1361-1366.

[30] M. Galin, *Polymer* **24** (1983) 865-870.

[31] Y. H. Chang, D. C. Bonner, *J. Appl. Polym. Sci.* **19** (1975) 2439.

[32] M. Tian, P. Munk, *J. Solution Chemistry* **24** (1995) 267-284.

[33] J. E. Mark, Physical Properties of Polymers, Handbook, Springer Verlag (2006).

[34] K. Adamska, A. Voelkel, *Journal of Chromatography A* **1132** (2006) 260-267.

[35] N. J. Rebello, H. K. Beech, B. D. Olsen, *ACS Macro Letters* **10** (2021) 531-537.

[36] C. Bunk, L. Löser, N. Fribiczer, H. Komber, L. Jackisch, R. Scholz, B. Voit, S. Seiffert, K. Saalwächter, M. Lang, F. Böhme, *Macromolecules* **55** (2022) 6573-6589.

[37] A. Sarac, D. Sakar. O. Cankurtaran, F. Y. Karaman, *Polymer Bull.* **53** (2005) 349-357.

[38] A. Sarac, Ö. Cankurtaran, F. Yilmaz, *Macromol. Symp.* **217** (2004) 301-306.

[39] M. Tian, P. Munk, *J. Chem. Eng. Data* **39** (1994) 742-755.

[40] C. Bordes, V. Freville, E. Ruffin, P. Marote, J. Y. Gauvrit, S. Briancon, P. Lanteri, *Int. J. Pharmaceutics* **383** (2010) 236-243.

[41] N. Schuld, B. A. Wolf in *Polymer Handbook*, Eds. J. Brandrup, E. H. Immergut, E. A. Grulke, 4th Edition, Wiley, New York (2003), Chapter VII pp 247-264.

[42] C. M. Hansen, *Hansen Solubility Parameters*, A User's Handbook, 2nd edition, Taylor & Francis Group, LLC (2007).

[43] J. Klein, H. E. Jeberien, *Makromol. Chem.* **181** (1980) 1237.

A.6. Supporting Information Chapter IV

A.6.1. ^{1}H NMR spectroscopy investigation of star block copolymer 2

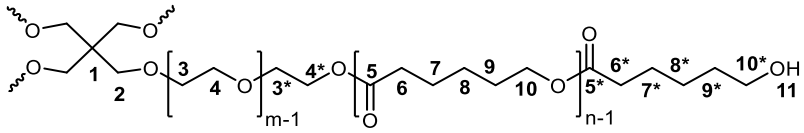

Hydroxy-terminated PEG-*b*-PCL star block copolymer **(2)**

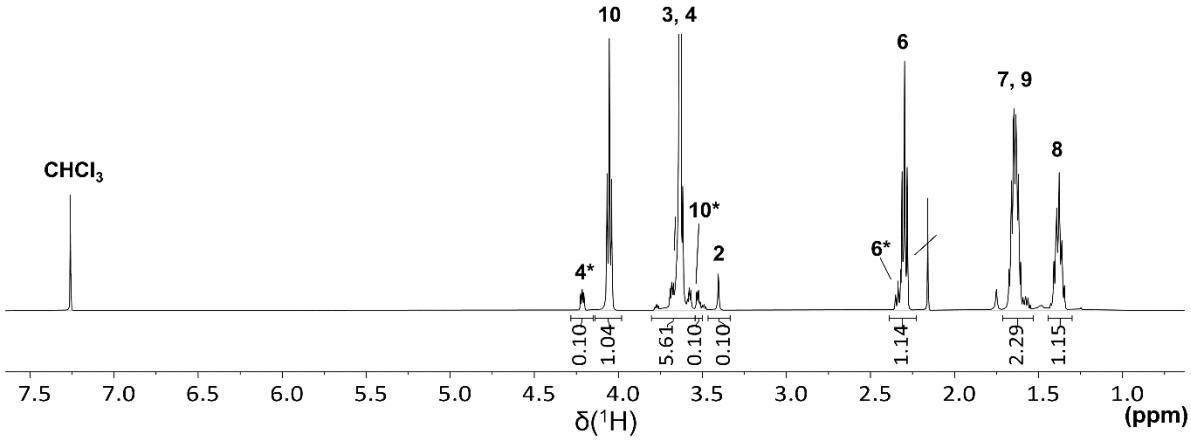

Figure A.6. 1: ^{1}H NMR spectrum of **2** with integral regions used to calculate the monomer units of the PEG block (m) and the PCL block (n) per arm as well as the number-average molar mass $M_{n,NMR}$ of **2** according to the following remarks (solvent: $CDCl_3$).

Calculation of the monomer units of the PEG block (m) and PCL block (n) per arm, and $M_{n,NMR}$:

$m = (0.25 \cdot (I_3 + I_4 + I_{4*})) / (0.5 \cdot I_2) = 1.43 / 0.05 = 29$ (estimated error: ± 2%)

$n = (0.5 \cdot (I_6 + I_{6*})) / (0.5 \cdot I_2) = 0.57 / 0.05 = 11$ (estimated error: ± 2%)

$M_{n,NMR} = 4 \cdot m \cdot M_{0,PEG} + 4 \cdot n \cdot M_{0,PCL} + M_{n,core} = 116 \cdot 44$ g mol^{-1} + $44 \cdot 114$ g mol^{-1} + 136 g mol^{-1} = 10.3 kg mol^{-1} (± 200 g mol^{-1})

A.6.2. ^{1}H NMR spectroscopic investigation of star block copolymer 3

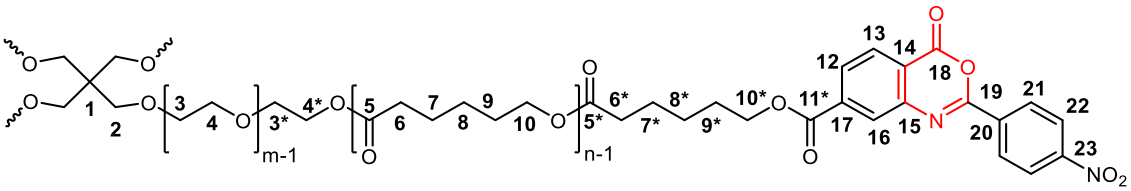

a) 2-(4-nitrophenyl)-benzoxazinone-terminated PEG-*b*-PCL star block copolymer **(3)**

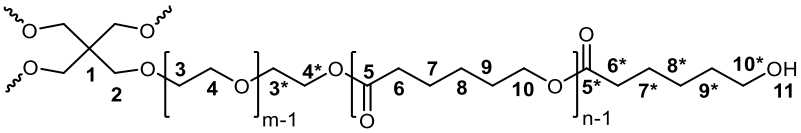

b) Hydroxy-terminated PEG-*b*-PCL star block copolymer **(2)**

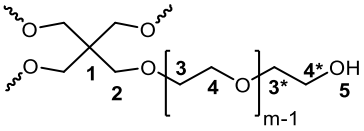

c) tetra-PEG-OH

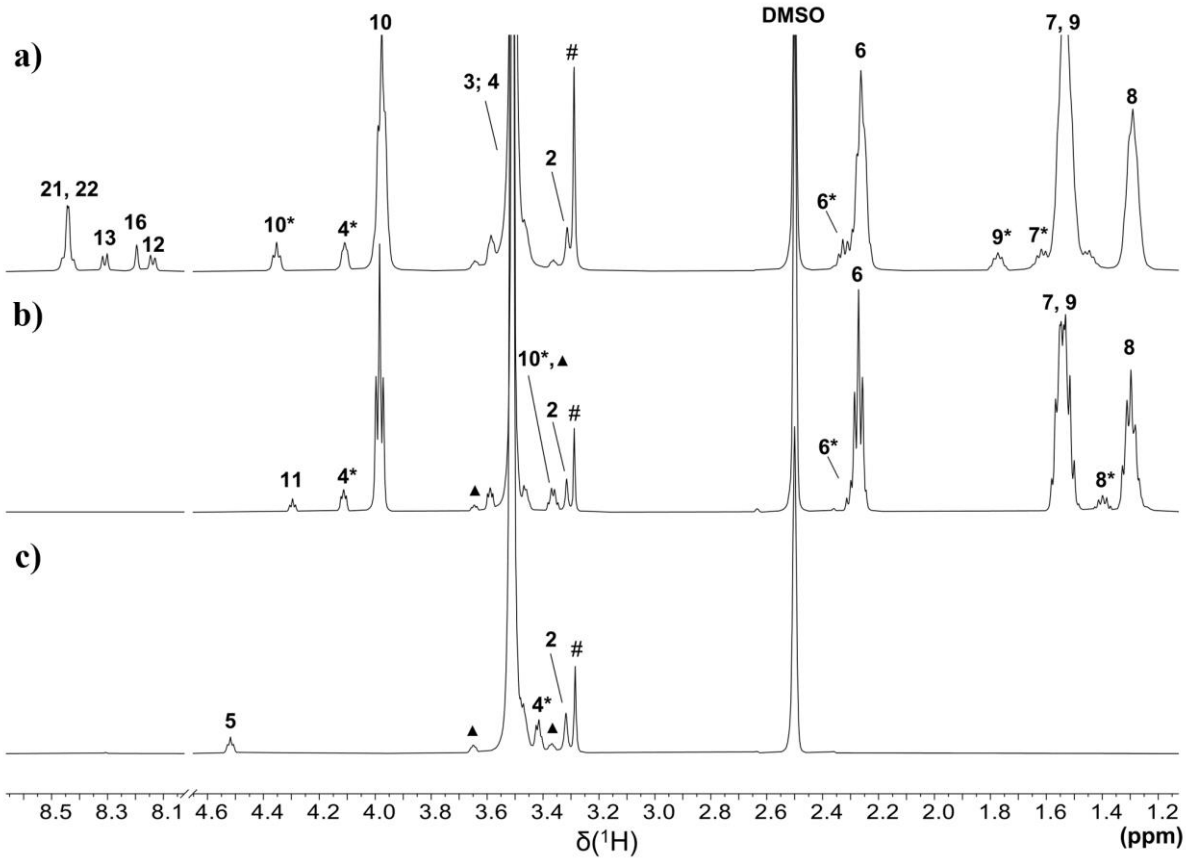

Figure A.6. 2: Chemical structures of star polymers **a)** tetra-PEG-OH, **b)** hydroxy-terminated PEG-*b*-PCL star block copolymer **(2)**, and **c)** 2-(4-nitrophenyl)-benzoxazinone-terminated PEG-*b*-PCL star block copolymer **(3)** (top) and the corresponding ^{1}H NMR spectra (bottom; solvent: DMSO-d_6). Symbol # resp. ▲ indicates H_2O resp. satellite signals.

A.6.3. ^{1}H NMR spectroscopic investigation of star block copolymer 4

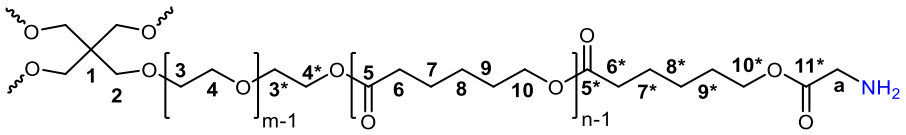

a) Amino-terminated PEG-*b*-PCL star block copolymer **(4)**

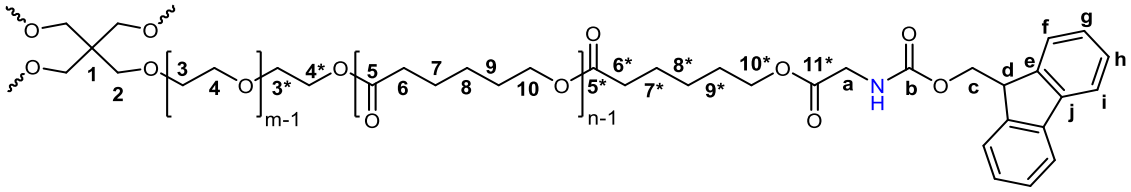

b) Fmoc-glycine-terminated PEG-*b*-PCL star block copolymer

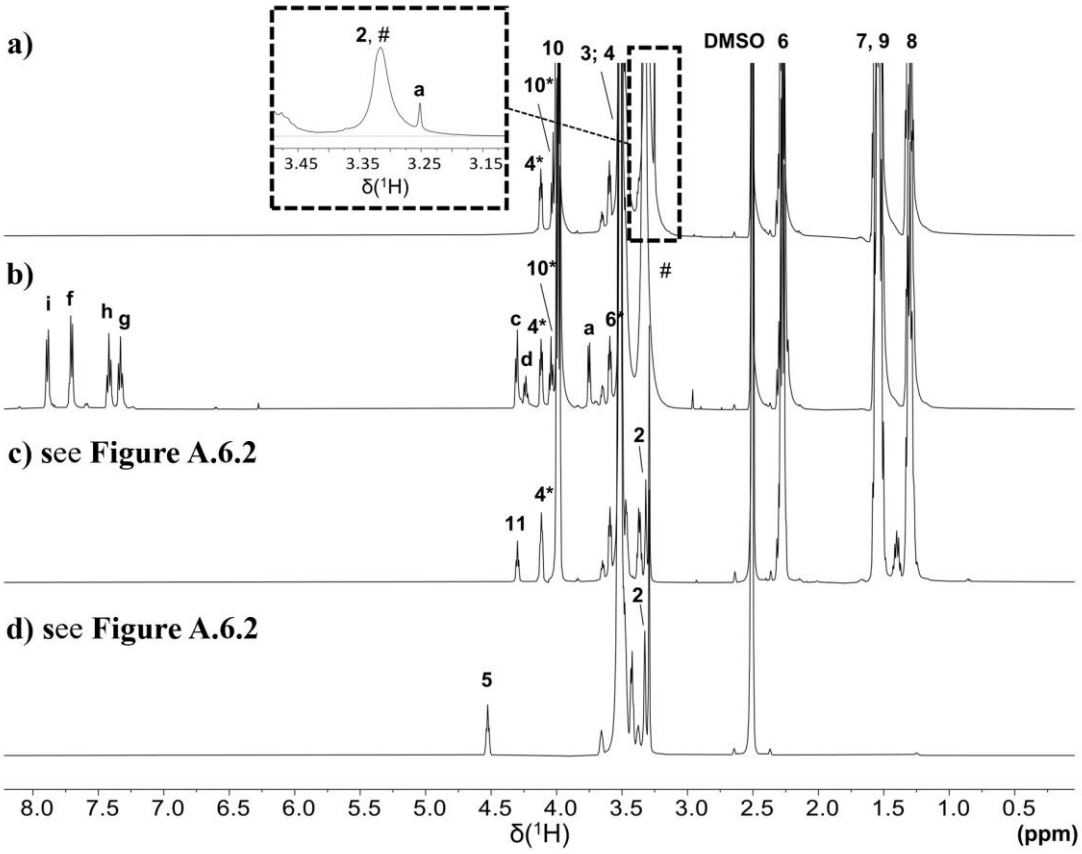

Figure A.6. 3: Chemical structures of star polymers **a)** of amino-terminated PEG-*b*-PCL star block copolymer **(4)**, **b)** hydroxy-terminated PEG-*b*-PCL star block copolymer **(2)**, and **c)** 2-(4-nitrophenyl)-benzoxazinone-terminated PEG-*b*-PCL star block copolymer **(3)** (top) and the corresponding ^{1}H NMR spectra (bottom; solvent: DMSO-d_6). Symbol # resp. ▲ indicates H_2O resp. satellite signals. Chemical structure of amino-terminated PEG-*b*-PCL star block copolymer **(4)** and the corresponding 2D ^{1}H NMR spectrum (solvent: DMSO-d_6). Symbol # indicates H_2O.

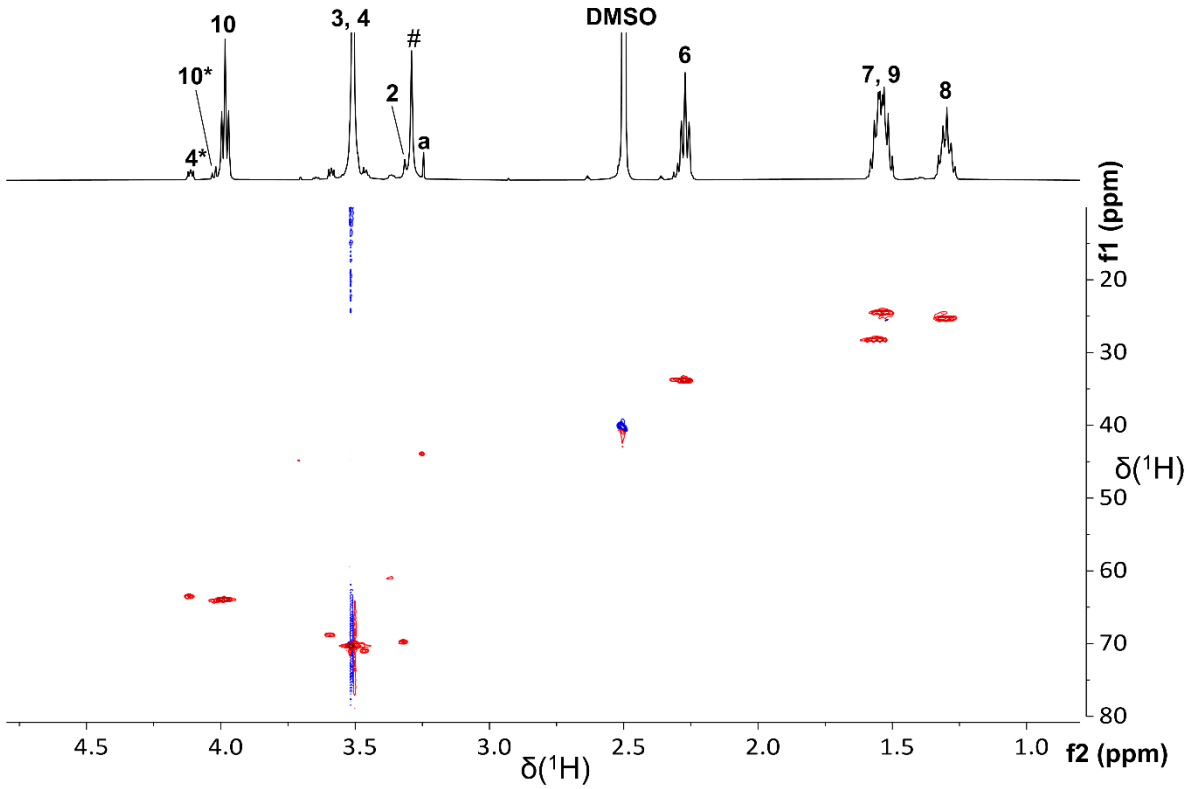

Figure A.6. 4: 2D ^{1}H NMR spectrum of **4** (solvent: DMSO-d_6). Symbol # indicates H_2O.

A.6.4. MALDI TOF MS

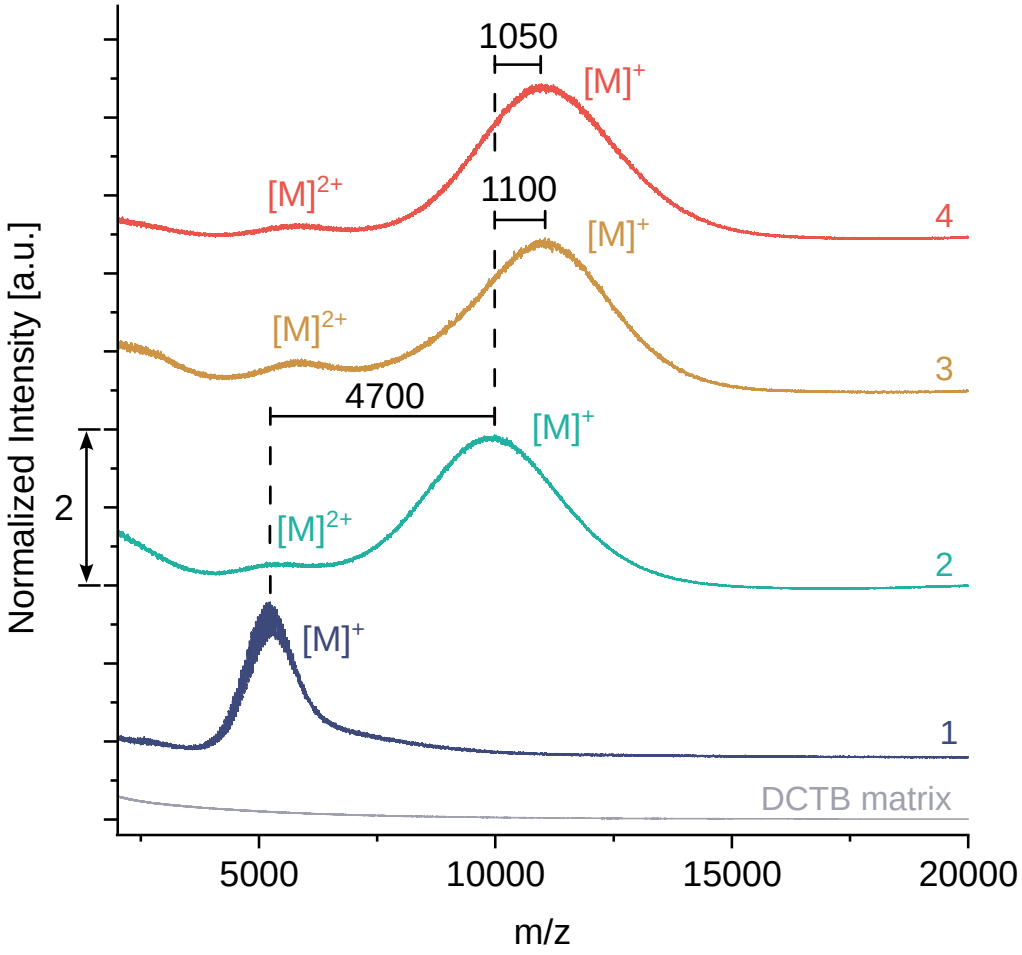

Figure A.6. 5: MALDI-TOF mass spectra of 1, 2, 3, 4 and the blank background mass spectrum of the matrix DCTB with potassium acetate measured in linear positive TOF mode. The molar mass of the star block (co)polymers was calculated for the single charged mass peak $[M]^+$ using background-subtracted mass spectra and peak deconvolution in order to correct for overlapping intensities of the double charged mass peak $[M]^{2+}$. The mass peaks are assigned only according to their charge state regardless of the adducts' nature. The relative mass difference measured between the peak apexes between 1 and 2 and between 2 and 3 is of $\Delta m/z \pm 100$ accuracy and between 2 and 2 of $\Delta m/z \pm 50$ accuracy.

A.6.5. MQ NMR spectroscopy

Table A.6. 1: Overview of the connectivity distribution of all ACNs synthesized.

ACN	f_{SL} [a]	f_{DL} [b]	f_{HOC} [c]	f_{defs} [d]	RDC_{SL} [e]	RDC_{DL} [f]	RDC_{HOC} [g]	RDC_{avg} [h]
	(%)				(Hz)			
5a	4	14	75	7	90	29	1.3	9
5b	33	38	26	3	123	48	2.4	59
5c	**34**	**44**	19	3	154	58	0.4	79
5d	**40**	**47**	11	1	183	72	32	109

[a] fraction of single links

[b] fraction of double links

[c] fraction of higher order connectivity defects

[d] defect and sol fraction

[e] Residual Dipolar Coupling (RDC) of the single links

[f] RDC of the double links

[g] RDC of the higher-order connectivity defects

[h] fraction-weighted average RDC

A.6.6. Rheology

Table A.6. 2: Overview of the gelation process of star polymer **3** and **4** as a function of both synthesis concentration and temperature.

c_{prep}	c (g L^{-1})	T (°C)	1st scope (min)	2nd scope = gel point (min)
0.5c*	38	30	21	75
c*	76	30	10	25
c*	76	45	10.8	19
c*	76	60	17.7	-
c*	76	80	12	-
1.5c*	114	30	10	20
2.5c*	190	30	8.5	14

A.6.7. Interaction parameter estimates for PEG and PCL in DMSO

Literature provides only indirect information about the interactions between DMSO and PEG or PCL. Classical references like the Polymer Handbook[1] do not cover these polymer solvent pairs and we attempt to estimate these interactions based upon the Hansen approach[2]. **Table A.6.3** compiles the most recent reference on the Hansen solubility parameters[3] and the estimate from Hansen's book for DMSO.[2] Regarding PEG and PCL we list several sources whereby we indicate in bold the preferred value (due to a direct measurement, consistency with other data, etc.).

Table A.6. 3: Hansen solubility parameters δ given in units of $MPa^{1/2}$. The table distinguishes between measured (m) and calculated (c) values, if this information was provided.

	δ_D	δ_P	δ_H	δ, δ_T	v_0 [cm^3/mol]	Refs.	κ [10^{-5}/K]
PEG	17	10	5	19.4 (c) / **20.4** (m) / 20.8	39	2, 4	71 [a]
PCL	19.6	5	8.4	19.2 / **20.2** / 19.9	**102.3** (m) 101.3 (c)	5, 2	64 [a]
DMSO	17.4	14.2	7.3	23.6	71.3	3	93 [b]
DMSO	18.4	16.4	10.2	26.7	71.3	2	93 [b]

v_0 is the volume of solvent molecule and κ is the thermal expansion coefficient.

[a] From Table 7.4 of Ref. 1 at the lowest available temperature.

[b] Average thermal expansion coefficient in the temperature interval 20 – 60 °C computed from the density data of Ref. 6

For the parameters of this table, we follow Hansen[2, 7] and decompose the total solubility parameter into three different contributions related to dispersion forces, polar cohesive energy, and hydrogen bonding

$$\delta_{\mathrm{T}}^2 = \delta_{\mathrm{D}}^2 + \delta_{\mathrm{P}}^2 + \delta_{\mathrm{H}}^2 \qquad (1)$$

From these contributions for a species *A* and *B*, one can compute the solubility parameter distance[2]

$$R_\alpha^2 = 4(\delta_{\mathrm{DA}} - \delta_{\mathrm{DB}})^2 + (\delta_{\mathrm{PA}} - \delta_{\mathrm{PB}})^2 + (\delta_{\mathrm{HA}} - \delta_{\mathrm{HB}})^2 \qquad (2)$$

The coefficient of 4 for the first term was introduced in later works for convenience:[8] with this empirical parameter, all miscible materials appear roughly within a sphere when interpreting the above differences as differences along the three axes of a cartesian coordinate system. Solubility parameters like the Hildebrand-Scott solubility parameter, δ, or the Hansen solubility parameter, δ_{T}, can be used to compute estimates for the Flory-Huggins interaction parameters

of different molecules. The Hildebrand-Scott solubility parameter for species $X = A, B$ is defined as[9]

$$\delta_X = \left(\frac{E_X}{v_X}\right)^{1/2} = \left(\frac{\Delta H_X - RT}{v_X}\right)^{1/2} \quad (3)$$

Here, R is the gas constant, T the absolute temperature, E_X is the energy of vaporization (cohesive energy), v_X the molar volume, and ΔH_X the enthalpy change of species X. Let us use A for the solvent and B for the polymer. For non-polar systems, a comparison of the solubility parameters provides a first estimate for the (enthalpic part) of the Flory interaction parameter

$$\chi_{\mathrm{H}} \approx \frac{v_{\mathrm{A}}}{RT}(\delta_{\mathrm{A}} - \delta_{\mathrm{B}})^2 \quad (4)$$

where T is the absolute temperature and v_{A} the molar volume of the solvent that establishes the unit volume of the Flory-Huggins lattice in the dilute case. Often, a correction is added on top of the enthalpic contribution[1] that is considered to be of entropic origin. Typically, a constant between 0.3 and 0.4 is chosen (most often 0.34),

$$\chi = 0.34 + \frac{v_{\mathrm{A}}}{RT}(\delta_{\mathrm{A}} - \delta_{\mathrm{B}})^2 \quad (5)$$

Mixing is expected if

$$\chi < \chi_{crit} = 1/2 \quad (6)$$

(or equivalently, if $\chi_H \leq 0.16$). A connection between the solubility parameter distance and the Flory-Huggins interaction parameter χ is established by computing[10]

$$\chi_\alpha = \alpha \frac{v_{\mathrm{A}} R_\alpha^2}{4RT} \quad (7)$$

which is proportional to χ_{H} in the absence of polar interactions and hydrogen bonding, however, the agreement is not quantitative. Lindvig[10] analyzed a large number of solubilities and proposed that a coefficient of $\alpha = 0.6$ leads to a better agreement with the Flory-Huggins parameter as compared to the original choice of $\alpha = 1.0$.

The solubility parameters given in **Table A.6. 3** were measured at room temperature. According to Ref. 2, one can extrapolate in approximation the temperature dependence of the different contributions to the solubility parameter by using

$$\frac{d\delta_D}{dT} = -\frac{5}{4}\kappa\delta_D \quad (8)$$

$$\frac{d\delta_P}{dT} = -\frac{1}{2}\kappa\delta_P \quad (9)$$

$$\frac{d\delta_H}{dT} = -\delta_H(0.00122 + \frac{\kappa}{2}) \quad (10)$$

Here, κ is the thermal coefficient of expansion. We have used these relations in combination with the available data to compute predictions for the Hansen interaction parameters at 80 °C for $\alpha = 0.6$.

All computed interaction parameters are summarized in **Table 6. 2** of the main text. According to the table, DMSO is a good solvent for PEG, while the estimates for PCL could be somewhat above or below theta conditions.

A.6.8. References

[1] J. E. Mark, *Physical properties of polymers handbook*, Springer, 2007.

[2] C. M. Hansen, *Hansen solubility parameters: a user's handbook*, CRC Press, Boca Raton, 2 edn., 2007.

[3] A. Alanazi, S. Alshehri, M. Altamimi and F. Shakeel, *J. Mol. Liq.*, 2020, **299**, 112211.

[4] E. Mannekens, The use of the Hansen Solubility Parameters (HSP) in the development of inkjet inks, www.hansen-solubility.com/contents/Inkjet_HSP_Chemstream.pdf

[5] https://polymerdatabase.com/polymers/polycaprolactone.html (21.11.2023).

[6] R. T. M. Bicknell, D. B. Davies and K. G. Lawrence, *Journal of the Chemical Society, Faraday Transactions 1: Physical Chemistry in Condensed Phases*, 1982, **78**, 1595-1601.

[7] C. M. Hansen, *Danish Technical: Copenhagen*, 1967, **14**.

[8] J. Camacho, E. Díez, I. Díaz and G. Ovejero, *Polym. Int.*, 2017, **66**, 1013-1020.

[9] M. Rubinstein and R. H. Colby, *Polymer physics*, Oxford University Press, New York, 2003.

[10] T. Lindvig, M. L. Michelsen and G. M. Kontogeorgis, *Fluid Phase Equilibria*, 2002, **203**, 247-260.

A.7. Supporting Information Chapter V

A.7.1. NMR and FTIR Spectroscopy

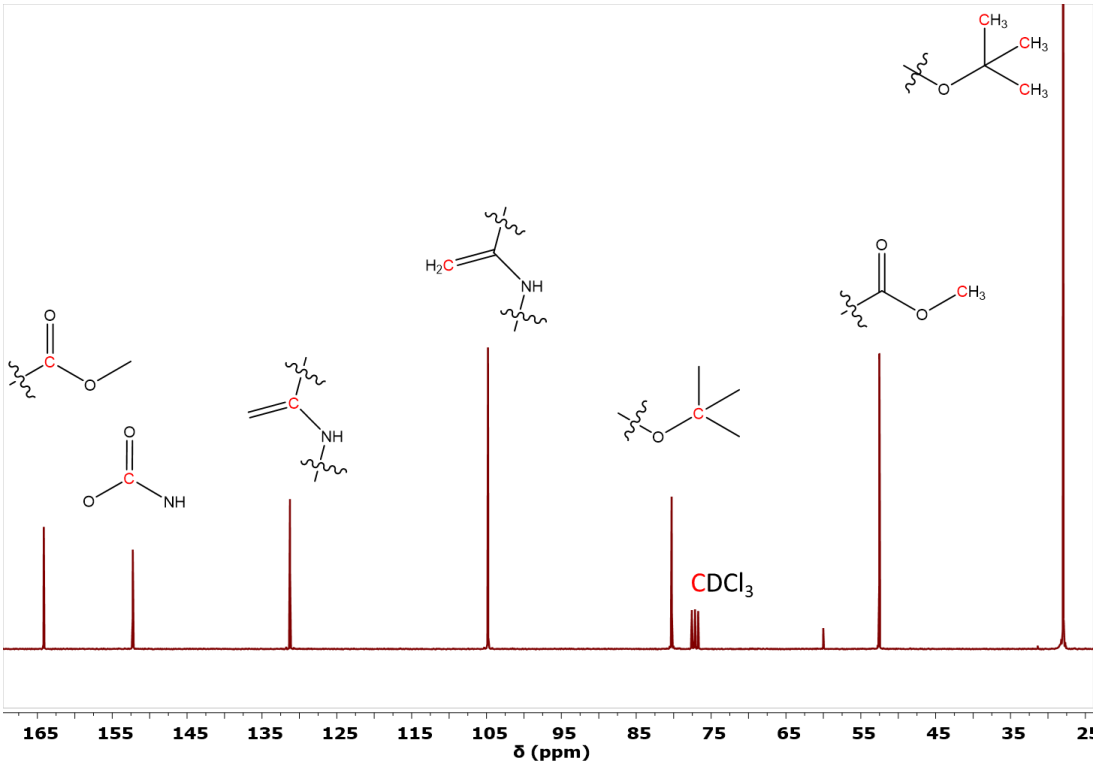

Figure A.7. 1: Exemplary ^{13}C-NMR spectrum of *t*BAMA ($CDCl_3$).

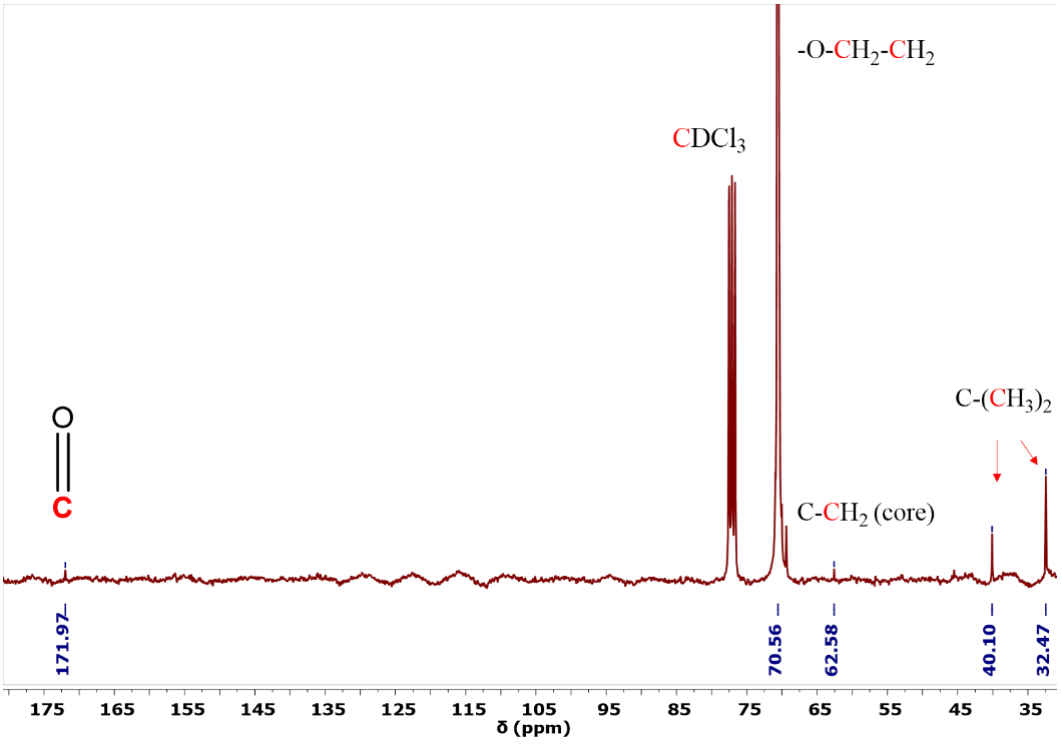

Figure A.7. 2: Exemplary ^{13}C-NMR spectrum of [PEG_{27}-amide-Br]$_4$ ($CDCl_3$).

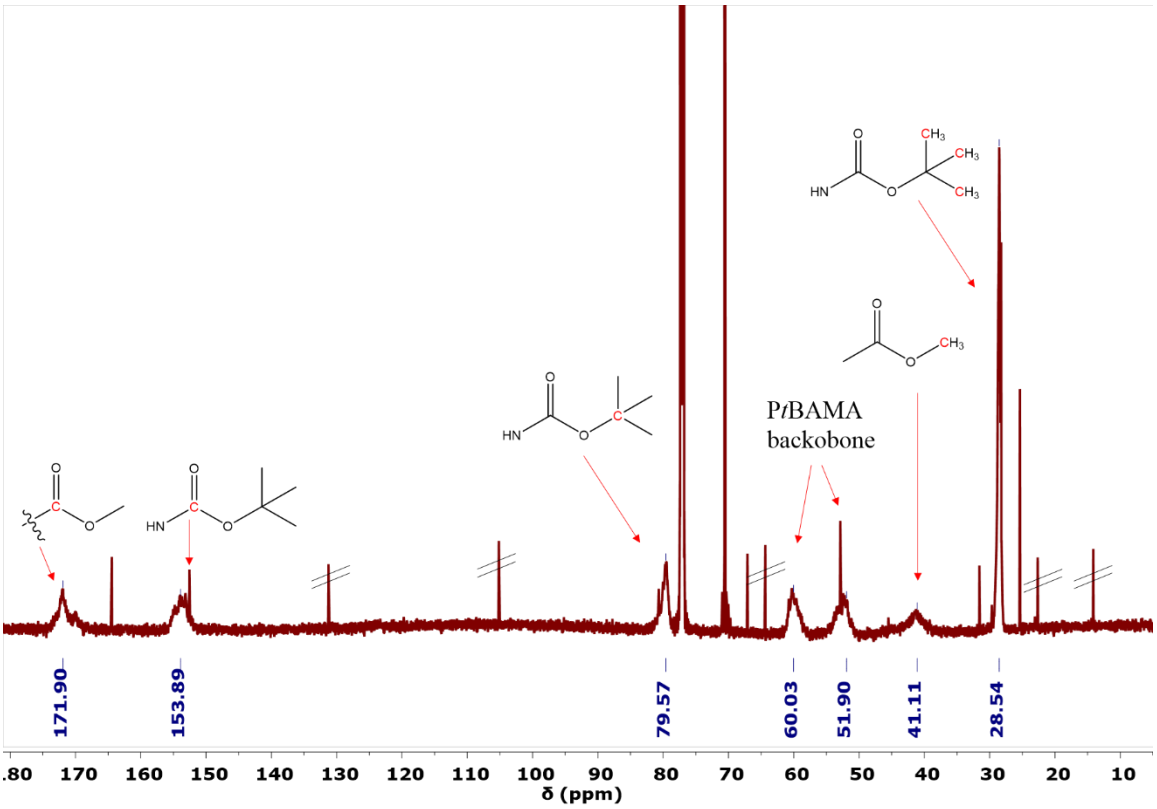

Figure A.7. 3: Exemplary ^{13}C-NMR spectrum of [PEG_{27}-*b*-PtBAMA]$_4$ ($CDCl_3$).

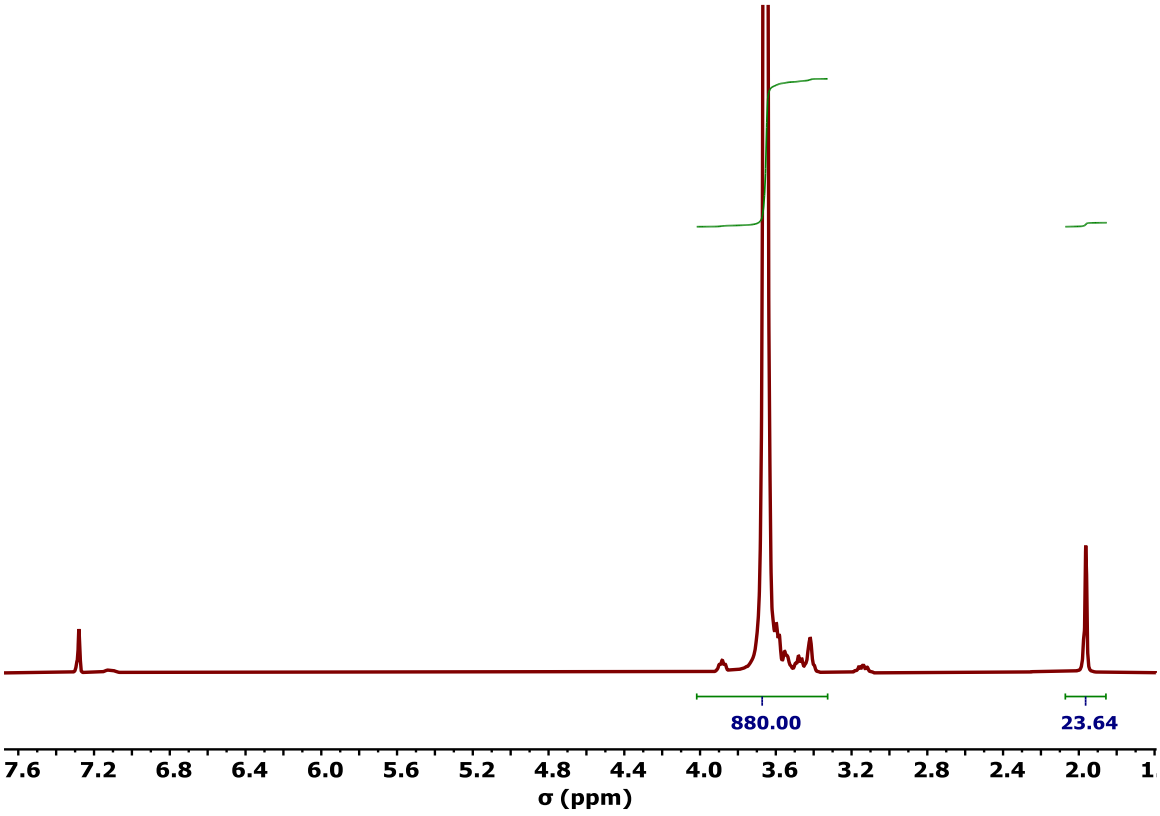

Figure A.7. 4: Exemplary ^{1}H-NMR spectrum of [PEG_{56}-amide-Br]$_4$ ($CDCl_3$).

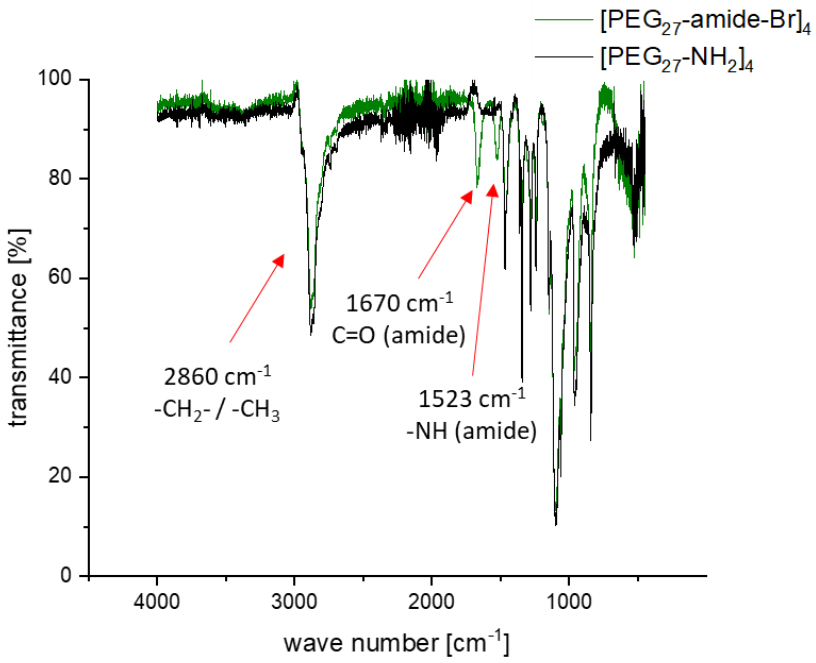

Figure A.7. 5: Exemplary overlay of FTIR measurements of $[PEG_{56}\text{-amide-Br}]_4$ and $[PEG_{56}\text{-}NH_2]_4$.

A.7.2. Dispersity optimization by added deactivator species

To overcome the loss of reaction control which results in higher *Đ*, the addition of different amounts of $CuCl_2$ as deactivator species was investigated. **Figure A.7. 6 A** shows the corresponding SEC traces of the block copolymers obtained after 4 h of reaction time while **Table A.7. 1** (entry 1-5) summarizes the conditions used.

Table A.7. 1: Reaction conditions used to synthesize [PEG27-*b*-PtBAMA$_y$]$_4$ via ATRP, showing the influence of amount deactivator and copper species used. Corresponding polymer properties are characterized by SEC and ^{1}H-NMR spectroscopy.

Entry	[I]	[Cu(I)X]	[Cu(II)X]	[*t*BAMA]	[L]	*T* [°C]	DPn, NMR /arm[b]	M_n [g/mol][a]	[*Đ*][a]
		X= Cl	X= Cl		[TPMA]				
1	1	4	**0**	400	8	60	13	22,800	1.46
2	1	4	**0.6**	400	8	60	13	28,000	1.53
3	1	4	**1.2**	400	8	60	11	22,400	1.27
4	1	4	**2**	400	8	60	12	19,500	1.18
5	1	4	**2.4**	400	8	60	12	17,000	1.40
6	1	4	**2**	400	8	60	20	15,600	1.50
		X= Cl	**X= Br**						
7	1	4	2	400	8	60	9	16,000	1,25
		X= Br	X=Cl						
8	1	4	2	400	8	60	14	16,000	1.29
		X= Br	X=Br						
9	1	**4**	**2**	400	8	60	12	14,100	1.34

[a] Determined by SEC (eluent: DMAc/LiCl [99.79/0.21], PMMA calibration) and by [b] ^{1}H-NMR spectroscopy. All reactions use a monomer concentration= 0.63 mmol/mL (ratio: dioxane/iso-propanol=1:8).

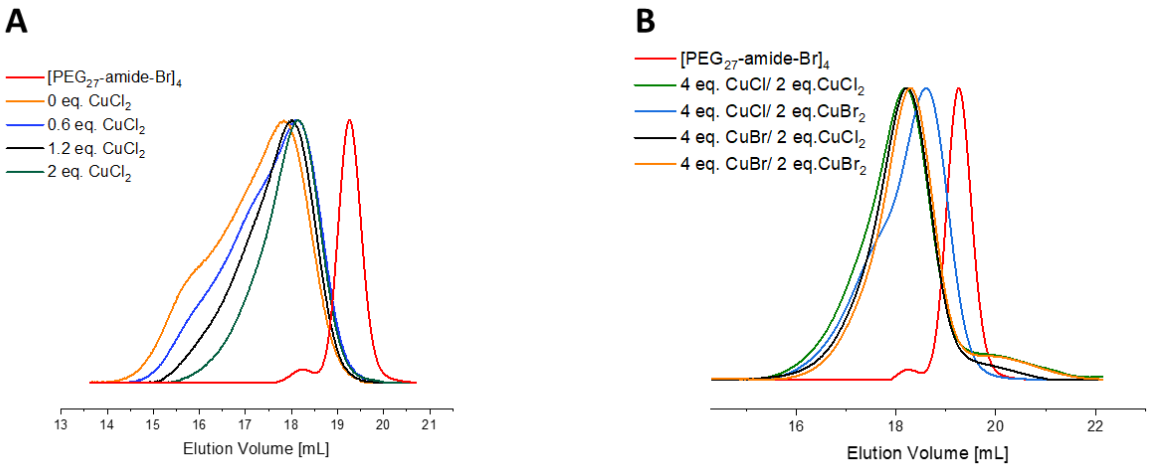

Figure A.7. 6: Comparison of experiments using different amounts of $CuCl_2$ as deactivator species (A); Comparison of experiments showing the influence of different Cu(I) and Cu(II)-species (B).

A.7.3. Influence of variation of Cu Species

In contrast to the CuCl/$CuCl_2$-system introduced before we were interested in the influence of the copper species used on the reaction control and the resulting conversion. Several experiments were compared using all possible combinations of CuCl, CuBr, $CuCl_2$, and $CuBr_2$. All experiments were carried out for 21 h. The new reaction conditions are summed up in **Table A.7. 1** (entry 6-9) and the corresponding SEC traces are shown in **Figure A.7. 6 B**.

A.7.4. Influence of Temperature

Next to the alkyl halide[1] , temperature,[2,3] pressure,[4,5] and the solvent, especially the polarity of the media[6] has the most pronounced influence on the conduction of ATRP reactions. Several temperatures were used to investigate the influence on the CuCl/$CuCl_2$-System (**Table A.7. 2** entry 1). Starting from room temperature (23 °C), the temperature was varied to 40, 50, 60 (used before), 70, or 80 °C (**Table A.7. 2** and **Figure A.7. 7**).

Table A.7. 2: Reaction conditions used to synthesize $[PEG_{27}\text{-}b\text{-}PtBAMA_y]_4$ via ATRP, showing the influence of temperature on the system. Corresponding polymer properties are characterized by SEC and ^{1}H-NMR spectroscopy.

Entry	[I]	[Cu(I)Cl]	[Cu(II)Cl]	[*t*BAMA]	[L]	*T* [°C]	DPn,NMR /arm[b]	M_n [g/mol][a]	[*Đ*][a]
1	1	4	**2**	400	8	60	20	15,600	1.50
2	1	4	2	400	8	**23**	20	24,800	1.65
3	1	4	2	400	8	**40**	17	18,400	1.18
4	1	4	2	400	8	**50**	15	22,000	1.24
5	1	4	2	400	8	**70**	12	15,400	1.16
6	1	4	2	400	8	**80**	20	12,200	1.7

[a] Determined by SEC (eluent: DMAc/LiCl [99.79/0.21], PMMA calibration) and by [b] ^{1}H-NMR spectroscopy. All reactions use a monomer concentration= 0.63 mmol/mL (ratio: dioxane/iso-propanol=1:8).

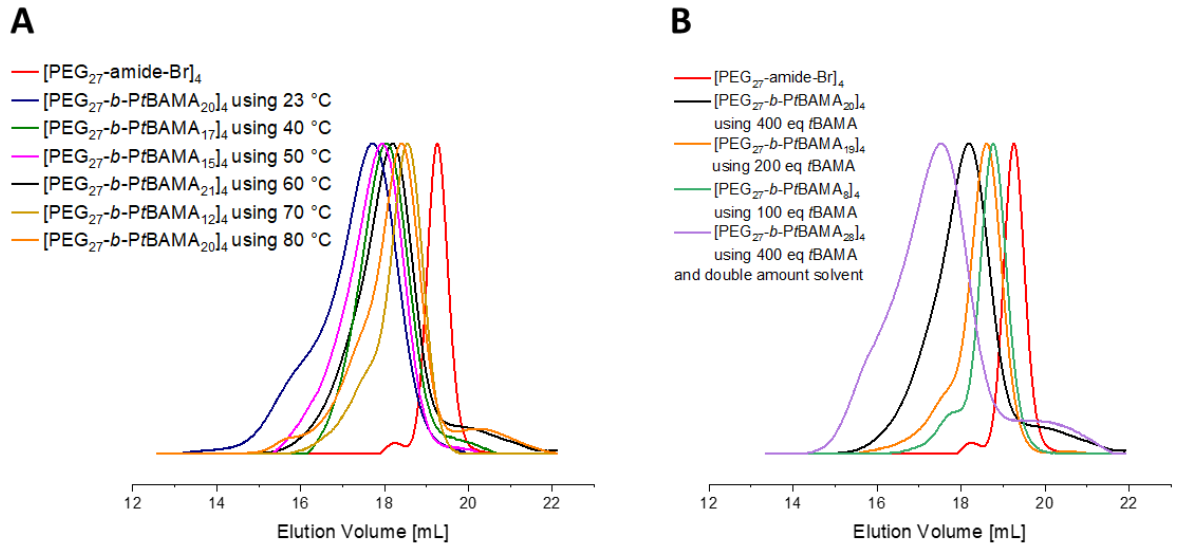

Figure A.7. 7: SEC elution traces (eluent: DMAc/LiCl [99.79/0.21]) corresponding to temperature variation experiments of **Table A.7. 2** (A); SEC elution traces (eluent: DMAc/LiCl [99.79/0.21]) corresponding to monomer concentration variation experiments (B, **Table A.7 .3**).

A.7.5. Influence of monomer concentration

To investigate the influence of initiator and monomer concentration on conversion and star-star coupling side reactions the monomer concentration was varied and the resulting polymers are compared via SEC and ^{1}H-NMR spectroscopy. **Table A.7. 3** summarizes the corresponding reactions performed. Starting with a monomer to initiator ratio of 1:400 the ratio was varied to either 1:200 or 1:100 keeping the initiator concentration constant. In contrast to that entry 4 of

Table A.7. 3 describes a constant initiator to monomer ratio of 400:1 while the initiator concentration itself is halved. **Figure A.7. 8** shows the corresponding SEC traces.

Table A.7. 3: Reaction conditions used to synthesize $[PEG_{27}$-*b*-$PtBAMA_y]_4$ via ATRP, showing the influence of monomer concentration on the system. Corresponding polymer properties are characterized by SEC and ^{1}H-NMR spectroscopy.

Entry	[I]	[Cu(I)Cl]	[Cu(II)Cl]	[*t*BAMA]	[L]	*T* [°C]	DPn,NMR /arm[b]	M_n [g/mol][a]	[*Đ*][a]
1	1	4	**2**	400	8	60	20	15,600	1.50
2	1	4	2	200	8	60	19	13,200	1,15
3	1	4	2	100	8	60	8	13,000	1,09
4	1	4	2	400	8	60	28	20,800	1.8

[a] Determined by SEC (eluent: DMAc/LiCl [99.79/0.21], PMMA calibration) and by [b] ^{1}H-NMR spectroscopy. All reactions use a solvent ratio of dioxane/iso-propanol=1:8 and an initiator concentration of 1.55 µmol/mL (expect entry 4 which is using a initiator concentration of 0.77 µmol/mL).

A.7.6. The right solvent: Key between long and short chains

Besides the temperature, the type of solvent used plays an important role in terms of reaction kinetics.[6] Therefore, different ratios of dioxane and iso-propanol as well as the use of pure alcohols with different polarities as reaction solvent were compared. Hence, we decided to use ethanol as a more polar solvent and 1-octanol as a rather unpolar solvent when compared to iso-propanol. **Figure A.7. 8 B** shows the corresponding SEC-traces for the ratio variation at dioxane/iso-propanol systems while **Figure A.7. 8**. **A** shows the SEC-traces of reaction variation using either pure ethanol, iso-propanol or 1-octanol as a reaction solvent. All reactions were performed under the same ratios of tBAMA:TPMA:CuCl: initiator = 400:8:4:1 with a monomer concentration of 0.63 mmol/mL for 4 h at 60 °C, except for the solvent variation discussed. In addition, the reaction in pure iso-propanol, used room temperature instead of 60 °C, which is why it can only serve as a limited comparison reaction considering that in our case lower temperatures are associated with higher Đ but comparable conversions to the one at 60 °C (see influence of temperature).

Table A.7. 4: Reaction conditions used to synthesize [PEG_{27}-*b*-$PtBAMA_y$]$_4$ via ATRP, showing the influence of solvent media used on the system. Corresponding polymer properties are characterized by SEC and ^{1}H-NMR spectroscopy.

Entry	Solvent [mL]	Cosolvent [mL]	Initiator concentration [µmol/mL]	*T* [°C]	DPn,NMR /arm[b]	M_n [g/mol][a]	[*Đ*][a]
1	Dioxane 0.5	*Iso*-propanole 4	1.55	60	20	15,600	1.50
2	Dioxane 2.25	*Iso*-propanole 2.25	1.55	60	32	16,300	2,72
3	Dioxane 4	*Iso*-propanole 0.5	1.55	60	16	13,100	2,02
4	*Iso*-propanol 4.5	-	1.55	23	20	23,900	1,76
5	Octanole 4.5	-	1.55	60	41	37,000	1.87
6	Ethanol 4.5	-	1.55	60	3	11,700	1.17

[a] Determined by SEC (eluent: DMAc/LiCl [99.79/0.21], PMMA calibration) and by [b] ^{1}H-NMR spectroscopy. All reactions use a monomer concentration= 0.63 mmol/mL (ratio: dioxane/iso-propanol=1:8).

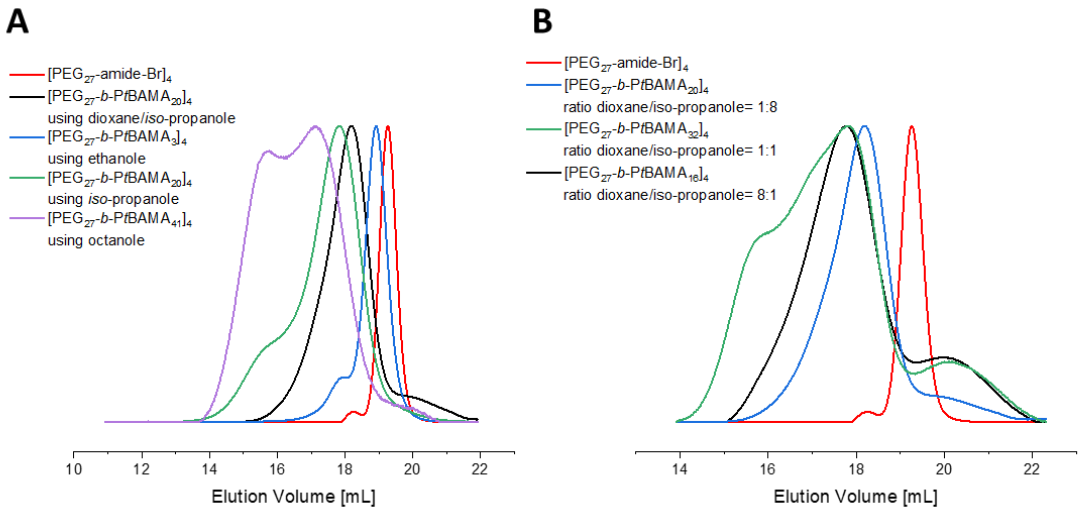

Figure A.7. 8: SEC elution traces (eluent: DMAc/LiCl [99.79/0.21]) of reaction variation using either pure ethanol, iso-propanol, or octanol as a reaction solvent (A); SEC elution traces (eluent: DMAc/LiCl [99.79/0.21]) showing the influence of ratio variation between the amounts of dioxan and iso-propanol used (B).

A.7.7. Towards increasing conversion

As shown before, the use of different solvents at 60 °C reaction temperature and a CuCl/$CuCl_2$ system reveal that the conversion can be drastically increased if pure alcohol with longer alkyl chains serves as solvent (ethanol < iso-propanol < 1-octanol). Additionally, with the higher conversion, the reaction lacks control due to the appearance of more star-star coupling side reactions which can be observed via SEC. As already mentioned before, alcohols as solvents

are well known to promote the disproportionation of Cu(I)X into Cu(0) and Cu(II)X which is a crucial step in SET-LRP.[7] Additionally, more recent work of avoiding star-star coupling reactions show that Cu(0) mediated controlled radical polymerization techniques combine high-end group fidelity with fewer star-star coupling reactions observed.[8–11] To overcome the problem of star-star-coupling, the reaction type was changed from ATRP to SET-LRP, comparing iso-propanol and 1-octanol as solvent. **Table A.7. 5** sums up the reaction conditions used and **Figure A.7. 9** shows the corresponding SEC traces.

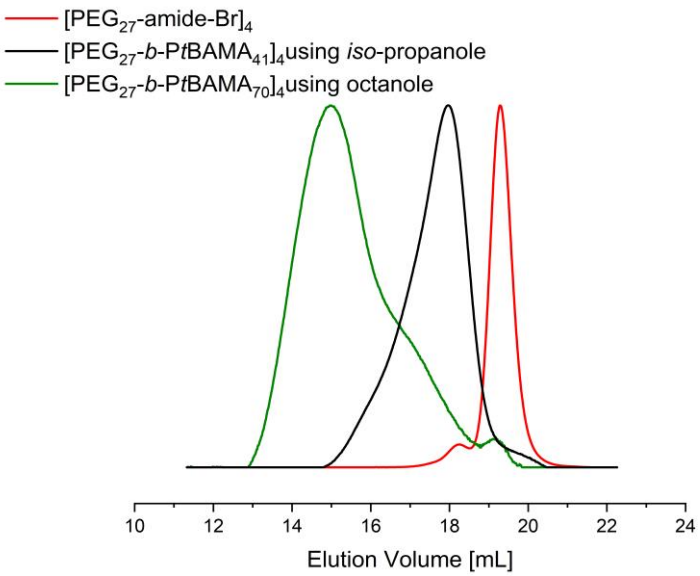

Figure A.7. 9: SEC-traces (eluent: DMAc/LiCl [99.79/0.21]) comparing different solvents used for block extension of $[PEG_{27}\text{-amide-Br}]_4$ with tBAMA via SET-LRP reactions.

Table A.7. 5: Reaction conditions used to synthesize $[PEG_{27}\text{-}b\text{-PtBAMA}_y]_4$ via SET-LRP, showing the influence of solvent used. The corresponding block copolymer characteristics were determined by SEC and ^{1}H-NMR spectroscopy.

Entry	[I]	[Cu(0)]	[Cu(II)Cl]	[*t*BAMA]	[L]	T [°C]	DPn,NMR /arm	M_n [g/mol]	[*Đ*]	Reaction time
1	1	4	0.8	400	8	RT	41	27,800	1.37	48 h
2	1	4	0.4	400	8	RT	70	69,400	2.49	24 h

[a] Determined by SEC (eluent: DMAc/LiCl [99.79/0.21], PMMA calibration) and by [b] ^{1}H-NMR spectroscopy. All reactions use a monomer concentration= 0.63 mmol/mL and either iso-propanol (entry 1) or 1-octanol (entry 2) as solvent.

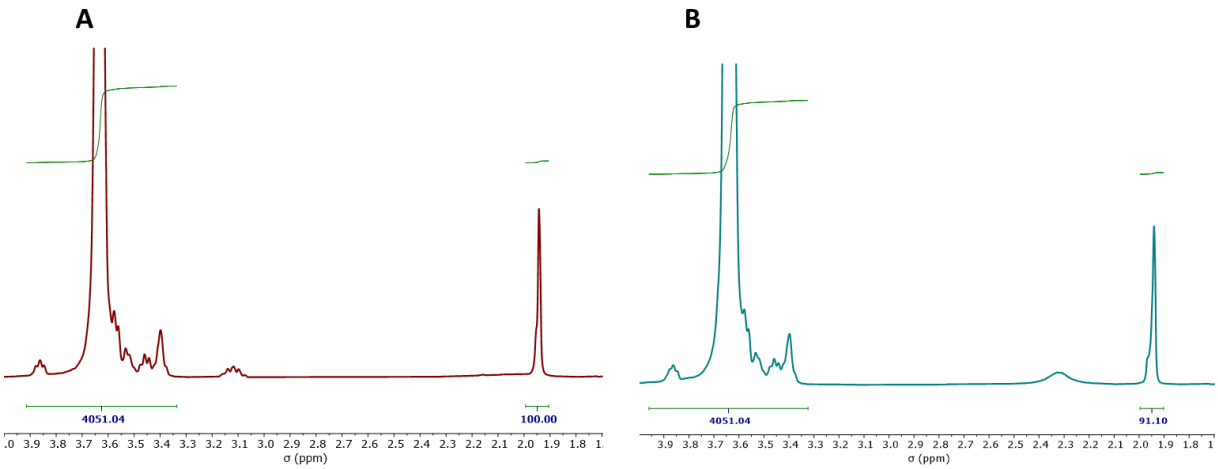

Figure A.7. 10: Example ^{1}H-NMR of [PEG$_{56}$-amide-Br]$_4$ before **(A)** treatment with TFA at 50 °C for 10 and after **(B)** using CDCl3.

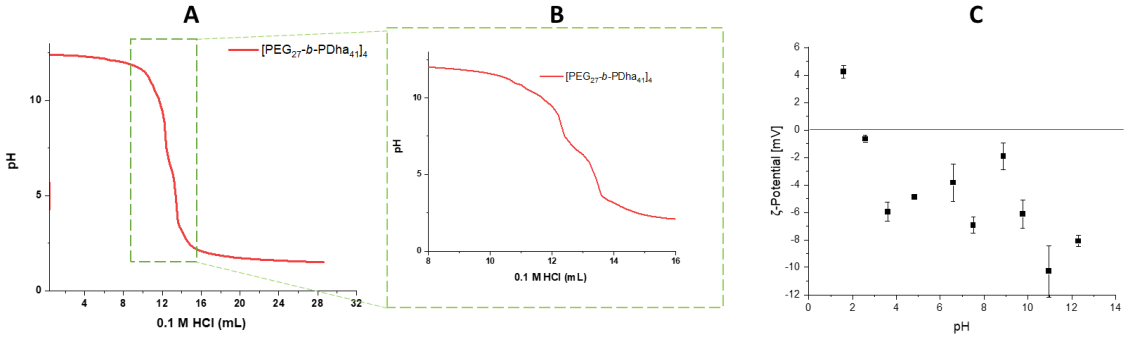

Figure A.7. 11: Potentiometric titration of [PEG$_{27}$-*b*-PDha$_{41}$]$_4$ dissolved in 0.1 M NaOH at a concentration of 0.2 mg/mL and titrated with 0.1 M HCl; B: Zoom of **Figure A.7. 11A** in the range of 8-16 mL; C: ζ-Potential of [PEG$_{27}$-*b*-PDha$_{41}$]$_4$ at different pH values determined by titration.

A.7.8. Dynamic Light Scattering

The amplitude correlation functions $g^{(1)}(q,\tau)$ received from the DLS were fitted with a biexponential function

$$g^{(1)}(q,\tau) = A_1 \cdot \exp\left(-\frac{\tau}{\tau_{\mathrm{R},1}}\right) + A_2 \cdot \exp\left(-\frac{\tau}{\tau_{\mathrm{R},2}}\right)$$

where A_i is the amplitude and $\tau_{\mathrm{R,i}}$ with i = 1, 2 is the characteristic relaxation time of the corresponding process . The diffusion coefficient is extracted from the relaxation time using the scattering vectors q of the respective scattering angle.

$$D = \left(\frac{1}{\tau_{\mathrm{R,i}} \cdot q^2}\right)$$

with the Boltzmann constant k_B, the absolute temperature T, and the viscosity of the solvent η_s. The results of this analysis are summarized in **Table A.7. 6**.

$$R_H = \frac{k_B T}{6\pi\eta_s D}$$

Table A.7. 6: Amplitudes (A_1, A_2) of the biexponential fits and extracted hydrodynamic radii at a scattering angle of 90° and c = 0.2 mg/mL corresponding to **Figure 7. 4A**. The correlation functions were normalized to unity.

Polymer	A_1	$R_{H,1}$ (nm)	A_2	$R_{H,2}$ (nm)	pH
[PEG$_{27}$-*b*-PDha$_6$]$_4$	0,21	29	0,79	92	13,0
[PEG$_{27}$-*b*-PDha$_{20}$]$_4$	0,28	27	0,72	72	13,0
[PEG$_{27}$-*b*-PDha$_{41}$]$_4$	0,26	26	0,74	73	13,1
[PEG$_{55}$-*b*-PDha$_6$]$_4$	0,21	22	0,78	76	13,1
[PEG$_{112}$-*b*-PDha$_7$]$_4$	0,27	21	0,73	69	13,1
[PEG$_{27}$-*b*-PDha$_6$]$_4$	0,70	88	0,30	242	5,1
[PEG$_{27}$-*b*-PDha$_{20}$]$_4$	0,39	21	0,61	163	5,0
[PEG$_{27}$-*b*-PDha$_{41}$]$_4$	0,43	23	0,56	102	4,9
[PEG$_{55}$-*b*-PDha$_6$]$_4$	0,35	66	0,65	200	4,9
[PEG$_{112}$-*b*-PDha$_7$]$_4$	0,29	30	0,71	163	5,0
[PEG$_{27}$-*b*-PDha$_6$]$_4$	0,60	115	0,40	721	3,0
[PEG$_{27}$-*b*-PDha$_{20}$]$_4$	0,76	44	0,24	533	3,0
[PEG$_{27}$-*b*-PDha$_{41}$]$_4$	0,10	305	0,90	3550	3,0
[PEG$_{55}$-*b*-PDha$_6$]$_4$	0,60	64	0,40	383	2,9
[PEG$_{112}$-*b*-PDha$_7$]$_4$	0,41	50	0,59	235	2,9

A.7.9. Atomic Force Microscopy

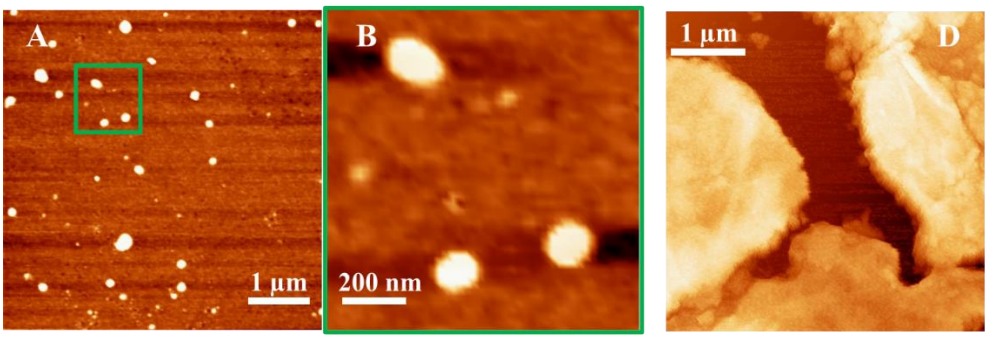

Figure A.7. 12: AFM height image showing the size distributions of [PEG$_{27}$-*b*-PDha$_6$]$_4$ aggregates at pH=13 at a concentration of 1.0 mg/mL **(A).** Zoomed in AFM height image for the region marked by the green box in **A (B)**; AFM height image showing the size distributions of [PEG$_{27}$-*b*-PDha$_{41}$]$_4$ aggregates at pH=3 at a concentration of 1.0 mg/mL **(C).**

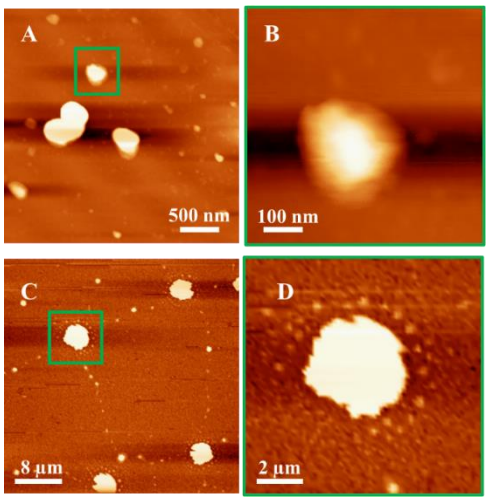

Figure A.7. 13: A and **C** AFM height images showing the size distributions of $[PEG_{27}\text{-}b\text{-}PDha_{41}]_4$ aggregates at pH= 3 and pH=13 at a concentration of 0.2 mg/mL respectively. **B**: Zoomed in AFM height image for the region marked by the green box in **A. D**: Zoomed in AFM height image for the region marked by the green box in **C**.

A.7.10. References

[1] W. Tang, Y. Kwak, W. Braunecker, N. V. Tsarevsky, M. L. Coote and K. Matyjaszewski, *J. Am. Chem. Soc.*, 2008, **130**, 10702-10713.

[2] F. Seeliger and K. Matyjaszewski, *Macromolecules*, 2009, **42**, 6050-6055.

[3] F. Seeliger and K. Matyjaszewski, *Macromolecules*, 2010, **43**, 5478-5478.

[4] J. Morick, M. Buback and K. Matyjaszewski, *Macromol. Chem. Phys.*, 2011, **212**, 2423-2428.

[5] L. Mueller, W. Jakubowski, K. Matyjaszewski, J. Pietrasik, P. Kwiatkowski, W. Chaladaj and J. Jurczak, *Eur. Polym. J.*, 2011, **47**, 730-734.

[6] W. A. Braunecker, N. V. Tsarevsky, A. Gennaro and K. Matyjaszewski, *Macromolecules*, 2009, **42**, 6348-6360.

[7] V. Percec, T. Guliashvili, J. S. Ladislaw, A. Wistrand, A. Stjerndahl, M. J. Sienkowska, M. J. Monteiro and S. Sahoo, *J. Am. Chem. Soc.*, 2006, **128**, 14156-14165.

[8] C. Boyer, A. Atme, C. Waldron, A. Anastasaki, P. Wilson, P. B. Zetterlund, D. Haddleton and M. R. Whittaker, *Polymer Chemistry*, 2013, **4**, 106-112.

[9] C. Boyer, A. Derveaux, P. B. Zetterlund and M. R. Whittaker, *Polymer Chemistry*, 2012, **3**, 117-123.

[10] B. G. van Ravensteijn, R. Bou Zerdan, M. E. Helgeson and C. J. Hawker, *Macromolecules*, 2018, **52**, 601-609.

[11] C. Waldron, A. Anastasaki, R. McHale, P. Wilson, Z. Li, T. Smith and D. M. Haddleton, *Polymer Chemistry*, 2014, **5**, 892-898.

A.8. Supporting Information Chapter VI

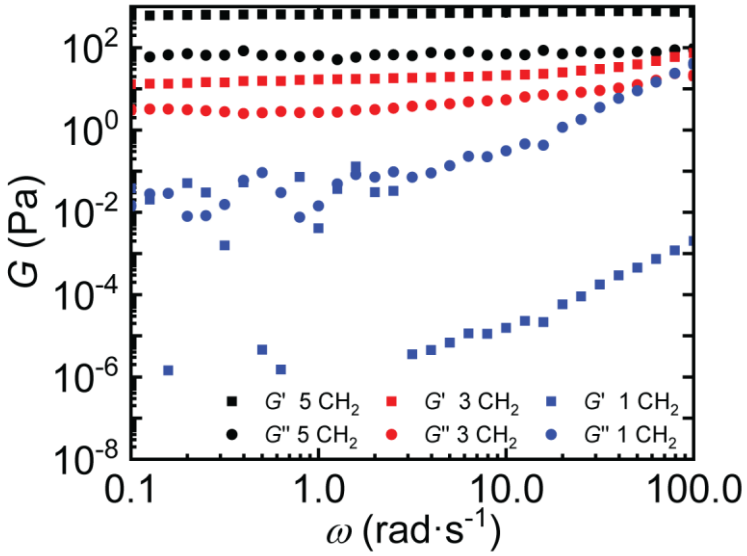

Figure A.8. 1: Oscillatory shear-rheology of gels at a concentration of 1 wt% synthesized at pH 3 (sulfuric acid), comparing different linker lengths of the betaine.

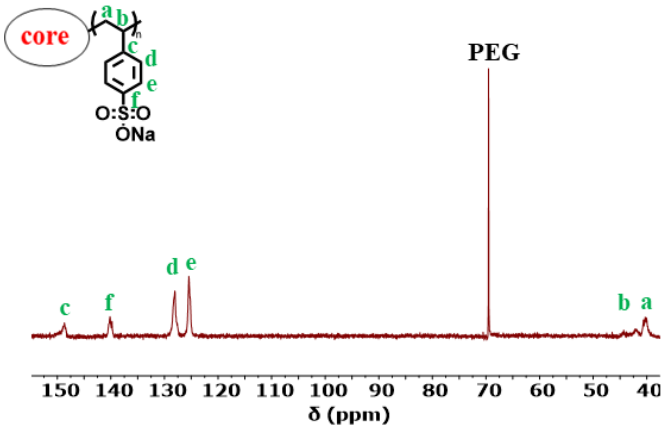

Figure A.8. 2: ^{13}C-NMR spectroscopy measurements (D_2O) of [PEG_{27}-b-$PSSNa_{100}$]$_4$.

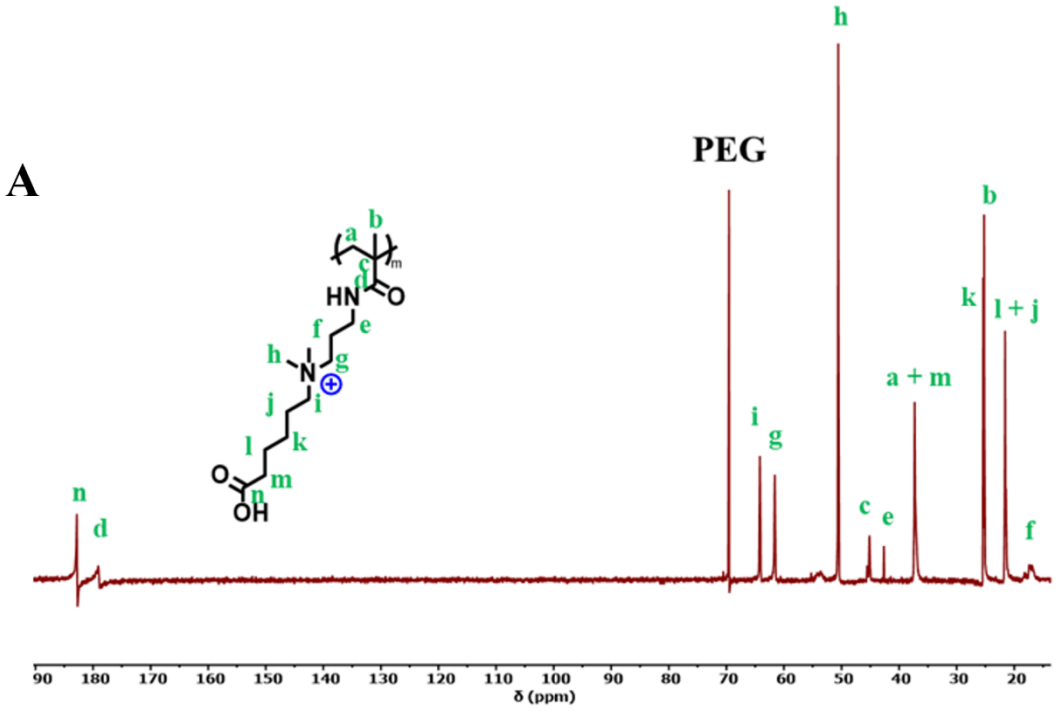

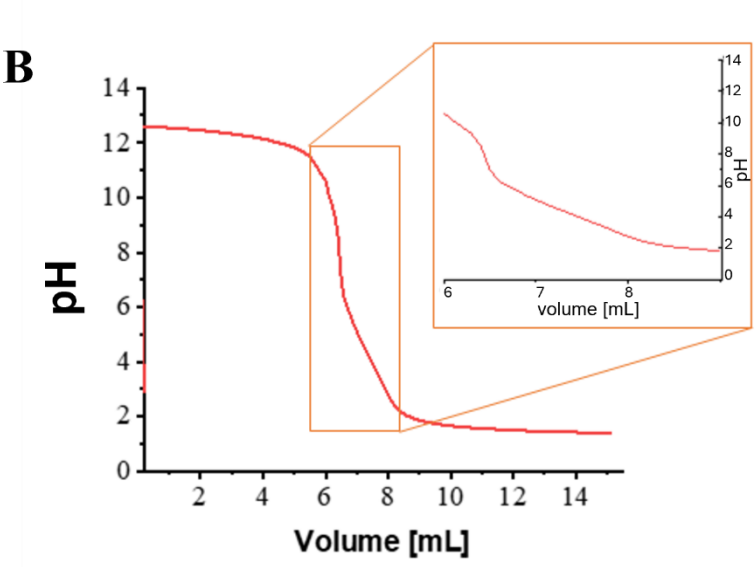

Figure A.8. 3: A: ^{13}C-NMR spectroscopy measurements (D_2O) of [PEG_{27}-b-($PDMAPMAAm_{26}$-g-$PCBAMAAm_{82}$)$_{108}$]$_4$, **B:** Potentiometric titration of [PEG_{27}-b-($PDMAPMAAm_{26}$-g-$PCBAMAAm_{82}$)$_{108}$]$_4$ dissolved in 0.1 M NaOH at a concentration of 10 mg/mL and titrated with 0.1 M HCl.

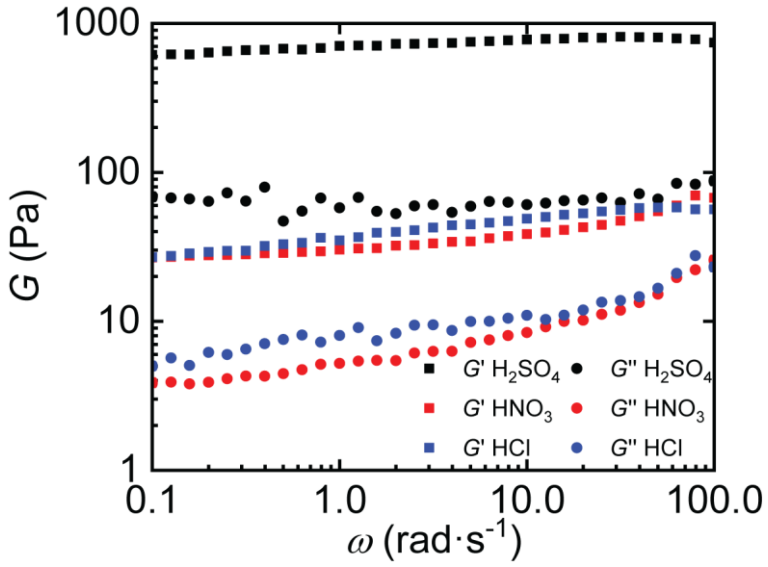

Figure A.8. 4: Oscillatory shear-rheology of gels at a concentration of 1 wt% synthesized at pH 3 with sulfuric acid, nitric acid and hydrochloric acid.

Viscometry

The specific viscosity η_{sp} was determined using a capillary viscometer of micro-Ubbelohde type I. The capillary was precleaned with hydrochloric acid, sodium hydroxide and water. Stock solutions of the respective polymers were prepared in aqueous sodium hydroxide solution (pH 13) and diluted to 12, 9, 6, 3, and 1 g·L^{-1}. Measurements were performed in a water bath at 20 °C.

The specific viscosity η_{sp} was calculated from the time t that a defined volume of the polymer solution needs to flow through the capillary and the corresponding time t_s for aqueous sodium hydroxide solution at pH 13 (1).

$$\eta_{sp} = \frac{\eta - \eta_s}{\eta_s} \approx \frac{t - t_s}{t_s} \quad (1)$$

The intrinsic viscosity $[\eta]$ is defined as (2) and was extrapolated according to the method of Schulz–Blaschke[1] (3).

$$[\eta] = \lim_{c \to 0} \frac{\eta_{sp}}{c} \quad (2)$$

$$\frac{\eta_{sp}}{c} = [\eta] + k_{SB}[\eta]\eta_{sp} \quad (3)$$

The Schulz–Blaschke constant k_{SB} provides qualitative information on the solvent quality; lower k_{SB} typically refers to better solvent quality.

The overlap concentration c^* is obtained from (4) and its error was estimated from the error propagation as (5).

$$c^* = \frac{1}{[\eta]} \tag{4}$$

$$\Delta c^* = \frac{1}{[\eta]^2} \cdot \Delta[\eta] \tag{5}$$

Results of viscosimetric analysis are summarized in **Table A.8. 1.**

Table A.8. 1: Overlap concentrations and Schulz–Blaschke constants from viscosimetric analysis for [PEG_{27}-b-$PSSNa_{100}$]$_4$ and [PEG_{27}-b-$PDMAPMAAm_{108}$]$_4$.

pH	**[PEG_{27}-*b*-$PDMAPMAAm_{108}$]$_4$**		**[PEG_{27}-*b*-$PSSNa_{100}$]$_4$**	
	k_{SB}	c^* (g·L^{-1})	k_{SB}	c^* (g·L^{-1})
13	0.14	39.7 ± 0.2	0.43	21.5 ± 0.5

References:

[1] G. V. Schulz, F. Blaschke, *J. Prakt. Chem.* **1941**, *158*, 130.

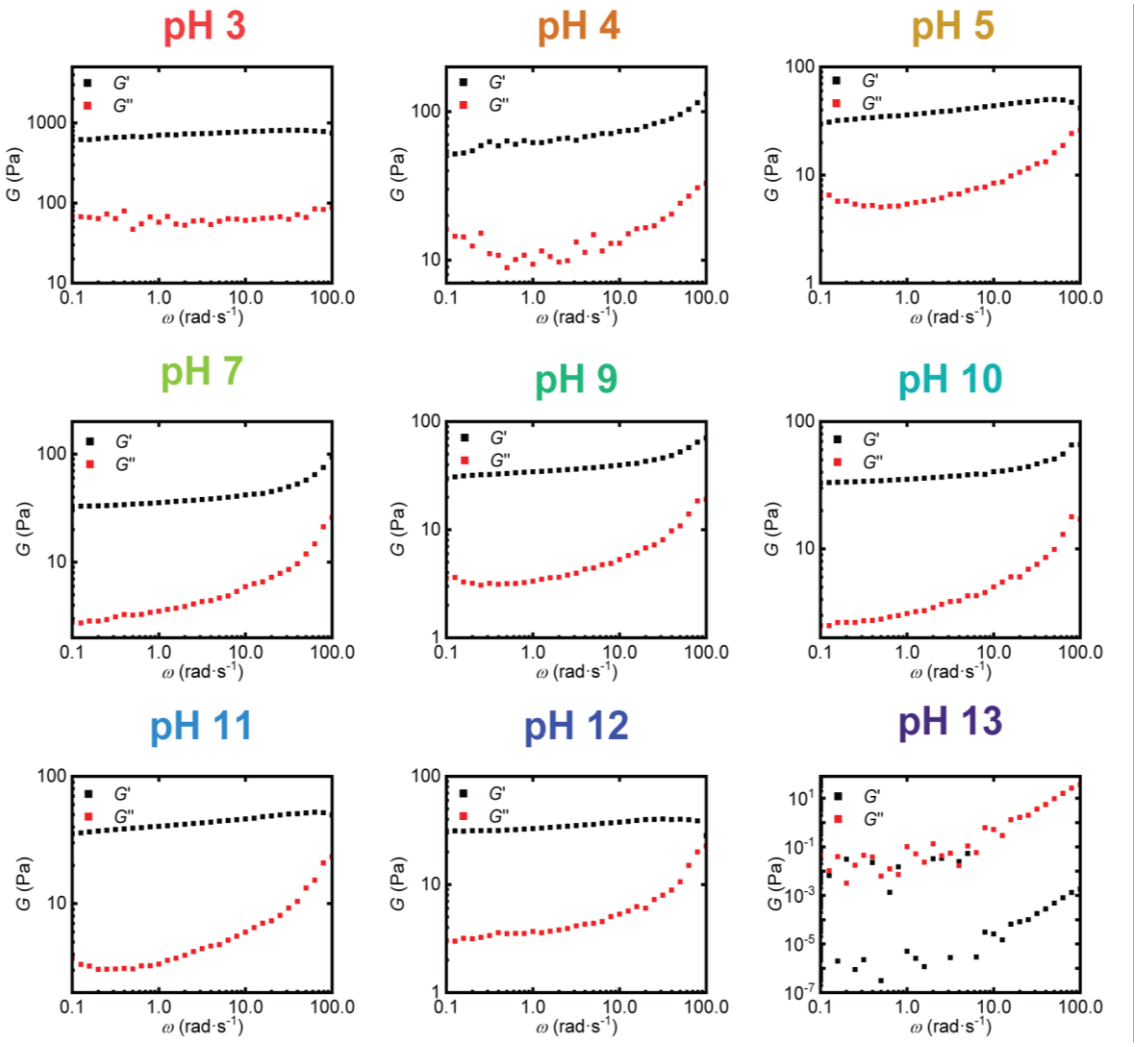

Figure A.8. 5: Oscillatory shear-rheology of the system at a concentration of 1 wt% synthesized at different pH using sulfuric acid and sodium hydroxide.

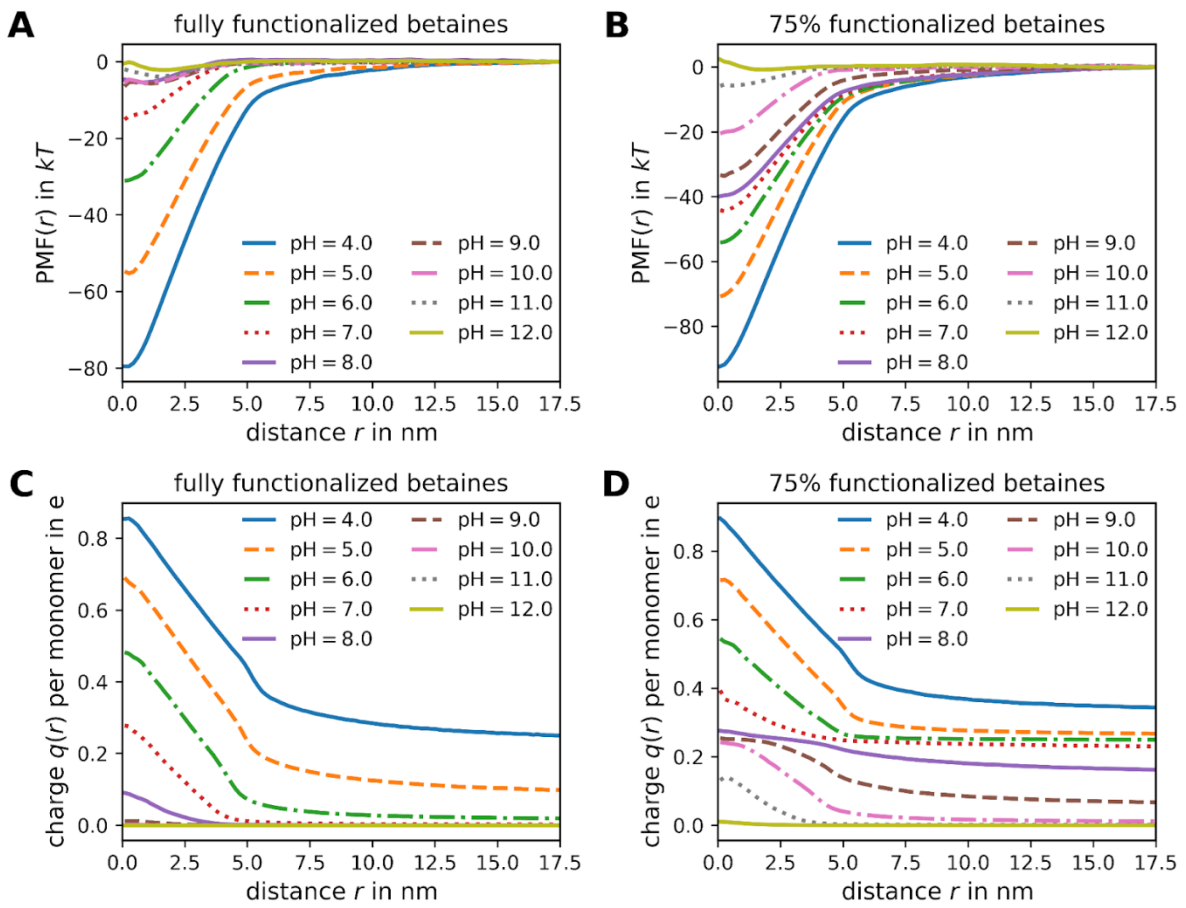

Figure A.8. 6: A&B: Plots of the PMF as a function of the distance between the centers of mass of the two chains for the case of full functionalization (**A**) and 75% functionalization (**B**). The minima at a small separation indicate an attractive interaction between the chains. The PMF is set to zero at the maximum separation between the chains. C&D: Plot of the mean charge per monomer as a function of the distance between the centers of mass of the two chains for the case of full functionalization (**C**) and 75% functionalization (**D**). The distance-dependent charging up of the monomers corresponds to the charge-regulation mechanism.

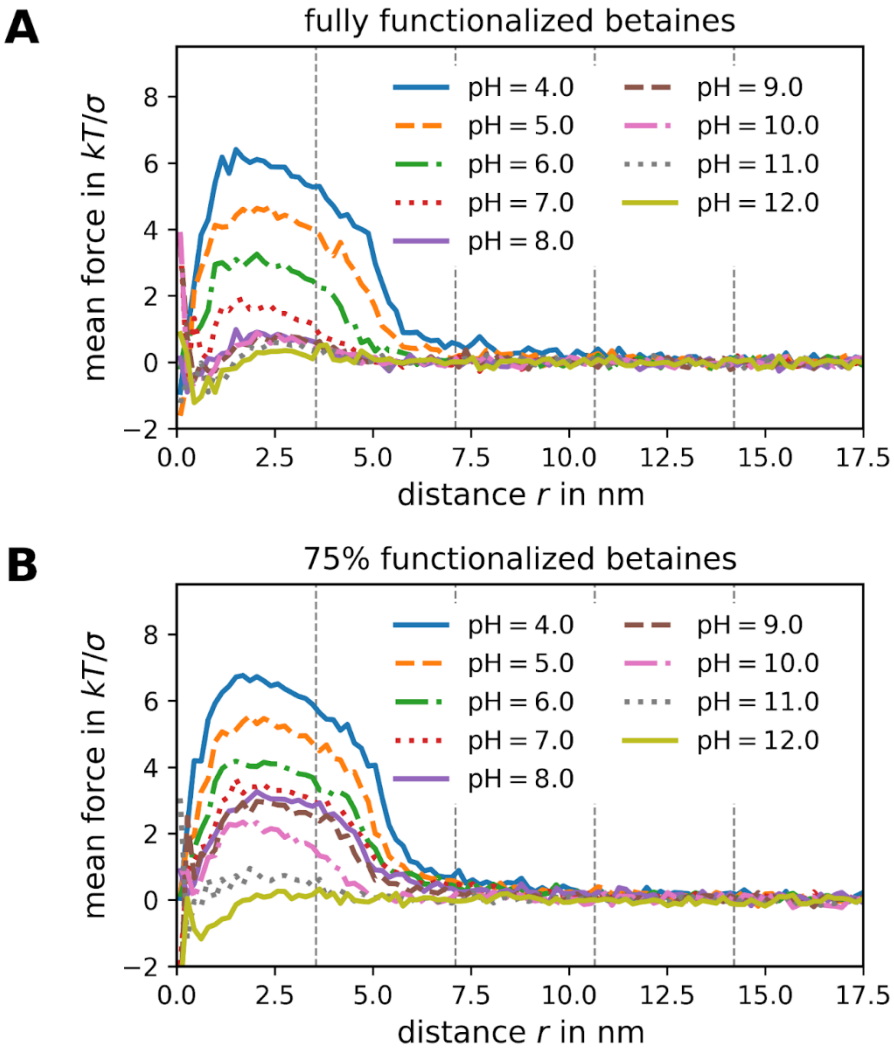

Figure A.8. 7: Plot of the measured mean force as a function of the distance between the centers of mass of the two chains for the fully functionalized case **A:** and the case of 75% functionalization **B:** The dashed vertical lines indicate the window boundaries. The continuity of the mean force across the window boundaries is an indicator that the stratification did not hinder the ergodic sampling of the phase space.

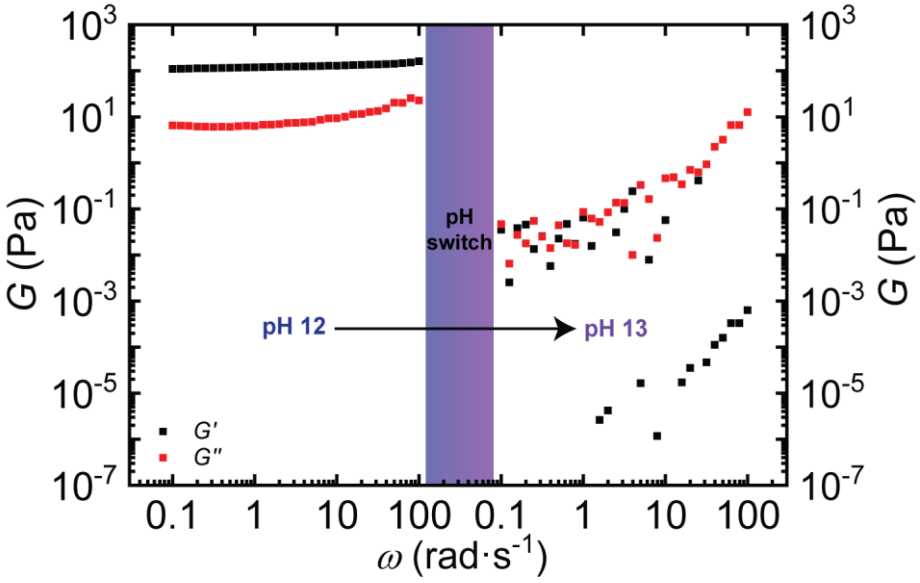

Figure A.8. 8: Oscillatory shear-rheology of the system synthesized at a concentration of 2 wt% at pH 12 and then switched to pH 13 leading to a gel with a concentration of 1.5 wt%.

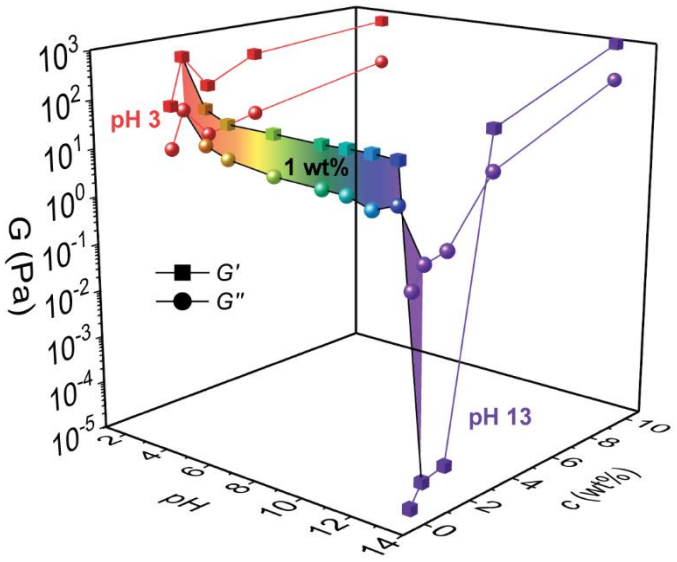

Figure A.8. 9: Overview of the rheological data obtained from measurements of the system at varied pH and concentrations.

[redacted]

CURRICULUM VITAE

NORA FRIBICZER

[redacted]

Work Experience

[redacted]

Education

[redacted]

Trainings & Certificates

[redacted]

Additional Skills & Activities

[redacted]